NMR studies on 2-oxoglutarate oxygenases

A thesis submitted to the Board of the faculty of Physical Sciences of the University of Oxford in partial fulfilment of degree of Doctor of Philosophy

Ivanhoe K. H. Leung
St Peter's College, University of Oxford
Trinity Term 2012

NMR studies on 2-oxoglutarate oxygenases

Ivanhoe K. H. Leung
St Peter's College, University of Oxford

D.Phil Thesis
Trinity Term 2012

Abstract

The work described in this Thesis has focused on the application of nuclear magnetic resonance (NMR) spectroscopy to study the Fe(II) and 2-oxoglutarate (2OG) dependent oxygenases, a family of structurally related enzymes that are ubiquitous in plants, micro-organisms and animals. The work included enzyme mechanistic studies, NMR method development, protein NMR and method development for inhibitor discovery.

NMR was applied to study human γ-butyrobetaine hydroxylase (BBOX), an enzyme involved in L-carnitine biosynthesis. The studies showed that BBOX exhibits remarkable substrate promiscuity and is able to accept a large number of alternative substrates including the catalytic product L-carnitine and its unnatural enantiomer D-carnitine. Inhibition and mechanistic studies have also been conducted with 3-(2,2,2-trimethylhydrazineyl)propionate (THP), a BBOX inhibitor that is clinically used for the treatments of myocardial infarction and angina. The studies showed that THP is actually a competitive substrate forming a number of products including 3-amino-4-(methylamino)butanoic acid that is observed as a formaldehyde adduct. NMR analyses using ^{13}C-labelled THP revealed that the reaction of THP involves a radical mechanism involving C-N fragmentation and C-C bond formation in a fashion similar to a Stevens rearrangement in organic chemistry.

The development and implementation of two competition-based NMR methodologies to study ligand binding to 2OG oxygenases are described. In the first method, 2OG was used as a reporter ligand and its signal was monitored by spin echo-edited ^{1}H experiments upon displacement by competitive ligand. An alternative version involving the use of ^{13}C-labelled 2OG as the reporter and heteronuclear spectra editing is also proposed. This displacement method was applied for ligand screening and for quantifying ligand binding affinities for several 2OG oxygenases including the hypoxia inducible factor (HIF) hydroxylases. It was also used to investigate the catalytic mechanism of deacetoxycephalosporin C synthase (DAOCS), which revealed that 2OG and penicillin (substrate) have distinct binding sites, arguing against the atypical mechanism previously proposed for this enzyme. In the second NMR method, water molecules were used as the reporter ligand. The basis of the method relies on the paramagnetic relaxation enhancement (PRE) effect. By replacing the active site metal of 2OG oxygenases by paramagnetic metal Mn(II), the relaxation rates of bulk water were increased. In the presence of a ligand, the accessibility of water molecules to the paramagnetic metal centre was hindered, leading to a decrease in the bulk water relaxation rates. This method was applied for ligand screening and for ligand binding constant measurements for HIF prolyl hydroxylase (PHD2).

Protein NMR was also applied to study substrate binding to PHD2. Isotopically labelled PHD2 was produced and protein resonance assignment was conducted for both the substrate-free and substrate-bound forms of PHD2. Comparison of the two sets of assignment provided solution state evidence for the substrate binding site that was previously identified by X-ray crystallography. The chemical shift perturbation data also suggested that a loop region at the *N*-terminal side of the core double-stranded β-helix fold of PHD2 is important for substrate binding. Unlike 2OG, the binding of the peptidyl substrate and the prolyl hydroxylated peptidyl product to PHD2 do not require the presence of an active site metal. In fact, the presence of 2OG inside the active site actually weakens the binding of the product whilst the binding of the substrate was not affected, which is likely due to steric clash between 2OG and the hydroxyproline residue.

The applicability of reversible boronate ester formation to protein-directed dynamic combinatorial chemistry for the discovery of protein ligands was also investigated. Using ^{11}B NMR, proof-of-principle studies demonstrated selective binding of boronate esters from a dynamic combinatorial library (DCL). The studies also identified factors that should be considered when designing a DCL involving boronate ester formation. The method was then applied to discover inhibitors for PHD2, and NMR was used as a verification and quantification technique. The studies have successfully led to the discovery of three novel potent PHD2 inhibitors that inhibit the enzyme at low nanomolar concentrations.

Contents

Abstract *I*
Contents *II*
Acknowledgements *VI*
Abbreviations and acronyms *VIII*

1 Introduction *1*
1.1 2-Oxoglutarate oxygenases *1*
1.1.1 General perspectives *1*
1.1.2 Catalytic mechanism *1*
1.1.3 Co-substrate and co-factor specificity *4*
1.1.4 Structural aspects *5*
1.1.5 Inhibition of 2OG oxygenases *7*
1.2 Biological applications of NMR spectroscopy *10*
1.2.1 Historical perspectives *10*
1.2.2 Protein-ligand interactions *12*
1.2.3 Direct ligand observation *13*
1.2.4 Reporter ligand displacement *13*
1.2.5 NOE-based binding experiments *14*
1.2.6 Protein-observed ligand binding experiments *18*
1.2.7 Protein backbone assignment *18*
1.3 Application of NMR spectroscopy to study 2OG oxygenases *19*
1.3.1 Objectives *20*
1.4 References *22*

2 Studies on human γ-butyrobetaine hydroxylase *33*
2.1 Introduction *33*
2.1.1 L-Carnitine *33*
2.1.2 L-Carnitine biosynthesis *34*
2.1.3 Inhibition of L-Carnitine biosynthesis *35*
2.1.4 Objectives *36*
2.2 Characterisation of human BBOX *37*
2.2.1 Characterisation of BBOX activity *37*
2.2.2 Substrate analogue analyses *39*
2.3 Studies on the BBOX inhibitor THP *43*
2.3.1 THP is a substrate for BBOX forming multiple products *43*
2.3.2 Further characterisation of THP rearrangement product *47*
2.3.3 Rearrangement mechanism *50*
2.4 Human BBOX as a therapeutic target *52*
2.4.1 THP-Orotate *52*
2.4.2 THP-Metformin *53*
2.4.3 2-Hydroxyglutarate *55*
2.4.4 Daminozide *56*
2.5 Development of alternative BBOX assays *57*
2.5.1 Development of a ^{19}F NMR assay *57*
2.5.2 Development of a F^- detection fluorescent assay *60*
2.6 Summary *65*

2.7 References *66*

3 Investigating protein-ligand interactions by NMR *72*
3.1 Introduction *72*
3.1.1 The human hypoxia signalling pathway *72*
3.1.2 The HIF hydroxylases as inhibition target *74*
3.1.3 Biophysical methods for 2OG oxygenases *74*
3.1.4 Ligand-observed competition-based NMR methods *75*
3.1.5 Objectives *75*
3.2 Reporter screening for 2OG oxygenases *75*
3.2.1 Methodology *75*
3.2.2 Screening *77*
3.2.3 Binding constant measurement *79*
3.2.4 HIF hydroxylases and TCA cycle intermediates *80*
3.2.5 HIF hydroxylases and 2-hydroxyglutarate *83*
3.2.6 2-Oxoadipate as an alternative co-substrate of PHD2 *86*
3.2.7 Hydroxylated CODD *88*
3.2.8 Applicability of the method to other 2OG oxygenases *89*
3.2.9 Application of the method to investigate enzyme mechanism *91*
3.3 Solvent water as reporter for 2OG oxygenase screening *97*
3.3.1 Paramagnetic relaxation enhancement *97*
3.3.2 Method development *98*
3.3.3 Metal binding *101*
3.3.4 Binding of PHD2 inhibitors *102*
3.3.5 Co-binding of co-substrate and substrate *104*
3.4 Summary *107*
3.5 References *109*

4 Protein NMR studies on HIF prolyl hydroxylase PHD2 *116*
4.1 Introduction *116*
4.1.1 Structural aspects of PHD2 *116*
4.1.2 Protein NMR spectroscopy *119*
4.1.3 Protein backbone assignment *120*
4.1.4 Objectives *122*
4.2 Preparation for protein NMR *123*
4.2.1 Production of PHD2 in minimal media *123*
4.2.2 Establishing conditions for NMR analyses *124*
4.3 Backbone resonance assignment of $PHD2_{181-402}$ *127*
4.3.1 Backbone resonance assignment *127*
4.4 PHD2-substrate interactions *142*
4.4.1 Free and complexed form of $PHD2_{181-402}$ *142*
4.4.2 Translation of assignment from $^{2}H,^{13}C,^{15}N$-labelled $PHD2_{181-402}$ to ^{15}N-labelled $PHD2_{181-402}$ *147*
4.4.3 Probing the CODD binding site through substrate variants *154*
4.4.4 CODD and hydroxylated CODD *162*
4.4.5 2OG and inhibitor binding site *165*
4.5 Conclusions and future works *167*
4.6 References *168*

5. NMR investigations on a dynamic combinatorial approach to enzyme inhibition using boronate esters *172*
5.1 Introduction *172*
5.1.1 Dynamic combinatorial chemistry *172*
5.1.2 Reversible reactions for protein-directed DCC *172*
5.1.3 Dynamic combinatorial library *174*
5.1.4 Screening of dynamic combinatorial library *174*
5.1.5 Boronate ester formation *175*
5.1.6 Boronic acids as serine protease inhibitors *175*
5.1.7 Objectives *176*
5.2 Investigation of reversible boronate ester formation in DCC *176*
5.2.1 Observation of the α-chymotrypsin-boronate ester ternary complex *176*
5.2.2 Amplification of the boronate ester species by αCT *179*
5.2.3 Selectivity between sugars *179*
5.2.4 Selectivity between boronic acids *183*
5.2.5 NMR as a potential screening method for boronate ester DCC *189*
5.3 Application of DCC using reversible boronate ester formation *190*
5.3.1 Human prolyl hydroxylase domain-containing enzyme 2 *190*
5.3.2 Design of the scaffold boronic acid ligand *191*
5.3.3 Design of the PHD2-directed DCC experiments *191*
5.3.4 PHD2-directed DCC leads to stable analogue inhibitors *194*
5.4 Summary *196*
5.5 References *197*

6. Materials and methods *204*
6.1 General NMR methods *204*
6.1.1 Materials *204*
6.1.2 Buffer for NMR experiments *204*
6.1.3 General sample preparation and handling *205*
6.1.4 Sample acquisition and processing *206*
6.1.5 Characterisation of compounds *206*
6.1.6 ^{1}H NMR *207*
6.1.7 ^{19}F NMR *207*
6.1.8 ^{11}B NMR *207*
6.2 Protein NMR experiments *207*
6.2.1 ^{1}H-^{15}N HSQC *207*
6.2.2 Triple resonance experiments *208*
6.2.3 ^{1}H-^{15}N TROSY-HSQC *209*
6.3 NMR Binding experiments *210*
6.3.1 CPMG displacement experiments *210*
6.3.2 1D HSQC displacement experiments *210*
6.3.3 Water relaxation experiment *210*
6.3.4 STD-NMR *211*
6.3.5 WaterLOGSY *212*
6.4 Data treatment *212*
6.4.1 ^{1}H NMR time course *212*
6.4.2 Kinetic parameters by NMR for BBOX *212*
6.4.3 IC_{50} measurement for BBOX inhibitor *213*

6.4.4 pK_a measurement *213*
6.4.5 Binding constant measurement *213*
6.5 Mass spectrometry *215*
6.5.1 Identification of BBOX catalysed reaction products *215*
6.6 General protein methods *215*
6.6.1 Materials *215*
6.6.2 Sodium dodecyl sulfate polyacrylamide gel electrophoresis *216*
6.6.3 Protein concentration determination *217*
6.7 Production and purification of PHD2$_{181-426}$ *217*
6.7.1 Transformation *217*
6.7.2 2TY growth media *218*
6.7.3 Starter culture *218*
6.7.4 Large scale growth *218*
6.7.5 Protein purification by cation exchange chromatography *219*
6.7.6 *Apo*-protein production *220*
6.7.7 Protein purification by size exclusion chromatography *220*
6.8 Production and purification of ^{15}N-labelled and ^{13}C,^{15}N-labelled PHD2$_{181-402}$ *221*
6.8.1 M9 minimal media *221*
6.8.2 Starter culture *222*
6.8.3 Large scale growth *222*
6.8.4 Protein purification using gravity flow nickel affinity chromatography *222*
6.8.5 Removal of the His-tag *223*
6.8.6 *Apo*-protein production *224*
6.8.7 Buffer exchange *224*
6.9 Production and purification of ^{2}H,^{13}C,^{15}N-labelled PHD2$_{181-402}$ *224*
6.9.1 M9 minimal media *224*
6.9.2 Starter culture *224*
6.9.3 Large scale growth *224*
6.9.4 Protein purification *225*
6.10 Expression trials *225*
6.10.1 Starter culture *225*
6.10.2 Expression trial for the production of ^{15}N-labelled PHD$_{181-402}$ *225*
6.10.3 Expression trial for the production of ^{15}N,^{13}C-labelled PHD$_{181-402}$ *226*
6.10.4 Expression trial for the production of ^{2}H,^{15}N,^{13}C-labelled PHD$_{181-402}$ *226*
6.10.5 Analysis *227*
6.11 References *228*

Appendix I Protein backbone assignment for PHD2$_{181-402}$-Zn(II)-2OG-alanine substituted CODD variants *i*

Appendix II Protein backbone assignments for PHD2$_{181-402}$-Zn(II), PHD2$_{181-402}$-Zn(II)-2OG and PHD2$_{181-402}$-Zn(II)-BIQ *xliii*

Appendix III Publications *xlix*

Acknowledgements

I would like to take this opportunity to thank my supervisors Dr Tim Claridge and Prof. Chris Schofield for their help and guidance in the last four years, especially for allowing me the freedom to explore different aspects of NMR and for the opportunity to participate in a large variety of different projects. I would also like to thank Tim for introducing me to biological NMR during my undergraduate times (*Organic and Biological Spectroscopy* supplementary subject and my Part II project) and Chris for accepting me into his research group and for funding my work.

I would like to thank my co-workers and collaborators for their contributions. In particular I am indebted to Dr Luc Henry for custom synthesising many compounds for me. His overall contribution in the BBOX project is invaluable. I want to thank Anna Rydzik for taking the BBOX project further especially in assay development. I would also like to thank Dr Emily Flashman for teaching me how to produce and purify PHD2 and answering many of my questions on 2OG oxygenases especially during my first year, and Dr Adam Hardy for teaching me how to produce and purify isotopic labelled PHD2 and for help in LG2. I also want to thank Andrea Szöllössi for helping me with trouble shooting in the water relaxation project, and it is her project that inspired the 2OG displacement method. Thanks also go to Dr Tom Brown for introducing me to the DCC project and for sharing his expertise on boronic acids and sugars, and to Marina Demetriades for taking the DCC project to the next step, designing and synthesising boronic acids and inhibitors for PHD2. Thanks also go to those who have collaborated and contributed on specific projects: (in alphabetical order) Jacob Bush, Mun Chiang Chan, Prof. Babur Chowdhry (Greenwich University), Dr Lars Hillringhaus, Manso Jubier, Dr Grazyna Kochan, Dr Clarisse Lejeune, Nikita Loik, Dr James McCullagh, Inga Pfeffer, Robin Procter, Dr Alexander Sagidullin (Oxford Instruments), Tristan Smart, Wendy Sobey, Colin Sparrow, Hanna Tarhonskaya, Dr Esther Woon and Dr Kar Kheng Yeoh. Individual contributions are acknowledged at the beginning of each Chapter and in the text.

Generally, I would like to thank Dr Richard Hopkinson for useful discussions and inspiring ideas on various projects (and yes I should have listened about formaldehyde), Dr Mike McDonough and Dr Rashed Chowdhury for discussions on the BBOX and PHD2 projects respectively. Rubén Gómez Castellanos, Adam,

Andrea, Sarah Davies and other CJS group members for helping me in LG2, such as how to run a gel properly. I want to thank Dr Despoina Mavridou, Dr Christina Redfield and Dr Peter Gierth (Bruker) for their advice on protein NMR. I would like to thank Tina Jackson, Maria Marshall and Dr Guo Liang Ping for maintaining the instruments and the NMR lab supply, and Wendy Sobey for keeping the lab tidy. I would also like to thank Dr Barbara Odell, Dr Ignacio Perez-Victoria and members of the Claridge Group for useful discussions on NMR during group meetings. I would like to thank all the NMR users, especially those who regularly use the AV700, for their understanding and flexibility when I need the machine for a long period of time. Thesis-wise, I want to thank Adam, Andrea, Anna, Luc, Marina and Richard for proof-reading multiple times. Finally, I want to thank all members of the Schofield Group and the Claridge Group past and present for their help and company in general.

I would like to take this opportunity to thank my friends who made my life easier in Oxford. Especially I want to thank Marina for her company, talking and her tolerance; Richard his company, for listening to my complaints and for introducing me to the Smurfs, Maggie for literally dragging me from the basement to the club for drinks, Rubén for organising social events, lunches and dinners at Hertford and Anna for not kicking me. I also like to thank Luc, Andrea, Tobias, Adam, Steve, Aman, Tom, Rashed, Mike and many others for Friday nights at the club and other social events. I would also like to thank those who regularly turn up to CJS football and I have a feeling that we will win the trophy next year. I also want to thank Marina, Richard, Rubén, Anna and Andrea for organising vacations and travelling the world together.

Finally, I really want to thank my parents for their continued love and support. Especially I would like to dedicate this Thesis to my father, who managed to complete his own PhD despite suffering from a life-changing illness – Now I know how tough it is to write a thesis. I also want to thank my mom and my grandma for their support and encouragement throughout.

Abbreviations and acronyms

2,4-PDCA	2,4-pyridinedicarboxylate
2HG	2-hydroxyglutarate
2OG	2-oxoglutarate
2TY	2-tryptone/yeast extract
5-C-8HQ	5-carboxy-8-hydroxyquinoline
αCT	α-chymotrypsin
ALDH9	aldehyde dehydrogenase 9
AlkB	alkylated DNA repair protein B
AMBA	3-amino-4-(methylamino)butanoic acid
APS	ammonium persulphate
B_0	applied magnetic field
BBOX	γ-butyrobetaine hydroxylase
BFBA	1-benzofuran-2-boronic acid
BNS	bicyclic naphthalenylsulfonyl inhibitor
BSA	bovine serum albumin
BTPBA	1-benzothiophen-2-ylboronic acid
BIQ	bicyclic isoquinolinyl inhibitor
CAD	*C*-terminal transactivation domain
CD	circular dichroism
CMCPBA	6-(1-carboxymethylcarbamoyl)-3-pyridinylboronic acid
CODD	*C*-terminal oxygen dependent degradation domain
COSY	correlation spectroscopy
CPMG	Carr-Purcell-Meiboom-Gill
DAOCS	deacetoxycephalosporin C synthase
DCC	dynamic combinatorial chemistry
DCL	dynamic combinatorial library
DOSY	diffusion ordered spectroscopy
DSBH	double-stranded β-helix
E. coli	*Escherichia coli*
EDTA	ethylenediaminetetraacetic acid
EPR	electron paramagnetic resonance
ESI-MS	non-denaturing electrospray ionisation mass spectrometry

EtBA	ethylboronic acid
FBDD	fragment based drug discovery
FBXL	F-box and leucine-rich repeat protein
FIH	factor inhibiting hypoxia inducible factor
GBB	γ-butyrobetaine
HEPES	4-(2-hydroxyethyl)-1-piperazineethanesulfonic acid
HIF	hypoxia inducible factor
HMBC	heteronuclear multiple-bond correlation spectroscopy
HMQC	heteronuclear multiple quantum correlation spectroscopy
HPLC	high-performance liquid chromatography
HSQC	heteronuclear single quantum coherence spectroscopy
HTBA	hydroxyphenylboronic acid
HTML	3-hydroxy-N^{ε}-trimethyllysine
HTMLA	3-hydroxy-N^{ε}-trimethyllysine aldolase
hyCODD	hydroxylated CODD
IC_{50}	half maximal inhibitory concentration
ICP-MS	inductively coupled plasma mass spectrometry
ILOE	inter-ligand Overhauser effect
ITC	isothermal titration calorimetry
IPNS	isopenicillin N synthase
IPTG	isopropyl β-D-1-thiogalactopyranoside
JMJD	Jumonji domain containing protein
k_{cat}	catalytic constant
K_D	dissociation constant
$K_{D,app}$	apparent dissociation constant
K_I	inhibition constant
K_M	Michaelis constant
LB	Luria-Bertani media
MES	2-(*N*-morpholino)ethanesulfonic acid
MS	mass spectrometry
NMR	nuclear magnetic resonance
NODD	*N*-terminal oxygen dependent degradation domain
NOE	nuclear Overhauser effect
NOESY	nuclear Overhauser effect spectroscopy

NOG	*N*-oxalylglycine
NTBA	naphthalen-2-ylboronic acid
OD_{600}	optical density
P4H	prolyl 4-hydroxylase
PDB	protein data bank
PHD	prolyl hydroxylase domain containing enzyme
PRE	paramagnetic relaxation enhancement
PROJECT	periodic refocusing of J evolution by coherence transfer
pVHL	von Hippel-Lindau protein
R_1	longitudinal relaxation rates
R_2	transverse relaxation rates
SAR	structure-activity relationships
SDS-PAGE	sodium dodecylsulfate polyacrylamide gel electrophoresis
SHMT	serine hydroxymethyltransferase
SOFAST-HMQC	band-selective optimized flip-angle short-transient HMQC
SPR	surface plasmon resonance
STD-NMR	saturation transfer difference NMR
T_1	longitudinal relaxation time constant
T_2	transverse relaxation time constant
TCA	tricarboxylic acid
TEMED	tetramethylethylenediamine
THP	3-(2,2,2-trimethylhydraziniumyl)propionate
TMABA	4-*N*-trimethylaminobutyraldehyde
TMABADH	4-*N*-trimethylaminobutyraldehyde dehydrogenase
TMLH	N^{ϵ}-trimethyllysine hydroxylase
TOCSY	total correlation spectroscopy
Tr-NOE	transferred nuclear Overhauser effect
Tris	tris(hydroxymethyl)aminomethane
TROSY	transverse relaxation-optimised spectroscopy
V_{max}	maximum velocity
waterLOGSY	water-ligand observation with gradient spectroscopy
WT	wild type

1. Introduction

1.1 2-Oxoglutarate oxygenases

1.1.1 General perspectives

2-Oxoglutarate (2OG) oxygenases belong to a family of structurally related non-haem Fe(II) dependent dioxygenases that are ubiquitous in plants, micro-organisms and animals.[1,2] 2OG oxygenases, especially those found in plants and micro-organisms, catalyse a wide range of oxidation reactions including hydroxylations, ring expansions, ring closures and desaturations.[3–6] However, to date, the only known reactions that 2OG oxygenases catalyse in animals are hydroxylation and demethylation reactions.[7] Given the range of chemical reactions 2OG oxygenases catalyse, they often have important roles in many biological processes and functions, ranging from antibiotic biosynthesis in prokaryotes to gibberellin biosynthesis in plants.[7,8] In humans, they are involved in biosyntheses (*e.g.* collagen biosynthesis and L-carnitine biosynthesis), post-translational modifications (*e.g.* protein hydroxylation) and epigenetic regulations (*e.g.* nucleic acid demethylation).[7,8]

1.1.2 Catalytic mechanism

In general, 2OG oxygenases catalyse oxidation reactions by incorporating a single oxygen atom from molecular oxygen into their substrates. This is always coupled with 2OG oxidation into succinate and carbon dioxide (Figure 1-1).[9–11]

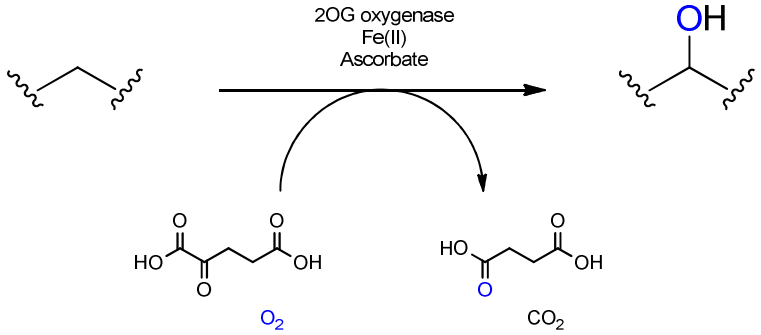

Figure 1-1 2OG oxygenases catalyse oxidation reactions such as hydroxylations. The co-substrates are 2OG and oxygen and the co-products are succinate and CO_2. Reducing agents such as ascorbate often promote 2OG oxygenase activity.

Despite the wide range of oxidation reactions that 2OG oxygenases catalyse, they appear to employ a common general catalytic mechanism, which is outlined in Figure 1-2.[9–11] The first step of the catalytic cycle involves the binding of 2OG and substrate

to the enzyme.[12,13] 2OG coordinates to the metal centre inside the active site in a divalent manner by replacing two water ligands. The substrate binds in close proximity but does not directly coordinate to the metal, although it may be involved in the displacement of the third water molecule away from the active site Fe(II).[14] The next step involves the binding of molecular oxygen, which occupies a third site at the metal centre. An oxidative decarboxylation reaction then occurs to give carbon dioxide, succinate and a highly oxidising Fe(IV)-oxo intermediate.[15–18] One of the oxygen atoms from molecular oxygen is incorporated into succinate, and the other into the substrate,[19] with the reactive Fe(IV) species reduced back to Fe(III) and then Fe(II).[20]

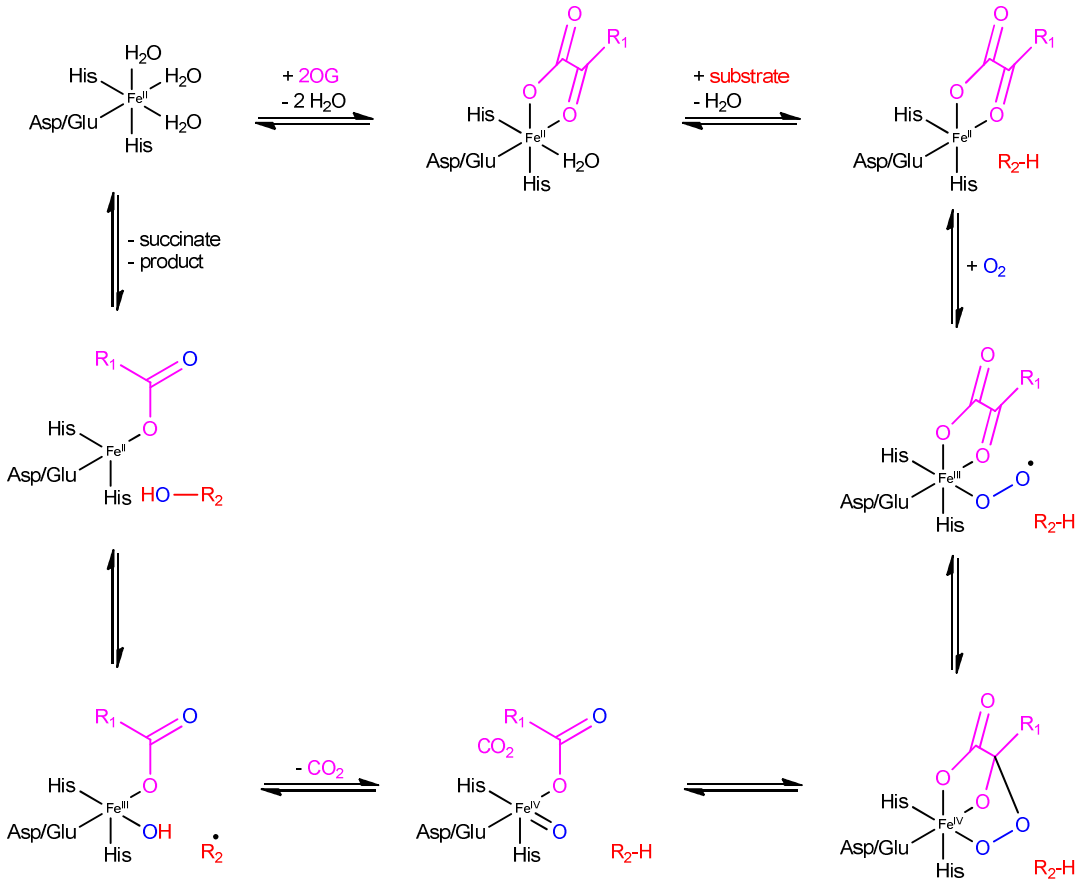

Figure 1-2 Mechanism for 2OG oxygenase catalysis. The binding of 2OG and substrate displaces three water molecules away from the active site Fe(II) and creates a vacant site for oxygen binding. The binding of oxygen probably happens last to minimise oxidative damage. The timing of CO_2 release and when the vacant sites are re-occupied by water molecules are unknown. There is evidence for all the intermediates shown, including the Fe(IV)-oxo species, except for the Fe(II)-O_2 complex and the Fe(III)-OH intermediate.

Many 2OG oxygenases are also capable of uncoupled turnover, in which oxidative decarboxylation of 2OG into succinate and carbon dioxide can proceed in the absence of a substrate or in the presence of a sub-optimal substrate.[2] The oxidising Fe(IV)-oxo

species generated may be reduced back to Fe(II) by reducing agents (such as ascorbate),[21] water (similar to Fenton chemistry),[22,23] buffer,[24] or in some cases amino acid residues in the active site (self-hydroxylation).[25,26]

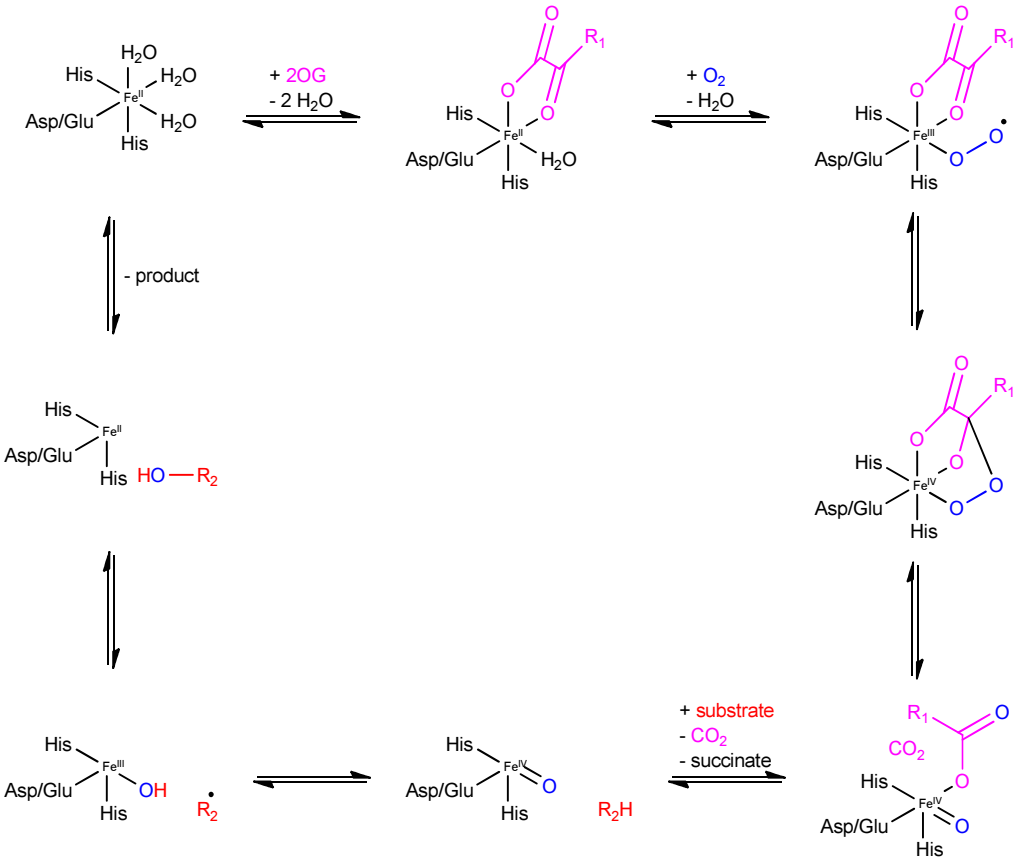

Figure 1-3 An alternative mechanism proposed for the 2OG oxygenase deacetoxycephalosporin C synthase (DAOCS). Due to a proposed overlap of the 2OG and substrate binding sites, the enzyme cannot form an enzyme-2OG-substrate complex. Instead, oxidative decarboxylation of 2OG happens first and results in the formation of succinate, CO_2 and the oxidising Fe(IV)-oxo intermediate. Succinate is proposed to stabilise the Fe(IV)-oxo species. Subsequent binding of the substrate displaces the succinate and completes the oxidative reaction.

An exception to the general mechanism has been proposed for a bacterial 2OG oxygenase deacetoxycephalosporin C synthase (DAOCS) based on structural and kinetic evidence using two sub-optimal substrates, penicillin G and ampicillin.[27] The proposed alternative mechanism (Figure 1-3) largely follows the uncoupled turnover pathway. In the first step, 2OG and oxygen bind to the Fe(II) in the enzyme active site in the absence of the substrate. Based on the proposed overlap of the 2OG and substrate binding sites, as apparently shown in the X-ray crystal structures (PDB ids: 1UOB and IUNB), simultaneous binding of 2OG and substrate to the enzyme is prevented. The next step involves uncoupled oxidation of 2OG to generate a reactive Fe(IV)-oxo species. This is followed by the release of succinate and carbon dioxide

from the active site, which frees up enough space for the binding and subsequent oxidation of the substrate to complete the catalytic cycle. Quantum mechanical calculations suggested the reactive Fe(IV)-oxo species is long-lived enough for the proposed mechanism to proceed, although at present further experimental evidence and rationalisation is required to support this atypical mechanism.

1.1.3 Co-substrate and co-factor specificity

The redox active Fe(II) inside the enzyme active site is apparently an absolute requirement for 2OG oxygenase activity. Although many transition metal ions, including but not limited to Mn(II), Co(II), Ni(II), Cu(II) and Zn(II), also bind to the active site of many 2OG oxygenases with similar affinity as Fe(II),[28] replacing the Fe(II) with these transition metals results in a loss of catalytic activity.[29–31] The active site metal is not released from the enzyme at the end of the catalytic cycle.[32] It is unclear whether there are any active transport mechanisms *in vivo* for Fe(II) delivery to 2OG oxygenases or whether the enzymes simply compete for free Fe(II) in cells.

2OG oxygenases generally have a relatively strict requirement for 2OG as the decarboxylation co-substrate. Only a handful of compounds, which are all 2OG analogues, have been reported as alternative co-substrates for certain 2OG oxygenases (Figure 1-3). For instance, 2-oxoadipate, a 5-carbon structural analogue of 2OG, can act as co-substrate for mammalian collagen prolyl 4-hydroylase with reduced activity.[33,34] D-2-Hydroxyglutarate (D-2HG), a reduced form of 2OG, has been shown to promote substrate hydroxylation *via* oxidation into 2OG for the human hypoxia inducible factor (HIF) prolyl hydroxylase domain containing enzyme (PHD) isoforms 1, 2 and 3.[35]

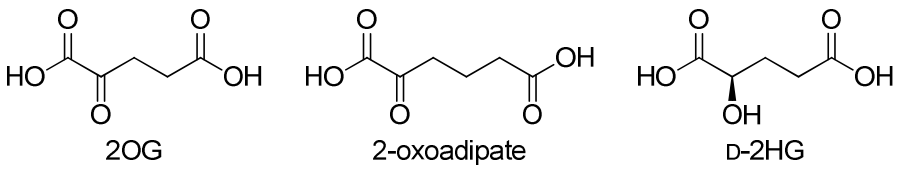

Figure 1-4 2-Oxoadipate and D-2HG may act as alternative co-substrate for some 2OG oxygenases.

2OG oxygenases show various degrees of dependencies on reducing agents (especially ascorbate),[21,36] as they can (but not always) promote the rates of both uncoupled and coupled turnover,[21,36] even in cases in which the coupling ratio between 2OG oxidation and substrate oxidation is stoichiometric.[36] The exact roles of reducing agents in 2OG oxygenase catalysis are not fully understood. Their proposed

roles include the facilitation of complete uncoupled turnover cycles and/or for the maintenance of a pool of free Fe(II) in solution.[21,36–38] There are also contradicting reports implying ascorbate may[39] or may not[40] bind to 2OG oxygenases. Ascorbate may also influence the coupling ratio between 2OG oxidation and substrate oxidation.[41] The structures of the reducing agents are also important. For instance, in a study using HIF hydroxylases, glutathione and dithiothreitol (both of which are stronger reducing agents than ascorbate) show weaker effects on the stimulation of enzyme activities in a substrate dependent manner.[36] In another study with the chick embryo collagen prolyl 4-hydroxylase, the reaction was reported to be completely dependent on ascorbate which could not be replaced by the reducing agents dithiothreitol or tetrahydrofolic acid.[42] Previous studies have shown that excess ascorbate may actually inhibit enzyme activity for some 2OG oxygenases.[41,42]

1.1.4 Structural aspects

All structurally characterised 2OG oxygenases contain a conserved double-stranded β-helix (DSBH) core fold, which is formed from two β-sheets in a squashed barrel structure (for reviews see references 43–46; Figure 1-5). The DSBH core support a highly conserved 2-His-1-carboxylate (HXD/E...H) amino acid residue triad for the coordination of a single high-spin six-coordinated Fe(II) ion at the enzyme active site (Figure 1-6).[47] The active site Fe(II) is held by two histidine residues and one aspartic acid or glutamic acid residue, with the other three sites occupied by water ligands. Kinetic and structural studies have suggested the two histidine residues are important in Fe(II) binding.[48] In addition to the core DSBH structure, 2OG oxygenases usually contain different extra structural features. These usually include at least one *C*-terminal helix, and an insert between the βIV and βV strands of the DSBH, which can range from a small loop of a few amino acids to an entire protein domain.[43–46]

An induced fit mechanism has been implied for some 2OG oxygenases based on X-ray crystallographic evidence. For instance, significant protein structural changes have been observed upon substrate binding for PHD2,[49,50] a human 2OG oxygenase, and isopenicillin N synthase (IPNS),[51] a microbial 2OG oxygenase.

The binding of the co-substrate 2OG may also induce structural changes to some 2OG oxygenases. Different folded states have been observed for the *E. coli* alkylated DNA repair protein AlkB by nuclear magnetic resonance (NMR) spectroscopy and other

biophysical measurements.[52,53] In its *apo* form, the enzyme is essentially unstructured. Addition of either metal ion or 2OG alone does not significantly alter the protein structure. However, substantial structural changes (into a folded and structured protein) can be observed upon the binding of both metal and 2OG.[52,53]

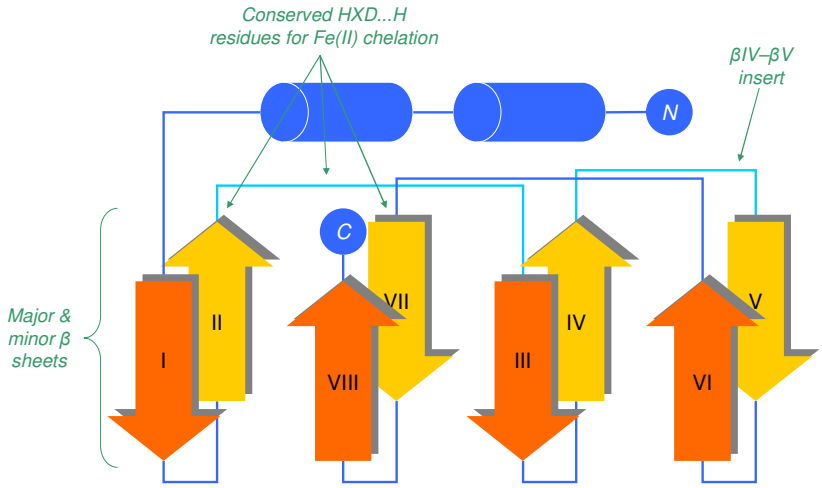

Figure 1-5 A schematic representation of the DSBH core fold of 2OG oxygenases. The orange and the yellow colour represents the two β-sheets that form the DSBH core. Roman numerals indicate the eight strands of the DSBH according to Stirk *et al.*[45]

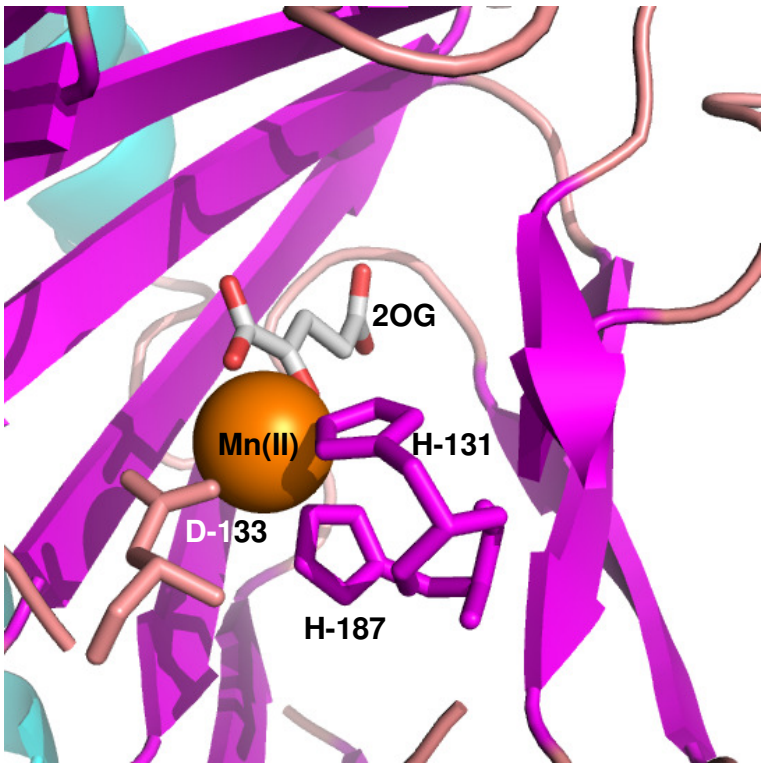

Figure 1-6 View from a crystal structure of *E. coli* alkylated DNA repair protein AlkB (PDB id: 3I3Q). The active site metal ion is held by two histidine residues and one aspartic acid residue (or for some 2OG oxygenases, a glutamic acid residue). In the crystal structure, Mn(II) was used instead of the native Fe(II).

1.1.5 Inhibition of 2OG oxygenases

Many 2OG oxygenases are current inhibition targets for commercial and therapeutic applications. For instance the plant 2OG oxygenase gibberellin C-20 oxidase is an inhibition target of commercially used herbicides.[54] Several human 2OG oxygenases, such as the hypoxia inducible factor (HIF) hydroxylases that are involved in human oxygen sensing, are inhibition targets for diseases including cancer, ischemia, inflammation and anaemia.[55–58] The inhibition of γ-butyrobetaine hydroxylase (BBOX), a 2OG oxygenase involved in human carnitine biosynthesis, is targeted clinically for the treatment of angina and myocardial infarction.[59–62] There are two main types of 2OG oxygenase inhibitors; the first predominantly act as 2OG competitors and the other as prime substrate mimics (for review see reference 63).

To date, most small molecule-based 2OG oxygenase inhibitors are 2OG competitors and bind to the active site Fe(II).[63] They can broadly be classified into five main types: (1) *N*-oxalyl amino acids; (2) pyridine carboxylic acids; (3) bipyridyl compounds; (4) isoquinolinyl compounds and; (5) *N*-hydroxythiazoles (Figure 1-7).

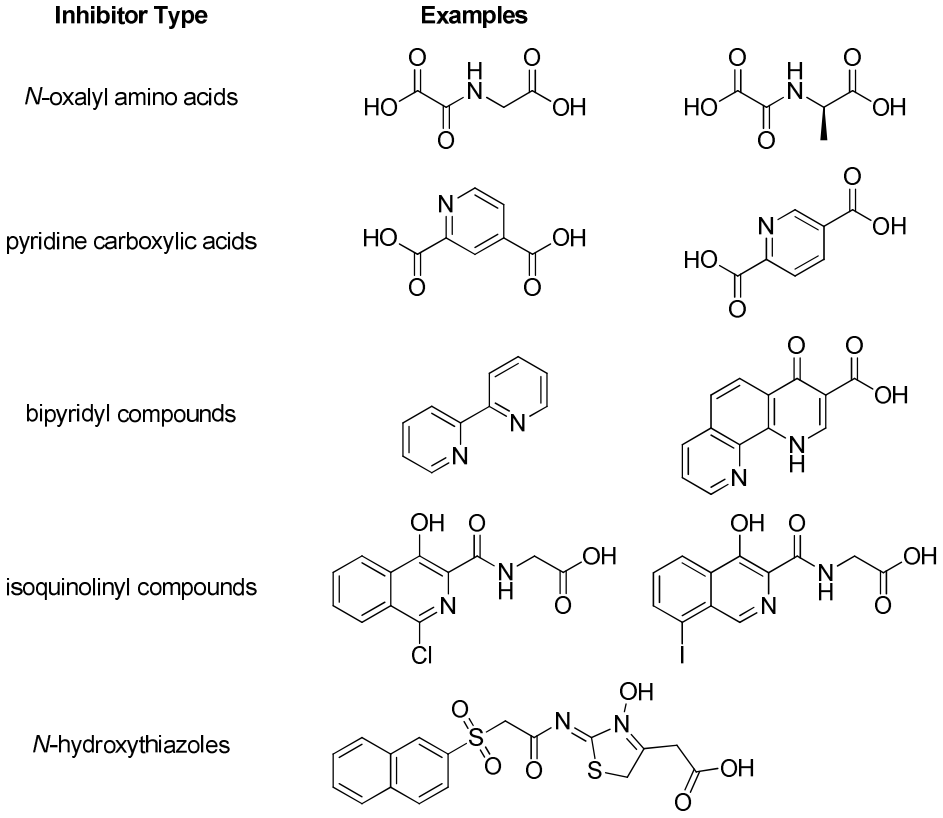

Figure 1-7 Structures and examples of common 2OG oxygenase inhibitors that are 2OG competitors.

The first two types (*N*-oxalyl amino acids and pyridine carboxylic acids) are essentially generic inhibitors of 2OG oxygenases. The simplest of which are *N*-oxalyl amino acids (such as *N*-oxalylglycine), which are direct structural mimics of 2OG.[34,64] Selectivity, for instance between HIF hydroxylases, can be achieved by replacing the glycine moiety with different D-/L- amino acids.[65] Pyridine carboxylic acids, such as 2,4-pyridinedicarboxylate, are also 2OG mimics. The pyridinecarboxylic acid group chelate to the Fe(II) in the active site and the other carboxylic acid is anchored by the same basic residues that anchor the C-5 carboxylic acid of 2OG (Figure 1-8).[66–68] Other 2OG structural mimic, such as 4,6-dioxoheptanoic acid, has also been shown to be good inhibitor of 2OG oxygenase by mimicking the same interactions.[69]

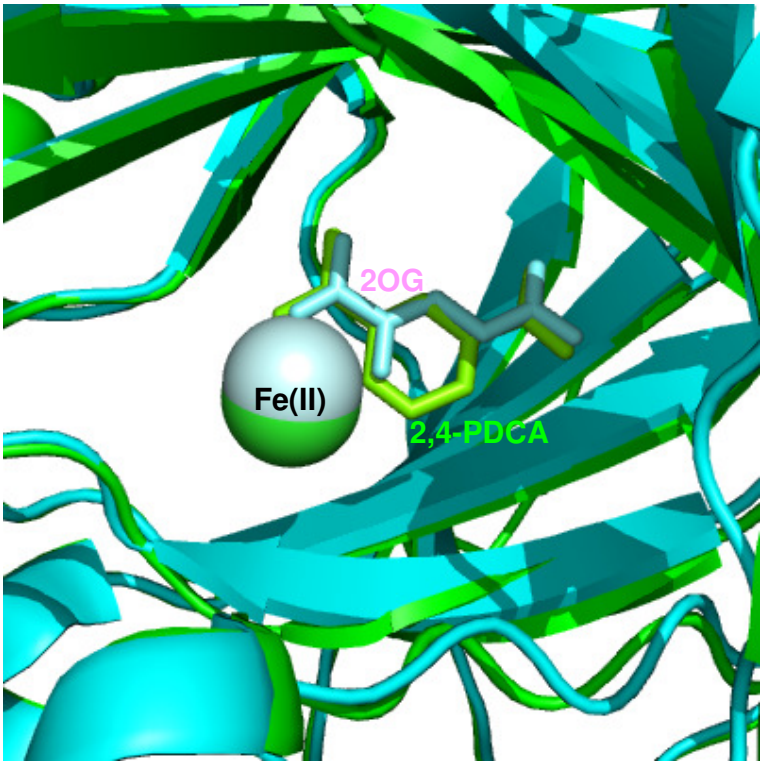

Figure 1-8 Views from crystal structures of HIF hydroxylase Factor Inhibiting HIF (FIH) in complex with Fe(II) and 2OG (PDB id: 1MZF; green) and with Fe(II) and 2,4-PDCA (PDB id: 2WoX; cyan). 2,4-PDCA is a structural mimic of 2OG and they bind to the active site metal in the same manner.

Bipyridyl compounds are a distinct group of 2OG oxygenase inhibitors. They are good metal chelators and their mode of action may in part due to chelation of free Fe(II) in solution. Selectivity between 2OG oxygenases can be achieved by altering the functionalisation of the bipyridyl template.[70–75] They are generic inhibitors of 2OG oxygenases and inhibit a wide range of 2OG oxygenases including collagen P4H,[70,71] the HIF hydroxylases[72–74] and the histone demethylases.[75]

Finally, isoquinolinyl compounds[66,76–79] and the closely related *N*-hydroxythiazoles[80,81] are two classes of very potent 2OG oxygenase inhibitors. Structurally, they are essentially extensions of the *N*-oxalyl amino acid scaffold. Similar to *N*-oxalyl amino acid, selectivity can be achieved by modifying the amino acid moiety of the compound, which has been demonstrated by a series of amino acid substituted bicyclic isoquinolinyl inhibitors towards the inhibition of PHD2.[79] Crystallographic studies have shown that these compounds not only chelate to the active site Fe(II) but also tend to bind towards the substrate binding pocket, which may be manipulated to improve their potency and selectivity to different 2OG oxygenases.[82]

Apart from the five main classes of inhibitor scaffold discussed above, there are also other templates that have been used to design inhibitors for 2OG oxygenases. For instance, hydroxyquinoline compounds have recently been shown to inhibit histone demethylases based on high-throughput screening (HTS).[83] In another HTS study, the hydantoin template has been identified as a potent PHD inhibitor.[84]

There are only a handful of reported 2OG oxygenases inhibitors that are prime substrate mimics, which include both peptides and small molecules. One of the reported prime substrate-based inhibitors was based on the HIF peptide fragment *C*-terminal oxygen dependent degradation domain (CODD; HIF-1$\alpha_{556\text{-}574}$), which is a substrate for the HIF hydroxylase PHD2. In that study, the proline residue on the hydroxylation site was replaced by unhydroxylable proline analogues including L-3,4-dehydroproline and L-4-thioproline (Figure 1-9). These CODD-based inhibitors showed that they selectively inhibit PHD2 over FIH, another HIF hydroxylase.[85]

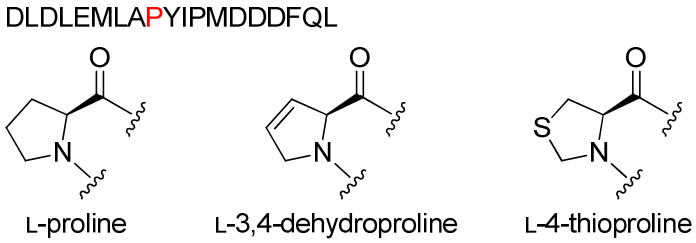

Figure 1-9 By replacing the proline residue on the hydroxylation site of CODD (red) with unhydroxylable proline analogues, the resultant peptides were found to selectively inhibit PHD2 over FIH.

BBOX was another inhibition target for several prime substrate-based inhibitors. The substrate for BBOX is γ-butyrobetaine and these prime substrate-based inhibitors were therefore all small molecules (Figure 1-10). 3-(2,2,2-

Trimethylhydraziniumyl)propionate is a direct structural mimic of γ-butyrobetaine, with a NH group replacing a CH_2 group at the C-4 position. It acts as a competitive substrate to BBOX.[86] 1-[2-(Trimethylammonio)ethyl]cyclopropanecarboxylate, a cyclopropyl-substituted γ-butyrobetaine analogue, is reported to be a non-competitive *Pseudomonas* BBOX inhibitor.[87] The authors speculated it may bind to an allosteric site. 3-(2,2-Dimethylcyclopropyl)propanoic acid, another cyclopropyl-substituted γ-butyrobetaine analogue, is reported to be a mechanism-based inhibitor of *Pseudomonas* BBOX, in which it reacts as a substrate and its speculated mode of inhibition includes cross-linking with the enzyme to deactivate it.[88]

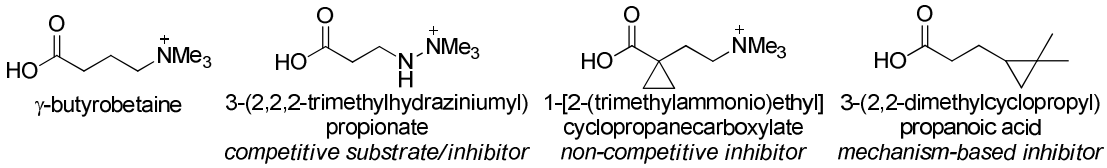

Figure 1-10 Several prime-substrate-based inhibitors have been reported for the inhibition of BBOX. The structure of the prime substrate (γ-butyrobetaine) is also shown.

Other reported 2OG oxygenase inhibitors include transition metal ions, which inhibit 2OG oxygenases by displacing and replacing the active site Fe(II).[29–31] Metal chelators such as ethylenediaminetetraacetic acid (EDTA) also inhibit 2OG oxygenases by removing the active site Fe(II), which have been demonstrated with P4H[42] and AlkB.[89] EDTA is also routinely used in biochemical assays involving 2OG oxygenases for reaction quenching.[90] Zinc ejecting compounds such as disulfiram and ebselen have also been shown to inactivate certain 2OG oxygenases such as histone demethylases by removing the structurally important Zn(II) present in these enzymes.[91] Nitric oxide has also been reported to inhibit 2OG oxygenases such as PHD2, presumably by competing with oxygen for the binding site.[92,93] Therefore, it is possible that nitric oxide acts as a natural inhibitor of HIF hydroxylase (and other 2OG oxygenases) in hypoxic conditions.[94]

1.2 Biological applications of NMR spectroscopy

1.2.1 Historical perspectives

The application of NMR spectroscopy to study biological systems dates back to the 1950s.[95–98] Early efforts focused mainly on the assignment and characterisation of biological related compounds and enzymatic products. For instance, the first NMR studies of amino acids and related compounds were published in 1957 and 1958.[99,100]

The first ^{1}H spectrum of the protein ribonuclease was reported in 1957,[101] for which the aliphatic and aromatic regions of the protein were clearly distinguished.[101] Jardetzky and Jardetzky further interpreted the aliphatic region of the spectrum into α protons and side chain protons.[102] In the same year, one of the first attempts to study the stereochemistry of an enzymatic product was also published. In that study, the stereochemistry of malate, which was formed as a result of the pig heart fumarase catalysed hydration of fumarate, was characterised.[103] The first attempt to apply NMR spectroscopy to study protein-ligand interactions was published in 1963, in which the binding of diphosphopyridine nucleotide to yeast alcohol dehydrogenase was studied by observing line width changes of the ligand.[104] The first applications of NMR spectroscopy for real time monitoring of enzymatic reactions were published in 1968 and 1969.[105,106] In the first study, the hydrolysis reaction of acetylcholine by horse serum cholinesterase was monitored by a series of ^{1}H spectra,[105] and in the second study, the isomerisation reaction of D-fructose-6-phosphate to D-glucose-6-phosphate by phosphoglucose isomerase was studied by ^{1}H NMR.[106]

The 1960s and 1970s saw rapid development of NMR technologies, including the application of the nuclear Overhauser effect (NOE) between nuclear spins,[107] pulse-Fourier transform NMR,[108] and two-dimensional NMR spectroscopy.[109] These developments allowed major discoveries in protein NMR to be made in the 1980s and 1990s. The first general strategy for sequential assignment of protein resonances and protein structure by using a combination of COSY and NOESY experiments was reported in 1982.[110] In 1985, the first NMR structure of a protein was reported, which was determined by more than 200 NOESY constraints along the protein polypeptide chain.[111] The system studied was proteinase inhibitor IIA from bull seminal plasma, which is a protein of 57 amino acids with a molecular weight of ~6 kDa.[111] In 1990, three-dimensional ^{1}H,^{15}N,^{13}C triple resonance NMR spectroscopy using ^{15}N,^{13}C-labelled protein was introduced.[112] The development of transverse relaxation-optimised spectroscopy (TROSY) in 1997 made resonance assignment and structure determination of large protein complexes of up to 800-900 kDa possible.[113] The use of NMR to study structure-activity relationships (SAR-by-NMR) was proposed in 1996,[114] and laid out the foundations for studying protein-ligand interactions by protein NMR.

During the same period, there was also significant development in ligand-based NMR methodologies for the study of protein-ligand interactions. The use of transferred NOE (tr-NOE) was initially proposed in 1972 and was applied to detect ligand binding and for the determination of bound ligand conformation.[115–117] Three major NOE-based methodologies were reported at the turn of the century. Saturation transfer difference NMR (STD-NMR) spectroscopy,[118] which allowed epitope mapping of ligands to the target protein, and the application of inter-ligand Overhauser effect (ILOE),[119] which allowed the study of relative orientation of simultaneous and proximately bound ligands, were reported in 1999. The water-ligand observation with gradient spectroscopy (waterLOGSY) method was reported in 2000 and allowed rapid screening of ligand mixtures.[120] The interligand NOE for pharmacophore mapping (INPHARMA) method was reported in 2005 which allows comparison and modelling of relative binding conformations from related ligands.[121] In addition, many activity-based and competition-based methodologies were also reported in the 2000s, which allowed the screening of high-affinity ligands. These included the use of ^{1}H NMR[122–124] or by monitoring other heteronuclei such as phosphorus[125] and fluorine.[126–128]

1.2.2 Protein-ligand interactions

Studies of the interactions between proteins and other molecules (ligands) are of fundamental importance in the area of chemical biology. These ligands can be small molecules, peptides, proteins, metal ions, nucleic acids or other biomolecules. Because binding interactions occur dynamically in solution, NMR can provide information on many aspects of these interactions, ranging from inhibitor screening, structural analyses, enzyme kinetics and drug discovery (for reviews see references 129–138).

There exists a large variety of NMR experiments providing different types of information on protein-ligand interactions. They can be broadly divided into two approaches. One is to observe the signals of a ligand (directly or through a reporter ligand),[139–143] the other to observe the signals of the protein (often using isotopically labelled proteins).[141–145] Consideration of factors such as exchange rate, binding affinity and molecular weight (of both ligands and proteins) are important, as there are different practical and technical difficulties associated with different experiments.

1.2.3 Direct ligand observation

Ligand binding can often be indicated by changes in the NMR parameters of the ligand in the presence and absence of the receptor protein, as the ligand molecule experiences different chemical environments and rotational correlation times (Figure 1-11). The NMR parameters that are usually used for direct observation include chemical shift, peak intensity, line width, and longitudinal (R_1) and transverse (R_2) relaxation rates.[146,147] The most common nuclei for direct observation are ^{1}H,[104,148] ^{13}C,[149] ^{19}F[126,148–151] and ^{31}P.[125] These methods are most sensitive when the difference in size is large between the ligand and the protein as there are greater changes in the observed NMR parameters. In addition, both ^{19}F and ^{31}P nuclei exhibit large chemical shift anisotropy so that even weak binding events may lead to line broadening owing to the strong R_2 dependent line broadening pathway.[125,152]

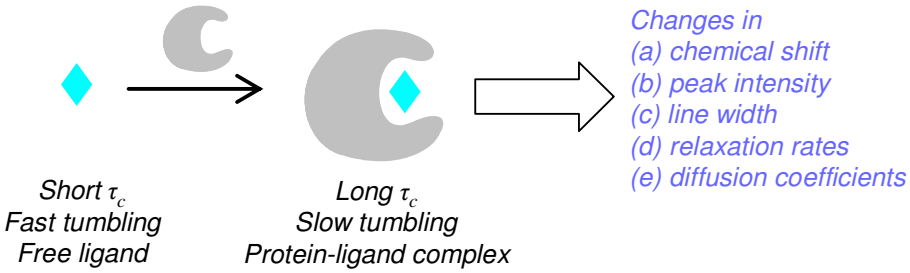

Figure 1-11 Scheme illustrating the principle of direct ligand observation in NMR screening.

Binding affinity, which is usually defined by the dissociation constant (K_D) of the ligand and the target protein, can be readily determined by titration experiments.[146,147] However, one drawback for direct ligand observation, especially when the nucleus is ^{1}H, is that it is only suitable for relatively weak binders (K_D ranges from high μM to mM) because accurate measurement of NMR parameters is necessary and therefore factors such as protein background may hide the ligand signal when the ligand and protein concentrations are similar (condition required for strong binder). It is also not possible to directly distinguish between specific and non-specific binding events.

1.2.4 Reporter ligand displacement

The NMR reporter screening method is a useful alternative to direct ligand observation. By observing changes in the NMR parameters of a reporter ligand, it can provide site-specific information about the binding of both high- and low-affinity ligands (Figure 1-12). Several nuclei, including ^{1}H,[122–124] ^{13}C,[153] ^{19}F[126,154] and ^{31}P[125] have been proposed for reporter screening by NMR. If the binding affinity of the

reporter ligand is known, K_D values for the ligands of interest can be obtained by titration.[146,147,155] However, because this method relies on reporter ligands that bind to specific binding sites, it can provide false negative results, for instance, with allosteric inhibitors because they do not compete for the same binding site as the reporter ligand.

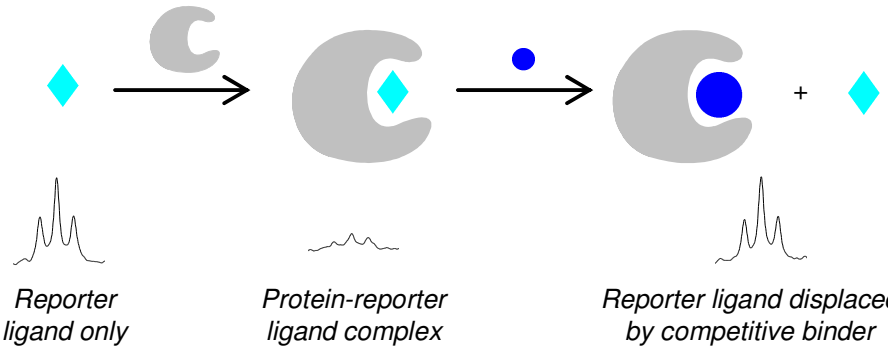

Figure 1-12 Scheme illustrating the principle of reporter ligand displacement method in NMR screening.

1.2.5 NOE-based binding experiments

Another approach to study protein-ligand interactions is to utilise the NOE. Several techniques were developed based on this concept, including transferred NOE (tr-NOE),[115–117,156] STD-NMR[118] and waterLOGSY.[120]

Tr-NOE relies on the difference in rotational correlation time between protein-bound and protein-free ligands.[156] When a small molecule ligand is free in solution, it generally has short rotational correlation times and exhibits small and positive intra-ligand NOEs, whilst when the ligand is bound to a protein, it behaves as part of a large molecule and exhibits large and negative NOEs due to increase of correlation time. The resulting tr-NOE signal is an average between the free and the bound states (Figure 1-13). Practically, tr-NOE experiments require stringent experiment conditions. These include mixing time, molecular weight of the ligand and the ratio of ligand excess. Due to these limitations, tr-NOE is generally less useful as a screening tool, but it can provide useful information about the bound conformation of the ligand.[117] A closely related method, ILOE,[119] which is based on the same principle and provides information about the relative binding orientation of two (or more) proximally bound ligands. ILOE has been applied in the area of fragment based drug discovery (FBDD) to provide information about the linking of proximally bound fragments to produce stronger and more 'drug-like' protein ligands.[157]

Figure 1-13 Scheme illustrating the principle of tr-NOE.

The STD-NMR method is based on the NOE between proteins and ligands.[118] It is a combination of two experiments. In the first (on-resonance) experiment, radiofrequency pulses are applied to selected protein resonances, and by spin diffusion, all protein resonances become rapidly saturated (Figure 1-14). Magnetisation can also spread by the same process in an intermolecular fashion onto the bound ligands leading to (partial) saturation of ligand resonances. If the ligand dissociates sufficiently fast, this saturation can be detected as a reduction in signal intensity in the spectrum. A reference (off-resonance) spectrum, which is essentially a normal ^{1}H spectrum, is also recorded without protein saturation in otherwise the same experimental conditions. Subtraction of the two spectra leads to a difference spectrum in which only signals experiencing saturation are visible. STD-NMR was initially proposed as a screening tool.[118] It is also useful in providing information about the binding epitope of the ligand to the protein.[158] Together with tr-NOE, useful models of how ligands are bound inside the protein active site can be generated.[159] K_D values can also be obtained by STD-NMR,[160] although both epitope mapping and K_D determination are complicated by ligand rebinding,[160] ligand relaxation time,[161–163] protein saturation time[160] and non-specific binding.[164] Due to the reliance on ligand exchange between the free and bound states, STD-NMR generally does not work for very strong or very weak ligand systems. In order to reduce spectral overlap, to perform screening for complex mixtures and to avoid undesired direct ligand saturation, several alternative versions of STD-NMR have been reported. These included STD-TOCSY,[165] STD-DOSY,[166] ^{13}C observed STD[167,168] and isotope edited STD experiments.[169]

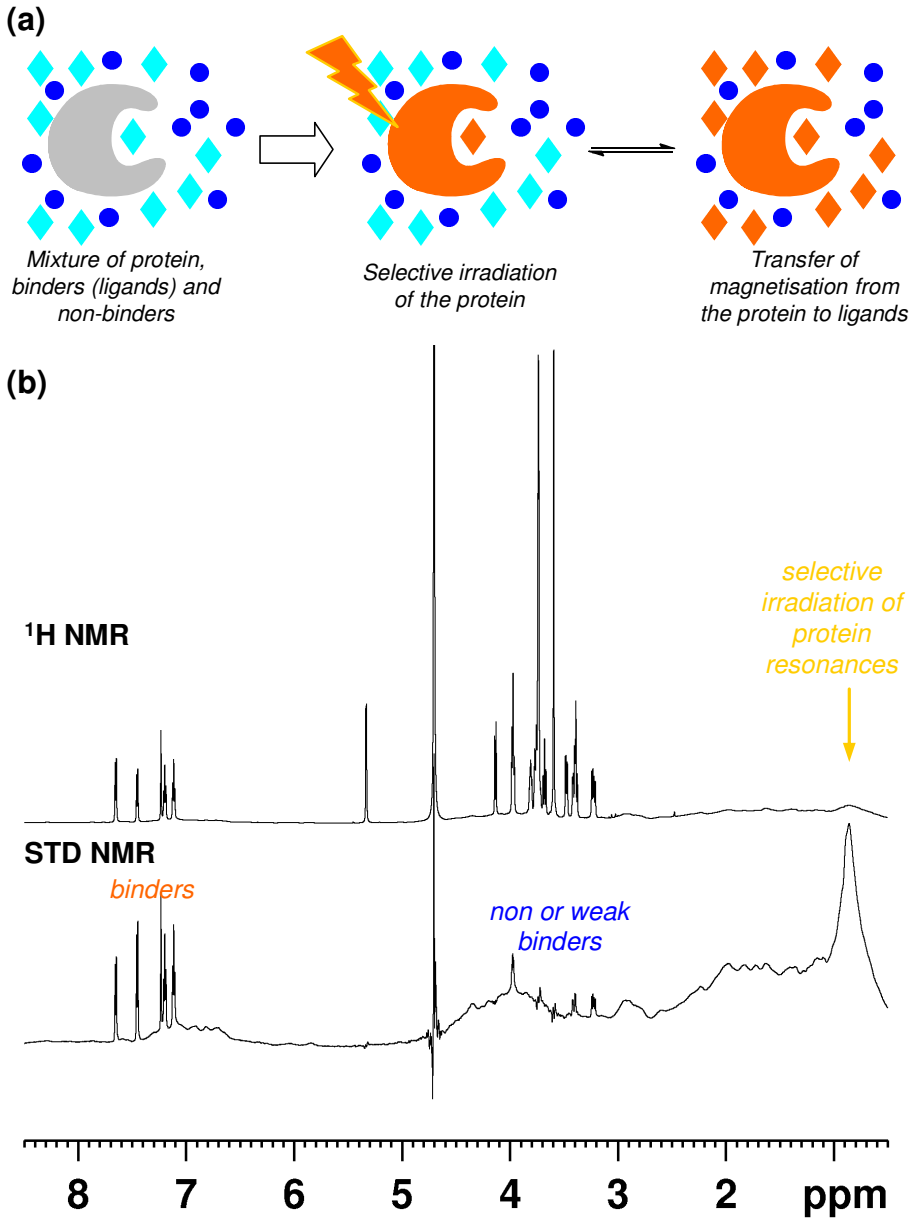

Figure 1-14 (a) Scheme illustrating the principle of STD-NMR; (b) A typical STD-NMR spectrum ran at 700 MHz. The mixture contained 100 µM bovine serum albumin (BSA), 10 mM tryptophan (binder) and 10 mM sucrose (non-binder).Selective on-resonance irradiation was applied at 0.86 ppm and off resonance irradiation was applied at 50 ppm. The saturation time was 2 seconds and the relaxation delay was also 2 seconds.

The waterLOGSY method is based on NOE between bulk water molecules, ligands and proteins.[120] The bulk water is saturated and magnetisation can spread intermolecularly to free ligands, bound ligands and proteins, with subsequent magnetisation transfer from the protein to bound ligands. Due to differences in rotational correlation times between free and bound components of the mixture (water molecules, ligands and proteins) and hence opposite signs of their intermolecular NOEs, binders and non-binders can usually be distinguished as opposite phased resonances on the waterLOGSY spectrum. WaterLOGSY is widely-used as a primary

screening tool.[170] K_D values can also be obtained by waterLOGSY,[170] although it has been shown that the accuracy may be influenced by protein concentrations.[171] WaterLOGSY can also provide information about solvent accessibility by conducting experiments with perdeuterated protein.[172,173] Similar to STD-NMR, waterLOGSY generally does not work for very strong or very weak ligand systems, as it relies on the exchange between free and bound ligands.

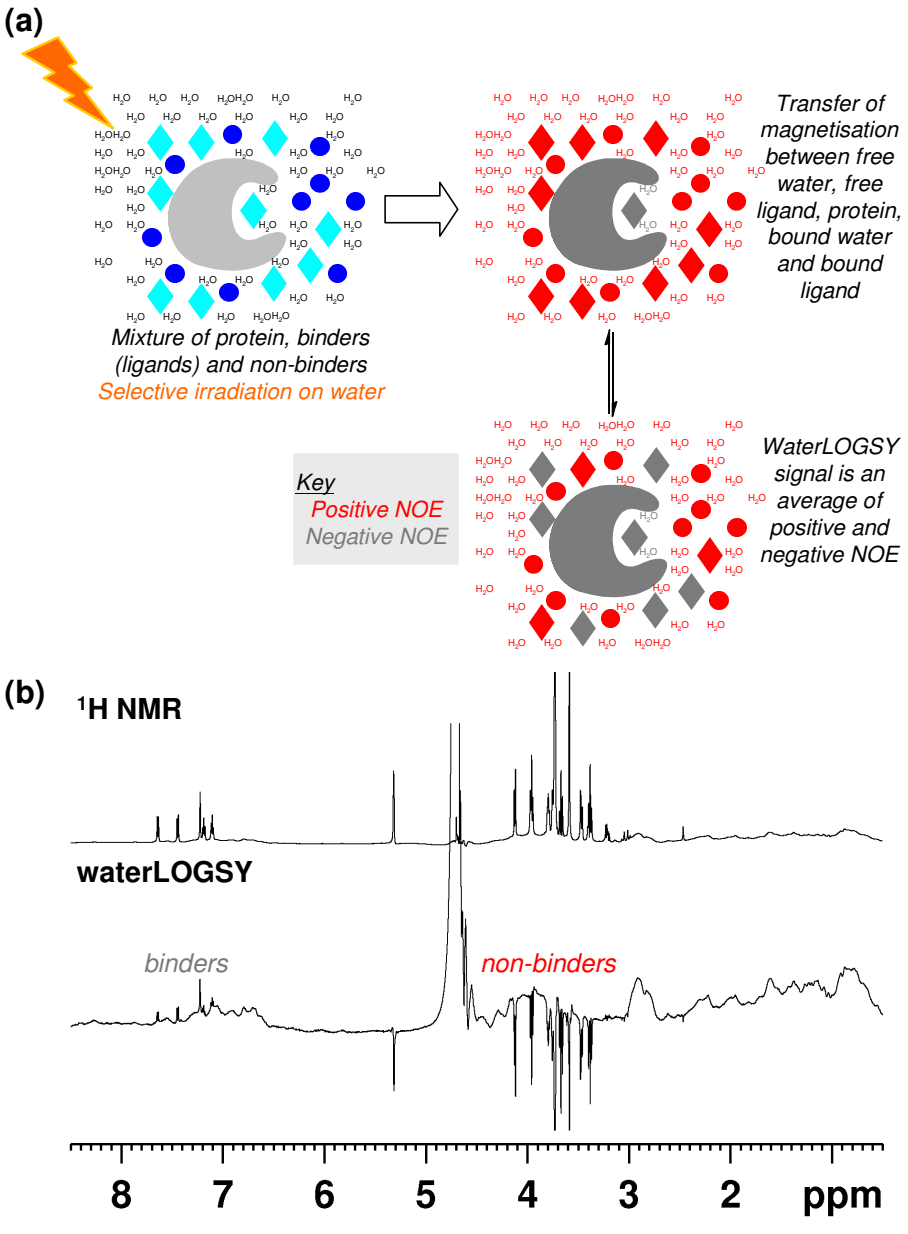

Figure 1-15 (a) Scheme illustrating the principle of waterLOGSY; (b) A typical waterLOGSY spectrum ran at 700 MHz. The mixture contained 100 µM bovine serum albumin (BSA), 2 mM tryptophan (binder) and 2 mM sucrose (non-binder) in 90% H_2O and 10% D_2O. Selective on-resonance irradiation was applied at 4.7 ppm. The mixing time was 1 second and the relaxation delay was 2 seconds.

1.2.6 Protein-observed ligand binding experiments

The most common method to study protein-ligand interactions by protein-observed NMR is by chemical shift perturbation of backbone amide protons.[129,138,174] Analyses are usually conducted using ^{1}H-^{15}N HSQC and the experiments require uniformly ^{15}N-labelled proteins. Each resonance on the HSQC spectrum represents a single amino acid (except for proline which has no NH). Side chain NH_2 groups (*e.g.* asparagine and glutamine) may also be present in the spectrum. Because amide chemical shifts are highly sensitive to perturbations in environment, they are good reporters of conformational change, solvent exposure and ligand binding. The mapping of the binding site on the protein can usually be readily obtained by ligand titration, although it may be complicated by protein dynamics such as slow exchange between the free and bound forms of the protein, and protein conformational change.[175] In such cases the cross saturation experiment and the related transferred cross saturation experiment,[176] which utilises transfer of magnetisation from the ligand (usually protein or peptide) to a ^{2}H,^{15}N-labelled protein for detection, can be applied. Other labelling schemes such as amino acid specific labelling[177] or ^{13}C-methyl labelling are also widely used especially in the study of large proteins,[178] which overcome problems including signal overlap and relaxation. It was also shown that at relatively high protein concentration (~1 mM), ligand binding can be monitored with unlabelled protein at natural abundance using the band-selective optimized flip-angle short-transient HMQC (SOFAST-HMQC) experiment.[179]

1.2.7 Protein backbone assignment

Before detailed information about protein-ligand interactions can be obtained, it is necessary to assign the protein backbone amide resonances to specific residues along the protein sequence (for reviews see references 180–182).

Backbone amide proton assignment for small proteins is now a relatively straightforward and semi-automated process, which usually requires only single ^{15}N-labelled proteins. The most common method of determining resonance assignment is known as the sequential assignment strategy.[183] The first step involves the recording and analyses of 3D heteronuclear-edited correlation spectra (such as TOCSY-^{1}H-^{15}N HSQC) to identify amino acid spin systems by tracing through-bond scalar interactions along the amino acid side chain. The next step involves the recording and

analyses of through-space dipolar interactions, usually using 3D heteronuclear-edited experiments such as the NOESY-^{1}H-^{15}N HSQC, to allow sequential NOE analysis along the protein sequence.

For larger proteins, the triple resonance assignment strategy,[184,185] which requires the use of ^{13}C,^{15}N-labelled protein, can be used. Although widely applied, it can still be a tedious and expensive process for proteins larger than 25 kDa especially if deuterium labelling is required to overcome signal losses due to ^{1}H-^{13}C dipole-dipole relaxation.[186] Triple resonance experiments rely on the relatively large ^{1}J (and in some cases ^{2}J) couplings between ^{1}H, ^{15}N and ^{13}C in the protein backbone spin system. The first step usually involves the recording of at least one set of the triple resonance experiments, such as HN(CO)CACB, which gives correlation information between $^{1}H_{i}$, $^{15}N_{i}$, $^{13}C\alpha_{i-1}$ and $^{13}C\beta_{i-1}$, and HNCACB, which gives correlation information between $^{1}H_{i}$, $^{15}N_{i}$, $^{13}C\alpha_{i}$, $^{13}C\beta_{i}$, $^{13}C\alpha_{i-1}$ and $^{13}C\beta_{i-1}$. This allows sequential linking of the amide protons. Amino acid types can then be identified by the ^{13}C chemical shifts of α and β carbons (such as those of alanine, glycine, serine and threonine). Other experiments such as TOCSY-^{1}H-^{15}N HSQC and HCCH-TOCSY may also help in the identification of amino acid types by mapping ^{1}H chemical shifts along the amino acid side chain. Further discussions about the specific triple resonance experiments can be found in Chapter 4.

1.3 Application of NMR spectroscopy to study 2OG oxygenases

NMR spectroscopy has previously been applied, though not extensively, to study 2OG oxygenases. One of the major applications has been reaction monitoring by small molecule NMR spectroscopy. NMR has a distinctive advantage as it can monitor both 2OG oxidation and substrate oxidation at the same time and in the same spectrum, which may be otherwise difficult by other biophysical techniques (such as the use of radiolabelled 2OG and substrate). For example, NMR was applied to monitor the coupling ratio between HIF peptide substrate hydroxylation and 2OG oxidation by the HIF hydroxylase PHD2.[187] It is also possible to identify the formation of multiple products, and characterise them *in situ* from the reaction mixture or *ex situ* as a purified compound. For instance, the identification of formaldehyde and the characterisation of different demethylation states of histone methyllysine as catalysed by the histone demethylase Jumonji domain containing

protein 2E (JMJD2E) have been followed by ^{1}H NMR.[188] Purified hydroxylated HIF peptide as a result of PHD2 catalysis has also been characterised by NMR.[189]

Protein NMR has also been, although not extensively, applied to study 2OG oxygenases. The *E. coli* DNA repair enzyme AlkB has been studied by protein NMR and other biophysical techniques to identify different dynamic states upon metal binding and co-substrate binding.[52,53] The *apo* and metal bound *holo* forms of AlkB were found to be largely unstructured, but the simultaneous binding of both metal and 2OG induced protein folding and significant conformational change of the protein structure as shown by both ^{1}H NMR and ^{1}H-^{15}N HSQC. In another study, human PHD2 was selectively labelled with ^{15}N-tryptophan and its interaction with a bicyclic inhibitor, labelled with ^{19}F and ^{13}C, was studied by both protein NMR (^{1}H-^{15}N HSQC) using paramagnetic shifts by replacing the active site Fe(II) by paramagnetic Co(II) and Ni(II) metal ions, and small molecule NMR by direct observation of the bound inhibitor using ^{13}C and ^{19}F NMR. The results revealed there are two different bound conformations of the inhibitor when bound to PHD2.[190]

Protein NMR studies have also been conducted using isotopically labelled protein substrates of 2OG oxygenases.[191,192] For instance, the stability of ^{15}N-labelled ankyrin repeat protein, which is a substrate for the HIF hydroxylase factor inhibiting HIF (FIH), was studied by ^{1}H-^{15}N HSQC, which found that hydroxylated ankyrin repeat proteins are significantly more stable than the unhydroxylated counterpart. Protein backbone assignment has also been conducted for HIF1$\alpha_{404–477}$,[193] which contained the *N*-terminal oxygen dependent degradation domain (NODD) of HIF1α. HIF1$\alpha_{404–477}$ is a substrate for HIF prolyl hydroxylases, which was found to be largely unstructured in solution by ^{1}H-^{15}N HSQC. However, no follow-up work has yet been reported for the system.

1.3.1 Objectives

The main objective of the work reported in this Thesis was to apply NMR spectroscopy to study different aspects of 2OG oxygenases.

In Chapter 2, NMR spectroscopy was applied to study the human oxygenase BBOX, an enzyme involved in L-carnitine biosynthesis. NMR was applied to monitor enzyme kinetics and to perform enzyme inhibition studies of various BBOX inhibitors. NMR was also applied to identify alternative BBOX substrates and for the characterisation

of enzymatic products *in situ*. Using ^{13}C-labelled substrate, the mechanism of a novel BBOX-catalysed C-C bond formation reaction was revealed. Finally, with the aid of NMR spectroscopy, the development of alternative and higher-throughput BBOX assays is also described.

In Chapter 3, two ligand-based NMR techniques were investigated and optimised to study ligand binding interactions to 2OG oxygenases. Both methods were essentially competition-based experiments. In the first method, 2OG was applied as a reporter ligand and in the second method, water molecules were used as reporter. The HIF hydroxylases PHD2 and FIH were used as model protein systems and the binding constants of various substrates and inhibitors were measured and compared.

In Chapter 4, the application of protein NMR to study the PHD2-substrate interactions was investigated. Protein backbone assignment was conducted for $PHD2_{181\text{-}402}$-Zn(II)-2OG and $PHD2_{181\text{-}402}$-Zn(II)-2OG-CODD. The PHD2 amino acid residues involved in substrate and co-substrate binding were identified. Finally, the binding of CODD (substrate) and hydroxylated CODD (product) to PHD2 was also investigated and the results revealed a mechanism for the release of the enzyme product.

In Chapter 5, NMR was applied to study the potential of using the protein-directed dynamic combinatorial chemistry (DCC) approach to discover novel protein ligands and inhibitors for 2OG oxygenases. First, the applicability of the reversible reaction of boronate ester formation to protein directed DCC was investigated by a combination of ^{11}B and ^{1}H experiments. Secondly, the method was applied to discover new inhibitors for the HIF prolyl hydroxylase PHD2, in which NMR was applied for hit validation and binding quantification.

In Chapter 6, experimental procedures are described.

1.4 References

1. Costas, M.; Mehn, M. P.; Jensen, M. P.; Que Jr., L. Dioxygen activation at mononuclear nonheme iron active sites: enzymes, models, and intermediates. *Chem. Rev.* **2004**, *104*, 939–986.
2. Hausinger, R. P. Fe(II)/α-ketoglutarate-dependent hydroxylases and related enzymes. *Crit. Rev. Biochem. Mol. Biol.* **2004**, *39*, 21–68.
3. Flashman, E.; Schofield, C. J. The most versatile of all reactive intermediates? *Nat. Chem. Biol.* **2007**, *3*, 86–87.
4. Ozer, A.; Bruick, R. K. Non-heme dioxygenases: cellular sensors and regulators jelly rolled into one? *Nat. Chem. Biol.* **2007**, *3*, 144–153.
5. Loenarz, C.; Schofield, C. J. Expanding chemical biology of 2-oxoglutarate oxygenases. *Nat. Chem. Biol.* **2008**, *4*, 152–156.
6. Kovaleva, E. G.; Lipscomb, J. D. Versatility of biological non-heme Fe(II) centers in oxygen activation reactions. *Nat. Chem. Biol.* **2008**, *4*, 186–193.
7. Loenarz, C.; Schofield, C. J. Physiological and biochemical aspects of hydroxylations and demethylations catalyzed by human 2-oxoglutarate oxygenases. *Trends Biochem. Sci.* **2010**, *36*, 7–18.
8. Prescott, A. G.; Lloyd, M. D. The iron(II) and 2-oxoacid-dependent dioxygenases and their role in metabolism. *Nat. Prod. Rep.* **2000**, *17*, 367–383.
9. Hewitson, K. S.; Granatino, N.; Welford, R. W. D.; McDonough, M. A.; Schofield, C. J. Oxidation by 2-oxoglutarate oxygenases: non-haem iron systems in catalysis and signalling. *Phil. Trans. R. Soc. A* **2005**, *363*, 807–828.
10. Hanauske-Abel, H. M.; Günzler, V. A Stereochemical concept for the catalytic mechanism of prolylhydroxylase: applicability to classification and design of inhibitors. *J. Theor. Biol.* **1982**, *94*, 421–455.
11. Sono, M.; Roach, M. P.; Coulter, E. D.; Dawson, J. H. Heme-containing oxygenases. *Chem. Rev.* **1996**, *96*, 2841–2887.
12. Solomon, E. I.; Decker, A.; Lehnert, N. Non-heme iron enzymes: contrasts to heme catalysis. *Proc. Natl. Acad. Sci. U. S. A.* **2003**, *100*, 3589–3594.
13. Myllylä, R.; Tuderman, L.; Kivirikko, K. I. Mechanism of the prolyl hydroxylase reaction. 2. Kinetic analysis of the reaction sequence. *Eur. J. Biochem.* **1977**, *80*, 349–357.
14. Zhou, J.; Gunsior, M.; Bachmann, B. O.; Townsend, C. A.; Solomon, E. I. Substrate binding to the α-ketoglutarate-dependent non-heme iron enzyme clavaminate synthase 2. Coupling mechanism of oxidative decarboxylation and hydroxylation. *J. Am. Chem. Soc.* **1998**, *120*, 13539–13540.
15. Price, J. C.; Barr, E. W.; Tirupati, B.; Bollinger Jr., J. M.; Krebs, C. The first direct characterization of a high-valent iron intermediate in the reaction of an α-ketoglutarate-dependent dioxygenase: a high-spin Fe(IV) complex in taurine/α-ketoglutarate dioxygenase (TauD) from *Escherichia coli*. *Biochemistry* **2003**, *42*, 7497–7508.
16. Proshlyakov, D. A.; Henshaw, T. F.; Monterosso, G. R.; Ryle, M. J.; Hausinger, R. P. Direct detection of oxygen intermediates in the non-heme Fe enzyme taurine/α-ketoglutarate dioxygenase. *J. Am. Chem. Soc.* **2004**, *126*, 1022–1023.
17. Riggs-Gelasco, P. J.; Price, J. C.; Guyer, R. B.; Brehm, J. H.; Barr, E. W.; Bollinger Jr., J. M.; Krebs, C. EXAFS spectroscopic evidence for an Fe=O unit in the Fe(IV) intermediate observed during oxygen activation by taurine:α-ketoglutarate dioxygenase. *J. Am. Chem. Soc.* **2004**, *126*, 8108–8109.
18. Hoffart, L. M.; Barr, E. W.; Guyer, R. B.; Bollinger Jr., J. M.; Krebs, C. Direct spectroscopic detection of a C-H-cleaving high-spin Fe(IV) complex in a prolyl-4-hydroxylase. *Proc. Natl. Acad. Sci. U. S. A.* **2006**, *103*, 14738–14743.

19. Welford, R. W. D.; Kirkpatrick, J. M.; McNeill, L. A.; Puri, M.; Oldham, N. J.; Schofield, C. J. Incorporation of oxygen into the succinate co-product of iron(II) and 2-oxoglutarate dependent oxygenases from bacteria, plants and humans. *FEBS Lett.* **2005**, *579*, 5170–5174.

20. Grzyska, P. K.; Appelman, E. H.; Hausinger, R. P.; Proshlyakov, D. A. Insight into the mechanism of an iron dioxygenase by resolution of steps following the Fe^{IV}=O species. *Proc. Natl. Acad. Sci. U. S. A.* **2010**, *107*, 3982–3987.

21. Myllylä, R.; Majamaa, K.; Günzler, V.; Hanauske-Abel, H. M.; Kivirikko, K. I. Ascorbate is consumed stoichiometrically in the uncoupled reactions catalyzed by prolyl 4-hydroxylase and lysyl hydroxylase. *J. Biol. Chem.* **1984**, *259*, 5403–5405.

22. Ryle, M. J.; Liu, A.; Muthukumaran, R. B.; Ho, R. Y. N.; Koehntop, K. D.; McCracken, J.; Que Jr., L.; Hausinger, R. P. O_2- and α-ketoglutarate-dependent tyrosyl radical formation in TauD, an α-keto acid-dependent non-heme Iron dioxygenase. *Biochemistry* **2003**, *42*, 1854–1862.

23. Barlow, J. N.; Zhang, Z.; John, P.; Baldwin, J. E.; Schofield, C. J. Inactivation of 1-aminocyclopropane-1-carboxylate oxidase involves oxidative modifications. *Biochemistry* **1997**, *36*, 3563–3569.

24. McCusker, K. P.; Klinman, J. P. Modular behaviour of tauD provides insight into the origin of specificity in α-ketoglutarate-dependent nonheme iron oxygenases. *Proc. Natl. Acad. Sci. U. S. A.* **2009**, *106*, 19791–19795.

25. Mantri, M.; Zhang, Z.; McDonough, M. A.; Schofield, C. J. Autocatalysed oxidative modifications to 2-oxoglutarate dependent oxygenases. *FEBS J.* **2012**, *279*, 1563–1575.

26. Mantri, M.; Webby, C. J.; Loik, N. D.; Hamed, R. B.; Nielsen, M. L.; McDonough, M. A.; McCullagh, J. S. O.; Böttger, A.; Schofield, C. J.; Wolf, A. Self-hydroxylation of the splicing factor lysyl hydroxylase, JMJD6. *Med. Chem. Commun.* **2012**, *3*, 80–85.

27. Valegård, K.; Terwisscha van Scheltinga, A. C.; Dubus, A.; Ranghino, G.; Öster, L. M.; Hajdu, J.; Andersson, I. The structural basis of cephalosporin formation in a mononuclear ferrous enzyme. *Nat. Struct. Mol. Biol.* **2004**, *11*, 95–101.

28. Mecinović, J.; Chowdhury, R.; Liénard, B. M. R.; Flashman, E.; Buck, M. R. G.; Oldham, N. J.; Schofield, C. J. ESI-MS Studies on prolyl hydroxylase domain 2 reveal a new metal binding site. *ChemMedChem* **2008**, *3*, 569–572.

29. Kalliri, E.; Grzyska, P. K.; Hausinger, R. P. Kinetic and spectroscopic investigation of Co^{II}, Ni^{II}, and *N*-oxalylglycine inhibition of the Fe^{II}/α-ketoglutarate dioxygenase, TauD. *Biochem. Biophys. Res. Lett.* **2005**, *338*, 191–197.

30. Hirsila, M.; Koivunen, P.; Xu, L.; Seeley, T.; Kivirkko, K. I.; Myllyharju, J. Effect of desferrioxamine and metals on the hydroxylases in the oxygen sensing pathway. *FASEB J.* **2005**, *19*, 1308–1310.

31. Sekirnik, R.; Rose, N. R.; Mecinović, J.; Schofield, C. J. 2-Oxoglutarate oxygenases are inhibited by a range of transition metals. *Metallomics* **2010**, *2*, 397–399.

32. Günzler, V.; Majamaa, K.; Hanauske-Abel, H. M.; Kivirikko, K. I. Catalytically active ferrous ions are not released from prolyl 4-hydroxylase under turnover conditions. *Biochim. Biophys. Acta* **1986**, *873*, 38–44.

33. Majamaa, K.; Hanauske-Abel, H. M.; Günzler, V.; Kivirikko, K. I. The 2-oxoglutarate binding site of prolyl 4-hydroxylase. Identification of distinct subsites and evidence for 2-oxoglutarate decarboxylation in a ligand reaction at the enzyme-bound ferrous ion. *Eur. J. Biochem.* **1984**, *138*, 239–245.

34. Cunliffe, C. J.; Franklin, T. J.; Hales, N. J.; Hill, G. B. Novel inhibitors of prolyl 4-hydroxylases. 3. Inhibition by the substrate analogue *N*-oxaloglycine and its derivatives. *J. Med. Chem.* **1992**, *35*, 2652–2658.

35. Koivunen, P.; Lee, S.; Duncan, C. G.; Lopez, G.; Lu, G.; Ramkissoon, S.; Losman, J. A.; Joensuu, P.; Bergmann, U.; Gross, S.; Travins, J.; Weiss, S.; Looper, R.; Ligon, K. L.;

Verhaak, R. G. W.; Yan, H.; Kaelin Jr, W. G. Transformation by the (*R*)-enantiomer of 2-hydroxyglutarate linked to EGLN activation. *Nature* **2012**, *483*, 484–488.

36. Flashman, E.; Davies, S. L.; Yeoh, K. K.; Schofield, C. J. Investigating the dependence of the hypoxia-inducible factor hydroxylases (factor inhibiting HIF and prolyl hydroxylase domain 2) on ascorbate and other reducing agents. *Biochem. J.* **2010**, *427*, 135–142.

37. De Jong, L.; Albracht, S. P.; Kemp, A. Prolyl 4-hydroxylase activity in relation of the oxidation state of enzyme-bound iron. The role of ascorbate in peptidyl proline hydroxylation. *Biochim. Biophys. Acta* **1982**, *704*, 326–332.

38. De Jong, L.; Kemp, A. Stoicheiometry and kinetics of the prolyl 4-hydroxylase partial reaction. *Biochim. Biophys. Acta* **1984**, *787*, 105–111.

39. Majamaa, K.; Günzler, V.; Hanauske-Abel, H. M.; Myllylä, R.; Kivirikko, K. I. Partial identity of the 2-oxoglutarate and ascorbate binding sites of prolyl 4-hydroxylase. *J. Biol. Chem.* **1986**, *261*, 7819–7823.

40. Kutnink, M. A.; Tolbert, B. M.; Richmond, V. L.; Baker, E. M. Efficacy of the ascorbic acid isomers in proline hydroxylation. *Proc. Soc. Exp. Biol. Med.* **1969**, *132*, 440–442.

41. Szöllössi, A. Mechanistic studies on 2-oxoglutarate dependent oxygenases. MSc (by research) Thesis. University of Oxford, July 2012.

42. Tuderman, L.; Myllylä, R.; Kivirikko, K. I. Mechanism of the prolyl hydroxylase reaction. 1. Role of co-substrates. *Eur. J. Biochem.* **1977**, *80*, 341–348.

43. Schofield, C. J.; Zhang, Z. Structural and mechanistic studies on 2-oxoglutarate-dependent oxygenases and related enzymes. *Curr. Opin. Struct. Biol.* **1999**, *9*, 722–731.

44. Clifton, I. J.; McDonough, M. A.; Ehrismann, D.; Kershaw, N. J.; Granatino, N.; Schofield, C. J. Structural studies on 2-oxoglutarate oxygenases and related double-stranded β-helix fold proteins. *J. Inorg. Biochem.* **2006**, *100*, 644–669.

45. Stirk, H. J.; Woolfson, D. N.; Hutchinson, E. G.; Thornton, J. M. Depicting topology and handedness in jellyroll structures. *FEBS Lett.* **1992**, *308*, 1–3.

46. McDonough, M. A.; Loenarz, C.; Chowdhury, R.; Clifton, I. J.; Schofield, C. J. Structural studies on human 2-oxoglutarate dependent oxygenases. *Curr. Opin. Struct. Biol.* **2010**, *20*, 659–672.

47. Hegg, E. L.; Que, L. The 2-his-1-carboxylate faciad triad – an emerging structural motif in mononuclear non-heme iron(II) enzymes. *Eur. J. Biochem.* **1997**, *250*, 625–629.

48. Hewitson, K. S.; Holmes, S. L.; Ehrismann, D.; Hardy, A. P.; Chowdhury, R.; Schofield, C. J.; McDonough, M. A. Evidence that two enzyme-derived histidine ligands are sufficient for iron binding and catalysis by factor inhibiting HIF (FIH). *J. Biol. Chem.* **2008**, *283*, 25971–25978.

49. McDonough, M. A.; Li, V.; Flashman, E.; Chowdhury, R.; Mohr, C.; Liénard, B. M. R.; Zondlo, J.; Oldham, N. J.; Clifton, I. J.; Lewis, J.; McNeill, L. A.; Kurzeja, R. J. M.; Hewitson, K. S.; Yang, E.; Jordan, S.; Syed, R. S.; Schofield, C. J. Cellular oxygen sensing: crystal structure of hypoxia-inducible factor prolyl hydroxylase (PHD2). *Proc. Natl. Acad. Sci. U. S. A.* **2006**, *103*, 9814–9819.

50. Chowdhury, R.; McDonough, M. A.; Mecinović, J.; Loenarz, C.; Flashman, E.; Hewitson, K. S.; Domene, C.; Schofield, C. J. Structural basis for binding of hypoxia-inducible factor to the oxygen-sensing prolyl hydroxylases. *Structure* **2009**, *17*, 981–989.

51. Roach, P. L.; Clifton, I. J.; Hensgens, C. M.; Shibata, N.; Schofield, C. J.; Hajdu, J.; Baldwin, J. E. Structure of isopenicillin N synthase complexed with substrate and the mechanism of penicillin formation. *Nature* **1997**, *387*, 827–870.

52. Bleijlevens, B.; Shivarattan, T.; Flashman, E.; Yang, Y.; Simpson, P. J.; Koivisto, P.; Sedgwick, B.; Schofield, C. J.; Matthews, S. J. Dynamic states of the DNA repair enzyme AlkB regulate product release. *EMBO Rep.* **2008**, *9*, 872–877.

53. Bleijlevens, B.; Shivarattan, T.; van den Boom, K. S.; de Haan, A.; van der Zwan, G.; Simpson, P. J.; Matthews, S. J. Changes in protein dynamics of the DNA repair dioxygenase AlkB upon binding of Fe^{2+} and 2-oxoglutarate. *Biochemistry* **2012**, *51*, 3334–3341.

54. Rademacher, W. Growth retardants: effects on gibberellin biosynthesis and other metabolic pathways. *Ann. Rev. Plant Physiol. Plant Mol. Biol.* **2000**, *51*, 501−531.

55. Semenza, G. L. Targeting HIF-1 for cancer therapy. *Nat. Rev. Cancer* **2003**, *3*, 721–732.

56. Nagel, S.; Talbot, N. P.; Mecinović, J.; Smith, T. G.; Buchan, A. M.; Schofield, C. J. Therapeutic manipulation of the HIF hydroxylases. *Antioxid. Redox Signal.* **2010**, *12*, 481–501.

57. Hewitson, K. S.; Schofield, C. J. The HIF pathway as a therapeutic target. *Drug Discov. Today* **2004**, *9*, 704–711.

58. Fraisl, P.; Aragonés, J.; Carmeliet, P. Inhibition of oxygen sensors as a therapeutic strategy for ischaemic and inflammatory disease. *Nat. Rev. Drug Discov.* **2009**, *8*, 139–152.

59. Sesti, C. Simkhovich, B. Z.; Kalvinsh, I. ; Kloner, R. A. Mildronate, a novel fatty acid oxidation inhibitor and antianginal agent, reduces myocardial infarct size without affecting hemodynamics. *J. Cardiovasc. Pharmacol.* **2006**, *47*, 493–499.

60. Liepinsh, E.; Vilskersts, R.; Loca, D.; Kirjanova, O.; Pugovichs, O.; Kalvinsh, I.; Dambrova, M. Mildronate, an inhibitor of carnitine biosynthesis, induces an increase in gamma-butyrobetaine contents and cardioprotection in isolated rat heart infarction. *J. Cardiovasc. Pharmacol.* **2006**, *48*, 314–319.

61. Hayashi, Y.; Kirimoto, T.; Asaka, N.; Nakano, M.; Tajima, K.; Miyake, H.; Matsuura, N. Beneficial effects of MET-88, a γ-butyrobetaine hydroxylase inhibitor in rats with heart failure following myocardial infarction. *Eur. J. Pharmacol.* **2000**, *395*, 217–224.

62. Rupp, H.; Zarain-Herzberg, A.; Maisch, B. The use of partial fatty acid oxidation inhibitors for metabolic therapy of angina pectoris and heart failure. *Herz* **2002**, *27*, 621–636.

63. Rose, N. R.; McDonough, M. A.; King, O. N. F.; Kawamura, A.; Schofield, C. J. Inhibition of 2-oxoglutarate dependent oxygenases. *Chem. Soc. Rev.* **2011**, *40*, 4364–4397.

64. Baader, E.; Tschank, G.; Baringhaus, K.-H.; Burghard, H.; Günzler, V. Inhibition of prolyl 4-hydroxylase by oxalyl amino acid derivatives *in vitro*, in isolated microsomes and in embryonic chicken tissues. *Biochem. J.* **1994**, *300*, 525–530.

65. McDonough, M. A.; McNeill, L. A.; Tilliet, M.; Papamicaël, C. A.; Chen, Q.-Y.; Banerji, B.; Hewitson, K. S.; Schofield, C. J. Selective inhibition of factor inhibiting hypoxia-inducible factor. *J. Am. Chem. Soc.* **2005**, *127*, 7680–7681.

66. Rose, N. R.; Ng, S. S.; Mecinović, J.; Liénard, B. M. R.; Bello, S. H.; Sun, Z.; McDonough, M. A.; Oppermann, U.; Schofield, C. J. Inhibitor scaffolds for 2-oxoglutarate-dependent histone lysine demethylases. *J. Med. Chem.* **2008**, *51*, 7053–7056.

67. Conejo-Garcia, A.; McDonough, M. A.; Loenarz, C.; McNeill, L. A.; Hewitson, K. S.; Ge, W.; Liénard, B. M.; Schofield, C. J.; Clifton, I. J. Structural basis for binding of cyclic 2-oxoglutarate analogues to factor-inhibiting hypoxia-inducible factor. *Bioorg. Med. Chem. Lett.* **2010**, *20*, 6125–6128.

68. Koski, M. K.; Hieta, R.; Böllner, C.; Kivirikko, K. I.; Myllyharju, J.; Wierenga, R. K. The active site of an algal prolyl 4-hydroxylase has a large structural plasticity. *J. Biol. Chem.* **2007**, *282*, 37112–37123.

69. Mecinović, J.; Loenarz, C.; Chowdhury, R.; Schofield, C. J. 2-Oxoglutarate analogue inhibitors of prolyl hydroxylase domain 2. *Bioorg. Med. Chem. Lett.* **2009**, *19*, 6192–6195.

70. Hales, N. J.; Beattie, J. F. Novel inhibitors of prolyl 4-hydroxylase. 5. The intriguing structure-activity relationships seen with 2,2'-bipyridine and its 5,5'-dicarboxylic acid derivatives. *J. Med. Chem.* **1993**, *36*, 3853–3858.

71. Franklin, T. J.; Morris, W. P.; Edwards, P. N.; Large, M. S.; Stephenson, R. Inhibition of prolyl 4-hydroxylase *in vitro* and *in vivo* by members of a novel series of phenanthrolinones. *Biochem. J.* **2001**, *353*, 333–338.

72. Hirsilä, M.; Koivunen, P.; Günzler, V.; Kivirikko, K. I.; Myllyharju, J. Characterization of the human prolyl 4-hydroxylases that modify the hypoxia-inducible factor. *J. Biol. Chem.* **2003**, *278*, 30772–30780.

73. Banerji, B.; Conejo-Garcia, A.; McNeill, L. A.; McDonough, M. A.; Buck, M. R. G.; Hewitson, K. S.; Oldham, N. J.; Schofield, C. J. The inhibition of factor inhibiting hypoxia-inducible factor (FIH) by β-oxocarboxylic acids. *Chem. Commun.* **2005**, 5438–5440.

74. Nangaku, M.; Izuhara, Y.; Takizawa, S.; Yamashita, T.; Fujii-Kuriyama, Y.; Ohneda, O.; Yamamoto, M.; van Ypersele de Strihou, C.; Hirayama, N.; Miyata, T. A novel class of prolyl hydroxylase inhibitors induces angiogenesis and exerts organ protection against ischemia. **Arterioscler. Thromb. Vasc. Biol.** *2007*, **27**, 2548-2554.

75. Chang, K.-H.; King, O. N. F.; Tumber, A.; Woon, E. C. Y.; Heightman, T. D.; McDonough, M. A.; Schofield, C. J.; Rose, N. R. Inhibition of histone demethylases by 4-carboxy-2,2'-bipyridyl compounds. *ChemMedChem* **2011**, *6*, 759–764.

76. Smirnova, N. A.; Rakhman, I.; Moroz, N.; Basso, M.; Payappilly, J.; Kazakov, S.; Hernandez-Guzman, F.; Gaisina, I. N.; Kozikowski, A. P.; Ratan, R. R.; Gazaryan, I. G. Utilization of an *in vivo* reporter for high throughput identification of branched small molecule regulators of hypoxic adaptation. *Chem. Biol.* **2010**, *17*, 380–391.

77. Warshakoon, N. C.; Wu, S.; Boyer, A.; Kawamoto, R.; Sheville, J.; Renock, S.; Xu, K.; Pokross, M.; Evdokimov, A. G.; Walter, R.; Mekel, M. A Novel Series of Imidazo[1,2-a]pyridine Derivatives as HIF-1α Prolyl Hydroxylase Inhibitors. *Bioorg. Med. Chem. Lett.* **2006**, *16*, 5598-5601.

78. Rosen, M. D.; Venkatesan, H.; Peltier, H. M.; Bembenek, S. D.; Kanelakis, K. C.; Zhao, L. X.; Leonard, B. E.; Hocutt, F. M.; Wu, X.; Palomino, H. L.; Brondstetter, T. I.; Haugh, P. V.; Cagnon, L.; Yan, W.; Liotta, L. A.; Young, A.; Mirzadegan, T.; Shankley, N. P.; Barrett, T. D.; Rabinowitz, M. H. Benzimidazole-2-pyrazole HIF prolyl 4-hydroxylase inhibitors as oral erythropoietin secretagogues. *ACS Med. Chem. Lett.* **2010**, *1*, 526–529.

79. Stubbs, C. J.; Loenarz, C.; Mecinović, J.; Yeoh, K. K.; Hindley, N.; Liénard, B. M.; Sobott, F.; Schofield, C. J.; Flashman, E. Application of a proteolysis/mass spectrometry method for investigating the effects of inhibitors on hydroxylase structure. *J. Med. Chem.* **2009**, *52*, 2799–2805.

80. Dao, J. H.; Kurzeja, R. J.; Morachis, J. M.; Veith, H.; Lewis, J.; Yu, V.; Tegley, C. M.; Tagari, P. Kinetic characterization and identification of a novel inhibitor of hypoxia-inducible factor prolyl hydroxylase 2 using a time-resolved fluorescence resonance energy transfer-based assay technology. *Anal. Biochem.* **2009**, *384*, 213-223.

81. Tegley, C. M.; Viswanadhan , V. N.; Biswas, K.; Frohn, M. J.; Peterkin, T. A. N.; Chang, C.; Bürli, R. W.; Dao, J. H.; Veith, H.; Rogers, N.; Yoder, S. C.; Biddlecome, G.; Tagari, P.; Allen, J. R.; Hungate, R. W. Discovery of Novel Hydroxy-Thiazoles as HIF-α Prolyl Hydroxylase Inhibitors: SAR, Synthesis, and Modeling Evaluation. *Bioorg. Med. Chem. Lett.* **2008**, *18*, 3925-3928.

82. Murray, J. K.; Balan, C.; Allgeier, A. M.; Kasparian, A.; Viswanadhan, V.; Wilde, C.; Allen, J. R.; Yoder, S. C.; Biddlecome, G.; Hungate, R. W.; Miranda, L. P. Dipeptidyl-quinolone derivatives inhibit hypoxia inducible factor-1α prolyl hydroxylase-1, -2, and -3 with altered selectivity. *J. Comb. Chem.* **2010**, *12*, 676–686.

83. King, O. N. F.; Li, X. S.; Sakurai, M.; Kawamura, A.; Rose, N. R.; Ng, S. S.; Quinn, A. M.; Rai, G.; Mott, B. T.; Beswick, P.; Klose, R. J.; Oppermann, U.; Jadhav, A.; Heightman, T. D.; Maloney, D. J.; Schofield, C. J.; Simeonov, A. Quantitative high-throughput screening identifies 8-hydroxyquinolines as cell-active histone demethylase inhibitors. *PLoS ONE* **2010**, *5*, e15535.

84. Vachal, P.; Miao, S.; Pierce, J. M.; Guiadeen, D.; Colandrea, V. J.; Wyvratt, M. J.; Salowe, S. P.; Sonatore, L. M.; Milligan, J. A.; Hajdu, R.; Gollapudi, A.; Keohane, C. A.; Lingham, R. B.; Mandala, S. M.; DeMartino, J. A.; Tong, X.; Wolff, M.; Steinhuebel, D.; Kieczykowski, G. R.; Fleitz, F. J.; Chapman, K.; Athanasopoulos, J.; Adam, G.; Akyuz, C. D.; Jena, D. K.; Lusen, J. W.; Meng, J.; Stein, B. D.; Xia, L.; Sherer, E. C.; Hale, J. J. 1,3,8-Triazaspiro[4.5]decane-2,4-diones as efficacious pan-inhibitors of hypoxia-inducible factor prolyl hydroxylase 1-3 (HIF PHD1-3) for the treatment of anemia. *J. Med. Chem.* **2012**, *55*, 2945–2959.

85. Kwon, H. S.; Choi, Y. K.; Kim, J. W.; Park, Y. K.; Yang, E. G.; Ahn, D.-R. Inhibition of a prolyl hydroxylase domain (PHD) by substrate analog peptides. *Bioorg. Med. Chem. Lett.* **2011**, *21*, 4325–4328.

86. Simkhovich, B. Z.; Shutenko, Z. V.; Meirena, D. V.; Khagi, K. B.; Mezapuķe, R. J.; Molodchina, T. N.; Kalviņs, I. J.; Lukevics, E.. 3-(2,2,2-Trimethylhydrazinium) Propionate (THP) - a novel gamma-butyrobetaine hydroxylase inhibitor with cardioprotective properties. *Biochem. Pharmacol.* **1988**, *37*, 195–202.

87. Petter, R. C.; Banerjee, S.; Englard, S. Inhibition of γ-butyrobetaine hydroxylase by cyclopropyl-substituted γ-butyrobetaines. *J. Org. Chem.* **1990**, *55*, 3088–3097.

88. Ziering, D. L.; Pascal Jr., R. A. Mechanism-based inhibition of bacterial γ-butyrobetaine hydroxylase. *J. Am. Chem. Soc.* **1990**, *112*, 834–838.

89. Begley, T. J.; Samson, L. D. AlkB mystery solved: oxidative demethylation of N1-methyladenine and N3-methylcytosine adducts by a direct reversal mechanism. *Trends Biochem. Sci.* **2003**, *28*, 2–5.

90. Hewitson, K. S.; Schofield, C. J.; Ratcliffe, P. J. Hypoxia-inducible factor prolyl-hydroxylase: purification and assays of PHD2. *Methods Enzymol.* **2007**, *435*, 25–42.

91. Sekirnik, R.; Rose, N. R.; Thalhammer, A.; Seden, P. T.; Mecinović, J.; Schofield, C. J. Inhibition of the histone lysine demethylase JMJD2A by ejection of structural Zn(II). *Chem. Commun.* **2009**, 6376-6378.

92. Metzen, E.; Zhou, J.; Jelkmann, W.; Fandrey, J.; Brüne, B. Nitric oxide impairs normoxic degradation of HIF-1α by inhibition of prolyl hydroxylases. *Mol. Biol. Cell* **2003**, *14*, 3470–3481.

93. Chowdhury, R.; Flashman, E.; Mecinović, J.; Kramer, H. B.; Kessler, B. M.; Frapart, Y. M.; Boucher, J.-L.; Clifton, I. J.; McDonough, M. A.; Schofield, C. J. Studies on the reaction of nitric oxide with the hypoxia-inducible factor prolyl hydroxylase domain 2 (EGLN1). *J. Mol. Biol.* **2011**, *410*, 268–279.

94. Levett, D. Z.; Fernandez, B. O.; Riley, H. L.; Martin, D. S.; Mitchell, K.; Leckstrom, C. A.; Ince, C.; Whipp, B. J.; Mythen, M. G.; Montgomery, H. E.; Grocott, M. P.; Feelisch, M.; Caudwell Extreme Everest Research Group. The role of nitrogen oxides in human adaptation to hypoxia. *Sci. Rep.* **2011**, *1*, 109.

95. Sogo, P. B.; Tolbert, B. M. Nuclear and electron paramagnetic resonance and its application to biology. *Adv. Biol. Med. Phys.* **1957**, *5*, 1–35.

96. Kowalsky, A.; Cohn, M. Application of nuclear magnetic resonance in biochemistry. *Annu. Rev. Biochem.* **1964**, *33*, 481–518.

97. Allerhand, A.; Trull, E. A. Nuclear magnetic resonance. *Annu. Rev. Phys. Chem.* **1970**, *21*, 317–348.

98. Jardetzky, O.; Wade-Jardetzky, N. G. Applications of nuclear magnetic resonance spectroscopy to the study of macromolecules. *Annu. Rev. Biochem.* **1971**, *40*, 605–634.

99. Takeda, M.; Jardetzky, O. Proton magnetic resonance of simple amino acids and dipeptides in aqueous solution. *J. Chem. Phys.* **1957**, *26*, 1346–1347.

100. Jardetzky, O.; Jardetzky, C. D. Proton magnetic resonance spectra of amino acids. *J. Biol. Chem.* **1958**, *233*, 383–387.

101. Saunders, M.; Wishnia, A.; Kirkwood, J. G. The nuclear magnetic resonance spectrum of ribonuclease. *J. Am. Chem. Soc.* **1957**, *79*, 3289–3290.

102. Jardetzky, O.; Jardetzky, C. D. An interpretation of the proton magnetic resonance spectrum of ribonuclease. *J. Am. Chem. Soc.* **1957**, *79*, 5322–5323.

103. Farrar, T. C.; Gutowsky, H. S.; Alberty, R. A.; Miller, W. G. The mechanism of the stereospecific enzymatic hydration of fumarate to L-malate. *J. Am. Chem. Soc.* **1957**, *79*, 3978–3980.

104. Jardetzky, O.; Wade, N. G.; Fischer, J. J. Proton magnetic resonance investigation of enzyme-coenzyme complexes. *Nature* **1963**, *197*, 183–184.

105. Kato, G. Studies on serum cholinesterase kinetics by nuclear magnetic resonance spectroscopy. *Mol. Pharmacol.* **1968**, *4*, 640–644.

106. Feather, M. S.; Lybyer, M. J. An NMR study of the phosphoglucose and phosphoribose isomerase reactions. *Biochem. Biophys. Res. Commun.* **1969**, *35*, 538–541.

107. Kaiser, R. Use of the nuclear Overhauser effect in the analysis of high-resolution nuclear magnetic resonance spectra. *J. Chem. Phys.* **1963**, *39*, 2435–2442.

108. Ernst, R. R.; Anderson, W. A. Application of Fourier transform spectroscopy to magnetic resonance. *Rev. Sci. Instrum.* **1966**, *37*, 93–102.

109. Aue; W. P.; Bartholdi, E.; Ernst, R. R. Two-dimensional spectroscopy. Application to nuclear magnetic resonance. *J. Chem. Phys.* **1976**, *64*, 2229–2246.

110. Wüthrich, K.; Wider, G.; Wagner, G.; Braun, W. Sequential resonance assignments as a basis for determination of spatial protein structures by high resolution proton nuclear magnetic resonance. *J. Mol. Biol.* **1982**, *155*, 311–319.

111. Williamson, M. P.; Havel, T. F.; Wüthrich, K. Solution conformation of proteinase inhibitor IIA from bull seminal plasma by ^{1}H nuclear magnetic resonance and distance geometry. *J. Mol. Chem.* **1985**, *182*, 295–315.

112. Kay, L. E.; Ikura, M.; Tschudin, R.; Bax, A. Three-dimensional triple-resonance NMR spectroscopy of isotopically enriched proteins. *J. Magn. Reson.* **1990**, *89*, 496–514.

113. Pervushin, K.; Riek, R.; Wider, G.; Wüthrich, K. Attenuated T_2 relaxation by mutual cancellation of dipole-dipole coupling and chemical shift anisotropy indicates an avenue to NMR structures of very large biological macromolecules in solution. *Proc. Nat. Acad. Sci. U. S. A.* **1997**, *94*, 12366–12371.

114. Shuker, S. B.; Hajduk, P. J.; Meadows, R. P.; Fesik, S. W. Discovering high-affinity ligands for proteins: SAR by NMR. *Science* **1996**, *274*, 1531–1534.

115. Balaram, P.; Bothner-By, A. A.; Dadok, J. Negative nuclear Overhauser effects as probes of macromolecular structure. *J. Am. Chem. Soc.* **1972**, *94*, 4015–4017.

116. Balaram, P.; Bothner-By, A. A.; Breslow, E. Localization of tyrosine at the binding site of neurophysin I1 by negative nuclear Overhauser effects. *J. Am. Chem. Soc.* **1972**, *94*, 4017–4018.

117. Albrand, J. P.; Birdsall, B.; Feeney, J.; Roberts, G. C. K.; Burgen, A. S. V. The use of transferred nuclear Overhauser effects in the study of the conformations of small molecules bound to proteins. *Int. J. Biol. Macromol.* **1979**, *1*, 37–41.

118. Mayer, M.; Meyer, B. Characterization of ligand binding by saturation transfer difference NMR spectroscopy. *Angew. Chem. Int. Ed.* **1999**, *38*, 1784–1788.

119. Li, D.; DeRose, E. F.; London, R. E. The inter-ligand Overhauser effect: A powerful new NMR approach for mapping structural relationships of macromolecular ligands. *J. Biomol. NMR* **1999**, *15*, 71–76.

120. Dalvit, C.; Pevarello, P.; Tató, M.; Veronesi, M.; Vulpetti, A.; Sundström, M. Identification of compounds with binding affinity to proteins via magnetization transfer from bulk water. *J. Biomol. NMR* **2000**, *18*, 65–68.

121. Sánchez-Pedregal, V. M.; Reese, M.; Meiler, J.; Blommers, M. J. J.; Griesinger, C.; Carlomagno, T. The INPHARMA method: protein-mediated interligand NOEs for pharmacophore mapping. *Angew. Chem. Int. Ed.* **2005**, *44*, 4172–4175.

122. Jahnke, W.; Floersheim, P.; Ostermeier, C.; Zhang, X.; Hemmig, R.; Hurth, K.; Uzunov, D. P. NMR reporter screening for the detection of high-affinity ligands. *Angew. Chem. Int. Ed.* **2002**, *41*, 3420–3423.

123. Dalvit, C.; Flocco, M.; Knapp, S.; Mostardini, M.; Perego, R.; Stockman, B. J.; Veronesi, M.; Varasi, M. High-throughput NMR-based screening with competition binding experiments. *J. Am. Chem. Soc.* **2002**, *124*, 7702–7709.

124. Dalvit, C.; Flocco, M.; Stockman, B. J.; Veronesi, M. Competition binding experiments for rapidly ranking lead molecules for their binding affinity to human serum albumin. *Comb. Chem. High Throughput Screen.* **2002**, *5*, 645–650.

125. Manzenrieder, F.; Frank, A. O.; Kessler, H. Phosphorus NMR spectroscopy as a versatile tool for compound library screening. *Angew. Chem. Int. Ed.* **2008**, *47*, 2608–2611.

126. Dalvit, C. Ligand- and substrate-based ^{19}F NMR screening: Principles and applications to drug discovery. *Prog. Nucl. Magn. Reson. Spectrosc.* **2007**, *51*, 243–271.

127. Dalvit, C.; Ardini, E.; Flocco, M.; Fogliatto, G. P.; Mongelli, N.; Veronesi, M. A general NMR method for rapid, efficient, and reliable biochemical screening. *J. Am. Chem. Soc.* **2003**, *125*, 14620–14625.

128. Stockman, B. J. 2-Fluoro-ATP as a versatile tool for ^{19}F NMR-based activity screening. *J. Am. Chem. Soc.* **2008**, *130*, 5870–5871.

129. *Protein-ligand interactions: structure and spectroscopy*; Harding, S. E., Chowdhry, B. Z., Eds.; Oxford University Press: Oxford, 2001.

130. Pellecchia, M.; Bertini, I.; Cowburn, D.; Dalvit, C.; Giralt, E.; Jahnke, W.; James, T. L.; Homans, S. W.; Kessler, H.; Luchinat, C.; Meyer, B.; Oschkinat, H.; Peng, J.; Schwalbe, H.; Siegal, G. Perspectives on NMR in drug discovery: a technique comes of age. *Nat. Rev. Drug Discov.* **2008**, *7*, 738–745.

131. Lepre, C. A.; Moore, J. M.; Peng, J. W. Theory and applications of NMR-based screening in pharmaceutical research. *Chem. Rev.* **2004**, *104*, 3641–3675.

132. Otting, G. Experimental NMR techniques for studies of protein-ligand interactions. *Curr. Opin. Struct. Biol.* **1993**, *3*, 760–768.

133. Jahnke, W. Perspectives of biomolecular NMR in drug discovery: the blessing and curse of versatility. *J. Biomol. NMR* **2007**, *39*, 87–90.

134. Jahnke, W.; Widmer, H. Protein NMR in biomedical research. *Cell. Mol. Life Sci.* **2004**, *61*, 580–599.

135. Heller, M.; Kessler, H. NMR spectroscopy in drug design. *Pure Appl. Chem.* **2001**, *73*, 1429–1436.

136. Powers, R. Advances in nuclear magnetic resonance for drug discovery. *Exp. Opin. Drug Discov.* **2009**, *4*, 1077–1098.

137. Blommers, M. J. J.; Flörsheimer, A.; Jahnke, W. Strategies for drug discovery using NMR. In *BioNMR in drug research. Methods and principle in medicinal chemistry*; Zerbe, O., Ed.; Wiley-VCH Verlag GmbH & Co. KGaA: Weinheim, 2002; Chapter 20, pp 439–457.

138. *NMR of biomolecules. Towards mechanistic systems biology*; Bertini, I., McGreevy, K. S., Parigi, G., Eds.; Wiley-VCH Verlag & Co.: Weinheim, 2012.

139. Meyer, B.; Peters, T. NMR spectroscopy techniques for screening and identifying ligand binding to protein receptors. *Angew. Chem. Int. Ed.* **2003**, *42*, 864–890.

140. Ludwig, C.; Guenther, U. L. Ligand based NMR methods for drug discovery. *Front. Biosci.* **2009**, *14*, 4565–4574.

141. Marchioro, C.; Davalli, S.; Provera, S.; Heller, M.; Ross, A.; Senn, H. Experiments in NMR-based screening. In *BioNMR in drug research. Methods and principle in medicinal chemistry*;

Zerbe, O., Ed.; Wiley-VCH Verlag GmbH & Co. KGaA: Weinheim, 2002; Chapter 14, pp 321–340.

142. Mercier, K. A.; Shortridge, M. D.; Powers, R. A multi-step NMR screen for the identification and evalution of chemical leads for drug discovery. *Comb. Chem. High Throughput Screen.* **2009**, *12*, 285–295.

143. Hajduk, P. J.; Meadows, R. P.; Fesik, S. W. NMR-based screening in drug discovery. *Quart. Rev. Biophys.* **1999**, *32*, 211–240.

144. Zuiderweg, E. R. P. Mapping protein-protein interactions in solution by NMR spectroscopy. *Biochemistry* **2002**, *41*, 1–7.

145. Zartler, E. R.; Shapiro, M. J. Protein NMR-based screening in drug discovery. *Curr. Pharm. Des.* **2006**, *12*, 3963–3972.

146. Fielding, L. NMR Methods for the determination of protein-ligand dissociation constants. *Curr. Top. Med. Chem.* **2003**, *3*, 39–53.

147. Fielding, L. NMR methods for the determination of protein–ligand dissociation constants. *Prog. Nucl. Magn. Reson. Spectrosc.* **2007**, *51*, 219–242.

148. Dalvit, C.; Gossert, A. D.; Coutant, J.; Piotto, M. Rapid acquisition of ^{1}H and ^{19}F NMR experiments for direct and competition ligand-based screening. *Magn. Reson. Chem.* **2011**, *49*, 199–202.

149. Krishna Sastry, M. V.; Swamy, M. J.; Surolia, A. Analysis of dynamics and mechanism of ligand binding to *Artocarpus integrifolia* agglutinin. A 13C and 19F NMR study. *J. Biol. Chem.* **1988**, *263*, 14826–14831.

150. Dalvit, C.; Flocco, M.; Veronesi, M.; Stockman, B. J. Fluorine-NMR competition binding experiments for high-throughput screening of large compound mixtures. *Comb. Chem. High Throughput Screen.* **2002**, *5*, 605–611.

151. Tengel, T.; Fex, T.; Emtenäs, H.; Almqvist, F.; Sethson, I.; Kihlberg, J. Use of ^{19}F NMR spectroscopy to screen chemical libraries for ligands that bind to proteins. *Org. Biomol. Chem.* **2004**, *2*, 725–731.

152. Dalvit, C.; Fagerness, P. E.; Hadden, D. T. A.; Sarver, R. W.; Stockman, B. J. Fluorine-NMR experiments for high-throughput screening: theoretical aspects, practical considerations, and range of applicability. *J. Am. Chem. Soc.* **2003**, *125*, 7696-7703.

153. Araç, D.; Murphy, T.; Rizo, J. Facile detection of protein-protein interactions by one-dimensional NMR spectroscopy. *Biochemistry* **2003**, *42*, 2774–2780.

154. Dalvit, C.; Mongelli, N.; Papeo, G.; Giordano, P.; Veronesi, M.; Moskau, D.; Kümmerle, R. Sensitivity improvement in ^{19}F NMR-based screening experiments: theoretical considerations and experimental applications. *J. Am. Chem. Soc.* **2005**, *127*, 13380–13385.

155. Cheng, Y.-C.; Prusoff, W. H. Relationship between the inhibition constant (KI) and the concentration of inhibitor which causes 50 per cent inhibition (I50) of an enzymatic reaction. *Biochem. Pharmacol.* **1973**, *22*, 3099–3108.

156. Ni, F. Recent developments in transferred NOE methods. *Prog. Nucl. Magn. Reson. Spectrosc.* **1994**, *26*, 517–606.

157. Pellecchia, M. NMR spectroscopy in fragment based drug design. *Top. Med. Chem.* **2009**, *5*, 125–139.

158. Biet, T.; Peters, T. Molecular Recognition of UDP-Gal by β-1,4-Galactosyltransferase T1. *Angew. Chem. Int. Ed.* **2001**, *40*, 4189–4192.

159. Angulo, J.; Rademacher, C.; Biet, T.; Benie, A. J.; Blume, A.; Peters, H.; Palcic, M.; Parra, F.; Peters, T. NMR analysis of carbohydrate-protein interactions. *Methods Enzymol.* **2006**, *416*, 12–30.

160. Angulo, J.; Enríquez-Navas, P. M.; Nieto, P. M. Ligand–receptor binding affinities from saturation transfer difference (STD) NMR spectroscopy: the binding isotherm of STD initial growth rates. *Chem. Eur. J.* **2010**, *16*, 7803–7812.

161. Yan, J.; Kline, A. D.; Mo, H.; Shapiro, M. J.; Zartler, E. R. The effect of relaxation on the epitope mapping by saturation transfer difference NMR. *J. Magn. Reson.* **2003**, *163*, 270–276.

162. Kemper, S.; Patel, M. K.; Errey, J. C.; Davis, B. G.; Jones, J. A.; Claridge, T. D. W. Group epitope mapping considering relaxation of the ligand (GEM-CRL): including longitudinal relaxation rates in the analysis of saturation transfer difference (STD) experiments. *J. Magn. Reson.* **2010**, *203*, 1–10.

163. Jayalakshmi, V.; Rama Krishna, N. Complete relaxation and conformational exchange matrix (CORCEMA) analysis of intermolecular saturation transfer effects in reversibly forming ligand-receptor complexes. *J. Magn. Reson.* **2002**, *155*, 106–118.

164. Ji, Z.; Yao, Z.; Liu, M. Saturation transfer difference nuclear magnetic resonance study on the specific binding of ligand to protein. *Anal. Biochem.* **2009**, *385*, 380–382.

165. Johnson, M. A.; Pinto, B. M. Saturation transfer difference 1D-TOCSY experiments to map the topography of oligosaccharides recognized by a monoclonal antibody directed against the cell-wall polysaccharide of group A *Streptococcus*. *J. Am. Chem. Soc.* **2002**, *124*, 15368–15374.

166. Kramer, M.; Kleinpeter, E. STD-DOSY: a new NMR method to analyze multi-component enzyme/substrate systems. *J. Magn. Reson.* **2010**, *202*, 245–249.

167. Nagaraja, C. S. Heteronuclear saturation transfer difference (HSTD) experiment for detection of ligand binding to proteins. *Chem. Phys. Lett.* **2006**, *420*, 340–346.

168. Räuber, C.; Berger, S. ^{13}C-NMR detection of STD spectra. *Magn. Reson. Chem.* **2010**, *48*, 91–93.

169. Fehér, K.; Groves, P.; Batta, G.; Jiménez-Barbero, J.; Muhle-Goll, C.; Kövér, K. E. Competition saturation transfer difference experiments improved with isotope editing and filtering schemes in NMR-based screening. *J. Am. Chem. Soc.* **2008**, *130*, 17148–17153.

170. Dalvit, C.; Fogliatto, G.; Stewart, A.; Veronesi, M.; Stockman, B. WaterLOGSY as a method for primary NMR screening: Practical aspects and range of applicability. *J. Biomol. NMR* **2001**, *21*, 349–359.

171. Fielding, L.; Rutherford, S.; Fletcher, D. Determination of protein-ligand binding affinity by NMR: observations from serum albumin model systems. *Magn. Reson. Chem.* **2005**, *43*, 463–470.

172. Ludwig, C.; Michiels, P. J. A.; Wu, X.; Kavanagh, K. L.; Pilka, E.; Jansson, A.; Oppermann, U.; Günther, U. L. SALMON: solvent accessibility, ligand binding, and mapping of ligand orientation by NMR spectroscopy. *J. Med. Chem.* **2008**, *51*, 1–3.

173. Ludwig, C.; Michiels, P. J. A.; Lodi, A.; Ride, J.; Bunce, C.; Günther, U. L. Evaluation of solvent accessibility epitopes for different dehydrogenase inhibitors. *ChemMedChem* **2008**, *3*, 1371–1376.

174. Cavanagh, J.; Fairbrother, W. J.; Palmer III, A. G.; Rance, M.; Skelton, N. J. Protein NMR spectroscopy. Principles and practice. Second Edition; Elsevier Academic Press: Burlington, 2007; pp 725–780.

175. Wishart, D. S. Interpreting protein chemical shift data. *Prog. Nucl. Magn. Reson. Spectrosc.* **2011**, *58*, 62–87.

176. Shimada, I.; Ueda, T.; Matsumoto, M.; Sakakura, M.; Osawa, M.; Takeuchi, K.; Nishida, N.; Takahashi, H. Cross-saturation and transferred cross-saturation experiments. *Prog. Nucl. Magn. Spectrosc. Reson.* **2009**, *54*, 123–140.

177. Ohki, S.-y.; Kainosho, M. Stable isotope labeling methods for protein NMR spectroscopy. *Prog. Nucl. Magn. Reson. Spectrosc.* **2008**, *53*, 208–226.

178. Tugarinov, V.; Kay, L. E. Methyl groups as probes of structure and dynamics in NMR studies of high-molecular-weight proteins. *ChemBioChem* **2005**, *6*, 1567–1577.

179. Quinternet, M.; Starck, J. P.; Delsuc, M. A.; Kieffer, B. Unraveling complex small-molecule binding mechanisms by using simple NMR spectroscopy. *Chem. Eur. J.* **2012**, *18*, 3969–3974.

180. Cavanagh, J.; Fairbrother, W. J.; Palmer III, A. G.; Rance, M.; Skelton, N. J. Protein NMR spectroscopy. Principles and practice. Second Edition; Elsevier Academic Press: Burlington, 2007; pp 781–812.

181. Dötsch, V. NMR strategies for protein assignments. In *BioNMR in drug research*; Zerbe, O., Ed.; Wiley-VCH Verlag GmbH & Co. KGaA: Weinheim, 2003; Chapter 4, pp 79–94.

182. Leopold, M. F.; Urbauer, J. L.; Wand, A. J. Resonance assignment strategies for the analysis of NMR spectra of proteins. *Mol. Biotechnol.* **1994**, *2*, 61–93.

183. Wüthrich, K. NMR of proteins and nucleic acids; John Wiley and Sons, Inc.: New York, 1986; pp 130–161.

184. Ikura, M.; Kay, L. E.; Bax, A. A novel approach for sequential assignment of ^{1}H, ^{13}C, and ^{15}N spectra of larger proteins: heteronuclear triple-resonance three-dimensional NMR spectroscopy. Application to calmodulin. *Biochemistry* **1990**, *29*, 4659–4667.

185. Sattler, M.; Schleucher, J.; Griesinger, C. Heteronuclear multidimensional NMR experiments for the structure determination of proteins in solution employing pulsed field gradients. *Prog. Nucl. Magn. Reson. Spectrosc.* **1999**, *34*, 93–158.

186. Kay, L. E.; Gardner, K. H. Solution NMR spectroscopy beyond 25 kDa. *Curr. Opin. Struct. Biol.* **1997**, *7*, 722–731.

187. Flashman, E.; Hoffart, L. M.; Hamed, R. B.; Bollinger Jr, J. M.; Krebs, C.; Schofield, C. J. Evidence for the slow reaction of hypoxia-inducible factor prolyl hydroxylase 2 with oxygen. *FEBS J.* **2010**, *277*, 4089–4099.

188. Hopkinson, R. J.; Hamed, R. B.; Rose, N. R.; Claridge, T. D. W.; Schofield, C. J. Monitoring the activity of 2-oxoglutarate dependent histone demethylases by NMR spectroscopy: direct observation of formaldehyde. *ChemBioChem* **2010**, *11*, 506–510.

189. McNeill, L. A.; Flashman, E.; Buck, M. R. G.; Hewitson, K. S.; Clifton, I. J.; Jeschke, G.; Claridge, T. D. W.; Ehrismann, D.; Oldham, N. J.; Schofield, C. J. Hypoxia-inducible factor prolyl hydroxylase 2 has a high affinity for ferrous iron and 2-oxoglutarate. *Mol. BioSyst.* **2005**, *1*, 321–324.

190. Poppe, L.; Tegley, C. M.; Li, V.; Lewis, J.; Zondlo, J.; Yang, E.; Kurzeja, R. J. M.; Syed, R. Different modes of inhibitor binding to prolyl hydroxylase by combined use of X-ray crystallography and NMR spectroscopy of paramagnetic complexes. *J. Am. Chem. Soc.* **2009**, *131*, 16654–16655.

191. Hardy, A. Structural studies on the hypoxic response. D.Phil Thesis. University of Oxford, July 2008.

192. Hardy, A. P.; Prokes, I.; Kelly, L.; Campbell, I. D.; Schofield, C. J. Asparaginyl β-hydroxylation of proteins containing ankyrin repeat domains influences their stability and function. *J. Mol. Biol.* **2009**, *392*, 994–1006.

193. Kim, D.-H.; Lee, S.-H.; Chi, S.-W.; Nam, K. H.; Han, K.-H. Backbone resonance assignment of a proteolysis-resistant fragment in the oxygen-dependent degradation domain of the hypoxia inducible factor 1α. *Mol. Cells* **2009**, *27*, 493–496.

2. Studies on human γ-butyrobetaine hydroxylase[†]

2.1 Introduction

2.1.1 L-Carnitine

L-Carnitine ((3*R*)-3-hydroxy-4-(trimethylammonio)butanoate, Figure 2-1) is essential for energy metabolism,[1–3] being present in many plants, micro-organisms and animals.[4–7] In humans, its most well-established role is the transportation of long-chain fatty acids from the cytoplasmic matrix into the mitochondrial matrix.[8–10] It is also involved in the storage of fatty acids,[11–13] the transport of β-oxidation products,[14,15] the excretion of toxic products[16] and the modulation of acyl-coenzyme-A/coenzyme-A homeostasis.[11,15] All known functions of L-carnitine involve the reversible esterification of the 3-hydroxyl group.[17,18]

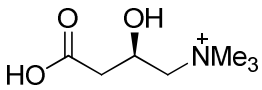

Figure 2-1 Structure of L-carnitine.

In humans, L-carnitine is obtained from both the diet (~75% total body L-carnitine) and by endogenous biosynthesis (~25%).[3,5,19] L-Carnitine is a popular dietary supplement because it is proposed to promote fatty acid metabolism,[20–22] and is produced commercially either by synthesis[23] or by fermentation.[24,25]

[†] *The work in this chapter was conducted in collaboration with Dr Grazyna T. Kochan, Dr Luc Henry, Anna M. Rydzik, Dr James S. O. McCullagh, Nikita D. Loik, Colin Sparrow and Robin Procter.*

G.T.K. produced and purified recombinant human BBOX, L.H. synthesised various GBB and THP analogues, trimethylaminoacetone, ^{13}C-labelled THP and AMBA. A.M.R. synthesised ^{19}F-labelled GBB analogues and the protected fluoresceine probe, initiated the development of the fluoride detection assay and performed experiment for the assays. J.S.O.M. and N.D.L. provided technical support for MS analysis. C.S. and R.P. performed accurate mass measurements.

Parts of the work from this chapter have been published as described:

1. Leung, I. K. H.; Krojer, T. J.; Kochan, G. T.; Henry, L.; von Delft, F.; Claridge, T. D. W.; Oppermann, U.; McDonough, M. A.; Schofield, C. J. Structural and mechanistic studies on γ-butyrobetaine hydroxylase. Chem. Biol. 2010, 17, 1316–1324.

2. Chowdhury, R.; Yeoh, K. K.; Tian, Y.-M.; Hillringhaus, L. Bagg, E. A.; Rose, N. R.; Leung, I. K. H.; Li, X. S.; Woon, E. C. Y.; Yang, M.; McDonough, M. A.; King, O. N.; Clifton, I. J.; Klose, R. J.; Claridge, T. D. W.; Ratcliffe, P. J.; Schofield, C. J.; Kawamura, A. The oncometabolite 2-hydroxyglutarate inhibits histone lysine demethylases. EMBO Rep. 2011, 12, 463–469.

3. Rydzik, A. M.; Leung, I. K. H.; Kochan, G. T.; Thalhammer, A.; Oppermann, U.; Claridge, T. D. W.; Schofield, C. J. Development and application of a fluoride-detection-based fluorescence assay for γ-butyrobetaine hydroxylase. ChemBioChem 2012, 13, 1559–1563.

4. Henry, L.; Leung, I. K. H.; Claridge, T. D. W.; Schofield, C. J. γ-Butyrobetaine hydroxylase catalyses a Stevens type rearrangement. Bioorg. Med. Chem. Lett. 2012, 22, 4975–4978.

5. Rose, N. R.; Woon, E. C.; Walport, L. J.; Chowdhury, R.; Li, X. S.; King, O. N. F.; Lejeune, C.; Tumber, A.; Ng, S. S.; Krojer, T.; Chan, M. C.; Rydzik, A. M.; Hopkinson, R. J.; Che, K. H.; Daniel, M.; Strain-Damerell, C.; Gileadi, C.; Kochan, G.; Leung, I. K. H.; Dunford, J.; Yeoh, K. K.; Ratcliffe, P. J.; Burgess-Brown, N.; von Delft, F.; Muller-Knapp, S.; Marsden, B.; Brennan, P. E.; McDonough, M. A.; Oppermann, U.; Klose, R. J.; Schofield, C. J.; Kawamura, A. The plant growth regulator daminozide is a selective inhibitor of the human KDM2/7 histone demethylases. J. Med. Chem. 2012, 55, 6639–6643.

2.1.2 L-Carnitine biosynthesis

A functional and highly conserved L-carnitine biosynthesis pathway occurs in many eukaryotes, such as plants and mammals, and some prokaryotes such as bacteria.[26–29] The starting point for the biosynthesis is N^{ε}-trimethyllysine.[30] Four enzymes are believed to be involved in the overall pathway (Figure 2-2).[30]

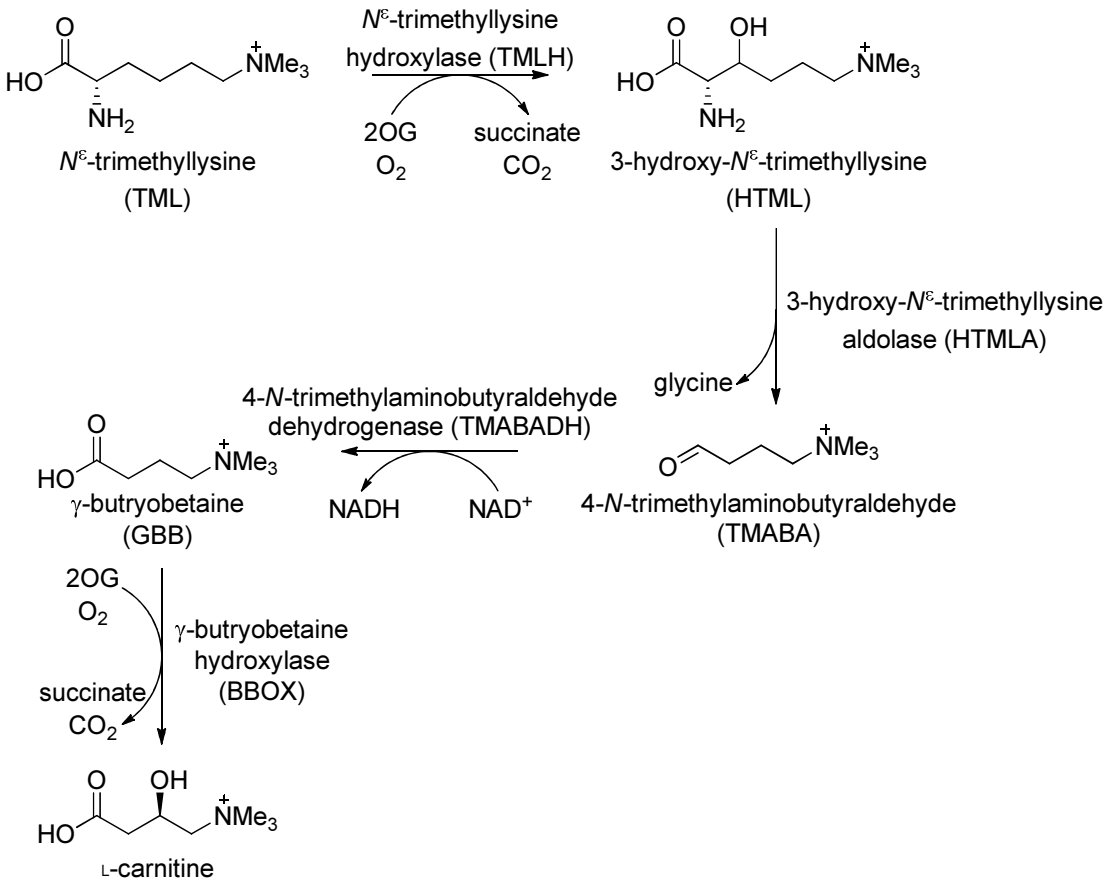

Figure 2-2 L-Carnitine biosynthesis pathway.

Firstly, N^{ε}-trimethyllysine hydroxylase (TMLH), which is a 2OG oxygenase,[31] catalyses the hydroxylation reaction of N^{ε}-trimethyllysine to 3-hydroxy-N^{ε}-trimethyllysine (HTML). It is speculated that N^{ε}-trimethyllysine originates from lysosomal or proteasomal degradation of methylated proteins including histones.[32–34] An enzymatic pathway involving N^{ε}-lysine methyltransferase has also been identified in the fungus *Neurospora crassa*.[35,36] There is also some evidence to suggest a similar enzymatic pathway is functional in humans.[37,38]

HTML aldolase (HTMLA), the second enzyme of the L-carnitine biosynthesis pathway,[30] catalyses the cleavage of HTML into 4-*N*-trimethylaminobutyraldehyde (TMABA) and glycine. A mammalian gene encoding HTMLA has so far not been

identified, although a recent study in yeast *Candida albicans* suggests that HTMLA may belong to the L-threonine aldolase family.[39] However, an *in vitro* study on serine hydroxymethyltransferase (SHMT) purified from rabbit liver has also demonstrated HTMLA activity.[40] There is also speculation that SHMT and L-threonine aldolase may be closely related.[41,42]

The third enzyme involved in L-carnitine biosynthesis is TMABA dehydrogenase (TMABADH),[43–45] which catalyses the dehydrogenation of TMADA into 4-*N*-trimethylaminobutyrate (γ-butyrobetaine or GBB). TMABADH has been identified and purified from rat liver[44] and the bacterium *Pseudomonas*.[45] There is considerable sequence similarity between rat TMABADH and human aldehyde dehydrogenase 9 (ALDH9; 92% positional identity).[43,44,46] It has also been shown that ALDH9 catalyses the dehydrogenation of γ-aminobutyraldehyde, a non-methylated analogue of TMADA, into γ-aminobutyric acid.[47,48]

The final step of L-carnitine biosynthesis is catalysed by γ-butryobetaine hydroxylase (BBOX), which is a 2OG oxygenase[49–53] that catalyses the stereospecific hydroxylation of GBB[54] to give L-carnitine (Figure 2-3).[55] BBOX has been purified from many sources, including the bacterium *Pseudomonas*,[26,56] rat liver,[57–59] calf liver[60], guinea pig liver,[61] and human kidney.[51]

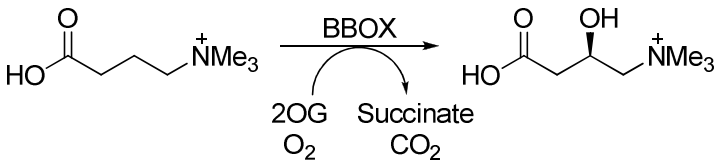

Figure 2-3 BBOX catalyses the stereospecific hydroxylation reaction of γ-butyrobetaine to L-carnitine.

2.1.3 Inhibition of L-carnitine biosynthesis

BBOX is an inhibition target for 3-(2,2,2-trimethylhydraziniumyl)propionate (THP, also known as Mildronate, MET-88, Meldonium or Quaterine; Figure 2-4).[62] THP is a clinically-used drug for the treatment of angina and myocardial infarction.[63–65] Some studies suggest that THP may be beneficial for the treatment of neurological conditions,[66,67] diabetes,[68] seizures and alcohol intoxication.[69]

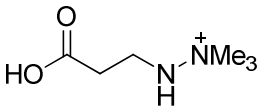

Figure 2-4 Structure of the BBOX inhibitor 3-(2,2,2-trimethylhydraziniumyl)propionate (THP).

The principal mechanism of action of THP is proposed to involve the inhibition of L-carnitine biosynthesis[70] and L-carnitine mediated transport into mitochondria,[71–73] thereby increasing glucose uptake and utilisation,[74] which leads to the reduction of oxidising species associated with fatty acid metabolism.[75]

Initially, THP was thought to be a non-competitive and non-reactive inhibitor of BBOX based upon kinetics analyses.[62] However, further kinetic studies performed by a different group suggested that THP is actually a competitive inhibitor of BBOX.[76] In the same study, the authors also suggested that THP may act as a substrate and speculated the formation of 3-hydroxy-THP, although 3-hydroxy-THP was never detected experimentally.[76]

2.1.4 Objectives

By applying NMR spectroscopy to conduct mechanistic and inhibition studies on recombinant human BBOX (prepared by Dr Grazyna T. Kochan), the objectives of the work described in this Chapter were to gain a better understanding of BBOX catalysis, in order to provide the basis for future development of improved inhibitors. A further objective is to develop alternative *in vitro* assays to monitor BBOX activity and to improve the throughput of inhibitor screening and quantification.

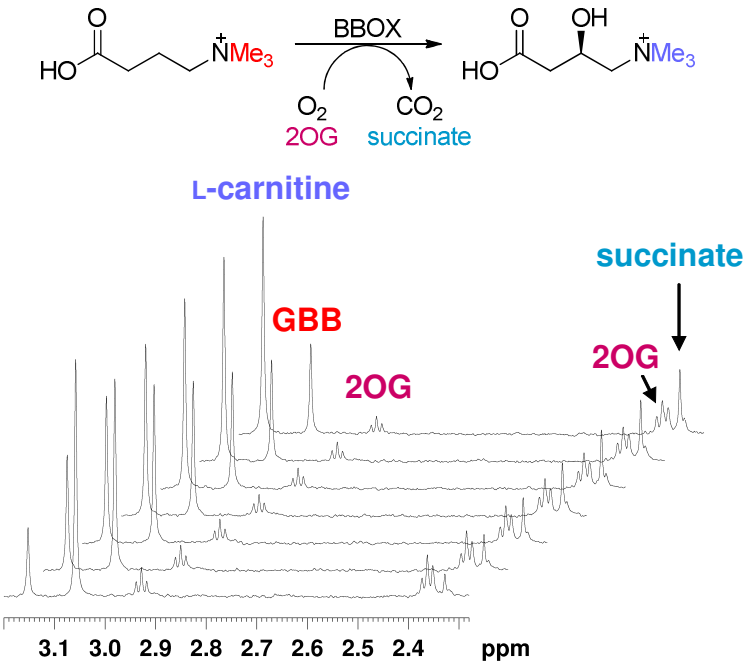

Figure 2-5 BBOX activity monitored by ^{1}H NMR. Spectra are shown in 4-minute intervals. The assay mixture contained 25 nM BBOX, 40 µM Fe(II), 40 µM GBB, 80 µM 2OG, 500 µM ascorbate, 80 mM KCl and 50 mM Tris-D11 (pH 7.5).

2.2 Characterisation of human BBOX

2.2.1 Characterisation of BBOX activity

A ^{1}H NMR-based assay was developed to measure BBOX activity by monitoring the *N*-methyl resonances of GBB and L-carnitine (Figure 2-5).

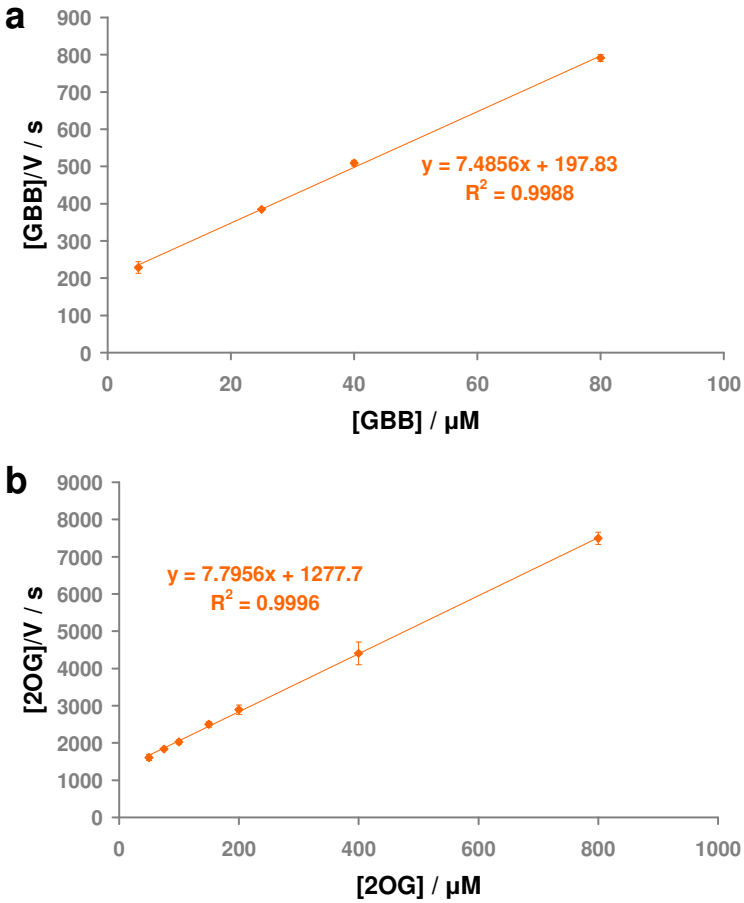

Figure 2-6 Hanes plot for the determination of BBOX kinetics parameters for GBB and 2OG: (a) Assay mixture contained 25 nM BBOX, 40 µM Fe(II), 400 µM 2OG, 500 µM ascorbate, 80 mM KCl and 50 mM Tris-D11 (pH 7.5). Percentage turnover is measured two minutes after mixing; (b) Assay mixture contained 25 nM BBOX, 40 µM Fe(II), 150 µM GBB, 500 µM ascorbate, 80 mM KCl and 50 mM Tris-D11 (pH 7.5). Percentage turnover is measured three minutes after mixing. The error bars indicate standard errors from at least three separate measurements. See also Table 2-1.

The results revealed that human BBOX is highly active (Figure 2-6 and Table 2-1). The catalytic activity was dependent on Fe(II) (Figure 2-7), and GBB hydroxylation was tightly coupled to 2OG oxidation (Figure 2-8). Substrate inhibition was observed at high GBB concentration (Figure 2-9), consistent with previous results obtained with *Pseudomonas* and rat liver BBOX.[56,59,77] Potassium ions were required for optimal BBOX activity in the experiments (Figure 2-10), as observed previously with rat liver BBOX.[77] The exact role of potassium ions is not known but previous studies

speculated that it may facilitate substrate binding.[77] Similar to other 2OG oxygenases, human BBOX activity was stimulated by reducing agents including ascorbate and glutathione (Figure 2-11), consistent with animal models reported previously.[61,78–80]

Substrate	Reaction time / Minutes	K_M / µM	V_{max} / µM s^{-1}	k_{cat} / s^{-1}	k_{cat}/K_M / M^{-1} s^{-1}
2OG	3	164	0.13	5.13	31×10^3
GBB	2	26.4	0.13	5.34	202×10^3

Table 2-1 Kinetics parameters obtained from measuring turnover for BBOX with 2OG and GBB as substrates. See also Figure 2-6.

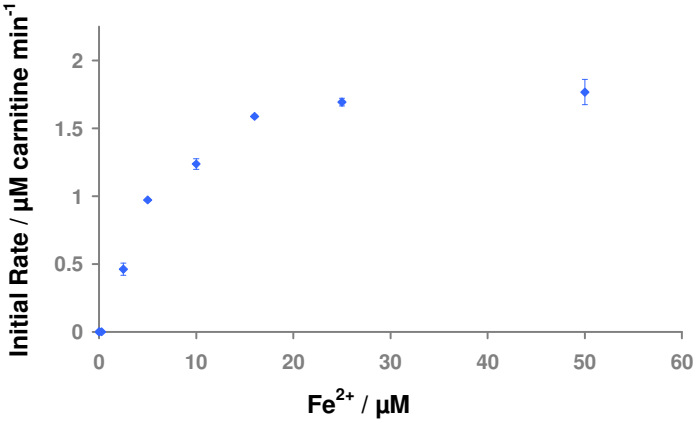

Figure 2-7 The effect of Fe(II) concentration on BBOX activity. At least 25 µM Fe(II) was required for optimal BBOX activity. The mixture contained 12.5 nM BBOX, 50 µM GBB, 1.5 mM 2OG, 5 mM ascorbate, 80 mM KCl and 50 mM Tris-D11 (pH 7.5). The error bars indicate standard errors from at least three separate measurements.

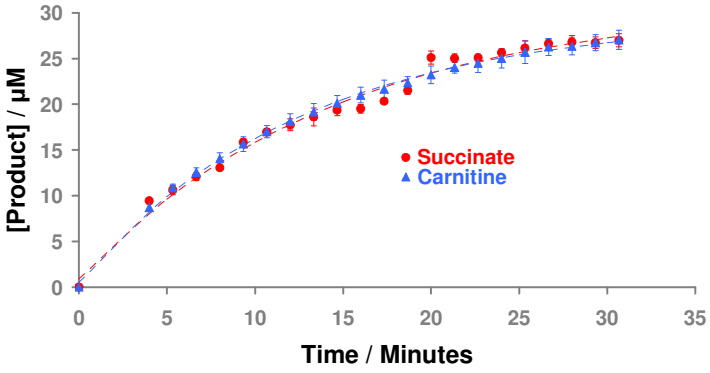

Figure 2-8 There is high coupling efficiency between 2OG oxidation and GBB hydroxylation, as monitored by ^{1}H NMR time course. The mixture included 25 nM BBOX, 40 µM Fe(II), 40 µM GBB, 80 µM 2OG, 500 µM ascorbate, 80 mM KCl and 50 mM Tris-D11 (pH 7.5). The error bars indicate standard errors from at least three separate measurements. Dashed lines are included to aid visualisation.

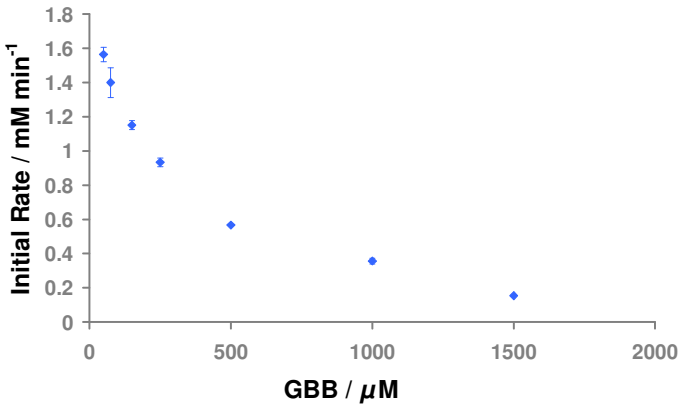

Figure 2-9 BBOX is subject to substrate inhibition at high GBB concentration. The mixture contained 12.5 nM BBOX, 50 μM Fe(II), 1.5 mM 2OG, 5 mM ascorbate, 80 mM KCl and 50 mM Tris-D11 (pH 7.5). The error bars indicate standard errors from at least three separate measurements.

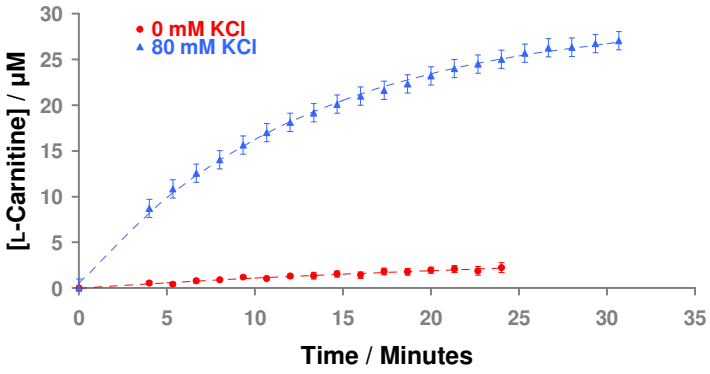

Figure 2-10 Potassium ions are required for BBOX activity: with 80 mM KCl activity is 1.77 ± 0.10 μM min^{-1}; with no KCl activity is 0.10 ± 0.02 μM min^{-1}. The mixture contained 25 nM BBOX, 40 μM Fe(II), 40 μM GBB, 80 μM 2OG, 500 μM ascorbate and 50 mM Tris-D11 (pH 7.5). The error bars indicate standard errors from at least three separate measurements. Dashed lines are included to aid visualisation.

2.2.2 Substrate analogue analyses

To date, little information has been reported on the substrate selectivity of human BBOX. To investigate the selectivity of recombinant human BBOX, a series of GBB analogues (synthesised by Dr Luc Henry) were screened as potential substrates (Figure 2-12).

Amongst all the tested compounds, no activity was observed with *N*,*N*,*N*-trimethylethanaminium, *N*,*N*,*N*-trimethylbutan-1-aminum and *N*,*N*,*N*-trimethylhexan-1-aminum ions, indicating the carboxylic group of GBB is required for activity. However the requirement for the trimethylamino group was less stringent. BBOX is able to accept substrates with the trimethylamino group substituted by a

dimethylamino group (4-(dimethylamino)butanoic acid, Table 2-2), but not with an isopropyl group (5-methylhexanoic acid). X-ray crystallographic analyses suggest the trimethylamino group is bound in an aromatic cage in the protein active site (PDB id: 3O2G). The NMR studies, however, imply the positive charge on the amino group also contributes to the binding. GBB analogues with one fewer or one extra carbon along the main carbon chain (*i.e.* 3-(trimethylammonio)propanoate and 5-(trimethylammonio)pentanoate respectively) were also hydroxylated (Table 2-2). However analogues with two fewer or two extra carbons (*i.e.* (trimethylammonio)acetate and 6-(trimethylammonio)hexanoate respectively) were not hydroxylated. Despite the relative sequence similarity between the BBOX and TMLH active sites,[81] which implies the folds and the actives site of the two enzymes are similar, N^{ε}-trimethyllysine was found not to be a substrate.

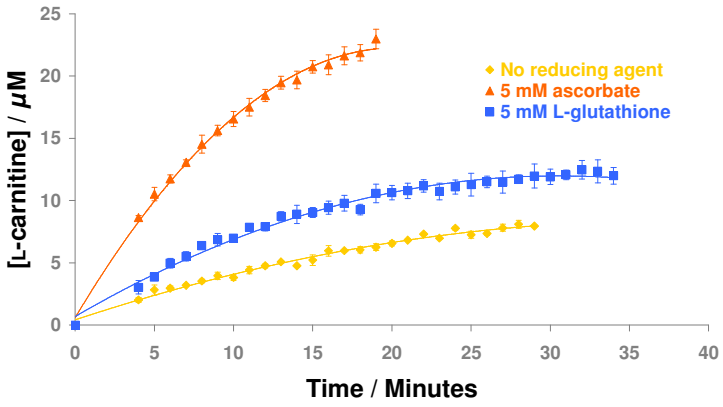

Figure 2-11 Reducing agents stimulate BBOX activity: with 5 mM ascorbate (1.77 ± 0.10 μM min^{-1}); with 5 mM glutathione (0.73 ± 0.02 μM min^{-1}); with no ascorbate (0.39 ± 0.01 μM min^{-1}). Reaction contained 12.5 nM BBOX, 50 μM Fe(II), 1.5 mM 2OG, 5 mM ascorbate, 80 mM KCl and 50 mM Tris-D11 (pH 7.5). The error bars indicate standard errors from at least three separate measurements. Dashed lines are included to aid visualisation.

Surprisingly L-carnitine, the natural product of BBOX, and D-carnitine, the unnatural enantiomer, were also found to be processed by BBOX. 3-Dehydrocarnitine was formed, which subsequently and spontaneously decarboxylated in the mixture to give trimethylaminoacetone (Figure 2-13 and Figure 2-14). The identity of trimethylaminoacetone was further confirmed by comparison with a synthetic standard (by Dr Luc Henry). Interestingly, D-carnitine was found to be a better substrate than L-carnitine (Table 2-3). The observation that L-carnitine can act as a substrate (albeit a poor one) implies that it could adopt a catalytically productive arrangement in the BBOX active site, other than that observed in the crystal structure of BBOX with GBB (PDB id: 3O2G).

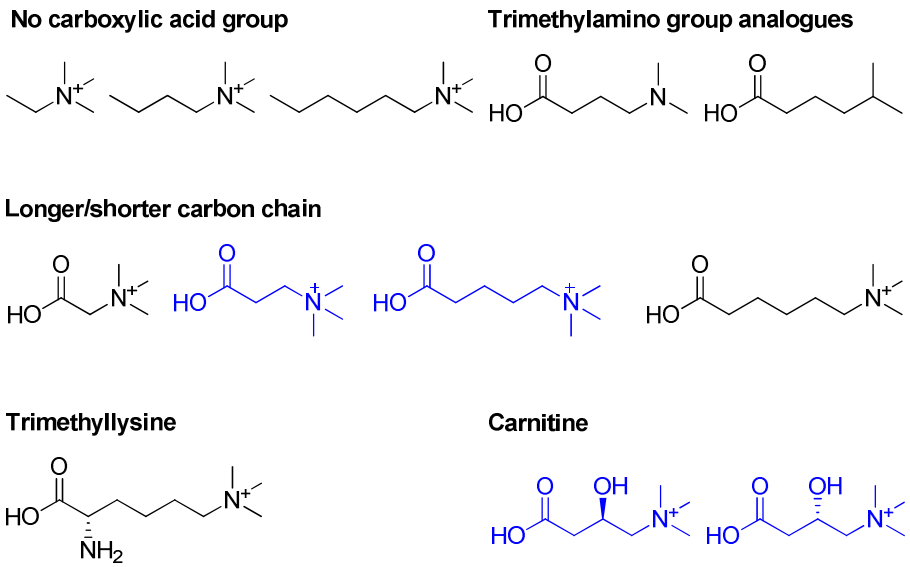

Figure 2-12 Compounds tested for BBOX activity. Compounds that can act as alternative BBOX substrates are highlighted in blue.

Substrate	Product(s)	Rate / μM product min^{-1}
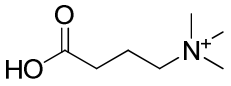	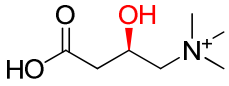	1.9 ± 0.05
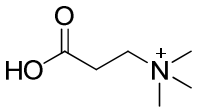	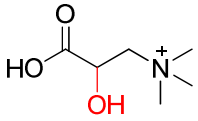	0.41 ± 0.05
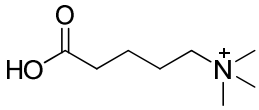	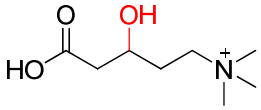	0.075 ± 0.003
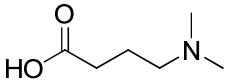	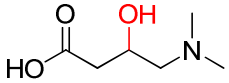	0.30 ± 0.01

Table 2-2 GBB analogues that can act as BBOX substrates. The assay mixture contained 12.5 nM BBOX, 50 μM Fe(II), 50 μM substrate, 1.5 mM 2OG, 5 mM ascorbate, 80 mM KCl and 50 mM Tris-D11 (pH 7.5). The errors indicate standard errors from at least three separate measurements. Products were identified by ^{1}H NMR and mass spectrometry analyses. Analytical data for the product of the reaction with 3-(trimethylammonio)propanoate (m/z = 148.0987; ^{1}H NMR (700 MHz, 100% D_2O, pH 7.5) δ(ppm) 3.65 (C-1, m), 4.47 (C-4, m), 3.17 (NMe_3, s); ^{13}C NMR (176 MHz) δ(ppm) 69.6 (C-1), 68.3 (C-2), 54.0 (NMe_3)). Analytical data for the product of the reaction with 5-(trimethylammonio)pentanoate (m/z = 176.1287; ^{1}H NMR (700 MHz, 100% D_2O, pH 7.5) δ(ppm) 3.41 (C-1, m), 1.92 (C-2, m), 3.99 (C-3, m), 2.38 (C-4, m), 3.07 (NMe_3, s). Analytical data for the product of the reaction with 4-(dimethylamino)butanoic acid: (m/z = 148.1; ^{1}H NMR (700 MHz, 100% D_2O, pH 7.5) δ(ppm) 2.37 (C-1, d), 4.29 (C-2, m), 3.14 (C-3, ddd), 2.87 (NMe_3, s); ^{13}C NMR (176 MHz) δ(ppm) 42.1 (C-1), 63.2 (C-2), 61.7 (C-3), 44.6 (NMe_3)).

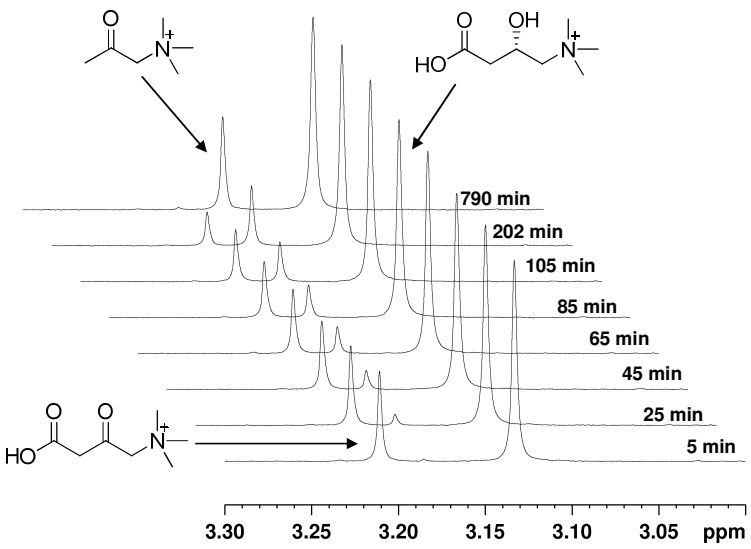

Figure 2-13 NMR analysis of the reaction of D-carnitine with BBOX. L-carnitine was found to react in a similar manner but at a much slower rate. The mixture included 1 μM BBOX, 25 μM Fe(II), 1 mM D-carnitine, 1.5 mM 2OG, 5 mM ascorbate, 80 mM KCl and 50 mM Tris-D11 (pH 7.5) in 95% H_2O and 5% D_2O. Analytical data for 3-dehydrocarnitine: m/z = 160.1; ^{1}H NMR (700 MHz, 95% H_2O/5% D_2O, pH 7.5) δ(ppm) 4.50 (C-2, s), 3.38 (C-4, s), 3.21 (NMe_3, s). Analytical data for trimethylaminoacetone: m/z = 116.1069; ^{1}H NMR δ(ppm) 4.44 (C-1, s), 2.15 (C-3, s), 3.19 (NMe_3, s); ^{13}C NMR (176 MHz) δ(ppm) 69.4 (C-1), 28.0 (C-3), 201.8 (C=O), 53.6 (NMe_3). The transient species 3-dehydrocarnitine is observed by mass spectrometry and ^{1}H NMR but does not stay in solution long enough for ^{1}H-^{13}C HSQC and ^{1}H-^{13}C HMBC analysis.

Substrate	Product	Assay protein concentration / nM	Rate / μM product min^{-1}
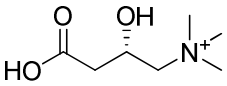	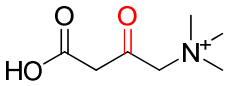	12.5	0.33 ± 0.03
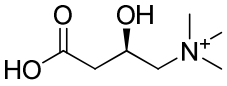	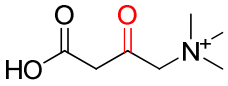	500	0.76 ± 0.03

Table 2-3 D-carnitine is a better substrate for BBOX than L-carnitine. The mixture contained BBOX at the concentration as shown in the table, 50 μM Fe(II), 50 μM substrate, 1.5 mM 2OG, 5 mM ascorbate, 80 mM KCl and 50 mM Tris-D11 (pH 7.5). The errors indicate standard errors from at least three separate measurements. A high concentration of enzyme was used for the L-carnitine reaction, as no measurable turnover was observed for L-carnitine when 12.5 nM enzyme was used.

Although trimethylaminoacetone was not found to be a BBOX inhibitor, from a biological perspective these observations are of interest because they may explain the results from a previous study that 2OG turnover increased (relative to uncoupled turnover) when L-, D-, or racemic carnitine was reacted with purified *Pseudomonas* γ-butyrobetaine hydroxylase.[82] This work also, at least in part, may rationalise the results from another study using a rat model, in which an increased level of trimethylaminoacetone was observed as a metabolite when the rats were fed with either racemic or D-carnitine.[2,83]

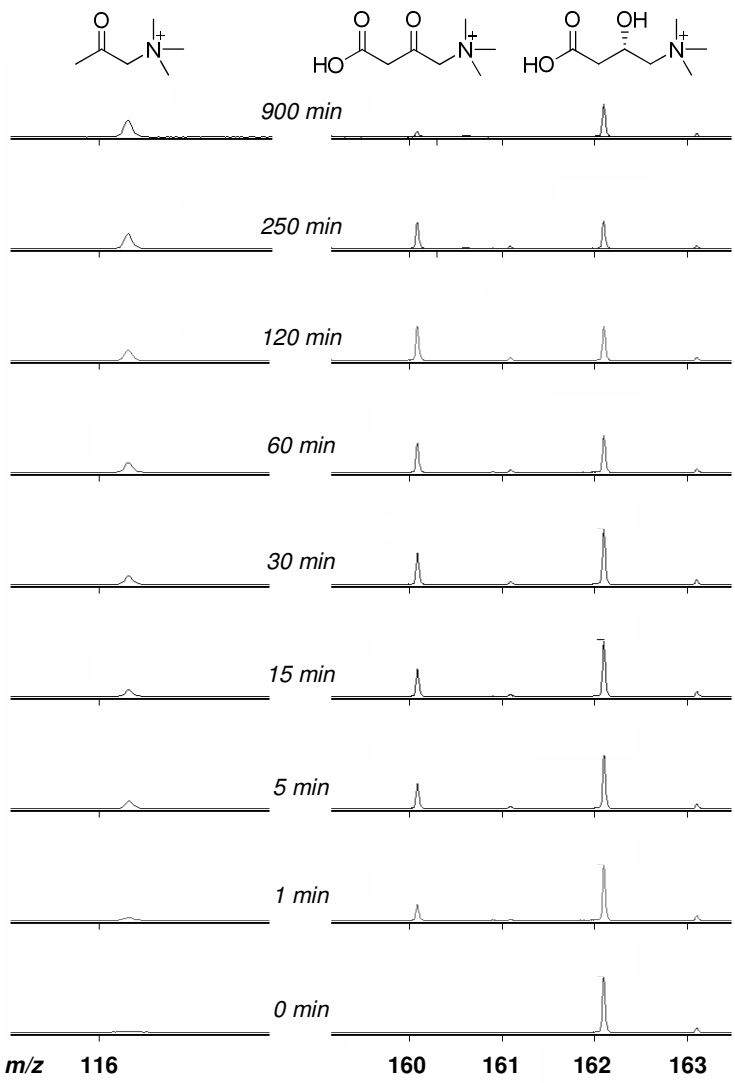

Figure 2-14 Mass spectrometric analysis of the reaction of D-carnitine with BBOX. 3-Dehydrocarnitine was initially formed from D-carnitine, which was then spontaneously decarboxylated to form trimethylaminoacetone. The mixture contained 1 μM BBOX, 25 μM Fe(II), 1 mM D-carnitine, 1.5 mM 2OG, 5 mM ascorbate, 80 mM KCl and 50 mM Tris (pH 7.5). The reaction was quenched by addition of 80% MeCN.

2.3 Studies on the BBOX inhibitor THP

2.3.1 THP is a substrate for BBOX forming multiple products

3-(2,2,2-trimethylhydraziniumyl)propionate (THP) is a clinically-used inhibitor for human BBOX.[62] An IC_{50} value of 66 μM was obtained for THP by NMR assay (Figure 2-15), a value which is comparable to values obtained from previous studies on recombinant human BBOX (62 μM)[84] and enzymes purified from rat liver (13 μM).[59]

^{1}H NMR studies revealed THP is a substrate of human BBOX with the same cofactor requirement as GBB. Initial analyses indicated the formation of multiple products, which were not observed with GBB or other GBB analogues

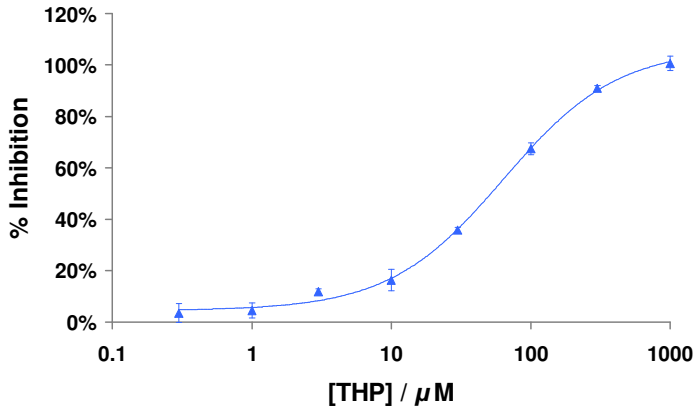

Figure 2-15 THP inhibits BBOX activity (IC_{50} = 66.1 ± 6.2 μM). The mixture included 25 nM BBOX, 40 μM Fe(II), 40 μM 2OG, 40 μM GBB, 500 μM ascorbate, 80 mM KCl and 50 mM Tris-D11 (pH 7.5). Percentage turnover of GBB to L-carnitine is measured 13 minutes after mixing. Percentage inhibition is defined as percentage turnover of GBB to L-carnitine when inhibitor is present divided by the percentage turnover of GBB to L-carnitine when no inhibitor is present. The error bars indicate standard errors from at least three separate measurements.

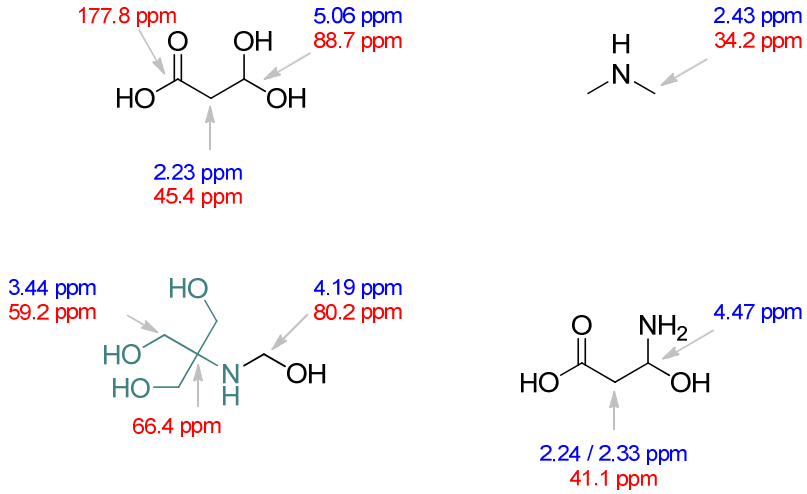

Figure 2-16 Malonic acid semialdehyde, dimethylamine and formaldehyde (observed as a Tris adduct, dark grey) were identified from the THP-BBOX Assay mixture. ^{1}H chemical shifts are shown in blue and ^{13}C chemical shifts are in red. Spectra are recorded at 700 MHz buffered in Tris/Tris-D11 (pH 7.5) in 95% H_2O and 5% D_2O at 280 K.

Using a combination of 1D-TOCSY, COSY, ^{1}H-^{13}C HSQC and ^{1}H-^{13}C HMBC experiments, several products were identified including the hydrated form of malonic acid semialdehyde (which decarboxylates to give acetaldehyde), dimethylamine and formaldehyde (observed as a Tris-D11 buffer adduct) (Figure 2-16). The identities of dimethylamine and formaldehyde were confirmed using pure standards. The ^{13}C shifts of malonic acid semialdehyde were compared with the deprotected product of 3,3-

dimethoxypropanoic acid in acid in solution. 3-amino-3-hydroxypropanoic acid was tentatively assigned (Figure 2-16), although it is too unstable to be characterised fully. NMR analyses also indicated the formation of a rearrangement product, which was assigned as 3-amino-4-(methylamino)butanoic acid (AMBA, Figure 2-17, see below) and was observed as a formaldehyde adduct (Figure 2-18; see also Sections 2.3.2 and 2.3.3).

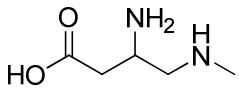

Figure 2-17 Structure of 3-amino-4-(methylamino)butanoic acid (AMBA).

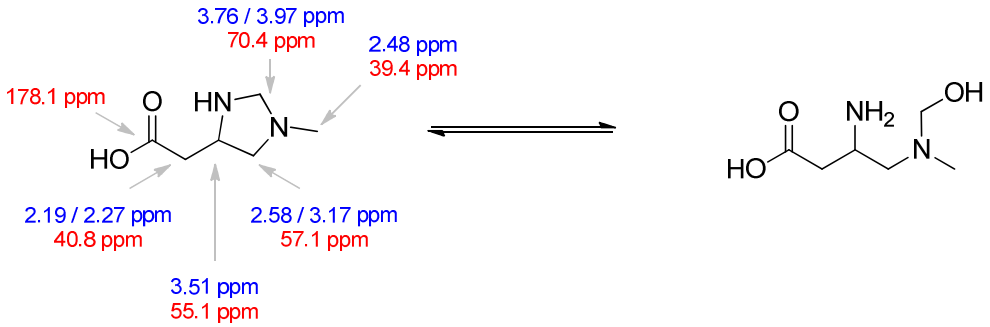

Figure 2-18 Proposed structure of the THP derived rearrangement product that was observed as AMBA-formaldehyde adduct. ^{1}H chemical shifts are shown in blue and ^{13}C chemical shifts are in red. Spectra are recorded at 700 MHz buffered in Tris/Tris-D11 (pH 7.5) in 95% H_2O and 5% D_2O at 280 K. At pH 7.5, the ^{1}H resonances of C-4 protons and -NCH_2OH protons are non-equivalent and broad, indicating dynamics between the ring opened and closed forms.

^{1}H-^{13}C HMBC showed that the rearrangement product (AMBA) has a terminal carboxylic group. 1D-TOCSY and COSY experiments suggest that there are four carbon atoms along the carbon backbone (*i.e.* an additional carbon-carbon bond when compared to THP, Figure 2-19 and Figure 2-20). Multiplicity-edited ^{1}H-^{13}C HSQC showed that C-3 is likely to be connected to a nitrogen atom (δ^{13}C = 55.1 ppm), and the ^{13}C chemical shift of C-4 (δ^{13}C = 57.1 ppm) indicated it is likely to be connected to another nitrogen atom. The ^{1}H resonances of the two protons on C-4 were non-equivalent and broad, suggesting exchange dynamics.

Two ^{1}H-^{13}C HMBC correlations can be observed from an unassigned methyl resonance across the nitrogen atom to C-4 and to an unassigned CH_2 (*i.e.* C-4 is connected to a substituted methylamine group, Figure 2-21). The ^{13}C chemical shift of the unassigned CH_2 (δ^{13}C = 70.4 ppm) suggested it was connected with two heteroatoms, possibly nitrogen and oxygen, or two nitrogens. The CH_2 ^{1}H resonances in the spectrum were broad and diastereotopic, suggesting that the aminal/hemiaminal

on the methylamine group was likely dynamic (between the linear and the cyclic form; Figure 2-18). No HMBC correlations were observed from the CH_2 owing to its broad ^1H resonances.

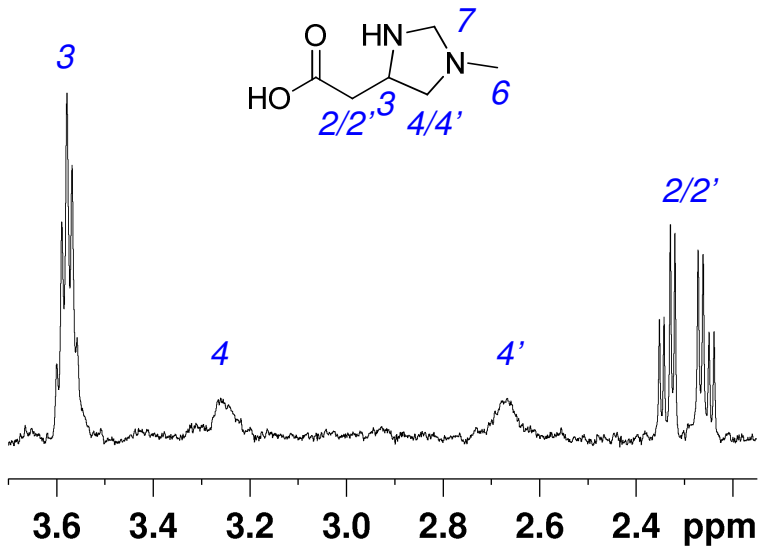

Figure 2-19 1D-TOCSY confirming the four carbon chain of the AMBA-formaldehyde adduct. Selective irradiation is applied at 3.58 ppm. Spectra were recorded at 700 MHz buffered in Tris/Tris-D11 (pH 7.5) in 95% H_2O and 5% D_2O at 280 K.

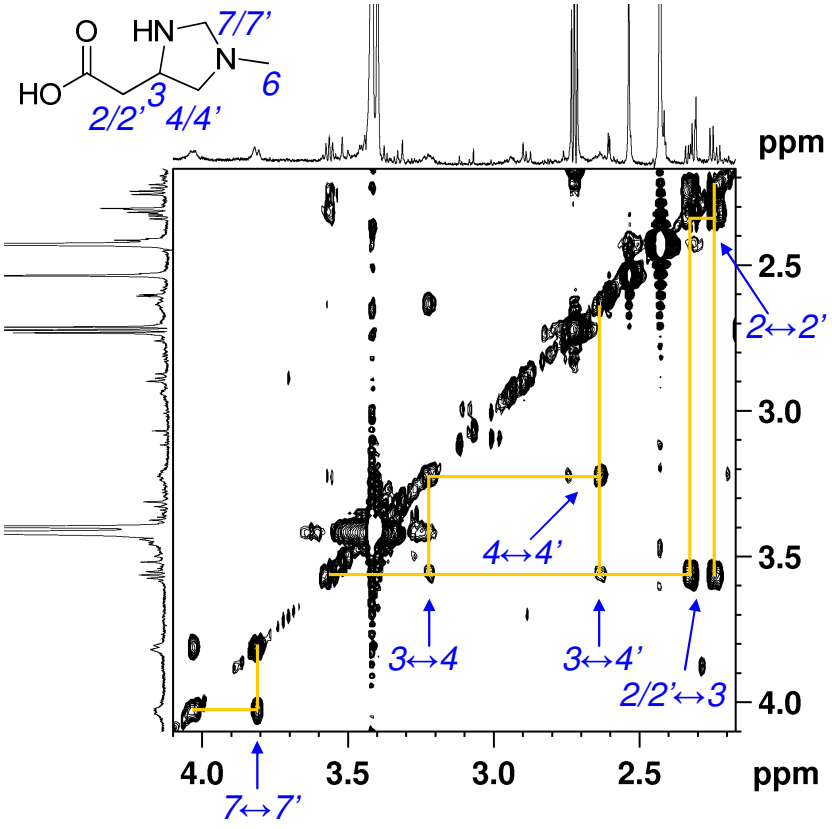

Figure 2-20 COSY confirming the four carbon chain of the AMBA-formaldehyde adduct. Spectra were recorded at 700 MHz buffered in Tris/Tris-D11 (pH 7.5) in 95% H_2O and 5% D_2O at 280 K.

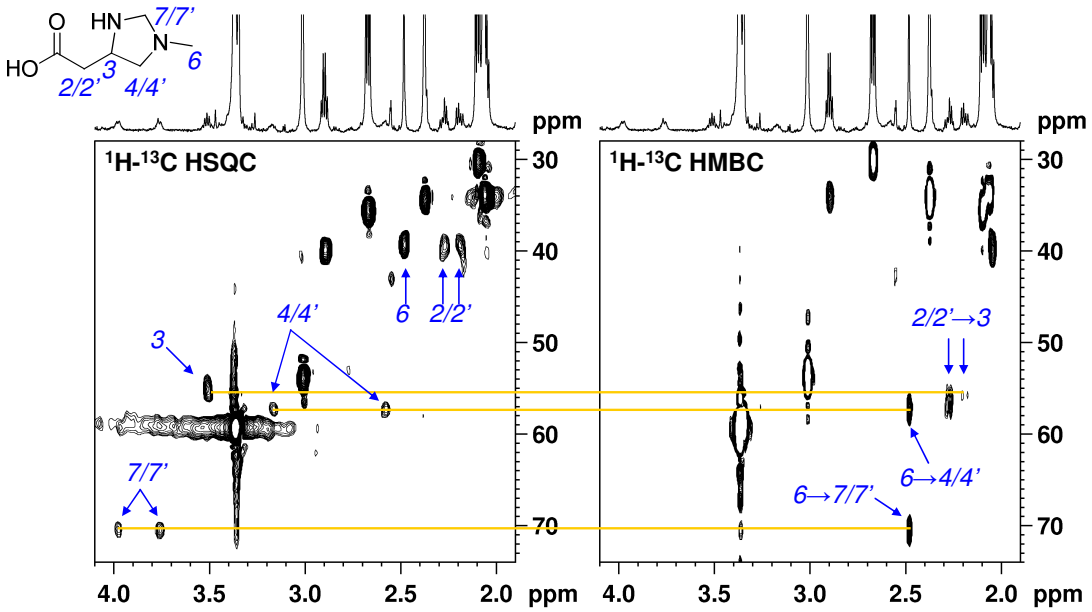

Figure 2-21 ^{1}H-^{13}C HMBC and ^{1}H-^{13}C HSQC correlations of the AMBA-formaldehyde adduct. The HMBC correction between *N*-methyl (6) and the hemiaminal/aminal CH_2 (7/7′) suggested the methylamine moiety of AMBA is substituted. No HMBC correlations between 3 and 7/7′, and 4/4′ and 7/7′ were observed owing to the broad resonances. Spectra were recorded at 700 MHz buffered in Tris/Tris-D11 (pH 7.5) in 95% H_2O and 5% D_2O at 275.5 K.

2.3.2 Further characterisation of THP rearrangement product

In order to confirm the identity of the THP rearrangement product was indeed AMBA, and to probe the proposed equilibrium between the aminal and hemiaminal forms of the AMBA-formaldehyde adduct, synthetic AMBA was prepared (by Dr Luc Henry) as a standard for NMR analyses.

A near stoichiometric amount of formaldehyde was added to AMBA to generate the AMBA-formaldehyde adduct. When comparing the NMR spectra of free AMBA and the AMBA-formaldehyde adduct, the most striking differences are the ^{13}C shifts of C-3 ($\delta^{13}C_{AMBA}$ = 46.1 ppm and $\delta^{13}C_{AMBA\text{-formaldehyde}}$ = 55.1 ppm) and *N*-methyl ($\delta^{13}C_{AMBA}$ = 33.3 ppm and $\delta^{13}C_{AMBA\text{-formaldehyde}}$ = 39.4 ppm), which differ by ~9 ppm and ~6 ppm respectively. This observation suggests both nitrogens on the AMBA-formaldehyde adduct are likely substituted (Figure 2-22). At pH 7.5, the ^{1}H and ^{13}C chemical shifts and correlations were identical to those observed in the BBOX Assay mixture, thus confirming the initial assignment (Figure 2-22, Figure 2-23 and Figure 2-24). However, no HMBC correlation can be observed from C-3 to the aminal/hemiaminal CH_2 owing to the broad resonances, as predicted for a cyclic structure.

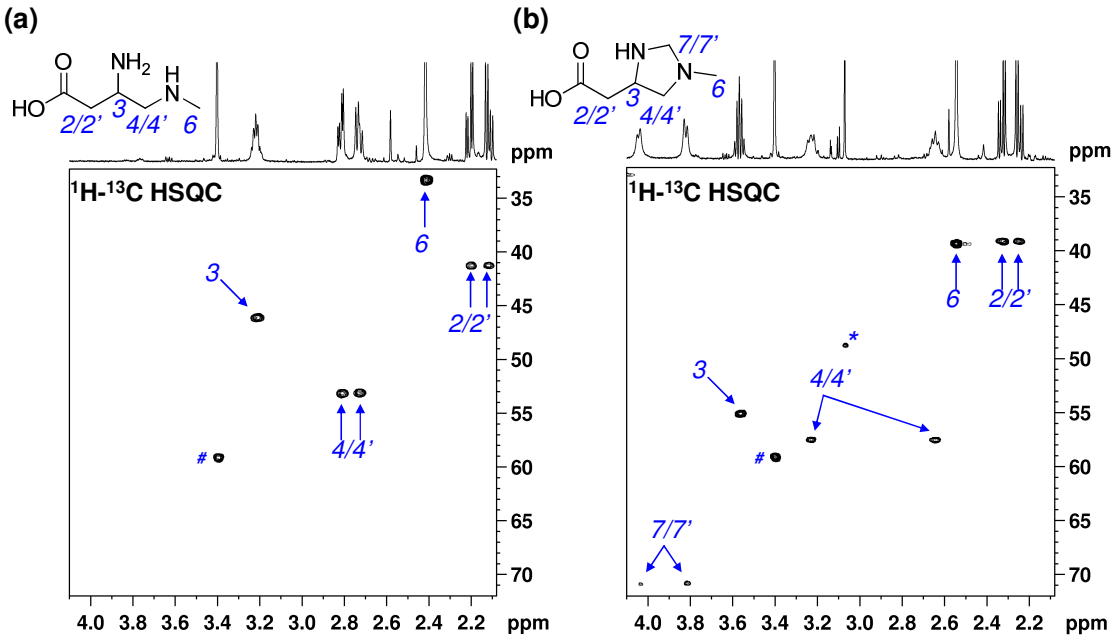

Figure 2-22 ^{1}H-^{13}C HSQC correlations for (a) 1 mM 3-amino-4-(methylamino)butanoic acid, and (b) 1 mM 3-amino-4-(methylamino)butanoic acid with 0.9 mM formaldehyde. Spectra were recorded at 700 MHz buffered in Tris-D11 (pH 7.5) in 95% H_2O and 5% D_2O at 280 K. # is Tris-D11 and * is an impurity from the formaldehyde stock solution.

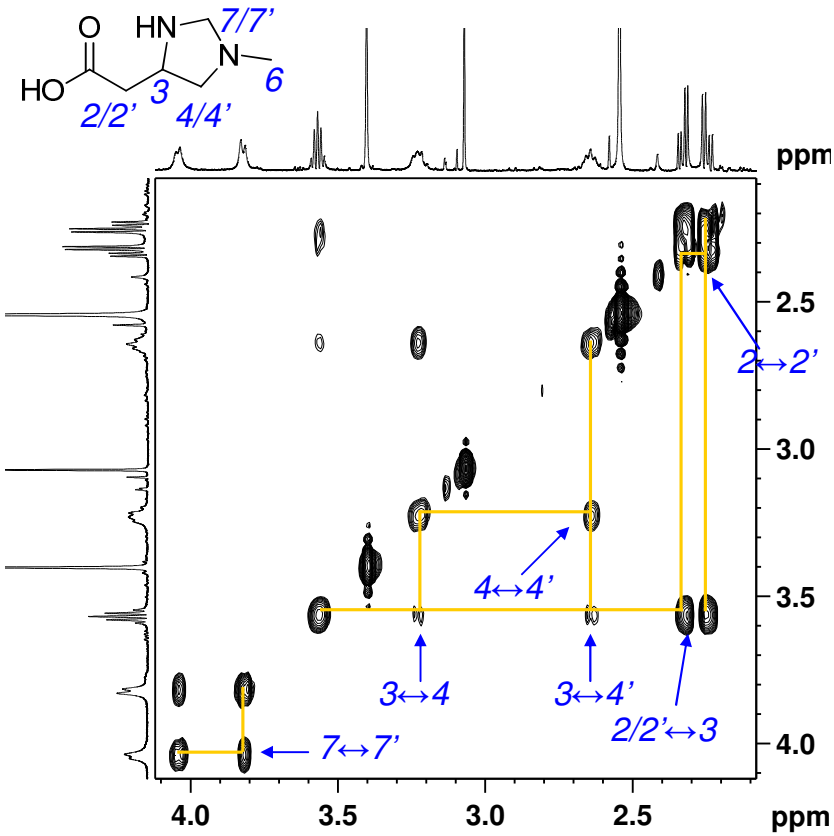

Figure 2-23 COSY of 1 mM 3-amino-4-(methylamino)butanoic acid with 0.9 mM formaldehyde. Spectra were recorded at 700 MHz buffered in Tris-D11 (pH 7.5) in 95% H_2O and 5% D_2O at 280 K.

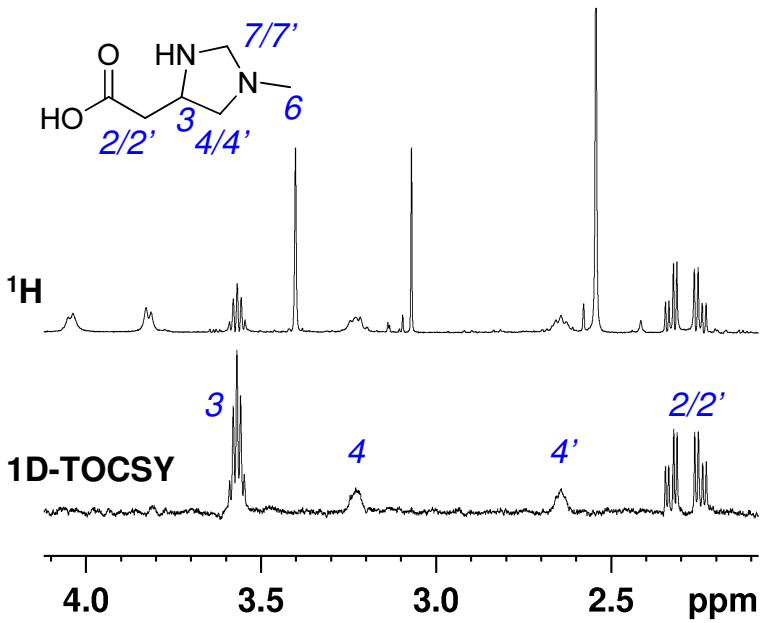

Figure 2-24 1D-TOCSY of 1 mM 3-amino-4-(methylamino)butanoic acid with 0.9 mM formaldehyde. Spectra are recorded at 700 MHz buffered in Tris-D11 (pH 7.5) in 95% H_2O and 5% D_2O at 280 K. Selection irradiation is applied at 3.57 ppm.

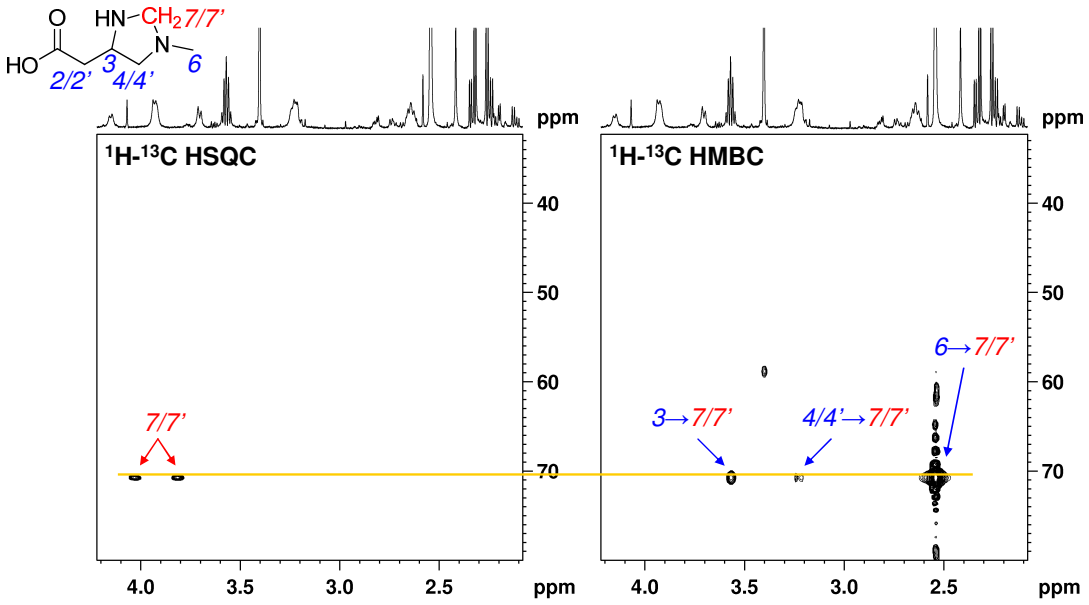

Figure 2-25 ^{1}H-^{13}C HSQC and ^{1}H-^{13}C HMBC correlations of 1 mM 3-amino-4-(methylamino)butanoic acid with 0.9 mM ^{13}C-labelled formaldehyde. Spectra are recorded at 700 MHz buffered in Tris-D11 (pH 7.5) in 95% H_2O and 5% D_2O at 280 K.

In order to observe the anticipated HMBC correlation between C-3 to the aminal/hemiaminal CH_2, ^{13}C-labelled formaldehyde was then reacted with AMBA. ^{1}H-^{13}C HSQC revealed that the only signals labelled in the resulting compound is the aminal/hemiaminal CH_2 (Figure 2-25). More importantly, HMBC correlations are observed between C-3 and the aminal/hemiaminal CH_2, confirming the formation of a ring structure (Figure 2-25).

2.3.3 Rearrangement mechanism

The crystal structures of BBOX show that L-carnitine and THP bind to the active site in essentially the same manner (PDB id: 3O2G and 3MS5 respectively), suggesting their reaction may follow similar reaction mechanisms, *i.e.* formation of 3-hydroxy-THP followed by fragmentation. Although the observation of malonic acid semialdehyde seemed to be consistent with this proposal, the absence of the 1,1,1-trimethylhydrazinium ion or trimethylamine suggested a more complex mechanism.

In order to determine the origin of the new carbon-carbon bond of AMBA, a reaction was conducted with 1,2,3,4-^{13}C labelled 2OG. The ^{13}C label was transferred only onto succinate, indicating there is no cross-linking between 2OG and THP. THP with one of its *N*-methyl groups labelled with ^{13}C was also prepared (by Dr Luc Henry). The result suggested that the ^{13}C label was transferred into C-4, *N*-methyl and the aminal/hemiaminal C-7 (Figure 2-26 and Figure 2-27), therefore suggesting a rearrangement mechanism. The ^{13}C label could also be observed on formaldehyde and dimethylamine, indicating formaldehyde production is likely *via* *N*-dimethyl hydroxylation followed by fragmentation. Formaldehyde production has been observed previously with another class of 2OG oxygenase histone N^{ϵ}-methyllysine demethylase, possibly by hydroxylation followed by fragmentation.[85,86] In addition, the reaction of THP and BBOX also involves N-N fragmentation and a C-C bond forming rearrangement.

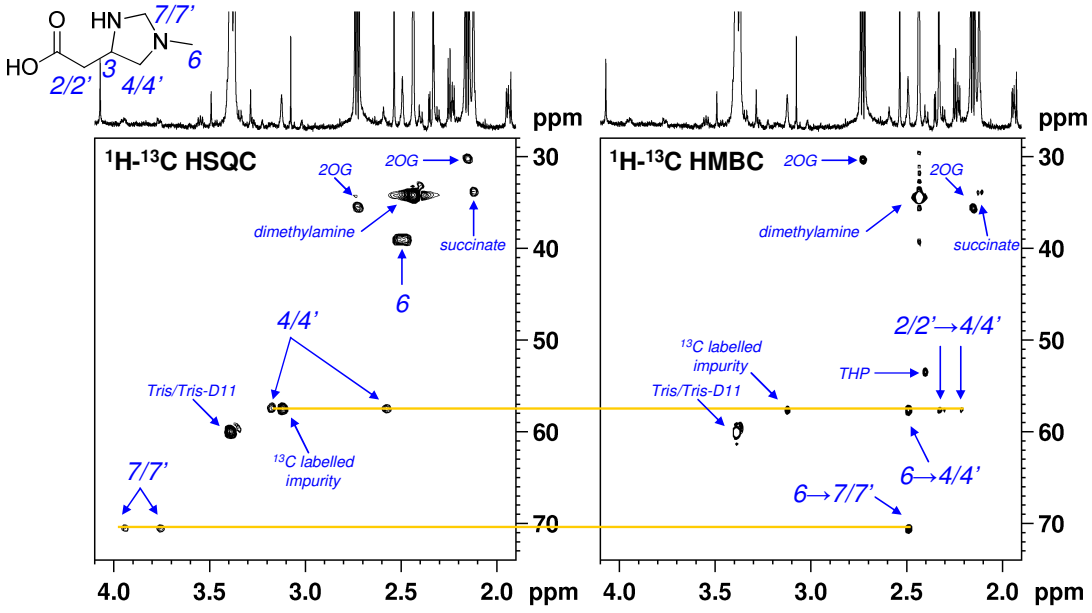

Figure 2-26 ^{1}H-^{13}C HMBC and ^{1}H-^{13}C HSQC correlations of the Assay mixture between ^{13}C-labelled THP and BBOX. Spectra are recorded at 700 MHz buffered in Tris/Tris-D11 (pH 7.5) in 95% H_2O and 5% D_2O at 280 K.

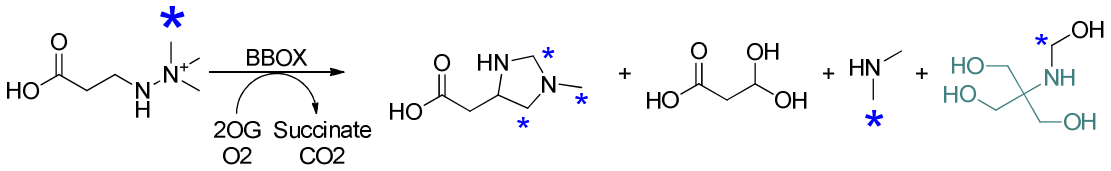

Figure 2-27 ^{13}C label (*) is transferred to the rearrangement product, dimethylamine and formaldehyde (as observed as a Tris adduct, dark grey).

In order to investigate the mechanism of the THP rearrangement reaction, the *tert*-butyl and isopropyl THP analogues were prepared and were reacted with BBOX. In both cases the reactions followed the normal hydroxylation pathway forming *tert*-butylamine and isopropylamine (Table 2-4). The identities of both products were confirmed using pure standards.

Substrate	Product	Assay protein concentration / nM	Rate / μM product min^{-1}
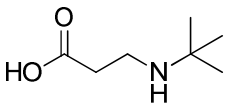	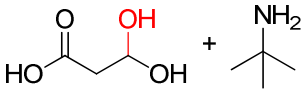	12.5	0.33 ± 0.06
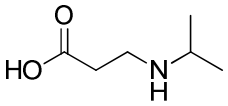	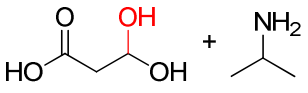	500	1.9 ± 0.04

Table 2-4 The *tert*-butyl and isopropyl THP analogues followed the normal hydroxylation pathway, which is then followed by fragmentation.

Overall, the evidence suggests the rearrangement reaction of THP must involve formation of an initial radical at C-3 (Figure 2-28). The presence of a secondary amine can then enable N-N fragmentation of the radical intermediate to give an imine and a trimethylamine radical cation. A 1,2-hydrogen shift of the trimethylamine radical cation can then give a methylene radical. The methylene radical can either react *via* a rebound process generating hydroxyl-trimethylamine (Figure 2-28 Route A), which subsequently fragments into formaldehyde and dimethylamine. Alternatively, the methylene radical can add into the imine to generate the rearranged C-C framework (Figure 2-28 Route B) and subsequent 1,5-hydrogen abstraction on one of the *N*-methyl groups by the resultant amine radical, followed by rebound hydroxylation, gives the rearrangement product. The closest parallel reaction in organic chemistry is the Stevens rearrangement, in which a quaternary amine is deprotonated to form an ylide, which then undergoes an *N*-alkyl migration rearrangement to give a secondary amine.[87] However, in contrast to the harsh

conditions used in organic chemistry,[88] this BBOX-catalysed reaction occurs at room temperature in aqueous solution. It should be noted that this also is a rare, possibly unique, example of human 2OG oxygenase catalysed C-C bond formation.

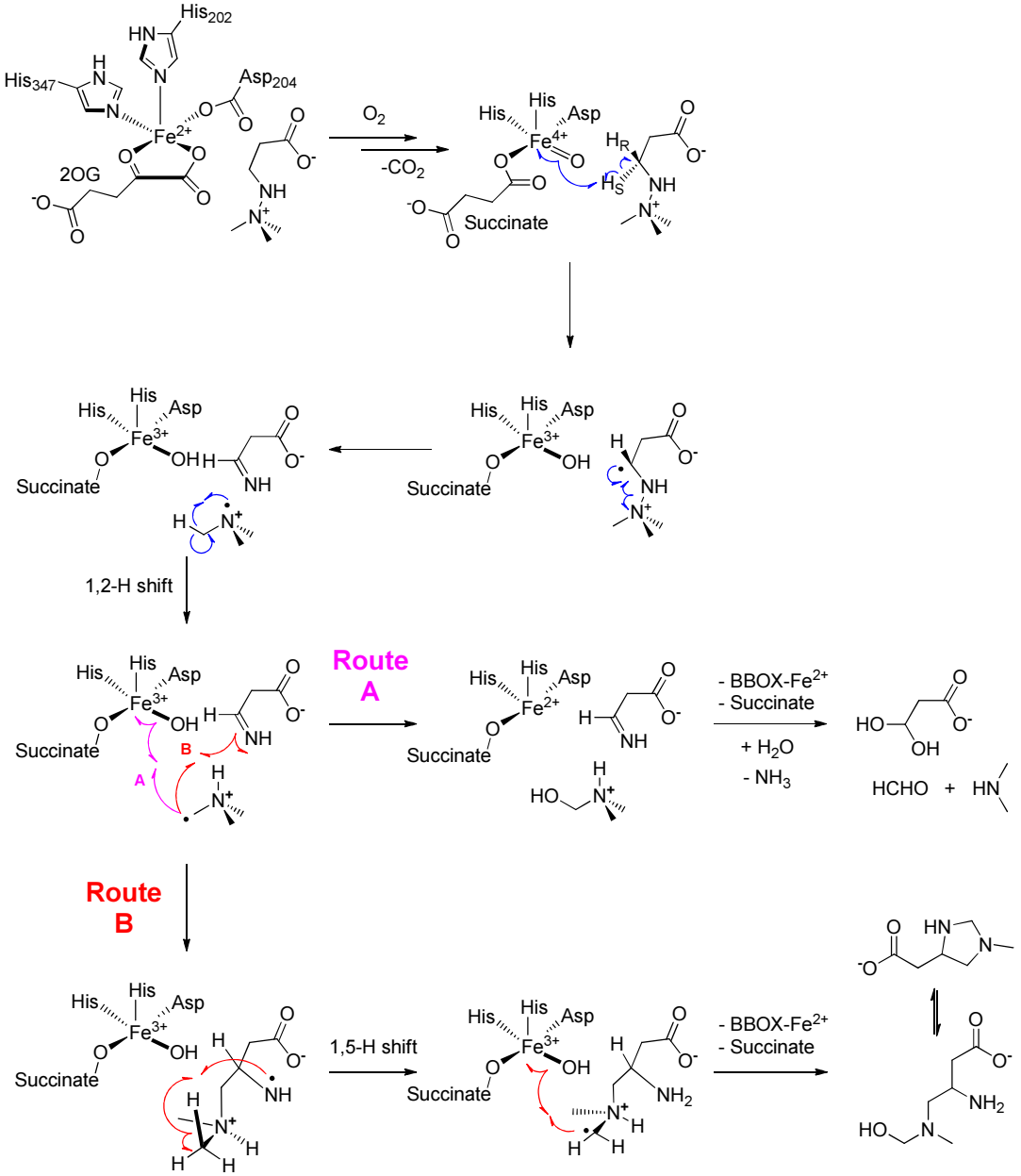

Figure 2-28 Proposed THP mechanism with BBOX. Two divergent reaction pathways give rise to all the observed products. NH_3 was never observed, although it is expected to be formed in path A.

2.4 Human BBOX as a therapeutic target

2.4.1 THP-Orotate

Recent studies and patent applications have described synergic properties of the orotate, succinate and fumarate salts of THP.[89,90] Orotate (Figure 2-29), succinate and fumarate may act as metal chelators at the 2OG binding site of BBOX. It was thus

proposed that this synergic effect may be due to dual inhibition of BBOX by both 2OG and GBB mimics. Orotate on its own has also shown cardioprotective effect in rats.[91]

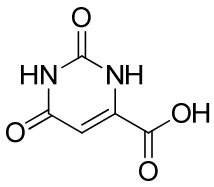

Figure 2-29 Structure of orotate.

Inhibition studies suggested orotate is a weak BBOX inhibitor (IC_{50} = 1.5 mM; Figure 2-30). There was no additive effect between THP and orotate in terms of BBOX inhibition (IC_{50} of THP = 66.1 μM; IC_{50} of THP-orotate = 64.5 μM; Figure 2-30). To further study this proposed synergic effect, inhibition studies using a 1:1 mixture of NOG, a structural analogue of 2OG which acts as a generic inhibitor of 2OG oxygenases, and THP were performed. The result suggested the potential effect of dual inhibition of BBOX is likely to be non-existent (IC_{50} of NOG = 25.7 μM; IC_{50} of THP-NOG = 25.6 μM; Figure 2-31).

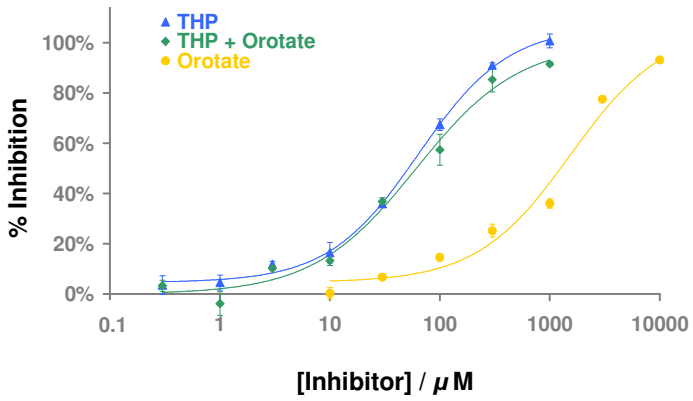

Figure 2-30 The effect of orotate and THP-orotate on BBOX inhibition (IC_{50} of THP = 66.1 ± 6.2 μM; IC_{50} of orotate = 1.54 ± 0.04 mM; IC_{50} of THP-orotate = 64.5 ± 11.5 μM). The mixture contained 25 nM BBOX, 40 μM Fe(II), 40 μM 2OG, 40 μM GBB, 500 μM ascorbate, 80 mM KCl and 50 mM Tris-D11 (pH 7.5). Percentage turnover of GBB to L-carnitine is measured by NMR 13 minutes after mixing. The error bars indicate standard errors from at least three separate measurements.

2.4.2 THP-Metformin

A recent study involving rat models suggested that THP may be useful for the treatment of diabetes by lowering blood glucose,[92] possibly by inhibiting L-carnitine biosynthesis and transportation, therefore stimulating glucose uptake and utilisation.

The anti-diabetic effect is more apparent when THP is applied alongside metformin (Figure 2-32), a widely-used diabetes drug.[93]

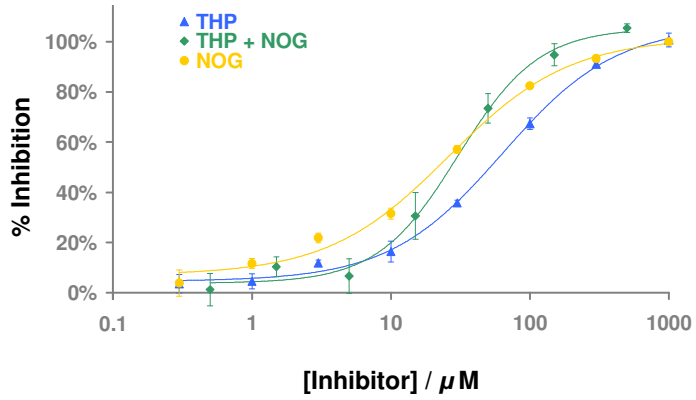

Figure 2-31 The effect of THP-NOG on BBOX inhibition (IC_{50} of THP = 66.1 ± 6.2 μM; IC_{50} of NOG = 25.7 ± 3.1 μM; IC_{50} of THP-NOG = 25.6 ± 4.5 μM). The mixture contained 25 nM BBOX, 40 μM Fe(II), 40 μM 2OG, 40 μM GBB, 500 μM ascorbate, 80 mM KCl and 50 mM Tris-D11 (pH 7.5). Percentage turnover of GBB to L-carnitine is measured by NMR 13 minutes after mixing. The error bars indicate standard errors from at least three separate measurements.

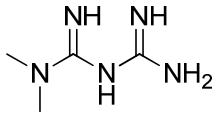

Figure 2-32 Structure of metformin.

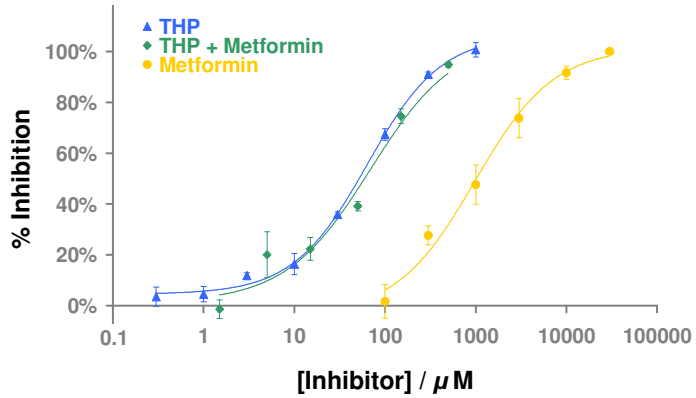

Figure 2-33 The effect of metformin and THP-metformin on BBOX inhibition (IC_{50} of THP = 66.1 ± 6.2 μM; IC_{50} of metformin = 1.11 ± 0.4 mM; IC_{50} of THP-metformin = 69.4 ± 3.9 μM). Reaction contained 25 nM BBOX, 40 μM Fe(II), 40 μM 2OG, 40 μM GBB, 500 μM ascorbate, 80 mM KCl and 50 mM Tris-D11 (pH 7.5). Percentage turnover of GBB to L-carnitine is measured by NMR 13 minutes after mixing. The error bars indicate standard errors from at least three separate measurements.

Inhibition studies suggest that metformin is a weak inhibitor of BBOX (IC_{50} = 1.1 mM; Figure 2-33), and there was no synergic effect observed on BBOX inhibition when a 1:1 mixture of THP and metformin was used (IC_{50} of THP = 66.1 μM; IC_{50} of

THP-metformin = 69.4 μM; Figure 2-33). This is in agreement with the rat model study which showed that the additional anti-diabetic effect of THP is likely due to metformin and THP targeting two separate pathways.[92]

2.4.3 2-Hydroxyglutarate

Recent studies have suggested the accumulation of 2-hydroxyglutarate (2HG; Figure 2-34) is associated with glioma, malignant glioblastoma and acute myeloid leukaemia (brain tumour).[94,95] The concentration of 2HG may be as high as 10 mM in cancer cells.[94] 2HG is a 2OG analogue and a good metal chelator, as indicated by broadening of the ^{1}H peaks in the presence of Fe(II). Therefore, 2HG may act as a competitive inhibitor of 2OG oxygenases.[96]

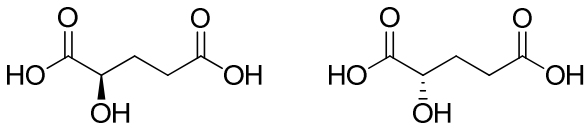

Figure 2-34 Structures of the D- and L-2-hydroxyglutarate.

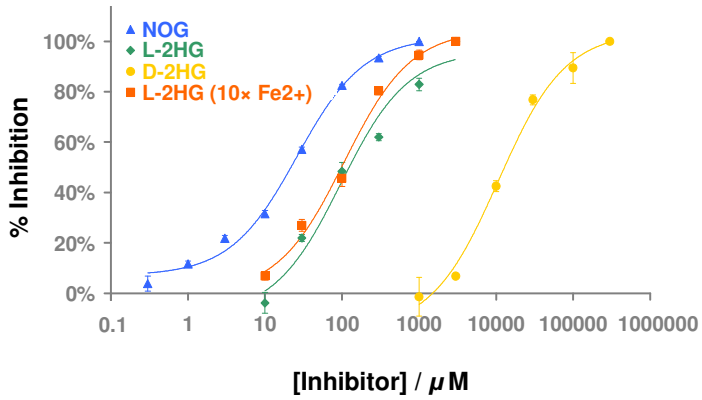

Figure 2-35 The effect of 2HG on BBOX inhibition (IC_{50} of L-2HG = 96.6 ± 2.7 μM; IC_{50} of D-2HG = 11.3 ± 0.1 mM; IC_{50} of L-2HG at 10× Fe(II) = 106.7 ± 1.4 μM; IC_{50} of NOG = 29.2 ± 1.2 μM). The mixture contained 25 nM BBOX, 40 μM Fe(II), 40 μM 2OG, 40 μM GBB, 500 μM ascorbate, 80 mM KCl and 50 mM Tris-D11 (pH 7.5). Percentage turnover of GBB to L-carnitine is measured by NMR 13 minutes after mixing. The error bars indicate standard errors from at least three separate measurements.

BBOX1 has recently been identified as a potential cancer gene on the basis of large scale microarray analysis.[97] Inhibition studies were therefore conducted to investigate the effect of 2HG on BBOX inhibition. The results suggest both L-2HG and D-2HG aree weak BBOX inhibitors (IC_{50} of L-2HG = 96.6 μM; IC_{50} of D-2HG = 11.3 mM; Figure 2-35). Inhibition of BBOX by L-2HG is ~7 times weaker than with NOG and D-2HG is ~700 times weaker than with NOG. As both enantiomers of 2HG are a good

Fe(II) chelator in solution, further inhibition studies were conducted using 10 times more metal. The same IC_{50} value was obtained at the higher Fe(II) concentration, which suggests the mode of inhibition is not predominately metal sequestration (IC_{50} of L-2HG at 10× Fe(II) concentration = 106.7 μM; Figure 2-35).

2.4.4 Daminozide

Daminozide (4-(2,2-dimethylhydrazinyl)-4-oxobutanoic acid) was a widely-used plant growth regulator in the agricultural and farming industries in the 1960s[98] until concerns about its possible carcinogenicity were reported (Figure 2-36).[99] One of its modes of action was proposed to be the inhibition of plant 2OG oxygenases that are involved in gibberellin biosynthesis.[100] Daminozide may also inhibit human 2OG oxygenases; recently a protein crystal structure of daminozide bound to the histone demethylase PHF8 was deposited (PDB id: 4DO0). As daminozide shares a similar structure to THP, the inhibitory effects of daminozide and its analogues against BBOX were investigated (Figure 2-36).

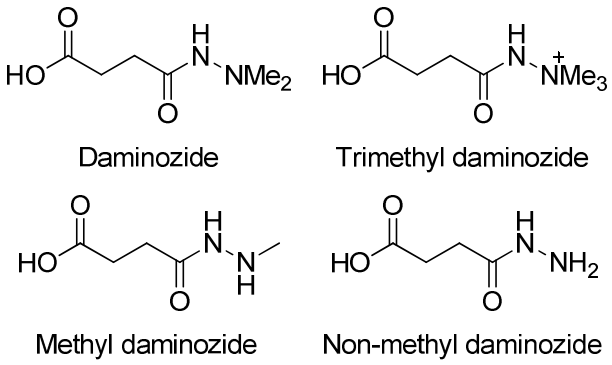

Figure 2-36 Structures of Daminozide and its analogues

Daminozide was found to be a very weak BBOX inhibitor with an IC_{50} value of 6.3 mM (Figure 2-37). The trimethyl analogue of daminozide is a slightly better inhibitor with an IC_{50} value of 1.7 mM (Figure 2-37). These results suggest that despite their structural similarities to THP, the extra carbonyl group at C-4 possibly obstructs their binding to the substrate binding pocket of BBOX, although they may also bind to the 2OG binding pocket of BBOX.

No IC_{50} values could be accurately determined for the methyl and non-methyl analogues of daminozide, as they were found to be highly unstable in aqueous solution (pH 7.5 buffered by 50 mM Tris). Methyl daminozide has a half life of ~23 hours and decomposes into multiple products. Non-methyl daminozide was found to

almost fully hydrolyse into succinate after 10 minutes in buffer. In fact, the IC_{50} value obtained for the supposedly "non-methyl daminozide" is 636 µM, which is suspiciously similar to the IC_{50} value of succinate (615 µM).

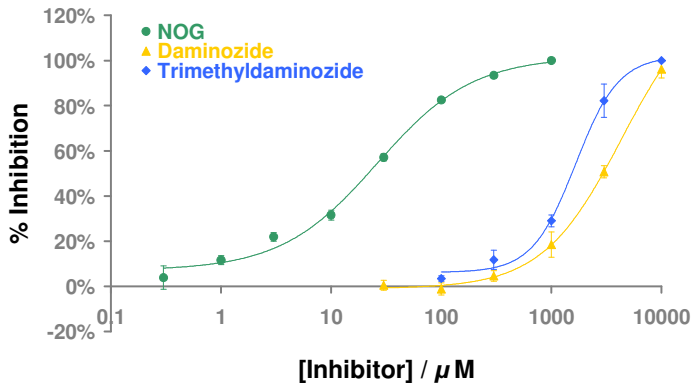

Figure 2-37 The effect of daminozide and trimethyl daminozide on BBOX inhibition (IC_{50} of daminozide = 6.3 ± 0.1 mM; IC_{50} of trimethyl daminozide = 1.7 ± 0.1 mM; IC_{50} of NOG = 29.2 ± 1.2 µM). The mixture included 25 nM BBOX, 40 µM Fe(II), 40 µM 2OG, 40 µM GBB, 500 µM ascorbate, 80 mM KCl and 50 mM Tris-D11 (pH 7.5). Percentage turnover of GBB to L-carnitine is measured by NMR 13 minutes after mixing. The error bars indicate standard errors from at least three separate measurements.

2.5 Development of alternative BBOX assays

2.5.1 Development of a ^{19}F NMR assay

The accuracy of ^{1}H NMR-based inhibition assays may be compromised in the case of signal overlap with solvent or with inhibitor resonances. The detection of a different nuclide would be desirable in such scenarios. ^{19}F NMR offers comparable (83%) sensitivity to ^{1}H NMR due to its 100% natural abundance and high magnetogyric ratio. ^{19}F chemical shifts span a very wide range and fluorine resonances are very sensitive to the local environment. In addition, ^{19}F spectra are usually free of undesirable background, which allows analyses to be conducted in the presence of protonated buffers and solvents. ^{19}F NMR has also been applied for high-throughput screening of macromolecular ligands.[101,102]

Fluoromethyl-GBB (4-[(fluoromethyl)(dimethyl)ammonio]butanoate) was therefore prepared (by Anna M. Rydzik) and assayed with BBOX (Figure 2-38). Fluoromethyl-carnitine (4-[(fluoromethyl)(dimethyl)ammonio]-3-hydroxybutanoate) was observed as the only product (Figure 2-39 and Figure 2-40), with a comparable rate of production to GBB (Figure 2-41).

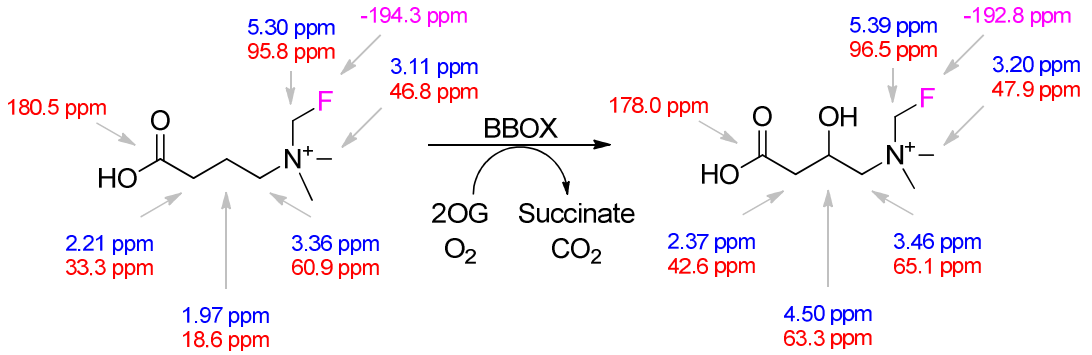

Figure 2-38 BBOX catalyses the reaction of fluoromethyl-GBB to fluoromethyl-carnitine. Spectra were recorded at 280 K buffered by 50 mM Tris-D11 at pH 7.5.

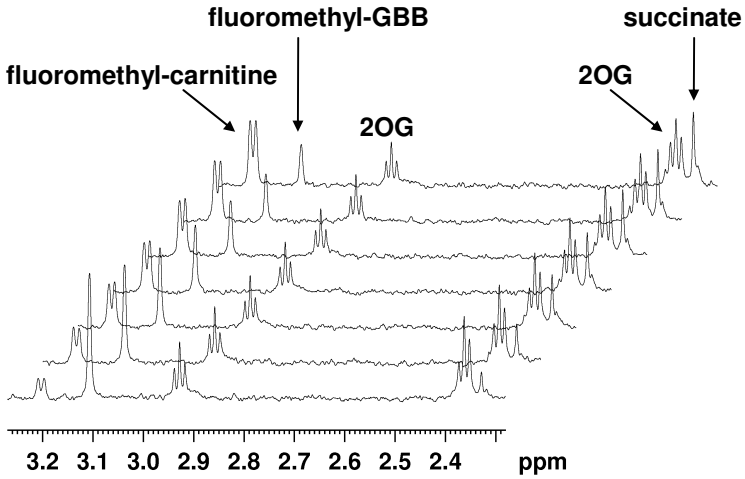

Figure 2-39 ^{1}H NMR assay to monitor BBOX activity with fluoromethyl-GBB. Spectra are shown in 4-minute intervals. The mixture contained 25 nM BBOX, 40 µM Fe(II), 40 µM fluoromethyl-GBB, 80 µM 2OG, 500 µM ascorbate, 80 mM KCl and 50 mM Tris-D11 (pH 7.5). Note that the two methyl peaks of fluoromethyl-carnitine are non-equivalent due to the introduction of a stereogenic centre upon hydroxylation.

A potential ^{19}F NMR-based strategy was derived for BBOX inhibition studies. Assay mixtures were prepared in water and protonated buffer, which were then quenched with deuterated organic solvent (such as methanol-D4 or acetonitrile-D3). Samples could then be stored and subsequently analysed in an automatic fashion using a robotic autosampler.

As a proof-of-principle study, the inhibition of BBOX by THP was measured by analysing percentage turnover of fluoromethyl-GBB to fluoromethyl-carnitine over time. Reactions were quenched with 20% (final volume) acetonitrile-D3 after ten minutes. A relatively high concentration of fluoromethyl-GBB was used because of the relatively low sensitivity of the room temperature ^{1}H/^{19}F inverse probe used, although a lower (and more biologically relevant) concentration could be achieved if a

commercially available ^{19}F cryoprobe was used.[103,104] The result from the assay was found to be comparable with data from other methods (Figure 2-42).

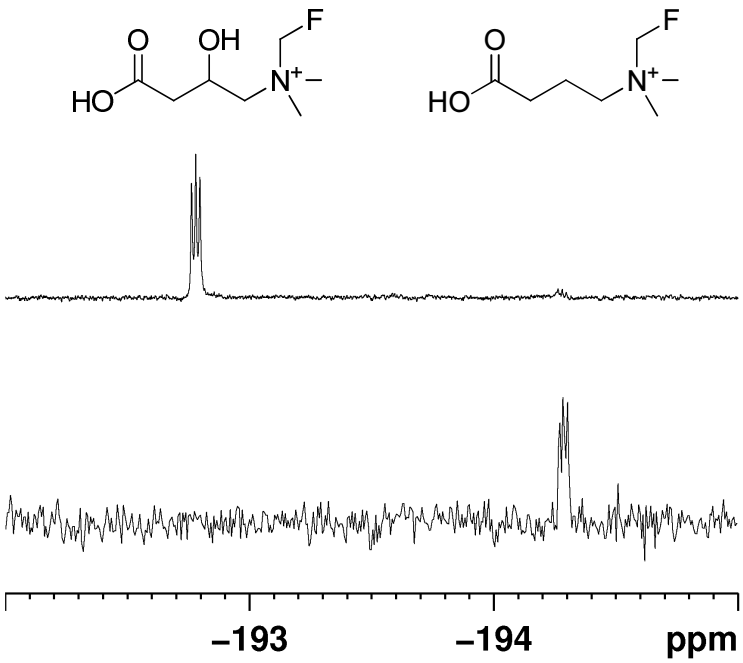

Figure 2-40 ^{1}H-coupled ^{19}F NMR spectra showing the chemical shifts of fluoromethyl-GBB and fluoromethyl-carnitine.

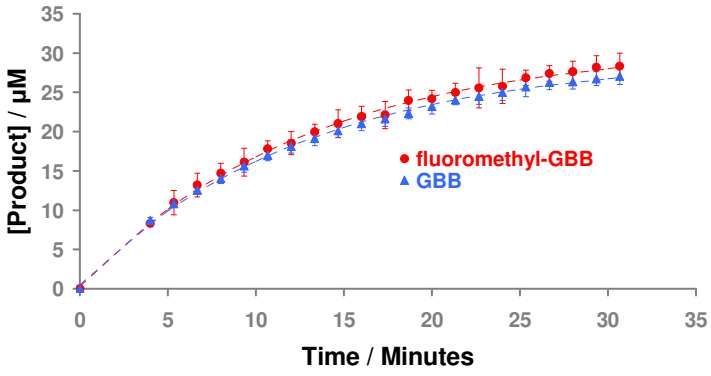

Figure 2-41 The rates of the reaction of fluoromethyl-GBB and GBB with BBOX, as monitored by ^{1}H NMR, are comparable. Reaction contained 25 nM BBOX, 40 µM Fe(II), 40 µM GBB/fluoromethyl-GBB, 80 µM 2OG, 500 µM ascorbate, 80 mM KCl and 50 mM Tris-D11 (pH 7.5). The error bars indicate standard errors from at least three separate measurements. Dashed lines are included to aid visualisation.

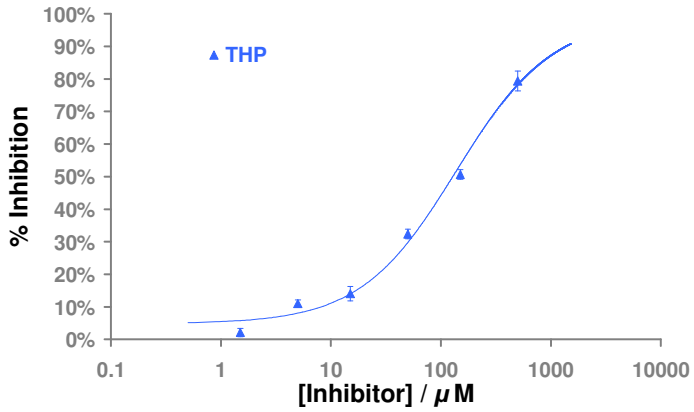

Figure 2-42 Inhibition measurement using fluoromethyl-GBB and ^{19}F NMR (IC_{50} of THP = 138.9 ± 19 μM). Reaction contained 25 nM BBOX, 40 μM Fe(II), 100 μM 2OG, 150 μM fluoromethyl-GBB, 500 μM ascorbate, 80 mM KCl and 50 mM Tris-D11 (pH 7.5). The reaction was quenched with 20% acetonitrile-D3 10 minutes after mixing. Percentage turnover of fluoromethyl-GBB to fluoromethyl-carnitine is measured by ^{19}F NMR. The error bars indicate standard errors from at least three separate measurements.

2.5.2 Development of a F^- detection fluorescent assay

Despite NMR being useful for the study of BBOX, especially for identifying novel substrates and characterising unexpected products, NMR is intrinsically labour intensive. The development of an alternative high-throughput assay for routine screening of inhibitor compounds is therefore desirable.

Recently, Gorres and Raines described a fluoride detection assay with collagen prolyl 4-hydroxylase (P4H), a 2OG oxygenase that catalyses the prolyl hydroxylation reaction from (2*S*)-proline to (2*S*, 4*R*)-4-hydroxyproline.[105] The assay is conducted with (2*S*, 4*S*)-4-fluoroproline to form (2*S*)-4-ketoproline and inorganic fluoride (Figure 2-43a).

The BBOX-catalysed D-carnitine hydroxylation reaction, which produced water and 3-dehydrocarnitine as products, provided a good starting point for the development of a BBOX specific fluoride probe (Figure 2-43b).

D-3-Fluoro-GBB ((3*S*)-3-fluoro-4-(trimethylammonio)butanoate, Figure 2-43c) was prepared (by Anna M. Rydzik). ^{19}F NMR confirmed the only fluorinated species formed with BBOX was a fluoride ion (Figure 2-44a), and ^{1}H NMR showed the formation of 3-dehydrocarnitine and trimethylaminoacetone (Figure 2-44b). Under standard reaction conditions, D-3-fluoro-GBB reacted at a slightly faster rate than D-carnitine (Figure 2-45). Unlike the natural substrate GBB, a lower coupling efficiency between 2OG oxidation and substrate oxidation was observed, *i.e.* there is excess

2OG oxidation (uncoupled turnover) above D-3-fluoro-GBB hydroxylation (Figure 2-46, Figure 2-47, Table 2-5). The deviation from 'perfect coupling' with unnatural substrate has been observed previously with other (small molecule) 2OG oxygenases,[106,107] and may be due to the unnatural substrates usually having lower binding efficiencies than the natural substrate. Also the unnatural substrate may adopt alternative uncooperative binding modes in the substrate binding pocket.

a.

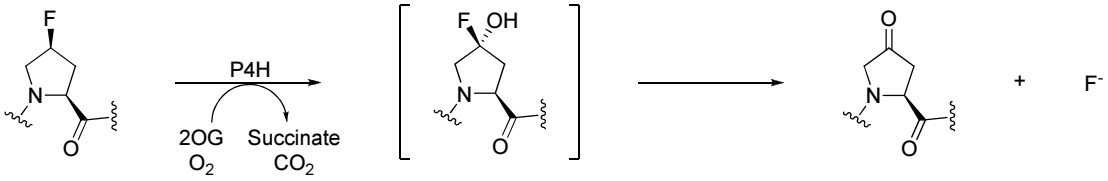

b.

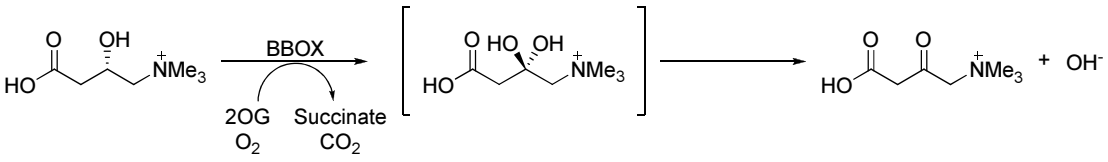

c.

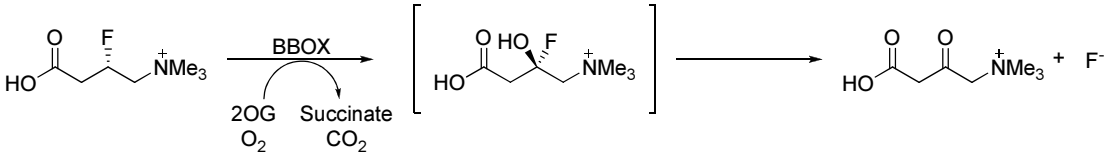

Figure 2-43 (a) Fluoride release in the reaction of (2*S*, 4*S*)-4-fluoroproline and P4H as described in reference 105; (b) The formation of water and 3-dehydrocarnitine in the reaction of D-carnitine and BBOX; (c) Fluoride release in the reaction of D-3-fluoro-GBB and BBOX.

A *tert*-butyldimethylsilyl-protected fluoresceine probe[108] was used to detect fluoride ions released in the reaction between D-3-fluoro-GBB and BBOX (Figure 2-48 and Figure 2-49; Synthesis of the probe and fluorescent experiments were performed by Anna M. Rydzik). A proportional increase of fluorescence was observed with increasing fluoride concentration *via* the fluoride ion dependent removal of the silyl protecting group.[108] The IC_{50} of THP was measured by this method; the value obtained by the fluorescence assay (25 μM) is in good agreement with the values measured by NMR (62 μM), demonstrating its potential as an alternative inhibition assay for BBOX.

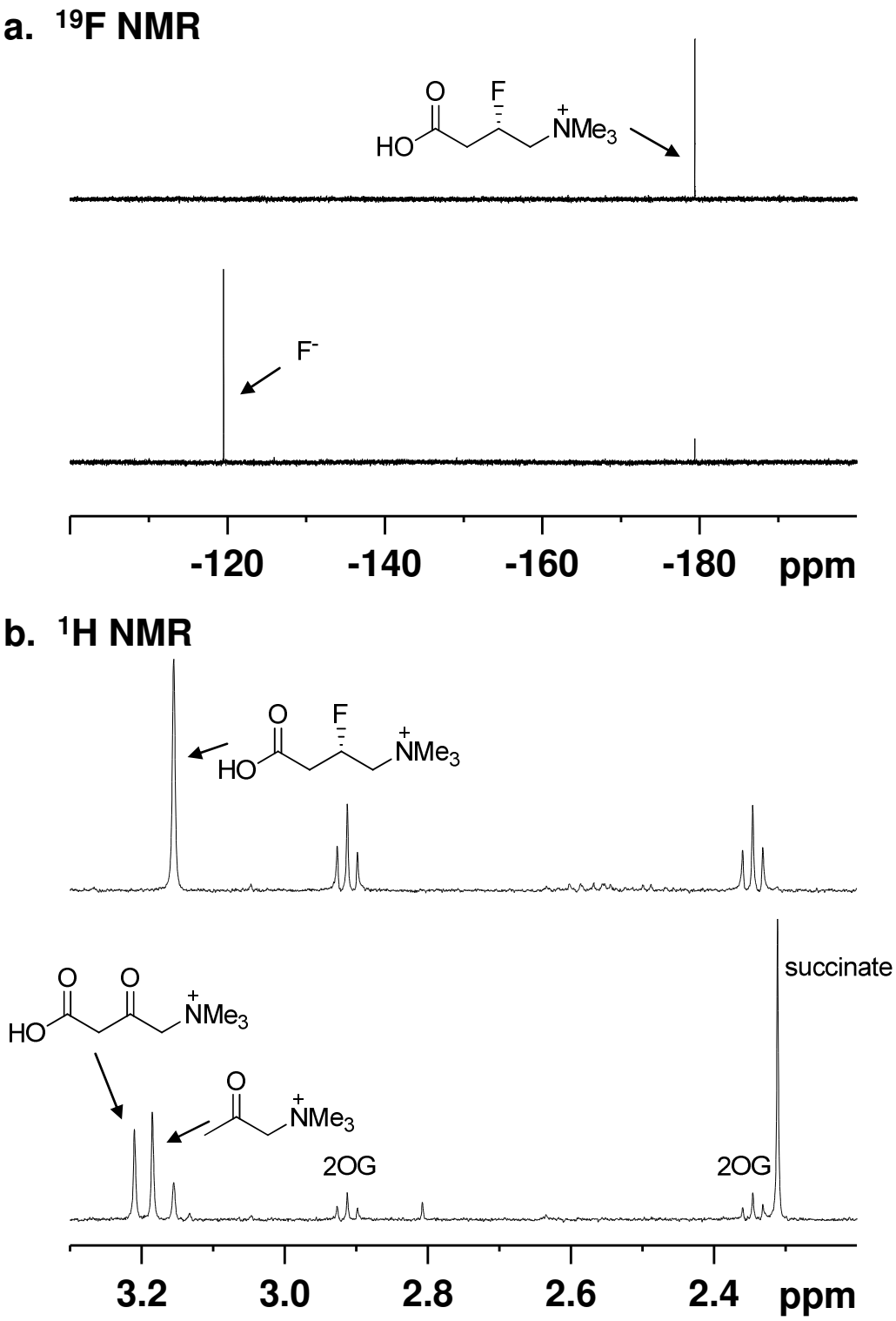

Figure 2-44 (a) ^{19}F NMR showing the formation of fluoride ions. The identity of fluoride ion is confirmed against pure standard (NaF); (b) ^{1}H NMR showing the formation of 3-dehydrocarnitine and trimethylaminoacetone.

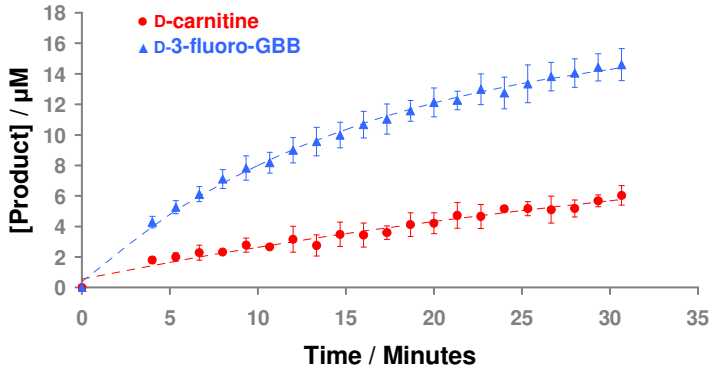

Figure 2-45 D-3-fluoro-GBB reacts slightly faster than D-carnitine. Mixture included 100 nM BBOX, 40 µM Fe(II), 40 µM D-fluoro-GBB/D-carnitine, 80 µM 2OG, 500 µM ascorbate, 80 mM KCl and 50 mM Tris-D11 (pH 7.5). The error bars indicate standard errors from at least three separate measurements. Dashed lines are included to aid visualisation.

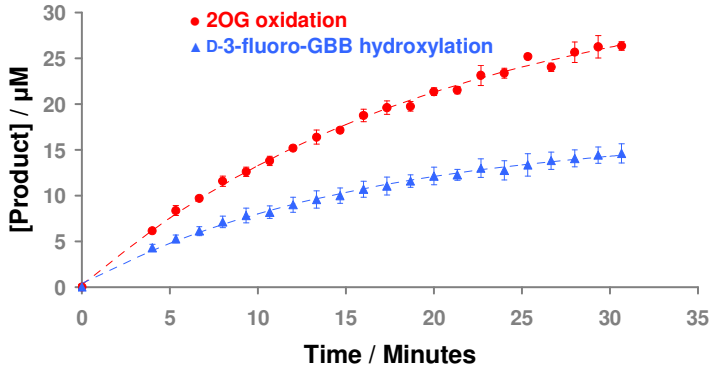

Figure 2-46 Excess 2OG oxidation over D-3-fluoro-GBB hydroxylation. Mixture included 100 nM BBOX, 40 µM Fe(II), 40 µM D-fluoro-GBB/D-carnitine, 80 µM 2OG, 500 µM ascorbate, 80 mM KCl and 50 mM Tris-D11 (pH 7.5). The error bars indicate standard errors from three separate measurements. Dashed lines are included to aid visualisation.

Substrate	Reaction time / Minutes	K_M / µM	V_{max} / µM s^{-1}	k_{cat} / s^{-1}	k_{cat}/K_M / M^{-1} s^{-1}
2OG	4.5	154	0.037	0.37	2.4×10^3
D-3-fluoro-GBB	6.5	12.0	0.010	0.10	7.5×10^3

Table 2-5 Kinetics parameters for BBOX with 2OG and D-3-fluoro-GBB as substrates. Measurements were conducted by ^{1}H NMR. See also Figure 2-47.

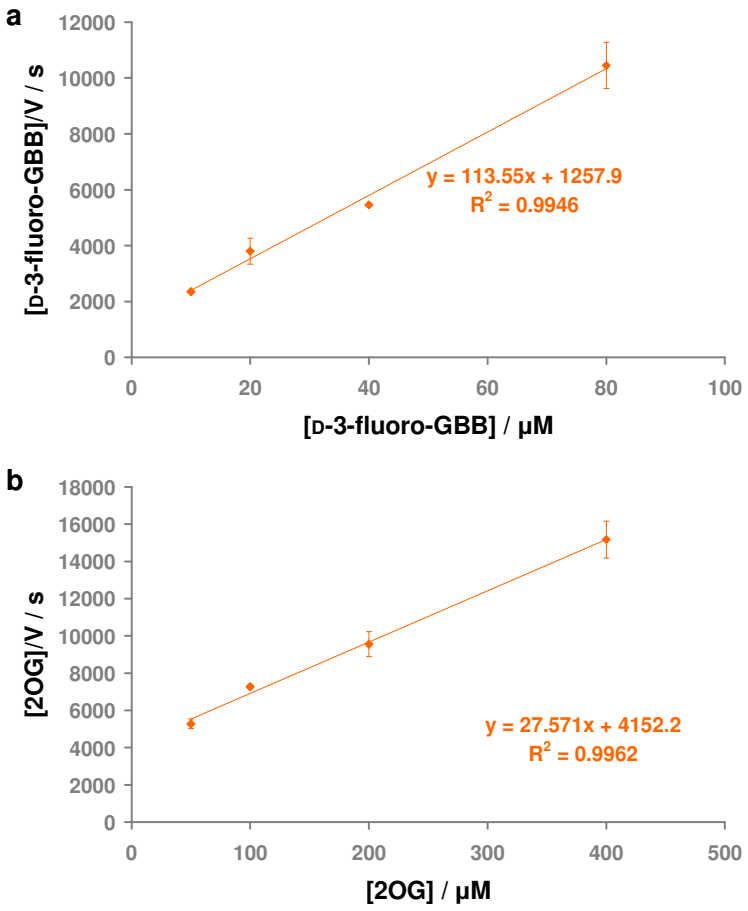

Figure 2-47 Hanes plot for the determination of BBOX kinetics parameters for D-3-fluoro-GBB and 2OG: (a) Mixture included 100 nM BBOX, 40 µM Fe(II), 625 µM 2OG, 500 µM ascorbate, 80 mM KCl and 50 mM Tris-D11 (pH 7.5). Percentage turnover is measured nine minutes after mixing; (b) Mixture included 100 nM BBOX, 40 µM Fe(II), 150 µM D-3-fluoro-GBB, 500 µM ascorbate, 80 mM KCl and 50 mM Tris-D11 (pH 7.5). Percentage turnover is measured five minutes after mixing. The error bars indicate standard errors from three separate measurements. See also Table 2-5.

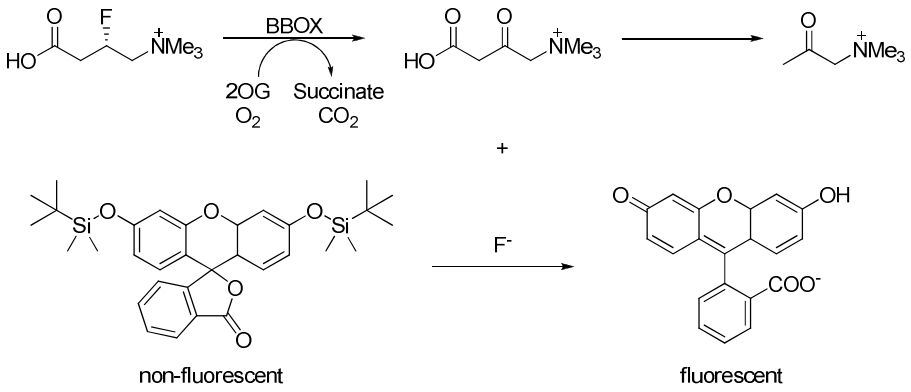

Figure 2-48 The fluoride ion dependent cleavage of the Si-O bond on the protected fluoresceine probe to generate the fluorescent species for detection.

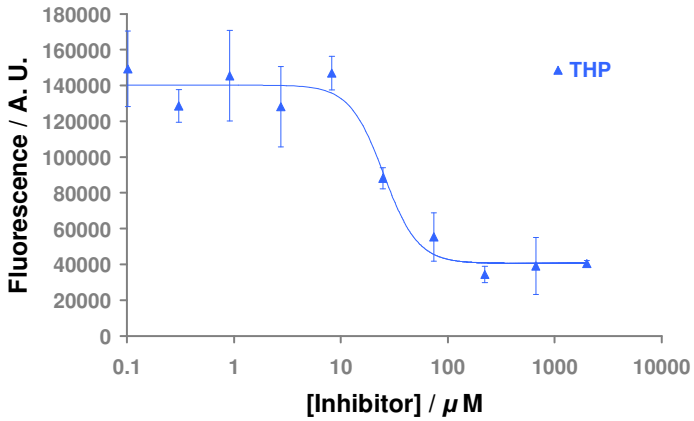

Figure 2-49 Inhibition measurement using D-3-fluoro-GBB and fluorescent assay (IC_{50} of THP = 25.2 ± 1.4 μM). Reaction contained 200 nM BBOX, 40 μM Fe(II), 500 μM 2OG, 40 μM D-3-fluoro-GBB, 250 μM ascorbate, 160 mM KCl and 50 mM Tris-D11 (pH 7.0). Reactions were quenched with 20% acetonitrile (final concentration) 10 minutes after mixing. Samples were then incubated with 4 μM protected fluoresceine probe in 80% DMSO (final concentration) for 60 minutes, and the fluorescence signal was measured immediately after the incubation. The assay was performed by Anna M. Rydzik. The error bars indicate standard errors from four separate measurements.

2.6 Summary

Overall, the work described in this Chapter has applied NMR spectroscopy to the study of recombinant human BBOX. BBOX was found to be a highly active 2OG oxygenase requiring potassium ions and ascorbate for optimal activity. BBOX was shown to be promiscuous with respect to substrate selectivity, processing a number of modified substrates including L- and D-carnitine. THP, a clinically used BBOX inhibitor, was also found to be a BBOX substrate forming multiple products including malonic acid semialdehyde, dimethylamine, formaldehyde and AMBA. BBOX is unique among human 2OG oxygenases in that it catalyses hydroxylation, demethylation and C-C bond forming reactions. As BBOX is a current inhibition target for medicinal applications, a ^{1}H NMR based inhibition assay was developed and a number of compounds, such as 2HG, were tested for BBOX inhibition. Finally, the development of alternative BBOX assays was also investigated. These included a ^{19}F NMR based assay and a fluoride detection fluorescence assay.

2.7 References

1. Fraenkel, G.; Friedman, S. Carnitine. *Vitam. Horm.* **1957**, *15*, 73–118.
2. Bremer, J. Carnitine – metabolism and functions. *Physiol. Rev.* **1983**, *63*, 1420–1480.
3. Steiber, A.; Kerner, J.; Hoppel, C. L. Carnitine: a nutritional, biosynthetic, and functional perspective. *Mol. Aspects Med.* **2004**, *25*, 455–473.
4. Panter, R. A. Carnitine levels in some higher plants. *FEBS Lett.* **1969**, *5*, 169–170.
5. Rebouche, C. J. Carnitine function and requirements during the life cycle. *FASEB J.* **1992**, *6*, 3379–3386.
6. Kleber, H. P. Bacterial carnitine metabolism. *FEMS Microbiol. Lett.* **1997**, *147*, 1–9.
7. Rebouche, C. J.; Seim, H. Carnitine metabolism and its regulation in microorganisms and mammals. *Annu. Rev. Nutr.* **1998**, *18*, 39–61.
8. McGarry, J. D.; Brown, N. F. The mitochondrial carnitine palmitoyltransferase system. From concept to molecular analysis. *Eur. J. Biochem.* **1997**, *244*, 1–14.
9. Kerner, J.; Hoppel, C. Fatty acid import into mitochondria. *Biochim. Biophys Acta.* **2000**, *1486*, 1-17.
10. Ramsay, R. R.; Gandour, R. C.; van der Leij, F. R. Molecular enzymology of carnitine transfer and transport. *Biochim. Biophys. Acta* **2001**, *1546*, 21–43.
11. Fritz, I. B. Carnitine and its role in fatty acid metabolism. *Adv. Lipid Res.* **1963**, *1*, 285–334.
12. Fritz, I. B. The effect of muscle extracts on the oxidation of palmitic acid by liver slices and homogenates. *Acta Physiol. Scand.* **1955**, *34*, 367–385.
13. Bremer, J. Carnitine in intermediary metabolism. The metabolism of fatty acid esters of carnitine by mitochondria. *J. Biol. Chem.* **1962**, *237*, 3628–3632.
14. Hoppel, C.L. Carnitine and carnitine palmitoyltransferase in fatty acid oxidation and ketosis. *Fed. Proc.* **1982**, *41*, 2853–2857.
15. Jakobs, B. S.; Wanders, R. J. Fatty acid β-oxidation in peroxisomes and mitochondria: the first, unequivocal evidence for the involvement of carnitine in shuttling propionyl-CoA from peroxisomes to mitochondria. *Biochem. Biophys. Res. Commun.* **1995**, *213*, 1035–1041.
16. Duran, M.; Loof, N. E.; Ketting, D.; Dorland, L. Secondary Carnitine Deficiency. *J. Clin. Chem. Clin. Biochem.* **1990**, *28*, 359–363.
17. Bremer, J. Carnitine in intermediary metabolism. Reversible acetylation of carnitine by mitochondria. *J. Biol. Chem.* **1962**, *237*, 2228–2231.
18. Friedman, S.; Fraenkel, G. Reversible enzymatic acetylation of carnitine. *Arch. Biochem. Biophys.* **1955**, *59*, 491–501.
19. Lennon, D. L.; Shrago, E. R.; Madden, M.; Nagle, F. J.; Hanson, P. Dietary carnitine intake related to skeletal muscle and plasma carnitine concentrations in adult men and women. *Am. J. Clin. Nutr.* **1986**, *43*, 234–238.
20. Brass, E. P.; Hoppel, C. L.; Hiatt, W. R. Effect of intravenous L-carnitine on carnitine homeostasis and fuel metabolism during exercise in humans. *Clin. Pharm. Ther.* **1994**, *55*, 681–692.
21. Brass, E. P.; Hiatt, W. R. The role of carnitine and carnitine supplementation during exercise in man and in individuals with special needs. *J. Am. Coll. Nutr.* **1998**, *17*, 207–215.
22. Brass, E. P. Supplemental carnitine and exercise. *Am. J. Clin. Nutr.* **2000**, *72*, 618S–623S.
23. Tinti, M. O.; Piccolo, O.; Bonifacio, F.; Crescenzi, C.; Penco, S. W. Industrial Process for the Production of L-Carnitine. PCT. Int. Appl. WO 2000029370, **2000**.
24. Kulla, H.; Lehky, P; Squaratti, A. Process for the Continuous Production of L-Carnitine. U. S. Patent 4708936, **1987**.
25. Naidu, G. S. N.; Lee, I. Y.; Lee, E. G. ; Kang, G. H.; Park, Y. H. Microbial and enzymatic production of L-carnitine. *Bioprocess Eng.* **2000**, *23*, 627–635.

26. Lindstedt, G.; Lindstedt, S.; Midtvedt, T.; Tofft, M. The formation and degradation of carnitine in *Pseudomonas*. *Biochemistry* **1967**, *6*, 1262–1270.

27. Vaz, F. M.; Wanders, R. J. A. Carnitine biosynthesis in mammals. *Biochem. J.* **2002**, *361*, 417–429.

28. Rippa, S.; Zhao, Y.; Merlier, F.; Charrier, A.; Perrin, Y. The carnitine biosynthetic pathway in *Arabidopsis thaliana* shares similar features with the pathway of mammals and fungi. *Plant Physiol. Biochem.* **2012**, *60*, 109–114.

29. Strijbis, K.; Vaz, F, M.; Distel, B. Enzymology of the carnitine biosynthesis pathway. *IUBMB Life* **2010**, *62*, 357–362.

30. Hulse, J. D.; Ellis, S. R.; Henderson, L. M. Carnitine biosynthesis. β-Hydroxylation of trimethyllysine by an α-ketoglutarate-dependent mitochondrial dioxygenase. *J. Biol. Chem.* **1978**, *253*, 1654–1659.

31. Vaz, F. M.; Ofman, R.; Westinga, K.; Back, J. W.; Wanders, R. J. A. Molecular and biochemical characterization of rat ε-N-trimethyllysine hydroxylase, the first enzyme of carnitine biosynthesis. *J. Biol. Chem.* **2001**, *276*, 33512–33517.

32. Bremer, J. Biosynthesis of carnitine *in vivo*. *Biochim. Biophys. Acta* **1961**, *48*, 622–624.

33. Wolf, G.; Berger, C. R. A. Studies on the biosynthesis and turnover of carnitine. *Arch. Biochem. Biophys.* **1961**, *92*, 360–365.

34. Paik, W. K.; Nochumson, S.; Kim, S. Carnitine biosynthesis via protein methylation. *Trends Biochem. Sci.* **1977**, *2*, 159–161.

35. Rebouche, C. J.; Broquist, H. P. Carnitine biosynthesis in *Neurospora crassa*: enzymatic conversion of lusine to ε-*N*-trimethyllysine. *J. Bacteriol.* **1976**, *126*, 1207–1214.

36. Borum, P. R.; Broquist, H. P. Purification of *S*-adenosylmethionine: ε-*N*-L-lysine methyltransferase. The first step in carnitine biosynthesis. *J. Biol. Chem.* **1977**, *252*, 5651–5655.

37. Khan-Siddiqui, L.; Bamji, M. S. Lysine-carnitine conversion in normal and undernourished adult man – suggestion of a nonpeptidyl pathway. *Am. J. Clin. Nutr.* **1983**, *37*, 93–98.

38. Vijayasarathy, C.; Khan-Siddiqui, L.; Murthy, S. N.; Bamji, M. S. Rise in plasma trimethyllysine levels in humans after oral lysine load. *Am. J. Clin. Nutr.* **1987**, *46*, 772–777.

39. McNeil, J. B.; Flynn, J.; Tsao, N.; Monschau, N.; Stahmann, K. P.; Haynes, R. H.; McIntosh, E. M.; Pearlman, R. E. Glycine metabolism in Candida albicans: characterization of the serine hydroxymethyltransferase (SHM1, SHM2) and threonine aldolase (GLY1) genes. *Yeast* **2000**, *16*, 167–175.

40. Schirch, L.; Peterson, D. Purification and properties of mitochondrial serine hydroxymethyltransferas. *J. Biol. Chem.* **1980**, *255*, 7801–7806.

41. Ogawa, H.; Gomi, T.; Fujioka, M. Serine hydroxymethyltransferase and threonine aldolase: are they identical? *Int. J. Biochem. Cell Biol.* **2000**, *32*, 289–301.

42. Constestabile, R.; Paiardini, A.; Pascarella, S.; di Salvo, M. L. ; D'Aguanno, S. ; Bossa, F. L-Threonine aldolase, serine hydroxymethyltransferase and fungal alanine racemase. A subgroup of strictly related enzymes specialized for different functions. *Eur. J. Biochem.* **2001**, *268*, 6508–6525.

43. Hulse, J. D.; Henderson, L. M. Carnitine biosynthesis. Purification of 4-*N*'-trimethylaminobutyraldehyde dehydrogenase from beef liver. *J. Biol. Chem.* **1980**, *255*, 1146–1151.

44. Vaz, F. M.; Fouchier, S. W.; Ofman, R. ; Sommer, M.; Wanders, R. J. A. Molecular and biochemical characterization of rat γ-trimethylaminobutyraldehyde dehydrogenase and evidence for the involvement of human aldehyde dehydrogenase 9 in carnitine biosynthesis. *J. Biol. Chem.* **2000**, *275*, 7390–7394.

45. Hassan, M.; Okada, M.; Ichiyanagi, T.; Mori, N. 4-*N*-Trimethylaminobutyraldehyde dehydrogenase: purification and characterization of an enzyme from *Pseudomonas* sp. 13CM. *Biosci. Biotechnol. Biochem.* **2008**, *72*, 155–162.

46. Lin, S. W.; Chen, J. C.; Hsu, L. C.; Hsieh, C. L.; Yoshida, A. Human γ-aminobutyraldehyde dehydrogenase (ALDH9): cDNA sequence, genomic organization, polymorphism, chromosomal localization, and tissue expression. *Genomics* **1996**, *34*, 376–380.

47. Abe, T.; Takada, K.; Ohkawa, K.; Matsuda, M. Purification and characterization of a rat brain aldehyde dehydrogenase able to metabolize γ-aminobutyraldehyde to γ-aminobutyric acid. *Biochem. J.* **1990**, *269*, 25–29.

48. Kikonyogo, A.; Pietruszko, R. Aldehyde dehydrogenase from adult human brain that dehydrogenates γ-aminobutyraldehyde: purification, characterization, cloning and distribution. *Biochem. J.* **1996**, *316*, 317–324.

49. Vaz, F. M.; van Gool, S.; Ofman, R.; Ijlst, L.; Wanders, R. J. Carnitine Biosynthesis: Identification of the cDNA Encoding Human γ-Butyrobetaine Hydroxylase. *Biochem. Biophys. Res. Commun.* **1998**, *250*, 506–510.

50. Rigault, C.; Le Borgne, F.; Demarquoy, J. Genomic structure, alternative maturation and tissue expression of the human BBOX1 gene. *Biochim. Biophys. Acta* **2006**, *1761*, 1469–1481.

51. Lindstedt, G.; Lindstedt, S.; Nordin, I. γ-Butyrobetaine hydroxylase in human kidney. *Scand. J. Clin. Lab. Invest.* **1982**, *42*, 477–485.

52. Lindstedt, G.; Lindstedt, S.; Olander, B.; Tofft, M. α-ketoglutarate and hydroxylation of γ-butyrobetaine. *Biochim. Biophys. Acta* **1968**, *158*, 503–505.

53. Lindstedt, G.; Lindstedt, S. Cofactor requirements of γ-butyrobetaine hydroxylase from rat liver. *J. Biol. Chem.* **1970**, *245*, 4178–4186.

54. Lindstedt, G.; Lindstedt S. On the biosynthesis and degradation of carnitine. *Biochem. Biophys. Res. Commun.* **1961**, *6*, 319–323.

55. Englard, S.; Blanchard, J. S.; Midelfort, C. F. γ-Butyrobetaine hydroxylase: stereochemical course of the hydroxylation reaction. *Biochemistry* **1985**, *24*, 1110–1116.

56. Lindstedt, G.; Lindstedt, S.; Tofft, S. γ-Butyrobetaine hydroxylase from *Pseudomonas* sp AK 1. *Biochemistry* **1970**, *9*, 4336–4342.

57. Lindstedt, G. Hydroxylation of γ-butyrobetaine to carnitine in rat liver. *Biochemistry* **1967**, *6*, 1271–1282.

58. Paul, H. S.; Sekas, G.; Adibi, S. A. Carnitine biosynthesis in hepatic peroxisomes. Demonstration of γ-butyrobetaine hydroxylase activity. *Eur. J. Chem.* **1992**, *203*, 599–605.

59. Galland, S.; Leborgne, F.; Guyonnet, D.; Clouet, P.; Demarquoy, J. Purification and characterization of the rat liver γ-butyrobetaine hydroxylase. *Mol. Cell. Biochem.* **1998**, *178*, 163–168.

60. Kondo, A.; Blanchard, J. S.; Englard, S. Purification and properties of calf liver γ-butyrobetaine hydroxylase. *Arch. Biochem. Biophys.* **1981**, *212*, 338–346.

61. Dunn. W. A.; Rettura, G.; Seifter, E.; Englard, S. Carnitine biosynthesis from γ-butyrobetaine and from exogenous protein-bound 6-*N*-trimethyl-L-lysine by the perfused guinea pig liver. *J. Biol. Chem.* **1984**, *259*, 10764–10770.

62. Simkhovich, B. Z.; Shutenko, Z. V.; Meirena, D. V.; Khagi, K. B.; Mezapuķe, R. J.; Molodchina, T. N.; Kalviņs, I. J.; Lukevics, E.. 3-(2,2,2-Trimethylhydrazinium) Propionate (THP) - a novel gamma-butyrobetaine hydroxylase inhibitor with cardioprotective properties. *Biochem. Pharmacol.* **1988**, *37*, 195–202.

63. Sesti, C. Simkhovich, B. Z.; Kalvinsh, I. ; Kloner, R. A. Mildronate, a novel fatty acid oxidation inhibitor and antianginal agent, reduces myocardial infarct size without affecting hemodynamics. *J. Cardiovasc. Pharmacol.* **2006**, *47*, 493–499.

64. Liepinsh, E.; Vilskersts, R.; Loca, D.; Kirjanova, O.; Pugovichs, O.; Kalvinsh, I.; Dambrova, M. Mildronate, an inhibitor of carnitine biosynthesis, induces an increase in gamma-

butyrobetaine contents and cardioprotection in isolated rat heart infarction. *J. Cardiovasc. Pharmacol.* **2006**, *48*, 314–319.

65. Hayashi, Y.; Kirimoto, T.; Asaka, N.; Nakano, M.; Tajima, K.; Miyake, H.; Matsuura, N. Beneficial effects of MET-88, a γ-butyrobetaine hydroxylase inhibitor in rats with heart failure following myocardial infarction. *Eur. J. Pharmacol.* **2000**, *395*, 217–224.
66. Sjakste, N.; Gutcaits, A.; Kalvinsh, I. Mildronate: an antiischemic drug for neurological indications. *CNS Drug Rev.* **2005**, *11*, 151–161.
67. Pupurea, J.; Isajevsb, S.; Skaparec, E.; Rumaksa, J.; Svirskisa, S.; Svirinab, D.; Kalvinshc, I.; Klusaa, V. Neuroprotective Properties of Mildronate, a Mitochondria-Targeted Small Molecule. *Neurosci. Lett.* **2010**, *470*, 100–105.
68. Liepinsh, E.; Skapare, E.; Svalbe, B.; Makrecka, M.; Cirule, H.; Dambrova, M. Anti-diabetic effects of mildronate alone or in combination with metformin in obese Zucker rats. *Eur. J. Pharmacol.* **2011**, *658*, 277–283.
69. Zvejniece, L.; Svalbe, B.; Makrecka, M.; Liepinsh, E.; Kalvinsh, I.; Dambrova, M. Mildronate exerts acute anticonvulsant and antihypnotic effects *Behav. Pharmacol.* **2010**, *21*, 548–555.
70. Dambrova, M.; Liepinsh, E.; Kalvinsh, I. Mildronate: Cardioprotective action through carnitine-lowering effect. *Trends Cardiovasc. Med.* **2002**, *12*, 275–279.
71. Georges, B.; Le Borgne, F.; Galland, S. ; Isoir, M. ; Ecosse, D. ; Grand-Jean, F. ; Demarquoy, J. Carnitine transport into musclar cells. Inhibition of transport and cell growth by Mildronate. *Biochem. Pharmacol.* **2000**, *59*, 1357–1363.
72. Oppedisano, F.; Fanello, D.; Calvani, M.; Indiveri, C. Interaction of Mildronate with the mitochondrial carnitine/acylcarnitine transport protein. *J. Biochem. Mol. Toxicol.* **2008**, *22*, 8–14.
73. Jaudzems, K.; Kuka, J.; Gutsaits, A.; Zinovjevs, K.; Kalvinsh, I.; Liepinsh, E.; Liepinsh, E.; Dambrova, M. Inhibition of carnitine acetyltransferase by mildronate, a regulator of energy metabolism. *J. Enzyme Inhib. Med. Chem.* **2009**, *24*, 1269–1275.
74. Liepinsh, E.; Vilskersts, R.; Skapare, E.; Svalbe, B.; Kuka, J.; Cirule, H.; Pugovics, O.; Kalvinsh, I.; Dambrova, M. Mildronate decreases carnitine availability and up-regulates glucose uptake and related gene expression in the mouse heart. *Life Sci.* **2008**, *83*, 613–619.
75. Asaka, N.; Muranaka, Y.; Kirimoto, T.; Miyake, H. Cardioprotective profile of MET-88, an inhibitor of carnitine synthesis and insulin during hypoxia in isolated perfused rat hearts. *Fundam. Clin. Pharmacol.* **1998**, *12*, 158–163.
76. Spaniol, M.; Brooks, H.; Auer, L.; Zimmermann, A.; Solioz, M.; Stieger, B.; Krähenbühl, S. Development and characterization of an animal model of carnitine deficiency. *Eur. J. Biochem.* **2001**, *268*, 1876–1887.
77. Wehbie, R. S.; Punekar, N. S.; Lardy, H. A. Rat liver γ-butyrobetaine hydroxylase catalyzed reaction : influence of potassium, substrates, and substrate analogues on hydroxylation and decarboxylation. *Biochemistry* **1988**, *27*, 2222–2228.
78. Nelson, P. J.; Pruitt, R. E.; Henderson, L. L. ; Jenness, R. ; Henderson, L. M. Effect of ascorbic acid deficiency on the *in vivo* synthesis of carnitine. *Biochim. Biophys. Acta* **1981**, *672*, 123–127.
79. Rebouche, C. J. Ascorbic acid and carnitine biosynthesis. *Am. J. Clin. Nutr.* **1991**, *54*, 1147S–1152S.
80. Furusawa, H.; Sato, Y.; Tanaka, Y.; Inai, Y.; Amano, A.; Iwama, M.; Kondo, Y.; Handa, S.; Murata, A.; Nishikimi, M.; Goto, S.; Maruyama, N.; Takahashi, R.; Ishigami, A. Vitamin C is not essential for carnitine biosynthesis *in vivo*: verification in vitamin C-depleted senescence marker protein-30/gluconolactonase knockout mice. *Biol. Pharm. Bull.* **2008**, *31*, 1673–1679.
81. McDonough, M. A. ; Loenarz, C.; Chowdhury, R.; Clifton, I. J.; Schofield, C. J. Structural studies on human 2-oxoglutarate dependent oxygenases. *Curr. Opin. Struct. Biol.* **2010**, *20*, 659–672.

82. Holme, E.; Lindstedt, S.; Nordin, I. Uncoupling in the γ-butyrobetaine hydroxylase reaction by D- and L-carnitine. *Biochem. Biophys. Res. Commun.* **1982**, *107*, 518–524.

83. Seim, H.; Löster, H.; Strack, E. Kataboler carnitinstoffwechsel. Reaktionsprodukte der carnitin-decarboxylase und der carnitin-dehydrogenase in vivo. *Hoppe-Seyler's Z. Physiol. Chem.* **1980**, *361*, 1427–1435.

84. Tars, K.; Rumnieks, J.; Zeltins, A.; Kazaks, A.; Kotelovica, S.; Leonciks, A.; Saripo, J.; Viksna, A.; Kuka, J.; Liepinsh, E.; Dambrova, M. Crystal structure of human gamma-butyrobetaine hydroxylase. *Biochem. Biophys. Res. Commun.* **2010**, *298*, 634–639.

85. Ng, S. S.; Kavanagh, K. L.; McDonough, M. A.; Butler, D. Pilka, E. S.; Lienard, B. M. R.; Bray, J. E.; Savitsky, P.; Gileadi, O.; von Delft, F.; Rose, N. R.; Offer, J.; Scheinost, J. C.; Borowski, T.; Sundstrom, M. Schofield, C. J.; Oppermann, U. Crystal structures of histone demethylase JMJD2A reveal basis for substrate specificity. *Nature* **2007**, *448*, 87–92.

86. Hopkinson, R. J.; Hamed, R. B.; Rose, N. R.; Claridge, T. D. W.; Schofield, C. J. Monitoring the activity of 2-oxoglutarate dependent histone demethylases by NMR spectroscopy: direct observation of formaldehyde. *ChemBioChem* **2010**, *11*, 506–510.

87. Stevens, T. S.; Creighton, E. M.; Gordon, A. B.; MacNicol, M. CCCCXXIII. – Degradation of quaternary ammonium salt. Part I. *J. Chem. Soc.* **1928**, 3193–3197.

88. Vanecko, J. A.; Hayley, W.; West, F.G. Recent advances in the Stevens rearrangement of ammonium ylides. *Tetrahedron* **2006**, *62*, 1043–1062.

89. Vilskersts, R.; Liepinsh, E.; Kuka, J.; Cirule, H.; Veveris, M.; Kalvinsh, I.; Dambrova, M. Myocardial infarct size-limiting and anti-arrhythmic effects of mildronate orotate in the rat heart. *Cardiovasc. Drugs Ther.* **2009**, *23*, 281–288.

90. Stonans, I.; Kalvins, I.; Vilskersts, R.; Liepins, E.; Dambrova, M. Medical use of 3-(2,2,2-trimethylhydrazinism)propionate orotate. PCT. Int. Appl. WO 2009074498, **2009**.

91. Munsch, C.; Williams, J. F.; Rosenfeldt, F. L. The impaired tolerance of the recently infarcted rat heart to cardioplegic arrest: The protective effect of orotic acid. *J. Mol. Cell. Cardiol.* **1989**, *21*, 751–754.

92. Liepinsh, E.; Skapare, E.; Svalbe, B.; Makrecka, M.; Cirule, H.; Dambrova, M. Anti-diabetic effects of mildronate alone or in combination with metformin in obese Zucker rats. *Eur. J. Pharmacol.* **2011**, *658*, 277–283.

93. Bailey, C. J.; Turner, R. C. Metformin. *N. Engl. J. Med.* **1996**, *334*, 574–579.

94. Dang, L.; White, D. W.; Gross, S.; Bennett, B. D.; Bittinger, M. A.; Driggers, E. M.; Fantin, V. R.; Jang, H. G.; Jin, S.; Keenan, M. C.; Marks, K. M.; Prins, R. M.; Ward, P. S.; Yen, K. E.; Liau, L. M.; Rabinowitz, J. D.; Cantley, L. C.; Thompson, C. B.; Vander Heiden, M. G.; Su, S. M. Cancer-associated IDH1 mutations produce 2-hydroxyglutarate. *Nature* **2009**, *462*, 739–744.

95. Reitman, Z. J.; Yan, H. Isocitrate dehydrogenase 1 and 2 mutations in cancer: alterations at a crossroads of cellular metabolism. *J. Natl. Cancer Inst.* **2010**, *102*, 932–941.

96. Xu, W.; Yang, H.; Liu, Y.; Yang, Y.; Wang, P.; Kim, S.-H.; Ito, S.; Yang, C.; Wang, P.; Xiao, M.-T.; Liu, L.-X.; Jiang, W.-Q.; Liu, J.; Zhang, J.-Y.; Wang, B.; Frye, S.; Zhang, Y.; Xu, Y.-H.; Lei, Q.-Y.; Guan, K.-L.; Zhao, S.-M.; Xiong, Y. Oncometabolite 2-hydroxyglutarate is a competitive inhibitor of α-ketoglutarate-dependent dioxygenases. *Cancer Cell* **2011**, *19*, 17–30.

97. Dawany, N. B.; Dampier, W. N.; Tozeren, A. Large-scale integration of microarray data reveals genes and pathways common to multiple cancer types. *Int. J. Cancer* **2011**, *128*, 2881–2891.

98. Riddell, J. A.; Hageman, H. A.; J'Anthony, C. M.; Hubbard, W. L. Retardation of plant growth by a new group of chemicals. *Science* **1962**, *136*, 391.

99. Cabral, R.; Hasegawa, R.; Hoshiya, T.; Hakoi, K.; Ogiso, T.; Boonyaphiphat, P.; Shirai, T.; Ito, N. Carcinogenic potential of some pesticides in a mediumterm multi-organ bioassay in rats. *Int. J. Cancer* **1993**, *54*, 489–493.

100. Brown, R. G. S.; Kawaide, H.; Yang, Y.-Y.; Rademacher, W.; Kamiya, Y. Daminozide and prohexadione have similar modes of action as inhibitors of the late stages of gibberellin metabolism. *Physiol. Plant* **1997**, *101*, 309–313.

101. Dalvit, C.; Fagerness, P. E.; Hadden, D. T. A.; Sarver, R. W.; Stockman, B. J. Fluorine-NMR experiments for high-throughput screening: theoretical aspects, practical considerations, and range of applicability. *J. Am. Chem. Soc.* **2003**, *125*, 7696–7703

102. Tengel, T.; Fex, T.; Emtenäs, H.; Almqvist, F.; Sethson, I.; Kihlberg, J. Use of ^{19}F NMR spectroscopy to screen chemical libraries for ligands that bind to proteins. *Org. Biomol. Chem.* **2004**, *2*, 725–731.

103. Kovacsa, H.; Moskaua, D.; Spraul, M. Cryogenically cooled probes – a leap in NMR technology. *Prog. Nucl. Magn. Reson. Spectrosc.* **2005**, *46*, 131–155.

104. Dalvit, C.; Mongelli, N.; Papeo, G.; Giordano, P.; Veronesi, M.; Moskau, D,; Kümmerle, R. Sensitivity improvement in ^{19}F NMR-based screening experiments: theoretical considerations and experimental applications. *J. Am. Chem. Soc.* **2005**, *127*, 13380–13385.

105. Gorres, K. L.; Raines, R. T. Direct and continuous assay for prolyl 4-hydroxylase. *Anal. Biochem.* **2009**, *386*, 181–185.

106. Valegård, K.; Terwisscha van Scheltinga, A. C.; Dubus, A.; Ranghino, G.; Öster, L. M.; Hajdu, J.; Andersson, I. The structural basis of cephalosporin formation in a mononuclear ferrous enzyme. *Nat. Struct. Mol. Biol.* **2004**, *11*, 95–101.

107. Zhou, J.; Kelly, W. L.; Bachmann, B. O.; Gunsior, M.; Townsend, C. A.; Solomon, E. I. Spectroscopic studies of substrate interactions with clavaminate synthase 2, a multifunctional α-KG-dependent non-heme iron enzyme: correlation with mechanisms and reactivities. *J. Am. Chem. Soc.* **2001**, *123*, 7388–7392

108. Yang, X.-F.; Ye, S.-J.; Bai, Q.; Wang, X.-Q. A fluorescein-based fluorogenic probe for fluoride ion based on the fluoride-induced cleavage of *tert*-butyldimethylsilyl ether. *J. Fluoresc.* **2007**, *17*, 81–87.

3. Investigating protein-ligand interactions by NMR[†]

3.1 Introduction

3.1.1 The human hypoxia signalling pathway

In humans and other animals, the hypoxia inducible factor (HIF) is a heterodimeric transcriptional complex involved in the response to changes in cellular oxygen availability.[1–5] There are three human isoforms of HIFα. HIF1α and HIF2α are closely related at the amino acid sequence level and may have related but different roles in oxygen sensing,[6] whereas HIF3α is more distantly related.[7] HIF1α is ubiquitously expressed but HIF2α and HIF3α have a more restricted expression pattern.[1–7]

The HIF isoforms are conserved amongst mammalian species and exist as α/β-heterodimers.[8] The HIF β-subunit (HIFβ) is a constitutive nuclear protein but the HIF α-subunit (HIFα) is found in both the cytoplasm and the nucleus.[9–11] HIFα is constantly expressed and its concentration in cells is highly regulated by oxygen.[9,11] In contrast, HIFβ degradation is not oxygen dependent.[10,11]

In hypoxia, HIFα binds to HIFβ and transcriptional co-activating protein(s), such as p300, in the nucleus and triggers subsequent hypoxic responses (*e.g.* growth of new blood vessels and stimulation of red blood cell production, etc).[10,12–14] In normoxia, however, the HIFα subunit is rapidly degraded by the ubiquitin-proteasome pathway.[8,9,11]

The activities of HIF in cells are regulated by factors including the binding between HIFα and its transcriptional co-activators and the availability of HIFα, both of which

---

[†] *The work in this chapter is conducted in collaboration with Dr Emily Flashman, Dr Lars Hillringhaus, Marina Demetriades, Dr Adam P. Hardy, Hanna Tarhonskaya, Andrea Szöllössi, Tristan J. Smart, Dr. Grazyna T. Kochan, Dr Kar Kheng Yeoh, Dr Esther C. Y. Woon, Dr Clarisse Lejeune, Dr Luc Henry, Jacob T. Bush, Inga Pfeffer, Dr Alexander I. Sagidullin (Oxford Instruments) and Prof. Babur Z. Chowdhry (Greenwich University).*

E.F., L.H. and M.D. helped produced and purified PHD2. A.P.H. provided FIH. H.T. provided mutant PHD2 enzymes. A.S. provided DAOCS. T.J.S. provided FBXL11. G.T.K. provided BBOX. M.D. and K.K.Y. synthesised BIQ. K.K.Y. synthesised BIQ analogues. E.C.Y.W. synthesised NOG analogues. C.L. synthesised 5-C-8HQ. L.H. synthesised ^{13}C-labelled NOG and ^{13}C-labelled penicillin G. J.T.B. synthesised penicillin N. I.P. performed T_m shift measurements. A.I.S. performed low field NMR measurements. B.Z.C. performed trace metal concentration measurements.

The methods developed in this chapter have been published or applied as described:

1. Leung, I. K. H.; Flashman, E.; Yeoh, K. K.; Schofield, C. J.; Claridge, T. D. W. Using NMR solvent water relaxation to investigate metalloenzyme–ligand binding interactions. J. Med. Chem. 2010, 53, 867–875.

2. Rotili, D.; Altun, M.; Kawamura, A.; Wolf, A.; Fischer, R.; Leung, I. K. H.; Mackeen, M. M.; Tian, Y.-M.; Ratcliffe, P. J.; Mai, A.; Kessler, B. M.; Schofield, C. J. A photoreactive small-molecule probe for 2-oxoglutarate oxygenases. Chem. Biol. 2011, 18, 642–654.

3. Leung, I. K. H.; Demetriades, M.; Hardy, A. P.; Lejeune, C.; Smart, T. J.; Szöllössi, A.; Kawamura, A.; Schofield, C. J.; Claridge, T. D. W. Reporter ligand NMR screening method for 2-oxoglutarate oxygenase inhibitors. J. Med. Chem. 2013, 56, 547–555.

in turn are regulated by HIF hydroxylases (Figure 3-1).[15–17] The HIF hydroxylases belong to the 2OG oxygenase family.[18–21] In humans, there are four HIF hydroxylases. They comprise factor inhibiting HIF (FIH) and three prolyl hydroxylase domain containing protein (PHD) isoforms 1–3.[18–21] The PHDs catalyse the hydroxylation of HIFα at two conserved proline residues and FIH catalyses the hydroxylation of an asparagine residue.[18–21] Among the four HIF hydroxylases, PHD2 has been identified as the most important oxygen sensor in humans. PHD2 reacts unusually slowly with oxygen relative to other human 2OG oxygenases, a property that may be associated with its function as an oxygen sensor.[22]

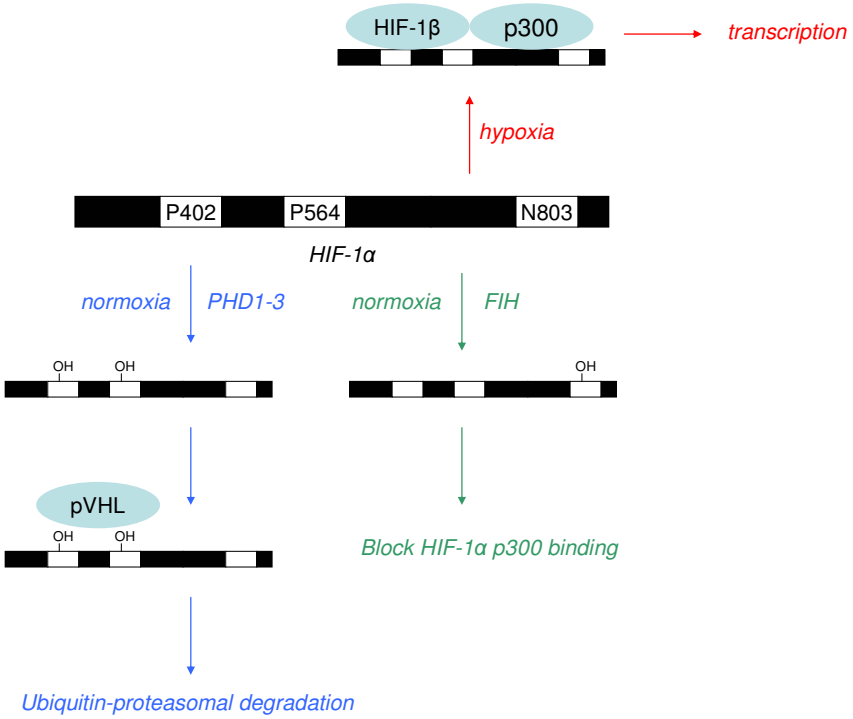

Figure 3-1 The human hypoxia signalling pathway is regulated by HIF hydroxylases.

In normoxia, the PHDs initiate the oxygen dependent degradation of HIFα by catalysing the hydroxylation of two prolyl residues (positions 402 and 564 in human HIF1α).[23,24] These two hydroxylation sites are often termed the *N*-terminal oxygen-dependent degradation domain (HIF1α$_{395\text{-}413}$, NODD) and the *C*-terminal oxygen-dependent degradation domain (HIF1α$_{556\text{-}574}$, CODD) respectvely. The prolyl hydroxylated HIFα is then recognised by the von Hippel-Lindau protein (pVHL), which is a targeting element of E3-ubiquitin ligase.[25] The binding between prolyl hydroxylated HIFα and pVHL triggers subsequent degradation of HIFα by ubiquitin-proteasomes.[8,9,11]

FIH catalyses the oxygen dependent hydroxylation of an asparaginyl residue on the *C*-terminal transactivation domain (CAD) of HIFα (position 803 in HIF1α).[26–29] The hydroxylation of CAD introduces steric constraints on HIFα,[30] and stops its interaction with its transcriptional co-activating protein and, as a result, HIF activity cannot be activated.[31] A schematic representation of this pathway is shown in Figure 3-1.

3.1.2 The HIF hydroxylases as inhibition target

Due to the central role HIF plays in human oxygen homeostasis, the HIF pathway has become an attractive target for therapeutic intervention.[32–35] There are several points on the HIF pathway that are potential targets. In particular, the inhibition of HIF hydroxylases has been shown to be useful for the treatment of diseases including ischemia,[36] inflammation,[36,37] anaemia[38] and cancer.[39–44] Although peer-reviewed data have not yet been published, several PHD inhibitors are currently undergoing clinical trials.[45]

3.1.3 Biophysical methods for 2OG oxygenases

Studies on the inhibition and mechanisms of the HIF hydroxylases (and other 2OG oxygenases) would benefit from efficient binding and screening assays. Several biophysical methods have been applied in order to study ligand (including metal ions, small molecules and other biomolecules) binding to 2OG oxygenases. Methods applied include non-denaturing electrospray ionisation mass spectrometry (ESI-MS; for examples see references 46–50), protein X-ray crystallography (for reviews see references 51 and 52), isothermal titration calorimetry (ITC),[53] surface plasmon resonance (SPR),[54] circular dichroism (CD) spectroscopy,[53] electron paramagnetic resonance (EPR)[55] and protein NMR spectroscopy.[53,56] Whilst many of these techniques can provide detailed information on binding interactions (*e.g.* structure, thermodynamics, kinetics, etc), many are specialist and not suitable for general screening purposes.[57,58] Among these methodologies, non-denaturing ESI-MS is one of the more 'generic' methods, and can be applied as a simple and rapid primary screening tool for 2OG oxygenase inhibitors. However, because non-covalent protein-ligand complexes may not always survive the transition from solution phase to gas phase,[59] the search for alternative, simple and complementary solution-based screening techniques is ongoing.

3.1.4 Ligand-observed competition-based NMR methods

Ligand-observed NMR methods are widely used for the study of protein-ligand interactions (such as screening and binding constant measurement) because they do not require isotopically labelled protein and are relatively quick and sensitive (for reviews see references 60 and 61). There are two main types of ligand-observed NMR binding experiments. One method monitors the bulk ligand that is in exchange with the bound ligand (directly or through NOE-based experiments). Another method monitors a reporter ligand, which is in competition with the ligand-of-interest for the same binding site.

Although widely applied, exchange-based experiments suffer from limited detection ranges of binding affinities (false negatives), unspecific binding (false positives)[62] and, in some cases, complications with binding constant determination.[63,64] Provided the binding site is known and a good reporter ligand is available, competition based methods can be good alternatives. By observing changes in the NMR parameters of a reporter ligand in the presence and absence of the ligand-of-interest, this method can provide qualitative and quantitative site-specific information of both high- and low-affinity ligands. Several nuclei, including proton[65–67] and hetero-nuclei such as phosphorus,[68] fluorine[69] and carbon[70] have been proposed for observation.

3.1.5 Objectives

The objective of the work described in this Chapter was to develop ligand-observed competition based solution NMR methods for the qualitative and quantitative screening and measurement of binders for HIF hydroxylases and other 2OG oxygenases. In Section 3.2, work using 2OG as a reporter is described, and in Section 3.3, the use of water as reporter ligand is described.

3.2 Reporter screening for 2OG oxygenases

3.2.1 Methodology

For the work described in this Section, the HIF hydroxylases PHD2 ($PHD2_{181-426}$; provided by Dr Emily Flashman, Dr Lars Hillringhaus and Marina Demetriades) and FIH (provided by Dr Adam P. Hardy) were chosen as model proteins because of the therapeutic interest in their chemical inhibition. 2OG was chosen as the potential reporter ligand because all 2OG oxygenases utilise 2OG as a co-substrate. In order to

stop turnover of 2OG into succinate *via* uncoupled turnover, the catalytic Fe(II) inside the PHD2 and FIH active sites was substituted by the diamagnetic and non-catalytically active metal ion Zn(II).[48]

Both PHD2-Zn(II) and FIH-Zn(II) form stable complexes with 2OG that saturate at a ~1:1 ratio. Under these conditions, the ^{1}H NMR spectrum is dominated by signals from the protein. The Carr-Purcell-Meiboom-Gill (CPMG) sequence was applied for spectral editing to remove any broad (protein) resonances (Figure 3-2).[71–73] In particular, the recently proposed periodic refocusing of J evolution by coherence transfer (PROJECT) method,[74] which uses an additional $90_{y}°$ pulse at the midpoint of a double spin echo to refocus and suppress J modulation, provides cleaner line shapes and was therefore used in assays described in this Section.

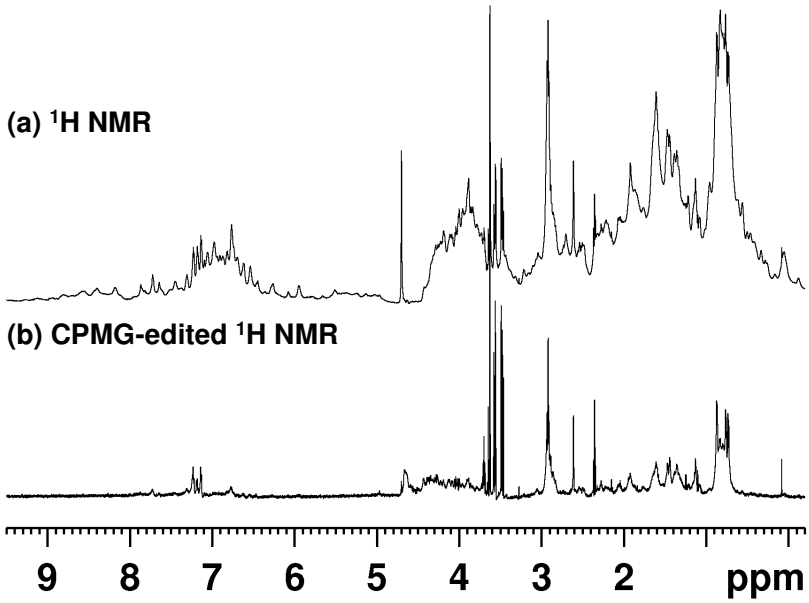

Figure 3-2 The broad protein background is removed in a CPMG-edited ^{1}H experiment with a total echo time of 40 ms. Sample contained 150 µM PHD2, 300 µM Zn(II), 150 µM 2OG, 600 µM bicyclic naphthalenylsulfonyl inhibitor (BNS) and 50 mM Tris-D11 pH 7.5 in D_2O.

The CPMG-editing method also provides a means to distinguish free and bound 2OG. When 2OG is bound to PHD2, significant broadening of the 2OG resonances is observed due to a high transverse relation rate in the bound state, so the resultant CPMG-edited spectrum showed near-complete loss of the 2OG signal intensity (Figure 3-3). In the presence of a competitive binder, however, 2OG is displaced from the binding site, leading to sharpening of the signals and recovery of 2OG signal intensity (Figure 3-3). The simplicity and sensitivity of the experiment makes it a good candidate for a primary screening method for 2OG oxygenases.

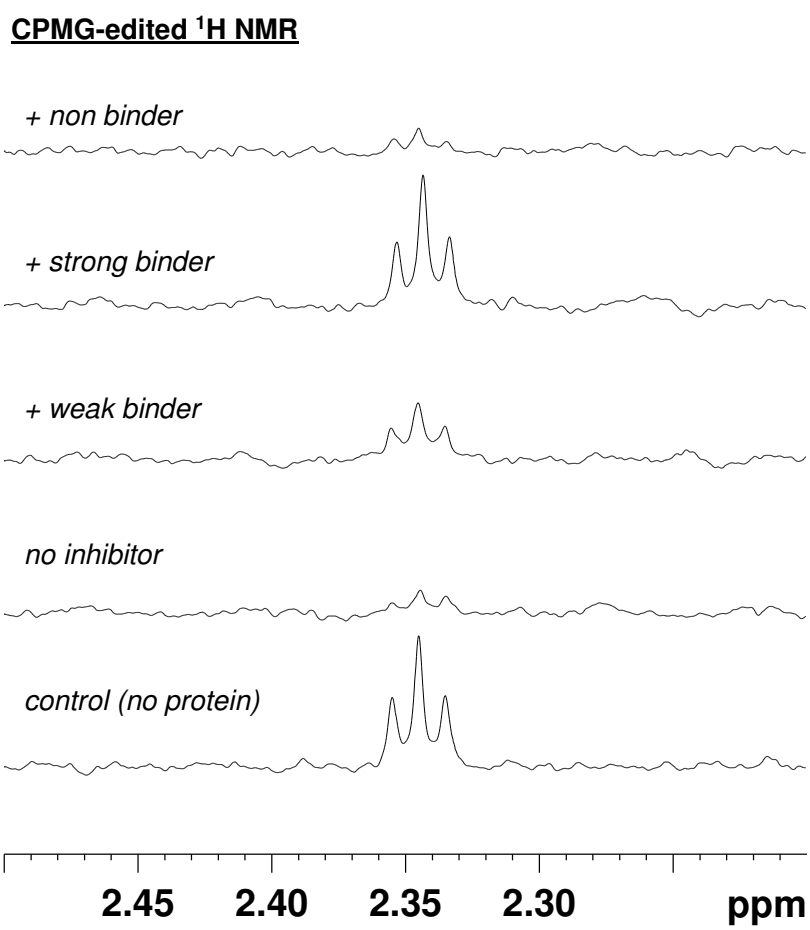

Figure 3-3 2OG displacement monitored by the PROJECT CPMG-edited ^{1}H experiment. The total echo time is 40 ms. Unless otherwise stated, samples contained 10 μM PHD2, 80 μM Zn(II), 10 μM 2OG, 400 μM inhibitor and 50 mM Tris-D11 pH 7.5 in 90% H_2O + 10 D_2O. The C-4 proton resonance of 2OG is monitored. The non-binder is *cis*-aconitate; the strong binder is the bicyclic naphthalenylsulfonyl inhibitor (BNS; see Figure 3-4) and the weak binder is fumarate. See below for further discussion.

3.2.2 Screening

By monitoring the level of 2OG displacement, it is possible to screen and compare the strength of binding for different compounds at a single concentration in an efficient manner. This is demonstrated by work with several 2OG oxygenase inhibitors (Figure 3-4). The inhibitors tested included the broad spectrum 2OG oxygenase inhibitors *N*-oxalylglycine (NOG)[75] and 2,4-pyridine dicarboxylic acid (2,4-PDCA),[76] as well as PHD2 selective inhibitors including the bicyclic isoquinolinyl inhibitor (BIQ; Synthesised by Dr Kar Kheng Yeoh and Marina Demetriades)[77] and the bicyclic naphthalenylsulfonyl inhibitor (BNS).[78] 5-carboxy-8-hydroxyquinoline (5-C-8-HQ; Synthesised by Dr Clarisse Lejeune), an inhibitor of histone demethylases, was also tested.[79] Compounds were screened at a concentration of 400 μM in the presence of 10 μM enzyme and 10 μM 2OG.

The percentage 2OG displacement is defined as:

$$\%\ 2\text{OG displacement} = \frac{I_{2\text{OG}} - I_{2\text{OG}(0)}}{I_{2\text{OG(blank)}} - I_{2\text{OG}(0)}} \times 100\%$$

In which $I_{2\text{OG}}$ stands for the integral of the 2OG signal in the presence of both the inhibitor and the protein, $I_{2\text{OG}(0)}$ stands for the integral of 2OG in the presence of the protein but in the absence of the inhibitor, and $I_{2\text{OG(blank)}}$ is the integral of 2OG in the absence of the protein or inhibitor.

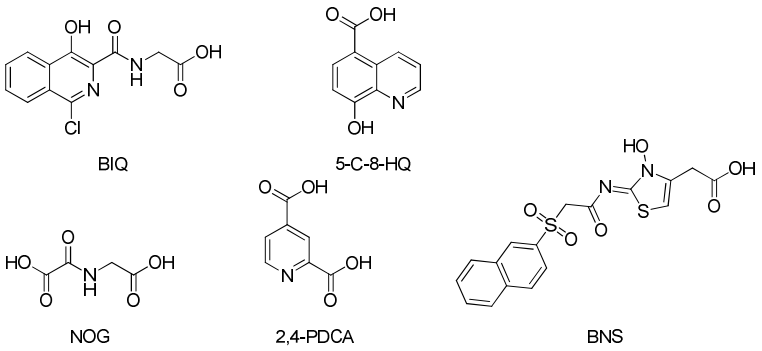

Figure 3-4 2OG oxygenase inhibitors tested in the 2OG displacement study.

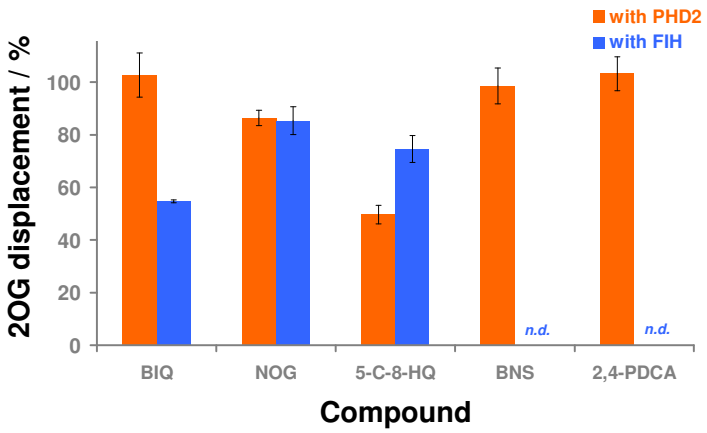

Figure 3-5 Competitive screening experiments using 2OG as reporter ligand. The assay mixture contained 10 μM *apo*-PHD2/FIH, 80 μM Zn(II), 10 μM 2OG, 400 μM inhibitor and 50 mM Tris-D11 pH 7.5 in 10% D_2O and 90% H_2O. Experiments were performed 3 times.

NOG, which is a largely non-selective 2OG oxygenase inhibitor, gave ~85% 2OG displacement for both PHD2 and FIH (Figure 3-5). In contrast, BIQ is a potent and selective PHD2 inhibitor.[77] The results confirm that BIQ is more selective for PHD2 over FIH, as BIQ gave complete 2OG displacement for PHD2 but only ~50% for FIH (Figure 3-5). 5-C-8-HQ, which is a generic inhibitor for histone demethylases,[79] binds relatively weakly to both PHD2 and FIH (~50% and ~75% 2OG displacement with PHD2 and FIH respectively; Figure 3-5). Finally, the assay was also tested with 2,4-

PDCA and BNS on PHD2. Both compounds caused complete 2OG displacement when tested with PHD2 (Figure 3-5), consistent with their previous assignment as potent inhibitors.

3.2.3 Binding constant measurement

Provided the dissociation constant ($K_{D,rep}$) of the reporter ligand (2OG) is known, it is possible to obtain the dissociation constant (K_D), of the inhibitors of interest by titration (see also Chapter 6).[66,80,81] The K_D values of 2OG to PHD2 and FIH used in this study were obtained using the solvent water relaxation method (See Section 3.3), in which the native Fe(II) was replaced by the paramagnetic Mn(II). The binding constants of 2OG to PHD2-Mn(II) (900 nM) and PHD2-Zn(II) (<5 μM obtained by ^{1}H-^{15}N HSQC titration; See Chapter 4) were essentially the same.

The K_D values for the inhibitors tested are summarised in Table 3-1. An example of the titration data is shown in Figure 3-6. The K_D values obtained for NOG with PHD2 and FIH are 3 μM and 4 μM respectively, which are comparable to the reported inhibition constant (K_I) values determined by activity assays (8 μM for PHD2 and 2 μM for FIH).[82] As discussed in the last section, BIQ is a selective inhibitor for PHD2. The K_D obtained for BIQ with PHD2 is 80 nM, which is ~1800 times lower than the value obtained with FIH (140 μM). The K_D values obtained for 5-C-8-HQ are 60 μM and 30 μM with PHD2 and FIH respectively, supporting the result obtained with the single concentration screening.

	Binding to PHD2		Binding to FIH	
Compound	K_D	Reported IC_{50} (or K_D)	K_D	Reported IC_{50} (or K_D)
NOG	3 ± 1 μM	20 μM (3 μM)	4 ± 1 μM	50 μM (2 μM)
BIQ	80 ± 10 nM	70 nM (< 1 μM)	140 ± 15 μM	> 25 μM
5-C-8-HQ	60 ± 5 μM	15 μM	30 ± 10 μM	20 μM
BNS	100 ± 10 nM	20 nM (< 1 μM)	not determined	-
2,4-PDCA	420 ± 130 nM	2 μM	not determined	-
fumarate	200 ± 70 μM	220 μM	no binding	-
L-2HG	> 600 μM	420 μM	360 ± 60 μM	190 μM
D-2HG	> 1000 μM	7300 μM	> 2300 μM	1500 μM

Table 3-1 Binding constants (K_D) measured in this study. 2HG stands for 2-hydroxyglutarate (see Section 3.2.5). The accuracy of the binding constants listed here is based on the assumption that the K_D of 2OG to PHD2 is 900 nM and the K_D of 2OG to FIH is 4 μM.

Titrations were also conducted for BNS and 2,4-PDCA with PHD2. The K_D obtained for BNS is 100 nM. BNS is reported as a potent PHD2 inhibitor (IC_{50} 20 nM),[78] and the low K_D value obtained here confirms that it is a very strong binder to PHD2 and that it binds in the 2OG binding pocket. The K_D obtained for 2,4-PDCA is 420 nM, supporting previous inhibition studies which reported 2,4-PDCA as a weaker inhibitor than BIQ, but more potent than NOG.

3.2.4 HIF hydroxylases and TCA cycle intermediates

The HIF pathway is a potentially important target for the management and treatment of cancers, as hypoxia may promote both tumour growth and apoptosis in different cancer cells.[39–44] There is evidence that TCA cycle intermediates may influence the regulation of HIF hydroxylase activities,[49,83] therefore information about the binding of TCA cycle intermediates to HIF hydroxylases (and other 2OG oxygenases) is of biological significance. Screening was therefore conducted with tricarboxylic acid (TCA) cycle intermediates (except succinyl coenzyme A; Figure 3-7). The results are summarised in Figure 3-8.

At an inhibitor concentration of 400 μM, the only TCA cycle intermediate that shows significant 2OG displacement is fumarate binding to PHD2. This is in agreement with previous inhibition data, which found that fumarate is the only compound among TCA cycle intermediates that inhibits PHD2 in the micromolar range.[49] A titration was also conducted for fumarate with PHD2. The K_D value obtained was 200 μM (Figure 3-9) confirming it is a weak PHD2 binder, however its role may become more significant, for instance, in cancer cells where there are mutations to fumarate hydratase (and therefore cellular fumarate levels are raised).[84–86] Succinate and isocitrate have also been reported as inhibitors of PHD2 with IC_{50} values greater than 10 mM.[49] However, at the tested concentration (40 fold molar excess), no 2OG displacement by these compounds was observed. Under the screening conditions, citrate, isocitrate and malate did not appear to displace 2OG, although previous non-denaturing ESI-MS data suggests that they form binary complexes with PHD2 but not ternary complexes with PHD2 and its peptidyl substrate.[49] The overall evidence suggests that citrate, isocitrate and malate do not bind to the 2OG binding pocket, but may form unspecific binding interactions to PHD2 (possibly to the peptidyl substrate binding site). In agreement with previous inhibition data,[49] none of the TCA cycle intermediates appeared to bind to FIH to any significant extent. It is worth noting that

all binding experiments conducted here were conducted with Zn(II) instead of the native Fe(II), but nonetheless the results are in good agreement with previously published data.

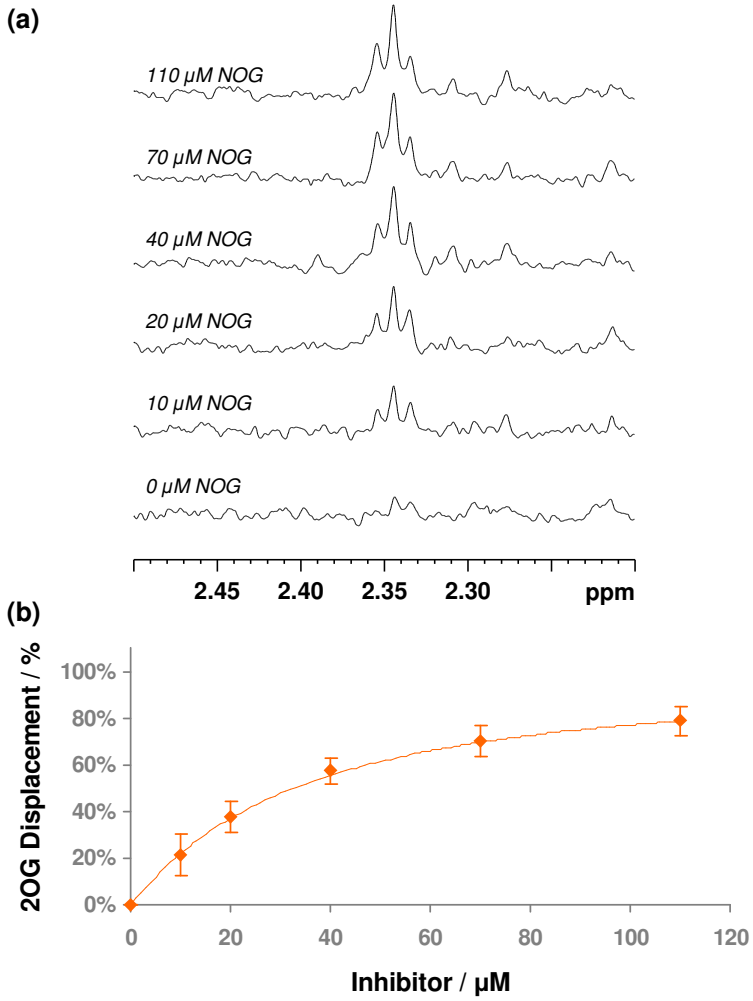

Figure 3-6 (a) Competitive titration experiment monitoring 2OG signal recovery at different inhibitor (NOG) concentrations; (b) Corresponding plot of the NOG titration data. Samples contained 10 µM *apo*-PHD2, 80 µM Zn(II), 10 µM 2OG and 50 mM Tris-D11 pH 7.5 in 90% H_2O and 10% D_2O. Experiments were performed 3 times.

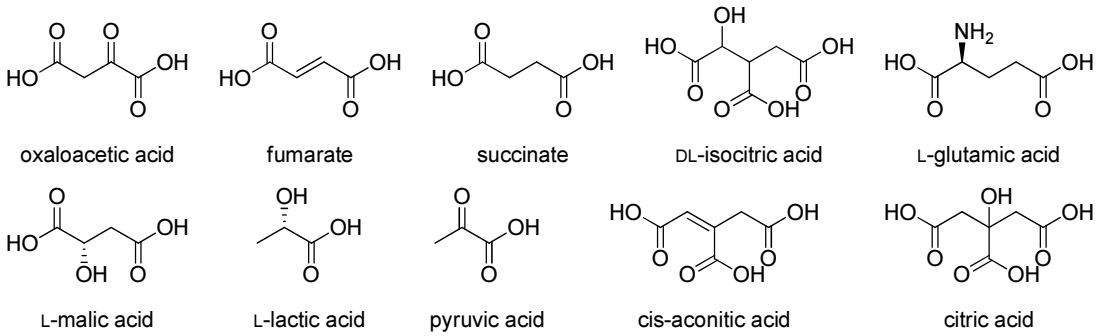

Figure 3-7 Structures of the TCA cycle intermediates used in this study.

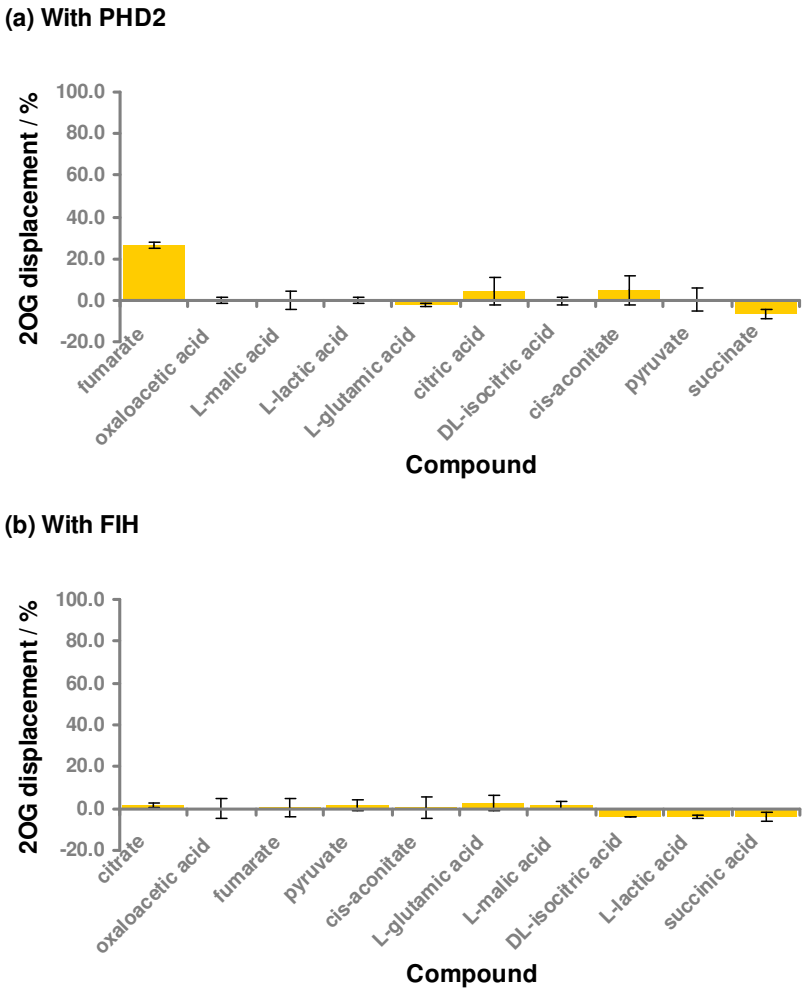

Figure 3-8 Competitive reporter screening experiments using 2OG as reporter ligand. The assay mixture contained 10 µM *apo*-PHD2/FIH, 80 µM Zn(II), 10 µM 2OG, 400 µM TCA cycle intermediate and 50 mM Tris-D11 pH 7.5 in 10% D_2O and 90% H_2O. Error bars indicate standard errors from 3 experiments.

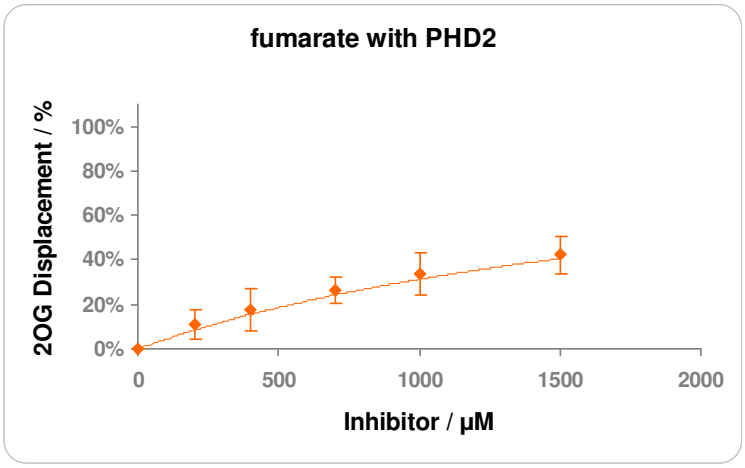

Figure 3-9 Competitive titration to monitor fumarate binding to PHD2. The assay mixture contained 10 µM *apo*-PHD2, 80 µM Zn(II) and 10 µM 2OG in 50 mM Tris-D11 (pH 7.5) 10% D_2O and 90% H_2O. Experiments were performed 3 times. The K_D obtained is 200 ± 70 µM.

3.2.5 HIF hydroxylases and 2-hydroxyglutarate

Mutations to the TCA cycle enzyme isocitrate dehydrogenase (IDH1/2) occur with a high prevalence in certain brain tumours and leukaemia,[87,88] and lead to the accumulation of the D-isomer of 2-hydroxyglutarate (2HG).[89] Mutation of 2HG dehydrogenases also led to neurometabolic disorder by accumulating either D- or L-2HG.[90,91] Previous studies have shown that both D- and L-2HG are weak inhibitors of HIF hydroxylases in cells.[92] A recent report suggests that D-2HG may act as a co-substrate for PHD2 with a Michaelis constant (K_M) of 210 μM *via* PHD2 catalysed oxidation of D-2HG into 2OG.[93]

In order to test whether 2HG binds to PHD2 and FIH, the reporter screening method was applied. Because some batches of commercially available 2HG contain trace amounts of 2OG as impurities (Figure 3-10), all batches were checked by ^{1}H NMR to test for the presence of 2OG. All batches of 2HG used in this study are free of 2OG or contain only negligible amounts (<<1 μM) of 2OG under the experimental conditions.

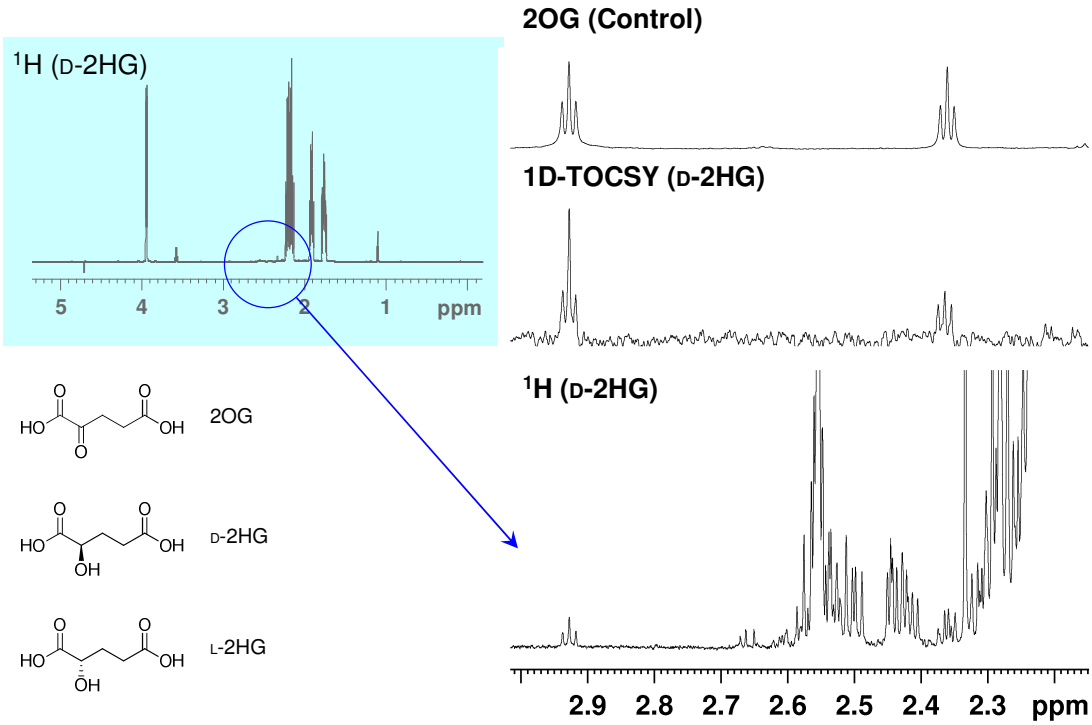

Figure 3-10 Some commercial available 2HG samples contained trace amounts of 2OG. For instance in the batch shown above, there was ~0.02% (by molarity) 2OG compared to 2HG (by integration), which, under the titration conditions as shown in Figure 3-13 and Figure 3-15, was significant (10 mM 2HG would result in 2 μM 2OG, *i.e.* 20% of the reporter ligand concentration). The peaks between 2.4 to 2.6 ppm are also impurities in the 2HG sample.

At 400 µM concentration, L-2HG but not D-2HG was found to bind to FIH (Figure 3-11). L-2HG was also found to bind to PHD2 albeit very weakly. Titrations for D- and L-2HG with PHD2 and FIH suggest that L-2HG is the stronger binder than D-2HG for both enzymes. With PHD2, the K_D obtained for L-2HG is >600 µM (Table 3-1; Figure 3-12) and for D-2HG it is >1 mM (Figure 3-13). With FIH, K_D for L-2HG is 360 µM (Figure 3-14) and for D-2HG it is >2.3 mM (Figure 3-15). Although both 2HG isomers are very weak PHD2 binders (for instance, D-2HG binds to PHD2 at least 30000 times weaker than the PHD2 inhibitor BIQ; Table 3-1), the K_D values obtained here indicate that their binding to HIF hydroxylases may be biologically relevant because reported concentrations of D-2HG in IDH1/2 mutated cells may be as high as 10 mM.

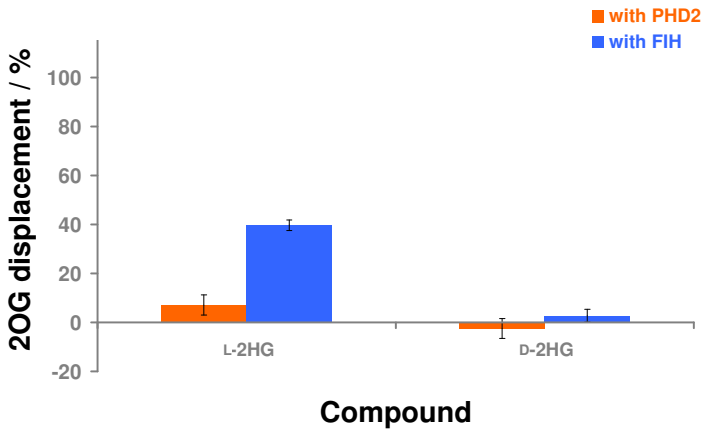

Figure 3-11 Competitive reporter screening experiments using 2OG as reporter ligand. The assay mixture contained 10 µM *apo*-PHD2/FIH, 80 µM Zn(II), 10 µM 2OG, 400 µM 2HG and 50 mM Tris-D11 pH 7.5 in 10% D_2O and 90% H_2O. Experiments were performed 3 times.

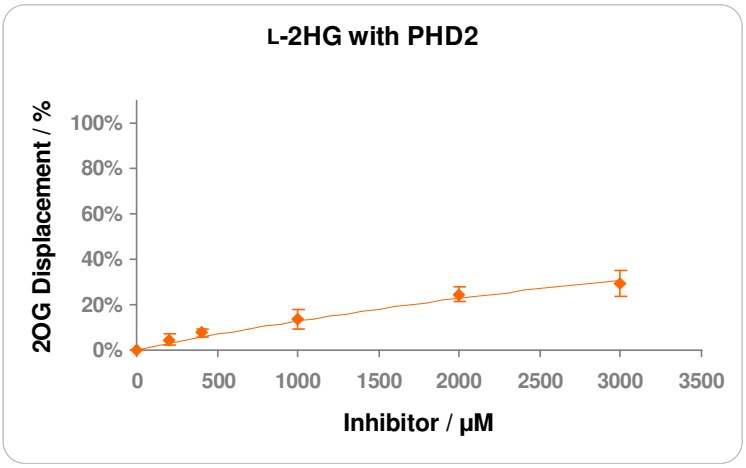

Figure 3-12 Competitive titration to monitor L-2HG binding to PHD2. The assay mixture contained 10 µM *apo*-PHD2, 80 µM Zn(II) and 10 µM 2OG in 50 mM Tris-D11 (pH 7.5) 10% D_2O and 90% H_2O. Experiments were performed 3 times. K_D obtained is >600 µM.

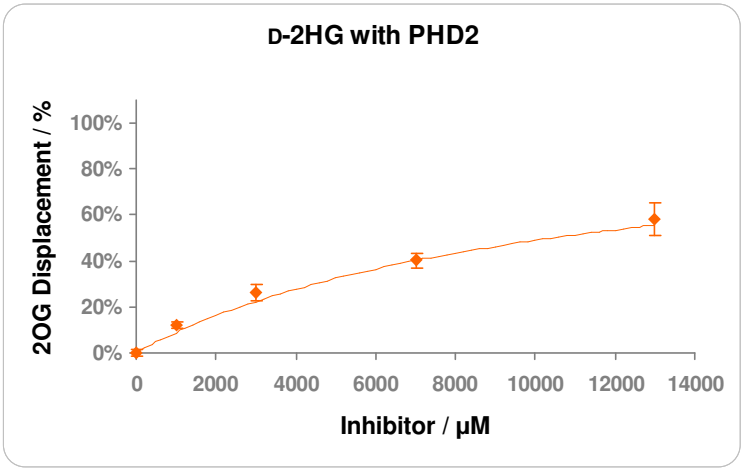

Figure 3-13 Competitive titration to monitor D-2HG binding to PHD2. The assay mixture contained 10 µM *apo*-PHD2, 80 µM Zn(II) and 10 µM 2OG in 50 mM Tris-D11 (pH 7.5) 10% D_2O and 90% H_2O. Experiments were performed 3 times. K_D obtained is >1 mM.

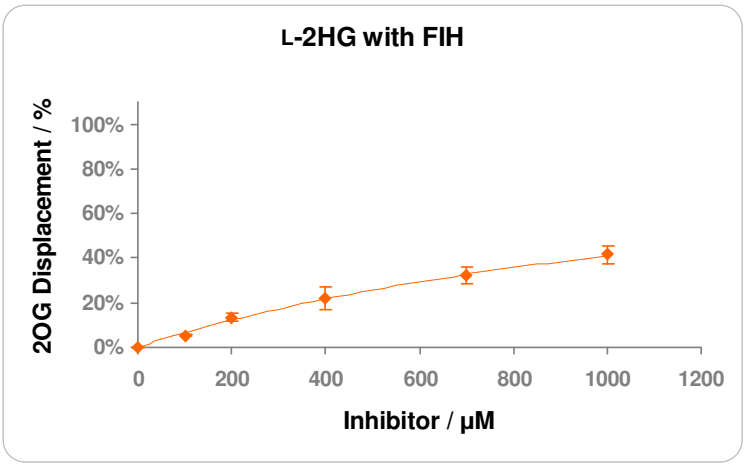

Figure 3-14 Competitive titration to monitor L-2HG binding to FIH. The assay mixture contained 10 µM *apo*-FIH, 80 µM Zn(II) and 10 µM 2OG in 50 mM Tris-D11 (pH 7.5) 10% D_2O and 90% H_2O. Experiments were performed 3 times. K_D obtained is 360 ± 60 µM.

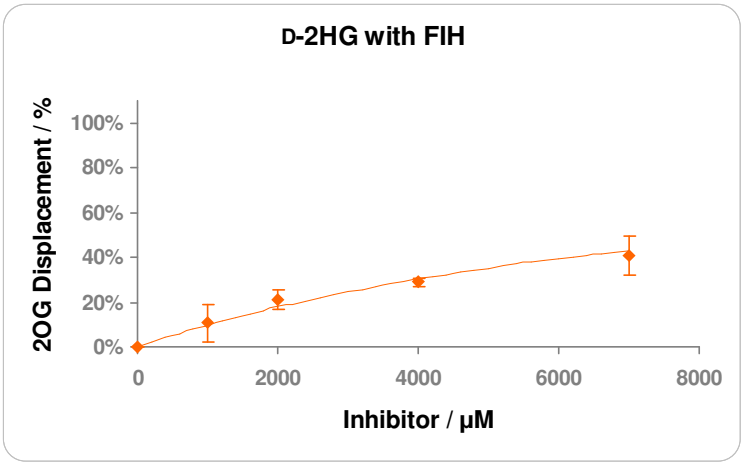

Figure 3-15 Competitive titration to monitor D-2HG binding to FIH. The assay mixture contained 10 µM *apo*-FIH, 80 µM Zn(II) and 10 µM 2OG in 50 mM Tris-D11 (pH 7.5) 10% D_2O and 90% H_2O. Experiments were performed 3 times. K_D obtained is >2.3 mM.

3.2.6 2-Oxoadipate as an alternative co-substrate of PHD2

Previous studies have suggested that analogues of 2OG, such as 2-oxoadipate, can act as alternative co-substrate (in place of 2OG) for some 2OG oxygenases.[94] However, this observation is not universal among the whole 2OG oxygenase family. For example, whilst mammalian collagen prolyl 4-hydroxylase takes 2-oxoadipate as a co-substrate,[94] the small molecule proline 4-hydroxylase found in bacterium *Streptomyces griseoviridus* does not.[95] The understanding of co-substrate selectivity could be biologically interesting, for instance, in situations when 2OG is limiting. 2-Oxoadipate was therefore tested as a binder and substrate of PHD2. Reporter screening experiments suggest 2-oxoadipate competes for the same binding site as 2OG. The K_D value of 2-oxoadipate with PHD2 measured by titration was 40 μM (Figure 3-16), which is in agreement with the value obtained by the water relaxation method (15 μM, see Section 3.3). This is also in agreement with data obtained by a differential scanning fluorimetry thermal shift assay (T_m shift; performed by Inga Pfeffer), which indicates increased stabilisation of PHD2 in the presence of 2-oxoadipate.

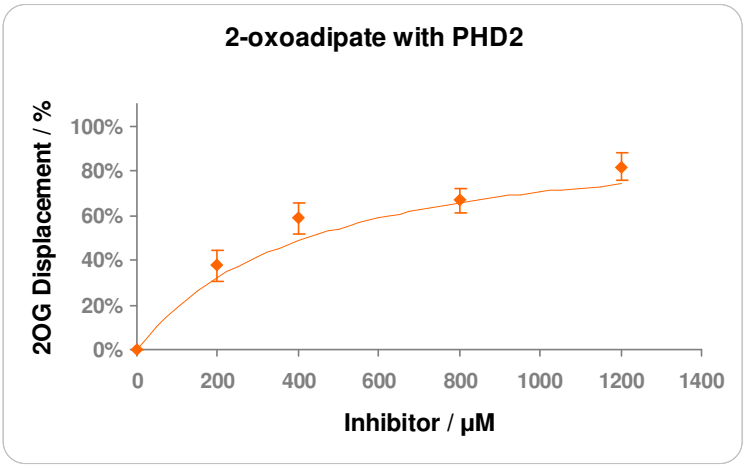

Figure 3-16 Competitive titration to monitor 2-oxoadipate binding to PHD2. The assay mixture contained 10 μM *apo*-PHD2, 80 μM Zn(II) and 10 μM 2OG in 50 mM Tris-D11 (pH 7.5) 10% D_2O and 90% H_2O. Experiments were performed 3 times. K_D obtained is 40 ± 10 μM.

After showing binding to PHD2, 2-oxoadipate was then tested as a PHD2 co-substrate. Indeed, 2-oxoadipate was shown to be a co-substrate for both uncoupled and coupled turnover (Figure 3-17), forming glutaric acid as a co-product (Figure 3-18). However, in the presence of a 1:1 ratio of 2OG, 2OG is taken as the preferential co-substrate, reflecting the differences in their binding constants to PHD2 (2OG <2 μM). Finally, 2-oxoadipate was also tested with FIH and BBOX (see

Chapter 2; BBOX is provided by Dr Grazyna T. Kochan). The data suggests that 2-oxoadipate is a co-substrate for FIH but not BBOX (Figure 3-19), demonstrating that some human 2OG oxygenases have stricter requirements for 2OG than the others.

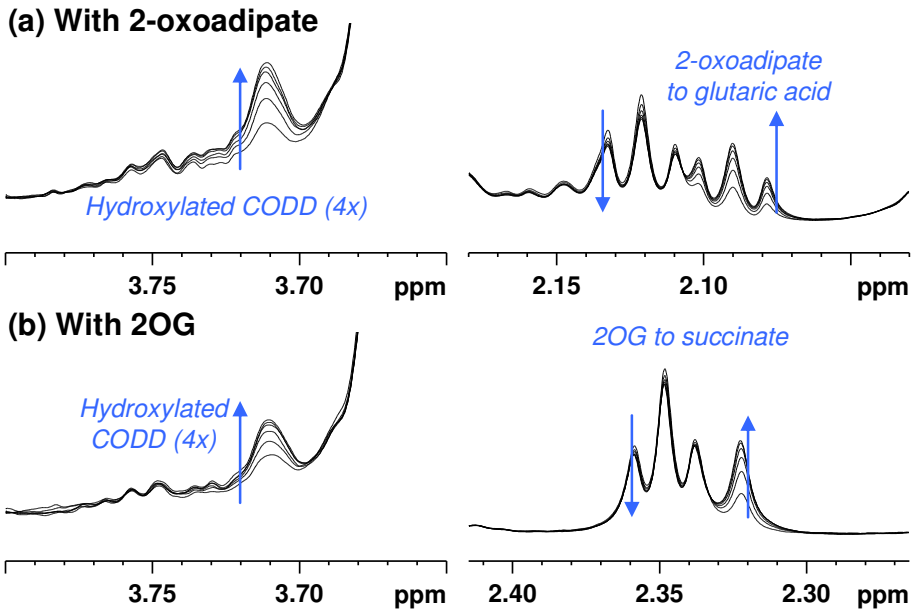

Figure 3-17 ^{1}H NMR experiments demonstrating 2-oxoadipate can act as a co-substrate of PHD2. (a) Reaction mixture contained 10 µM PHD2, 50 µM Fe(II), 500 µM CODD, 750 µM 2-oxoadipate and 4 mM ascorbate, 50 mM Tris-D11 pH 7.5 in 90% H_2O and 10% D_2O. CODD is a 19-mer peptide substrate for PHD2; (b) Same condition except 2-oxoadipate is replaced by 2OG. The first ^{1}H spectrum is recorded 5 minutes 30 seconds after mixing and spectra are shown at 4-minute intervals.

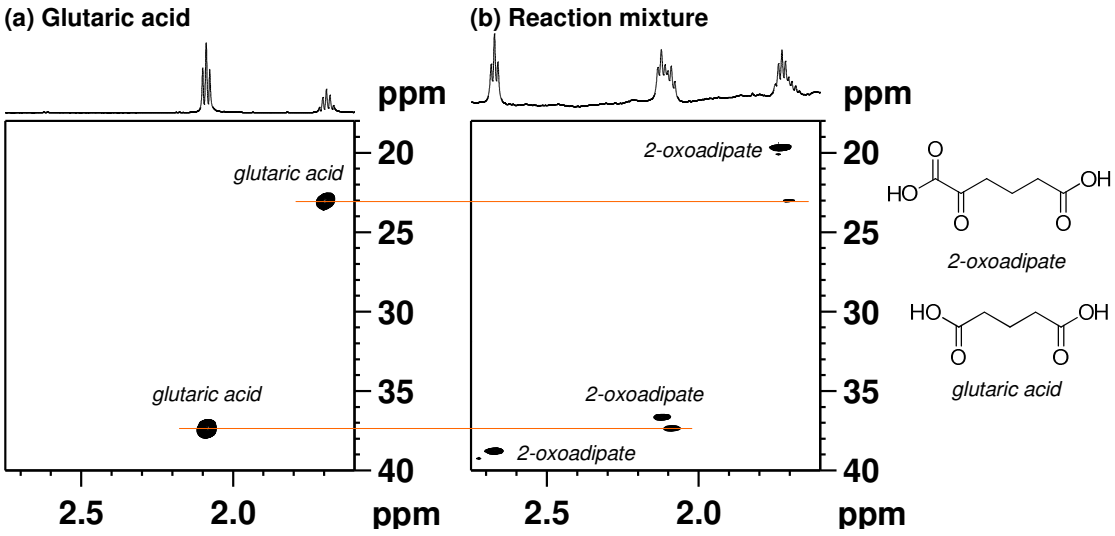

Figure 3-18 ^{1}H-^{13}C HSQC confirming glutaric acid is the product of PHD2 catalysed 2-oxoadipate oxidation reaction. Reaction mixture contained 10 µM PHD2, 50 µM Fe(II), 750 µM 2-oxoadipate and 4 mM ascorbate, 50 mM Tris-D11 pH 7.5 in 90% H_2O and 10% D_2O and is incubated at 298K overnight.

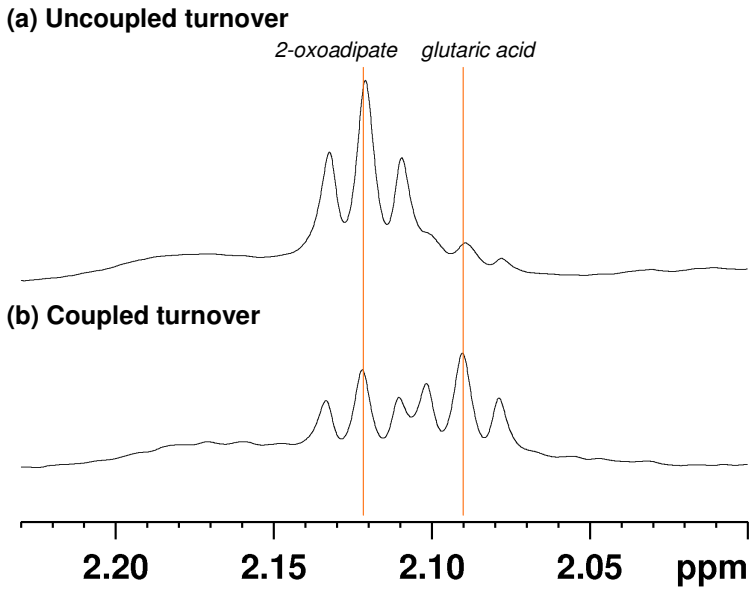

Figure 3-19 2-Oxoadipate is a co-substrate of FIH. (a) The reaction included 10 μM FIH, 50 μM Fe(II), 750 μM 2-oxoadipate and 4 mM ascorbate, 50 mM Tris-D11 pH 7.5 in 90% H_2O and 10% D_2O. The spectrum was recorded 1 hour after mixing; (b) Reaction mixture included 10 μM FIH, 50 μM Fe(II), 500 μM ankyrin peptide (substrate for FIH); 750 μM 2-oxoadipate and 4 mM ascorbate, 50 mM Tris-D11 pH 7.5 in 90% H_2O and 10% D_2O. The spectrum is recorded 5 minutes after sample mixing. The corresponding MALDI experiment (performed by Dr Adam P. Hardy) shows a mass shift of +16 indicating hydroxylation of the ankyrin peptide substrate (peptide only: 2161.74; reaction mixture with 2OG as co-substrate: 2178.56; reaction mixture with 2-oxoadipate as co-substrate: 2178.44).

3.2.7 Hydroxylated CODD

The 19-mer HIF peptide CODD (HIF1$\alpha_{556–574}$) is a substrate of PHD2. Previous work suggested that hydroxylated CODD (hyCODD) is a weak inhibitor of PHD2.[96] To investigate this potential feedback mechanism, hyCODD was subjected to displacement analysis.

Indeed, hyCODD was found to displace 2OG under standard screening conditions (10 μM PHD2, 80 μM Zn(II), 10 μM 2OG and 400 μM peptide). Under the same conditions, CODD does not displace 2OG (Figure 3-20). Although an exact K_D value could not be obtained by titration owing to the limited solubility of hyCODD at high concentration, a K_D value of ~50 μM was estimated for hyCODD with PHD2-Zn(II) based on the single point measurement. This value is comparable to the value obtained for CODD with PHD2-Mn(II) (~15 μM; See Section 3.3). This is in agreement with protein NMR studies, which suggested CODD and hyCODD bind to PHD2-Zn(II) with similar affinity (see Chapter 4). These observations suggest a new feedback mechanism, in which hyCODD not only competes with CODD for the peptidyl substrate binding site, but also competes with 2OG in the 2OG binding site,

and therefore reducing uncoupled turnover, potentially leading to oxidative damage (See also Chapter 4).

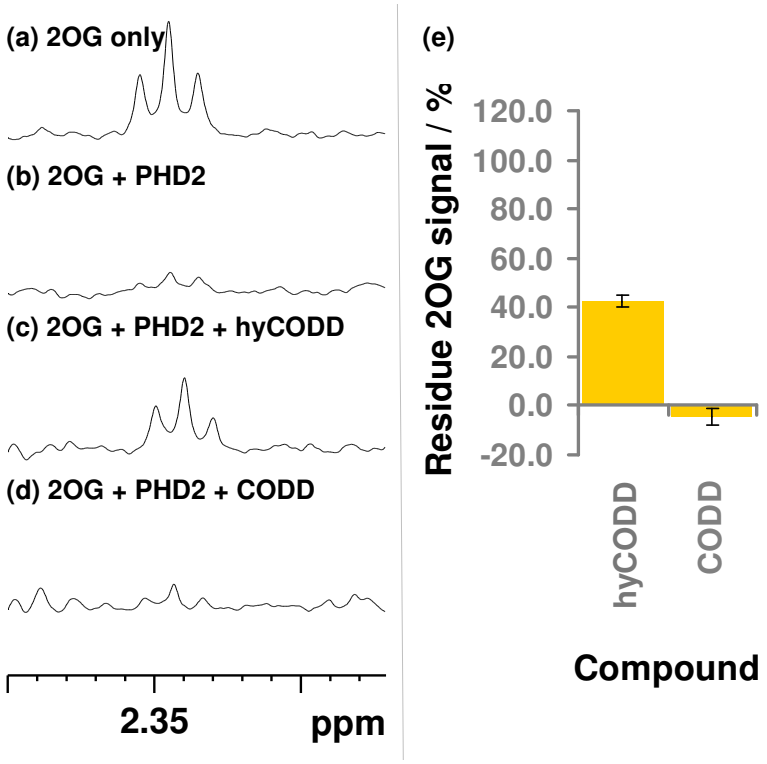

Figure 3-20 CPMG reporter displacement experiments showing hyCODD competes against 2OG for binding to PHD2. (a) 10 μM 2OG (control); (b) 10 μM PHD2, 80 μM Zn(II) and 10 μM 2OG (control); (c) 10 μM PHD2, 80 μM Zn(II), 10 μM 2OG and 400 μM hyCODD; (d) 10 μM PHD2, 80 μM Zn(II), 10 μM 2OG and 400 μM CODD; (e) Bar chart showing the amount of 2OG displacement. All samples were buffered with 50 mM Tris-D11 pH 7.5 in 90% H_2O and 10% D_2O.

3.2.8 Applicability of the method to other 2OG oxygenases

In order to test the wider applicability of the 2OG displacement method across the 2OG oxygenase family, it was tested qualitatively with the histone demethylase F-box and leucine-rich repeat protein 11 (FBXL11; provided by Tristan J. Smart).[97] Histone lysine methylation and demethylation is strongly linked to cancer,[98] and therefore a good screening assay would be useful for future inhibitor development against FBXL11 and other related demethylases.

In the experiments, excess enzyme was found to be needed to ensure most of the 2OG population was in the protein-bound form (Figure 3-21), indicating FBXL11 is a relatively weak 2OG binder. Single point screening experiments (at 800 μM inhibitor concentration) were tested using five known 2OG oxygenase inhibitors: NOG, 5-C-8-HQ, 2,4-PDCA, BNS and BIQ (Figure 3-22).

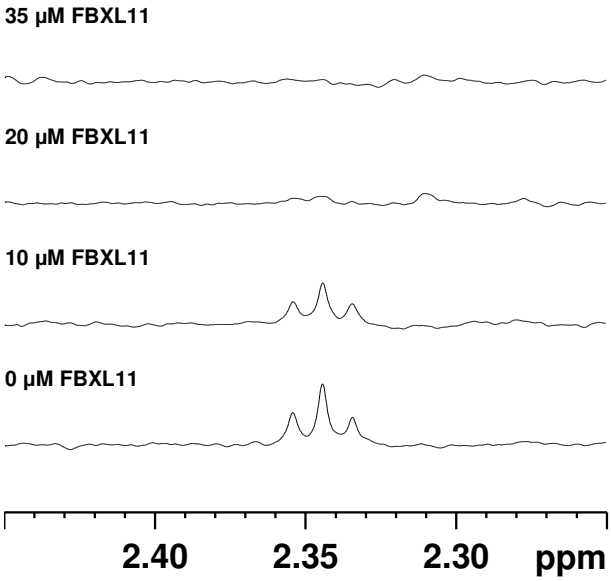

Figure 3-21 CPMG experiments showing excess FBXL11 is required to ensure most of the 2OG population is in the bound form. The assay mixture contained varying concentration of *apo*-FBXL11, 80 µM Zn(II), 10 µM 2OG and 50 mM Tris-D11 pH 7.5 in 10% D_2O and 90% H_2O.

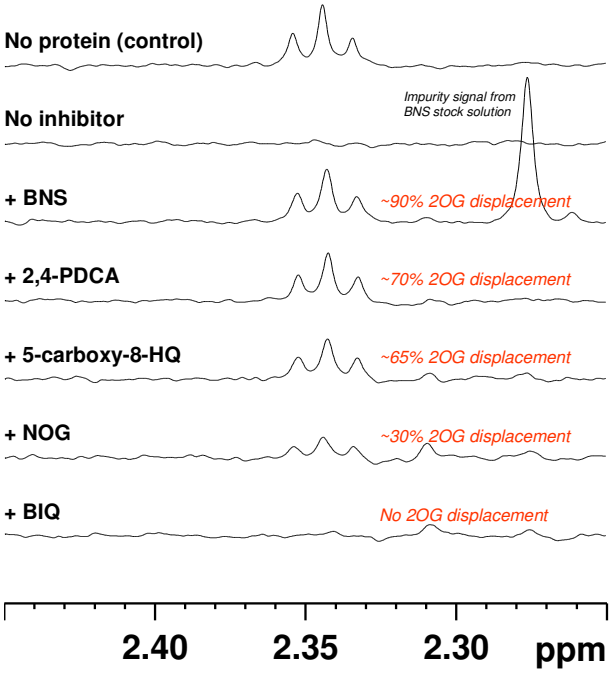

Figure 3-22 CPMG qualitative reporter screening experiments with FBXL11 at a single inhibitor concentration. The assay mixture contained 35 µM *apo*-FBXL11, 80 µM Zn(II), 10 µM 2OG, 800 µM inhibitor and 50 mM Tris-D11 pH 7.5 in 10% D_2O and 90% H_2O.

The results reveal that BNS and 2,4-PDCA, two potent PHD2 inhibitors, are relatively strong binders to FBXL11. NOG, the generic 2OG oxygenase inhibitor, and 5-C-8-HQ, a histone demethylase specific inhibitor, are also binders of FBXL11. Interestingly, the potent PHD2 bicyclic inhibitor BIQ, did not seem to displace 2OG

when tested with FBXL11. These results will hopefully provide basis for future FBXL11 inhibitor development.

3.2.9 Application of the method to investigate enzyme mechanism

Deacetoxycephalosporin C synthase (DAOCS) is a bacterial 2OG oxygenase that catalyses the first step of the biosynthesis of cephalosporins from penicillins.[99,100] The natural substrate of DAOCS is penicillin N,[101] although it will also accept less optimal substrates such as penicillin G.[102] Previous work employing steady-state kinetics, quantum mechanical calculation and X-ray crystallography as tools and penicillin G and ampicillin as model compounds, suggested that DAOCS may follow an abnormal sequential mechanism rather than the general 'consensus' mechanism (see Chapter 1).[103] In the proposed mechanism, the binding of 2OG and oxygen to DAOCS happens in the first step. Uncoupled turnover of 2OG to succinate results in the formation of the reactive Fe(IV)-oxo species inside the DAOCS active site. Following the release of carbon dioxide and succinate from the active site, the substrate then binds to the enzyme, triggering subsequent oxidation reactions. The key piece of evidence for this mechanism arises from the crystal structures of DAOCS, which appeared to show overlapping binding sites of substrate and 2OG, so that the enzyme-2OG-substrate complex (that is required for the 'consensus' mechanism) cannot be formed (PDB ids: 1UOB shows overlapping 2OG and penicillin G binding and 1UNB shows similar result with ampicillin and 2OG).

If DAOCS does indeed operate *via* the unusual sequential mechanism, the binding of penicillin should weaken the binding of 2OG (and vice versa) as suggested by the authors in the crystallography work.[103] In the original publication, evidence for this was based on steady state kinetics, in which substrate inhibition and co-substrate inhibition were observed.[103] However, it is also known that substrate inhibition is not uncommon among 2OG oxygenase family members that follow the general 'consensus' mechanism, including but not limited to γ-butyrobetaine hydroxylase (BBOX; see Chapter 2),[104] FIH[105] and anthocyanidin synthase (ANS).[106] It was considered that the 2OG reporter screening method may provide insights into the DAOCS mechanism. It was also hoped that binding data would provide clearer evidence than kinetics, because there is less interference from co-factors and co-substrates present during 2OG oxygenase catalysis.

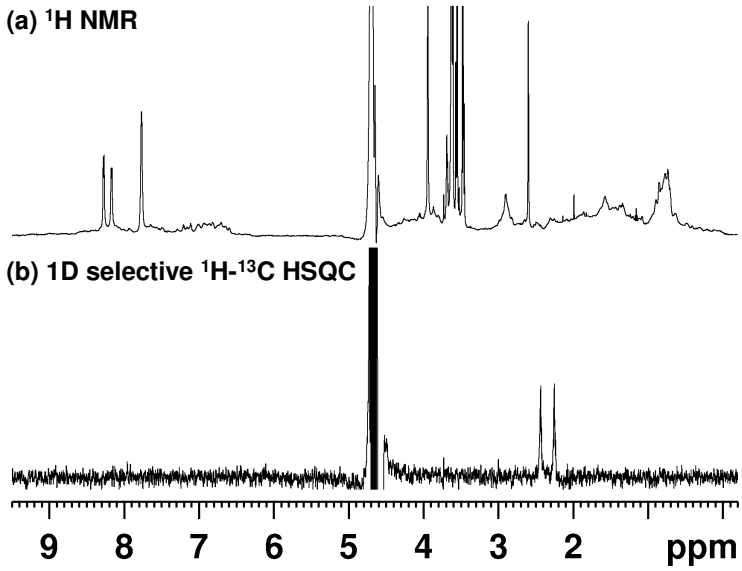

Figure 3-23 Editing using 1D selective ^{1}H-^{13}C HSQC experiment (at 30.5 ppm C-4 position of 2OG). Samples contained 40 µM PHD2, 100 µM Zn(II), 40 µM 1,2,3,4-13C 2OG, 800 µM bicyclic isoquinolinyl inhibitor (BIQ) and 50 mM Tris-D11 pH 7.5 in 90% H_2O + 10% D_2O.

A minor variation of the original method is presented here involving the use of ^{13}C-labelled reporters. The ^{13}C-label acts as a handle for spectral editing so that this method can be applied when there is significant signal overlap between the reporter ^{1}H resonances and the ^{1}H resonances from the ligand-of-interest. However the penalty is a loss of sensitivity, and a loss of addition T_2 filtering (as in the CMPG edited experiments) to distinguish the free and bound ligands. In order to tackle this, the 1D ^{1}H-^{13}C HSQC was chosen in favour of direct carbon observation (Figure 3-23). A broadband 1D ^{1}H-^{13}C HSQC was usually used, however in cases in which there was significant signal overlap, a ^{13}C selective version was used instead. In the selective version of the experiment, a Q3 shaped 180º pulse was applied as the selective pulse. The 1D ^{1}H-^{13}C HSQC experiments were conducted without ^{13}C decoupling to prevent sample heating during the long acquisition timeframe. Generally, a slightly higher concentration of protein and 2OG is used so that a reasonable signal-to-noise ratio can be achieved whilst keeping the experiment short (<30 minutes).

A proof-of-principle study was first conducted involving use of the commercially available 1,2,3,4-^{13}C labelled 2OG as the reporter and PHD2 as the model system. By applying the selective irradiation applied on C-4 (δ^{13}C = 30.5 ppm), the free and protein-bound 2OG can be easily distinguished using selective 1D HSQC (Figure 3-24). Titrations were conducted for BNS and NOG with PHD2 (Figure 3-25). The K_D values obtained (~100 nM for BNS and ~2 µM for NOG; Figure 3-26 and Figure

3-27) are comparable to those obtained using CPMG-edited ^{1}H NMR (100 nM and 3 µM respectively).

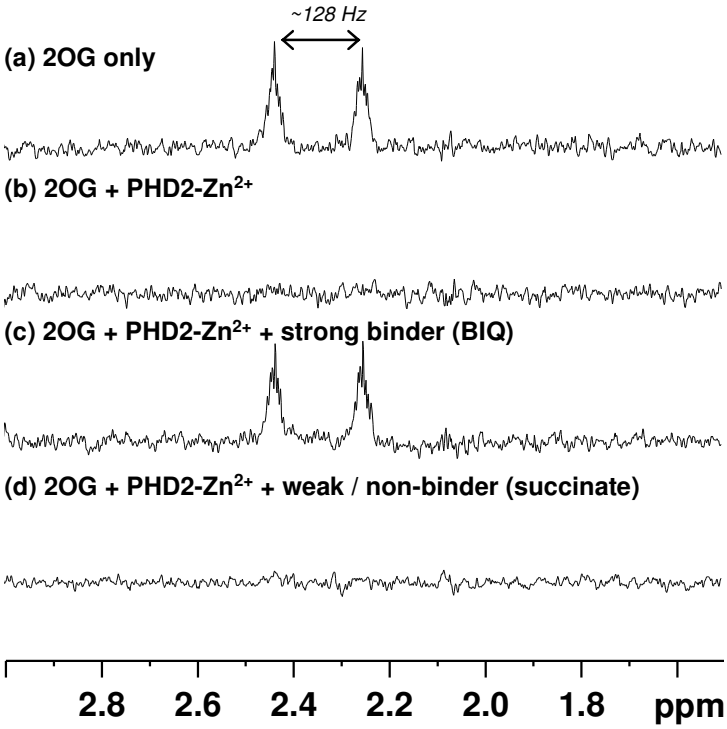

Figure 3-24 ^{13}C-labelled 2OG displacement experiments by the selective 1D ^{1}H-^{13}C HSQC at δ^{13}C = 30.5 ppm. (a) 40 µM ^{13}C-2OG (control); (b) 40 µM PHD2; 100 µM Zn(II) and 40 µM ^{13}C-2OG (control); (c) 40 µM PHD2; 100 µM Zn(II), 40 µM ^{13}C-2OG and 800 µM BIQ (complete 2OG displacement); (d) 40 µM PHD2; 100 µM Zn(II), 40 µM ^{13}C-2OG and 1500 µM succinate (no 2OG displacement). The assay mixtures contained 50 mM Tris-D11 pH 7.5 in 90% H_2O and 10% D_2O.

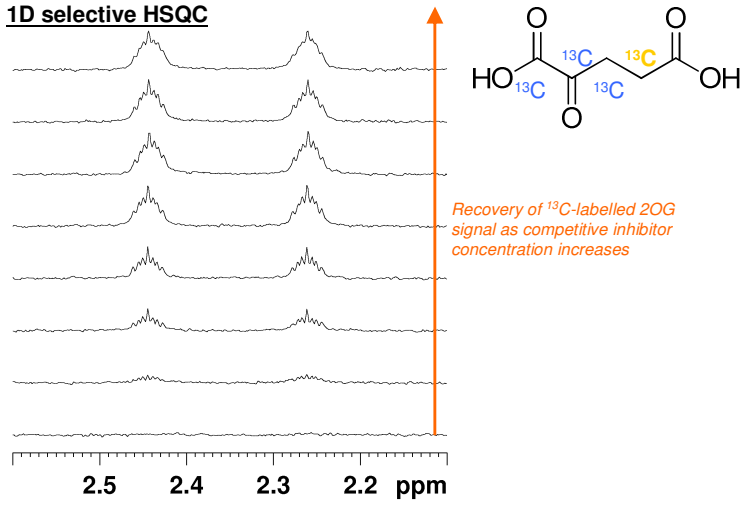

Figure 3-25 Titration experiments using ^{1}H-^{13}C HSQC. The assay mixture contained 150 µM *apo*-PHD2, 300 µM Zn(II), 150 µM ^{13}C-labelled 2OG and 50 mM Tris-D11 pH 7.5 in 10% D_2O and 90% H_2O, and varying concentrations of BNS. The signal being observed is highlighted in orange.

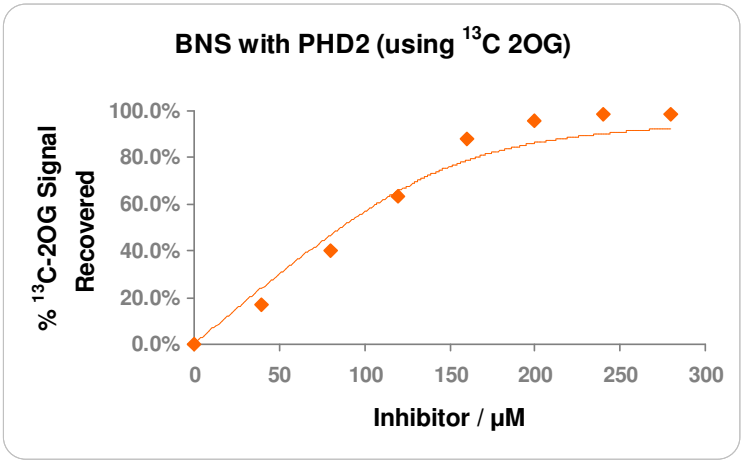

Figure 3-26 K_D determination by titration. The assay mixture contained 150 µM *apo*-PHD2, 300 µM Zn(II), 150 µM 2OG and 50 mM Tris-D11 pH 7.5 in 10% D_2O and 90% H_2O. K_D obtained ~110 nM.

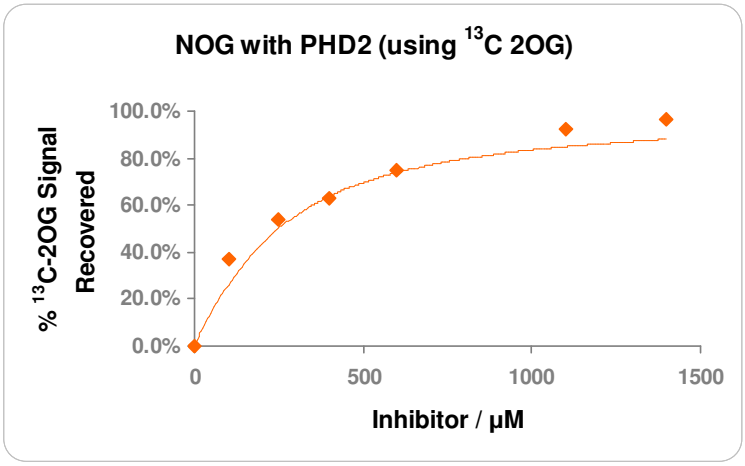

Figure 3-27 K_D determination by titration. The assay mixture contained 150 µM *apo*-PHD2, 300 µM Zn(II), 150 µM 2OG and 50 mM Tris-D11 pH 7.5 in 10% D_2O and 90% H_2O. K_D obtained ~2 µM.

This method was then applied to DAOCS (provided by Andrea Szöllössi). The 1,2,3,4-^{13}C labelled 2OG was found to bind to DAOCS, as indicated by the disappearance of the signal in the 1D HSQC spectrum (Figure 3-28). As a positive control, addition of the PHD2 inhibitor BIQ resulted in full recovery of the 2OG signal, indicating 2OG had been displaced from the DAOCS active site. However, no displacement of 2OG was observed when penicillin G or penicillin N were added to the mixture, even at a 1000 fold molar excess. A similar result was also observed with when ^{13}C-labelled NOG (Figure 3-29; synthesised by Dr Luc Henry), was used in place of ^{13}C-labelled 2OG.

In contrast, when ^{13}C-labelled penicillin G (synthesised by Dr Luc Henry) was added to DAOCS and Zn(II) (without 2OG/NOG), only a slight decrease of the penicillin G signal was observed in the absence of 2OG or NOG, indicating penicillin G only

binds weakly to DAOCS (Figure 3-30). However, when NOG was added to the mixture, complete disappearance of the penicillin G signal was observed. This indicates the binding of penicillin G actually improves when NOG is present. Some 2OG oxygenases, such as AlkB, experience large conformational changes upon metal and co-substrate (2OG/NOG) binding.[53] The observation with DAOCS may be explained by this induced fit theory, *i.e.* NOG (or analogous 2OG) binding induces conformational change of the protein which then enables better binding of penicillin G. As a positive control, addition of penicillin N (synthesised by Jacob T. Bush) to the DAOCS-penicillin G mixture led to full recovery of the penicillin G signal, thus providing further evidence that the penicillin G and the co-substrate binding site do not overlap.

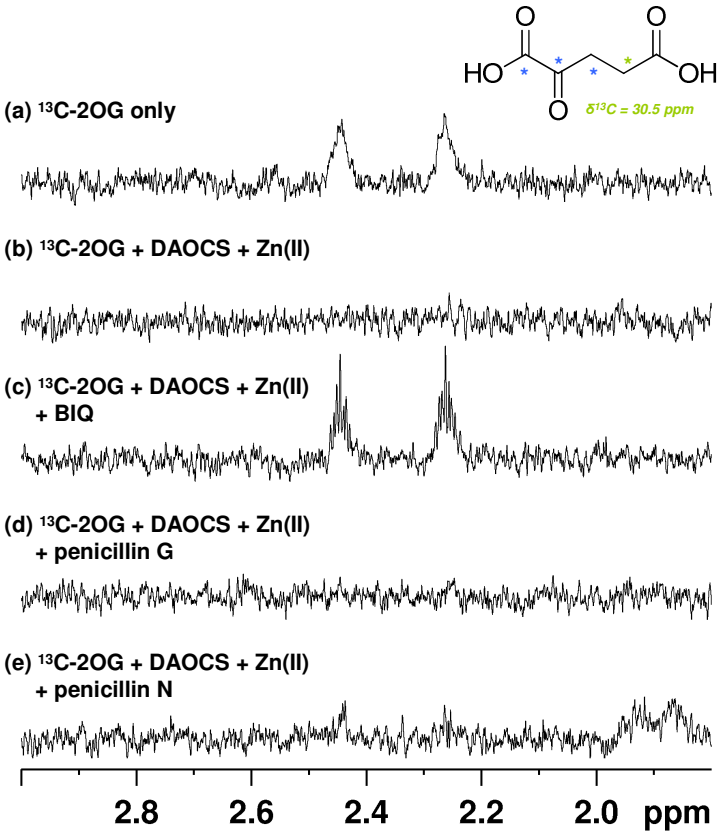

Figure 3-28 Selective 1D ^{1}H-^{13}C HSQC with selective irradiation applied at $\delta^{13}C$ = 30.5 ppm using ^{13}C-labelled 2OG. (a) 50 µM ^{13}C-2OG only; (b) 50 µM ^{13}C-2OG + 50 µM DAOCS and 100 µM Zn(II); (c) 50 µM ^{13}C-2OG + 50 µM DAOCS + 100 µM Zn(II) and 500 µM BIQ; (d) 50 µM ^{13}C-2OG + 50 µM DAOCS + 100 µM Zn(II) and 50 mM penicillin G; (e) 50 µM ^{13}C-2OG + 50 µM DAOCS + 100 µM Zn(II) and 50 mM penicillin N. All samples are buffered in 50 mM Tris-D11 pH 7.5 in D_2O.

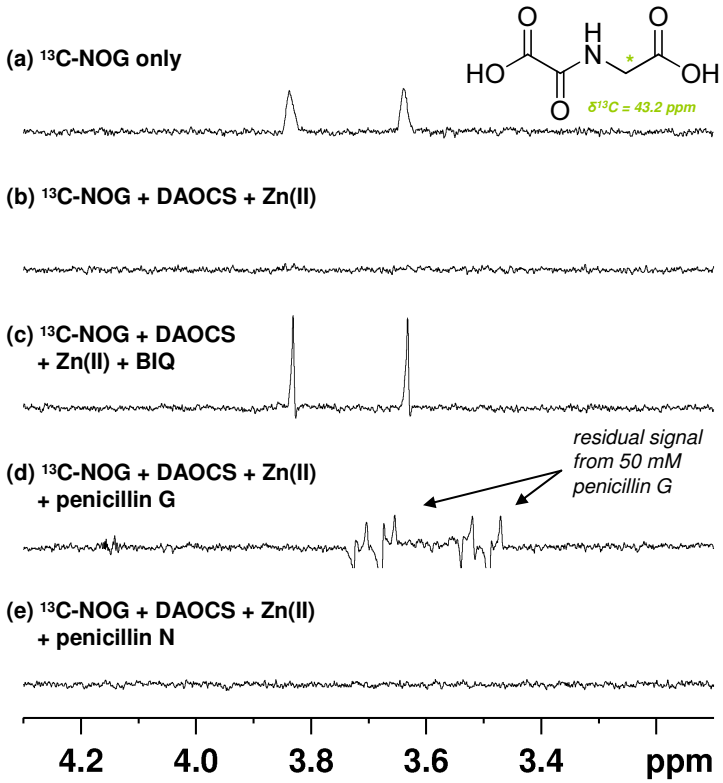

Figure 3-29 Selective 1D ^{1}H-^{13}C HSQC with selective irradiation applied at $\delta^{13}C$ = 43.2 ppm using ^{13}C-labelled NOG. (a) 50 µM ^{13}C-NOG only; (b) 50 µM ^{13}C-NOG + 50 µM DAOCS and 100 µM Zn(II); (c) 50 µM ^{13}C-NOG + 50 µM DAOCS + 100 µM Zn(II) and 500 µM BIQ; (d) 50 µM ^{13}C-NOG + 50 µM DAOCS + 100 µM Zn(II) and 50 mM penicillin G; (e) 50 µM ^{13}C-NOG + 50 µM DAOCS + 100 µM Zn(II) and 50 mM penicillin N. All samples are buffered in 50 mM Tris-D11 pH 7.5 in D_2O.

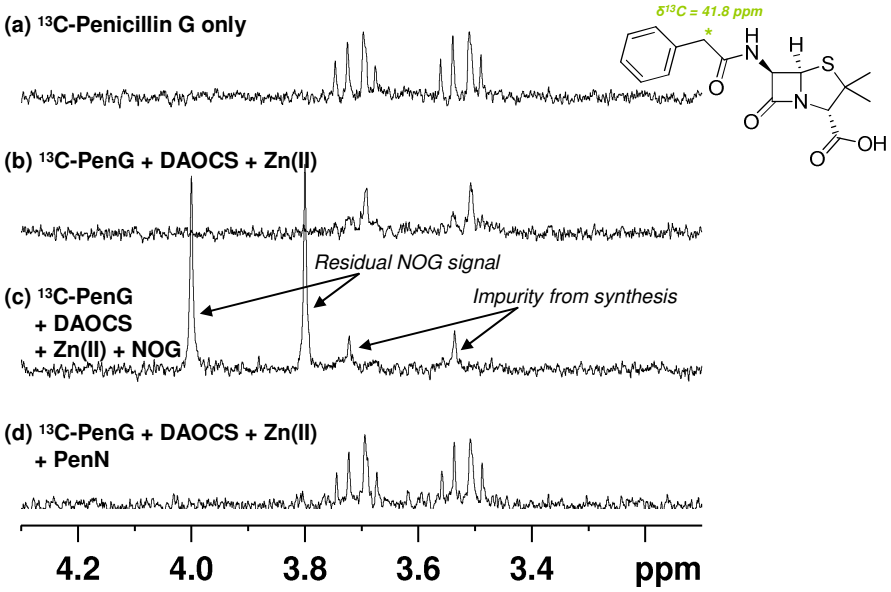

Figure 3-30 Selective 1D ^{1}H-^{13}C HSQC with selective irradiation applied at $\delta^{13}C$ = 41.8 ppm using ^{13}C-labelled penicillin G (PenG). (a) 50 µM ^{13}C-PenG only; (b) 50 µM ^{13}C-PenG + 50 µM DAOCS and 100 µM Zn(II); (c) 50 µM ^{13}C-PenG + 50 µM DAOCS + 100 µM Zn(II) and 5 mM NOG; (d) 50 µM ^{13}C-PenG + 50 µM DAOCS + 100 µM Zn(II) and 50 mM penicillin N (PenN); (e) 50 µM ^{13}C-PenG + 50 µM DAOCS + 100 µM Zn(II) and 500 µM BIQ. All samples are buffered in 50 mM Tris-D11 pH 7.5 in D_2O.

Overall, these results do not support the unusual mechanism proposed by Valegård *et al.*[103] In fact, the binding of penicillin G to DAOCS-Zn(II) actually increases in the presence of NOG. The formation of a DAOCS-Zn(II)-NOG-penicillin G complex is a prerequisite for the 'consensus' mechanism, and the results here provide further evidence for this being the mechanism employed by DAOCS, in common with most other reported 2OG oxygenases.

3.3 Solvent water as reporter for 2OG oxygenase screening

3.3.1 Paramagnetic relaxation enhancement

Paramagnetic relaxation enhancement (PRE) has been used as a tool to study paramagnetic metalloprotein-ligand interactions since the early 1960s.[107] The technique is based on the fact that the magnetic moment of an electron is 658 times greater than that of a proton nuclear spin.[108] Therefore in the presence of a paramagnetic metalloprotein, and provided the ligand binds close enough to the paramagnetic centre, the longitudinal and transverse relaxation rates of the binding ligand nuclei may be enhanced, whilst for non-binders the relaxation rates will remain unchanged. Through exchange between the free and the bound states, relaxation information is transferred and binding can be identified by monitoring changes in relaxation rate of bulk ligand nuclei. PRE can also be observed through solvent water proton relaxation rates, and has been applied to study paramagnetic metal binding with proteins and other macromolecules.[109–115] The same concept can also be applied to ligand screening of paramagnetic metalloproteins by competition-based method and using water as the reporter ligand (Figure 3-31).[116] The changes in paramagnetic relaxation behaviour depend on factors including the applied magnetic field (B_0), molecular correlation times, accessibility of the active site, and the properties of the paramagnetic metal itself. [107,117,118]

As a proof-of-principle study on the application of using water as the reporter ligand for ligand screening to 2OG oxygenases, the HIF hydroxylase PHD2 was chosen as a model system. The Fe(II) metal ion inside PHD2 (and other 2OG oxygenases) can be substituted by different transition metals.[48] Mn(II) forms a 1:1 complex with *apo*-PHD2,[48] and was selected as the metal of choice because of its favourable paramagnetic properties.[107,119]

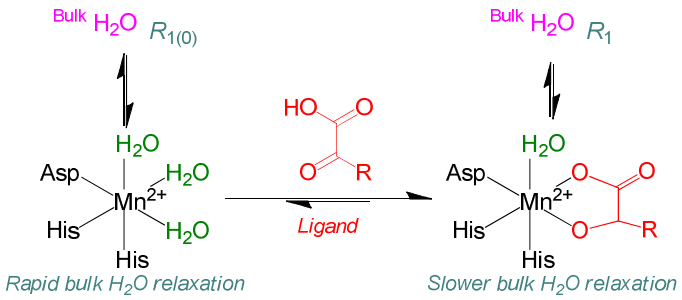

Figure 3-31 Monitoring ligand binding to paramagnetic metalloprotein by observing changes in the bulk solvent water relaxation rate.

3.3.2 Method development

Longitudinal relaxation time constants (T_1) were measured at 500 MHz using the standard inversion recovery or the saturation recovery schemes. Solvent water T_1 constants were measured directly in a H_2O-D_2O mixture, as opposed to the originally proposed method in which samples are measured in 100% H_2O and primarily using low field instruments.[116] In general, longer T_1 values are observed the more D_2O is used (and hence longer experiment time), whilst radiation damping may occur if the amount of H_2O is too high. In the experiments described here, a H_2O:D_2O ratio of 12.5% to 87.5% was chosen so that the range of T_1 values could be kept under five seconds, in order to keep the length of experiments reasonably short. Typically in a titration experiment (see Section 3.3.4), the T_1 values vary between 2 to 5 seconds when a 1:1 mixture of 50 μM *apo*-PHD2 and 50 μM Mn(II) was used, and between 1.8 to 3 seconds when 50 μM *apo*-PHD2 and 100 μM Mn(II) was used. Conventional 3 mm tubes were used to strike a balance between the ease of titration and avoiding radiation damping that may arise from the intense H_2O resonance. The small proportion of H_2O to D_2O also assists in avoiding radiation damping. The reduction of filling factor when using a 5 mm probe was not of concern because of the strong HDO signal being measured.

The absolute R_1 values are strongly influenced by variations in the concentrations of paramagnetic ion and protein, and the proportion of H_2O and D_2O (Figure 3-32). The actual parameter of interest is the relative change in observed relaxation rate on titration of the ligand and these variations can be normalised by the initial relaxation rate when no ligand is added ($R_{1(0)}$). A more accurate comparison can therefore be made by plotting the relative relaxation rates $1–R_1/R_{1(0)}$ against the titrated ligand concentration (Figure 3-32).

The amount of protein required for this relaxation method is either comparable to, or less than, other NMR based screening techniques because it is the intense HDO signal that is being measured. There is trade-off between protein concentration, total experiment time and the sensitivity of the method (Figure 3-33). When using ~25 µM protein and 100 µM Mn(II), the experiment time is shortened because there is a higher concentration of free Mn(II) in solution that is readily accessible to water molecules, thus leading to faster relaxation rates ($R_{1(0)}$ ~0.60 s^{-1}). However, in this case the reduction in relaxation rates upon ligand addition is diminished with the titration curve plateauing at around 90%, reducing the separation between the curves of similar affinity ligands. In contrast, by using ~75 µM protein with 100 µM Mn(II), the variation in rates is enhanced, plateauing at around 65%. One consequence of this, however, is that the time required for the experiment is greater due to the higher concentration of protein bound Mn(II) species with correspondingly fewer free ions in solution ($R_{1(0)}$ ~0.41 s^{-1}). By comparison, the water relaxation rate observed for the *apo*-PHD2 solution (50 µM, 12.5 % H_2O) in the absence of Mn(II) was 0.11 s^{-1}.

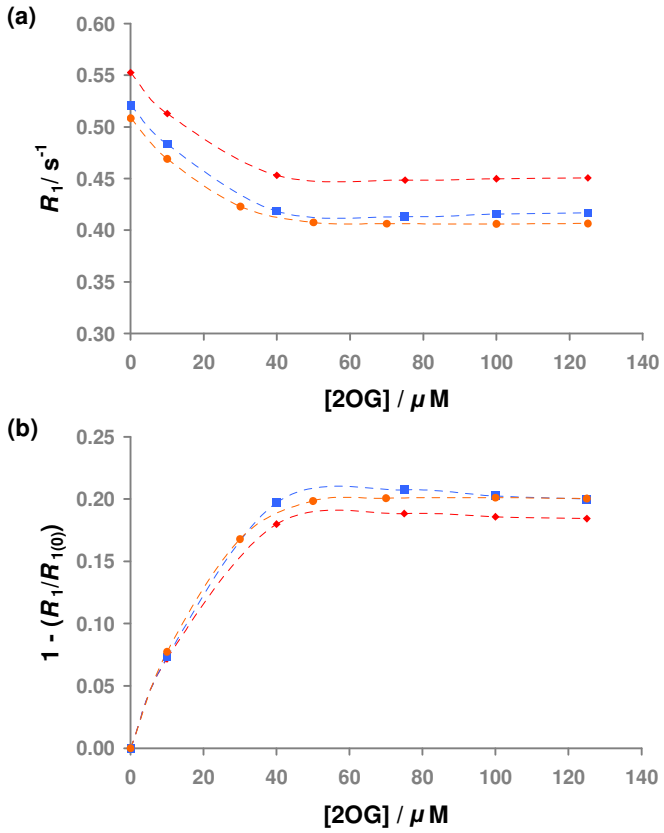

Figure 3-32 Titrations of 2OG in three separate sample preparations into 50 µM PHD2. Plotted against ligand concentration is (a) the directly measured solvent relaxation rate (R_1) and (b) the relative relaxation rate 1 - $R_1/R_{1(0)}$, in which $R_{1(0)}$ is the initial relaxation rate when no ligand is added. Slight differences in Mn(II) and protein concentrations from different sample preparations complicate comparisons across samples, but by normalising the rates, binding differences are made apparent. Dotted lines are added to aid visualisation.

It was also found that the water T_1 of the Mn(II) solution (50 μM concentration; with or without buffer or protein) increases by shaking the NMR tube (typically around 5% increase). However, no change in the water T_1 value was observed when conducting the measurement in a plastic NMR tube. It was subsequently proposed that metal adsorption onto the glass surface[120] of an NMR tube may reduce the absolute amount of paramagnetic species in solution and therefore lead to an increase of the T_1 value. In order to test this theory, inductively coupled plasma mass spectrometry (ICP-MS; Experiments performed by Prof. Babur Z. Chowdhry, Greenwich University) was used to quantify changes in Mn(II) concentration in solution. A ~6% reduction of Mn(II) concentration (from a 50 μM Mn(II) solution) was observed when the solution is moved along a glass NMR tube while ~0.1% reduction was observed when a plastic NMR tube was used. Previous reports suggested that the adsorption of trace metal onto glass surfaces can be minimised by the addition of a competing metal ion, such as sodium.[120] To test this theory, a solution containing 50 μM Mn(II) and 125 mM NaCl was prepared and moved along a glass NMR tube, ICP-MS experiments suggested <0.1% reduction in Mn(II) concentration was observed (as opposed to ~6% reduction without NaCl as shown by ICP-MS). It was therefore decided to conduct water relaxation experiments at high salt concentration to avoid false positive readings.

In order to investigate the validity and sensitivity of this method at high field, as opposed to conducting the experiments at low field as in the work of Bertini *et al.*, both high field (500 MHz) and low field (23 MHz) experiments were conducted for comparison (Figure 3-34; Experiments were conducted by Dr Alexander I. Sagidullin). Three PHD2-ligand systems were analysed, including mixtures containing 2OG, NOG and BNS. The low field experiments were conducted in 100% H_2O at 23 MHz, and both high and low field experiments were measured at 313 K.

As anticipated, the minimum relaxation rate is smaller at low field, indicating greater sensitivity under these conditions; however, the relative change of R_1 between the three ligands, and hence the calculated K_D values, are essentially the same at both low and high field (Figure 3-34). Qualitatively, the results obtained at high and low fields confirm that the bicyclic inhibitor BNS is a much stronger binder than 2OG and NOG. Quantitatively, the K_D values obtained for 2OG at both low and high field are ~2 μM, whilst for NOG they are ~3 μM. Thus, both qualitative screening and the

quantitative determination of binding kinetics appear feasible at high field and with conventional NMR instrumentation.

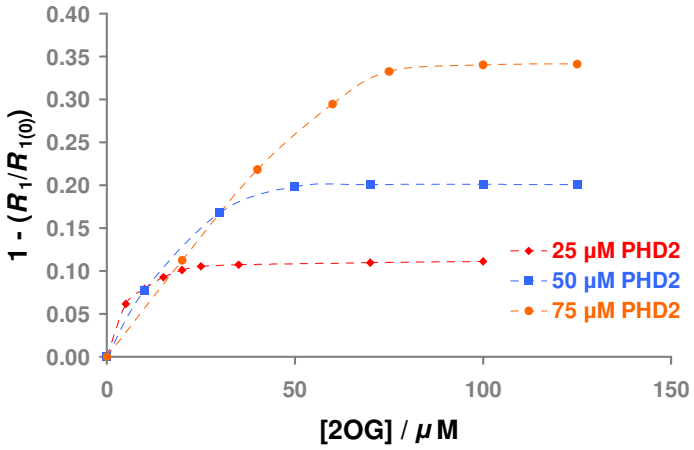

Figure 3-33 Titration of 2OG into 25 µM, 50 µM and 75 µM PHD2 with 100 µM Mn(II). The minimum R_1 value depends on the residual relaxation rate of the H_2O/D_2O mixture, which in turn is dependent upon the amount of free Mn(II) present in solution. Dotted lines are added to aid visualisation.

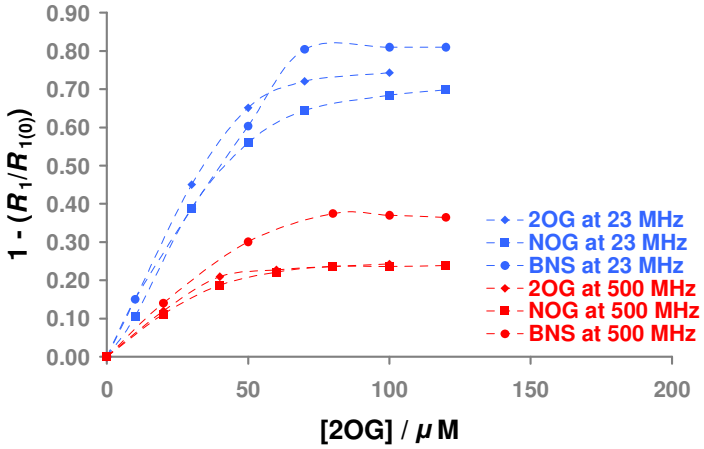

Figure 3-34 Titration of 2OG, NOG and BNS into 50 µM PHD2 with 100 µM Mn(II). The data plotted in red and blue are conducted at 500 and 23 MHz respectively. Dotted lines are added to aid visualisation.

3.3.3 Metal binding

By titrating *apo*-protein to a fixed concentration of Mn(II), it is possible to monitor metal binding to PHD2 with the solvent relaxation method. This was investigated with WT PHD2 and two PHD2 mutants (R383K and D315E; Figure 3-35; Mutant enzymes were provided by Hanna Tarhonskaya). In agreement with previously published ESI-MS data, WT PHD2 showed strong binding to Mn(II) with a K_D value of 0.62 µM. R383K is involved in 2OG binding and therefore the R383K mutation was not expected to affect metal binding.[121] The water relaxation technique suggests it has the same metal affinity as WT. However, the experiment with the D315E mutant

showed significant decrease in metal binding affinity (K_D = 240 μM). This is not surprising given that D315, being part of the HXD/E...H metal chelating amino acid triad, is involved in direct coordination of the metal inside the PHD2 active site (see also Chapter 4).[121]

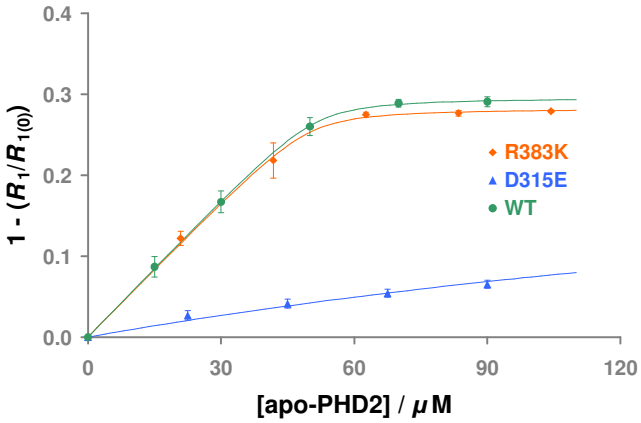

Figure 3-35 Solvent water relaxation to monitor Mn(II) binding to PHD2. The assay mixture contained 50 μM Mn(II) and 125 mM NaCl in 50 mM Tris-D11 (pH 7.5) 10% D_2O and 90% H_2O. *Apo*-PHD2 was titrated into the solution mixture. Experiments were performed 3 times. K_Ds obtained for WT PHD2, R383K PHD2 and D315E PHD2 are 60 ± 40 nM, 60 ± 20 nM and 240 ± 30 μM respectively. Solid line indicates fitting of the data to the binding isotherm.

3.3.4 Binding of PHD2 inhibitors

Most HIF hydroxylase inhibitors have amino acid side chains that bind in the 2OG binding pocket, and the selectivity of these inhibitors can be modified by varying the amino acid moiety.[122] A series of D- and L-amino acid substituted NOG and BIQ analogues (NOG analogues were provided by Dr Esther C. Y. Woon; BIQ analogues were provided by Dr Kar Kheng Yeoh) were therefore analysed using this solvent relaxation technique (Table 3-2 and Figure 3-36).

The results with the BIQ analogues suggest that the introduction of a methyl group (alanine derivative) alters the selectivity of BIQ binding significantly, with L-Ala-BIQ binding to PHD2 in a similar fashion to BIQ, whereas D-Ala-BIQ was a much weaker binder. The relatively weaker binding of D-Ala-BIQ is likely due, at least in part, to steric hindrance with the side chain of valine-376 in the 2OG binding pocket.[121,123] Solvent relaxation experiments gave K_D values of < 1 μM and ~22 μM for L-Ala-BIQ and D-Ala-BIQ respectively, consistent with the binding data obtained from non-denaturing ESI-MS. The substitution of the glycine moiety of BIQ by bulky amino acids such as valine also sterically weakens the binding of BIQ inhibitors to PHD2. In fact, both D- and L-Val BIQ show very similar levels of weak binding as indicated by

MS analyses. Solvent relaxation experiments gave K_D values of ~33 μM and ~35 μM for D- and L-Val BIQ respectively.

Ligand	Structure	K_D	IC_{50}
2OG	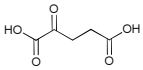	900 ± 100 nM	N/A
NOG	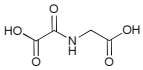	3 ± 1 μM	20 μM
Succinate	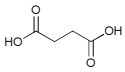	> 100 μM	85 μM
BNS	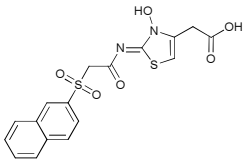	<1 μM	20 nM
BIQ	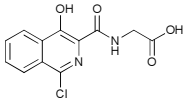	<1 μM	70 nM
L-Ala-BIQ	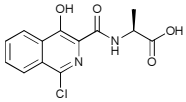	<1 μM	500 nM
D-Ala-BIQ	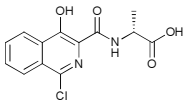	~20 μM	230 μM
L-Val-BIQ	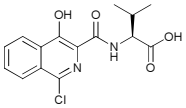	~35 μM	> 400 μM
D-Val-BIQ	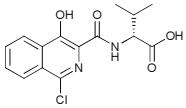	~35 μM	> 400 μM

Table 3-2 Dissociation constants (K_D) determined by the solvent relaxation technique at 298 K and reported IC_{50} values for 2OG, succinate and a range of inhibitors.

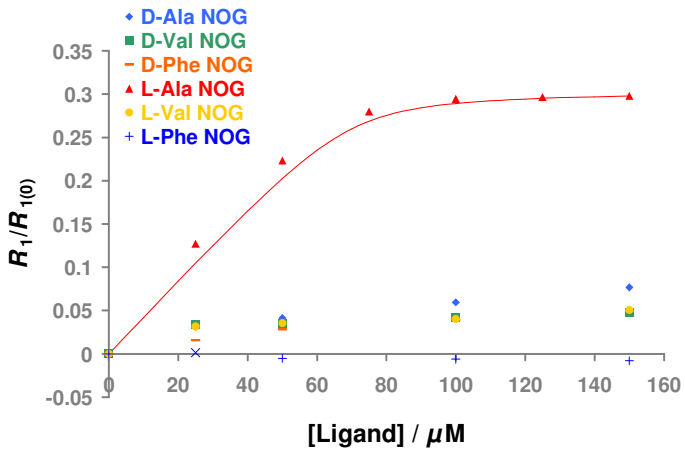

Figure 3-36 Solvent water relaxation to monitor amino acid substituted NOG analogues binding to PHD2. The assay mixture contained ~100 μM *apo*-PHD2 and 100 μM Mn(II) in 50 mM Tris-D11 (pH 7.5) 87.5% D_2O and 12.5% H_2O. NOG analogues were titrated into the solution mixture. Only the L-Ala-NOG data was fitted, with K_D ~1.7 μM. All other NOG analogues have K_D > 300 μM. Solid line indicates fitting of the data to the binding isotherm.

Amino acid substituted NOG analogues showed more selectivity against PHD2. Only the L-alanine substituted NOG (L-Ala-NOG) shows any significant binding to PHD2, with a K_D value of ~2.4 μM. This is consistent with the BIQ data, in which PHD2 prefers to bind to the L-amino acid substituted compound, and that the bulkiness of the valine and phenylalanine substitution hindered binding to PHD2.

After demonstrating that this method works efficiently for PHD2, it was tested with another HIF hydroxylase FIH (Figure 3-37). The results of these experiments suggest FIH is a strong 2OG binder albeit weaker than PHD2, with a K_D of 4 μM.

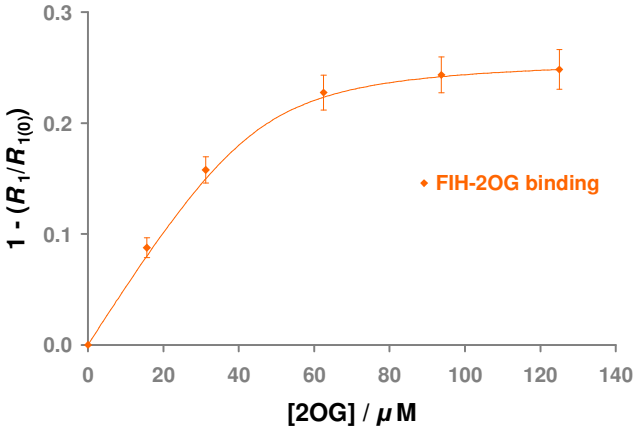

Figure 3-37 Solvent water relaxation to monitor 2OG binding to FIH-Mn(II). The assay mixture contained 50 μM *apo*-FIH, 50 μM Mn(II) and 125 mM NaCl in 50 mM Tris-D11 (pH 7.5) 87.5% D_2O and 12.5% H_2O. 2OG was titrated into the solution mixture. Solid line indicates fitting of the data to the binding isotherm. Experiments were performed 3 times. K_D obtained is 4 ± 1 μM.

3.3.5 Co-binding of co-substrate and substrate

Previous biophysical and kinetic studies have shown that PHD2 has a preference for hydroxylating CODD over NODD, with K_M values of 37 μM and 44 μM respectively.[96] The results from solvent relaxation experiments suggest CODD is a significantly stronger binder than NODD, with K_D values of ~15 μM and ~85 μM, respectively. Because neither CODD nor NODD directly chelates the metal centre, these data demonstrate that it is possible to screen for compounds that bind in the vicinity of the active site metal yet need not interact with the metal directly, provided that their association displaces water molecules from the active site metal or alters their exchange with bulk water. These data are also consistent with the proposed 2OG oxygenase mechanism of hydroxylation which involves displacement of water complexed to the active site iron upon substrate binding, such that a coordination position becomes free for an oxygen molecule to coordinate to the metal prior to the oxidative decarboxylation step.

The application of this technique to study co-binding was also investigated. CODD binds to PHD2 in a well-defined cleft, adopting a loose and extended conformation, whilst 2OG chelates directly to the metal centre in a bidentate fashion.[124] A clear additive effect is observed by the water relaxation technique when CODD is added to PHD2-2OG or when 2OG is added to PHD2-CODD (Figure 3-38). The titration of an equimolar mixture of 2OG-CODD into PHD2 yields a similar net effect. The observation of these sequential binding profiles is consistent with previously reported mechanistic and structural studies of PHD2, in which PHD2 forms a ternary complex with 2OG and CODD, and in which 2OG and CODD are observed to bind to neighbouring sites in the protein active site.[124] It also provides insights into the extent of water accessibility upon the binding of individual substrates. The K_Ds for 2OG in the absence and presence of CODD were measured as 900 nM and 1 μM, respectively. Similar titration behaviour was also observed in ternary systems involving PHD2-2OG-NODD. Interestingly, however, 2OG appeared to bind more strongly in the presence of CODD to the R383K PHD2 mutant (Figure 3-39). R383 is involved in binding 2OG by forming hydrogen bonds and electrostatic interactions with the C-5 carboxylic group of 2OG. This result suggests the dynamics of PHD2 binding induced by CODD binding may, at least in the case of the R383K mutant, hold the 2OG in the right place for catalysis.

This additive effect also allows the study of different modes of inhibition (Figure 3-40). NOG is an unreactive analogue of 2OG, which competes with 2OG for binding to the active site metal. As for 2OG, additive effects were observed when CODD was added to PHD2-NOG, indicating the formation of a ternary complex. In contrast, when CODD is added to PHD2-BNS inhibitor complexes, no additive effects were observed. BNS chelates directly to the metal centre and therefore competes with 2OG binding, but in addition they also appear able to block CODD from approaching the active site metal, consistent with crystallography studies. Thus, the additional steric bulk associated with these ligands also offers a second mode of inhibition through blocking substrate binding. Such information may prove valuable in inhibitor optimisation.

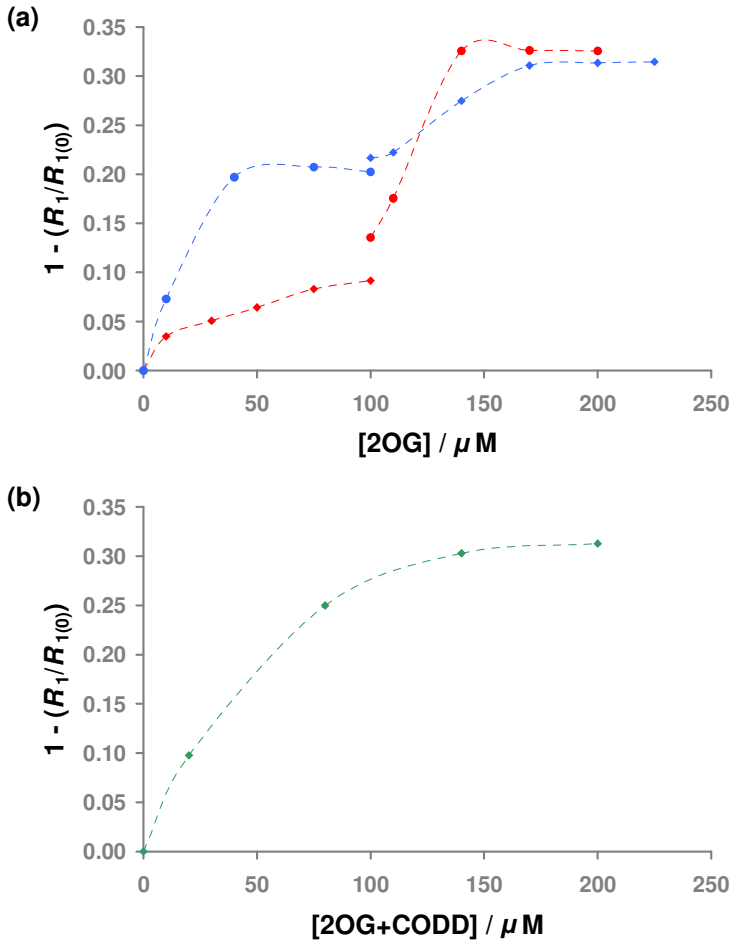

Figure 3-38 (a) The sequential titration of CODD (♦) and 2OG (•), and (b) simultaneous titration of equal molar CODD and 2OG into 50 μM PHD2 as a function of total ligand concentrations. For (a) different colours are used to represent different sequences of addition (red: CODD then 2OG, blue: 2OG then CODD). Dotted lines are added to aid visualisation.

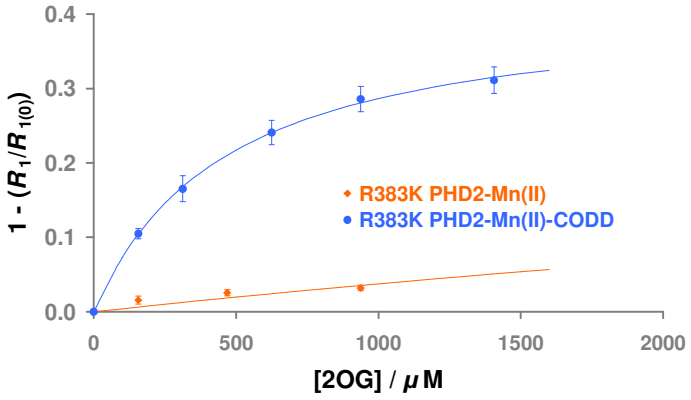

Figure 3-39 Solvent water relaxation to monitor 2OG binding to R383K PHD2 with and without CODD. The assay mixture contained 50 μM R383K PHD2, 50 μM Mn(II), 125 μM CODD where applicable and 125 mM NaCl in 50 mM Tris-D11 (pH 7.5) 87.5% D_2O and 12.5% H_2O. 2OG was titrated into the solution mixture. Experiments were performed 3 times. K_Ds obtained for 2OG binding to R383K PHD2 without CODD and with CODD are >10 mM and 430 ± 30 μM respectively. Solid line indicates fitting of the data to the binding isotherm.

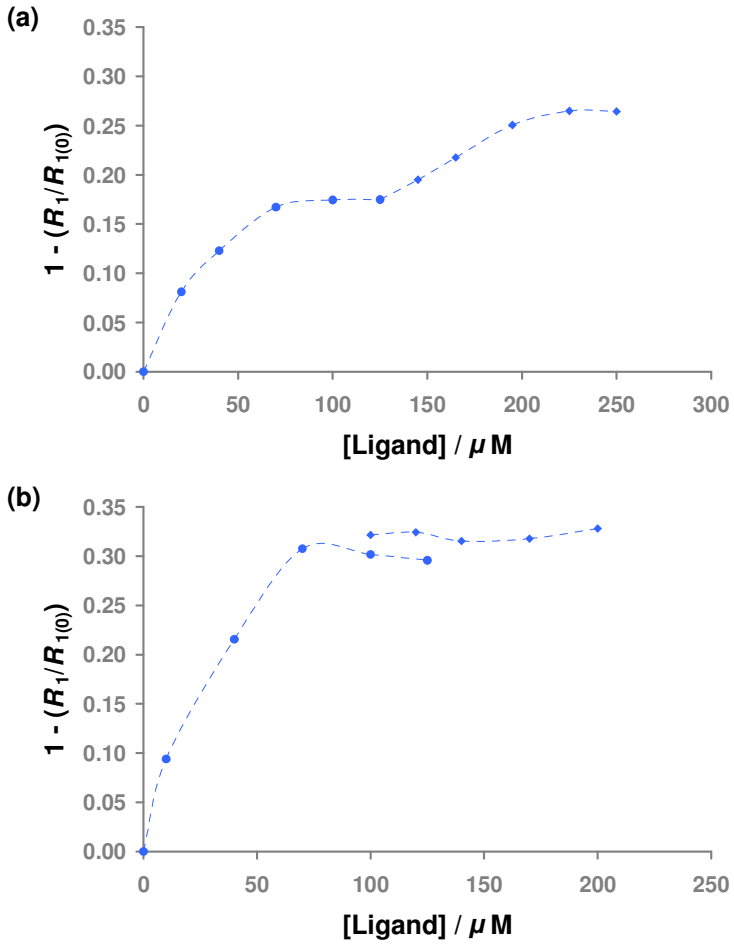

Figure 3-40 Binding titration curves showing (a) the titration of CODD (♦) into a solution of PHD2 + NOG (•) and (b) the titration of CODD (♦) into a solution of PHD2 + BNS (•). Additive effects can be observed in (a) indicating the formation of a PHD2-NOG-CODD complex, while in (b) the BNS inhibitor blocks CODD approaching the PHD2 active site metal. Dotted lines are added to aid visualisation.

3.4 Summary

Overall, the work described in this Chapter has demonstrated the potential of using ligand observed competition based solution NMR methods to study protein-ligand interactions.

In the first experiment, 2OG was used as a reporter, and the PROJECT CPMG method was used for spectral editing. This method can provide site-specific binding information in an efficient fashion. It can also provide accurate determination of dissociation constants for both strong and weak binders, which is otherwise difficult to estimate using other ligand-based NMR techniques. It is also demonstrated that signal overlap, a problem associated with many ^{1}H NMR based screening methods, can be overcome by the use of commercially available ^{13}C-labelled 2OG and 1D selective HSQC experiments. This method has been applied to different members of

the 2OG oxygenase superfamily, including HIF hydroxylases (PHD2 and FIH) and histone demethylases (FBXL11).

In the second method, the general applicability of ligand screening with PHD2 substituted with paramagnetic metal through the study of bulk water relaxation was investigated. This method can readily provide information including metal binding to *apo*-enzyme and ligand binding to paramagnetic metalloenzyme. The method is highly sensitive to ligand binding events directly at, and in the vicinity of, the paramagnetic metal centre. It enables the differentiation of binding affinities between ligands and, in favourable cases, allows the value of dissociation constants to be determined.

3.5 References

1. Wenger, R. H. Mammalian oxygen sensing, signalling and gene regulation. *J. Exp. Biol.* **2000**, *203*, 1253–1263.
2. Semenza, G. L. Hypoxia-inducible factor 1 (HIF-1) pathway. *Sci. STKE* **2007**, *407*, cm8.
3. Ke, Q.; Costa, M. Hypoxia-Inducible Factor-1 (HIF-1). *Mol. Pharmacol.* **2006**, *70*, 1469–1480.
4. Brahimi-Horn, M. C.; Pouysségur, J. HIF at a glance. *J. Cell Sci.* **2009**, *122*, 1055–1057.
5. Chowdhury, R.; Hardy, A.; Schofield, C. J. The Human Oxygen Sensing Machinery and its Manipulation. *Chem. Soc. Rev.* **2008**, *37*, 1308–1319.
6. Ratcliffe, P. J. HIF-1 and HIF-2: working alone or together in hypoxia? *J. Clin. Invest.* **2007**, *117*, 862–865.
7. Maynard, M. A.; Qi, H.; Chung, J.; Lee, E. H. L.; Kondo, Y.; Hara, S.; Conaway, R. C.; Conaway, J. W.; Ohh, M. Multiple splice variants of the human HIF-3α locus are targets of the von Hippel-Lindau E3 ubiquitin ligase complex. *J. Biol. Chem.* **2003**, *278*, 11032–11040.
8. Wang, G. L.; Jiang, B. H.; Rue, E. A.; Semenza, G. L. Hypoxia-inducible factor 1 is a basic-helix-loop-helix-PAS heterodimer regulated by cellular O_2 tension. *Proc. Natl. Acad. Sci. U. S. A.* **1995**, *92*, 5510–5514.
9. Salceda, S.; Caro, J. Hypoxia-inducible factor 1α (HIF-1α) protein is rapidly degraded by the ubiquitin-proteasome system under normoxic conditions. Its stabilization by hypoxia depends on redox-induced changes. *J. Biol. Chem.* **1997**, *272*, 22642–22647.
10. Kallio, P. J.; Pongratz, I.; Gradin, K.; McGuire, J.; Poellinger, L. Activation of hypoxia-inducible factor 1α: Posttranscriptional regulation and conformational change by recruitment of the Arnt transcription factor. *Proc. Natl. Acad. Sci. U. S. A.* **1997**, *94*, 5667–5672.
11. Bárdos, J. I.; Ashcroft, M. Negative and positive regulation of HIF-1: A complex network. *Biochim. Biophys. Acta* **2005**, *1755*, 107–120.
12. Gradin, K.; McGuire, J.; Wenger, R. H.; Kvietikova, I.; Whitelaw, M. L.; Toftgård, R.; Tora, L.; Gassmann, M.; Poellinger, L. Functional interference between hypoxia and dioxin signal transduction pathways: competition for recruitment of the Arnt transcription factor. *Mol. Cell. Biol.* **1996**, *16*, 5221–5231.
13. Wood, S. M.; Gleadle, J. M.; Pugh, C. W.; Hankinson, O.; Ratcliffe, P. J. The role of the aryl hydrocarbon receptor nuclear translocator (ARNT) in Hypoxic Induction of Gene Expression. Studies in ARNT-deficient cells. *J. Biol. Chem.* **1996**, *271*, 15117–15123.
14. Kallio, P. J.; Okamoto, K.; O'Brien, S.; Carrero, P.; Makino, Y.; Tanaka, H. Poellinger, L. Signal transduction in hypoxic cells: inducible nuclear translocation and recruitment of the CBP/p300 coactivator by the hypoxia-inducible factor-1α. *EMBO J.* **1998**, *17*, 6573–6586.
15. Schofield, C. J.; Ratcliffe, P. J. Signalling hypoxia by HIF hydroxylases. *Biochem. Biophys. Res. Commun.* **2005**, *338*, 617–626.
16. Schofield, C. J.; Ratcliffe, P. J. Oxygen sensing by HIF hydroxylases. *Nat. Rev. Mol. Cell Biol.* **2004**, *5*, 343–354.
17. Masson, N.; Ratcliffe, P. J. HIF prolyl and asparaginyl hydroxylases in the biological response to intracellular O_2 levels. *J. Cell Sci.* **2003**, *116*, 3041–3049.
18. Semenza, G. L. Hydroxylation of HIF-1: oxygen sensing at the molecular level. *Physiology* **2004**, *19*, 176–182.
19. Fandrey, J.; Gorr, T. A.; Gassmann, M. Regulating cellular oxygen sensing by hydroxylation. *Cardiovasc. Res.* **2006**, *71*, 642–651.
20. Koivunen, P.; Hirsila, M.; Gunzler, V.; Kivirikko, K. I.; Myllyharju, J. Catalytic properties of the asparaginyl hydroxylase (FIH) in the oxygen sensing pathway are distinct from those of its prolyl 4-hydroxylases. *J. Biol. Chem.* **2004**, *279*, 9899–9904.

21. Loenarz, C.; Chowdhury, R.; Schofield, C. J.; Flashman, E. Oxygenases for oxygen sensing. *Pure Appl. Chem.* **2008**, *80*, 1837–1847.

22. Berra, E.; Benizri, E.; Ginouves, A.; Volmat, V.; Roux, D.; Pouyssegur, J. HIF prolyl-hydroxylase 2 is the key oxygen sensor setting low steady-state levels of HIF-1α in normoxia. *EMBO J.* **2003**, *22*, 4082–4090.

23. Epstein, A. C. R.; Gleadle, J. M.; McNeill, L. A.; Hewitson, K. S.; O'Rourke, J.; Mole, D. R.; Mukherji, M.; Metzen, E.; Wilson, M. I.; Dhanda, A.; Tian, Y. M.; Masson, N.; Hamilton, D. L.; Jaakkola, P.; Barstead, R.; Hodgkin, J.; Maxwell, P. H.; Pugh, C. W.; Schofield, C. J.; Ratcliffe, P. J. *C. elegans* EGL-9 and mammalian homologs define a family of dioxygenases that regulate HIF by prolyl hydroxylation. *Cell* **2001**, *107*, 43–54.

24. Bruick, R. K.; McKnight, S. L. Oxygen sensing gets a second wind. *Science* **2002**, *295*, 807–808.

25. Illingworth, C. J. R.; Loenarz, C.; Schofield, C. J.; Domene, C. Chemical basis for the selectivity of the von Hippel Lindau tumor suppressor pVHL for prolyl-hydroxylated HIF-1α. *Biochemistry* **2010**, *49*, 6936–6944.

26. Dann, C. E. III; Bruick, R. K.; Deisenhofer J. Structure of factor inhibiting hypoxia-inducible factor 1: an asparaginyl hydroxylase involved in the hypoxic response pathway. *Proc. Natl. Acad. Sci. U. S. A.* **2002**, *99*, 15351–15356.

27. Hewitson, K. S.; McNeill, L. A.; Riordan, M. V.; Tian, Y. M.; Bullock, A. N.; Welford, R. W.; Elkins, J. M.; Oldham, N. J.; Bhattacharya, S.; Gleadle, J. M.; Ratcliffe, P. J.; Pugh, C. W.; Schofield, C. J. Hypoxia inducible factor (HIF) asparagine hydroxylase is identical to factor inhibiting HIF (FIH) and is related to the cupin structural family. *J. Biol. Chem.* **2002**, *277*, 26351–26355.

28. Elkins, J. M.; Hewitson, K. S.; McNeill, L. A.; Seibel, J. F.; Schlemminger, I.; Pugh, C. W.; Ratcliffe, P. J.; Schofield, C. J. Structure of factor inhibiting hypoxia-inducible factor (HIF) reveals mechanism of oxidative modification of HIF-1α. *J. Biol. Chem.* **2003**, *278*, 1802–1806.

29. McNeill, L. A.; Hewitson, K. S.; Claridge, T. D.; Seibel, J. F.; Horsfall, L. E.; Schofield, C. J. Hypoxia-inducible factor asparaginyl hydroxylase (FIH-1) catalyses hydroxylation at the beta-carbon of asparagine-803. *Biochem. J.* **2002**, *367*, 571–575

30. Dames, S. A.; Martinez-Yamout, M.; De Guzman, R. N.; Dyson, H. J.; Wright, P. E. Structural basis for Hif-1α/CBP recognition in the cellular hypoxic response. *Proc. Natl. Acad. Sci. U. S. A.* **2002**, *99*, 5271–5276.

31. Lando, D.; Peet, D. J.; Gorman, J. J.; Whelan, D. A.; Whitelaw, M. L.; Bruick, R. K. FIH-1 is an asparaginyl hydroxylase enzyme that regulates the transcriptional activity of hypoxia-inducible factor. *Genes Dev.* **2002**, *16*, 1466–1471.

32. Huang, L. E.; Bunn, H. F. Hypoxia-inducible factor and its biomedical relevance. *J. Biol. Chem.* **2003**, *278*, 19575–19578.

33. Giaccia, A.; Siim, B. G.; Johnson, R. S. HIF-1 as a target for drug development. *Nat. Rev. Drug Discov.* **2003**, *2*, 803–811.

34. Hewitson, K. S.; Schofield, C. J. The HIF pathway as a therapeutic target. *Drug Discov. Today* **2004**, *9*, 704–711.

35. Semenza, G. L. HIF-1 and human disease: one highly involved factor. *Genes Dev.* **2000**, *14*, 1983–1991.

36. Fraisl, P.; Aragonés, J.; Carmeliet, P. Inhibition of oxygen sensors as a therapeutic strategy for ischaemic and inflammatory disease. *Nat. Rev. Drug Discov.* **2009**, *8*, 139–152.

37. Koeppen, M.; Eckle, T.; Eltzschig, H. K. The hypoxia–inflammation link and potential drug targets. *Curr. Opin. Anaesthesiol.* **2011**, *24*, 363–369.

38. Muchnik, E.; Kaplan, J. HIF prolyl hydroxylase inhibitors for anemia. *Expert Opin. Investig. Drugs.* **2011**, *20*, 645–656.

39. Yeo, E.-J.; Chun, Y.-S.; Park, J.-W. New anticancer strategies targeting HIF-1. *Biochem. Pharmacol.* **2004**, *68*, 1061–1069.

40. Patiar, S; Harris, A. L. Role of hypoxia-inducible factor-1α as a cancer therapy target. *Endocr. Relat. Cancer* **2006**, *13*, S61–S75.

41. Hong, S.-S.; Lee, H.; Kim, K.-W. HIF-1α: a valid therapeutic target for tumor therapy. *Cancer Res. Treat.* **2004**, *36*, 343–353.

42. Maxwell, P. J. The HIF pathway in cancer. *Semin. Cell Dev. Biol.* **2005**, *16*, 523–530.

43. Poon, E.; Harris, A. L.; Ashcroft, M. Targeting the hypoxia-inducible factor (HIF) pathway in cancer. *Expert Rev. Mol. Med.* **2009**, *11*, e26.

44. Semenza, G. L. Targeting HIF-1 for cancer therapy. *Nat. Rev. Cancer* **2003**, *3*, 721–732.

45. Smith, T. G.; Talbot, N. P. Prolyl hydroxylases and therapeutics. *Antioxid. Redox Signal.* **2010**, *12*, 431–433.

46. Rose, N. R.; Woon, E. C. Y.; Kingham, G. L.; King, O. N. F.; Mecinović, J.; Clifton, I. J.; Ng, S. S.; Talib-Hardy, J.; Oppermann, U.; McDonough, M. A.; Schofield, C. J. Selective inhibitors of the JMJD2 histone demethylases: combined nondenaturing mass spectrometric screening and crystallographic approaches. *J. Med. Chem.* **2010**, *53*, 1810–1818.

47. Mecinović, J.; Loenarz, C.; Chowdhury, R.; Schofield, C. J. 2-Oxoglutarate analogue inhibitors of prolyl hydroxylase domain 2. *Bioorg. Med. Chem. Lett.* **2009**, *19*, 6192–6195.

48. Mecinović, J.; Chowdhury, R.; Liénard, B. M. R.; Flashman, E.; Buck, M. R. G.; Oldham, N. J.; Schofield, C. J. ESI-MS studies on prolyl hydroxylase domain 2 reveal a new metal binding site. *ChemMedChem* **2008**, *3*, 569–572.

49. Hewitson, K. S.; Liénard, B. M. R.; McDonough, M. A.; Clifton, I. J.; Butler, D.; Soares, A. S.; Oldham, N. J.; McNeill, L. A.; Schofield, C. J. Structural and mechanistic studies on the inhibition of the hypoxia-inducible transcription factor hydroxylases by tricarboxylic acid cycle intermediates. *J. Biol. Chem.* **2007**, *282*, 3293–3301.

50. McNeill, L. A.; Flashman, E.; Buck, M. R. G.; Hewitson, K. S.; Clifton, I. J.; Jeschke, G.; Claridge, T. D. W.; Ehrismann, D.; Oldham, N. J.; Schofield, C. J. Hypoxia-inducible factor prolyl hydroxylase 2 has a high affinity for ferrous iron and 2-oxoglutarate. *Mol. BioSyst.* **2005**, *1*, 321–324.

51. McDonough, M. A.; Loenarz, C.; Chowdhury, R.; Clifton, I. J.; Schofield, C. J. Structural studies on human 2-oxoglutarate dependent oxygenases. *Curr. Opin. Struct. Biol.* **2010**, *20*, 659–672.

52. Clifton, I. J.; McDonough, M. A.; Ehrismann, D.; Kershaw, N. J.; Granatino, N.; Schofield, C. J. Structural studies on 2-oxoglutarate oxygenases and related double-stranded β-helix fold proteins. *J. Inorg. Biochem.* **2006**, *100*, 644–669.

53. Bleijlevens, B.; Shivarattan, T.; Flashman, E.; Yang, Y.; Simpson, P. J.; Koivisto, P.; Sedgwick, B.; Schofield, C. J.; Matthews, S. J. Dynamic states of the DNA repair enzyme AlkB regulate product release. *EMBO Rep.* **2008**, *9*, 872–877.

54. Ehrismann, D.; Flashman, E.; Genn, D. N.; Mathioudakis, N.; Hewitson, K. S.; Ratcliffe, P. J.; Schofield, C. J. Studies on the activity of the hypoxia-inducible-factor hydroxylases using an oxygen consumption assay. *Biochem. J.* **2007**, *401*, 227–234.

55. Flagg, S. C.; Martin, C. B.; Taabazuing, C. Y.; Holmes, B. E.; Knapp, M. J. Screening chelating inhibitors of HIF-Prolyl Hydroxylase Domain 2 (PHD2) and Factor Inhibiting HIF (FIH). *J. Inorg. Biochem.* **2012**, *113*, 25–30.

56. Hardy, A. P.; Prokes, I.; Kelly, L.; Campbell, I. D.; Schofield, C. J. Asparaginyl β-hydroxylation of proteins containing ankyrin repeat domains influences their stability and function. *J. Mol. Biol.* **2009**, *392*, 994–1006.

57. *Protein-ligand interactions: structure and spectroscopy*; Harding, S. E., Chowdhry, B. Z., Eds.; Oxford University Press: Oxford, 2001.

58. *Protein-ligand interactions: hydrodynamics and calorimetry*; Harding, S. E., Chowdhry, B. Z., Eds.; Oxford University Press: Oxford, 2001.

59. Loo, J. A. Studying noncovalent protein complexes by electrospray ionization mass spectrometry. *Mass Spectrom. Rev.* **1997**, *16*, 25–49.

60. Meyer, B.; Peters, T. NMR spectroscopy techniques for screening and identifying ligand binding to protein receptors. *Angew. Chem. Int. Ed.* **2003**, *42*, 864–890.

61. Skinner, A. L.; Laurence, J. S. High-field solution NMR spectroscopy as a tool for assessing protein interactions with small molecule ligands. *J. Pharm. Sci.* **2008**, *97*, 4670–4695.

62. Ji, Z.; Yao, Z.; Liu, M. Saturation transfer difference nuclear magnetic resonance study on the specific binding of ligand to protein. *Anal. Biochem.* **2009**, *385*, 380–382.

63. Angulo, J.; Enríquez-Navas, P. M.; Nieto, P. M. Ligand-receptor binding affinities from saturation transfer difference (STD) NMR spectroscopy: the binding isotherm of STD initial growth rates. *Chem. Eur. J.* **2010**, *16*, 7803–7812.

64. Fielding, L.; Rutherford, S.; Fletcher, D. Determination of protein-ligand binding affinity by NMR: observation from serum albumin model systems. *Magn. Reson. Chem.* **2005**, *43*, 463–470.

65. Jahnke, W.; Floersheim, P.; Ostermeier, C.; Zhang, X.; Hemmig, R.; Hurth, K.; Uzunov, D. P. NMR reporter screening for the detection of high-affinity ligands. *Angew. Chem. Int. Ed.* **2002**, *41*, 3420–3423.

66. Dalvit, C.; Flocco, M.; Knapp, S.; Mostardini, M.; Perego, R.; Stockman, B. J.; Veronesi, M.; Varasi, M. High-throughput NMR-based screening with competition binding experiments. *J. Am. Chem. Soc.* **2002**, *124*, 7702–7709.

67. Dalvit, C.; Flocco, M.; Stockman, B. J.; Veronesi, M. Competition binding experiments for rapidly ranking lead molecules for their binding affinity to human serum albumin. *Comb. Chem. High Throughput Screening* **2002**, *5*, 645–650.

68. Manzenrieder, F.; Frank, A. O.; Kessler, H. Phosphorus NMR spectroscopy as a versatile tool for compound library screening. *Angew. Chem. Int. Ed.* **2008**, *47*, 2608–2611.

69. Dalvit, C. Ligand- and substrate-based ^{19}F NMR screening: Principles and applications to drug discovery. *Prog. Nucl. Magn. Reson. Spectrosc.* **2007**, *51*, 243–271.

70. Araç, D.; Murphy, T.; Rizo, J. Facile detection of protein-protein interactions by one-dimensional NMR spectroscopy. *Biochemistry* **2003**, *42*, 2774–2780.

71. Carr, H. Y.; Purcell, E. M. Effects of diffusion on free precession in nuclear magnetic resonance experiments. *Phys. Rev.* **1954**, *94*, 630–638.

72. Meiboom, S; Gill, D. Modified spin-echo method for measuring nuclear relaxation times. *Rev. Sci. Instrum.* **1958**, *29*, 688–691.

73. Hajduk, P. J.; Olejniczak, E. T.; Fesik, S. W. One-dimensional relaxation- and diffusion-edited NMR methods for screening compounds that bind to macromolecules. *J. Am. Chem. Soc.* **1997**, *119*, 12257–12261.

74. Aguilar, J. A.; Nilsson, M.; Bodenhausen, G.; Morris, G. A. Spin echo NMR spectra without J modulation. *Chem. Commun.* **2012**, *48*, 811–813.

75. Mole, D. R.; Schlemminger, I.; McNeill, L. A.; Hewitson, K. S.; Pugh, C. W.; Ratcliffe, P. J.; Schofield, C. J. 2-Oxoglutarate Analogue Inhibitors of HIF Prolyl Hydroxylase. *Bioorg. Med. Chem. Lett.* **2003**, *13*, 2677–2680.

76. Hirsila, M.; Koivunen, P.; Gunzler, V.; Kivirikko, K. I.; Myllyharju, J. Characterization of the human prolyl 4-hydroxylases that modify the hypoxia-inducible factor. *J. Biol. Chem.* **2003**, *278*, 30772–30780.

77. Warshakoon, N. C.; Wu, S.; Boyer, A.; Kawamoto, R.; Sheville, J.; Renock, S.; Xu, K.; Pokross, M.; Evdokimov, A. G.; Walter, R.; Mekel, M. A Novel Series of Imidazo[1,2-a]pyridine Derivatives as HIF-1α Prolyl Hydroxylase Inhibitors. *Bioorg. Med. Chem. Lett.* **2006**, *16*, 5598–5601.

78. Tegley, C. M.; Viswanadhan , V. N.; Biswas, K.; Frohn, M. J.; Peterkin, T. A. N.; Chang, C.; Bürli, R. W.; Dao, J. H.; Veith, H.; Rogers, N.; Yoder, S. C.; Biddlecome, G.; Tagari, P.; Allen, J. R.; Hungate, R. W. Discovery of Novel Hydroxy-Thiazoles as HIF-α Prolyl Hydroxylase Inhibitors: SAR, Synthesis, and Modeling Evaluation. *Bioorg. Med. Chem. Lett.* **2008**, *18*, 3925–3928.

79. King, O. N. F.; Li, X. S.; Sakurai, M.; Kawamura, A.; Rose, N. R.; Ng, S. S.; Quinn, A. M.; Rai, G.; Mott, B. T.; Beswick, P.; Klose, R. J.; Oppermann, U.; Jadhav, A.; Heightman, T. D.; Maloney, D. J.; Schofield, C. J.; Simeonov, A. Quantitative high-throughput screening identifies 8-hydroxyquinolines as cell-active histone demethylase inhibitors. *PLoS ONE* **2010**, *5*, e15535.

80. Nikolovska-Coleska, Z.; Wang, R.; Fang, X.; Pan, H.; Tomita, Y.; Li, P.; Roller, P. P.; Krajewski, K.; Saito, N. G.; Stuckey, J. A.; Wang, S. Development and optimization of a binding assay for the XIAP BIR3 domain using fluorescence polarization. *Anal. Biochem.* **2004**, *332*, 261–273.

81. Cer, R. Z.; Mudunuri, U.; Stephens, R.; Lebeda, F. J. IC_{50}-to-K_i: a web-based tool for converting IC_{50} to K_i values for inhibitors of enzyme activity and ligand binding. *Nucl. Acids Res.* **2009**, *37*, W441–W445.

82. Koivunen, P.; Hirsila, M.; Gunzler, V.; Kivirikko, K. I.; Myllyharju, J. Catalytic properties of the asparaginyl hydroxylase (FIH) in the oxygen sensing pathway are distinct from those of its prolyl 4-hydroxylases. *J. Biol. Chem.* **2004**, *279*, 9899–9904.

83. Koivunen, P.; Hirsilä, M.; Remes, A. M.; Hassinen, I. E.; Kivirikko, K. I.; Myllyharju, J. Inhibition of hypoxia-inducible factor (HIF) hydroxylases by citric acid cycle intermediates. Possible links between cell metabolism and stabilization of HIF. *J. Biol. Chem.* **2007**, *282*, 4524–4532.

84. Isaacs, J. S.; Jung, Y. J.; Mole, D. R.; Lee, S.; Torres-Cabala1, C.; Chung, Y.-L.; Merino, M.; Trepel, J.; Zbar, B.; Toro, J.; Ratcliffe, P. J.; Linehan, W. M.; Neckers, L. HIF overexpression correlates with biallelic loss of fumaratehydratase in renal cancer: Novel role of fumarate in regulation of HIF stability. *Cancer Cell* **2005**, *8*, 143–153.

85. King, A.; Selak, M. A.; Gottlieb, E. Succinate dehydrogenase and fumarate hydratase: linking mitochondrial dysfunction and cancer. *Oncogene* **2006**, *25*, 4675–4682.

86. Sudarshan, S.; Linehan, W. M.; Neckers, L. HIF and fumarate hydratase in renal cancer. *B. J. Cancer* **2007**, *96*, 403–407.

87. Reitman, Z. J.; Yan, H. Isocitrate dehydrogenase 1 and 2 mutations in cancer: alterations at a crossroads of cellular metabolism. *J. Natl. Cancer Inst.* **2010**, *102*, 932–941.

88. Dang, L.; Jin, S.; Su, S. M. IDH mutations in glioma and acute myeloid leukemia. *Trends Mol. Med.* **2010**, *16*, 387–397.

89. Dang, L.; White, D. W.; Gross, S.; Bennett, B. D.; Bittinger, M. A.; Driggers, E. M.; Fantin, V. R.; Jang, H. G.; Jin, S.; Keenan, M. C.; Marks, K. M.; Prins, R. M.; Ward, P. S.; Yen, K. E.; Liau, L. M.; Rabinowitz, J. D.; Cantley, L. C.; Thompson, C. B.; Vander Heiden, M. G.; Su, S. M. Cancer-associated IDH1 mutations produce 2-hydroxyglutarate. *Nature* **2009**, *462*, 739–744.

90. Struys, E. A. D-2-Hydroxyglutaric aciduria: unravelling the biochemical pathway and the genetic defect. *J. Inherit. Metab. Dis.* **2006**, *29*, 21–29.

91. Barth, P. G.; Hoffmann, G. F.; Jaeken, J.; Lehnert, W.; Hanefeld, F.; Van Gennip, A. H.; Duran, M.; Valk, J.; Schutgens, R. B. H.; Trefz, F. K.; Reimann, G.; Hartung, H.-P. L-2-Hydroxyglutaric acidemia: a novel inherited neurometabolic disease. *Ann. Neurol.* **1992**, *32*, 66–71.

92. Xu, W.; Yang, H.; Liu, Y.; Yang, Y.; Wang, P.; Kim, S.-H.; Ito, S.; Yang, C.; Wang, P.; Xiao, M.-T.; Liu, L.-x.; Jiang, W.-q.; Liu, J.; Zhang, J.-y.; Wang, B.; Frye, S.; Zhang, Y.; Xu, Y.-h.; Lei, Q.-y.; Guan, K.-L.; Zhao, S.-m.; Xiong, Y. Oncometabolite 2-hydroxyglutarate is a

competitive inhibitor of α-ketoglutarate-dependent dioxygenases. *Cancer Cell* **2011**, *19*, 17–30.

93. Koivunen, P.; Lee, S.; Duncan, C. G.; Lopez, G.; Lu, G.; Ramkissoon, S.; Losman, J. A.; Joensuu, P.; Bergmann, U.; Gross, S.; Travins, J.; Weiss, S.; Looper, R.; Ligon, K. L.; Verhaak, R. G. W.; Yan, H.; Kaelin Jr, W. G. Transformation by the (*R*)-enantiomer of 2-hydroxyglutarate linked to EGLN activation. *Nature* **2012**, *483*, 484–488.

94. Majamaa, K.; Hanauske-Abel, H. M.; Gübzler, V.; Kivirikko, K. I. The 2-oxoglutarate binding site of prolyl 4-hydroxylase. *Eur. J. Biochem.* **1984**, *138*, 239–245.

95. Lawrence, C. C.; Sobey, W. J.; Field, R. A.; Baldwin, J. E.; Schofield, C. J. Purification and initial characterization of proline 4-hydroxylase from Streptomyces griseoviridus P8648: a 2-oxoacid, ferrous-dependent dioxygenase involved in etamycin biosynthesis. *Biochem. J.* **1996**, *313*, 185–192.

96. Flashman, E.; Bagg, E. A. L.; Chowdhury, R.; Mecinović, J.; Loenarz, C.; McDonough, M. A.; Hewitson, K. S.; Schofield, C. J. Kinetic rationale for selectivity toward N- and C-terminal oxygen-dependent degradation domain substrates mediated by a loop region of hypoxia-inducible factor prolyl hydroxylases. *J. Biol. Chem.* **2008**, *283*, 3808–3815.

97. Tsukada, Y.-I.; Fang, J.; Erdjument-Bromage, H.; Warren, M. E.; Borchers, C. H.; Tempst, P.; Zhang, Y. Histone demethylation by a family of JmjC domain-containing proteins. *Nature* **2006**, *439*, 811–816.

98. Varier, R. A. Timmers, H. T. Histone lysine methylation and demethylation pathways in cancer. *Biochim. Biophys. Acta* **2010**, *1815*, 75–89.

99. Kovacevic, S.; Weigel, B. J.; Tobin, M. B.; Ingolia, T. D.; Miller, J. R. Cloning, characterization, and expression in Escherichia coli of the Streptomyces clavuligerus gene encoding deacetoxycephalosporin C synthetase. *J. Bacteriol.* **1989**, *171*, 754–760.

100. Lloyd, M. D.; Lee, H.-J.; Harlos, K.; Zhang, Z. H.; Baldwin, J. E.; Schofield, C. J.; Charnock, J. M.; Garner, C. D.; Hara, T.; Terwisscha van Scheltinga, A. C.; Valegård, K.; Viklund, J. A. C.; Hajdu, J.; Andersson, I.; Danielsson, Å.; Bhikhabhai, R. Studies on the active site of deacetoxycephalosporin C synthase. *J. Mol. Biol.* **1999**, *287*, 943–960.

101. Lipscomb, S. J.; Lee, H.-J.; Mukherji, M.; Baldwin, J. E.; Schofield, C. J.; Lloyd, M. D. The role of arginine residues in substrate binding and catalysis by deacetoxycephalosporin C synthase. *Eur. J. Biochem.* **2002**, *269*, 2735–2739.

102. Lloyd, M. D.; Lipscomb, S. J.; Hewitson, K. S.; Hensgens, C. M. H.; Baldwin, J. E.; Schofield, C. J. Controlling the substrate selectivity of deacetoxycephalosporin/deacetylcephalosporin C synthase. *J. Biol. Chem.* **2004**, *279*, 15420–15426.

103. Valegård, K.; Terwisscha van Scheltinga, A. C.; Dubus, A.; Ranghino, G.; Öster, L. M.; Hajdu, J.; Andersson, I. The structural basis of cephalosporin formation in a mononuclear ferrous enzyme. *Nat. Struct. Mol. Biol.* **2004**, *11*, 95–101.

104. Wehbie, R. S.; Punekar, N. S.; Lardy, H. A. Rat liver γ-butyrobetaine hydroxylase catalyzed reaction: influence of potassium, substrates, and substrate analogues on hydroxylation and decarboxylation. *Biochemistry* **1988**, *27*, 2222–2228.

105. McNeill, L. A.; Bethge, L.; Hewitson, K. S.; Schofield, C. J. A fluorescence-based assay for 2-oxoglutarate-dependent oxygenases. *Anal. Biochem.* **2005**, *336*, 125–131.

106. Welford, R. W. D.; Clifton, I. J.; Turnbull, J. J.; Wilson, S. C.; Schofield, C. J. Structural and mechanistic studies on anthocyanidin synthase catalysed oxidation of flavanone substrates: the effect of C-2 stereochemistry on product selectivity and mechanism. *Org. Biomol. Chem.* **2005**, *3*, 3117–3126.

107. Burton, D. R.; Forsen, S.; Karlstrom, G.; Dwek R. A. Proton relaxation enhancement (PRE) in biochemistry: a critical survey. *Prog. Nucl. Magn. Reson. Spectrosc.* **1979**, *13*, 1–45.

108. Mohr, P. J.; Taylor B. N.; Newell, D. B. CODATA recommended values of the fundamental physical constants: 2006. *Rev. Mod. Phys.* **2008**, *80*, 633–730.

109. Eisinger, J.; Shulman, R. G.; Blumberg, W. E. Relaxation enhancement by paramagnetic ion binding to deoxyribonucleic acid solutions. *Nature* **1961**, *192*, 963–964.

110. Mildvan, A. S.; Cohn, M. Magnetic resonance studies of the interaction of the manganous ion with bovine serum albumin. *Biochemistry* **1963**, *2*, 910–919.

111. Danchim, A.; Guéron, M. Proton magnetic relaxation study of the manganese-transfer-RNA complex. *J. Chem. Phys.* **1970**, *53*, 3599–3609.

112. Sherry, A. D.; Birnbaum, E. R.; Darnall, D. W. Proton relaxation studies in H_2O-D_2O mixtures the binding of manganese(II) to bovine serum albumin. *Anal. Biochem.* **1973**, *52*, 415–420.

113. Budak, H. Water proton relaxation rate enhancements and association constants for Mn(II) to serum proteins determined by NMR T_1 measurements. *Z. Naturforsch.* **2005**, *60c*, 807-812.

114. Yilmaz, A.; Koylu, Z.; Uysal, E. Proton NMR relaxation in albumin solutions doped with Mn(II). *Appl. Magn. Reson.* **2009**, *35*, 601–612.

115. Köylü, M. Z.; Asubay, S.; Yilmaz, A. Determination of proton relaxivities of Mn(II), Cu(II) and Cr(III) added to solutions of serum proteins. *Molecules* **2009**, *14*, 1537–1545.

116. Bertini, I.; Fragai, M.; Luchinat, C; Talluri, E. Water-based ligand screening for paramagnetic metalloproteins. *Angew. Chem. Int. Ed.* **2008**, *47*, 4533–4537.

117. Mildvan A. S.; Engle J. L. Nuclear relaxation measurements of water protons and other ligands. *Methods Enzymol.* **1972**, *26*, 654–682.

118. Mildvan A. S.; Gupta R. K. Nuclear relaxation measurements of the geometry of enzyme-bound substrates and analogs. *Methods Enzymol.* **1978**, *49*, 322–359.

119. Niccolai, N.; Tiezzi, E.; Valensin, G. Manganese(II) as magnetic relaxation probe in the study of biomechanisms and of biomacromolecules. *Chem. Rev.* **1982**, *82*, 359–384.

120. Smith, A. E. A study of the variation with pH of the solubility and stability of some metal ions at low concentrations in aqueous solution. Part 1. *Analyst* **1973**, *88*, 65–68.

121. McDonough, M. A.; Li, V.; Flashman, E.; Chowdhury, R.; Mohr, C.; Liénard, B. M. R.; Zondlo, J.; Oldham, N. J.; Clifton, I. J.; Lewis, J.; McNeill, L. A.; Kurzeja, R. J. M.; Hewitson, K. S.; Yang, E.; Jordan, S.; Syed, R. S.; Schofield, C. J. Cellular oxygen sensing: crystal structure of hypoxia-inducible factor prolyl hydroxylase (PHD2). *Proc. Natl. Acad. Sci. U. S. A.* **2006**, *103*, 9814–9819.

122. McDonough, M. A.; McNeill, L. A.; Tilliet, M.,; Papamicaël, C. A.; Chen, Q. Y.; Banerji, B.; Hewitson, K. S., Schofield, C. J. Selective inhibition of factor inhibiting hypoxia-inducible factor. *J. Am. Chem. Soc.* **2005**, *127*, 7680–7681.

123. Stubbs, C. J.; Loenarz, C.; Mecinović, J.; Yeoh, K. K.; Hindley, N.; Liénard, B. M.; Sobott, F.; Schofield, C. J.; Flashman, E. Application of a proteolysis/mass spectrometry method for investigating the effects of inhibitors on hydroxylase structure. *J. Med. Chem.* **2009**, *52*, 2799–2805.

124. Chowdhury, R.; McDonough, M. A.; Mecinović, J.; Loenarz, C.; Flashman, E.; Hewitson, K. S.; Domene, C.; Schofield, C. J. Structural basis for binding of hypoxia-inducible factor to the oxygen-sensing prolyl hydroxylases. *Structure* **2009**, *17*, 981–989.

4. Protein NMR studies on HIF prolyl hydroxylase PHD2[†]

4.1 Introduction

4.1.1 Structural aspects of PHD2

Progress in the molecular understanding of how HIF prolyl hydroxylases (PHDs), in particular the key human oxygen sensor PHD2, interact with their co-substrates and substrates has mainly been driven by X-ray crystallography.[1,2] The first crystal structure of PHD2 in complex with a (bicyclic) inhibitor was published in 2006 (PDB id: 2G19).[1] The structure revealed that, similar to all other biologically characterised 2OG oxygenases,[3–5] PHD2 contains a core double-stranded β-helix (DSBH) fold, which forms two β-sheets adopting a sandwich-like structure (major sheet: β1, β8, β5, β10, β4 and minor sheet: β7, β6, β9, βII; Figure 4-1). The structure reveals that the active site is located at the open end of the squashed DSBH barrel between the two β-sheets that form the DSBH. The Fe(II)-binding residues (His-313, Asp-315 and His-374) are located in a conserved HXD/E...H metal binding motif;[3–5] two of these (His-313, Asp-315) immediately after βII, with one (His-374) preceding β9. In a manner similar to other 2OG oxygenases,[5] PHD2 contains extra structural features in addition to the DSBH core. In the catalytic domain, these include one helix (α4) to the *C*-terminal side of the DSBH, and a small loop of eight residues between β6 and β7 of the DSBH. Human PHD2 also contains a non-catalytic MYND (myeloid, Nervy, and DEAF-1) type zinc finger at the *N*-terminal side of the DSBH (Figure 4-2).

A crystal structure of PHD2 in complex with a 19-residue peptide substrate, the *C*-terminal oxygen-dependent degradation domain (CODD) of HIF-1α (HIF-1$\alpha_{556\text{-}574}$; Sequence: DLDLEMLAPYIPMDDDFQL), was reported in 2009 (PDB id: 3HQR).[2] The CODD peptide was found to bind in a cleft on the PHD2 surface. An induced fit mechanism was indicated from the structure, in which residues 237-254 appear to adopt a closed loop conformation,[2] whilst in the structure without CODD, the same residues adopted an open finger-like "β2β3" conformation (Figure 4-3).[1] It is worth

---

[†] *The work in this Chapter was conducted in collaboration with Dr Adam P. Hardy and Dr Richard J. Hopkinson.*

A.P.H. provided technical support in the production and purification of isotopic labelled PHD2. R.J.H. synthesised and purified P564G CODD.

noting that although PHD2 exists (at least predominantly) as a monomer in solution, the substrate-free PHD2 structure crystallised as a homotrimer.[1]

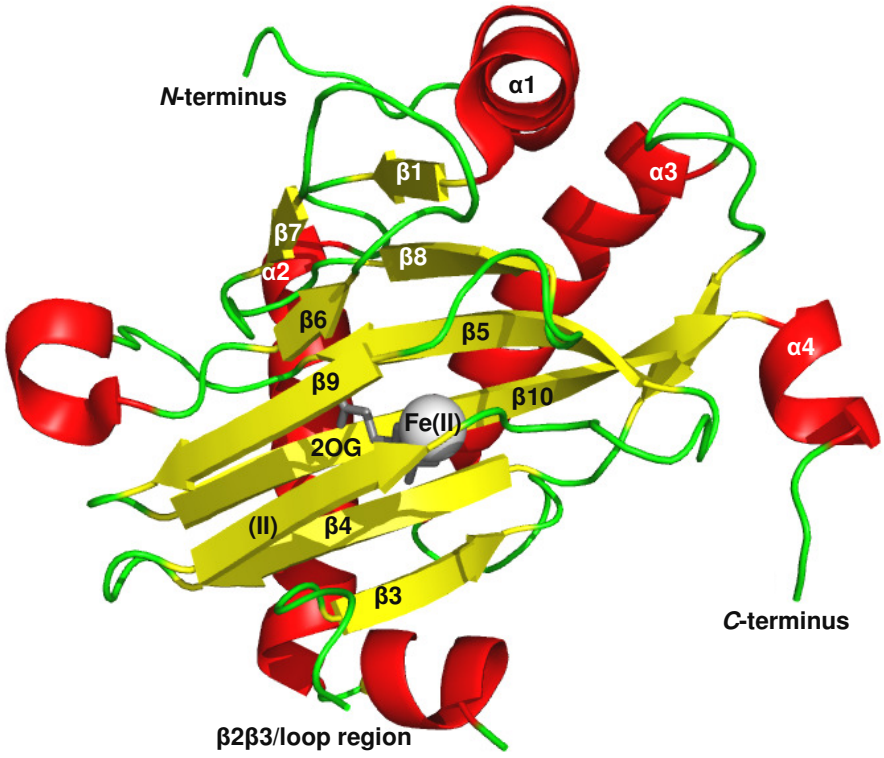

Figure 4-1 A view of the PHD2 X-ray crystal structure in complex with Fe(II) and 2OG (PDB id: 3OUJ). Red represents α-helix and yellow represents β-strand regions.

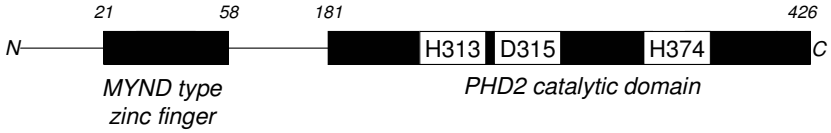

Figure 4-2 Schematic representation of the PHD2 sequence. The *N*-terminus contains a MYND type zinc finger and the catalytic domain is located in the *C*-terminus. The Fe(II)-binding residues (His-313, Asp-315 and His-374) are located in a conserved HXD/E...H metal binding motif.

In 2010, another crystal structure of PHD2 in complex with Fe(II) and 2OG (PDB id: 3OUJ) was reported.[6] In the reported structure, the β2β3/loop region of PHD2 was not visible, which implies dynamics in this region (Figure 4-1). Further evidence to support the existence of different dynamic states of PHD2 upon substrate/co-substrate binding came from a preliminary solution NMR study.[7] In that study, the methyl region of PHD2-Fe(II) and PHD2-Co(II) was monitored by ^{1}H NMR spectroscopy. Significant changes in the methyl region were observed upon co-substrate (2OG) or co-product (succinate) binding, thus implying dynamics in the PHD2 system.[7] Recently, a study using long-term molecular dynamics simulations revealed that the β2β3/loop region is flexible in the substrate free form (PHD2-Fe(II)-2OG), but is

more rigid when the substrate is bound (PHD2-Fe(II)-2OG-CODD),[8] thus providing further evidence about its role in substrate selectivity and the stabilisation of substrate binding.

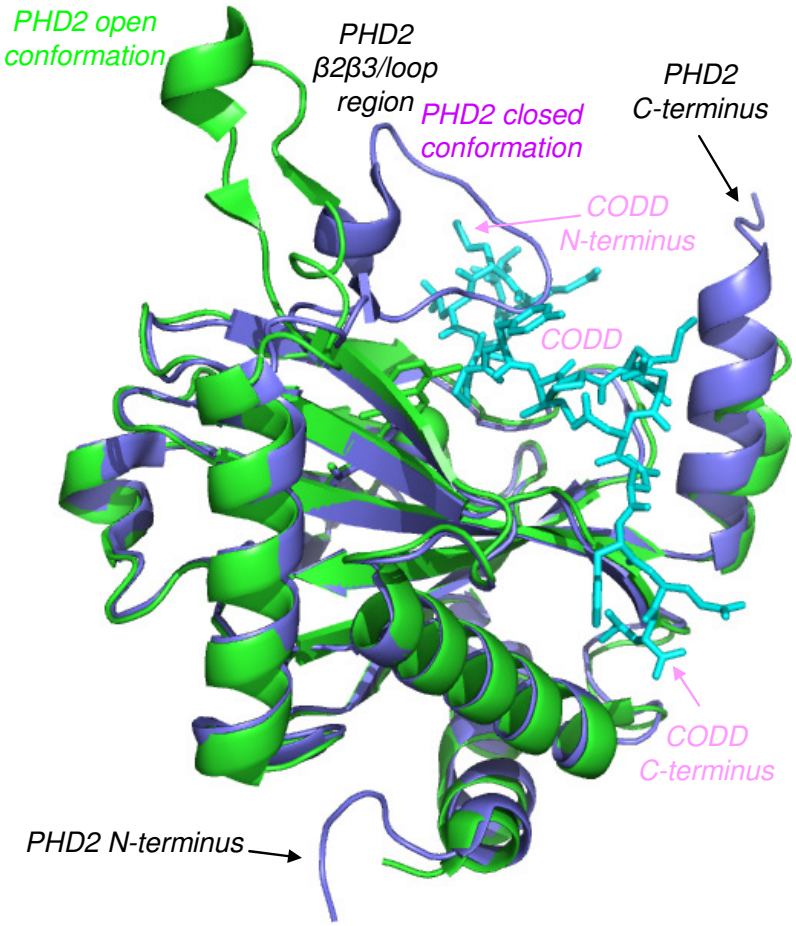

Figure 4-3 Alignment of two reported PHD2 X-ray crystal structures (PDB ids: 2G19 and 3HQR). The substrate-free structure (PHD2-Fe(II)-inhibitor; green) shows that residues 237-254 of PHD2 adopt an open "β2β3" like conformation. The CODD-complexed structure (PHD2-Mn(II)-2OG-CODD; blue) showed that it adopts a more closed "loop" conformation that envelopes the substrate residues. The substrate CODD is shown in cyan.

In addition to protein structures, pioneering work investigating the conformations of the HIF proline (Pro-564) and hydroxyproline residues on the hydroxylation site of CODD was also reported in 2009.[9] The work implies that although the proline residue exists in both C^4-*endo* and C^4-*exo* conformations in solution, it primarily exists in the C^4-*endo* form when it is bound to PHD2 (Figure 4-4). However, the hydroxyproline residue in hydroxylated CODD (hyCODD; product of CODD hydroxylation) favours a C^4-*exo* conformation due to the stereoelectronic *gauche* effect.[10,11] Similar effects have also been reported for the hydroxylated proline residue of the procollagen substrate for human collagen prolyl 4-hydroxylase.[12–14]

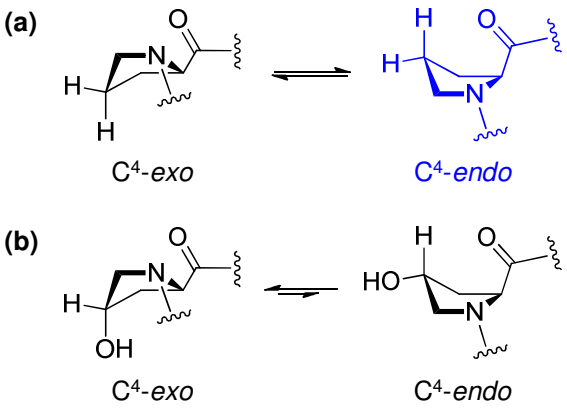

Figure 4-4 (a) When CODD (sequence: DLDLEMLAPYIPMDDDFQL) is free in solution, the proline residue at the hydroxylation site of CODD adopts both C^4-*exo* and C^4-*endo* conformations. When CODD is bound to PHD2, the proline residue primarily adopts the C^4-*endo* conformation, which is highlighted in blue; (b) The conformation the hydroxyproline residue in hydroxylated CODD is biased towards the C^4-*exo* conformation due to the stereoelectronic *gauche* effect.

4.1.2 Protein NMR spectroscopy

Protein NMR spectroscopy often involves the studies of protein-ligand interactions, protein structures and protein dynamics by the observation of protein resonances as opposed to ligand resonances (for reviews see references 15–18). The most common way to conduct protein NMR spectroscopy is to monitor ^{1}H-^{15}N one-bond correlations of amide protons from the protein backbone in uniformly isotopically ^{15}N-labelled proteins. In theory each amino acid residue gives one such correlation in a ^{1}H-^{15}N HSQC spectrum, except for proline which gives no signal due to the lack of amide proton. Some residues, such as asparagine and glutamine, give extra signals arising from side chain amide NH resonances. Backbone amide chemical shifts are sensitive to changes in both local environment and the overall secondary structure of proteins, therefore making them good probes for protein studies. Although protein NMR is probably best suited to the study of relatively small proteins (<25 kDa) because amide proton relaxation rates increase with protein molecular weight,[19] the development of transverse relaxation optimised spectroscopy (TROSY)[20,21] allows the study of ^{1}H-^{15}N correlations of protein complexes up to 800–900 kDa.[22,23] For very large proteins, the use of ^{1}H-$^{13}C_{methyl}$ correlation has gained increasing popularity because $^{13}C_{methyl}$ chemical shifts are a very sensitive probe to protein structure and dynamics, partly due to the favourable relaxation properties (slower relaxation) of methyl groups.[24,25] Protein complexes of up to 810 kDa in molecular weight have been studied using this method.[26]

In the context of protein-ligand interactions, the most common parameter used for observation is chemical shift.[27] Provided the exchange between the ligand-free and ligand-bound forms of the protein is fast on the NMR timescale, chemical shift perturbations allow the determination of binding constants as a function of ligand concentration without the need of prior protein assignment.[28] In addition, if the assignment of the protein backbone (see Section 4.3) is known, information such as ligand binding site on the protein and the amino acid residues involved in the binding interaction can be readily mapped out.[29,30] By using a series of structurally similar ligands, the relative binding orientations and structure-activity relationship of these binding ligands to the target protein can also identified (SAR-by-NMR).[31]

4.1.3 Protein backbone assignment

The most simple method of conducting sequential protein backbone assignment for a protein of the size of $PHD2_{181-402}$ (~25 kDa) is to apply the standard ^{1}H,^{13}C,^{15}N triple resonance strategy (for reviews 32–37). These 3D triple resonance experiments rely primarily on the relatively large ^{1}J (and sometimes ^{2}J) couplings in the protein backbone spin system (Figure 4-5) for coherent transfer of magnetisation. There are many types and variations of triple resonance experiments, the most typical experiments included HNCO,[35] HN(CA)CO,[38] HN(CO)CA,[35] HNCA,[35] HN(CO)CACB[39] and HNCACB.[40] The nomenclature of these experiments reflects the magnetisation transfer pathways (spins for which chemical shifts are not evolved are put in brackets; Figure 4-6).

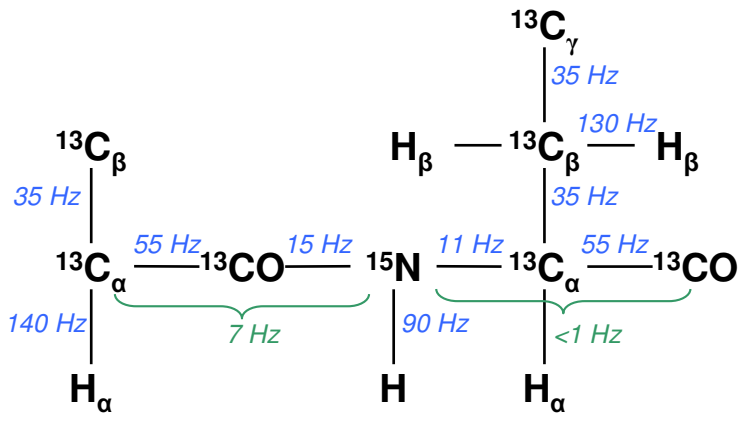

Figure 4-5 Typical $^{1}J/^{2}J$ coupling constants in a protein backbone spin system (adapted from reference 37). The blue numbers are ^{1}J and the green numbers are ^{2}J coupling constants respectively.

The easiest way to visualise a 3D spectrum is to consider it as a 2D spectrum (*e.g.* ^{1}H-^{15}N HSQC) extended into a third dimension (*e.g.* ^{13}C; Figure 4-7). Triple resonance

experiments usually work in pairs, with one experiment showing only inter-residue correlations and the other showing both inter- and intra-residue correlations (Figure 4-6 and Figure 4-8).

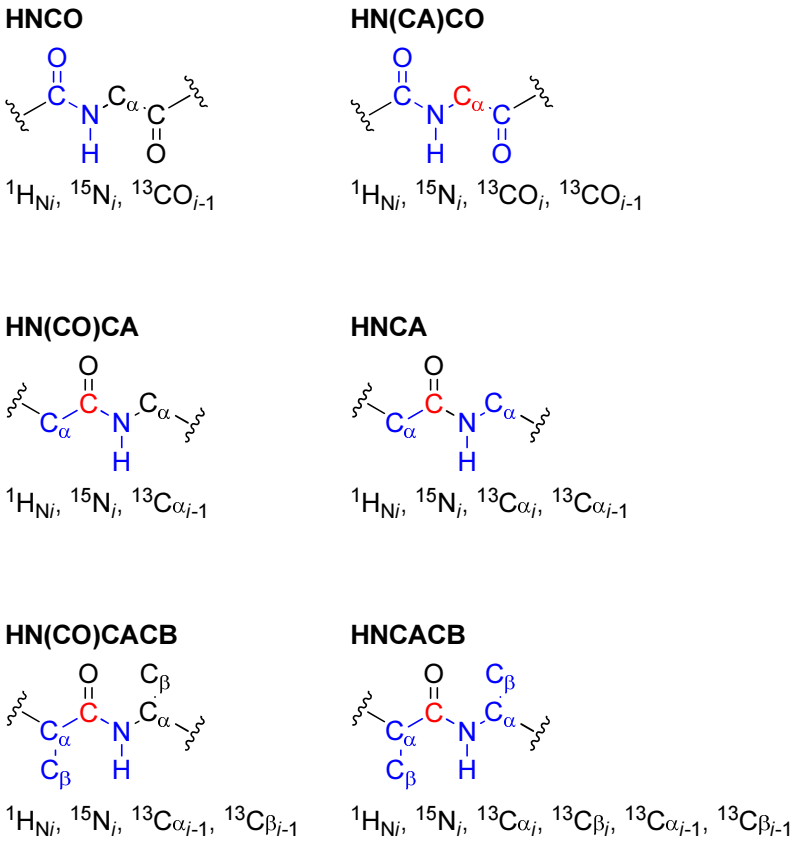

Figure 4-6 Triple resonance strategy for the sequential assignment of protein backbone resonances. The nomenclature of these experiments reflects their magnetisation transfer pathways (blue). Spins for which chemical shifts are not evolved are put in brackets (red).

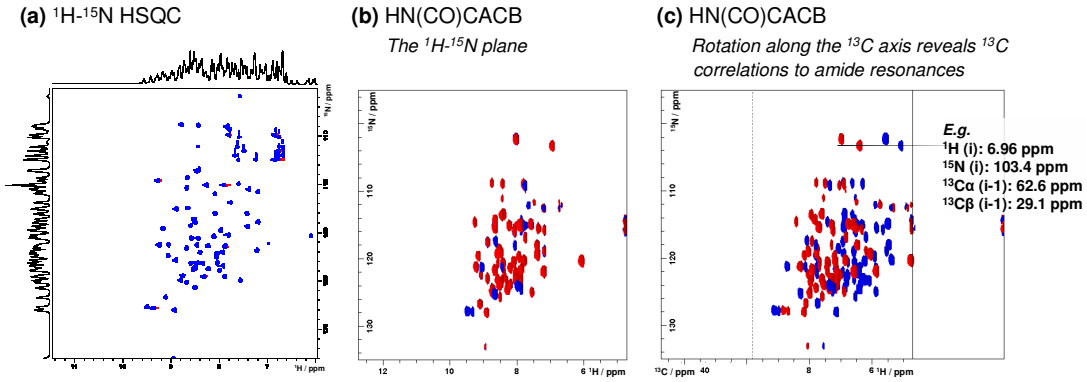

Figure 4-7 Example of a 3D triple resonance experiment. (a) ^{1}H-^{15}N HSQC of human ubiquitin; (b) HN(CO)CACB of the same sample (^{1}H-^{15}N plane). Note that many side chain amide resonances were edited away by the experiment; (c) The same HN(CO)CACB spectrum but rotated along the ^{13}C axis, and correlations to the α and β carbons of the previous residue can be obtained readily. Sample mixture contained 2.17 mM human ubiquitin in 50 mM phosphate buffer (pH 7.0) in 10% D_2O and 90% H_2O.

A common way of conducting protein assignment is by a "sequential walk" through the ^{1}H-^{13}C plane/strip of different ^{15}N resonances (Figure 4-8). For example, HNCO gives correlations between $^{1}H_{Ni}$, $^{15}N_{i}$ and $^{13}CO_{i-1}$, and HN(CA)CO gives correlations between $^{1}H_{Ni}$, $^{15}N_{i}$, $^{13}CO_{i-1}$ and $^{13}CO_{i}$. Therefore, the HNCO ^{1}H-^{13}C strip of residue *i* at $^{15}N_{i}$ ppm contains the ^{13}CO correlations of residue *i*-1, whilst the same ^{1}H-^{13}C strip of the corresponding HN(CA)CO spectrum contains the ^{13}CO correlations of both residues *i* and *i*-1 (Figure 4-8).

The $^{13}C_{\beta}$ chemical shift obtained from the HN(CO)CACB and HNCACB experiments also provides signature chemical shifts for certain amino acids such as alanine, serine and threonine, or in case of glycine, the lack of any $^{13}C_{\beta}$ chemical shift.

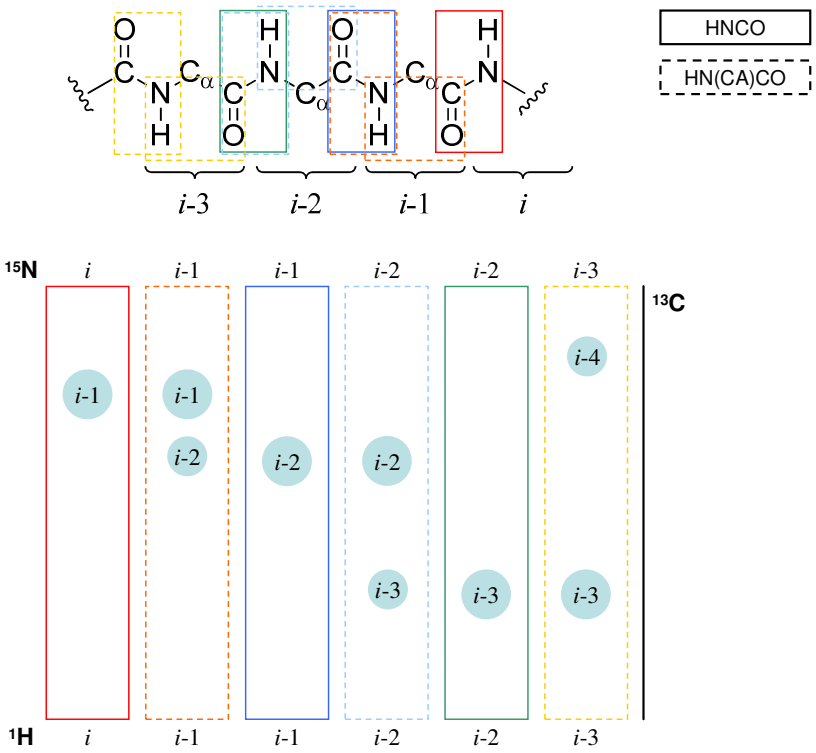

Figure 4-8 An illustration of a sequential walk along the ^{1}H-^{13}C plane of the HNCO (solid line) and NH(CA)CO (dotted line) experiments. HNCO shows correlation between the amide resonance of the current residue (*i*) and the CO resonance of the previous residue (*i*-1), whilst HN(CA)CO shows correlations between the amide resonance of the current residue (*i*) and the CO resonances of both the current (*i*) and the previous residues (*i*-1).

4.1.4 Objectives

The objectives of the work described in this Chapter were to produce and purify isotopically enriched PHD2 in order to conduct protein backbone assignments for PHD2, and to apply protein NMR spectroscopy to investigate conformational changes resulting from substrate binding to PHD2.

4.2 Preparation for protein NMR

4.2.1 Production of PHD2 in minimal media

In order to conduct protein NMR spectroscopy, it is necessary to produce ^{15}N-labelled protein in sufficient quantity (for reviews see references 41–43). A *C*- and *N*-terminal truncated construct of the catalytic domain of PHD2 ($PHD2_{181-402}$) was used in order to minimise spectral overlap and to reduce transverse relaxation losses to a minimum. Previous studies have indicated that there were minimal differences, at least *in vitro*, in the catalytic activity between $PHD2_{181-402}$ and the *N*-terminal truncated $PHD_{181-426}$ that was used elsewhere in the works described in this Thesis.[44]

Expression trials were carried out with glucose enriched M9 minimal medium (10 g glucose per litre) and the commercially available algal based Spectra 9 medium. Previous studies suggested the use of excess glucose may enhance the yield of labelled recombinant protein production in minimal media.[45] Spectra 9 is essentially a rich growth medium with a growth rate similar to LB and 2TY.[46] Expression trial used the following general procedure (for full experimental details see Chapter 6). An *E. coli* BL21(DE3) glycerol stock (obtained from Dr Adam P. Hardy) was first inoculated into 2TY and incubated at 37 °C overnight.[47,48] The starting culture was then divided and inoculated into the minimal and the algal media separately. Induction was initiated by addition of isopropyl β-D-1-thiogalactopyranoside (IPTG) when the cell density reached an optical density (OD_{600}) of 0.6–0.8. Protein production levels of both the insoluble and soluble fractions were analysed using sodium dodecylsulphate polyacrylamide gel electrophoresis (SDS-PAGE).

Variables	Conditions tested	
Media	Spectra 9	M9
IPTG	200 μM	500 μM
Temperature	28 ºC	37 ºC

Table 4-1 Expression variables tested for the production of ^{15}N-labelled $PHD2_{181-402}$. The best conditions were highlighted in blue. The M9 minimal media was enriched with 10 g/L glucose.

Several variables were investigated with respect to optimisation of recombinant protein production including temperature, IPTG concentration and incubation time (Table 4-1). Surprisingly, despite the fast growth rate in Spectra 9 medium, no $PHD2_{181-402}$ production was observed. The best conditions obtained involved the use of glucose enriched minimal medium, 200 μM IPTG concentration and overnight

incubation at 28 °C upon induction. Although previous studies have suggested that the addition of ferrous sulphate may improve cell density and expression,[49] this was not found to be required. Under the optimised condition typically around 15–20 mg of purified *apo*-^{15}N-PHD2$_{181\text{-}402}$ was obtained from 7.2 litres of media.

4.2.2 Establishing conditions for NMR analyses

Following the production of ^{15}N-labelled PHD2$_{181\text{-}402}$, initial ^{1}H-^{15}N HSQC analyses suggested that both *apo*-PHD2$_{181\text{-}402}$, PHD2$_{181\text{-}402}$-Zn(II) and PHD2$_{181\text{-}402}$-Zn(II)-2OG were apparently folded, with a spread of ^{1}H chemical shift from 6.3 ppm to 11.7 ppm, and ^{15}N chemical shift between 106.5 ppm and 132.5 ppm. The region between 7.4 ppm and 8.8 ppm was relatively crowded in the spectra and may contained resonances for some unstructured elements. Because the initial data looked promising, sample preparation procedures and other experimental considerations were investigated.[50,51]

Protein NMR is often conducted with protein solutions at a slightly acidic pH because at neutral or basic pH rapid exchange between amide protons and solvent H_2O may lead to exchange broadening. Two ^{15}N-labelled PHD2$_{181\text{-}402}$-Zn(II) samples, which were buffered at pH 7.5 and pH 6.6 respectively, were subjected to ^{1}H-^{15}N HSQC analyses (Figure 4-9). Sharper signals were observed with the sample that was buffered at pH 6.6. This condition was therefore used in all further experiments described in this Chapter.

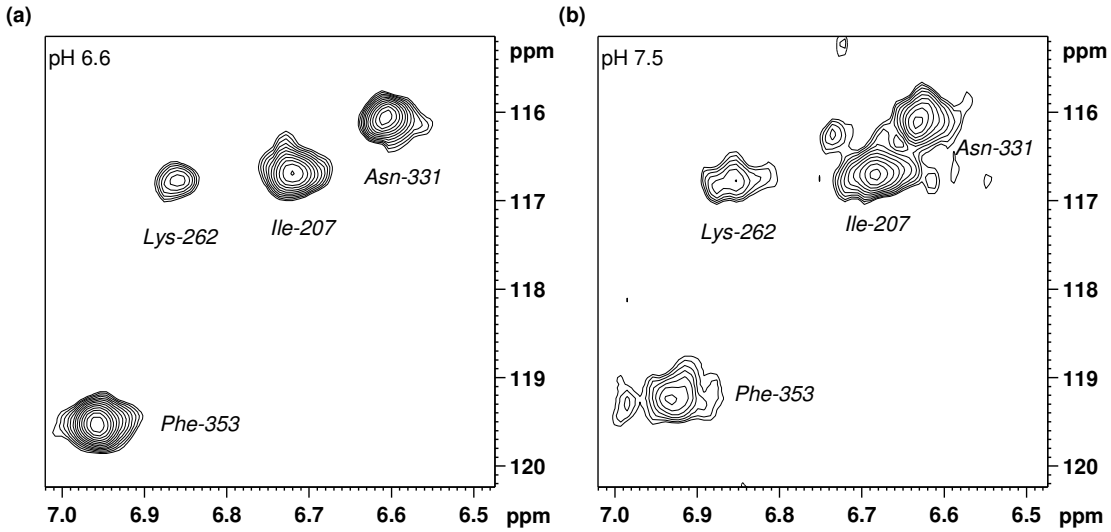

Figure 4-9 A region of the ^{1}H-^{15}N HSQC of PHD2$_{181\text{-}402}$-Zn(II) at pH 6.6 and 7.5 recorded at 700 MHz. The peaks are sharper and the signal-to-noise ratio is better at pH 6.6. The mixture contained 50 µM *apo*-^{15}N-PHD2$_{181\text{-}402}$, 50 µM Zn(II) and 50 mM Tris-D11 in 90% H_2O and 10% D_2O.

The long term stability of ^{15}N-PHD2$_{181-402}$ in solution at room temperature was also tested because of the length of the NMR experiments for protein assignment (days to weeks; Figure 4-10). It was found that *apo*-PHD2$_{181-402}$ was unstable and significant precipitation of *apo*-PHD2$_{181-402}$ was observed in less than 24 hours. However, in the presence of the metal ion Zn(II) and co-substrate 2OG, the sample remained unchanged after 12 days. In fact, it was subsequently found that it remained stable and apparently folded (as judged by ^{1}H-^{15}N HSQC) after half a year stored at 4 °C.

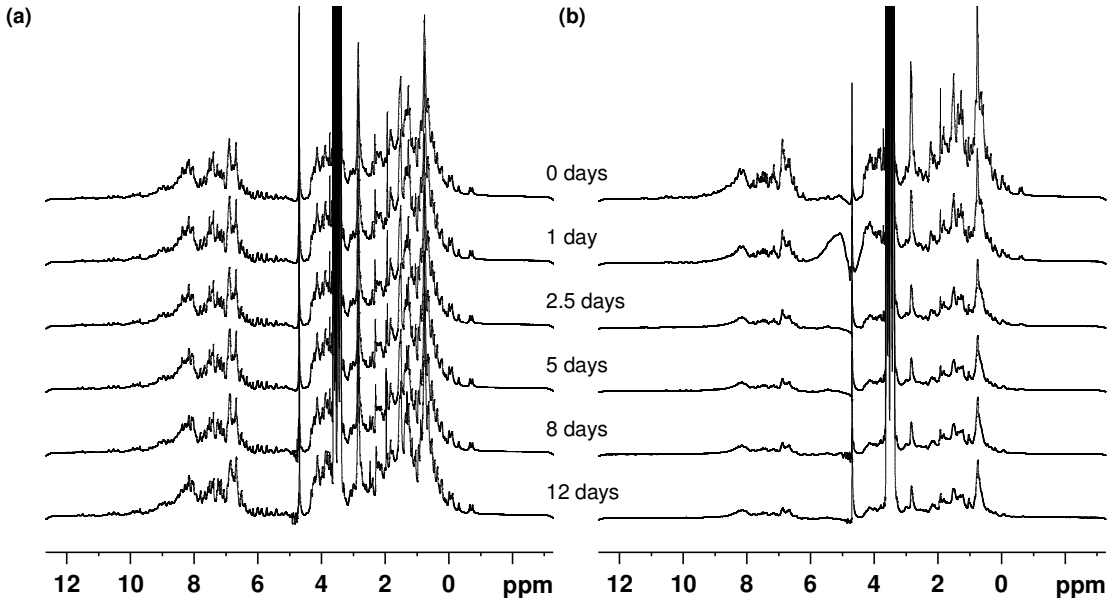

Figure 4-10 Stability of PHD2$_{181-402}$ at room temperature. (a) ^{15}N-PHD2$_{181-402}$-Zn(II)-2OG; (b) *apo*-^{15}N-PHD2$_{181-402}$ only. The drop in intensity is due to protein precipitation. The mixture contained ~1 mM *apo*-^{15}N-PHD2$_{181-402}$, 2 mM Zn(II), 3.5 mM 2OG and 50 mM Tris-D11 in 95% H_2O and 5% D_2O pH 6.6 where applicable.

Temperature is often a crucial parameter in protein NMR. In general, sharper peaks are observed at a higher temperature due to increase in the tumbling rate (reduced correlation times) of the protein. However, an increase in temperature may decrease the long term stability of the protein. Investigations were therefore carried out with ^{15}N-labelled PHD2$_{181-402}$-Zn(II)-2OG at different temperatures (Figure 4-11). At 5 °C, the amide proton signals were broadened and the overall signal-to-noise of the spectrum was poor. With increasing temperature (up to 37 °C), the amide proton signals became increasingly sharp and the spectral quality improved. Although sharpest signal was observed at 37 ºC, it was decided that for the work described in this Chapter, experiments would be conducted at 19 °C in order to achieve balance between protein stability and the quality of the spectra.

Finally, the performance between ^{1}H-^{15}N HSQC and ^{1}H-^{15}N TROSY-HSQC was compared. TROSY is a family of experiments that is routinely applied for the study of

large proteins at high fields. TROSY utilises the interference between ^{1}H-^{15}N dipolar coupling and chemical shift anisotropy to enable the recording of sharp amide signals.[20,21] Dipole-dipole interactions are field independent but chemical shift anisotropy is field dependent. For amide protons on a protein, the field to achieve the best cancellation is around 23.5 T (~1000 MHz in ^{1}H frequency). However the penalty for sharper signals is a loss of signal intensity from the editing process because TROSY only selects the narrowest component (1 out of 4 of the ^{1}H-^{15}N coupled amide resonances). With ^{15}N-labelled PHD2$_{181\text{-}402}$-Zn(II) at 700 MHz, there was no significant difference in the line widths observed between the HSQC and the TROSY-HSQC spectra (Figure 4-12). It was therefore decided to use the normal HSQC sequence for the further work described in this Chapter.

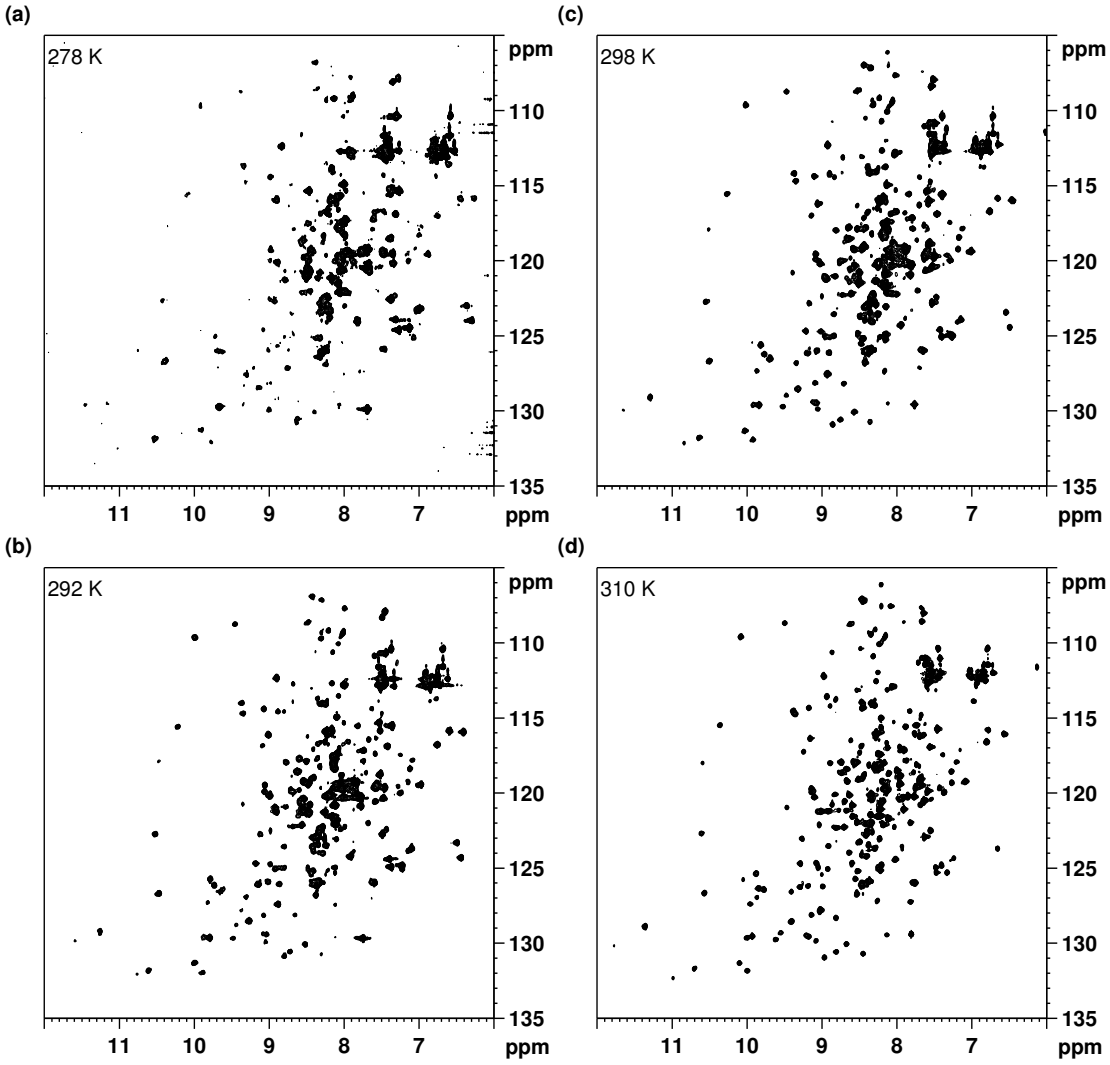

Figure 4-11 ^{1}H-^{15}N HSQC spectra of PHD2$_{181\text{-}402}$-Zn(II)-2OG at four different temperatures. The peaks are sharper as the temperature increases, especially in the region between 7.5 ppm and 9 ppm. The mixture contained 300 µM *apo*-^{15}N-PHD2$_{181\text{-}402}$, 500 µM Zn(II), 750 µM 2OG and 50 mM Tris-D11 in 95% H_2O and 5% D_2O pH 6.6. The spectra were recorded at 700 MHz.

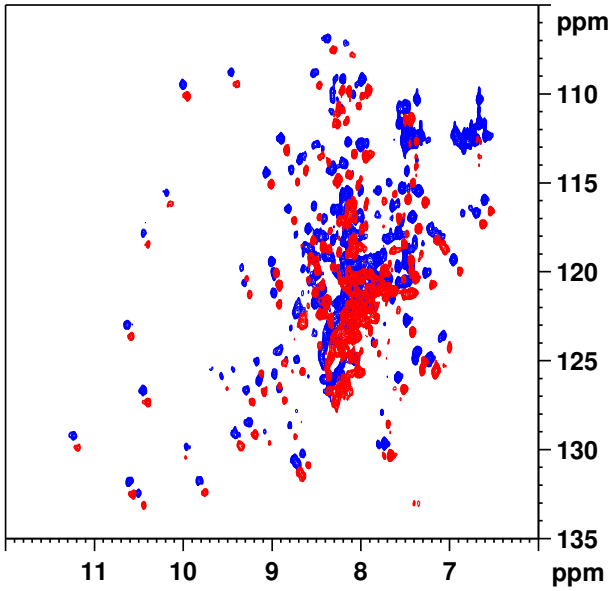

Figure 4-12 ^{1}H-^{15}N HSQC (blue) and ^{1}H-^{15}N TROSY-HSQC (red) of PHD2$_{181-402}$-Zn(II) at 700 MHz. The mixture contained 50 µM *apo*-^{15}N-PHD2$_{181-402}$, 50 µM Zn(II) and 50 mM Tris-D11 in 95% H_2O and 5% D_2O pH 6.6. Relaxation delay for ^{1}H-^{15}N HSQC is 1 second and for ^{1}H-^{15}N TROSY-HSQC is 2 seconds. Because a longer relaxation delay is required to obtain an optimal TROSY-HSQC spectrum, the total experiment time is essentially doubled. Note the chemical shift differences between ^{1}H-^{15}N HSQC (with ^{1}H decoupling during ^{15}N evolution and ^{15}N decoupling during ^{1}H acquisition) and the ^{1}H-^{15}N TROSY-HSQC (no decoupling, with selective observation of the slowest relaxing component).

4.3 Backbone resonance assignment of PHD2$_{181-402}$

4.3.1 Backbone resonance assignment

Double labelled (^{13}C and ^{15}N) protein was a prerequisite for the planned triple resonance experiments for protein assignment. The production of doubly ^{13}C and ^{15}N labelled protein requires the use of uniformly ^{13}C-labelled glucose as the sole carbon source in the minimal media. The same growth conditions that were used for ^{15}N-labelled PHD2 were applied for ^{13}C-labelled PHD2 production, except 4 g/L ^{13}C-glucose was added to the M9 minimal media (instead of 10 g/L unlabelled glucose; as judged by expression trial) due to the cost of the ^{13}C-labelled sugar. About 4 mg of *apo*-^{13}C,^{15}N-labelled PHD2$_{181-402}$ was obtained from 5 litres of doubly labelled minimal media.

The ^{1}H-^{15}N HSQC spectra of *apo*-^{15}N-PHD2$_{181-402}$ and *apo*-^{13}C,^{15}N-PHD2$_{181-402}$ were found to be very similar (Figure 4-13), indicating there are minimal ^{13}C-isotopic shifts to the backbone amide resonances. Triple resonance experiments were then conducted with *apo*-^{13}C,^{15}N-PHD2$_{181-402}$. A relatively high initial concentration (~1 mM) of protein was used due to the high degradation/precipitation rate (see also Section 4.2.2). HNCO was the most sensitive experiment and most of the expected cross

peaks were observed (Figure 4-14). However, in the corresponding HN(CA)CO experiment, many cross peaks were missing, and the spectral qualities of the HN(CO)CA and HNCA experiments were also poor. Because triple resonance experiments rely on one or two bond scalar couplings between ^{1}H, ^{13}C and ^{15}N, the missing cross peaks and poor spectral quality were likely due to fast relaxation of all participating spins, especially ^{13}C, arising from the size of the protein (25 kDa), and protein degradation/precipitation (due to the use of *apo*-protein).

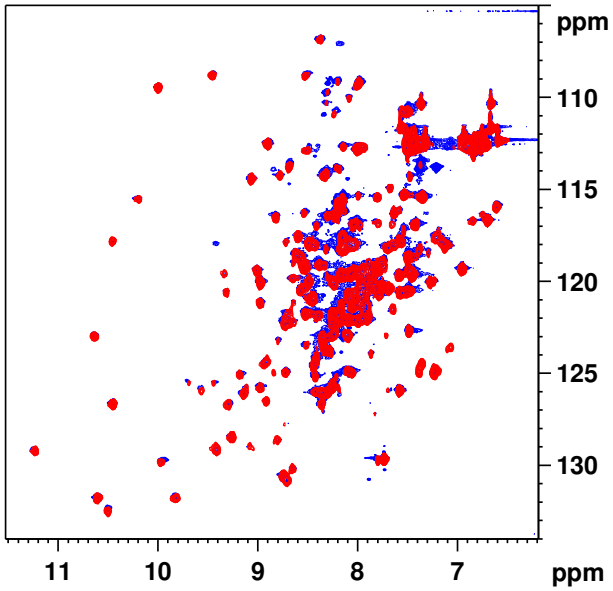

Figure 4-13 Overlaying the ^{1}H-^{15}N HSQC spectra of *apo*-^{15}N-PHD2$_{181\text{-}402}$ (red) and *apo*-^{13}C,^{15}N-PHD2$_{181\text{-}402}$ (blue), indicating there are minimal ^{13}C-isotopic shifts on amide resonances. Sample contained 1 mM *apo*-^{13}C,^{15}N-PHD2$_{181\text{-}402}$ or 150 µM *apo*-^{15}N-PHD2$_{181\text{-}402}$ buffered with 50 mM Tris-D11 (pH 6.6) in 95% H_2O and 5% D_2O.

A method to decrease the relaxation rate is by protein perdeuteration because deuterium has a lower magnetogyric ratio than proton (γ^2H/γ^1H = 0.15). The replacement of all the non-exchangeable protons with deuteriums essentially eliminates the dominant ^{1}H-^{13}C relaxation pathway. Expression trials were therefore conducted in D_2O with glucose-enriched minimal media with a glucose concentration of 4 g/L. Several variables, including IPTG concentration, cell density (OD_{600}) for induction, incubation time and temperature, were investigated (Table 4-2). In the expression trials, normal glucose was used instead of the expensive doubly ^{2}H,^{13}C-labelled glucose. Similar to the expression conditions of the single/double labelled PHD2$_{181\text{-}402}$, the starting culture was incubated in 2TY, but the incubation temperature was lowered to 30 °C to minimise the stress applied to *E. coli*.[48] No bacterial adaptation to deuterated medium was performed. No unfolding/re-folding of the purified protein was attempted due to the instability of *apo*-PHD2$_{181\text{-}402}$. About 9 mg

of *apo*-^{2}H,^{13}C,^{15}N-PHD2$_{181-402}$ was obtained from 5 L of medium under the optimised conditions.

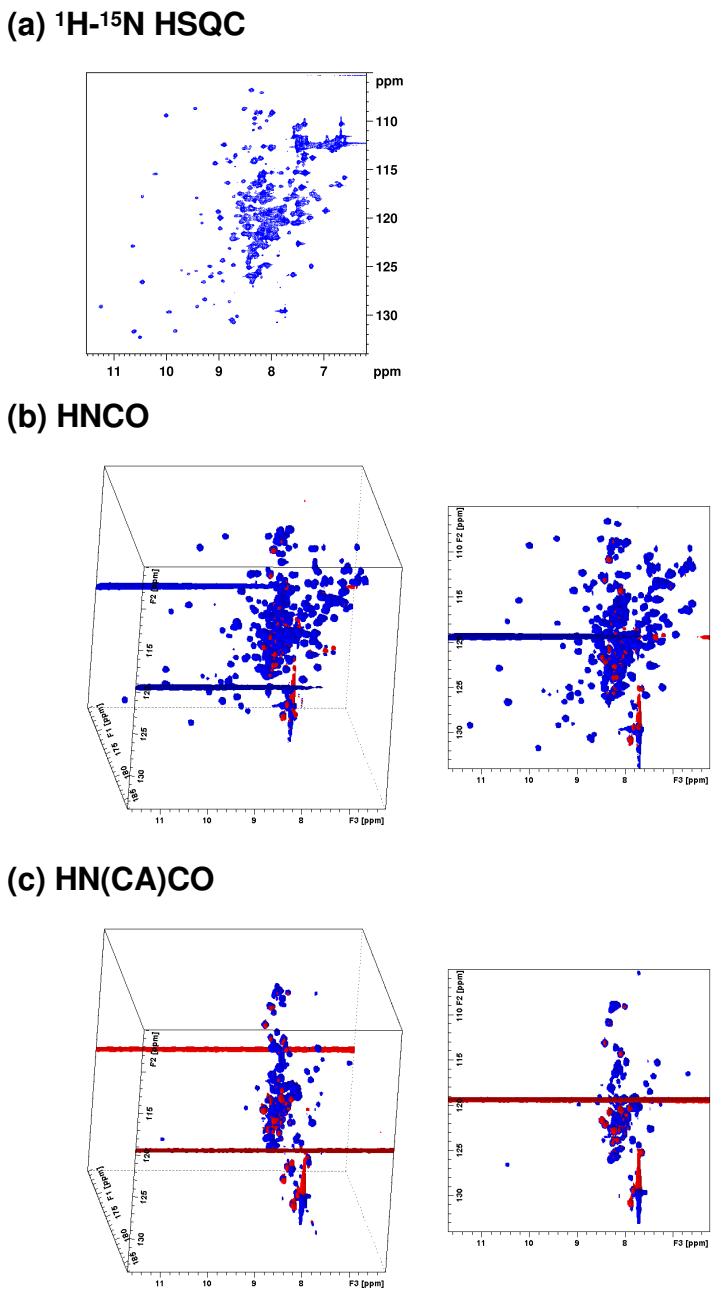

Figure 4-14 (a) ^{1}H-^{15}N HSQC spectrum of the *apo*-^{13}C,^{15}N-PHD2$_{181-402}$; (b) The corresponding HNCO spectrum and the ^{1}H-^{15}N projection; (c) The corresponding HN(CA)CO spectrum and the ^{1}H-^{15}N projection. The mixture contained ~1 mM enzyme and 50 mM Tris-D11 pH 6.6.

Variables	Conditions tested		
Cell density (OD_{600})	0.6–0.8	1.0	
IPTG	200 µM	500 µM	
Temperature	15 °C	28 °C	
Incubation Time	15 hours	24 hours	48 hours

Table 4-2 Expression variables tested for the production of ^{2}H,^{13}C,^{15}N-labelled PHD2$_{181-402}$. Normal glucose (4 g/L) instead of the doubly labelled ^{2}H,^{13}C-glucose was used in the expression trial. The best conditions are highlighted in blue.

NMR experiments were then conducted with the triple labelled $PHD2_{181-402}$ in the presence of Zn(II) and 2OG in order to improve protein stability (see Section 4.2.2). The resultant ^{1}H-^{15}N HSQC spectrum of the triple labelled protein indicated significantly narrower line shapes and sharper peaks for all amide resonances than the corresponding spectrum of the single labelled protein (Figure 4-15). Triple resonance experiments including HNCO, HN(CA)CO, HN(CO)CA, HNCA, HN(CO)CACB and HNCACB were conducted. All six experiments gave the expected cross peaks and sequential assignments were performed (Figure 4-16) by tracing through matching pairs of ^{13}CO, $^{13}C_{\alpha}$ and $^{13}C_{\beta}$ resonances. Chemical shift prediction values, which were calculated based on the published crystal structure (PDB id: 2G19), were also obtained using the programme ShiftX2.[52] The assigned chemical shifts, especially those of $^{13}C_{\alpha}$ and $^{13}C_{\beta}$, were checked against the predicted values as controls. Short links (usually 2-4 residues) were "assigned" by comparing the observed chemical shifts with the predicted chemical shift values.

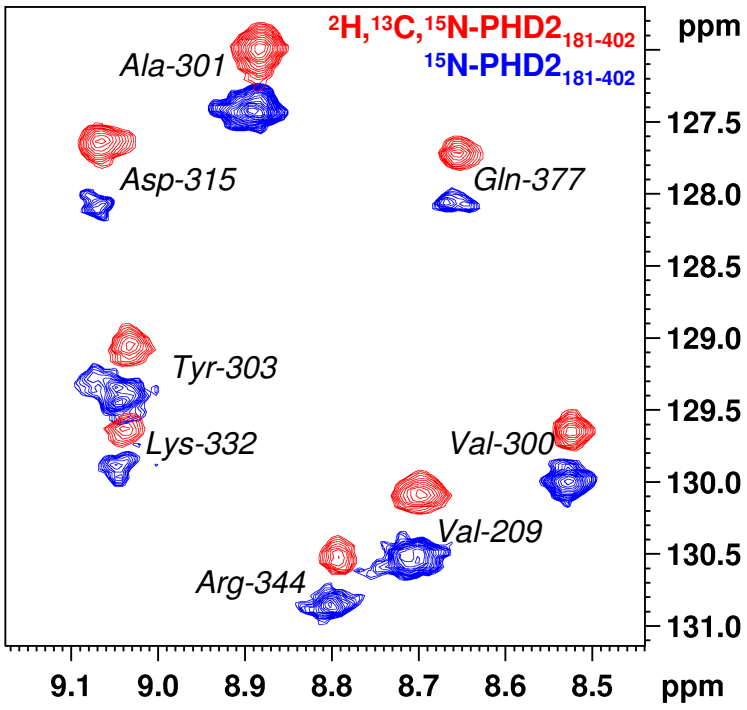

Figure 4-15 A region of the ^{1}H-^{15}N HSQC spectra of ^{15}N-$PHD2_{181-402}$-Zn(II)-2OG (blue) and $^{2}H,^{13}C,^{15}N$-$PHD2_{181-402}$-Zn(II)-2OG (red). The mixture contained ~1 mM *apo*-$PHD2_{181-402}$, 2 mM Zn(II), 3.5 mM 2OG and 50 mM Tris-D11 in 95% H_2O and 5% D_2O. Note the deuterium isotopic shift of the amide protons in the perdeuterated sample.

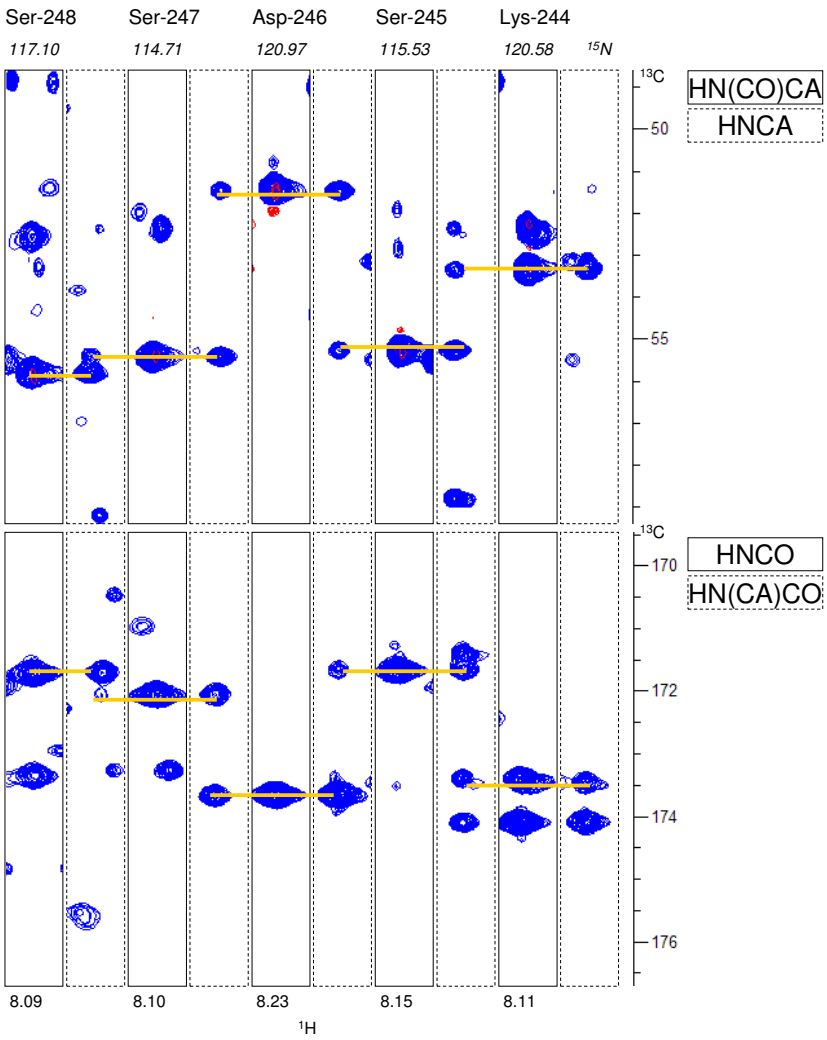

Figure 4-16 Illustrative stretches of sequential walk (for residues Lys-244 to Ser-248 in PHD2$_{181-402}$-Zn(II)-2OG) through ^{1}H-^{13}C planes of (a) HN(CO)CA and HNCA, and (b) HNCO and HN(CA)CO.

Overall, 256 peaks were identified in the ^{1}H-^{15}N HSQC spectrum, of which 36 were unassigned. 221 peaks were assigned to 172 residues, *i.e.* 80% of the 216 non-proline/*N*-terminal residues of PHD2$_{181-402}$ were assigned (Table 4-3). The relatively low level of assignment was in part due to the limited number of matching pairs of cross peaks in the triple resonance experiments. There were 43 residues that have multiple resonances assigned to them (Figure 4-17). These multiple (mostly duplicate) peaks often have different ^{1}H-^{15}N shifts but almost identical ^{13}C shifts for C_α and C_β. The observation of multiple peaks assigned to the same residues implies the presence of multiple local conformations that are in slow exchange with each other; however it is also worth noting that most of the multiple peaks had significantly lower intensities (usually <10%) than the corresponding main peaks. The residues that have multiple peaks assigned to them were concentrated at the *N*-terminal region, including α1 and the region between β1 and α2. The *N*-terminal region also includes a GSHMAS

sequence that is encoded by *E. coli*. Multiple assigned residues were also observed between residues 232 and 249. This region was proposed to adopt different conformations (β2β3/loop) between the free and complexed form of $PHD2_{181-402}$,[2,8] and might be involved in substrate selectivity.[44] Multiple assigned residues were also observed in the regions between α3 and β4 and between βII and β5. Duplicate peaks were also observed for residues at the *C*-terminus, confirming crystallographic and molecular dynamics simulation evidence that it might be dynamic.[2,8]

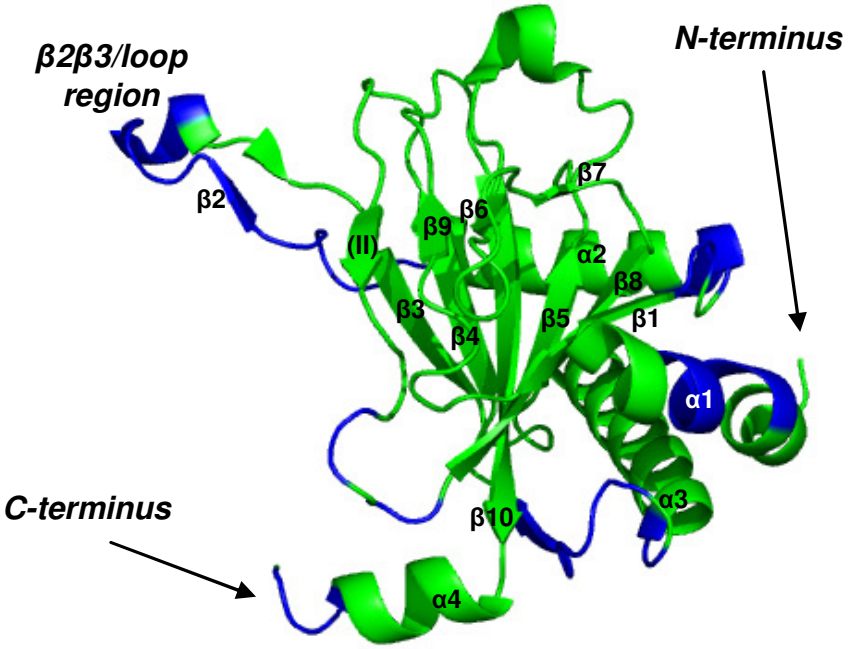

Figure 4-17 View from an X-Ray structure of $PHD2_{181-426}$-Fe(II)-bicyclic inhibitor (PDB id: 2G19). Regions for which multiple assigned residues were observed in the ^{1}H-^{15}N HSQC spectrum are highlighted in blue.

	Main assignment				
Residue	^{1}H	^{15}N	Cα	Cβ	CO
G			40.11		167.41
S	8.53	115.27	55.05	60.44	171.51
H	8.56	120.59	52.47	25.80	
M	8.27	122.73	52.11	29.67	172.56
A	8.35	125.82	48.87	16.02	174.39
S	8.23	115.76	52.99	60.09	170.27
P181			60.39	28.31	174.11
N182	8.31	117.93	50.14	35.49	173.02
G183	8.19	108.93	42.25		171.25
Q184	8.08	119.48	52.39	26.07	173.27
T185	8.07	116.87	59.26	66.47	170.47
K186	7.98	121.88	49.50	30.14	172.10
P187			57.52	23.93	171.42
L188	7.31	117.64	53.05	37.90	173.65
P189			59.76	28.31	173.66
A190	8.18	123.86	48.91	15.60	174.83
L191					
K192					
L193					
A194					
L195			51.16	37.63	173.42
E196	8.32	120.49	53.38	26.48	
Y197			57.00		173.73
I198	8.60	120.84	62.35	33.71	174.69

V199	8.45	115.88	65.42	26.12	172.54
P200			62.14	26.67	176.91
C201	7.67	116.09	60.81	23.90	175.21
M202	8.57	117.39	52.92	25.83	176.67
N203	8.37	116.49	53.26	34.33	174.26
K204	7.77	117.36	55.33	29.86	174.81
H205	8.35	113.02	52.79	29.46	174.30
G206	8.40	110.48	43.96		168.08
I207	6.57	115.59	56.78	40.80	172.87
C208	9.29	126.52	55.89	26.45	168.82
V209	8.69	130.12	58.54	30.01	172.38
V210			58.18	30.16	171.21
D211	8.40	125.34	51.17	39.99	172.82
D212	8.59	117.30	51.63	35.83	174.30
F213	8.41	116.87	56.93		173.54
L214			51.17	40.25	176.46
G215	10.19	115.24	40.54		170.97
K216	8.11	117.65		28.96	175.67
E217	8.51	118.89	57.08	25.15	176.88
T218	8.61	118.28	63.28	64.12	173.79
G219	8.47	108.25	45.08		
Q220	8.44	120.47	55.58	24.70	175.23
Q221	7.47	119.91	55.94	24.84	176.41
I222	7.99	119.49	62.92	33.33	175.30
G223	8.30	106.81	44.69		173.18
D224	8.38	122.51	54.34	36.25	176.83
E225	8.08	122.52	56.53	25.53	177.93
V226	8.53	119.88	63.63	27.46	174.85
R227	8.19	119.95	56.81	26.14	175.75
A228	7.77	120.62	52.08	14.00	178.44
L229	7.61	119.30	54.44	38.75	176.09
H230	8.13	118.83	55.28	26.04	176.30
D231	8.91	121.13	53.48	36.89	174.37
T232	7.44	107.77	59.29	66.72	173.22
G233	7.47	108.01	43.52		173.05
K234	7.51	115.60	53.01	28.60	174.51
F235	8.44	119.05	53.44	35.01	173.91
T236	9.34	113.80	56.90	68.22	171.69
D237	8.49	120.84	53.23	37.06	175.05
G238	8.85	114.06	43.19		171.77
Q239	8.38	118.73	53.29	25.50	173.42
L240	7.58	119.52	52.74	38.26	175.86
V241	7.87	119.06	60.37	28.38	174.29
S242	7.76	116.90	55.49	60.34	171.92
Q243	8.15	121.25		25.64	173.46
K244	8.11	120.57	53.29	29.09	174.10
S245	8.15	115.53		60.47	171.66
D246	8.23	120.97	51.50	37.42	173.66
S247	8.10	114.71	55.40	60.07	172.06
S248	8.09	117.09	55.81	60.19	171.71
K249	8.10	121.85	52.59	28.95	173.35
D250	8.09	121.41	51.46	37.21	172.95
I251	8.05	122.18	58.26	34.78	172.14
R252					
G253			41.67		170.17
D254	9.03	115.91	49.13	34.95	173.58
K255	8.59	121.08	50.51	30.52	173.02
I256	9.34	114.51	55.83	40.61	173.32
T257	8.06	113.35	58.28	66.66	167.78
W258	7.92	123.99	52.37	27.56	173.93
I259	9.79	125.41	53.77	36.68	172.03
E260	11.23	128.77	54.46	27.57	175.00
G261	9.98	109.39	41.47		169.61
K262	6.77	116.59	51.91	29.33	173.39
E263	10.45	126.31	53.52	23.54	171.78
P264			60.37	27.67	175.42
G265	9.04	113.95	42.35		172.09
C266	7.55	115.06	54.75	25.13	172.62
E267	8.97	119.92	57.75	25.44	176.86
T268	10.39	122.20	62.83		
I269			63.39	33.93	176.04
G270	8.39	106.54	44.68		173.73

L271	7.58	125.66	54.97	37.37	177.60
L272					
M273			56.27	30.44	174.97
S274	8.30	113.63	58.45	59.19	174.60
S275	8.19	119.91	59.52		
M276					
D277					
D278					
L279					
I280					
R281			56.58	25.88	177.19
H282	7.58	115.63	55.24	23.89	172.81
C283	7.49	114.65	57.89	24.19	171.97
N284	7.56	116.93	51.77	34.72	172.85
G285	8.65	111.95	42.72		172.41
K286	7.90	116.22	52.17	30.56	173.62
L287	7.61	120.29	50.15	37.25	172.23
G288	8.78	114.29	43.68		170.58
S289	7.68	118.31			
Y290	7.26	119.74	55.10	35.84	173.71
K291	9.13	125.79	51.94	28.47	172.35
I292	8.39	124.82	58.18	33.56	175.23
N293	8.37	126.43	49.34	36.46	171.60
G294	8.00	108.99	41.49		167.93
R295	7.99	112.60	51.29	28.05	174.09
T296	8.08	109.80	58.86	69.65	173.04
K297	7.81	115.19	54.81	30.64	172.32
A298	8.45	120.91	48.33	15.47	173.57
M299	9.73	125.85	50.85	29.70	172.48
V300	8.53	129.68	58.77	27.47	171.06
A301	8.89	127.02	47.12	21.18	173.11
C302	9.09	119.70	52.45	27.87	172.56
Y303	9.05	129.13		33.65	173.24
P304					
G305					
N306			50.07	34.99	172.06
G307	8.67	113.60	43.67		170.83
T308			58.89	66.41	172.58
G309	8.33	110.78	42.17		171.28
Y310					
V311			59.43	29.23	171.24
R312	8.31	122.11	53.65	26.28	172.56
H313	8.78	123.16	52.06	27.36	168.33
V314	8.03	118.49	56.57	31.22	174.05
D315	9.07	127.66	55.07	36.76	172.34
N316	7.52	110.44	46.07	35.93	170.59
P317			60.06	29.15	174.47
N318	8.16	117.17	49.53	36.05	172.28
G319	8.14	112.41	44.36		172.91
D320	9.06	119.18	50.60	37.44	173.88
G321	9.42	108.43	41.33		171.30
R322	8.00	119.98	54.44	25.73	172.77
C323	9.34	120.40	53.36	26.51	172.50
V324	7.21	124.77	59.18	33.41	170.94
T325					
C326			51.93	25.64	171.28
I327	8.24	121.33	54.46	37.70	173.38
Y328					
Y329					
L330			51.69		173.29
N331	6.41	115.50	51.35	35.84	170.36
K332	9.04	129.65	54.60	29.00	173.54
D333	8.99	122.20	52.06	35.90	171.97
W334	7.56	119.15		25.49	
D335					
A336					
K337					174.97
V338	6.76	113.41	59.82	29.78	
S339	8.24	113.73	55.87	59.22	
G340					
G341			43.82		171.26
I342	7.30	119.46	58.55	34.54	172.18

L343	7.64	126.74	50.51	37.82	170.70
R344	8.79	130.54	50.99	28.25	
I345	8.84	125.79	56.49	36.17	171.63
F346	8.44	125.07	50.87	34.84	169.97
P347			60.02	28.29	176.73
E348	9.17	124.16	54.91	26.41	175.10
G349	8.88	111.95	42.34		171.40
K350	7.53	118.65	51.19	29.81	173.34
A351	8.31	122.44	49.98	15.35	174.90
Q352	7.36	115.34	51.82	26.68	172.36
F353	6.96	119.06		36.33	171.61
A354	8.99	124.34	47.75	17.15	171.38
D355	8.22	123.06	50.18	38.18	173.40
I356	9.66	126.28		33.93	172.45
E357					
P358			58.56	24.80	172.97
K359	7.42	122.13	53.43	30.77	170.22
F360	7.11	118.89	56.02	36.03	172.64
D361	7.63	125.51	51.62	37.14	169.03
R362			52.68	29.24	173.29
L363	8.23	125.07	51.86	38.43	
L364					
F365					
F366			54.46	36.85	172.57
W367	7.07	117.44	53.56	27.66	175.74
S368	7.62	114.08	56.93	60.55	171.19
D369	7.78	119.96	49.74	36.74	
R370	7.60	110.60	54.50	25.66	173.18
R371	8.19	119.63	56.41	27.90	
N372	7.45	110.31	47.71	37.38	170.91
P373			60.75	27.41	173.33
H374	8.76	117.62	52.13	28.11	168.43
E375	9.09	116.50	50.07	30.84	171.00
V376	9.13	122.44	59.02	28.05	174.26
Q377	8.66	127.74	52.11	22.66	168.76
P378			60.24	28.16	174.85
A379	8.39	123.10	51.96	15.58	175.54
Y380			54.54	34.71	170.92
A381	7.65	121.62	47.24	18.34	172.44
T382	8.19	115.69	61.64	64.97	170.41
R383	8.31	130.36	50.84	31.11	172.12
Y384	9.81	126.85	54.08	40.92	173.74
A385	8.55	121.70	49.11	19.23	172.36
I386	8.80	120.71	57.18		
T387					
V388			59.39	28.66	172.55
W389	7.89	130.28	53.97	27.89	178.15
Y390			54.98	37.25	
F391					
D392	8.66	119.61	49.64	40.77	173.65
A393	9.25	128.05	52.02	15.97	177.56
D394	8.12	117.57	53.83	37.14	175.51
E395	8.70	121.93	56.59	26.90	176.36
R396	8.49	117.61	55.05	26.55	174.91
A397	7.44	119.35	51.05	14.69	176.82
R398	7.41	116.63	54.05	26.88	174.14
A399	7.48	122.39	49.89	15.22	175.20
K400	7.81	119.03	53.23	28.83	173.82
V401	7.76	120.13	59.05		172.46
K402	7.73	129.31	54.54	29.85	178.43

Duplicate 1

Residue	^{1}H	^{15}N	Cα	Cβ	CO
M			52.04		
A	8.27	125.65	48.99	15.82	173.89
S	8.00	114.99	52.61	60.51	170.35
P181			59.89	30.61	173.35
N182	8.59	119.42	50.42	35.81	172.82
G183	8.29	109.10	42.27		171.32
Q184	8.10	119.51	52.51	25.92	173.48
T185	8.13	116.09	58.80	66.39	171.45
K186	8.24	125.16	50.95	28.81	
E196			53.47	26.01	173.91

Y197	7.25	117.14	57.09	37.24	171.34
I198			62.34		174.71
V199	8.60	115.99	65.40	25.91	172.55
P200			62.19	26.17	177.02
C201	7.60	115.79	60.86		175.15
V210			58.15	29.99	171.32
D211	8.36	125.39	51.28	39.73	173.02
D212	8.63	117.84		36.00	174.26
G215			40.49		170.83
K216	8.07	117.41	56.87	29.06	175.70
E217			57.14	25.15	176.91
T218	8.68	118.61	63.17	64.09	
T232			58.88	66.30	172.62
G233	8.36	110.79	42.16		171.10
K234	7.89	120.25	52.87	29.41	173.51
F235			54.44	35.96	173.34
T236	8.00	115.28	58.47	66.57	171.39
Q239			52.65	25.82	173.27
L240	8.13	122.68	52.25	38.28	174.74
V241			59.18	28.94	173.49
S242	8.20	118.87	55.11	60.19	171.70
Q243			52.48	25.88	173.14
K244	8.24	122.50	53.18	29.30	173.93
S245	8.29	117.05	55.09	60.45	171.56
D246			51.15	37.69	173.80
S247	8.26	116.58	55.57		172.26
S248	8.27	117.69		60.12	171.98
K249	8.00	122.01	53.14	29.10	173.43
N284			51.88	34.88	172.90
G285	8.65	113.15	42.57		172.35
K286					
L287			50.03	37.37	172.21
G288	8.70	113.86	43.63		170.68
S289	7.74	118.45	53.83	59.49	171.87
Y290	7.43	120.11	55.14	35.72	173.61
K291	9.10	125.51	51.78	28.58	172.33
I292	8.52	125.29	58.04	33.23	175.26
N293			49.36	36.40	171.51
G294	8.06	109.34	41.45		167.97
P317			59.54	28.47	173.85
N318	8.32	123.20	49.79		172.74
D320			51.57	37.52	174.10
G321	8.26	108.83	42.38		171.62
K400			53.13	29.42	173.65
V401	8.22	122.60	59.25	29.12	172.48
K402	7.82	129.22	54.66	29.86	178.38

Duplicate 2

Residue	^{1}H	^{15}N	Cα	Cβ	CO
H			52.25	25.77	171.53
M	8.30	122.08		29.44	172.77
A	8.32	125.65	49.02	15.70	174.62
S	8.25	116.32	53.05	59.86	170.40
P181			60.42	28.25	174.02
N182	8.14	117.91	50.29	35.63	173.03
G183	8.28	109.35			
Q184	8.06	119.30	52.37	26.09	173.39
T185	8.15	115.64		66.33	
K186	8.13	124.73	50.83	28.96	171.17

Duplicate 3

Residue	^{1}H	^{15}N	Cα	Cβ	CO
A			49.02	15.70	174.58
S	8.21	116.44	53.11	59.91	170.10
N182					173.77
G183	7.97	107.33	42.37		171.34
Q184	8.16	119.48	52.51	25.94	173.46
T185	8.12	116.08	58.83	66.38	171.43
K186	8.21	124.92	50.90	28.77	

Table 4-3 Partial assignment for ^{2}H,^{13}C,^{15}N-labelled PHD2$_{181-402}$-Zn(II)-2OG. The gaps indicate missing assignments.

The assignment of the $PHD2_{181-402}$-Zn(II)-2OG-CODD complex was then attempted. The same sets of triple resonance experiments were conducted, except a lower enzyme concentration (300 μM *cf.* 1 mM) was used due to the limited solubility of CODD (<1 mM). Overall, 277 peaks were picked from the ^{1}H-^{15}N HSQC spectrum, of which 78 were unassigned. Out of the 216 assignable residues of $PHD2_{181-402}$, 157 residues (73%) were assigned and there were 42 residues that have multiple peaks assigned to them (Table 4-4). The low level of assignment was in part due to the relatively low concentrations of protein used owing to limited CODD solubility. Multiple assigned residues were observed in almost the same regions as for $PHD2_{181-402}$-Zn(II)-2OG (Figure 4-17 and Figure 4-18), further confirming these regions might exist in different dynamic states.[2] An interesting observation was that the residues in the β2β3/loop region still exhibit multiple conformations even when the substrate CODD is bound. This result provides further evidence for a dynamic role of the β2β3/loop, which was proposed to be involved in substrate recognition and substrate selectivity based on kinetics and mutagenesis studies.[44]

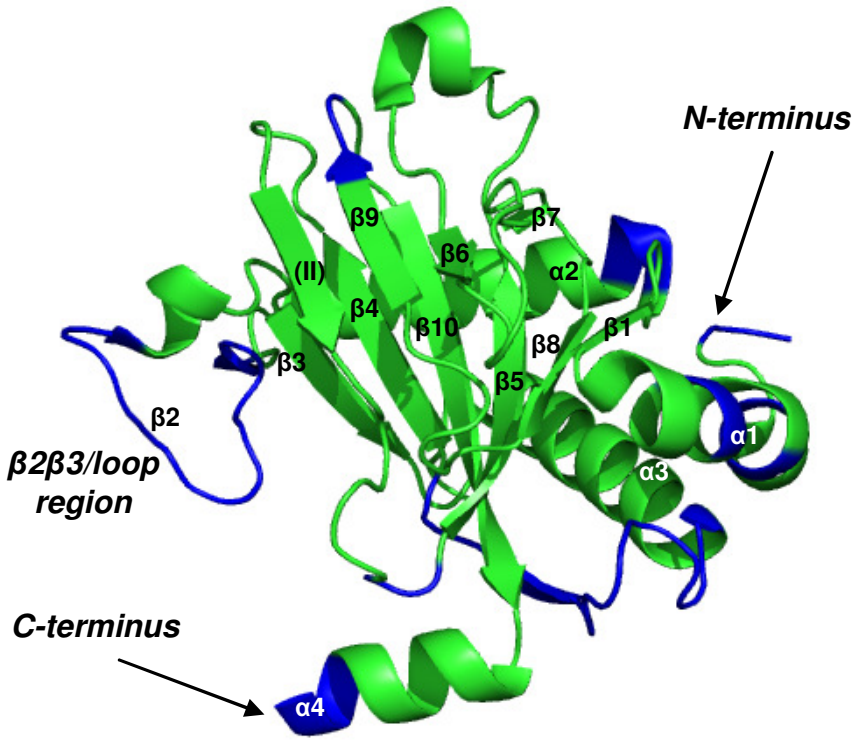

Figure 4-18 X-Ray structure of CODD-complexed PHD2 (PDB id: 3HQR). Regions for which multiple assigned residues were observed in the ^{1}H-^{15}N HSQC spectrum are highlighted in blue.

	Main assignment				
Residue	^{1}H	^{15}N	Cα	Cβ	C=O
G			40.08		167.38
S	8.53	115.28	55.04	60.45	
H	8.59	120.41	52.17	25.56	171.45
M	8.3	122.56		29.61	172.65

A	8.35	125.78	48.91	15.94	174.46
S	8.24	115.96	53.01	60.01	170.3
P181			59.9	30.61	173.36
N182	8.59	119.41	50.43	35.87	172.8
G183	8.29	109.07	42.33		171.36
Q184	8.16	119.47	52.54	25.94	173.44
T185	8.11	116.07	58.84	66.38	171.38
K186	8.16	124.8	50.87	28.9	
P187					
L188					
P189			60.25	27.92	174.8
A190	8.35	123.03	51.75	15.49	175.7
L191	7.89	116.76	55.01	38.09	175.42
K192	7.19	117.28	55.55	28.94	
L193			54.3	38.55	173.3
A194	8.04	119.63	52.45	15.84	174.59
L195	7.97	112.55	54.11	38.15	176.52
E196			53.4	26	173.86
Y197	7.24	117.14	57.09	37.3	171.4
I198	8.61	120.8	62.28	33.71	174.67
V199	8.41	115.77	65.43	26.2	172.49
P200			62.14	26.62	176.85
C201	7.65	115.99	60.81	23.88	175.28
M202	8.54	117.43	52.89	25.81	176.66
N203	8.4	116.51	53.34	34.34	174.47
K204	7.83	117.04	55.28	29.77	174.87
H205	8.36	112.48	52.43	28.7	173.88
G206	8.47	110.82	44.01		168.08
I207	6.56	115.57	56.79	40.7	172.78
C208			55.82	26.38	168.8
V209	8.69	130.06	58.52	30.08	172.43
V210			58.16	30.09	171.34
D211	8.38	125.36	51.21	39.88	172.91
D212	8.58	117.26	51.56	35.58	174.22
F213	8.39	116.87	57	35.85	173.52
L214			51.13	40.19	176.37
G215	10.17	115.23	40.56		170.99
K216	8.11	117.69	57	29.02	175.69
E217	8.46	118.99		25.06	176.82
T218	8.61	118.28	63.26	64.02	
G219	8.48	108.29	45.05		173.77
Q220	8.44	120.52	55.58	24.69	175.26
Q221	7.47	119.79	55.93	24.89	176.46
I222	7.97	119.54	62.92	33.28	175.28
G223	8.31	106.84	44.71		173.12
D224	8.42	122.33	54.21	36.13	176.76
E225	8.1	122.14	56.42	25.4	177.73
V226			63.63	27.48	174.83
R227	8.17	120.08	56.87	26.03	175.74
A228	7.79	120.72	52.1	13.97	178.55
L229	7.72	118.94	54.41	38.92	176.68
H230	8.38	119.36	55.73	25.08	175.91
D231	8.79	121.29	53.35	36.73	174.17
T232	7.35	108.06	59.75	67.1	173.43
G233	7.45	107.84	43.25		172.98
K234	7.45	115.67	53.1	28.74	174.36
F235	8.55	120.7	53.79	34.6	173.88
T236	9.4	113.29	56.65	68.49	171.42
D237	8.45	120.76	52.97	36.93	175.09
G238	8.03	108.97	42.27		170.06
Q239					
L240					
V241					
S242					
Q243					
K244			52.86	29.44	173.96
S245	8.12	115.93	55.3	60.46	171.71
D246	8.37	120.68	51.7	36.99	173.5
S247	7.98	113.69	54.87	60.32	172.55
S248	8.45	119.64	56.39	60.07	172.74
K249	7.93	121.55	54.18	28.18	173.69
D250	8.03	116.97	51.83	36.44	172.89

I251	7.72	121.53	59.26	35.46	171.9
R252	7.9	113.83	50.56	28.15	172.41
G253	8.71	110.16	41.93		170.23
D254	9.35	116.11	48.88	34.76	173.48
K255			50.25	31.14	173.31
I256	9.58	114.69	55.09	40.73	
T257	7.92	112.85	58.27	67.02	167.9
W258	7.88	124.54	52.27	27.53	174.07
I259	9.76	125.83	53.56	36.56	171.96
E260	11.21	128.73	54.28	27.17	174.89
G261	9.9	109.15	41.38		169.65
K262	6.7	116.46	51.95	29.39	173.44
E263	10.54	126.4	53.52	23.5	171.83
P264			60.41	27.69	175.42
G265	8.99	113.7	42.39		172.11
C266	7.56	114.92	54.75	25.15	172.61
E267	9	120.13	57.66	25.15	176.82
T268	9.97	121.17	62.78		
I269	8.11	125.45	63.37	33.87	175.86
G270	8.36	106.5	44.65		173.62
L271	7.54	125.37	54.92	37.38	177.58
L272					
M273					
S274					
S275					
M276					
D277					
D278					
L279					
I280					
R281			57.45	26.12	177.5
H282	7.59	113.98	55.31	25.18	172.3
C283	7.56	115.45	57.99	24.18	171.82
N284	7.51	116.82			
G285	8.61	112.64	42.7		172.41
K286	7.91	116.02	52.1	30.53	173.63
L287	7.57	120.14	50.05	37	172.18
G288	8.68	113.91	43.62		170.54
S289	7.71	118.82	53.66	59.45	176.71
Y290	7.17	119.91	54.96	36.03	173.62
K291	9.06	125.74	52.02	28.54	172.24
I292	8.47	124.73	58.42	33.66	173.97
N293	8.27	124.88	48.91	36.45	173.09
G294	7.78	108.51	43.15		168.09
R295	9.04	115.03	52.23	28.47	172.67
T296	7.86	108.39	58.38	70.17	173.97
K297	7.9	115.19	54.68	30.34	172.45
A298	8.32	120.59	48.54	15.55	173.83
M299	9.71	124.66	50.79	29.85	172.11
V300	8.49	129.5	58.88	27.36	171
A301	8.89	127.35	47.49	21.09	173.21
C302	9.14	119.93	52.81	27.41	172.87
Y303	9.03	129.72			173.23
P304					
G305					
N306					
G307					
T308			58.94	66.29	172.82
G309	8.35	110.74	42.17		171.19
Y310			52.57		173.92
V311	8.09	119.2	58.93	29.21	170.68
R312	8.04	119.93	53.57	26.17	172.51
H313	8.69	121.67	52.13	28.34	168.43
V314	8.16	116.8	56.6	31.7	174.13
D315	9.11	128.53	54.73	37.06	171.06
N316	7.13	105.92	45.66	36.28	171.46
P317			59.95	29.49	174.08
N318	8.32	118.48	49.53	36.26	172.07
G319	8.19	112.61	44.38		172.5
D320	8.91	119.21	50.43	37.32	
G321	9.2	106.46	41.37		172.13
R322			55.29	28.77	173.37

C323	9.69	120.86	53.29	25.77	172.17
V324	7.28	125.45	59.32	33.44	170.95
T325					
C326					
I327					
Y328					
Y329					
L330					
N331					
K332					
D333					
W334					
D335					
A336					
K337					
V338					
S339					
G340					
G341			43.86		171.21
I342	7.3	119.5	58.53	34.51	172.2
L343	7.63	126.82	50.54	37.74	170.73
R344	8.82	130.59	51.04	28.28	171.63
I345	8.8	125.72	56.47	36.23	
F346	8.5	125.1	50.92	34.94	170
P347			60.16	28.27	176.71
E348	9.23	123.62	54.81	25.97	174.89
G349	8.89	111.6	42.41		171.43
K350	7.56	118.84	51.31	29.61	173.26
A351	8.26	122.17	49.99	15.37	174.98
Q352	7.35	115.51	52.01	26.49	172.31
F353	6.98	118.92	51.8	36.48	171.61
A354	9.01	124.33	47.74	17.18	171.39
D355	8.23	123	50.15	38.22	173.38
I356	9.7	126.39	55.37	33.77	172.4
E357	8.3	125.33	51		173.7
P358			58.52	24.92	173.02
K359	7.43	122.09	53.35	30.68	170.22
F360	7.1	118.94	55.97	36.05	172.62
D361	7.62	125.4	51.66	37.13	169.04
R362					
L363					
L364					
F365					
F366			54.47	36.9	172.64
W367	7.15	117.44	53.53	27.55	175.69
S368	7.52	114.01	56.98	61	170.94
D369	7.74	119.17	49.86	36.39	173.03
R370	7.63	110.4	54.86		173.52
R371	8.27	118.47	56.39	27.91	173.19
N372	7.37	110.41	47.65	37.32	170.83
P373			60.72	27.45	173.14
H374	8.94	118.06	52.08	28.11	168.3
E375	9.02	115.99	49.98	30.41	171.02
V376	9.21	122.77	59.06	27.98	174.3
Q377	8.66	127.51	52.16	22.77	168.81
P378					
A379					
Y380			54.59	34.76	170.85
A381	7.63	121.49	47.22	18.38	172.38
T382	8.17	115.72	61.63	65.37	
R383	8.37	130.14	50.94	31.04	172.06
Y384	9.71	126.6	54.1	40.94	173.81
A385	8.51	121.52	49.1	19.17	172.52
I386					
T387					
V388					
W389					
Y390			54.9	36.97	173.56
F391	8.72	120.85	52.5	38.06	172.87
D392	8.34	119.17	49.78	41.36	173.55
A393	9.34	128.41	52.2	16.07	178.06
D394	8.26	117.74	53.89	37.08	175.7

E395	8.78	121.87	56.67	27.06	176.16
R396	8.75	118	53.64	27.12	173.97
A397	7.38	118.18	51.72	14.29	178.48
R398	7.42	116.78	55.36	26.52	175.56
A399	7.64	121.03	50.66	15.06	176.03
K400	7.07	114.62	53.74	29.16	173.87
V401	7.19	117.72			
K402	7.57	129.32	54.52	29.79	178.42

Duplicate 1

Residue	^{1}H	^{15}N	Cα	Cβ	C=O
S			55.62	60.07	172.28
H	8.25	117.7		25.56	171.41
M	8.32	122.11		29.45	172.8
A	8.33	125.69	49.03	15.71	174.63
S	8.25	116.32	53.05	59.86	170.39
P181			60.38	28.32	174.1
N182	8.31	117.94	50.14	35.52	173.01
G183	8.19	108.92	42.22		171.19
Q184	7.86	120.11	52.91	29.32	173.45
T185	8.22	120.87	54.46		
L193			53.24	42.2	173.61
A194	8.05	123.59	49.41	15.39	175.12
L195	7.95	120.33	52.33		174.74
P200			62.11	26.58	176.91
C201	7.6	115.77	60.84	23.91	175.24
G215			40.56		170.85
K216	8.06	117.43	56.99	28.97	175.67
E217	8.49	118.86		25.04	176.82
T236			55.08	69.3	173.36
D237	7.97	122.16	52.35	38.02	175.18
G238	8	108.91	42.32		171.52
Q239	8.02	119.28	52.61	25.93	173.25
L240	8.13	122.57	52.13	38.3	174.74
V241	7.99	120.92	59.19	28.96	173.47
S242	8.19	118.77	55.13	60.19	
S245			55.14	60.32	170.75
D246	8.31	122.24	51.11	37.67	173.77
S247	8.26	116.57	55.54		170.17
C283			57.94	24.22	171.86
N284	7.44	116.93	51.71	34.86	172.78
G285	8.63	111.82	42.76		172.57
I292			60.39	28.27	174.04
N293	8.2	117.95	50.27	35.6	173.03
G294	8.25	109.23	42.28		171.3
R295	8.07	119.35	52.41	26.03	173.36
T296	8.14	115.74	58.83	66.42	171.45
K297	8.23	125.08	50.96	28.79	173.29
D320			51.53	37.39	174.06
G321	8.26	108.8	42.27		171.63
P378			59.79	28.3	173.81
A379	8.17	123.74	48.95	15.52	175.02
Y380	8.04	121.45	51.91	38.57	174.45
K400			53.28		173.85
V401	7.76	120.16	59.17	28.66	172.48
K402	7.74	129.21	54.51	29.78	178.39

Duplicate 2

Residue	^{1}H	^{15}N	Cα	Cβ	C=O
M			52.05	29.47	172.73
A	8.29	125.69	49.01	15.82	173.88
S	7.99	114.98	52.61	60.53	170.34
Q184			52.37	26.06	173.25
T185	8.07	116.85	59.24	66.5	170.5
K186	7.97	121.81	49.41	30.19	172.13
N284					171.6
G285	8.1	111.83	42.78		172.56
K286	7.87	115.95	52.13	30.52	173.66
K400			53.12	26.2	173.32
V401	8.07	122.17	59.37	28.67	172.56
K402	7.9	130.1	53.94		178

Duplicate 3

Residue	^{1}H	^{15}N	Cα	Cβ	C=O
G183			42.19		

Q184	8.07	120.47	52.49	25.94	173.72
T185	8.13	116.18	58.85	66.4	171.43
K186	8.21	124.93	50.91		
V401			59.21	29.12	172.46
K402	7.82	129.12	54.63	29.87	178.28
		Duplicate 4			
Residue	^{1}H	^{15}N	Cα	Cβ	C=O
G183			42.25		171.37
Q184	8.11	119.51	52.52	25.93	

Table 4-4 Partial assignment for ^{2}H,^{13}C,^{15}N-labelled PHD2$_{181-402}$-Zn(II)-2OG-CODD. The gaps indicate missing assignments.

Overall, isotopically labelled PHD2$_{181-402}$ was successfully produced recombinantly and partial protein assignment was conducted for both the substrate free (PHD2$_{181-402}$-Zn(II)-2OG) and substrate bound (PHD2$_{181-402}$-Zn(II)-2OG-CODD) forms of PHD2$_{181-402}$. Multiple assigned residues were observed for both forms, and these regions included the *N*-terminal α1 helix, the β2β3/loop region, the regions between β1 and α2, between α3 and β4 and between βII and β5, and the α4 helix at the *C*-terminus. Further analysis can be found in Section 4.4.1.

4.4 PHD2-substrate interactions

4.4.1 Free and complexed form of PHD2$_{181-402}$

Titration analysis with ^{15}N-labelled PHD2$_{181-402}$-Zn(II)-2OG at different CODD concentration suggested the rate of exchange between the substrate-free (PHD2$_{181-402}$-Zn(II)-2OG) and substrate-complexed (PHD2$_{181-402}$-Zn(II)-2OG-CODD) forms was slow or slow-intermediate on the NMR time scale (Figure 4-19). The determination of the dissociation constant (K_D) of CODD was attempted by integrating the peaks corresponding to the substrate-free and substrate-bound forms of PHD2$_{181-402}$, and the data was subjected to non-linear fitting using the equation as described by Morton *et al.* (Chapter 6).[53] However, poor fitting was obtained and therefore an accurate K_D value could not be determined. This may be due in part to poor signal-to-noise ratio of the resonances that correspond to the minor component in the ^{1}H-^{15}N HSQC spectrum, which may in turn be due to line broadening as a result of slow-intermediate exchange dynamics.

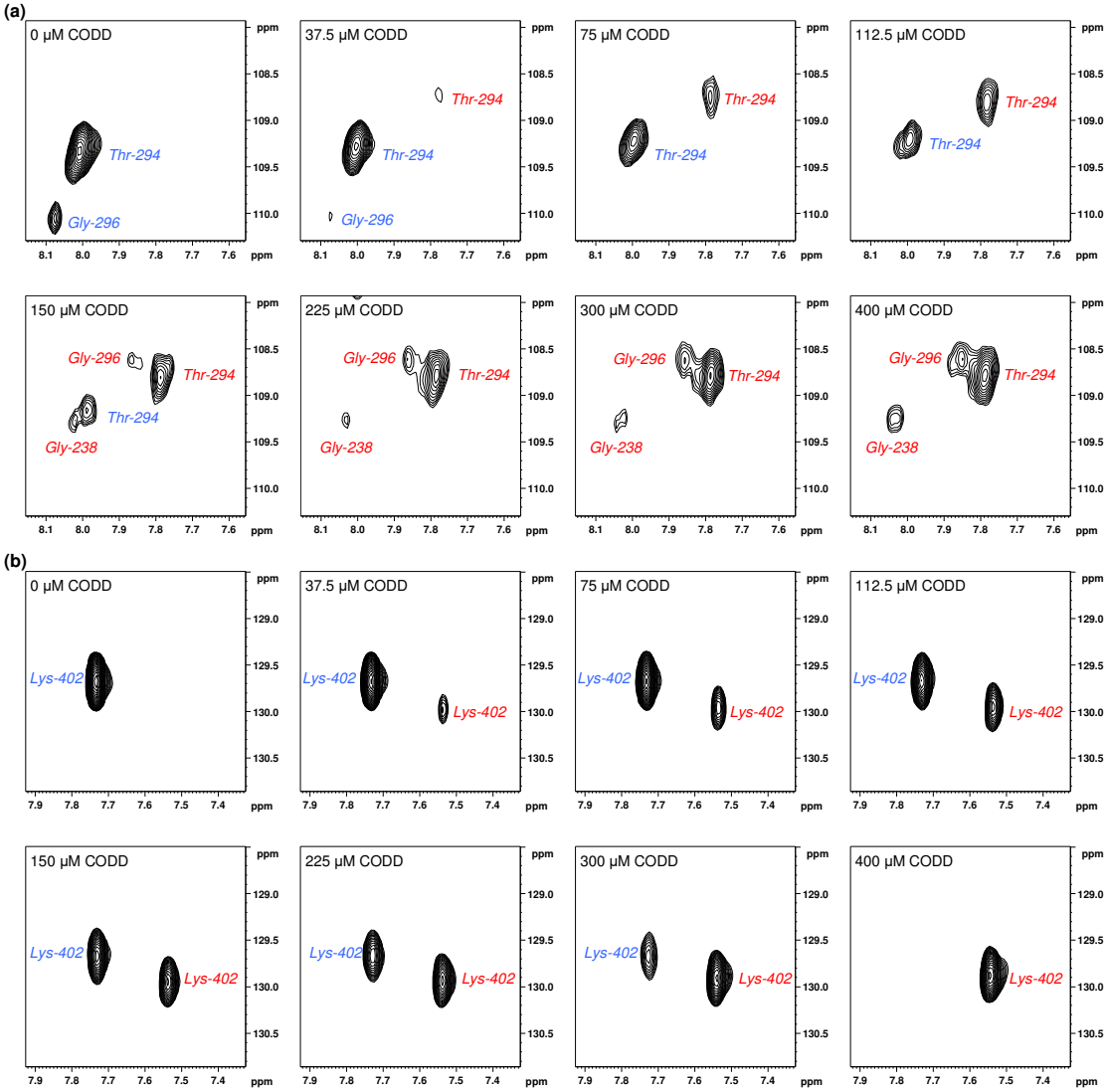

Figure 4-19 Examples of the slow or slow-intermediate exchange kinetics between PHD2$_{181\text{-}402}$-Zn(II)-2OG and PHD2$_{181\text{-}402}$-Zn(II)-2OG-CODD. (a) Peaks corresponding to T294 and G296; (b) Peak corresponding to the *C*-terminal K402. Mixture contained 150 μM *apo*-^{15}N-PHD2$_{181\text{-}402}$, 150 μM Zn(II), 300 μM 2OG and 50 mM Tris-D11 pH 6.6 in 95% H_2O and 5% D_2O.

Addition of CODD to ^{15}N-labelled PHD2$_{181\text{-}402}$-Zn(II)-2OG induced significant changes in the ^{1}H-^{15}N HSQC spectrum (Figure 4-20), which are likely due to peptide binding resulting in changes in the protein conformation. In order to study the effect of substrate binding to PHD2, changes in backbone amide chemical shifts ($\Delta\delta$, in ppm) between PHD2$_{181\text{-}402}$-Zn(II)-2OG and PHD2$_{181\text{-}402}$-Zn(II)-2OG-CODD were compared. A scaling factor of 10 was used to normalise the ^{15}N chemical shift with the following formula as described by Cavanagh *et al.*:[54]

$$\Delta\delta = \sqrt{(\Delta\delta^{1}\mathrm{H})^{2} + (\frac{\Delta\delta^{15}\mathrm{N}}{10})^{2}}$$

A $\Delta\delta$ cut-off of 0.18 ppm was used for the assessment of significant resonance shift changes. For residues that had missing assignment from either or both forms of the protein, $\Delta\delta$ were defined as 0 ppm. In cases where multiple peaks were assigned to the same residues, only the main peaks were considered. The data was then mapped onto the protein crystal structure of PHD2-Mn(II)-2OG-CODD (PDB id: 3HQR).[2] The results indicated that most changes in chemical shift appeared to originate from direct contacts between CODD and PHD2$_{181\text{-}402}$-Zn(II)-2OG (Figure 4-21 and Figure 4-22). Two notable regions that involve significant chemical shift changes which are not directly involved in CODD contact include the β2β3/loop and the *C*-terminal helix α4. The overall NMR data thus provided further supporting evidence of the X-ray crystal structures,[2] which identifies the same two regions existing as different dynamic states between the free and complexed forms of PHD2.

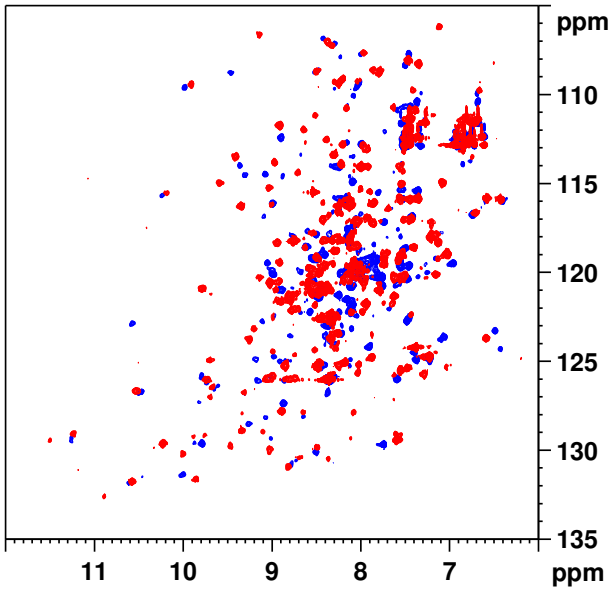

Figure 4-20 ^{1}H-^{15}N HSQC spectra of the ^{15}N-PHD2$_{181\text{-}402}$-Zn(II)-2OG (blue) and ^{15}N-PHD2$_{181\text{-}402}$-Zn(II)-2OG-CODD (red). The mixture contained 150 μM *apo*-^{15}N-PHD2$_{181\text{-}402}$, 300 μM Zn(II), 400 μM 2OG, 500 μM CODD (if applicable) and 50 mM Tris-D11 in 95% H_2O and 5% D_2O pH 6.6.

As a result of gaps in the assignment of PHD2$_{181\text{-}402}$-Zn(II)-2OG (80% assigned) and PHD2$_{181\text{-}402}$-Zn(II)-2OG-CODD (75% assigned), it cannot be ruled out that residues involved in these gaps are involved in substrate binding. Out of the 216 assignable residues, the chemical shifts of 138 peaks were compared (64%). Regions that cannot be compared included residues 187-197 (α1), 206-210 (β1), 272-281 (α3), 304-311 (between β4 and βII), 322-341 (β5), 362-366 (β8), 378-382 (between β9 and β10) and 386-390 (β10). Although most of these regions were not apparently involved in the binding of CODD or protein dynamics (as indicated by the X-ray crystal structure;

Figure 4-21), further work, including the use of ^{1}H-^{15}N NOESY-HSQC, are needed so that a more complete picture can be obtained.

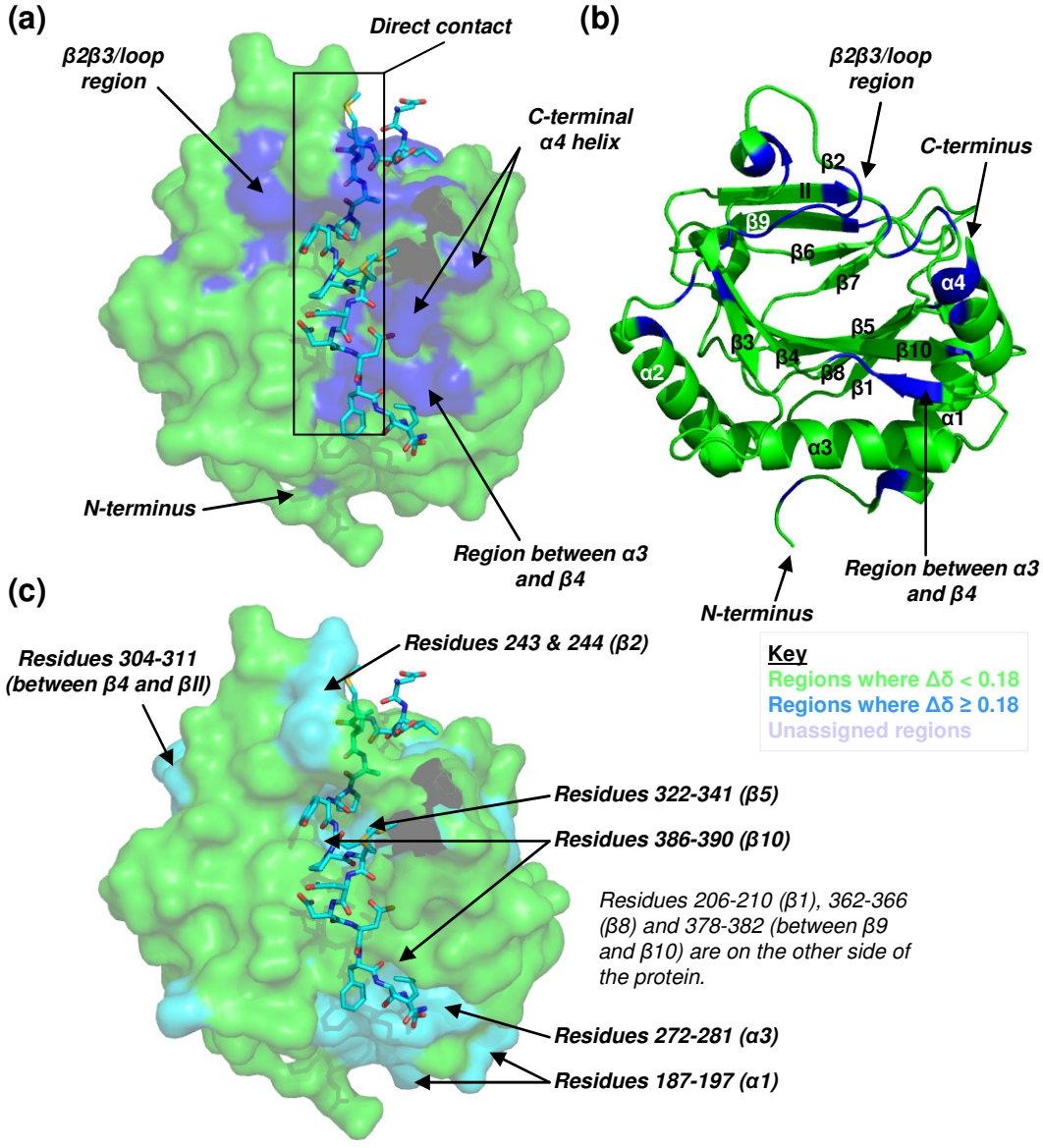

Figure 4-21 View from a X-ray structure of PHD2-Mn(II)-2OG-CODD (PDB id: 3HQR). (a) Surface view: Residues that have $\Delta\delta$ larger than 0.18 ppm between $PHD2_{181-402}$-Zn(II)-2OG and $PHD2_{181-402}$-Zn(II)-2OG-CODD were highlighted in blue; (b) The corresponding view in ribbon form; (c) Areas highlighted in cyan indicate missing assignments (including proline) from either or both $PHD2_{181-402}$-Zn(II)-2OG and $PHD2_{181-402}$-Zn(II)-2OG-CODD, in such cases $\Delta\delta$ were defined as 0 ppm.

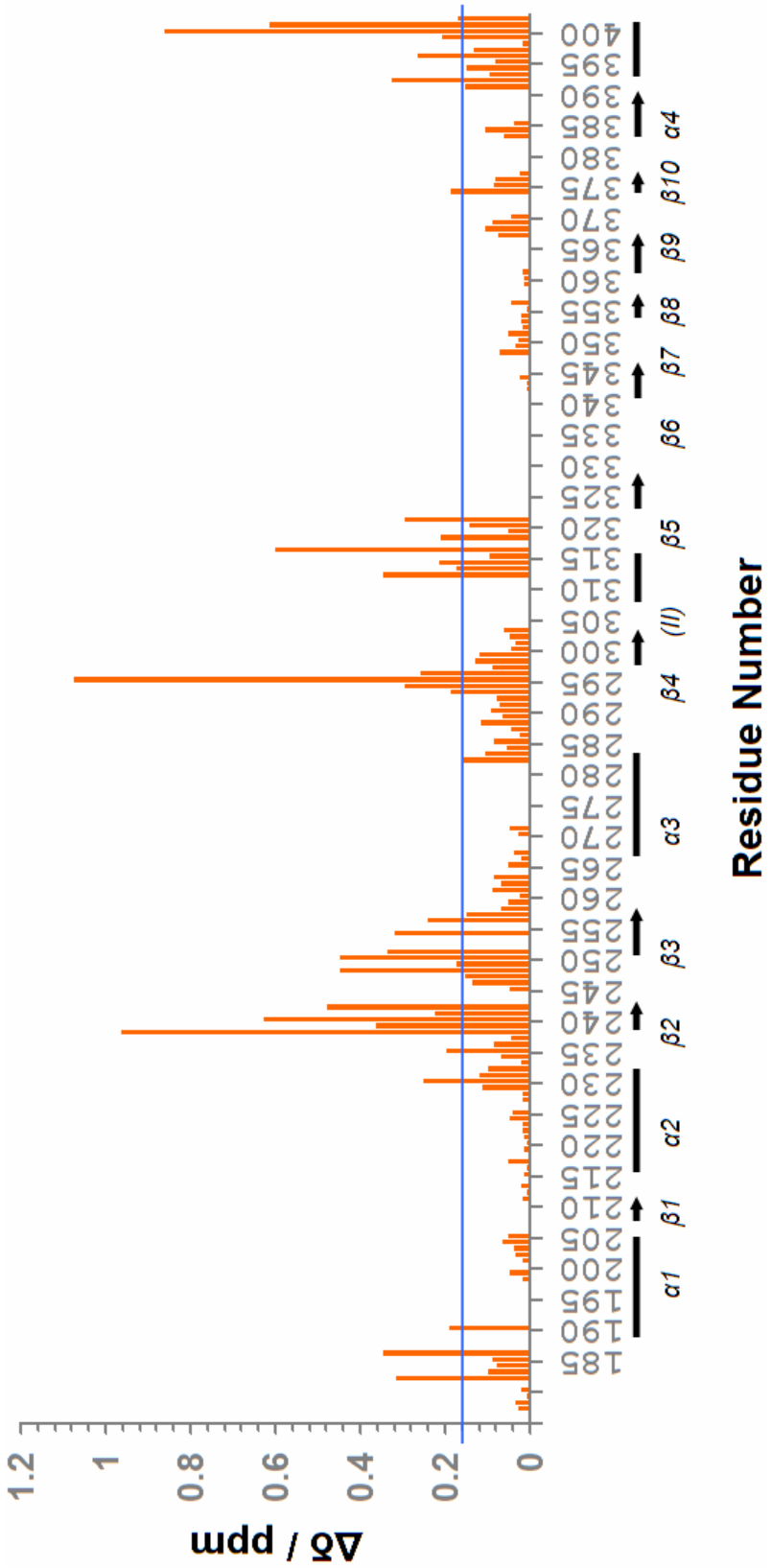

Figure 4-22 Bar chart showing Δδ (ppm) against residue number for the free and CODD-complexed forms of $PHD2_{181-402}$. Note that for cases in which there are missing assignments from either or both forms Δδ are defined as 0 ppm.

4.4.2 Translation of assignment from $^{2}H,^{13}C,^{15}N$-labelled $PHD2_{181-402}$ to ^{15}N-labelled $PHD2_{181-402}$

It has been reported that deuterium isotope shifts can be significant for spins located within three or four bonds of the site of deuteration.[55,56] Because the assignments of both $PHD2_{181-402}$-Zn(II)-2OG and $PHD2_{181-402}$-Zn(II)-2OG-CODD were conducted with $^{2}H,^{13}C,^{15}N$-labelled proteins, whilst routine binding experiments were conducted with ^{15}N-labelled proteins, translation of the assignment from the triple labelled to the single labelled proteins was therefore conducted. Only the ^{1}H and ^{15}N chemical shifts of the major form were transferred, which are summarised in Table 4-5 and Table 4-6.

Transfer of ^{1}H and ^{15}N assignment				
	$^{2}H,^{13}C,^{15}N$-labelled		^{15}N-labelled	
Residue	^{1}H	^{15}N	^{1}H	^{15}N
G				
S	8.53	115.27	8.54	115.50
H	8.56	120.59	8.57	121.01
M	8.27	122.73	8.27	123.11
A	8.35	125.82	8.37	126.20
S	8.23	115.76	8.23	115.93
P181				
N182	8.31	117.93	8.32	118.24
G183	8.19	108.93	8.21	109.14
Q184	8.08	119.48	8.08	119.69
T185	8.07	116.87	8.07	117.04
K186	7.98	121.88	7.99	122.23
P187				
L188	7.31	117.64	7.33	117.93
P189				
A190	8.18	123.86		
L191				
K192				
L193				
A194				
L195				
E196	8.32	120.49	8.36	121.28
Y197				
I198	8.60	120.84	8.60	121.33
V199	8.45	115.88	8.48	116.22
P200				
C201	7.67	116.09	7.68	116.47
M202	8.57	117.39	8.59	117.70
N203	8.37	116.49	8.36	116.80
K204	7.77	117.36	7.76	117.79
H205	8.35	113.02	8.36	113.52
G206	8.40	110.48	8.51	111.36
I207	6.57	115.59	6.59	115.84
C208	9.29	126.52	9.31	126.94
V209	8.69	130.12	8.72	130.54
V210				
D211	8.40	125.34	8.41	125.88
D212	8.59	117.30	8.61	117.51
F213	8.41	116.87	8.41	117.09
L214				
G215	10.19	115.24	10.21	115.54
K216	8.11	117.65	8.12	117.86
E217	8.51	118.89	8.54	119.19
T218	8.61	118.28	8.62	118.55
G219	8.47	108.25	8.48	108.64
Q220	8.44	120.47	8.45	120.75
Q221	7.47	119.91	7.48	120.29
I222	7.99	119.49	8.01	119.75

G223	8.30	106.81	8.30	107.14
D224	8.38	122.51	8.37	122.87
E225	8.08	122.52	8.10	123.00
V226	8.53	119.88	8.54	120.35
R227	8.19	119.95	8.22	120.23
A228	7.77	120.62	7.78	120.90
L229	7.61	119.30	7.60	119.60
H230	8.13	118.83	8.13	119.24
D231	8.91	121.13	8.91	121.30
T232	7.44	107.77	7.45	107.94
G233	7.47	108.01	7.49	108.27
K234	7.51	115.60	7.51	115.83
F235	8.44	119.05	8.46	119.39
T236	9.34	113.80	9.36	113.99
D237	8.49	120.84	8.51	121.24
G238	8.85	114.06	8.88	114.59
Q239	8.38	118.73	8.40	118.95
L240	7.58	119.52	7.59	119.99
V241	7.87	119.06	7.87	119.20
S242	7.76	116.90	7.74	117.16
Q243	8.15	121.25	8.16	121.51
K244	8.11	120.57	8.12	120.82
S245	8.15	115.53	8.16	115.83
D246	8.23	120.97	8.25	121.25
S247	8.10	114.71	8.10	114.93
S248	8.09	117.09	8.09	117.35
K249	8.10	121.85	8.11	122.10
D250	8.09	121.41	8.10	121.79
I251	8.05	122.18	8.05	122.43
R252				
G253				
D254	9.03	115.91	9.02	116.10
K255	8.59	121.08	8.62	121.52
I256	9.34	114.51	9.35	114.73
T257	8.06	113.35	8.07	113.52
W258	7.92	123.99	7.91	124.20
I259	9.79	125.41	9.78	125.69
E260	11.23	128.77	11.25	129.19
G261	9.98	109.39	9.99	109.64
K262	6.77	116.59	6.76	116.80
E263	10.45	126.31	10.47	126.65
P264				
G265	9.04	113.95	9.07	114.35
C266	7.55	115.06	7.53	115.28
E267	8.97	119.92	8.99	120.18
T268	10.39	122.20	10.48	122.61
I269				
G270	8.39	106.54	8.42	106.91
L271	7.58	125.66	7.60	125.94
L272				
M273				
S274	8.30	113.63	8.30	114.02
S275	8.19	119.91	8.21	120.22
M276				
D277				
D278				
L279				
I280				
R281				
H282	7.58	115.63	7.58	116.14
C283	7.49	114.65	7.50	114.77
N284	7.56	116.93	7.59	117.27
G285	8.65	111.95	8.68	112.47
K286	7.90	116.22	7.92	116.49
L287	7.61	120.29	7.59	120.53
G288	8.78	114.29	8.81	114.62
S289	7.68	118.31	7.70	118.53
Y290	7.26	119.74	7.25	119.99
K291	9.13	125.79	9.14	126.12
I292	8.39	124.82	8.41	125.14
N293	8.37	126.43	8.37	126.80
G294	8.00	108.99	8.01	109.28

R295	7.99	112.60	8.00	112.82
T296	8.08	109.80	8.08	110.05
K297	7.81	115.19	7.82	115.54
A298	8.45	120.91	8.46	121.29
M299	9.73	125.85	9.73	126.15
V300	8.53	129.68	8.53	130.02
A301	8.89	127.02	8.88	127.41
C302	9.09	119.70	9.08	119.95
Y303	9.05	129.13	9.04	129.44
P304				
G305				
N306				
G307	8.67	113.60	8.69	113.91
T308				
G309	8.33	110.78	8.40	110.65
Y310				
V311				
R312	8.31	122.11	8.34	122.46
H313	8.78	123.16	8.80	123.54
V314	8.03	118.49	8.04	118.82
D315	9.07	127.66	9.07	128.11
N316	7.52	110.44	7.51	110.66
P317				
N318	8.16	117.17	8.16	117.57
G319	8.14	112.41	8.16	112.67
D320	9.06	119.18	9.06	119.46
G321	9.42	108.43	9.45	108.73
R322	8.00	119.98	8.02	120.29
C323	9.34	120.40	9.36	120.76
V324	7.21	124.77	7.22	125.34
T325				
C326				
I327	8.24	121.33	8.25	121.67
Y328				
Y329				
L330				
N331	6.41	115.50	6.41	115.93
K332	9.04	129.65	9.05	129.91
D333	8.99	122.20	8.98	122.44
W334	7.56	119.15	7.56	119.47
D335				
A336				
K337				
V338	6.76	113.41	6.76	113.64
S339	8.24	113.73	8.24	114.08
G340				
G341				
I342	7.30	119.46	7.29	119.57
L343	7.64	126.74	7.64	127.06
R344	8.79	130.54	8.79	130.86
I345	8.84	125.79	8.86	126.06
F346	8.44	125.07	8.44	125.41
P347				
E348	9.17	124.16	9.17	124.57
G349	8.88	111.95	8.90	112.29
K350	7.53	118.65	7.52	118.78
A351	8.31	122.44	8.34	122.86
Q352	7.36	115.34	7.36	115.55
F353	6.96	119.06	6.98	119.39
A354	8.99	124.34	8.98	124.72
D355	8.22	123.06	8.24	123.50
I356	9.66	126.28	9.65	126.56
E357				
P358				
K359	7.42	122.13	7.43	122.39
F360	7.11	118.89	7.15	119.23
D361	7.63	125.51	7.64	125.87
R362				
L363	8.23	125.07	8.23	125.20
L364				
F365				
F366				

W367	7.07	117.44	7.08	117.80
S368	7.62	114.08	7.63	114.37
D369	7.78	119.96	7.84	119.84
R370	7.60	110.60	7.60	110.89
R371	8.19	119.63	8.19	120.16
N372	7.45	110.31	7.45	110.69
P373				
H374	8.76	117.62	8.78	117.94
E375	9.09	116.50	9.09	116.84
V376	9.13	122.44	9.12	122.73
Q377	8.66	127.74	8.65	128.12
P378				
A379	8.39	123.10	8.42	123.58
Y380				
A381	7.65	121.62	7.68	121.99
T382	8.19	115.69		
R383	8.31	130.36	8.31	130.72
Y384	9.81	126.85	9.82	127.26
A385	8.55	121.70	8.56	122.05
I386	8.80	120.71	8.79	120.92
T387				
V388				
W389	7.89	130.28		
Y390				
F391				
D392	8.66	119.61	8.67	119.90
A393	9.25	128.05	9.27	128.50
D394	8.12	117.57	8.13	117.87
E395	8.70	121.93	8.68	122.22
R396	8.49	117.61	8.50	117.89
A397	7.44	119.35	7.45	119.62
R398	7.41	116.63	7.42	116.87
A399	7.48	122.39	7.49	122.74
K400	7.81	119.03	7.83	119.31
V401	7.76	120.13	7.77	120.35
K402	7.73	129.31	7.75	129.65

Table 4-5 Transfer of ^{1}H and ^{15}N assignment from $^{2}H,^{13}C,^{15}N$-PHD2$_{181-402}$-Zn(II)-2OG to ^{15}N-PHD2$_{181-402}$-Zn(II)-2OG.

Transfer of ^{1}H and ^{15}N assignment				
	$^{2}H,^{13}C,^{15}N$-PHD2$_{181-402}$-Zn(II)-2OG-CODD		^{15}N-PHD2$_{181-402}$-Zn(II)-2OG-CODD	
Residue	^{1}H	^{15}N	^{1}H	^{15}N
G				
S	8.53	115.28	8.54	115.47
H	8.59	120.41	8.61	120.70
M	8.3	122.56	8.32	122.67
A	8.35	125.78	8.36	126.06
S	8.24	115.96	8.25	116.25
P181				
N182	8.59	119.41	8.60	119.73
G183	8.29	109.07	8.30	109.27
Q184	8.16	119.47	8.16	119.61
T185	8.11	116.07		
K186	8.16	124.8	8.19	125.08
P187				
L188				
P189				
A190	8.35	123.03	8.32	123.08
L191	7.89	116.76	7.94	116.86
K192	7.19	117.28	7.21	117.45
L193				
A194	8.04	119.63	8.06	119.86
L195	7.97	112.55	7.97	112.82
E196				
Y197	7.24	117.14	7.21	117.10
I198	8.61	120.8	8.63	121.20
V199	8.41	115.77	8.44	116.09
P200				
C201	7.65	115.99	7.70	116.41
M202	8.54	117.43	8.54	117.76
N203	8.4	116.51	8.43	117.02
K204	7.83	117.04	7.86	117.25
H205	8.36	112.48	8.40	112.54
G206	8.47	110.82	8.52	111.15
I207	6.56	115.57	6.58	115.82
C208				

V209	8.69	130.06	8.69	130.40
V210				
D211	8.38	125.36	8.36	125.70
D212	8.58	117.26	8.57	117.75
F213	8.39	116.87	8.42	117.37
L214				
G215	10.17	115.23	10.19	115.52
K216	8.11	117.69	8.12	117.94
E217	8.46	118.99	8.47	119.25
T218	8.61	118.28	8.64	118.59
G219	8.48	108.29	8.50	108.66
Q220	8.44	120.52	8.44	120.83
Q221	7.47	119.79	7.51	120.11
I222	7.97	119.54	7.99	119.90
G223	8.31	106.84	8.33	107.24
D224	8.42	122.33	8.45	122.58
E225	8.1	122.14	8.11	122.24
V226				
R227	8.17	120.08	8.20	120.42
A228	7.79	120.72	7.79	121.00
L229	7.72	118.94	7.74	119.21
H230	8.38	119.36	8.41	119.59
D231	8.79	121.29	8.80	121.52
T232	7.35	108.06	7.35	108.27
G233	7.45	107.84	7.47	108.03
K234	7.45	115.67	7.45	115.88
F235	8.55	120.7	8.55	121.08
T236	9.4	113.29	9.40	113.47
D237	8.45	120.76	8.48	121.18
G238	8.03	108.97	8.04	109.25
Q239				
L240				
V241				
S242				
Q243				
K244				
S245	8.12	115.93	8.13	116.16
D246	8.37	120.68	8.37	120.83
S247	7.98	113.69	8.00	114.05
S248	8.45	119.64	8.47	119.99
K249	7.93	121.55	7.94	121.75
D250	8.03	116.97	8.03	117.11
I251	7.72	121.53	7.75	121.72
R252	7.9	113.83	7.92	114.05
G253	8.71	110.16	8.73	110.46
D254	9.35	116.11	9.35	116.28
K255				
I256	9.58	114.69	9.59	114.96
T257	7.92	112.85	7.93	113.06
W258	7.88	124.54	7.88	124.78
I259	9.76	125.83	9.74	126.04
E260	11.21	128.73	11.23	129.03
G261	9.9	109.15	9.91	109.41
K262	6.7	116.46	6.71	116.63
E263	10.54	126.4	10.54	126.65
P264				
G265	8.99	113.7	8.98	113.83
C266	7.56	114.92	7.54	115.01
E267	9	120.13	9.03	120.57
T268	9.97	121.17	9.79	120.90
I269	8.11	125.45		
G270	8.36	106.5	8.38	106.99
L271	7.54	125.37	7.55	125.49
L272				
M273				
S274				
S275				
M276				
D277				
D278				
L279				
I280				
R281				
H282	7.59	113.98	7.58	113.99
C283	7.56	115.45	7.57	115.76
N284	7.51	116.82	7.52	117.03
G285	8.61	112.64	8.63	112.69
K286	7.91	116.02	7.91	116.16
L287	7.57	120.14	7.56	120.34
G288	8.68	113.91	8.71	114.34
S289	7.71	118.82	7.70	118.88
Y290	7.17	119.91	7.16	120.13
K291	9.06	125.74	9.07	126.01
I292	8.47	124.73	8.48	125.11
N293	8.27	124.88	8.31	125.27
G294	7.78	108.51	7.79	108.73
R295	9.04	115.03	9.04	115.23

T296	7.86	108.39	7.86	108.60
K297	7.9	115.19	7.90	115.46
A298	8.32	120.59	8.34	121.00
M299	9.71	124.66	9.70	124.93
V300	8.49	129.5	8.49	129.83
A301	8.89	127.35	8.89	127.80
C302	9.14	119.93	9.14	120.27
Y303	9.03	129.72	9.03	129.91
P304				
G305				
N306				
G307				
T308				
G309	8.35	110.74		
Y310				
V311	8.09	119.2	8.07	119.18
R312	8.04	119.93	8.06	120.24
H313	8.69	121.67	8.72	122.03
V314	8.16	116.8	8.17	117.17
D315	9.11	128.53	9.11	128.94
N316	7.13	105.92	7.12	106.18
P317				
N318	8.32	118.48	8.36	118.78
G319	8.19	112.61	8.20	112.80
D320	8.91	119.21	8.92	119.45
G321	9.2	106.46	9.15	106.62
R322				
C323	9.69	120.86	9.69	121.22
V324	7.28	125.45	7.29	125.71
T325				
C326				
I327				
Y328				
Y329				
L330				
N331				
K332				
D333				
W334				
D335				
A336				
K337				
V338				
S339				
G340				
G341				
I342	7.3	119.5		
L343	7.63	126.82	7.63	127.15
R344	8.82	130.59	8.82	130.87
I345	8.8	125.72	8.82	125.98
F346	8.5	125.1	8.48	125.42
P347				
E348	9.23	123.62	9.25	123.75
G349	8.89	111.6	8.91	111.72
K350	7.56	118.84	7.55	119.05
A351	8.26	122.17	8.28	122.42
Q352	7.35	115.51	7.35	115.83
F353	6.98	118.92	7.03	118.96
A354	9.01	124.33	9.00	124.43
D355	8.23	123	8.25	123.39
I356	9.7	126.39	9.67	126.42
E357	8.3	125.33	8.31	125.65
P358				
K359	7.43	122.09	7.44	122.37
F360	7.1	118.94	7.14	119.19
D361	7.62	125.4	7.63	125.75
R362				
L363				
L364				
F365				
F366				
W367	7.15	117.44	7.15	117.83
S368	7.52	114.01	7.53	114.30
D369	7.74	119.17	7.74	119.49
R370	7.63	110.4	7.64	110.69
R371	8.27	118.47	8.30	118.79
N372	7.37	110.41	7.39	110.84
P373				
H374	8.94	118.06	8.95	118.35
E375	9.02	115.99	9.01	116.19
V376	9.21	122.77	9.21	123.12
Q377	8.66	127.51	8.66	127.84
P378				
A379				
Y380				
A381	7.63	121.49	7.65	121.78
T382	8.17	115.72	8.18	116.06

R383	8.37	130.14	8.37	130.46
Y384	9.71	126.6	9.70	127.04
A385	8.51	121.52	8.52	121.81
I386				
T387				
V388				
W389				
Y390				
F391	8.72	120.85	8.73	121.18
D392	8.34	119.17	8.36	119.49
A393	9.34	128.41	9.35	128.87
D394	8.26	117.74	8.28	118.05
E395	8.78	121.87	8.78	122.10
R396	8.75	118	8.75	118.22
A397	7.38	118.18	7.41	118.58
R398	7.42	116.78	7.44	116.98
A399	7.64	121.03	7.63	121.35
K400	7.07	114.62	7.09	114.94
V401	7.19	117.72	7.21	118.00
K402	7.57	129.32	7.60	129.41

Table 4-6 Transfer of ^{1}H and ^{15}N assignment from $^{2}H,^{13}C,^{15}N$-PHD2$_{181-402}$-Zn(II)-2OG-CODD to ^{15}N-PHD2$_{181-402}$-Zn(II)-2OG-CODD.

Some of the transferred assignment values might be compromised due to degenerate (or missing) peaks in the spectra corresponding to the single labelled protein (Figure 4-23) because single labelled proteins generally had faster amide proton transverse relaxation rates than perdeuterated proteins and therefore broader peaks. In some cases, extra peaks were observed in the single labelled protein spectrum but not in the triple labelled protein spectrum (Figure 4-23), which could correspond to amides that are buried (and hence solvent inaccessible) and might have very slow H/D exchange rates, resulting in diminished amplitude in the spectrum of the triple labelled sample.

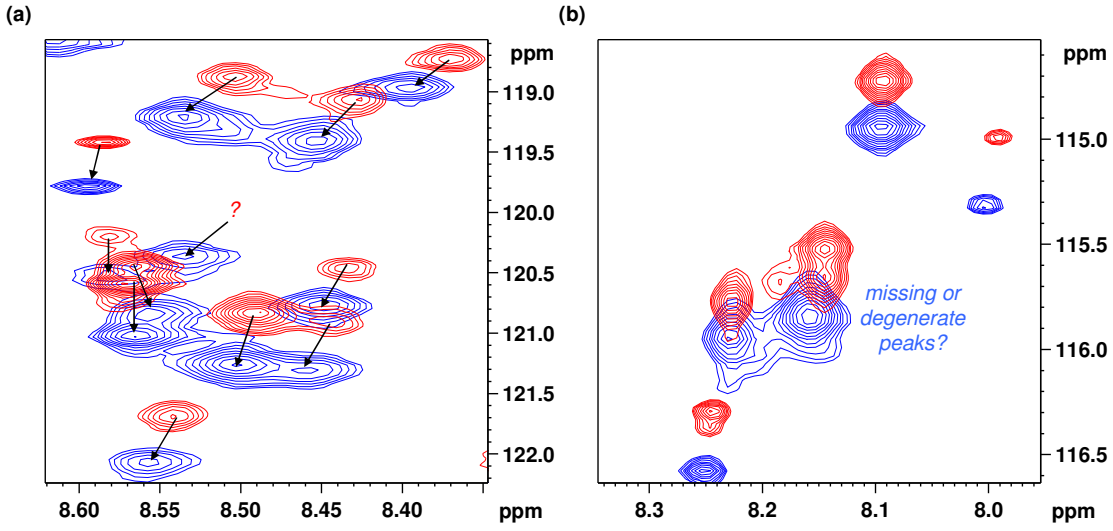

Figure 4-23 Chemical shift transfer from the $^{2}H,^{13}C,^{15}N$ labelled sample (red) to the ^{15}N labelled sample (blue). Potential errors included (a) missing peak in the triple labelled spectrum, and (b) missing/degenerate peaks in the single labelled sample.

4.4.3 Probing the CODD binding site through substrate variants

In order to identify the residues that were involved in PHD2-substrate recognition and interaction, the binding influence of a series of alanine variants of CODD to ^{15}N-PHD2$_{181-402}$-Zn(II)-2OG were investigated (Figure 4-24 and Appendix I).

The ^{1}H-^{15}N HSQC spectra of ^{15}N-labelled PHD2$_{181-402}$-Zn(II)-2OG in the presence of different CODD variants were then compared with the one of ^{15}N-PHD2$_{181-402}$-Zn(II)-2OG-CODD using the minimal shift approximation approach,[57,58] in which the assignment of the slow exchange perturbed peaks were made on a proximity basis by considering ^{1}H and ^{15}N shifts between the two spectra. A $\Delta\delta$ cut-off of 0.1 ppm was used for analyses and peaks that do not have an apparent slow exchange partner were not considered. The results are summarised in Table 4-7.

All the tested variants, except P564A CODD and D569A,D570A,D571A CODD, fully saturate PHD2$_{181-402}$-Zn(II)-2OG at the same concentration as CODD (at 2.7 fold molar excess) as judged by ^{1}H-^{15}N HSQC, indicating their binding affinities are not substantially affected by alanine substitution. This result is in agreement with previous kinetic studies which shows the length of the peptide was critical for catalysis[59,60] but (most) amino acid substitutions had minimal effect (which retained 80%–120% activities when compared to CODD).[61] The triple substituted variant D569A,D570A,D571A CODD showed only weak binding in fast exchange to PHD2$_{181-402}$-Zn(II)-2OG. Previous studies have identified these three negative charged aspartic acid residues were crucial for catalysis and that if two or all of them were substituted to alanine, hydroxylation is reduced significantly (*e.g.* the triple alanine CODD variant retained <10% activity).[61] The other alanine CODD variant that showed weak binding to PHD2$_{181-402}$-Zn(II)-2OG in fast exchange was P564A CODD. This is relatively surprising because previous studies had shown that CODD variants, in which the P564 residue was substituted by different proline like analogues such as L-3,4-dehydroproline, may be used as PHD2 inhibitors (reported IC_{50} = 8.5 μM).[62] Because alanine may not be the best mimic for proline, P564G CODD (obtained from Dr Richard J. Hopkinson) was also tested. Similar to the alanine variant, the binding of P564G CODD to PHD2$_{181-402}$-Zn(II) was weak as judged by ^{1}H-^{15}N HSQC. As glycine (and alanine) is smaller and more flexible than proline, the result obtained here suggests that the (relatively rigid) conformation of the proline might play an important role in the binding of CODD to PHD2.

HIF-1α$_{556-574}$ (CODD): DLDLEMLAPYIPMDDDFQL

D556A CODD: **A**LDLEMLAPYIPMDDDFQL
L557A CODD: D**A**DLEMLAPYIPMDDDFQL
D558A CODD: DL**A**LEMLAPYIPMDDDFQL
L559A CODD: DLD**A**EMLAPYIPMDDDFQL
E560A CODD: DLDL**A**MLAPYIPMDDDFQL
M561A CODD: DLDLE**A**LAPYIPMDDDFQL
L562A CODD: DLDLEM**A**APYIPMDDDFQL
P564A CODD: DLDLEMLA**A**YIPMDDDFQL
Y565A CODD: DLDLEMLAP**A**IPMDDDFQL
I566A CODD: DLDLEMLAPY**A**PMDDDFQL
P567A CODD: DLDLEMLAPYI**A**MDDDFQL
M568A CODD: DLDLEMLAPYIP**A**DDDFQL
D569A,D570A,D571A CODD: DLDLEMLAPYIPM**AAA**FQL
F572A CODD: DLDLEMLAPYIPMDDD**A**QL
Q573A CODD: DLDLEMLAPYIPMDDDF**A**L
L574A CODD: DLDLEMLAPYIPMDDDFQ**A**

Figure 4-24 Alanine substituted CODD variants that were used in this study.

CODD mutants	PHD2 residues with $\Delta\delta$ > 0.1 ppm					Possible reasons
D556A	*T268*					
L557A	None					
D558A	*S248*	*T268*	*D320*			
L559A	None					
E560A	*T268*	*G321*				
M561A	D246	*S248*	D250	*T268*	*G321*	D246, S248 and D250 are part of the β2β3/loop
L562A	*S248*	*T268*	R312			$R312_{PHD2}$-$L562_{CODD}$ = 3.3 Å
P564A	Weak binding					
Y565A	*T268*	*G321*	K400	V401		*C* -terminal α4 helix
I566A	F391					$F391_{PHD2}$-$I566_{CODD}$ = 3.5 Å
P567A	*T268*					
M568A	K400	V401				$K400_{PHD2}$-$M568_{CODD}$ = 3.4 Å; *C* -terminal α4 helix
D569A,D570A,D571A	Weak binding					
F572A	E260	G261	K262	R295	F391	$K262_{PHD2}$-$F572_{CODD}$ = 4.2 Å; $R295_{PHD2}$-$F572_{CODD}$ = 2.8 Å; $F391_{PHD2}$-$F572_{CODD}$ = 5.6 Å
Q573A	N293	G294				$N293_{PHD2}$-$Q573_{CODD}$ = 3.6 Å ($\Delta\delta$ > 0.05)
L574A	*S248*	H374	A393	D394	A397	H374 = Fe(II) binding; A393, D394, A397 and A398 are
	A398					part of the *C* -terminal α4 helix

Table 4-7 Table summarising the differences between the ^{1}H-^{15}N HSQC spectra of PHD2$_{181-402}$-Zn(II)-2OG-CODD and PHD2$_{181-402}$-Zn(II)-2OG-alanine substituted CODD variants. Residues with $\Delta\delta$ > 0.1 ppm difference between the two forms were listed here, except in the case of Q573A CODD, in which the $\Delta\delta$ cut-off was 0.05 ppm due to small overall changes between the two spectra. The residues in *italic* are always altered in different spectra, which may due to solvent effect.

Amongst CODD and the CODD variants that bind to PHD2$_{181-402}$-Zn(II)-2OG with similar affinity as CODD, they all induce very similar chemical shift changes in PHD2 (when comparing the substrate free and substrate bound spectra). This indicates that CODD and the CODD variants induce the same global conformational changes to PHD2$_{181-402}$ (*e.g.* the β2β3/loop). Only minimal and localised changes between the ^{1}H-^{15}N HSQC spectra of these PHD2$_{181-402}$-Zn(II)-2OG-CODD variants and PHD2$_{181-}$

$_{402}$-Zn(II)-2OG-CODD were observed (Table 4-7; Figure 4-25 to Figure 4-32). Most of these localised differences were observed when alanine was substituted at the *C*-terminal side of CODD, indicating there may be a well-defined binding site on PHD2$_{181\text{-}402}$ for the *C*-terminal of CODD. Interestingly, the M561A CODD variant, in which an alanine was substituted at the *N*-terminal side of CODD, actually induces chemical shift changes to residues located on the β2β3/loop (D246 and D250; Figure 4-25). These results are in agreement with a previous molecular dynamics stimulation study, which suggested that the *C*-terminal side of CODD binds relatively strongly to PHD2-Fe(II)-2OG whilst the *N*-terminal side of CODD binds to PHD2 relatively weakly and is stabilised by the β2β3/loop region.

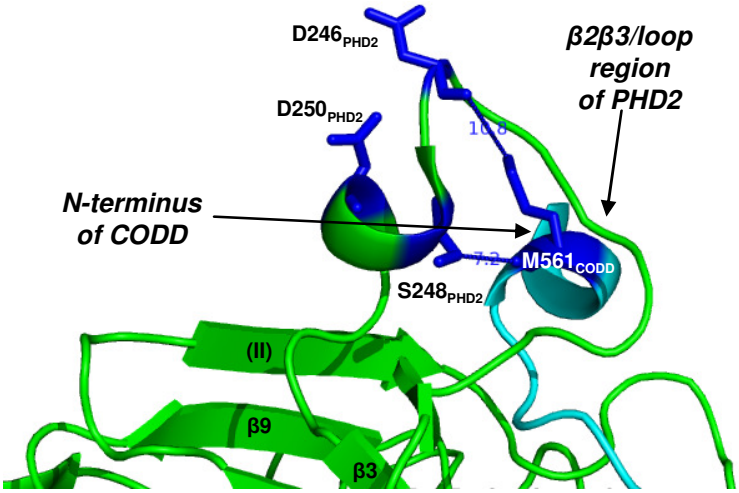

Figure 4-25 A view of the X-ray structure of PHD2-Mn(II)-2OG-CODD (PDB id: 3HQR) showing the interactions between M561$_{CODD}$ and PHD2. Residues with $\Delta\delta$ > 0.1 ppm difference between PHD2$_{181\text{-}402}$-Zn(II)-2OG-CODD and PHD2$_{181\text{-}402}$-Zn(II)-2OG-M561A CODD were highlighted in blue. The protein is shown in green and the CODD peptide is shown in cyan.

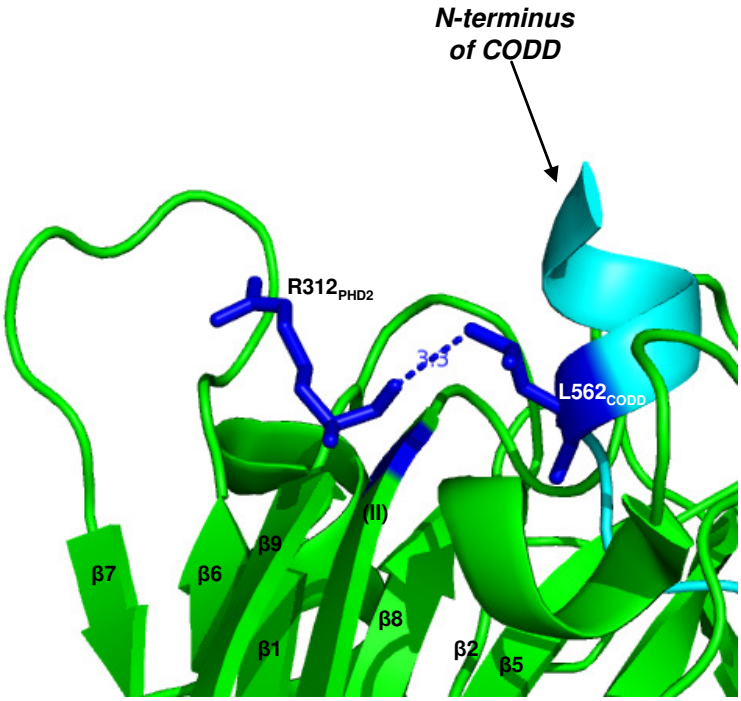

Figure 4-26 A view of the X-ray structure of PHD2-Mn(II)-2OG-CODD (PDB id: 3HQR) showing the interactions between $L562_{CODD}$ and PHD2. Residues with $\Delta\delta$ > 0.1 ppm difference between $PHD2_{181-402}$-Zn(II)-2OG-CODD and $PHD2_{181-402}$-Zn(II)-2OG-L562A CODD were highlighted in blue. The protein is shown in green and the CODD peptide is shown in cyan.

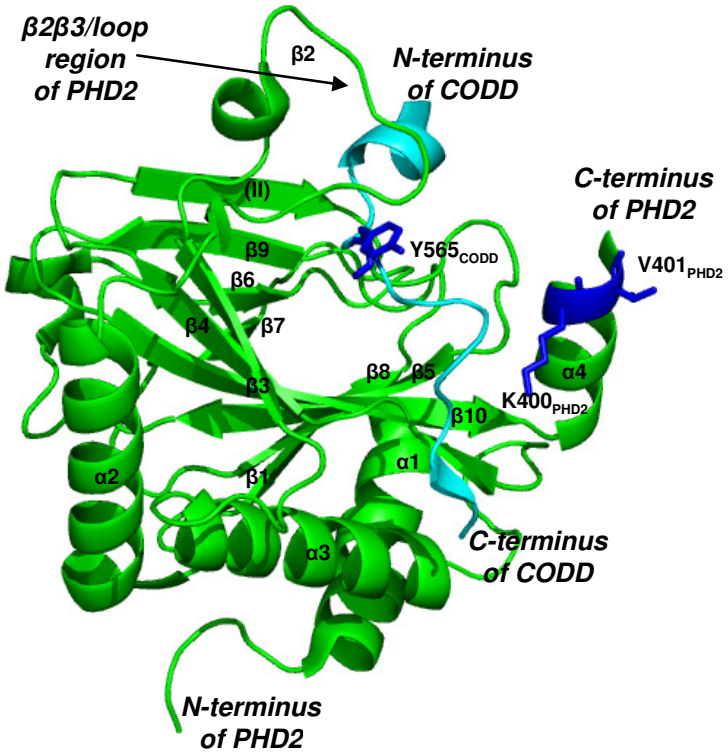

Figure 4-27 A view of the X-ray structure of PHD2-Mn(II)-2OG-CODD (PDB id: 3HQR) showing the interactions between $Y565_{CODD}$ and PHD2. Residues with $\Delta\delta$ > 0.1 ppm difference between $PHD2_{181-402}$-Zn(II)-2OG-CODD and $PHD2_{181-402}$-Zn(II)-2OG-Y565A CODD were highlighted in blue. The protein is shown in green and the CODD peptide is shown in cyan.

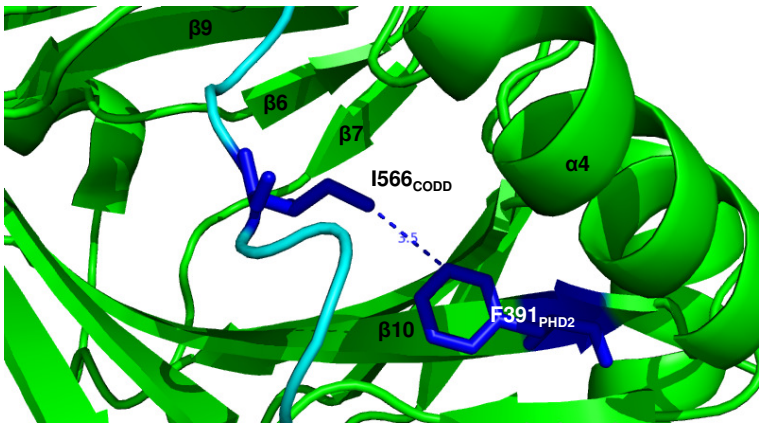

Figure 4-28 A view of the X-ray structure of PHD2-Mn(II)-2OG-CODD (PDB id: 3HQR) showing the interactions between $I566_{CODD}$ and PHD2. Residues with $\Delta\delta$ > 0.1 ppm difference between $PHD2_{181-402}$-Zn(II)-2OG-CODD and $PHD2_{181-402}$-Zn(II)-2OG-I566A CODD were highlighted in blue. The protein is shown in green and the CODD peptide is shown in cyan.

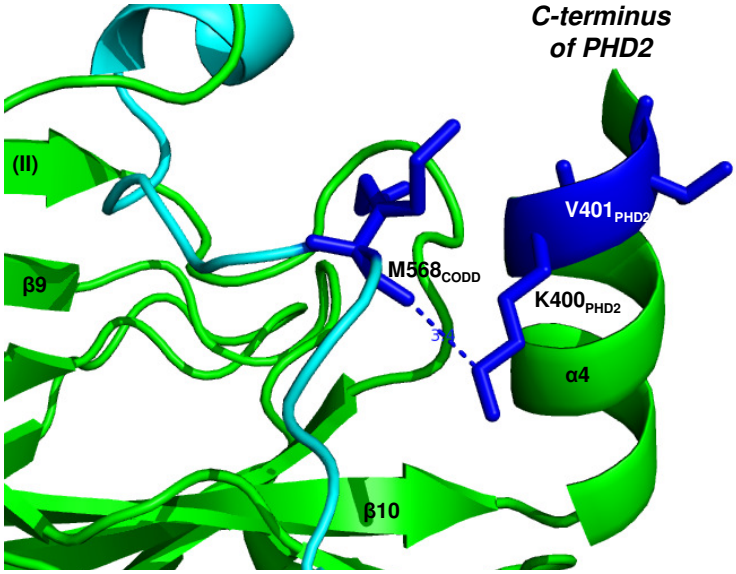

Figure 4-29 A view of the X-ray structure of PHD2-Mn(II)-2OG-CODD (PDB id: 3HQR) showing the interactions between $M568_{CODD}$ and PHD2. Residues with $\Delta\delta$ > 0.1 ppm difference between $PHD2_{181-402}$-Zn(II)-2OG-CODD and $PHD2_{181-402}$-Zn(II)-2OG-M568A CODD were highlighted in blue. The protein is shown in green and the CODD peptide is shown in cyan.

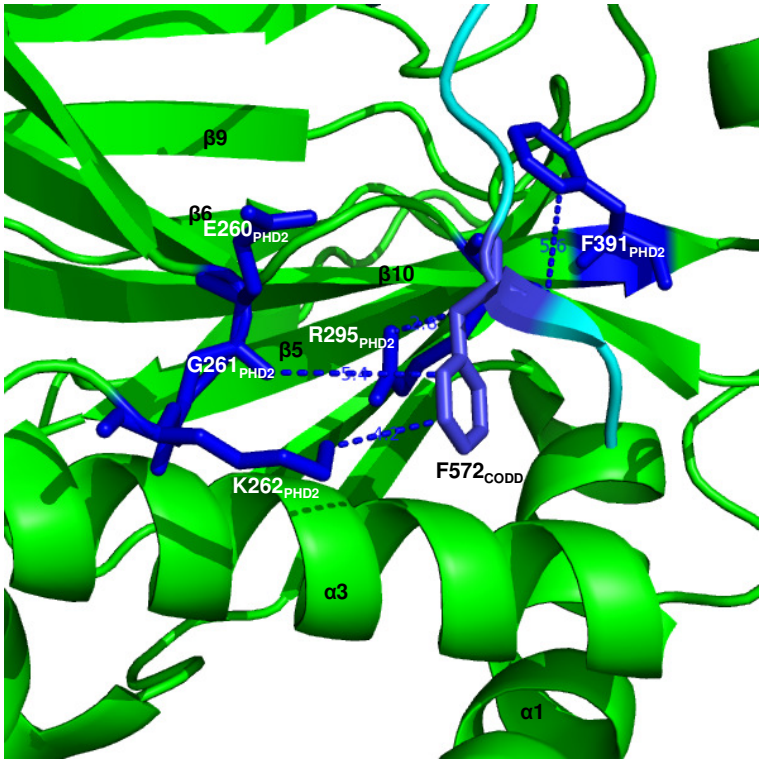

Figure 4-30 A view of the X-ray structure of PHD2-Mn(II)-2OG-CODD (PDB id: 3HQR) showing the interactions between $F572_{CODD}$ and PHD2. Residues with $\Delta\delta$ > 0.1 ppm difference between $PHD2_{181-402}$-Zn(II)-2OG-CODD and $PHD2_{181-402}$-Zn(II)-2OG-F572A CODD were highlighted in blue. The protein is shown in green and the CODD peptide is shown in cyan.

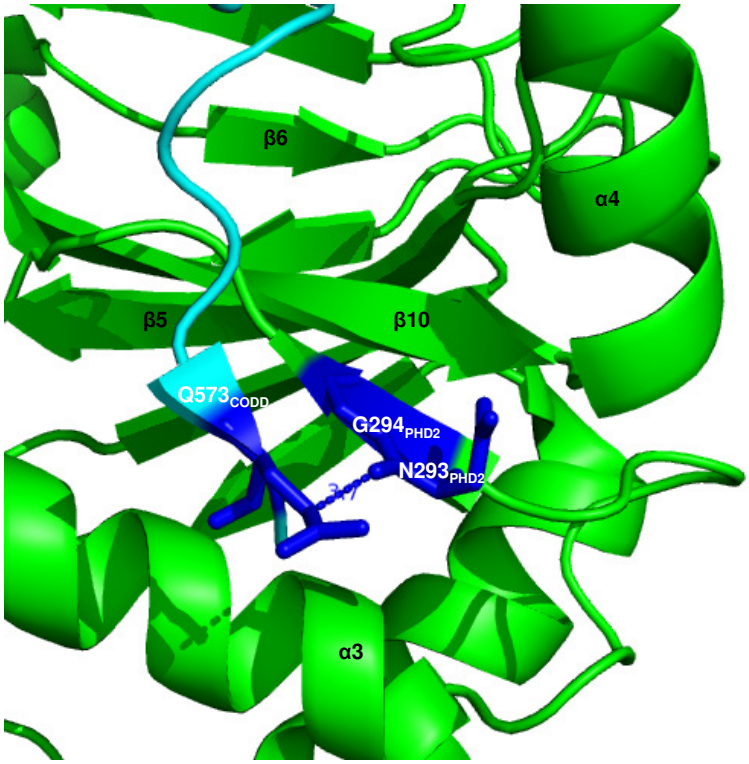

Figure 4-31 A view of the X-ray structure of PHD2-Mn(II)-2OG-CODD (PDB id: 3HQR) showing the interactions between $Q573_{CODD}$ and PHD2. Residues with $\Delta\delta$ > 0.05 ppm difference between $PHD2_{181-402}$-Zn(II)-2OG-CODD and $PHD2_{181-402}$-Zn(II)-2OG-Q573A CODD were highlighted in blue. The protein is shown in green and the CODD peptide is shown in cyan.

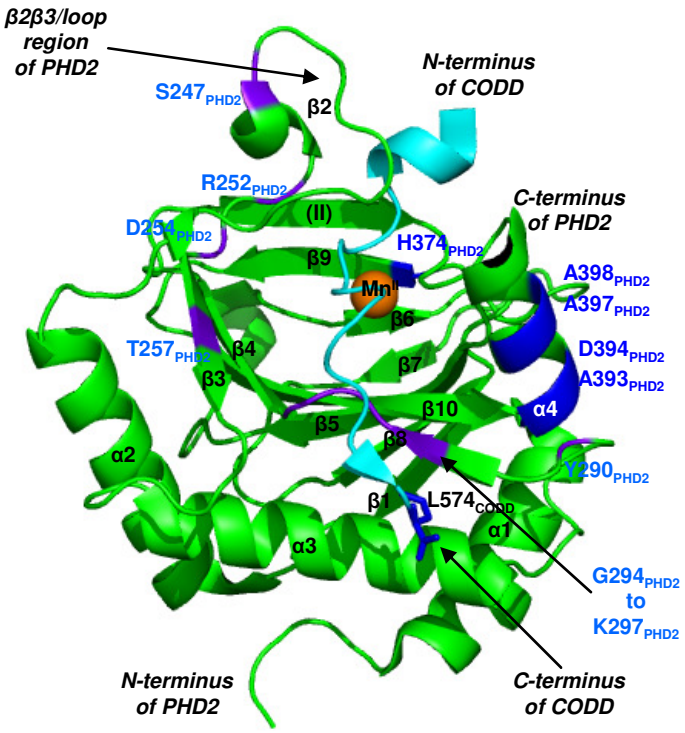

Figure 4-32 A view of the X-ray structure of PHD2-Mn(II)-2OG-CODD (PDB id: 3HQR) showing the interactions between $L574_{CODD}$ and PHD2. Residues with $\Delta\delta$ > 0.1 ppm difference between $PHD2_{181-402}$-Zn(II)-2OG-CODD and $PHD2_{181-402}$-Zn(II)-2OG-L574A CODD were highlighted in blue and peaks that disappear were highlightd in skyblue. The protein is shown in green and the CODD peptide is shown in cyan.

One exception was L574A CODD. The replacement of $L574_{CODD}$ by alanine induced relatively large chemical shift changes to the peaks corresponding to the PHD2 *C*-terminal α4 helix (Figure 4-32). This is interesting because previous studies have suggested $L574_{CODD}$ is important for PHD2 catalysis, and revealed that binding of CODD to PHD2 is decreased when $L574_{CODD}$ is deleted or changed to a serine.[61,63] Note that there are nine peaks that are apparently missing in the $PHD2_{181-402}$-Zn(II)-2OG-L574A CODD spectrum when compared to the corresponding spectrum with CODD. These include five residues just before β4 ($Y290_{PHD2}$ and $G294_{PHD2}$–$K297_{PHD2}$) and four residues on β3 ($S247_{PHD2}$, $R252_{PHD2}$, $D254_{PHD2}$ and $T257_{PHD2}$). This observation indicates that these residues are involved (and therefore broadened) in the binding of L574A CODD.

Finally, it was observed that the ^{1}H and ^{15}N chemical shifts of residues $S248_{PHD2}$, $T268_{PHD2}$, $D320_{PHD2}$ and $G321_{PHD2}$ were varied in different spectra (Figure 4-33). The exact reason for this observation is unknown but this might reflect solvent exposures.

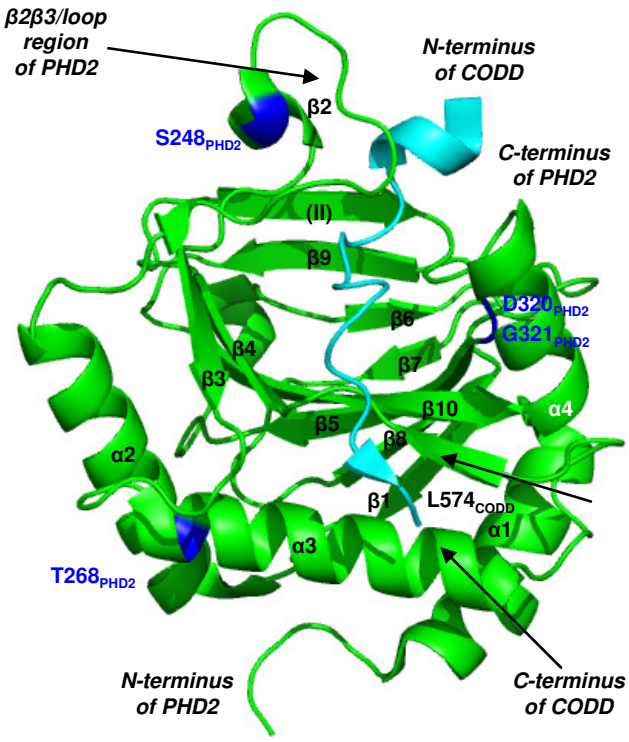

Figure 4-33 A view of the X-ray structure of PHD2-Mn(II)-2OG-CODD (PDB id: 3HQR). S248, T268, D320 and G321, which often varied in different spectra, were highlighted in blue. The protein is shown in green and the CODD peptide is shown in cyan.

4.4.4 CODD and hydroxylated CODD

In order to probe the mechanism of PHD2-substrate recognition and product release, the binding of CODD and hyCODD to $PHD2_{181-402}$ was investigated by protein NMR as assessed by changes in ^{1}H-^{15}N HSQC.

Unlike 2OG, the binding of CODD or hyCODD to PHD2 was found to be independent of metal. Both CODD and hyCODD saturated *apo*-$PHD2_{181-402}$ or $PHD2_{181-402}$-Zn(II) at 2.7 fold molar excess (Figure 4-34) with slow exchange kinetics on the NMR time scale, indicating the binding affinities of CODD and hyCODD were essentially the same with or without the active site metal.

However, hyCODD showed only weak binding in fast exchange in the presence of the metal Zn(II) and cofactor 2OG ($PHD2_{181-402}$-Zn(II)-2OG) as judged by ^{1}H-^{15}N HSQC titration (Figure 4-35). Under the same conditions with CODD at 2.7 fold molar excess, the complex of $PHD2_{181-402}$-Zn(II)-2OG-CODD was formed (Figure 4-19). In a corresponding experiment, it was found that the ^{1}H-^{15}N HSQC spectra of *apo*-PHD2-hyCODD and *apo*-$PHD2_{181-402}$-2OG-hyCODD (without Zn(II)) were essentially the same (Figure 4-36). Because 2OG does not bind to *apo*-PHD2,[64] these

results imply hyCODD binding is perturbed by the presence of 2OG inside the PHD2 active site, but that binding of CODD is not affected.

The results obtained here provide a possible mechanism for product release from PHD2. When CODD is bound to PHD2, the proline residue primarily adopts the C^4-*endo* conformation, possibly due to steric constraints inside the PHD2 active site.[2,9] With hyCODD, the hydroxyproline residue favours the C^4-*exo* conformation due to the stereoelectronic *gauche* effect. The adoption of the C^4-*exo* conformation creates a steric clash between hyCODD and 2OG inside the protein active site. Because both 2OG and Zn(II) (or other metal ions) bind better to PHD2 than CODD (as reflected by their binding constants; Chapter 3), at a 1:1:1:1 PHD2-metal-2OG-hyCODD complex, hyCODD will be displaced from the protein.

In addition, as shown in Chapter 3, if there was an accumulation of hyCODD in solution (for instance, due to the blockage of the von Hippel–Lindau tumor suppressor protein), 2OG might be displaced from PHD2 by the formation of the PHD2-metal-hyCODD complex. The displacement of 2OG might act as a feedback mechanism to prevent uncoupled turnover and unnecessary oxidative damage.

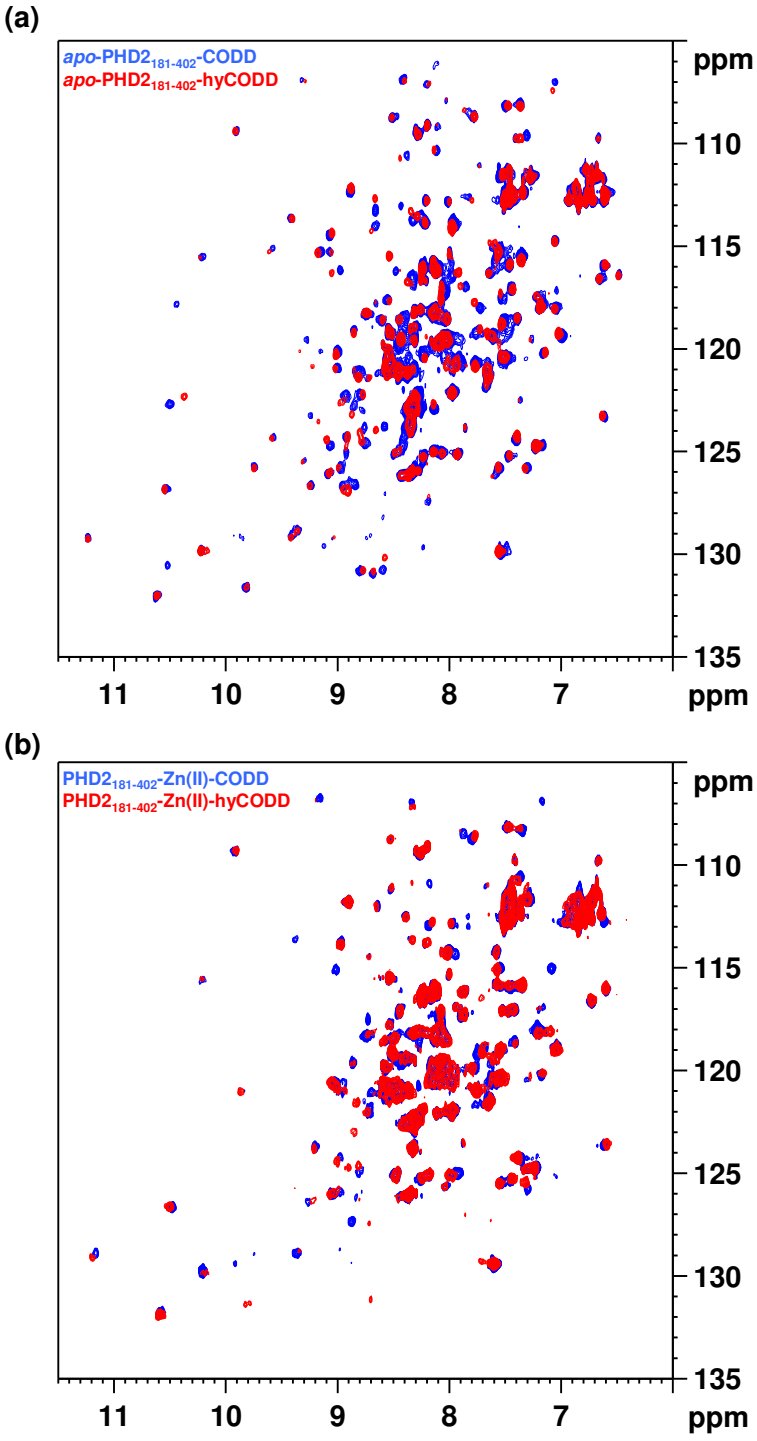

Figure 4-34 (a) Overlaying the ^{1}H-^{15}N HSQC spectra for *apo*-^{15}N-PHD2$_{181\text{-}402}$-CODD (blue) and *apo*-^{15}N-PHD2$_{181\text{-}402}$-hyCODD (red). Mixture contained 150 µM *apo*-^{15}N-PHD2$_{181\text{-}402}$ and 700 µM CODD or 550 µM hyCODD; (b) Overlaying the ^{1}H-^{15}N HSQC spectra for ^{15}N-PHD2$_{181\text{-}402}$-Zn(II)-CODD (blue) and ^{15}N-PHD2$_{181\text{-}402}$-Zn(II)-hyCODD (red). Mixture contained 150 µM *apo*-^{15}N-PHD2$_{181\text{-}402}$, 300 µM Zn(II) and 400 µM CODD/hyCODD. All samples were buffered with 50 mM Tris-D11 at pH 6.6 in 95% H_2O and 5% D_2O.

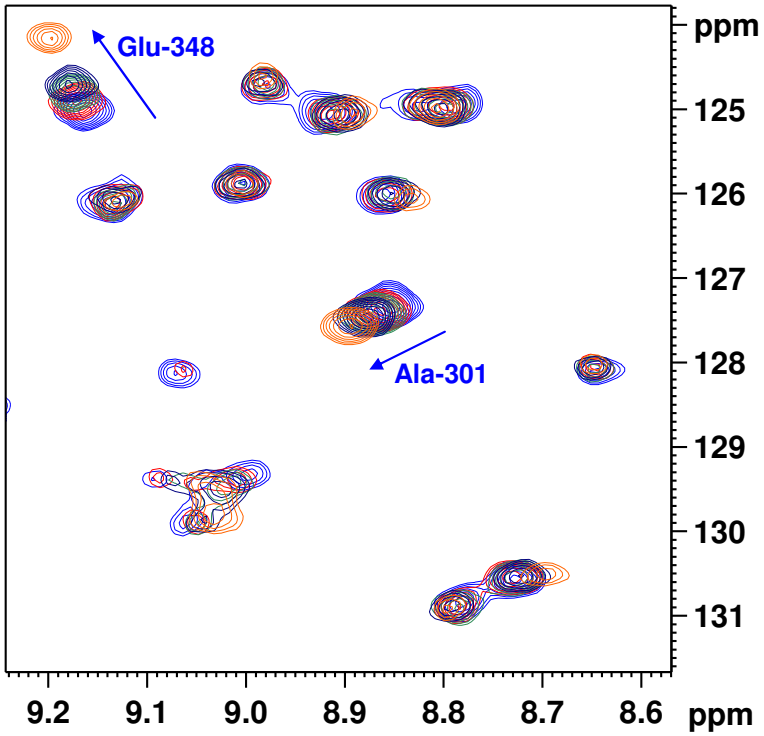

Figure 4-35 Overlaying a region of the ^{1}H-^{15}N HSQC spectra for ^{15}N-PHD2$_{181-402}$-Zn(II)-2OG with 0 µM hyCODD (blue), 75 µM hyCODD (red), 112.5 µM hyCODD (green) , 150 µM hyCODD (purple) and 300 µM hyCODD (orange). All samples were buffered with 50 mM Tris-D11 at pH 6.6 in 95% H_2O and 5% D_2O.

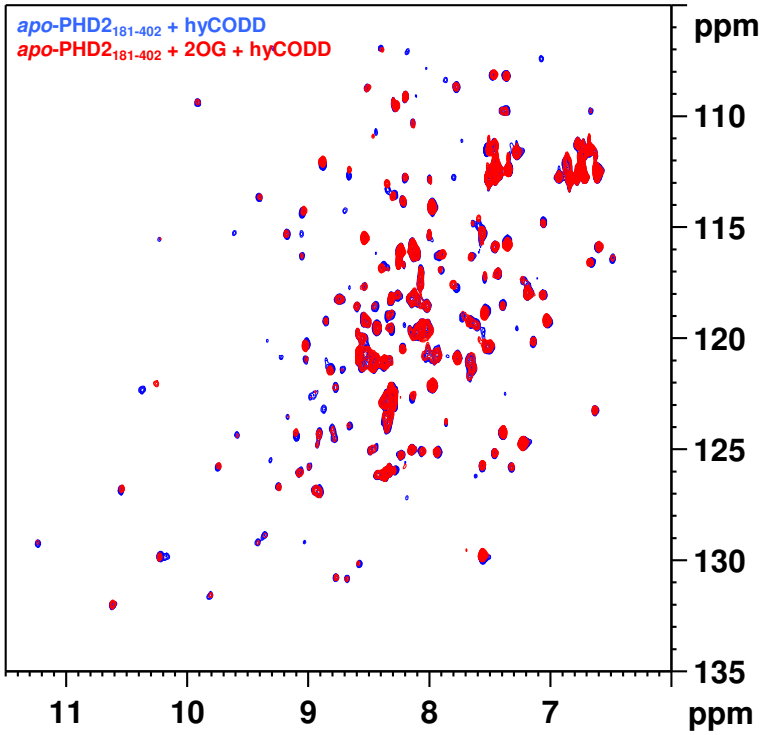

Figure 4-36 Overlaying the ^{1}H-^{15}N HSQC spectra containing 150 µM *apo*-^{15}N-PHD2$_{181-402}$ and 400 µM hyCODD (blue), 150 µM *apo*-^{15}N-PHD2$_{181-402}$, 300 µM 2OG and 400 µM hyCODD (red). All samples were buffered with 50 mM Tris-D11 at pH 6.6 in 95% H_2O and 5% D_2O.

4.4.5 2OG and inhibitor binding site

The protein NMR studies also enabled the identification of the binding sites for co-substrate 2OG and PHD2 inhibitors. Preliminary experiments were conducted with 2OG and the bicyclic inhibitor BIQ (see also Appendix II).

The titration of 2OG to ^{15}N-labelled PHD2$_{181-402}$ was conducted and chemical shift changes were followed by ^{1}H-^{15}N HSQC. The binding kinetics of 2OG to PHD2$_{181-402}$-Zn(II) was found to be slow on the NMR time scale. The K_D of 2OG to PHD2$_{181-402}$-Zn(II) was found to be ~1.1 μM (Figure 4-37), which is comparable to the values obtained with PHD2$_{181-426}$-Mn(II) (~0.9 μM; See Chapter 3). By comparing the ^{1}H-^{15}N HSQC spectra of ^{15}N-PHD2$_{181-402}$-Zn(II)-2OG and ^{15}N-PHD2$_{181-402}$-Zn(II) using the minimal shift approximation with a Δδ cut-off of 0.1 ppm,[57,58] the binding residues involved in the binding of 2OG can be readily mapped out and the changes are highlighted on the crystal structure of PHD2-Fe(II)-2OG (PDB id: 3OUJ; Figure 4-38). The data indicate that M299, A301 and R383 are directly involved in 2OG binding. M299 and A301 anchor the C-1 carboxylic group of 2OG, whilst R383 anchors the 2OG C-5 carboxylic group. Interestingly, R312, H313, V314 and H374 which are primarily involved in Fe(II) binding, also showed significant chemical changes upon 2OG binding, which suggests the binding of 2OG may 'lock' the active site Fe(II) in place. C323, I356 and F360 also showed chemical shift changes but are likely due to solvent effects.

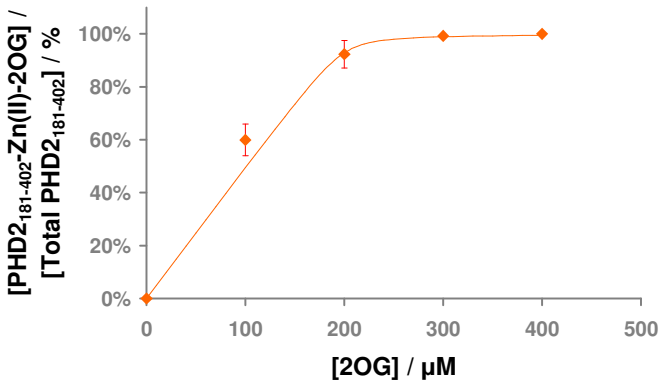

Figure 4-37 2OG titration into ^{15}N-PHD2$_{181-402}$-Zn(II). The mixture included ~200 μM *apo*-^{15}N-labelled PHD2$_{181-402}$; 500 μM Zn(II) and 50 mM Tris-D11 pH 6.6 in 90% H_2O and 10% D_2O. The protein spectra implied slow exchange between the signals of PHD2$_{181-402}$-Zn(II) and PHD2$_{181-402}$-Zn(II)-2OG. The y-axis is plotted as [PHD2$_{181-402}$-Zn(II)-2OG] / [Total PHD2$_{181-402}$], and is an average of three different sets of peaks. The K_D obtained for 2OG is <5 μM.

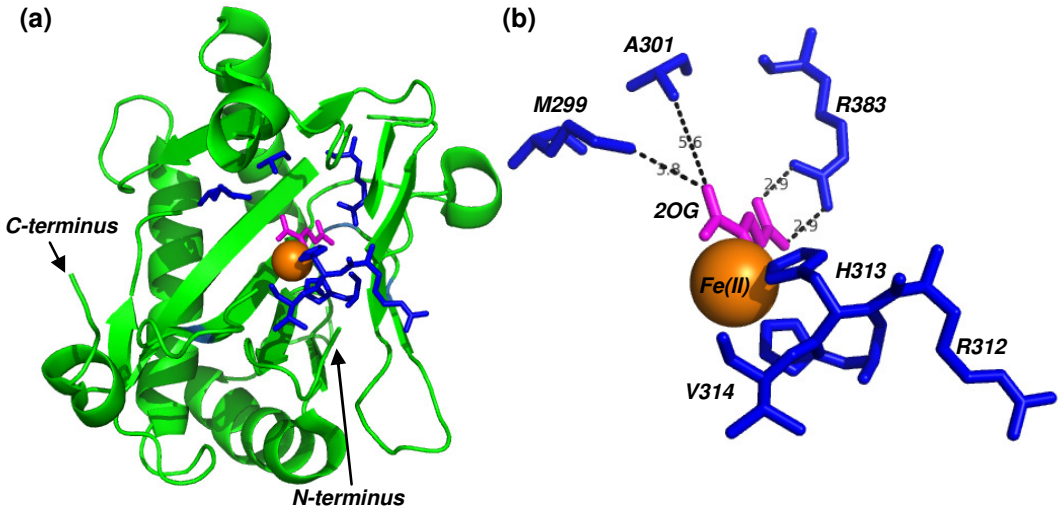

Figure 4-38 (a) X-Ray structure of PHD2-Fe(II)-2OG (PDB id: 3OUJ). Residues that have Δδ larger than 0.1 ppm between $PHD2_{181-402}$-Zn(II) and $PHD2_{181-402}$-Zn(II)-2OG are highlighted in blue. (b) Active site highlighting the perturbed residues.

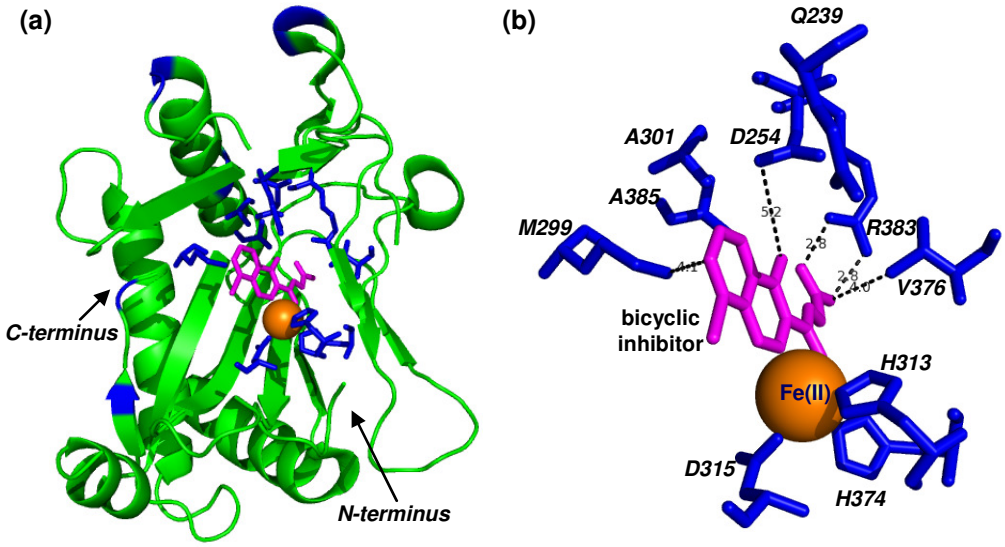

Figure 4-39 (a) X-Ray structure of PHD2-Fe(II)-bicyclic inhibitor (PDB id: 2G19). Residues that have Δδ larger than 0.1 ppm between $PHD2_{181-402}$-Zn(II) and $PHD2_{181-402}$-Zn(II)-BIQ are highlighted in blue. Note that some of the perturbed residues are far away from the binding site and they are likely due to solvent effects because DMSO-D6 was used as a solvent for BIQ; (b) Active site highlighting the perturbed residues.

The binding of the potent BIQ inhibitor to ^{15}N-$PHD2_{181-402}$-Zn(II) was then studied, and the data were mapped onto the crystal structure of PHD2-Fe(II)-bicyclic inhibitor (PDB id: 2G19; Figure 4-39). The data suggested Q239, D254, M299, A301, V376, R383 and A385 are involved in BIQ binding. The bicyclic ring of BIQ interacts with Q239, D254, M299, A301 and A385 whilst V376 and R383 interact with the terminal carboxylic group. Similar to the binding of 2OG, residues that are primarily involved in metal binding (H313, D315 and H374) also showed significant chemical shift changes. Residues G223, T232, G233, S247, S248, G294 and K297 also showed

chemical shift changes but they are likely due to solvent effects because DMSO-D6 was used as a solvent for BIQ (<3%).

4.5 Conclusions and future works

Overall, the work in this Chapter has applied protein NMR to study the binding of co-substrate (2OG), substrate (CODD) and inhibitor (BIQ) to PHD2$_{181-402}$-Zn(II). Uniformly isotopically labelled PHD2$_{181-402}$ (^{15}N; ^{13}C,^{15}N and ^{2}H,^{13}C,^{15}N) were successfully produced and partial protein assignments of PHD2$_{181-402}$-Zn(II)-2OG (80%) and PHD2$_{181-402}$-Zn(II)-2OG-CODD (73%) were determined using the standard triple resonance strategy. Chemical shift perturbation allowed the identification of the PHD2 residues involved in the binding of 2OG, CODD and BIQ. The overall NMR data have provided solution state evidence that supports previous proposals about the existence of different dynamic states of the catalytic domain of PHD2,[2,7] especially with the β2β3/loop region and the α4 helix upon the binding of CODD. However, the NMR results imply that the β2β3/loop is dynamic even when CODD is bound. In addition to binding, a potential mechanism for the release of the hydroxylated product (hyCODD) was also proposed based on steric clash between the hydroxyproline residue of CODD and 2OG in the active site.

In order to complete the several lines of investigation that have started from the work described in this Chapter, some future work is proposed. Firstly, in order to obtain a more complete protein backbone assignment of PHD2$_{181-402}$-Zn(II)-2OG (80%) and PHD2$_{181-402}$-Zn(II)-2OG-CODD, the use of ^{1}H-^{15}N NOESY-HSQC is proposed, which allows sequential assignment based on NOE signals between neighbouring amide protons. The use of perdeuterated protein should help in simplifying the spectrum and improving overall spectral quality. Secondly, once the full assignment is completed, the measurement of R_1, R_2 and heteronuclear NOE could be performed to further investigate the types of motion different residues (*e.g.* β2β3/loop) are exhibiting, in order to obtain more insight about their roles in substrate recognition and binding. Thirdly, binding experiments with the HIF *N*-terminal oxygen dependent degradation domain (NODD; HIF1α$_{395-413}$), another PHD2 substrate, should be performed in order to identify its binding site on PHD2, in order to obtain further insight about the structural basis of PHD2 substrate selectivity.

4.6 References

1. McDonough, M. A.; Li, V.; Flashman, E.; Chowdhury, R.; Mohr, C.; Liénard, B. M. R.; Zondlo, J.; Oldham, N. J.; Clifton, I. J.; Lewis, J.; McNeill, L. A.; Kurzeja, R. J. M.; Hewitson, K. S.; Yang, E.; Jordan, S.; Syed, R. S.; Schofield, C. J. Cellular oxygen sensing: crystal structure of hypoxia-inducible factor prolyl hydroxylase (PHD2). *Proc. Natl. Acad. Sci. U. S. A.* **2006**, *103*, 9814–9819.
2. Chowdhury, R.; McDonough, M. A.; Mecinović, J.; Loenarz, C.; Flashman, E.; Hewitson, K. S.; Domene, C.; Schofield, C. J. Structural basis for binding of hypoxia-inducible factor to the oxygen-sensing prolyl hydroxylases. *Structure* **2009**, *17*, 981–989.
3. Schofield, C. J.; Zhang, Z. Structural and mechanistic studies on 2-oxoglutarate-dependent oxygenases and related enzymes. *Curr. Opin. Struct. Biol.* **1999**, *9*, 722–731.
4. Clifton, I. J.; McDonough, M. A.; Ehrismann, D.; Kershaw, N. J.; Granatino, N.; Schofield, C. J. Structural studies on 2-oxoglutarate oxygenases and related double-stranded β-helix fold proteins. *J. Inorg. Biochem.* **2006**, *100*, 644–669.
5. McDonough, M. A.; Loenarz, C.; Chowdhury, R.; Clifton, I. J.; Schofield, C. J. Structural studies on human 2-oxoglutarate dependent oxygenases. *Curr. Opin. Struct. Biol.* **2010**, *20*, 659–672.
6. Rosen, M. D.; Venkatesan, H.; Peltier, H. M.; Bembenek, S. D.; Kanelakis, K. C.; Zhao, L. X.; Leonard, B. E.; Hocutt, F. M.; Wu, X.; Palomino, H. L.; Brondstetter, T. I.; Haugh, P. V.; Cagnon, L.; Yan, W.; Liotta, L. A.; Young, A.; Mirzadegan, T.; Shankley, N. P.; Barrett, T. D.; Rabinowitz, M. H. Benzimidazole-2-pyrazole HIF prolyl 4-hydroxylase inhibitors as oral erythropoietin secretagogues. *ACS Med. Chem. Lett.* **2010**, *1*, 526–529.
7. Bleijlevens, B.; Shivarattan, T.; Flashman, E.; Yang, Y.; Simpson, P. J.; Koivisto, P.; Sedgwick, B.; Schofield, C. J.; Matthews, S. J. Dynamic states of the DNA repair enzyme AlkB regulate product release. *EMBO Rep.* **2008**, *9*, 872–877.
8. Wick, C. R.; Lanig, H.; Jäger, C. M.; Burzlaff, N.; Clark, T. Structural insight into the prolyl hydroxylase PHD2: a molecular dynamics and DFT study. *Eur. J. Inorg. Chem.* **2012**, *31*, 4973–4985.
9. Loenarz, C.; Mecinović, J.; Chowdhury, R.; McNeill, L. A.; Flashman, E.; Schofield, C. J. Evidence for a stereoelectronic effect in human oxygen sensing. *Angew. Chem. Int. Ed.* **2009**, *48*, 1784–1787.
10. Wolfe, S. Gauche effect. Stereochemical consequences of adjacent electron pairs and polar bonds. *Acc. Chem. Res.* **1972**, *5*, 102–111.
11. Choudhary, A.; Pua, K. H.; Raines, R. T. Quantum mechanical origin of the conformational preferences of 4-thiaproline and its *S*-oxides. *Amino Acids* **2011**, *41*, 181–186.
12. Bretscher, L. E.; Jenkins, C. L.; Taylor, K. M.; DeRider, M. L.; Raines, R. T. Conformational stability of collagen relies on a stereoelectronic effect. *J. Am. Chem. Soc.* **2001**, *123*, 777–778.
13. Gorres, K. L.; Edupuganti, R.; Krow, G. R.; Raines, R. T. Conformational preferences of substrates for human prolyl 4-hydroxylase. *Biochemistry* **2008**, *47*, 9447–9455.
14. Shoulders, M. D.; Kotch, F. W.; Choudhary, A.; Guzei, I. A.; Raines, R. T. The aberrance of the 4*S* diastereomer of 4-hydroxyproline. *J. Am. Chem. Soc.* **2010**, *132*, 10857–10865.
15. Otting, G. Experimental NMR techniques for studies of protein-ligand interactions. *Curr. Opin. Struct. Biol.* **1993**, *3*, 760–768.
16. Montelione, G. T.; Zheng, D.; Huang, Y. J.; Gunsalus, K. C.; Szyperski, T. Protein NMR spectroscopy in structural genomics. *Nat. Struct. Biol.* **2000**, *7*, 982–985.
17. Heller, M.; Kessler, H. NMR spectroscopy in drug design. *Pure Appl. Chem.* **2001**, *73*, 1429–1436.
18. Jahnke, W.; Widmer, H. Protein NMR in biomedical research. *Cell. Mol. Life Sci.* **2004**, *61*, 580–599.

19. Kay, L. E.; Gardner, K. H. Solution NMR spectroscopy beyond 25 kDa. *Curr. Opin. Struct. Biol.* **1997**, *7*, 722–731.

20. Pervushin, K.; Riek, R.; Wider, G.; Wüthrich, K. Attenuated T_2 relaxation by mutual cancellation of dipole-dipole coupling and chemical shift anisotropy indicates an avenue to NMR structures of very large biological macromolecules in solution. *Proc. Natl. Acad. Sci. U. S. A.* **1997**, *94*, 12366–12371.

21. Riek, R. TROSY: Transverse relaxation-optimized spectroscopy. In *BioNMR in drug research*; Zerbe, O., Ed.; Wiley-VCH Verlag GmbH & Co. KGaA: Weinheim, 2003; Chapter 10, pp 227–242.

22. Riek, R.; Fiaux, J.; Bertelsen, E. B.; Horwich, A. L.; Wüthrich, K. Solution NMR techniques for large molecular and supramolecular structures. *J. Am. Chem. Soc.* **2002**, *124*, 12144–12153.

23. Fiaux, J.; Bertelsen, E. B.; Horwich, A. L.; Wüthrich, K. NMR analysis of a 900K GroEL GroES complex. *Nature* **2002**, *418*, 207–211.

24. Tugarinov, V.; Kay, L. E. Methyl groups as probes of structure and dynamics in NMR studies of high-molecular-weight proteins. *ChemBioChem* **2005**, *6*, 1567–1577.

25. Tzakos, A. G.; Grace, C. R. R.; Lukavsky, P. J.; Riek, R. NMR techniques for very large proteins and RNAs in solution. *Annu. Rev. Biophys. Biomol. Struct.* **2006**, *35*, 319–342.

26. Tugarinov, V.; Sprangers, R.; Kay, L. E. Line narrowing in methyl-TROSY using zero-quantum ^{1}H-^{13}C NMR spectroscopy. *J. Am. Chem. Soc.* **2004**, *126*, 4921–4925.

27. Wishart, D. S. Interpreting protein chemical shift data. *Prog. Nucl. Magn. Reson. Spectrosc.* **2011**, *58*, 62–87.

28. Clarkson, J.; Campbell, I. D. Studies of protein-ligand interactions by NMR. *Biochem. Soc. Trans.* **2003**, *31*, 1006–1009.

29. Shuker, S. B.; Hajduk, P. J.; Meadows, R. P.; Fesik, S. W. Discovering high-affinity ligands for proteins: SAR by NMR. *Science* **1996**, *274*, 1531–1534.

30. Rajagopal, P.; Waygood, E. B.; Reizer, J.; Saier Jr, M. H.; Klevit, R. E. Demonstration of protein-protein interaction specificity by NMR chemical shift mapping. *Protein Sci.* **1997**, *6*, 2624–2627.

31. Medek, A.; Hajduk, P. J.; Mack, J.; Fesik, S. W. The use of differential chemical shifts for determining the binding site location and orientation of protein-bound ligands. *J. Am. Chem. Soc.* **2000**, *122*, 1241–1242.

32. Dötsch, V. NMR strategies for protein assignments. In *BioNMR in drug research*; Zerbe, O., Ed.; Wiley-VCH Verlag GmbH & Co. KGaA: Weinheim, 2003; Chapter 4, pp 79–94.

33. Leopold, M. F.; Urbauer, J. L.; Wand, A. J. Resonance assignment strategies for the analysis of NMR spectra of proteins. *Mol. Biotechnol.* **1994**, *2*, 61–93.

34. Ikura, M.; Kay, L. E.; Bax, A. A novel approach for sequential assignment of ^{1}H, ^{13}C, and ^{15}N spectra of larger proteins: heteronuclear triple-resonance three-dimensional NMR spectroscopy. Application to calmodulin. *Biochemistry* **1990**, *29*, 4659–4667.

35. Kay, L. E.; Ikura, M.; Tschudin, R.; Bax, A. Three-dimensional triple-resonance NMR spectroscopy of isotopically enriched proteins. *J. Magn. Reson.* **1990**, *89*, 496–514.

36. Powers, R.; Gronenborn, A. M.; Clore, G. M.; Bax, A. Three-dimensional triple-resonance NMR of ^{13}C/^{15}N-enriched proteins using constant-time evolution. *J. Magn. Reson.* **1991**, *94*, 209–213.

37. Sattler, M.; Schleucher, J.; Griesinger, C. Heteronuclear multidimensional NMR experiments for the structure determination of proteins in solution employing pulsed field gradients. *Prog. Nucl. Magn. Reson. Spectrosc.* **1999**, *34*, 93–158.

38. Clubb, R. T.; Thanabal, V.; Wagner, G. A constant-time three-dimensional triple-resonance pulse scheme to correlate intraresidue $^{1}H^{N}$, ^{15}N, and ^{13}C' chemical shifts in ^{15}N-^{13}C-labelled proteins. *J. Magn. Reson.* **1992**, *97*, 213–217.

39. Grzesiek, S.; Bax, A. Correlating backbone amide and side chain resonances in larger proteins by multiple relayed triple resonance NMR. *J. Am. Chem. Soc.* **1992**, *114*, 6291–6293.

40. Grzesiek, S.; Bax, A. An efficient experiment for sequential backbone assignment of medium-sized isotopically enriched proteins. *J. Magn. Reson.* **1992**, *99*, 201–207.

41. Kainosho, M. Isotope labelling of macromolecules for structural determinations. *Nat. Struct. Biol.* **1997**, *4*, 858–861.

42. Patzelt, H.; Goto, N.; Iwai, H.; Lundstrom, K.; Fernholz, E. Modern methods for the expression of proteins in isotopically enriched form. In *BioNMR in drug research*; Zerbe, O., Ed.; Wiley-VCH Verlag GmbH & Co. KGaA: Weinheim, 2003; Chapter 1, pp 1–38.

43. Ohki, S.-y.; Kainosho, M. Stable isotope labeling methods for protein NMR spectroscopy. *Prog. Nucl. Magn. Reson. Spectrosc.* **2008**, *53*, 208–226.

44. Flashman, E.; Bagg, E. A. L.; Chowdhury, R.; Mecinović, J.; Loenarz, C.; McDonough, M. A.; Hewitson, K. S.; Schofield, C. J. Kinetic rationale for selectivity toward N- and C-terminal oxygen-dependent degradation domain substrates mediated by a loop region of hypoxia-inducible factor prolyl hydroxylases. *J. Biol. Chem.* **2008**, *283*, 3808–3815.

45. Hardy, A. Structural studies on the hypoxic response. D.Phil Thesis, University of Oxford, 2008.

46. Anderson, S.; Chiang, Y. W. Expression system compositions and methods. U.S. Patent 0,136,169, June 9, 2011.

47. Sivashanmugam, A.; Murray, V.; Cui, C.; Zhang, Y.; Wang, J.; Li, Q. Practical protocols for production of very high yields of recombinant proteins using *Escherichia coli*. *Protein Sci.* **2009**, *18*, 936–948.

48. Marley, J.; Lu, M.; Bracken, C. A method for efficient isotopic labeling of recombinant proteins. *J. Biomol. NMR* **2001**, *20*, 71–75.

49. Paliy, O.; Gunasekera, T. S. Growth of *E. coli* BL21 in minimal media with different gluconeogenic carbon sources and salt contents. *Appl. Microbiol. Biotechnol.* **2007**, *73*, 1169–1172.

50. Lian, L.-Y. NMR studies of protein-ligand interactions. In *Protein-ligand interactions: structure and spectroscopy*; Harding, S. E., Chowdhry, B. Z., Ed.; Oxford University Press: Oxford, 2001; Chapter 10, pp 383–405.

51. Oppenheimer, N. J. Sample preparation. *Methods Enzymol.* **1989**, *176*, 78–89.

52. Han, B.; Liu, Y.; Ginzinger, S. W.; Wishart, D. S. SHIFTX2: significantly improved protein chemical shift prediction. *J. Biomol. NMR* **2011**, *50*, 43–57.

53. Morton, C. J.; Pugh, D. J. R.; Brown, E. L. J.; Kahmann, J. D.; Renzoni, D. A. C.; Campbell, I. D. Solution structure and peptide binding of the SH3 domain from human Fyn. *Structure* **1996**, *4*, 705–714.

54. Cavanagh, J.; Fairbrother, W. J.; Palmer III, A. G.; Rance, M.; Skelton, N. J. Protein NMR spectroscopy. Principles and practice. Second Edition; Elsevier Academic Press: Burlington, 2007; pp 725–780.

55. Hansen, P. E. Isotope effects on nuclear shielding. *Annu. Rep. NMR Spectrosc.* **1984**, *15*, 105–234.

56. Hansen, P. E. Isotope effects in nuclear shielding. *Prog. Nucl. Magn. Reson. Spectrosc.* **1988**, *20*, 207–314.

57. Farmer II, B. T.; Constantine, K. L.; Goldfarb, V.; Friedrichs, M. S.; Wittekind, M.; Yanchunas Jr., J.; Robertson, J. G.; Mueller, L. Localizing the $NADP^+$ binding site on the MurB enzyme by NMR. *Nat. Struct. Biol.* **1996**, *3*, 995–997.

58. Mitton-Fry, R. M.; Anderson, E. M.; Hughes, T. R.; Lundblad, V.; Wuttke, D. S. Conserved structure for single-stranded telomeric DNA recognition. *Science* **2002**, *296*, 145–147.

59. Hirsilä, M.; Koivunen, P.; Günzler, V.; Kivirikko, K. I.; Myllyharju, J. Characterization of the human prolyl 4-hydroxylases that modify the hypoxia-inducible factor. *J. Biol. Chem.* **2003**, *278*, 30772–30780.

60. Koivunen, P.; Hirsilä, M.; Kivirikko, K. I.; Myllyharju, J. The length of peptide substrates has a marked effect on hydroxylation by the hypoxia-inducible factor prolyl 4-hydroxylases. *J. Biol. Chem.* **2006**, *281*, 28712–28720.

61. Li, D.; Hirsilä, M.; Koivunen, P.; Brenner, M. C.; Xu, L.; Yang, C.; Kivirikko, K. I.; Myllyharju, J. Many amino acid substitutions in a hypoxia-inducible transcription factor (HIF)-1α-like peptide cause only minor changes in its hydroxylation by the HIF prolyl 4-hydroxylases. Substitution of 3,4-dihydroproline or azetidine-2-carboxylic acid for the proline leads to a high rate of uncoupled 2-oxoglutarate decarboxylation. *J. Biol. Chem.* **2004**, *279*, 55051–55059.

62. Kwon, H. S.; Choi, Y. K.; Kim, J. W.; Park, Y. K.; Yang, E. G.; Ahn, D.-R. Inhibition of a prolyl hydroxylase domain (PHD) by substrate analog peptides. *Bioorg. Med. Chem. Lett.* **2011**, *21*, 4325–4328.

63. Kageyama, Y.; Koshiji, M.; To, K. K. W.; Tian, Y.-M.; Ratcliffe, P. J.; Huang, L. E. Leu-574 of human HIF-1α is a molecular determinant of prolyl hydroxylation. *FASEB J.* **2004**, *18*, 1028–1030.

64. McNeill, L. A.; Flashman, E.; Buck, M. R. G.; Hewitson, K. S.; Clifton, I. J.; Jeschke, G.; Claridge, T. D. W.; Ehrismann, D.; Oldham, N. J.; Schofield, C. J. Hypoxia-inducible factor prolyl hydroxylase 2 has a high affinity for ferrous iron and 2-oxoglutarate. *Mol. BioSyst.* **2005**, *1*, 321–324.

5. NMR investigations on a dynamic combinatorial approach to enzyme inhibition using boronate esters[†]

5.1 Introduction

5.1.1 Dynamic combinatorial chemistry

Protein-directed dynamic combinatorial chemistry (DCC) is a method for generating and identifying protein ligands *via* the reversible inter-conversions of simple building blocks under thermodynamic control in the presence of a target protein template (Figure 5-1).[1–14] The library of reversibly inter-converting building blocks is termed a dynamic combinatorial library (DCL),[15,16] and the distribution of these dynamically-generated components reflects their respective thermodynamic stabilities within the DCL. When a DCL is exposed to an 'external' influence, such as the presence of a protein, the equilibrium shifts and those components that interact with the 'external' influence are stabilised and amplified.

The design of any protein-directed DCC experiments usually includes a library of building blocks, a reversible reaction, a target protein and an analytical method.

5.1.2 Reversible reactions for protein-directed DCC

The development of appropriate reversible reactions for protein-directed DCC is not trivial because they must occur in aqueous solution at a biologically relevant pH and temperature, be compatible with biomacromolecules and be amenable to efficient screening.

Various dynamic reversible reactions have been proposed and applied in protein-directed DCC (Figure 5-2). Most notably is the use of addition-elimination reactions at carbonyl groups (such as imine and hydrazone formation),[17–30] and thiol exchange

---

[†] *The work in this chapter was conducted in collaboration with Dr Tom Brown Jr, Marina Demetriades and Mun Chiang Chan.*

T.B. initiated, designed and performed initial experiments for the αCT project. M.D. initiated and designed the PHD2 project, helped expressed and purified PHD2, synthesised boronic acids and stable analogues, and performed ESI-MS experiments. M.C.C. performed inhibition assay for PHD2.

Parts of the work from this chapter have been published as described:

1. Leung, I. K. H.; Brown Jr, T.; Schofield, C. J.; Claridge, T. D. W. An approach to enzyme inhibition employing reversible boronate ester formation. Med. Chem. Commun. 2011, 2, 390–395.

2. Demetriades, M.; Leung, I. K. H.; Chowdhury, R.; Chan, M. C.; Yeoh, K. K.; Tian, Y.-M.; Claridge, T. D. W.; Ratcliffe, P. J.; Woon, E. C. Y.; Schofield, C. J. Dynamic combinatorial chemistry employing boronic acids/boronate esters leads to potent oxygenase inhibitors. Angew. Chem. Int. Ed. 2012, 51, 6672–6675; Angew. Chem. 2012, 124, 6776–6779.

reactions (such as thiol-disulphide exchange,[31–39] thiol-enone reaction[40] and the hemithioacetal reaction[41,42]). Other organic based reversible reactions, including Diels-Alder[43] and alkene cross metathesis reactions,[44] have also been proposed or applied to protein-directed DCC *via* a pre-equilibrated approach, in which the DCL was initially generated in organic solvent, and then diluted into aqueous buffer containing the protein target.

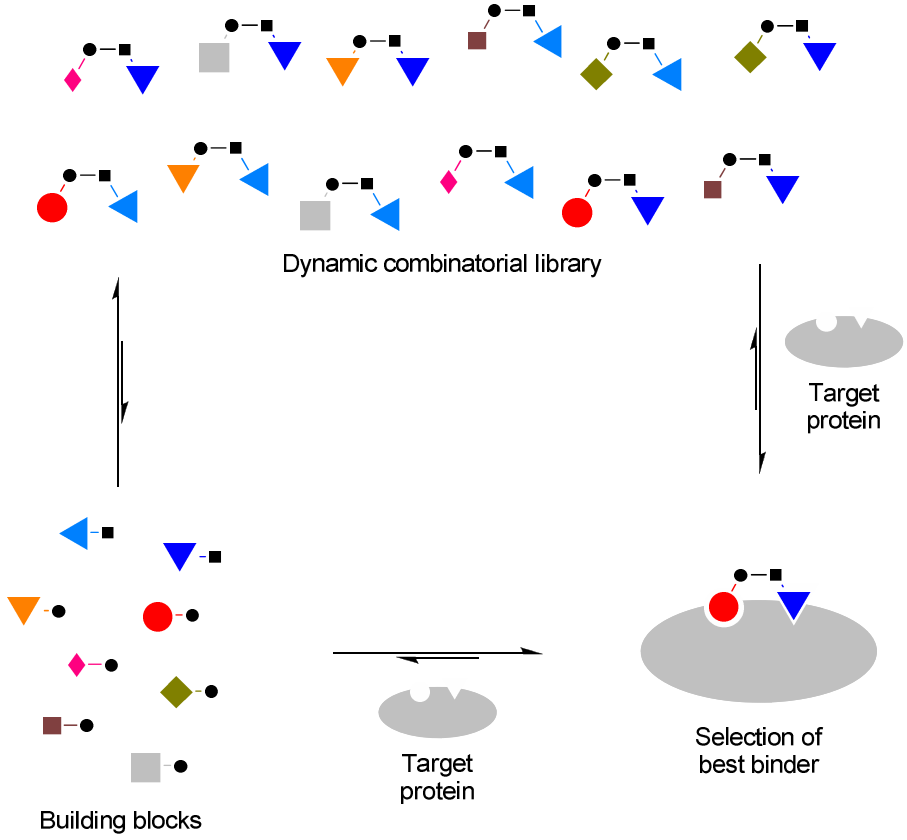

Figure 5-1 A graphical representation of protein-directed dynamic combinatorial chemistry.

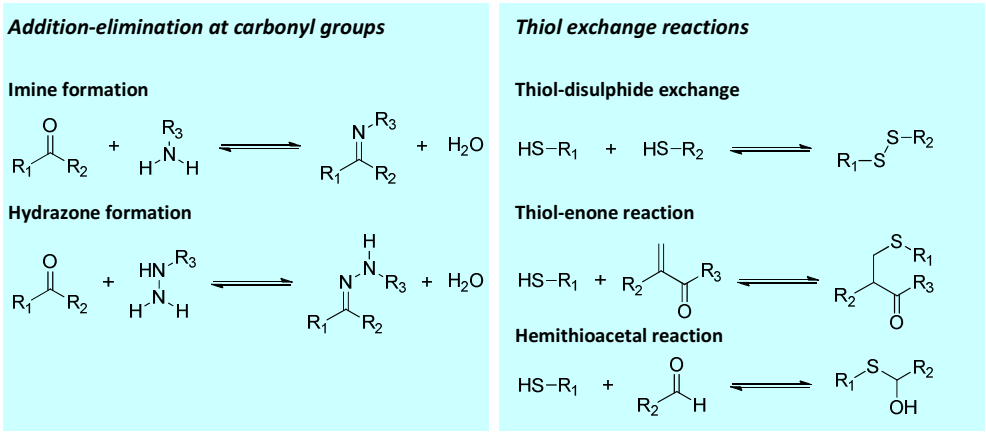

Figure 5-2 Reversible reactions that have been applied to protein-directed DCC.

Non-covalent exchange such as metal-ligand coordination has also been applied in protein-directed DCC to investigate the optimal ligand stereochemistry to the target binding site.[45,46] Enzyme-catalysed reversible reactions such as protease-catalysed amide bond formation/hydrolysis reactions[47] and aldolase-catalysed aldol addition/cleavage reactions[48,49] have also been investigated.

5.1.3 Dynamic combinatorial library

Two general strategies have been applied to the design of protein-directed DCL. One commonly-used strategy is to generate dimeric ligands from mono-functionalised building blocks (Figure 5-3a).[15] A second common strategy to the design of DCL involves bi-functionalised linker molecules and mono-functionalised head groups (Figure 5-3b).[16]

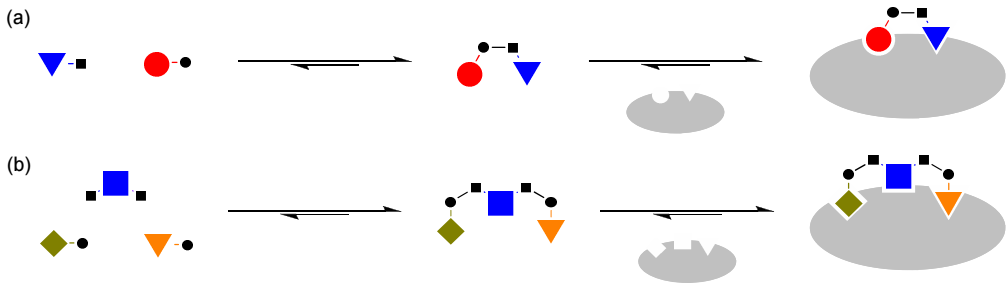

Figure 5-3 General strategies to the generation of protein-directed dynamic combinatorial library. (a) The use of mono-functionalised building blocks, and (b) the use of mono- and di-functionalised building blocks.

Protein-directed DCC may be performed in a random screening fashion, or may employ a scaffold/anchor molecule that can react reversibly with a library of small molecules. The scaffold molecule can be based on existing binders or by analyses of the target protein structure. A library of small molecules, which contain structures that cover different geometrical and functional spaces, is then added to generate the DCL.

5.1.4 Screening of dynamic combinatorial library

Various techniques have been applied to the analysis of protein-directed dynamic combinatorial libraries. Separation methods including high-performance liquid chromatography (HPLC) with UV or mass detection have been applied to isolate and quantify individual library members.[18–25,31–34,40,45–49] Biophysical techniques including mass spectrometry[29,37,38,44] and X-ray crystallography[26] have also been applied to study such interactions with target enzymes. Biological assays such as inhibition[17,25,28,42] and binding[35,36] assays have also been applied.

Ligand-based NMR techniques have also been employed in protein-directed DCC. WaterLOGSY[50] was applied as an initial screening method to characterise the binding of the scaffold ligand in a study involving thiol-disulphide exchange for the development of pantothenate synthase inhibitors.[34] STD-NMR[51] was applied extensively to screen members of a dynamic combinatorial library involving hemithioacetal reactions for the identification of novel β-galactosidase inhibitors.[41,42]

5.1.5 Boronate ester formation

Reversible boronate ester formation has been proposed as a potential new reaction class for protein-directed DCC.[6,52] Boronic acids (and the tetrahedral ions formed by their reaction with water) react with alcohols to form boronate esters (Figure 5-4).[53,54] In aqueous solution at biologically relevant pH the reaction of boronic acids with alcohols, including diols, is reversible, with the equilibrium position is dependent upon the pK_a values of the boronic acids and the alcohols.[55] The structure of the alcohols can also be important. Diols that are conformationally locked in a *syn*-periplanar arrangement form more stable complexes.[55]

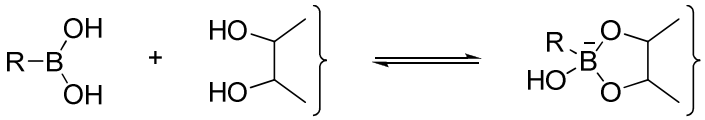

Figure 5-4 The reversible reaction between boronic acids and alcohols, such as diols, to form boronate esters.

5.1.6 Boronic acids as serine protease inhibitors

The electrophilic nature of boronic acids has been exploited for the inhibition of enzymes containing nucleophilic active site residues, including serine proteases[56–62] and serine β-lactamases.[63–65] Boronic acids react reversibly with an active site nucleophile to form a tetrahedral complex which acts as an analogue of the tetrahedral intermediates in catalysis (Figure 5-5).[61,62]

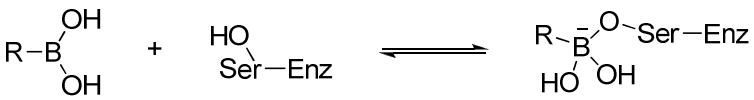

Figure 5-5 Boronic acids react reversibly with an active site nucleophile of enzymes such as serine proteases to form a tetrahedral complex which act as a transition stage analogue.

In several cases it has been reported that addition of certain diols or sugars improves the potency of boronic acids on serine protease inhibition (Figure 5-6),[66–69] but diols or sugars alone do not inhibit serine proteases. These observations imply some

boronate esters are better inhibitors than the corresponding boronic acid, and therefore support the proposal that the reversible boronate ester formation reaction may be useful for protein-directed DCC.

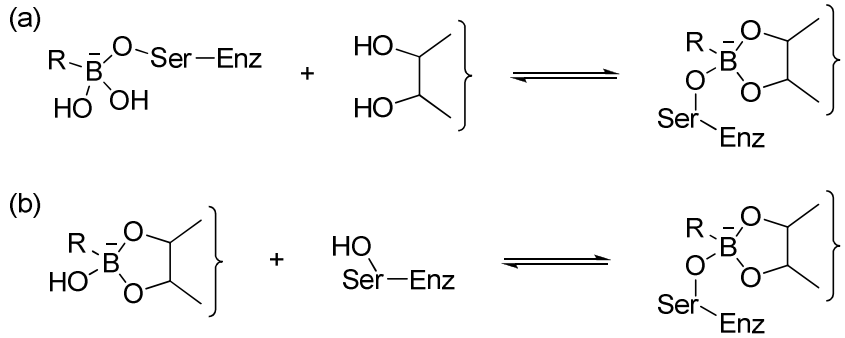

Figure 5-6 Proposed mechanisms for the binding of boronate esters to serine proteases.

5.1.7 Objectives

The objective for the work described in this Chapter was to apply NMR spectroscopy to investigate the applicability of reversible boronate ester formation in protein-directed DCC by using α-chymotrypsin as a model system. Subsequently, the principle was applied to design novel inhibitors for the HIF hydroxylase PHD2.

5.2 Investigation of reversible boronate ester formation in DCC

5.2.1 Observation of the α-chymotrypsin-boronate ester ternary complex

Initial experiments were performed to observe ternary complex formation between enzyme, boronic acid and diol. The serine protease α-chymotrypsin (αCT) and 1-benzothiophen-2-ylboronic acid (BTPBA; Figure 5-7), which is an inhibitor of serine proteases and β-lactamases,[65] was used as the model system for this study. Sugars such as D-fructose and L-sorbose (Figure 5-8) have been reported to improve the inhibition of boronic acids to serine proteases, whilst sugars such as D-glucose, L-glucose, L-fructose and D-sorbose have little effect.[66–69] Therefore these were used as positive and negative controls respectively.

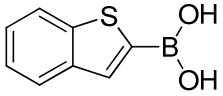

Figure 5-7 Structure of BTPBA.

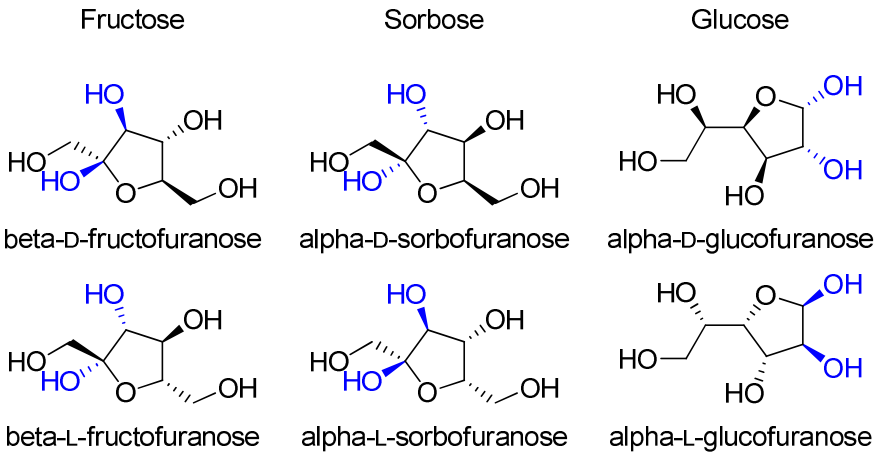

Figure 5-8 Structures of the sugars used in this study. Only the *cis*-diol geometry is shown.

^{11}B NMR has previously been applied to study free and protein-bound boron-species with serine proteases[70–72] and serine β-lactamases,[73] and has also been used to measure boronic acid pK_a.[74] ^{11}B is quadrupolar (I = 3/2) and this property can be exploited to probe the hybridisation state of the boron atom.[75] In ^{11}B NMR analyses, broad peaks are often observed if the ^{11}B nucleus is in a sp^2-hybridised planar trigonal environment, whereas relatively sharper peaks are often observed for the ^{11}B nucleus in the more highly symmetrical sp^3-hybridised tetrahedral environment.[75] The long rotational correlation time associated with protein-boronic acid or protein-boronate ester complexes may further contribute to line-narrowing.[76,77]

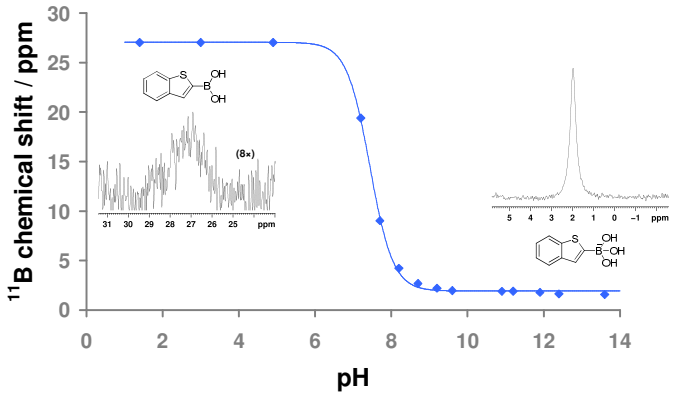

Figure 5-9 ^{11}B NMR titration to determine the pK_a value of BTPBA (pK_a ~7.4). The data was fitted using a standard sigmoid curve.

The pK_a of BTPBA was found to be ~7.4, as monitored by changes in the ^{11}B chemical shift at different pH (Figure 5-9), therefore experiments were conducted at pH 5.8 to ensure the free boronic acid was predominantly in the sp^2-hybridised form (Figure 5-10a: peak A; 26.4 ppm; linewidth >300 Hz). Upon addition of D-fructose to

BTPBA, the ^{11}B signal was sharpened and was shifted to lower ppm, indicating the formation of a tetrahedral, sp^3 boronate ester species (Figure 5-10b: peak B; 6.72 ppm; linewidth ~190 Hz). A similar sharpening and shift effect was observed when αCT was added to BTPBA to form a binary αCT-BTPBA binary complex (Figure 5-10c: peak C; 2.35 ppm; linewidth ~90 Hz), suggesting the boronic acid is in a tetrahedral boronate form when bound to αCT. The addition of D-fructose to the αCT-BTPBA binary complex further sharpened and shifted the ^{11}B signal (Figure 5-10d: peak D; 6.47 ppm; linewidth ~60 Hz), consistent with the formation of a ternary αCT-BTPBA-D-fructose complex in which the αCT-bound ^{11}B nucleus is in an sp^3-hydribised tetrahedral environment. The changes in ^{11}B linewidth and chemical shift are consistent with previous studies involving 3-dansylamidophenylboronic acid and the β-lactamase P99,[73] in which the boronic acid linewidth changes from ~580 Hz in its free form to ~160 Hz when it is bound to the enzyme, and a change in ^{11}B chemical shift of ~25 ppm. These results support previous studies employing kinetic and X-ray crystallographic analyses that reported evidence for the formation of ternary boronic acid-sugar complexes with nucleophilic enzymes.[66,67,78]

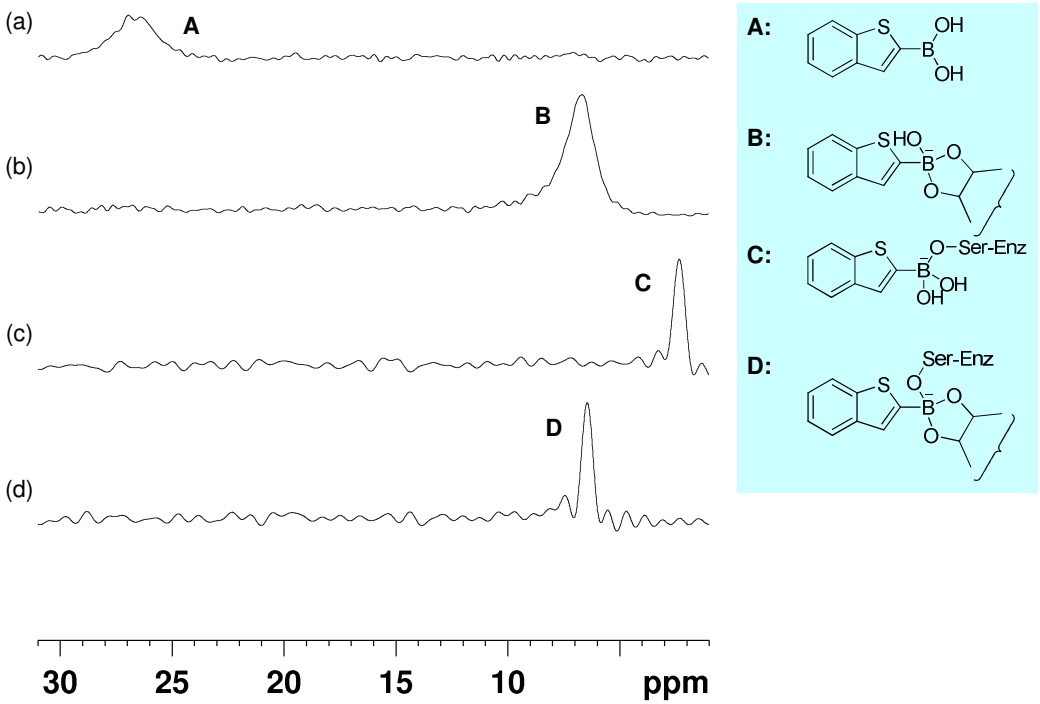

Figure 5-10 Monitoring ternary enzyme-boronic acid-sugar complex formation by ^{11}B NMR: (a) 5 mM BTPBA; (b) 5 mM BTPBA + 500 mM D-fructose; (c) 1 mM BTPBA + 33 mg/ml (~1.3 mM) αCT; (d) 1 mM BTPBA + 33 mg/ml (~1.3 mM) αCT + 2 mM D-fructose. The resonances correspond to BTPBA (peak A), the BTPBA-D-fructose boronate ester (peak B), αCT-BTPBA binary complex (peak C) and the αCT-BTPBA-D-fructose ternary complex (peak D).

5.2.2 Amplification of the boronate ester species by αCT

In the absence of αCT, ~140 mM D-fructose was required to fully form the BTPBA-D-fructose boronate ester with 1 mM BTPBA, but in the presence of 1 mM αCT, only ~2 mM D-fructose was required (Figure 5-11). Thus, the presence of αCT appeared to move the equilibrium towards the formation of the BTPBA-D-fructose boronate ester.

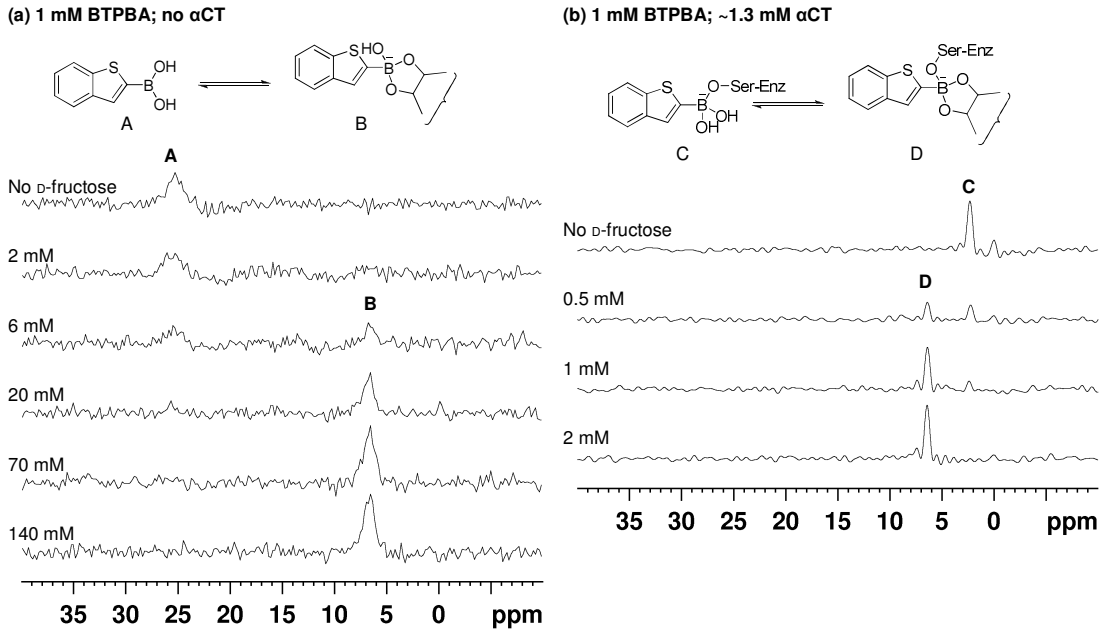

Figure 5-11 The presence of αCT moves the equilibrium position towards the formation of the BTPBA-D-fructose boronate ester. ^{11}B NMR spectra of (a) the addition of D-fructose to BTPBA and (b) the addition of D-fructose to BTPBA in the presence of one equivalent of αCT.

5.2.3 Selectivity between sugars

Sugars used in this study did not bind to αCT to any significant extent on their own, as monitored by STD-NMR (Figure 5-12).[51] This implies the formation of ternary αCT-boronic acid-sugar complexes may depend on both (i) the propensity of the boronate ester to form in solution and (ii) the affinity of the boronate ester complex for the enzyme.

The affinities of fructose and glucose for BTPBA were determined by conducting a series of titrations monitored by ^{1}H NMR (Figure 5-13). The affinities of D-fructose and L-fructose for BTPBA were similar (Figure 5-14; K_A = ~46 M^{-1}), but those of D-glucose and L-glucose were weaker (Figure 5-14; K_A = <2 M^{-1}). Therefore the relative increase in inhibition potency observed for D-fructose over both D- and L-glucose[66–69] may reflect, at least in part, the higher affinity of D-fructose for boronic acids in solution. This increased affinity may be due to the increased population (~25% of the

total) of the β-furanose form in which the C-1 and C-2 hydroxyl groups are in a *syn*-periplanar arrangement for D- (and L-) fructose, compared to the ~0.1% of the α-furanose form present in (both D- and L-) glucose solution.[79]

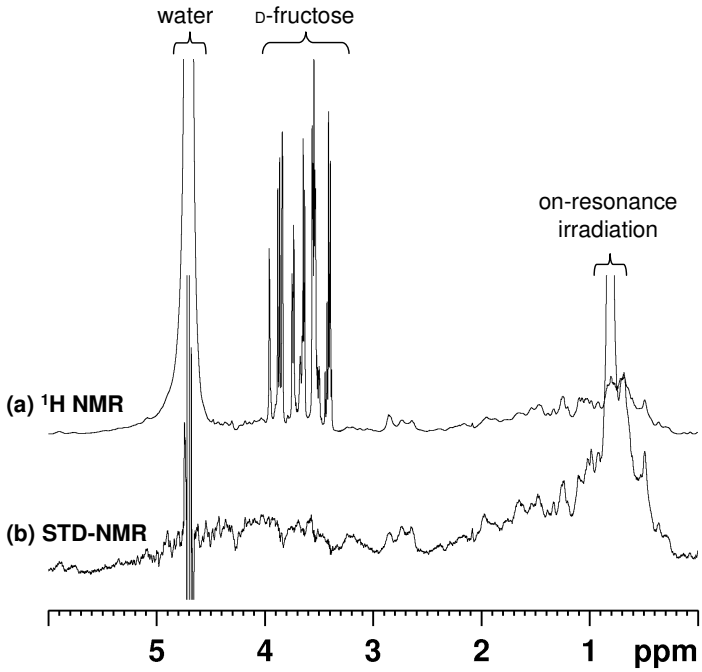

Figure 5-12 (a) ^{1}H NMR spectrum of a mixture of D-fructose and αCT; (b) The corresponding STD-NMR spectrum showing D-fructose on its own is a weak or non-binder of αCT. The experiment condition is as follows: 5 mM D-fructose; 90 μM αCT; 50 mM Tris-D11 pH 7.5 in D_2O. On-resonance irradiation is applied at 0.81 ppm and off-resonance irradiation is applied at 50 ppm. Saturation time is 5 seconds and relaxation delay is 7 seconds.

These data also suggest that the more potent inhibition observed in the presence of D-fructose relative to L-fructose[66–69] results from more efficient recognition of either D-fructose or of the D-fructose-boronate ester complex by αCT, as suggested previously by molecular modelling.[80] In accordance with this, using ^{11}B NMR titration, it was found that D-fructose readily forms a ternary αCT-BTPBA-fructose complex, whereas use of L-fructose resulted in the formation of only a small amount of a ternary complex under similar conditions (Figure 5-15). Titrations revealed that at least 30 times more L-fructose (than D-fructose) was required to fully form the ternary αCT-BTPBA-fructose complex. Similar stereoselectivity for boronate ester formation has also been observed with L-/D-sorbose, in which case the αCT-BTPBA-L-sorbose complex is preferentially formed over the αCT-BTPBA-D-sorbose complex (Figure 5-16 and Figure 5-17).

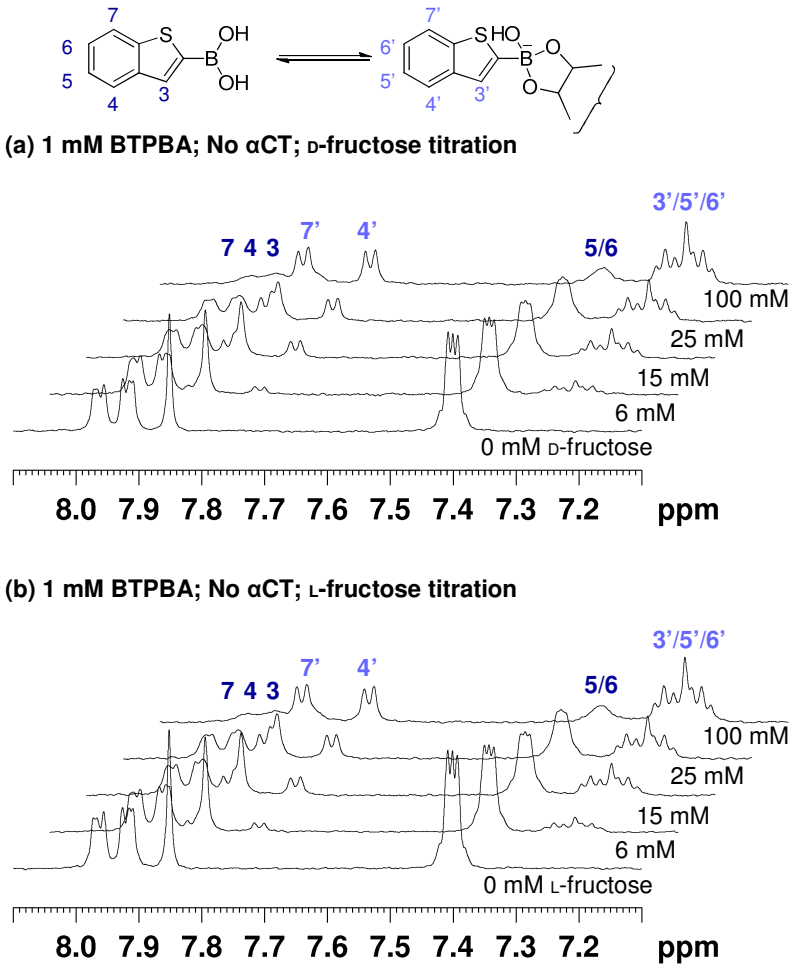

Figure 5-13 ^{1}H titration of (a) D- and (b) L-fructose to 1 mM BTPBA in the absence of αCT.

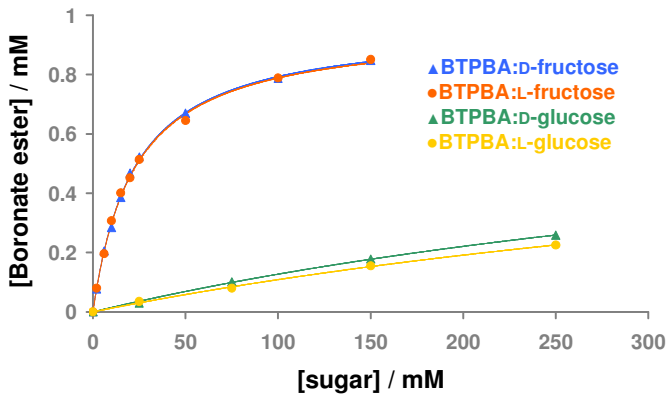

Figure 5-14 Binding curve of D- and L-fructose (K_A ~46 M^{-1}) and D- and L-gluctose (K_A <2 M^{-1}) to 1 mM BTPBA as determined by ^{1}H NMR.

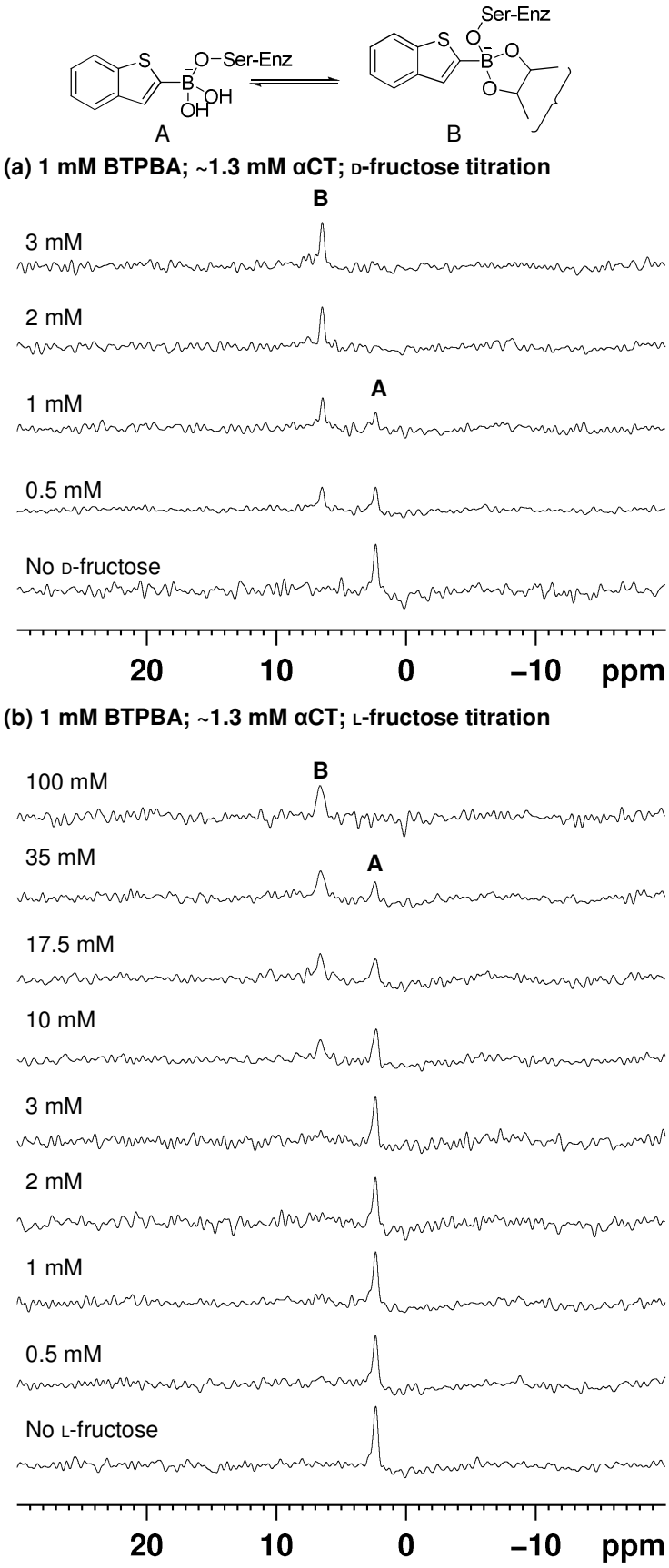

Figure 5-15 ^{11}B NMR showing the formation of an αCT-BTPBA-fructose ternary complex. More L-fructose than D-fructose is required to form the ternary complex.

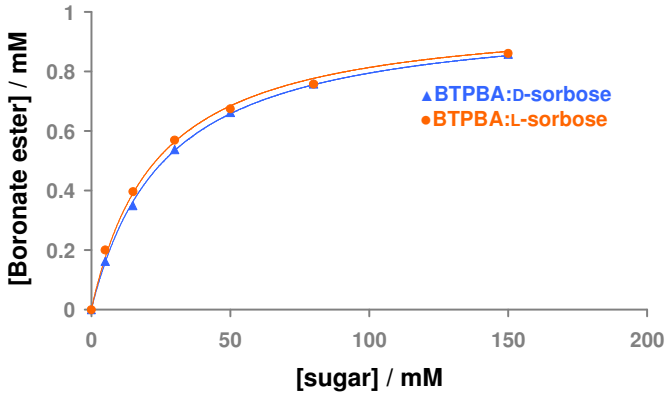

Figure 5-16 Binding curve of D- and L-sorbose (K_A ~40 M^{-1} for both systems) to 1 mM BTPBA as monitored by ^{1}H NMR.

5.2.4 Selectivity between boronic acids

When building a protein-directed boronate ester DCL, it is important to ensure that all the boronic acids should readily form boronate esters under the solution conditions appropriate to the target enzyme. The dynamics of boronate ester formation depends upon the structure and the pK_a of the boronic acid, and the solution pH.[55] For instance, the pK_a of naphthalen-2-ylboronic acid (NTBA) is ~8.9 (Figure 5-18). At pH 5.8, a ~1:500 NTBA to D-fructose ratio was required to form 50% of the NTBA-D-fructose boronate ester complex (compared to 1:6 for BTPBA), at pH 7.0 this was reduced to ~1:50, and at pH 8.0, ~1:10 (Figure 5-19). Thus, in addition to the selection of suitable chelating alcohols, the properties of the boronic acid should be appropriate for boronate ester formation to enable assessment of any enhanced inhibitory potency.

To investigate the dependencies on boronic acid structures and pK_as, we selected four structurally different bor(on)ic acids including BTPBA, ethylboronic acid (EtBA), 4-hydroxyphenylboronic acid (HPBA), and boric acid (Figure 5-20), and monitored the formation of ternary enzyme-boronic acid-sugar complexes by ^{11}B NMR at pH 5.8. Typically the pK_a values for arylboronic acids are <9 and for alkylboronic acids between 10 and 12.[81,82] Upon addition of αCT to the mixture of bor(on)ic acids (without sugar), BTPBA was identified as the only compound leading to an observable complex with αCT. Addition of D-fructose revealed the formation of an αCT-BTPBA-D-fructose ternary complex (Figure 5-21). In part this selectivity likely reflects the low efficacy of EtBA, HPBA and boric acid in forming boronate esters at

pH 5.8 due to their pK_a values and, in the case of HPBA, the electron-donating nature of its 4-hydroxyphenyl substituent.

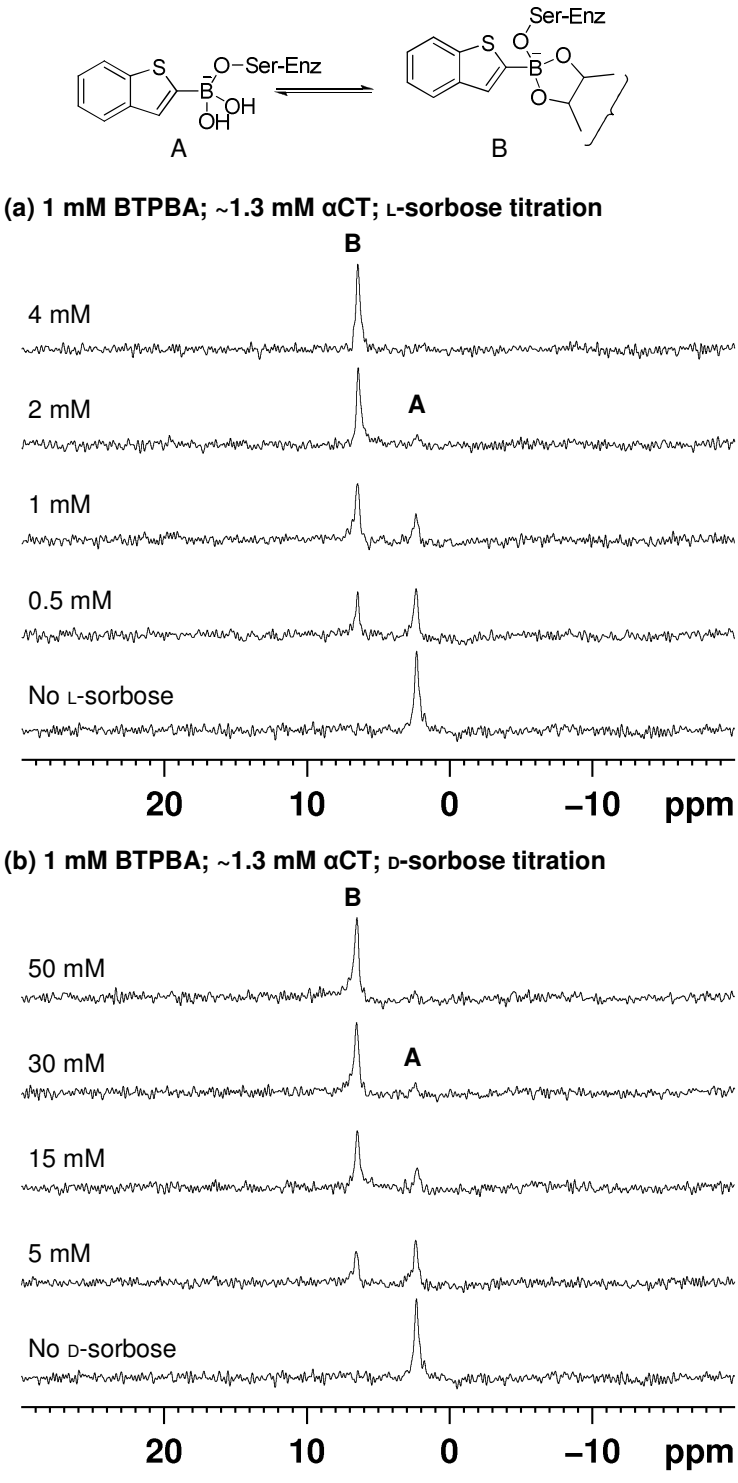

Figure 5-17 ^{11}B NMR showing the formation of an αCT-BTPBA-sorbose ternary complex, (a) with L-sorbose and (b) D-sorbose. More D-sorbose than L-sorbose is required to form the ternary complex.

In order to study the selectivity of the αCT active site for particular boronic acids, 1-benzofuran-2-boronic acid (BFBA; Figure 5-22), the oxygen analogue of BTPBA, was also used as a model boronic acid. BFBA is a good inhibitor of serine proteases and serine β-lactamases. It has a similar pK_a value to BTPBA (pK_a ~ 7.3; Figure 5-23) and both BFBA and BFPBA are equally reactive to boronate ester formation in solution (Figure 5-24 and Figure 5-25).

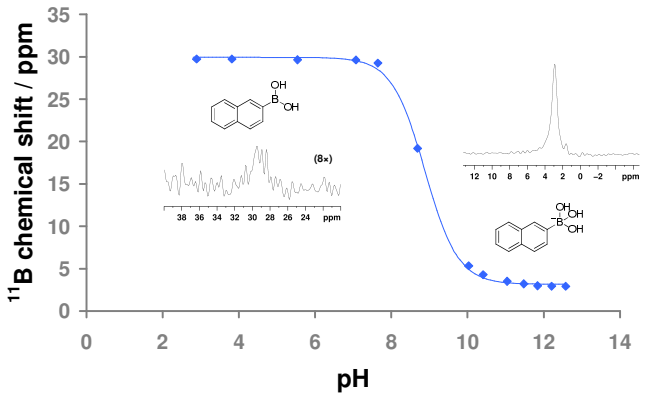

Figure 5-18 NTBA pK_a determination by ^{11}B NMR (pK_a ~8.9).

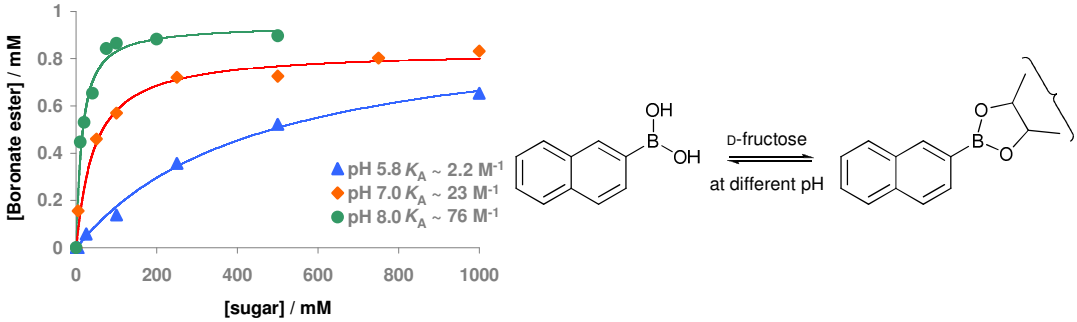

Figure 5-19 The dynamics of NTBA-D-fructose boronate ester formation depends on the solution pH.

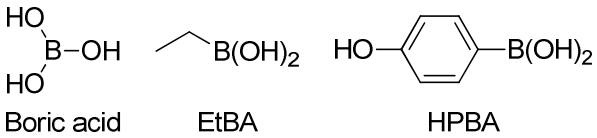

Figure 5-20 Structures of boric acid, ethylboronic acid, and 4-hydroxyphenylboronic acid.

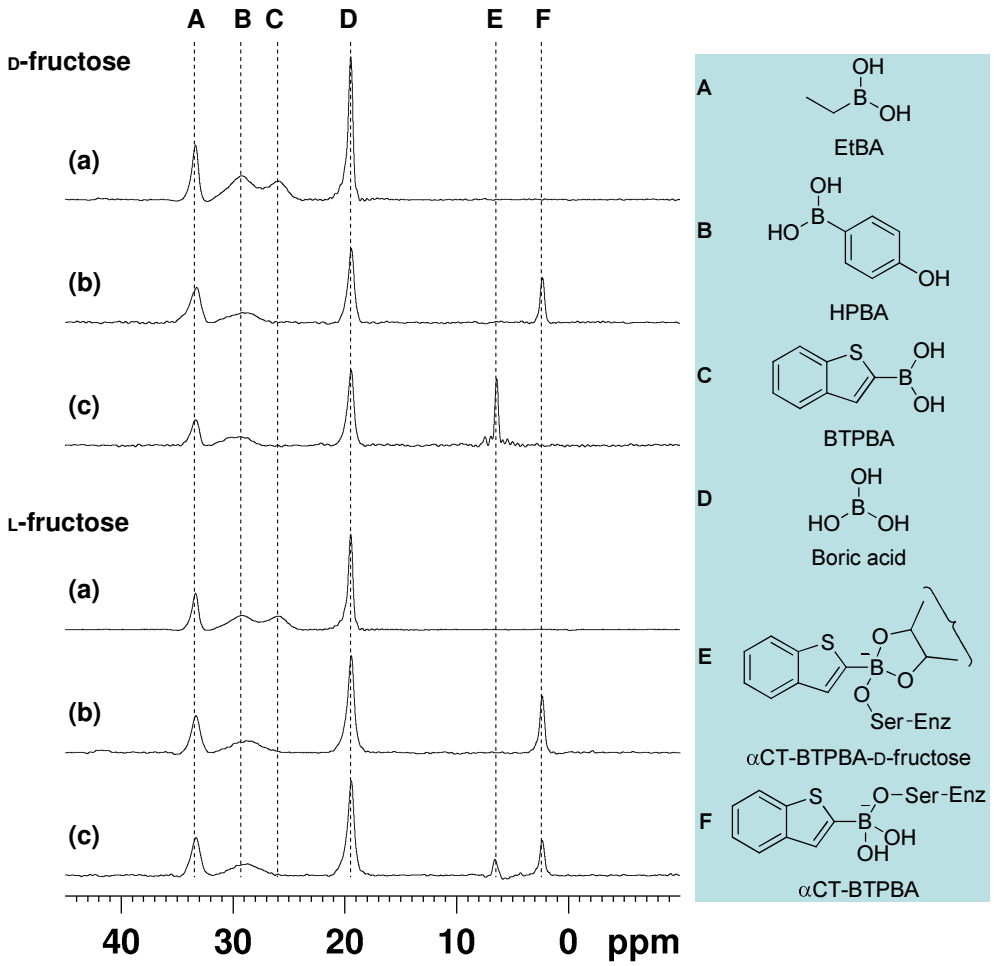

Figure 5-21 Equilibrium mixture analysis by ^{11}B NMR: (a) boronic acids only; (b) boronic acids + αCT; (c) boronic acids + αCT + D/L-fructose. Assays included the following bor(on)ic acids (at 2 mM concentration each): BTPBA (peak C), EtBA (peak A), HPBA (peak B), boric acid (peak D). Addition of αCT (~2 mM) led to the selective formation of a binary enzyme-boronic acid complex with BTPBA (peak F). Addition of fructose (12 mM) leads to the selective formation of a ternary αCT-boronic acid-fructose complex with BTPBA (peak E). Addition of D-fructose gives full conversion to the ternary αCT-BTPBA-D-fructose complex whilst <50% conversion is observed for L-fructose.

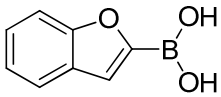

Figure 5-22 Structure of BFBA.

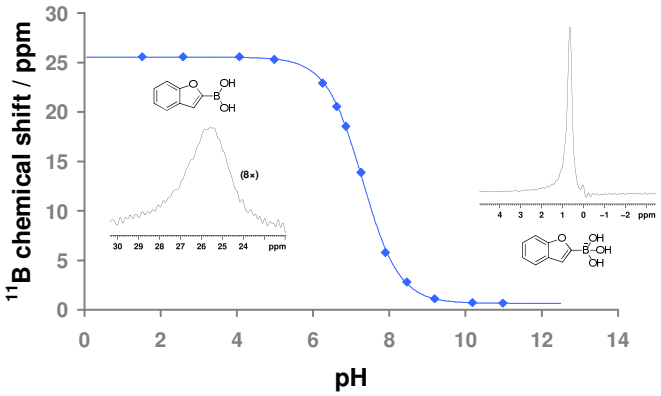

Figure 5-23 ^{11}B NMR titration to determine the pK_a value of BFBA (pK_a ~7.3).

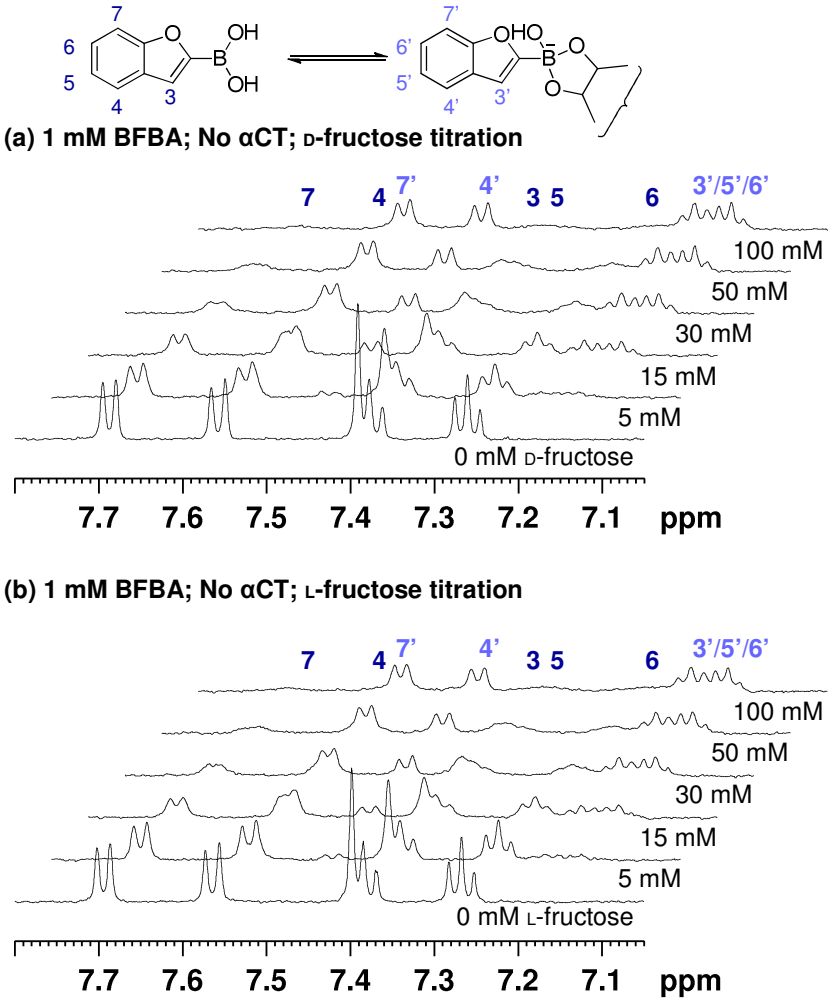

Figure 5-24 ^{1}H titration of (a) D- and (b) L-fructose to 1 mM BFBA in the absence of αCT.

^{11}B NMR was used to monitor the interactions between αCT, BTPBA and BFBA in the presence and absence of sugars (Figure 5-26). Addition of D-fructose revealed the preferential formation of the αCT-BTPBA-D-fructose over the αCT-BFBA-D-fructose ternary complex, implying differences in binding affinity to the complexes and

illustrating the potential of using reversible boronate ester formation in protein-directed DCC.

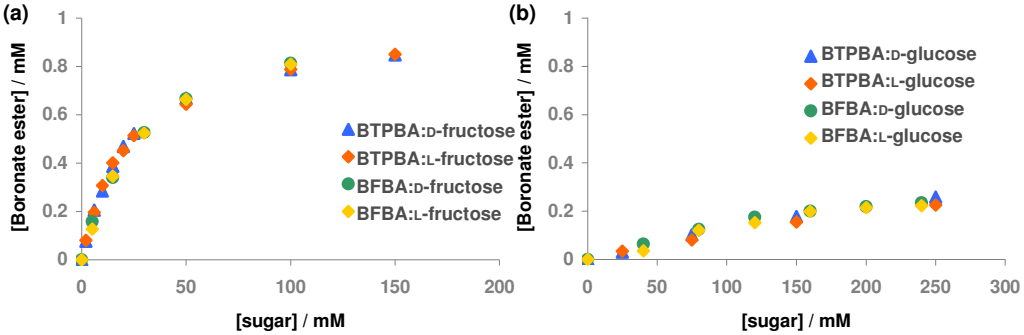

Figure 5-25 (a) Binding curves for D-fructose and L-fructose with BTPBA and BFBA (K_A ~ 52 M^{-1}); and (b) for D-glucose and L-glucose with BTPBA and BFBA (K_A < 2 M^{-1}) are shown. The concentrations of BTPBA and BFBA were 1 mM.

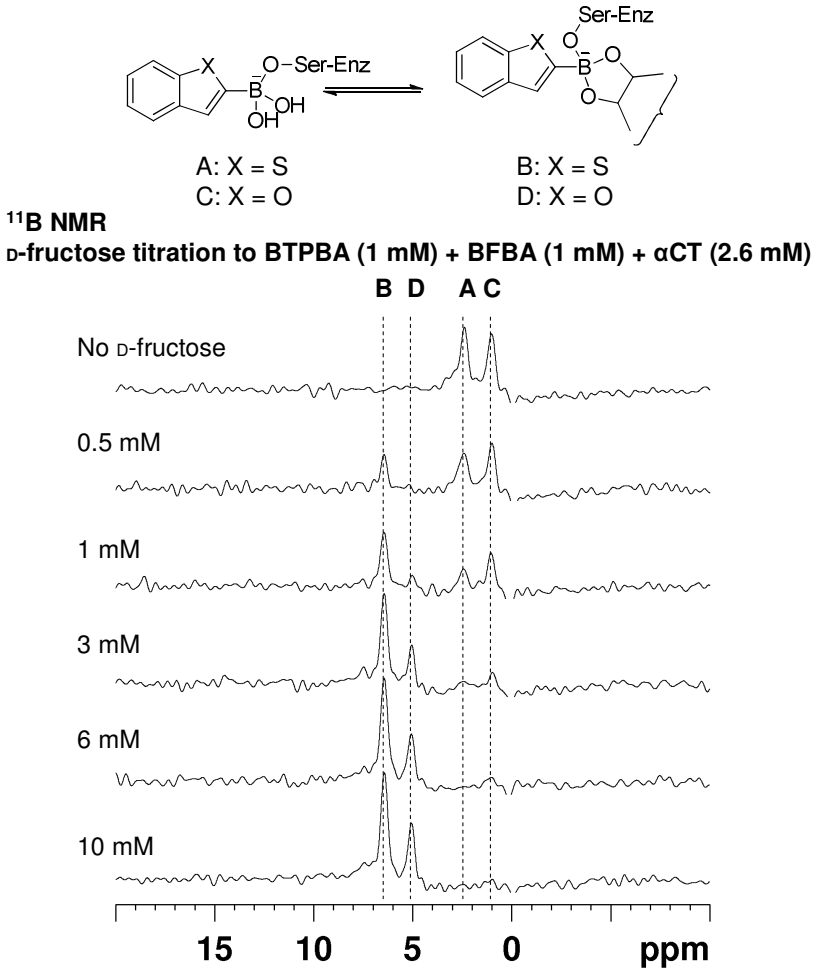

Figure 5-26 αCT preferentially binds to BTPBA and BTPBA-D-fructose boronate ester, as shown by ^{11}B NMR: Peak A: αCT-BTPBA binary complex; Peak B: αCT-BTPBA-D-fructose ternary complex; Peak C: αCT-BFBA binary complex; Peak D: αCT-BFBA-D-fructose ternary complex.

5.2.5 NMR as a potential screening method for boronate ester DCC

Ligand-based NMR screening methodologies such as the water-ligand observed *via* gradient spectroscopy (waterLOGSY)[50] and saturation transfer difference NMR (STD-NMR)[51] have been applied in protein-directed DCC to screen mixtures generated by the thiol-disulphide exchange or hemithioacetal reactions.[34,41,42]

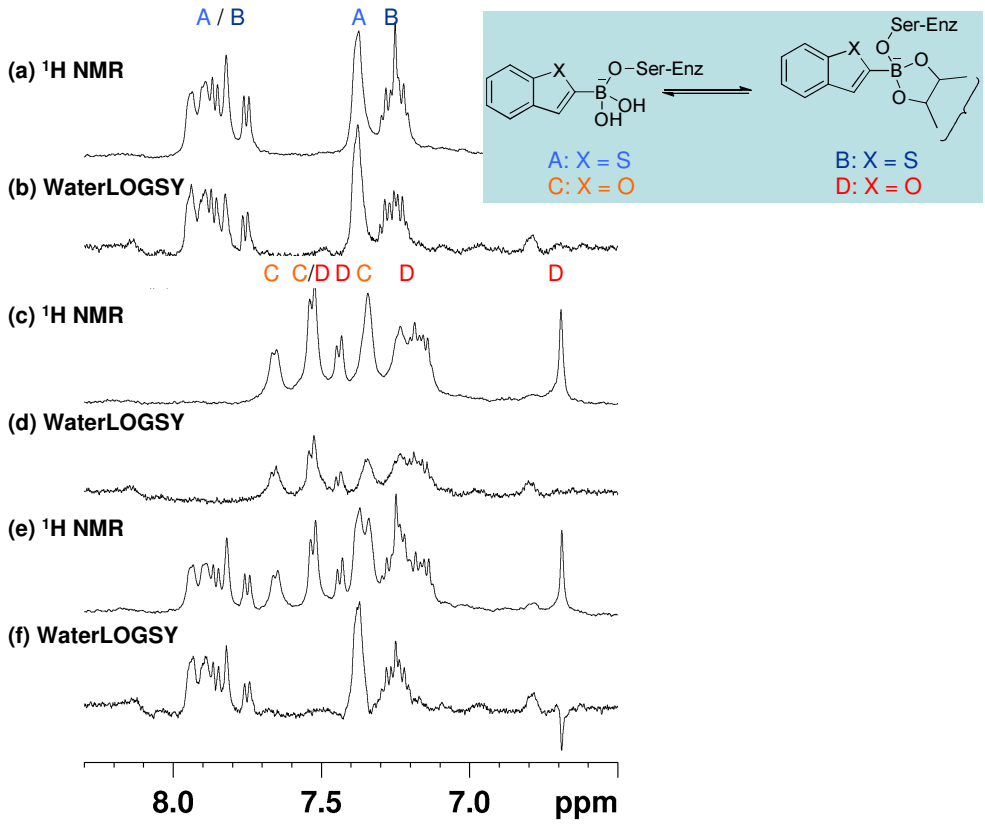

Figure 5-27 ^{1}H waterLOGSY analyses for the binding of BTPBA/BFBA and BTPBA/BFBA-D-fructose boronate ester to αCT. (a) and (b): Both BTPBA and BTPBA-D-fructose boronate ester bind to αCT; (c) and (d): Both BFBA and BFBA-D-fructose boronate ester bind to αCT; (e) and (f) in a mixture of BTPBA, BFBA, BTPBA-D-fructose boronate ester and BFBA-D-fructose boronate ester, only BTPBA and BTPBA-D-fructose boronate ester binds to αCT.

The applicability of waterLOGSY for protein-directed DCC involving reversible boronate ester formation was then investigated. The boronic acid pair BTPBA and BFBA was used for this purpose and a slight excess of D-fructose was used to ensure the formation of some boronate ester species. When conducting the experiment with either BTPBA or BFBA, waterLOGSY suggested all four species (BTPBA, BTPBA-D-fructose, BFBA and BFBA-D-fructose) bind to αCT. However, in a mixture containing all four species, waterLOGSY analyses revealed that αCT preferentially selects BTPBA and the BTPBA-D-fructose boronate ester over the BFBA and the BFBA-D-fructose boronate ester (Figure 5-27). In contrast, no selectivity was

observed in the equivalent waterLOGSY experiment with L-fructose (Figure 5-28); presumably all four components (BTPBA, BTPBA-L-fructose, BFBA and BFBA-L-fructose) bind weakly to αCT. These results suggest ligand-based NMR may be useful for the screening of DCL generated by the reversible boronate ester formation method.

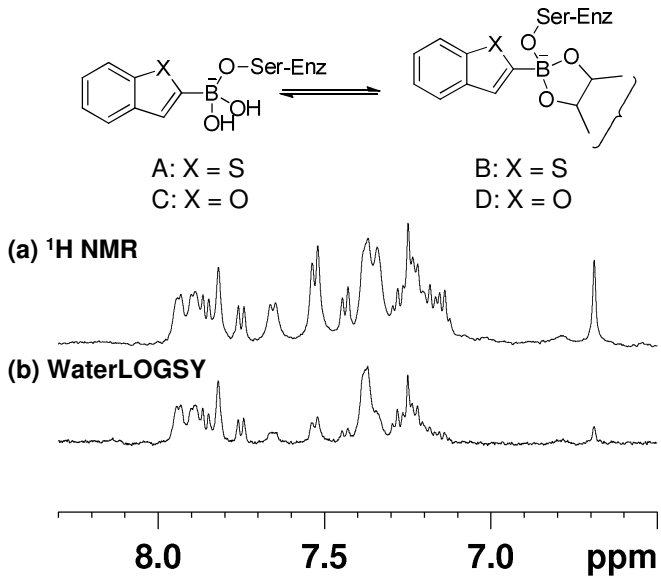

Figure 5-28 WaterLOGSY spectrum showing no selectivity is observed in the presence of L-fructose with BTPBA and BFBA to αCT.

5.3 Application of DCC using reversible boronate ester formation

5.3.1 Human prolyl hydroxylase domain-containing enzyme 2

Human prolyl hydroxylase domain-containing enzyme 2 (PHD2) is a 2OG oxygenase that plays a key role in human oxygen sensing.[83–86] PHD2 is a current inhibition target for new pharmaceutical treatments against ischemic disease and anaemia.[87–89] The human oxygen sensing/hypoxic pathway was also identified as a potential target for the treatment of cancer,[90–94] and recent reports have shown that the inhibition of PHD2 reduces the growth of tumour in mice.[95]

Following the finding that PHD2 activity is inhibited by *N*-oxalylglycine (NOG),[96–98] a 2OG analogue, several groups have described the identification of new inhibitors of PHD2.[99–106] However, due to the conserved nature of the active site geometry within the prolyl hydroxylase family,[107,108] the challenge to discover potent and selective PHD2 inhibitors remains elusive. Protein-directed DCC using reversible boronate ester formation therefore provides an attractive alternative for the identification of novel and potentially selective PHD2 inhibitors

5.3.2 Design of the scaffold boronic acid ligand

PHD2 forms a stable complex with iron and 2OG.[109] 2OG binds to the iron in a bidentate manner inside the PHD2 active site.[110] To date, most PHD2 inhibitors were designed to bind to the iron on the PHD2-iron complex and therefore act as 2OG competitors.[99–106,111] A good starting scaffold for the ligand therefore included a bidentate metal chelation functionality to maintain strong binding interactions to PHD2, and a boronic acid functionality so that improvement in binding may be explored with different alcohols. Following these requirements, 6-(1-carboxymethylcarbamoyl)-3-pyridinylboronic acid (CMCPBA) was designed and prepared (by Marina Demetriades) as the scaffold ligand (Figure 5-29).

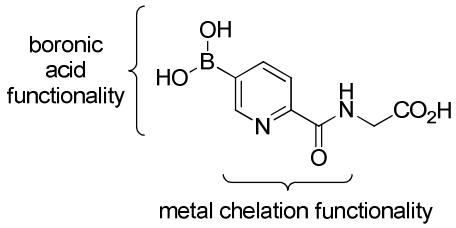

Figure 5-29 6-(1-carboxymethylcarbamoyl)-3-pyridinylboronic acid (CMCPBA) as the scaffold ligand for PHD2-directed DCC.

5.3.3 Design of the PHD2-directed DCC experiments

The pK_a of CMCPBA is ~7.4 (Figure 5-30); therefore all experiments were conducted at pH 7.5 to achieve efficient binding with alcohols.[55] Non-denaturing electrospray ionisation mass spectrometry (ESI-MS) was previously applied in the analysis of 2OG,[109] inhibitor[112] and metal[113] binding to PHD2 and was therefore selected as the primary analytical method.

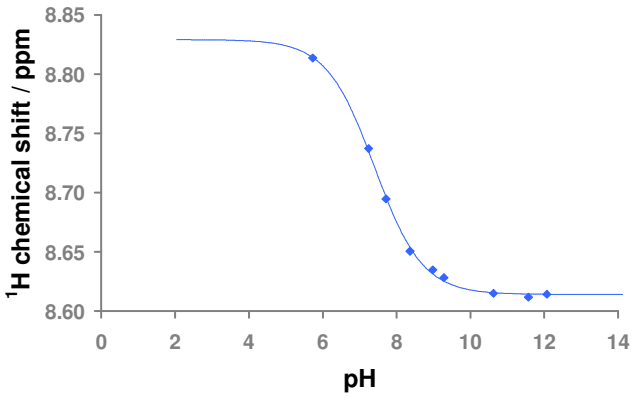

Figure 5-30 ^{1}H NMR titration to determine the pK_a value of CMCPBA (pK_a ~7.4).

Overall, forty diols (in groups of ten) were tested by ESI-MS in the presence of CMCPBA and PHD2-Fe(II) at a 1:1:1 molar ratio. Seven hits were identified from the initial DCC-MS screening (Table 5-1; experiment was designed and performed by Marina Demetriades). These hits were further characterised by NMR using the water relaxation technique (see Chapter 3),[114] in which CMCPBA was titrated into a mixture of PHD2-Mn(II) and five fold excess of alcohol, and apparent binding constant ($K_{D,app}$) values were obtained (Table 5-1). For instance, CMCPBA itself is a reasonable binder to PHD2 with a binding constant of 24.8 μM. Addition of 2,4-dihydroxybenzoate, one of the hits obtained from the DCC-MS analysis, gave a 30-fold improvement in binding ($K_{D,app}$ = 0.79 μM), possibly due to the formation of the CMCPBA-2,4-dihydroxybenzoate boronate ester species, and that the resultant CMCPBA-2,4-dihydroxybenzoate boronate ester is a stronger binder to PHD2-Mn(II) complex than CMCPBA or 2,4-dihydroxybenzoic acid alone. Addition of butane-2,3-diol or catechol gave little improvement in the binding to PHD2-Mn(II) (Table 5-1). Butane-2,3-diol do not form a boronate ester with CMCPBA (as judged by ^{1}H NMR), and whilst catechol formed a boronate ester with CMCPBA, the resultant CMCPBA-catechol boronate ester did not appear to bind significantly stronger to PHD2-Mn(II) than CMCPBA.

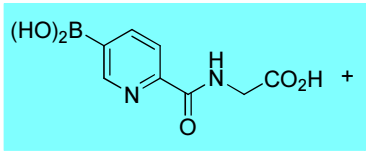

Alcohol	$K_{D,app}$ / μM	Alcohol	$K_{D,app}$ / μM
no alcohol	24.8 ± 2.4	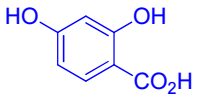	0.79 ± 0.1
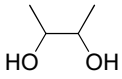	18.2 ± 0.9	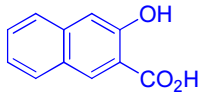	3.0 ± 0.4
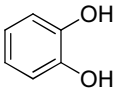	13.2 ± 2.1	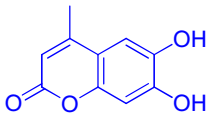	2.6 ± 0.4
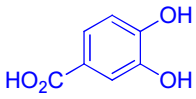	2.2 ± 0.5	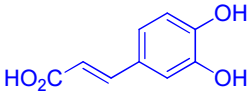	3.0 ± 0.2
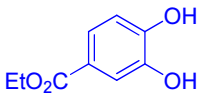	1.3 ± 0.1	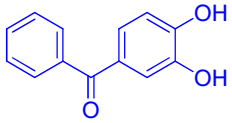	0.62 ± 0.2

Table 5-1 Hits obtained from PHD2-directed DCC analyses are highlighted in blue. Butane-2,3-diol and catechol are negative controls. The $K_{D,app}$ values listed represent the apparent K_D of the CMCPBA-diol boronate ester to PHD2-Mn(II), which is measured by the water relaxation method (Chapter 3). For each diol, CMCPBA was titrated into a sample mixture that contained 50 μM *apo*-PHD2, 50 μM Mn(II) and 350 μM diol. Solutions were buffered using 50 mM Tris-D11 (pH 7.5) in 12.5% H_2O and 87.5% D_2O.

It was reported that aromatic alcohols, such as catechol and 3,4-dihydroxybenzoate, may inhibit 2OG oxygenases.[115] In order to test whether the hits obtained from the DCC-MS experiment and that the improvement in $K_{D,app}$ described above is due to a genuine DCC effect, *i.e.* the binding of boronate ester to PHD2, rather than a combined effect of boronic acid inhibition and alcohol inhibition acting separately on PHD2, the NMR reporter screening method (see Chapter 3) was applied.

Screening experiments were conducted with 10 μM PHD2 and 80 μM Zn(II). At 50 μM concentration, CMCPBA appeared to cause ~50% 2OG displacement, confirming that it is a moderate binder to PHD2 and that it competes with 2OG for the co-substrate binding site (Figure 5-31). In the absence of CMCPBA, none of the diols (at 150 μM concentration) appeared to displace 2OG from PHD2-Zn(II) (Figure 5-31). However, in the presence of 50 μM CMCPBA and 150 μM diol hits, significant improvements in 2OG displacement were observed (~75% to ~85% 2OG displacement; Figure 5-31), which suggests the resultant CMCPBA-diol boronate esters are stronger binders to PHD2-Zn(II) than CMCPBA. As a negative control, no improvement in 2OG displacement was observed with 150 μM butane-2,3-diol and 50 μM CMCPBA (Figure 5-31); whilst with 150 μM catechol and 50 μM CMCPBA, only slight improvement in 2OG displacement was observed (~60%; Figure 5-31).

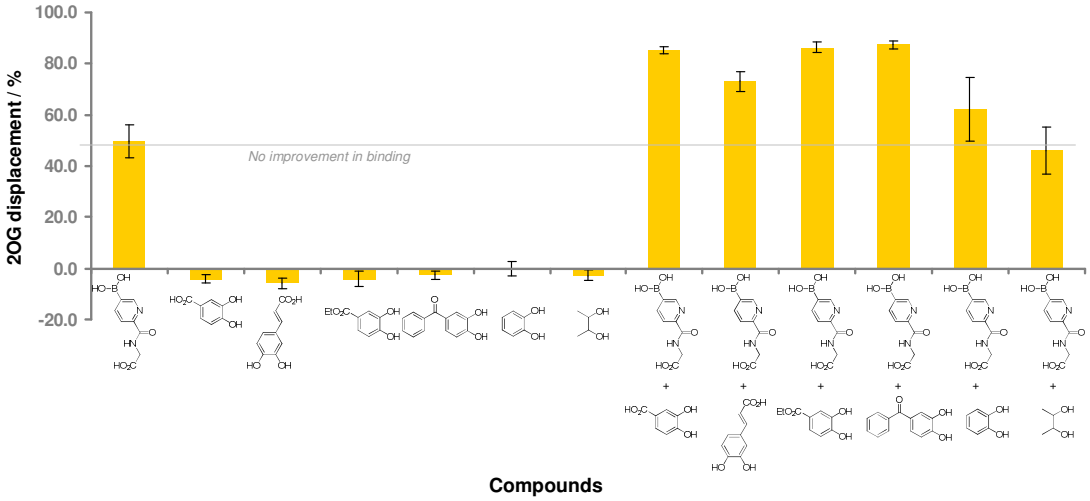

Figure 5-31 The addition of certain diols improve the binding of CMCPBA to PHD2-Zn(II), which is reflected by the improvement in 2OG displacement as monitored by the reporter ligand screening method (Chapter 3). Sample mixture contained 10 μM *apo*-PHD2, 80 μM Zn(II), 50 μM CMCPBA and 150 μM diol where applicable. Solutions were buffered using 50 mM Tris-D11 (pH 7.5) in 90% H_2O and 10% D_2O.

5.3.4 PHD2-directed DCC leads to stable analogue inhibitors

Overall, the PHD2-directed DCC screening experiments revealed that the binding of CMCPBA to PHD2 can be improved by the introduction of bulky aromatic groups (*e.g.* 3-hydroxy-2-naphthoic acid, Table 5-1) or substituted aromatic groups (*e.g.* 3,4-dihydroxybenzoic acid) at the 5-pyridinyl position, presumably due to better filling of the co-substrate binding pocket. The next stage was to design stable analogue inhibitors guided by these findings.

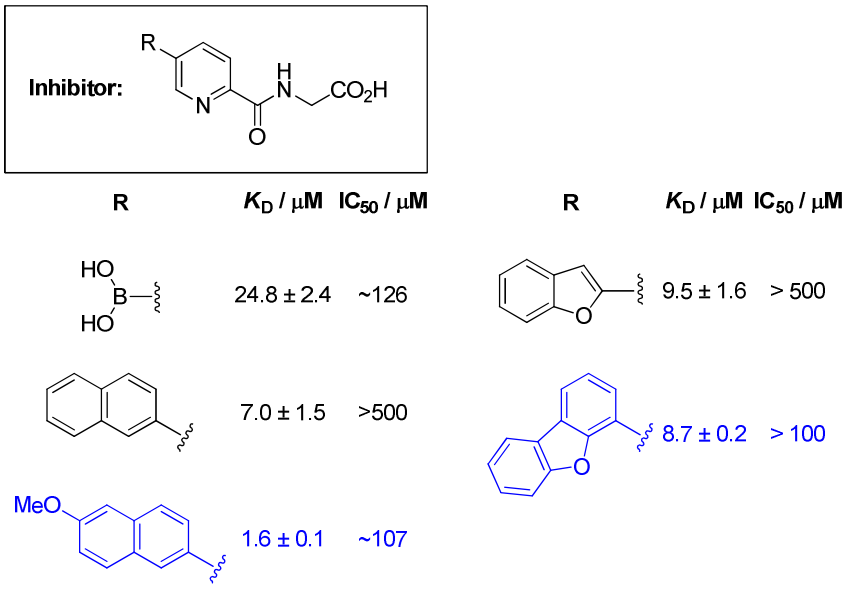

Table 5-2 First generation stable analogues (blue) and the negative controls (black). IC_{50} values were measured by Mun Chiang Chan. K_D values were measured by the water relaxation method (Chapter 3), in which the analyte was titrated into a mixture contained 50 μM *apo*-PHD2 and 50 μM Mn(II). Solutions were buffered using 50 mM Tris-D11 (pH 7.5) in 12.5% H_2O and 87.5% D_2O.

In order to mimic the hits obtained from the DCC-MS screening, two stable analogues were designed and synthesised (by Marina Demetriades; Table 5-2). The boronate ester bond was mimicked by both five and six membered aromatic groups. As negative controls, the benzofuran and the naphthalene-based analogues were also prepared (to mimic catechol; Table 5-2). Binding constants were obtained by the water relaxation method and all four stable analogue compounds showed improvement in binding when compared to CMCPBA. However, somewhat surprisingly, the discrimination between the stable analogues and the negative controls were minimal. In order to further investigate this observation, IC_{50} values were measured (by Mun Chiang Chan). The inhibition data revealed that there is a bigger discrimination between the stable analogues and the negative controls (than binding constants). This is likely due to the two stable analogue compounds (the -

OMe group and the bicyclic moiety) binding towards the peptidyl substrate binding site, which blocks substrate binding as well as co-substrate binding.

In order to further improve the binding of the stable analogues to PHD2, the crystal structure of a bicyclic isoquinolinyl inhibitor (BIQ; see Chapter 3), which is a potent PHD2 inhibitor,[111] was examined. One key contribution to the binding of BIQ to PHD2 is the interaction between a hydroxyl group and Tyr-303 in the PHD2 active site.[111] A second generation of the stable analogues, which includes a hydroxyl group at the 3-position of the pyridine ring in order to mimic this interaction with Tyr-303, was therefore designed and synthesised (by Marina Demetriades).

The binding constants of the second generation stable analogue inhibitors to PHD2 were then measured by the water relaxation technique. *N*-(pyridin-2-ylcarbonyl)glycine, which lacks the hydroxyl group, was found to have negligible binding to PHD2 whilst *N*-[(3-hydroxypyridin-2-yl)carbonyl]glycine was a good binder to PHD2 (K_D = 3.5 μM, Table 5-3). Furthermore, introduction of a bicyclic aromatic group, as suggested by the DCC screening analyses, led to significant improvements in both the binding and inhibition of PHD2. When compared to the original CMCPBA, the binding constants of all the second generation stable analogues are ~1000 times smaller and the inhibition constants are ~10000 times smaller (Table 5-3).

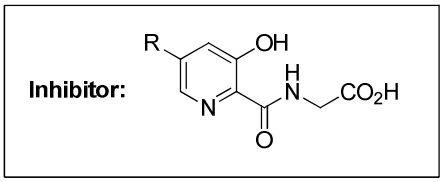

R	K_D / μM	IC_{50} / μM	R	K_D / μM	IC_{50} / μM
H—	3.5 ± 0.2	~409	HO	0.93 ± 0.1	~0.004
	0.45 ± 0.2	~0.017	MeO	0.82 ± 0.1	~0.013

Table 5-3 Second generation stable analogues. IC_{50} values were measured by Mun Chiang Chan. K_D values were measured by the water relaxation method (Chapter 3), in which the analyte was titrated into a mixture contained 50 μM *apo*-PHD2 and 50 μM Mn(II). Solutions were buffered using 50 mM Tris-D11 (pH 7.5) in 12.5% H_2O and 87.5% D_2O.

Overall, the PHD2-directed DCC analysis has led to the discovery of several novel and potent PHD2 inhibitors. The starting boronic acid (CMCPBA) is a moderate

binder and inhibitor to PHD2 that competes against 2OG for the co-substrate binding site. DCC analysis has led to the identification of the aromatic substituent as an important factor in PHD2 inhibition, presumably by binding towards the peptidyl substrate binding site. Further analysis of known PHD2 inhibitors has led to the introduction of a hydroxyl group at the 3-position of the pyridine ring, which further improved the binding and inhibition of these stable analogues.

5.4 Summary

Overall, the results described in this Chapter have validated the potential and successfully applied the reversible reactions between boronic acids and diols to produce boronate esters in protein-directed DCC. The results suggest the equilibrium between boronic acids, diols and boronate esters can be controlled by the addition of a target protein, in this case a serine protease αCT, which binds the boronic acid/boronate ester in a covalent manner. In the presence of the protein, the equilibrium shifted towards the most favourable combination of boronic acids and diols for the formation of a ternary enzyme-boronic acid-diol complex. It is also demonstrated that the observation of a ternary complex depends not only on the affinity of the boronate ester for the target protein, but also on the propensity of the boronate ester to form in solution, which in turn is dependent upon the pK_a of the boronic acid and on the solution pH.

The potential of applying reversible boronate ester formation in protein-directed DCC was further demonstrated using PHD2. In case of PHD2, the boronic acid binds non-covalently to the enzyme. Screening of the most favourable combinations of boronic acids and diols was conducted using ESI-MS and quantified by NMR. Stable analogues, which were derived on the results from the initial screening, were then prepared and optimised, which led to several novel and potent PHD2 inhibitors being identified.

5.5 References

1. Lehn, J.-M. Dynamic combinatorial chemistry and virtual combinatorial libraries. *Chem. Eur. J.* **1999**, *5*, 2455–2463.
2. Klekota, B.; Miller, B. L. Dynamic diversity and small-molecule evolution: a new paradigm for ligand identification. *Trends Biotechnol.* **1999**, *17*, 205–209.
3. Cousins, G. R. L.; Poulsen, S.-A.; Sanders, J. K. M. Molecular evolution: dynamic combinatorial libraries, autocatalytic networks and the quest for molecular function. *Curr. Opin. Chem. Biol.* **2000**, *4*, 270–279.
4. Karan, C.; Miller, B. L. Dynamic diversity in drug discovery: putting small-molecule evolution to work. *Drug Discov. Today* **2000**, *5*, 67–75.
5. Lehn, J.-M.; Eliseev, A. V. Dynamic combinatorial chemistry. *Science* **2001**, *291*, 2331–2332.
6. Ramström, O.; Lehn, J.-M. Drug discovery by dynamic combinatorial libraries. *Nat. Rev. Drug Discov.* **2002**, *1*, 26–36.
7. Rowan, S. J.; Cantrill, S. J.; Cousins, G. R. L.; Sanders, J. K. M.; Stoddart, J. F. Dynamic covalent chemistry. *Angew. Chem. Int. Ed.* **2002**, *41*, 898–952.
8. Ramström, O.; Bunyapaiboonsri, T.; Lohmann, S.; Lehn, J.-M. Chemical biology of dynamic combinatorial libraries. *Biochim. Biophys. Acta* **2002**, *1572*, 178–186.
9. Otto, S.; Furlan, R. L. E.; Sanders, J. K. M. Dynamic combinatorial chemistry. *Drug Discov. Today* **2002**, *7*, 117–125.
10. Arya, P.; Roth, H.-J. Combinatorial chemistry editorial review. *Curr. Opin. Chem. Biol.* **2005**, *9*, 229–231.
11. Corbett, P. T.; Leclaire, J.; Vial, L.; West, K. R.; Wietor, J.-L.; Sanders, J. K. M.; Otto, S. Dynamic combinatorial chemistry. *Chem. Rev.* **2006**, *106*, 3652–3711.
12. Ladame, S. Dynamic combinatorial chemistry: on the road to fulfilling the promise. *Org. Biomol. Chem.* **2008**, *6*, 219–226.
13. Hochgürtel, M.; Lehn, J.-M. Dynamic combinatorial diversity in drug discovery. In *Fragment-based approaches in drug discovery*; Jahnke, W., Erlanson, D. A., Ed.; Wiley-VCH Verlag GmbH & Co. KGaA: Weinheim, 2006; Chapter 16, pp 341–364.
14. Greaney, M. F.; Bhat, V. T. Protein-directed dynamic combinatorial chemistry. In *Dynamic combinatorial chemistry: in drug discovery, bioinorganic chemistry, and materials sciences*; Miller, B. L., Ed.; John Wiley & Sons, Inc.: New Jersey, 2010; Chapter 2, pp 43–82.
15. Lehn, J.-M.; Ramström, O. Generation and screening of a dynamic combinatorial library. PCT. Int. Appl. WO 20010164605, **2001**.
16. Steeneck, C.; Eliseev, A. V.; Hochguertel, M.; Kroth, H. A method of forming a dynamic combinatorial library using a scaffold. PCT. Int. Appl. WO 2003034071, **2003**.
17. Bunyapaiboonsri, T.; Ramström, O.; Lohmann, S.; Lehn, J.-M.; Peng, L.; Goeldner, M. Dynamic deconvolution of a pre-equilibrated dynamic combinatorial library of acetylcholinesterase inhibitors. *ChemBioChem* **2001**, *2*, 438–444.
18. Huc, I.; Lehn, J.-M. Virtual combinatorial libraries: dynamic generation of molecular and supramolecular diversity by self-assembly. *Proc. Natl. Acad. Sci. U. S. A.* **1997**, *94*, 2106–2110.
19. Hochgürtel, M.; Kroth, H.; Piecha, D.; Hofmann, M. W.; Nicolau, C.; Krause, S.; Schaaf, O.; Sonnenmoser, G.; Eliseev, A. V. Target-induced formation of neuraminidase inhibitors from *in vitro* virtual combinatorial libraries. *Proc. Natl. Acad. Sci. U. S. A.* **2002**, *99*, 3382–3387
20. Hochgürtel, M.; Niesinger, R.; Kroth, H.; Piecha, D.; Hofmann, M. W.; Krause, S.; Schaaf, O.; Nicolau, C.; Eliseev, A. V. Ketones as building blocks for dynamic combinatorial libraries: highly active neuraminidase inhibitors generated via selective pressure of the biological target. *J. Med. Chem.* **2003**, *46*, 356–358.

21. Zameo, S.; Vauzeilles, B.; Beau, J.-M. Dynamic combinatorial chemistry: lysozyme selects an aromatic motif that mimics a carbohydrate residue. *Angew. Chem. Int. Ed.* **2005**, *44*, 965–969.

22. Zameo, S.; Vauzeilles, B.; Beau, J.-M. Direct composition analysis of a dynamic library of imines in an aqueous medium. *Eur. J. Org. Chem.* **2006**, 5441–5444.

23. Valade, A.; Urban, D.; Beau, J.-M. Target-assisted selection of galatosyltransferase binders from dynamic combinatorial libraries. An unexpected solution with restricted amounts of the enzyme. *ChemBioChem* **2006**, *7*, 1023–1027.

24. Bugaut, A.; Toulmé, J.-J.; Rayner, B. SELEX and dynamic combinatorial chemistry interplay for the selection of conjugated RNA aptamers. *Org. Biomol. Chem.* **2006**, *4*, 4082–4088.

25. Bunyapaiboonsri, T.; Ramström, H.; Ramström, O.; Haiech, J.; Lehn, J.-M. Generation of bis-cationic heterocyclic inhibitors of *Bacillus subtilis* HPr kinase/phosphatase from a ditopic dynamic combinatorial library. *J. Med. Chem.* **2003**, *46*, 5803–5811.

26. Valade, A.; Urban, D.; Beau, J.-M. Two galatosyltransferases' selection of different binders from the same uridine-based dynamic combinatorial library. *J. Comb. Chem.* **2007**, *9*, 1–4.

27. Congreve, M. S.; Davis, D. J.; Devine, L.; Granata, C.; O'Reilly, M.; Wyatt, P. G.; Jhoti, H. Detection of ligands from a dynamic combinatorial library by X-ray crystallography. *Angew. Chem. Int. Ed.* **2003**, *42*, 4479–4482.

28. Ramström, O.; Lohmann, S.; Bunyapaiboonsri, T.; Lehn, J.-M. Dynamic combinatorial carbohydrate libraries: probing the binding site of the concanavalin A lectin. *Chem. Eur. J.* **2004**, *10*, 1711–1715.

29. Poulsen, S.-A. Direct screening of a dynamic combinatorial library using mass spectrometry. *J. Am. Soc. Mass Spectrom.* **2006**, *17*, 1074–1080.

30. Herrmann, A. Dynamic mixtures and combinatorial libraries: imines as probes for molecular evolution at the interface between chemistry and biology. *Org. Biomol. Chem.* **2009**, *7*, 3195–3204.

31. Ramström, O.; Lehn, J.-M. In situ generation and screening of a dynamic combinatorial carbohydrate library against concanavalin A. *ChemBioChem*, **2000**, *1*, 41–48.

32. Milanesi, L.; Hunter, C. A.; Sedelnikova, S. E.; Waltho, J. P. Amplification of bifunctional ligands for calmodulin from a dynamic combinatorial library. *Chem. Eur. J.* **2006**, *12*, 1081–1087.

33. Danieli, B.; Giardini, A.; Lesma, G.; Passarella, D.; Peretto, B.; Sacchetti, A.; Silvani, A.; Pratesi, G.; Zunino, F. Thiocolchicine-podophyllotoxin conjugates: dynamic libraries based on disulfide exchange reaction. *J. Org. Chem.* **2006**, *71*, 2848–2853.

34. Scott, D. E.; Dawes, G. J.; Ando, M.; Abell, C.; Ciulli, A. A fragment-based approach to probing adenosine recognition sites by using dynamic combinatorial chemistry. *ChemBioChem* **2009**, *10*, 2772–2779.

35. Pei, Z.; Larsson, R.; Aastrup, T.; Anderson, H.; Lehn, J.-M.; Ramström, O. Quartz crystal microbalance bioaffinity sensor for rapid identification of glycosyldisulfide lectin inhibitors from a dynamic combinatorial library. *Biosens. Bioelectron.* **2006**, *22*, 42–48.

36. André, S.; Pei, Z.; Siebert, H.-C.; Ramström, O.; Gabius, H.-J. Glycosyldisulfides from dynamic combinatorial libraries as *O*-glycoside mimetics for plant and endogenous lectins: their reactivities in solid-phase and cell assays and conformational analysis by molecular dynamics simulations. *Bioorg. Med. Chem.* **2006**, *14*, 6314–6326.

37. Liénard, B. M. R.; Selevsek, N.; Oldham, N. J.; Schofield, C. J. Combined mass spectrometry and dynamic chemistry approach to identify metalloenzyme inhibitors. *ChemMedChem* **2007**, *2*, 175–179.

38. Liénard, B. M. R.; Hüting, R.; Lassaux, P.; Galleni, M.; Frére, J.-M.; Schofield, C. J. Dynamic combinatorial mass spectrometry leads to metallo-β-lactamase inhibitors. *J. Med. Chem.* **2008**, *51*, 684–688.

39. Cancilla, M. T.; He, M. M.; Viswanathan, N.; Simmons, R. L.; Taylor, M.; Fung, A. D.; Cao, K.; Erlanson, D. A. Discovery of an Aurora kinase inhibitor through site-specific dynamic combinatorial chemistry. *Bioorg. Med. Chem. Lett.* **2008**, *18*, 3978–3981.

40. Shi, B.; Stevenson, R.; Campopiano, D. J.; Greaney, M. F. Discovery of glutathione S-transferase inhibitors using dynamic combinatorial chemistry. *J. Am. Chem. Soc.* **2006**, *128*, 8459–8467.

41. Caraballo, R.; Dong, H.; Ribeiro, J. P.; Jiménez-Barbero, J.; Ramström, O. Direct STD NMR identification of β-galactosidase inhibitors from a virtual dynamic hemithioacetal system. *Angew. Chem. Int. Ed.* **2010**, *49*, 589–539.

42. Caraballo, R.; Sakulsombat, M.; Ramström, O. Towards dynamic drug design: identification and optimisation of β-galactosidase inhibitors from a dynamic hemithioacetal system. *ChemBioChem* **2010**, *11*, 1600–1606.

43. Boul, P. J.; Reutenauer, P.; Lehn, J.-M. Reversible Diels-Alder reactions for the generation of dynamic combinatorial libraries. *Org. Lett.* **2005**, *7*, 15–18.

44. Poulsen, S.-A.; Bornaghi, L. F. Fragment-based drug discovery of carbonic anhydrase II inhibitors by dynamic combinatorial chemistry utilizing alkene cross metathesis. *Bioorg. Med. Chem.* **2006**, *14*, 3275–3284.

45. Sakai, S.; Shigemasa, Y.; Sasaki, T. A self-adjusting carbohydrate ligand for GalNAc specific lectins. *Tetrahedron Lett.* **1997**, *38*, 8145–8148.

46. Sakai, S.; Shigemasa, Y.; Sasaki, T. Iron(II)-assisted assembly of trivalent GalNAc clusters and their interactions with GalNAc-specific lectins. *Bull. Chem. Soc. Jpn.* **1999**, *72*, 1313–1319.

47. Swann, P. G.; Casanova, R. A.; Desai, A.; Frauenhoff, M. M.; Urbancic, M.; Slomczynska, U.; Hopfinger, A. J.; Le Breton, G. C.; Venton, D. L. Nonspecific protease-catalyzed hydrolysis/synthesis of a mixture of peptides: product diversity and ligand amplification by a molecular trap. *Biopolymers* **1996**, *40*, 617–625.

48. Lins, R. J.; Flitsch, S. L.; Turner, N. J.; Irving, E.; Brown, S. A. Enzymatic generation and in situ screening of a dynamic combinatorial library of sialic acid analogues. *Angew. Chem. Int. Ed.* **2002**, *41*, 3405–3407.

49. Lins, R. J.; Flitsch, S. L.; Turner, N. J.; Irving, E.; Brown, S. A. Generation of a dynamic combinatorial library using sialic acid aldolase and in situ screening against wheat germ agglutinin. *Tetrahedron* **2004**, *60*, 771–780.

50. Dalvit, C.; Pevarello, P.; Tató, M.; Veronesi, M.; Vulpetti, A.; Sundström, M. Identification of compounds with binding affinity to proteins via magnetization transfer from bulk water. *J. Biomol. NMR* **2000**, *18*, 65–68.

51. Mayer, M.; Meyer, B. Characterization of ligand binding by saturation transfer difference NMR spectroscopy. *Angew. Chem. Int. Ed.* **1999**, *38*, 1784–1788.

52. Katz, B. A.; Finer-Moore, J.; Mortezaei, R.; Rich, D. H.; Stroud, R. M. Episelection: novel K_i ~ nanomolar inhibitors of serine proteases selected by binding or chemistry on an enzyme surface. *Biochemistry* **1995**, *34*, 8264–8280.

53. Springsteen, G.; Wang, B. A detailed examination of boronic acid-diol complexation. *Tetrahedron* **2002**, *58*, 5291–5300.

54. Lorand, J. P.; Edwards, J. O. Polyol complexes and structure of the benzeneboronate ion. *J. Org. Chem.* **1959**, *24*, 769–774.

55. Yan, J.; Springsteen, G.; Deeter, S.; Wang, B. The relationship among pK_a, pH, and binding constants in the interactions between boronic acids and diols – it is not as simple as it appears. *Tetrahedron* **2004**, *60*, 11205–11209.

56. Antonov, V. K.; Ivanina, T. V. n-Alkylboronic acid as bifunctional reversible inhibitors of α-chymotrypsin. *FEBS Lett.* **1970**, *7*, 23–25.

57. Philipp, M.; Bender, M. L. Inhibition of serine proteases by arylboronic acids. *Proc. Natl. Acad. Sci. U. S. A.* **1971**, *68*, 478–480.

58. Kettner, C. A.; Bone, R.; Agard, D. A.; Bachovchin, W. W. Kinetic properties of the binding of α-lytic protease to peptide boronic acids. *Biochemistry* **1988**, *27*, 7682–7688.

59. Bachovchin, W. W.; Wong, W. Y. L.; Farr-Jones, S.; Shenvi, A. B.; Kettner, C. A. Nitrogen-15 NMR spectroscopy of the catalytic-triad histidine of a serine protease in peptide boronic acid inhibitor complexes. *Biochemistry* **1988**, *27*, 7689–7697.

60. Steiner, S. J.; Bien, J. T.; Smith, B. D. Diphenylboronic acid is a strong inhibitor of serine proteases. *Bioorg. Med. Chem. Lett.* **1994**, *4*, 2417–2420.

61. Matthews, D. A.; Alden, R. A.; Birktoft, J. J.; Freer, S. T.; Kraut, J. X-ray crystallographic study of boronic acid adducts with subtilisin BNP' (Novo). A model for the catalytic transition state. *J. Biol. Chem.* **1975**, *250*, 7120–7126.

62. Matteson, D. S.; Sadhu, K. M. (*R*)-l-Acetamido-2-phenylethaneboronic acid. A specific transition-state analogue for chymotrypsin. *Biochemistry* **1971**, *10*, 2477–2483.

63. Crompton, I. E.; Cuthbert, B. K. ; Lowe, G. ; Waley, S. G. *β*-Lactamase inhibitors. The inhibition of serine *β*-lactamases by specific boronic acids. *Biochem. J.* **1988**, *251*, 453–459.

64. Beesley, T.; Gascoyne, N.; Knott-Hunziker, V.; Petursson, S.; Waley, S. G.; Jurin, B.; Grundström, T. The inhibition of class C *β*-lactamases by boronic acids. *Biochem. J.* **1983**, *209*, 229–233.

65. Weston, G. S.; Blázquez, J.; Baquero, F.; Shoichet, B. K. Structure-based enhancement of boronic acid-based inhibitors of AmpC *β*-lactamase. *J. Med. Chem.* **1998**, *41*, 4577–4586.

66. Suenaga, H.; Mikami, M.; Yamamoto, H.; Harada, T.; Shinkai, S. Strong inhibitory effect of sugar·biphenylylboronic acid complexes on the hydrolytic activity of a-chymotrypsin. *J. Chem. Soc. Perkin Trans.* **1995**, 1733–1738.

67. Suenaga, H.; Nakashima, K.; Shinkai, S. Sugars intensify the inhibitory effect of phenylboronic acid on the hydrolytic activity of α-chymotrypsin. *J. Chem. Soc., Chem. Commun.* **1995**, 29–30.

68. London, R. E.; Gabel, S. A. Formation of a trypsin-borate-4-aminobutanol ternary complex. *Biochemistry* **2002**, *41*, 5963–5967.

69. Smoum, R.; Rubinstein, A.; Srebnik, M. A study of the effect on nucleophilic hydrolytic activity of pancreatic elastase, trypsin, chymotrypsin, and leucine aminopeptidase by boronic acids in the presence of arabinogalactan: a subsequent study on the hydrolytic activity of chymotrypsin by boronic acids in the presence of mono-, di-, and trisaccharides. *Bioorg. Chem.* **2003**, *31*, 464–474.

70. Baldwin, J. E.; Claridge, T. D. W.; Derome, A. E.; Schofield, C. J.; Smith, B. D. ^{11}B NMR studies of an aryl boronic acid bound to chymotrypsin and subtilisin. *Bioorg. Med. Chem. Lett.* **1991**, *1*, 9–12.

71. Zhong, S.; Jordan, F.; Kettner, C.; Polgar, L. Observation of tightly bound ^{11}B nuclear magnetic resonance signals on serine proteases. Direct solution evidence for tetrahedral geometry around the boron in the putative transition-state analogues. *J. Am. Chem. Soc.* **1991**, *113*, 9429–9435.

72. Tsilikounas, E.; Kettner, C. A.; Bachovchin, W. W. ^{11}B NMR spectroscopy of peptide boronic acid inhibitor complexes of α-lytic protease. Direct evidence for tetrahedral boron in both boron-histidine and boron-serine adduct complexes. *Biochemistry* **1993**, *32*, 12651–12655.

73. Baldwin, J. E.; Claridge, T. D. W.; Derome, A. E.; Smith, B. D.; Twyman, M.; Waley, S. G. Direct observation of a tetrahedral boronic acid-β-lactamase complex using ^{11}B NMR spectroscopy. *J. Chem. Soc., Chem. Commun.* **1991**, 573–574.

74. Kono, Y.; Ishihara, K.; Nagasawa, A.; Umemoto, K.; Saito, K. An ^{11}B NMR study of the kinetics of methylboronic acid-methylboronate interchange in aqueous solution. *Inorg. Chim. Acta* **1997**, *262*, 91–96.

75. Gupta, R. R.; Lechner, M. D. In *Chemical Shifts and Coupling Constants for Boron-11 and Phosphorus-31*; Springer-Verlag: 1997.

76. Bull, T. E. Nuclear magnetic relaxation of spin-3/2 nuclei involved in chemical exchange. *J. Magn. Reson.* **1972**, *8*, 344–353.

77. Hubbard, P. S. Nonexponential nuclear magnetic relaxation by quadrupole interactions. *J. Chem. Phys.* **1970**, *53*, 985–987.

78. Transue, T. R.; Krahn, J. M.; Gabel, S. A.; DeRose, E. F.; London, R. E. X-ray and NMR characterization of covalent complexes of trypsin, borate, and alcohols. *Biochemistry* **2004**, *43*, 2829–2839.

79. Angyal, S. J. The composition of reducing sugars in solution. *Adv. Carbohydr. Chem. Biochem.* **1984**, *42*, 15–68.

80. Nicholls, M. P.; Paul, P. K. C. Structures of carbohydrate-boronic acid complexes determined by NMR and molecular modelling in aqueous alkaline media. *Org. Biomol. Chem.* **2004**, *2*, 1434–1441.

81. Yabroff, D. L.; Branch, G. E. K.; Bettman, B. The relative strengths of some hydrocarbon derivatives of boric acid. *J. Am. Chem. Soc.* **1934**, *56*, 1850–1857.

82. Bettman, B.; Branch, G. E. K.; Yabroff, D. L. Dissociation constants of organic boric acids. *J. Am. Chem. Soc.* **1934**, *56*, 1865–1870.

83. Chowdhury, R.; Hardy, A.; Schofield, C. J. The human oxygen sensing machinery and its manipulation. *Chem. Soc. Rev.* **2008**, *37*, 1308–1319.

84. Semenza, G. L. HIF-1 and mechanisms of hypoxia sensing. *Curr. Opin. Cell Biol.* **2001**, *13*, 167–171.

85. Berra, E.; Ginouvés, A.; Pouysségur, J. The hypoxia-inducible-factor hydroxylases bring fresh air into hypoxia signalling. *EMBO Rep.* **2006**, *7*, 41–45.

86. Schofield, C. J.; Ratcliffe, P. J. Oxygen sensing by HIF hydroxylases. *Nat. Rev. Mol. Cell Biol.* **2004**, *5*, 343–354.

87. Fraisl, P.; Aragonés, J. Carmeliet, P. Inhibition of oxygen sensors as a therapeutic strategy for ischaemic and inflammatory disease. *Nat. Rev. Drug Discov.* **2009**, *8*, 139–152.

88. Hewitson, K. S.; Schofield, C. J. The HIF pathway as a therapeutic target. *Drug Discov. Today* **2004**, *9*, 704–711.

89. Hewitson, K. S.; McNeill, L. A.; Schofield, C. J. Modulating the hypoxia-inducible factor signaling pathway: Applications from cardiovascular disease to cancer. *Curr. Pharm. Des.* **2004**, *10*, 821–833.

90. Poon, E.; Harris, A. L.; Ashcroft, M. Targeting the hypoxia-inducible factor (HIF) pathway in cancer. *Expert Rev. Mol. Med.* **2009**, *11*, e26–e48.

91. Semenza, G. L. Targeting HIF-1 for cancer therapy. *Nat. Rev. Cancer* **2003**, *3*, 721–732.

92. Harris, A. L. Hypoxia – a key regulatory factor in tumour growth. *Nat. Rev. Cancer* **2002**, *2*, 38–47.

93. Pouysségur, J.; Dayan, F.; Mazure, N. M. Hypoxia signalling in cancer and approaches to enforce tumour regression. *Nature* **2006**, *441*, 437–443.

94. Maxwell, P. H. The HIF pathway in cancer. *Sem. Cell Dev. Biol.* **2005**, *16*, 523–530.

95. Klotzsche-von Ameln, A.; Muschter, A.; Mamlouk, S.; Kalucka, J.; Prade, I.; Franke, K.; Rezaei1, M.; Poitz, D. M.; Breier, G.; Wielockx, B. Inhibition of HIF prolyl hydroxylase-2 blocks tumor growth in mice through the antiproliferative activity of TGFβ. *Cancer Res.* **2011**, *71*, 3306–3316.

96. Jaakkola, P.; Mole, D. R.; Tian, Y. M.; Wilson, M. I.; Gielbert, J.; Gaskell, S. J.; von Kriegsheim, A.; Hebestreit, H. F.; Mukherji, M.; Schofield, C. J.; Maxwell, P. H.; Pugh, C. W.; Ratcliffe, P. J. Targeting of HIF-α to the von Hippel-Lindau ubiquitylation complex by O_2-regulated prolyl hydroxylation. *Science* **2001**, *292*, 468–472.

97. Mole, D. R.; Schlemminger, I.; McNeill, L. A.; Hewitson, K. S.; Pugh, C. W.; Ratcliffe, P. J.; Schofield, C. J. 2-Oxoglutarate analogue inhibitors of HIF prolyl hydroxylase. *Bioorg. Med. Chem. Lett.* **2003**, *13*, 2677–2680.

98. Mecinović, J.; Loenarz, C.; Chowdhury, R.; Schofield, C. J. 2-Oxoglutarate analogue inhibitors of prolyl hydroxylase domain 2. *Bioorg. Med. Chem. Lett.* **2009**, *19*, 6192–6195.

99. Ivan, M.; Haberberger, T.; Gervasi, D. C.; Michelson, K. S.; Günzler, V.; Kondo, K.; Yang, H.; Sorokina, I.; Conaway, R. C.; Conaway, J. W.; Kaelin, W. G., Jr. Biochemical purification and pharmacological inhibition of a mammalian prolyl hydroxylase acting on hypoxia-inducible factor. *Proc. Natl. Acad. Sci. U. S. A.* **2002**, *99*, 13459–13464.

100. Schlemminger, I.; Mole, D. R.; McNeill, L. A.; Dhanda, A.; Hewitson, K. S.; Tian, Y. M.; Ratcliffe, P. J.; Pugh, C. W.; Schofield, C. J. Analogues of Dealanylalahopcin are inhibitors of human HIF prolyl hydroxylases. *Bioorg. Med. Chem. Lett.* **2003**, *13*, 1451–1454.

101. McDonough, M. A.; McNeill, L. A.; Tilliet, M.; Papamicaël, C. A.; Chen, Q. Y.; Banerji, B.; Hewitson, K. S.; Schofield, C. J. Selective inhibition of factor inhibiting hypoxia-inducible factor. *J. Am. Chem. Soc.* **2005**, *127*, 7680–7681.

102. Tegley, C. M.; Viswanadhan, V. N.; Biswas, K.; Frohn, M. J.; Peterkin, T. A. N.; Chang, C.; Bürli, R. W.; Dao, J. H.; Veith, H.; Rogers, N.; Yoder, S. C.; Biddlecome, G.; Tagari, P.; Allen, J. R.; Hungate, R. W. Discovery of novel hydroxy-thiazoles as HIF-α prolyl hydroxylase inhibitors: SAR, synthesis, and modelling evaluation. *Bioorg. Med. Chem. Lett.* **2008**, *18*, 3925–3928.

103. Liénard, B. M.; Conejo-García, A.; Stolze, I.; Loenarz, C.; Oldham, N. J.; Ratcliffe, P. J.; Schofield, C. J. Evaluation of aspirin metabolites as inhibitors of hypoxia-inducible factor hydroxylases. *Chem. Commun.* **2008**, *47*, 6393–6395.

104. Dao, J. H.; Kurzeja, R. J. M.; Morachis, J. M.; Veith, H.; Lewis, J.; Yu, V.; Tegley, C. M.; Tagari, P. Kinetic characterization and identification of a novel inhibitor of hypoxia-inducible factor prolyl hydroxylase 2 using a time-resolved fluorescence resonance energy transfer-based assay technology. *Anal. Biochem.* **2009**, *384*, 213–223.

105. Rosen, M. D.; Venkatesan, H.; Peltier, H. M.; Bembenek, S. D.; Kanelakis, K. C.; Zhao, L. X.; Leonard, B. E.; Hocutt, F. M.; Wu, X.; Palomino, H. L.; Brondstetter, T. I.; Haugh, P. V.; Cagnon, L.; Yan, W.; Liotta, L. A.; Young, A.; Mirzadegan, T.; Shankley, N. P.; Barrett, T. D.; Rabinowitz, M. H. Benzimidazole-2-pyrazole HIF prolyl 4-hydroxylase inhibitors as oral erythropoietin secretagogues. *ACS Med. Chem. Lett.* **2010**, *1*, 526–529.

106. Frohn, M.; Viswanadhan, V.; Pickrell, A. J.; Golden, J. E.; Muller, K. M.; Bürli, R. W.; Biddlecome, G.; Yoder, S. C.; Rogers, N.; Dao, J. H.; Hungate, R.; Allen, J. R. Structure-guided design of substituted aza-benzimidazoles as potent hypoxia inducible factor-1α prolyl hydroxylase-2 inhibitors. *Bioorg. Med. Chem. Lett.* **2008**, *18*, 5023–5026.

107. Clifton, I. J.; McDonough, M. A.; Ehrismann, D.; Kershaw, H. J.; Granatino, N.; Schofield, C. J. Structural studies on 2-oxoglutarate oxygenases and related double-stranded β-helix fold proteins. *J. Inorg. Biochem.* **2006**, *100*, 644–669.

108. McDonough, M. A.; Loenarz, C.; Chowdhury, R.; Clifton, I. J.; Schofield, C. J. Structural studies on human 2-oxoglutarate dependent oxygenases. *Curr. Opin. Struct. Biol.* **2010**, *20*, 659–672.

109. McNeill, L. A.; Flashman, E.; Buck, M. R. G.; Hewitson, K. S.; Clifton, I. J.; Jeschke, G.; Claridge, T. D. W.; Ehrismann, D.; Oldham N. J.; Schofield, C. J. Hypoxia-inducible factor prolyl hydroxylase 2 has a high affinity for ferrous iron and 2-oxoglutarate. *Mol. BioSyst.* **2005**, *1*, 321–324.

110. Chowdhury, R.; McDonough, M. A.; Mecinović, J.; Loenarz, C.; Flashman, E.; Hewitson, K. S.; Domene, C.; Schofield, C. J. Structural basis for binding of hypoxia-inducible factor to the oxygen-sensing prolyl hydroxylases. *Structure* **2009**, *17*, 981–989.

111. McDonough, M. A.; Li, V.; Flashman, E.; Chowdhury, R.; Mohr, C.; Liénard, B. M. R.; Zondlo, J.; Oldham, N. J.; Clifton, I. J.; Lewis, J.; McNeill, L. A.; Kurzeja, R. J. M.;

Hewitson, K. S.; Yang, E.; Jordan, S.; Syed, R. S.; Schofield, C. J. Cellular oxygen sensing: Crystal structure of hypoxia-inducible factor prolyl hydroxylase (PHD2). *Proc. Natl. Acad. Sci. U. S. A.* **2006**, *103*, 9814–9819.

112. Hewitson, K. S.; Liénard, B. M. R.; McDonough, M. A.; Clifton, I. J.; Butler, D.; Soares, A. S.; Oldham, N. J.; McNeill, L. A.; Schofield, C. J. Structural and mechanistic studies on the inhibition of the hypoxia-inducible transcription factor hydroxylases by tricarboxylic acid cycle intermediates. *J. Biol. Chem.* **2007**, *282*, 3293–3301.

113. Mecinović, J.; Chowdhury, R.; Liénard, B. M. R.; Flashman, E.; Buck, M. R. G.; Oldham, N. J.; Schofield, C. J. ESI-MS studies on prolyl hydroxylase domain 2 reveal a new metal binding site. *ChemMedChem* **2008**, *3*, 569–572.

114. Bertini, I.; Fragai, M.; Luchinat, C.; Talluri, E. Water-based ligand screening for paramagnetic metalloproteins. *Angew. Chem. Int. Ed.* **2008**, *47*, 4533–4537.

115. Cunliffe, C. J.; Franklin, T. J. Inhibition of prolyl 4-hydroxylase by hydroxyanthraquinones. *Biochem. J.* **1986**, *239*, 311–315.

6. Materials and methods[†]

6.1 General NMR methods

6.1.1 Materials

All chemicals for NMR experiments were obtained from Sigma-Aldrich or Alfa Aesar, except those listed in Table 6-1 or where otherwise stated.

Chemicals	Suppliers
Tris-D11	Cambridge Isotope Laboratories or Euriso-Top
D_2O	Apollo Scientific or Euriso-Top
Acetonitrile-D3	Apollo Scientific
DMSO-D6	Merck Chemicals

Table 6-1 Suppliers of chemicals for NMR analyses.

6.1.2 Buffer for NMR experiments

Unless otherwise stated, all NMR experiments were carried out in solution buffered with 50 mM deuterated tris(hydroxymethyl)aminomethane (Tris-D11; pH 6.6 or 7.5) or 100 mM 2-(*N*-morpholino)ethanesulfonic acid (MES; pH 5.8). The buffer compositions are listed in Table 6-2 and Table 6-3.

Component	Amount per 100 mL
Tris-D11	660 mg
NaN_3	20 mg

Table 6-2 Tris-based NMR buffer contained 50 mM Tris-D11 and 0.02% (w/v) NaN_3 (pH 6.6 or 7.5).

Component	Amount per 100 mL
MES hydrate	1.95 g

Table 6-3 MES-based NMR buffer contained 100 mM MES (pH 5.8).

Buffers were made up in Milli-Q H_2O or in D_2O. Milli-Q H_2O was obtained from an Elix Reverse Osmosis system coupled with a Milli-Q Synthesis system and a 0.22 μm filter (Millipore). For H_2O-based buffer, pH was adjusted using HCl and NaOH. In case of the D_2O-based buffer, DCl and NaOD were used. The following equation was used to convert pH meter reading into pD, as proposed by Glasoe and Long:[1]

[†] *The work in this Chapter was conducted in collaboration with Dr Adam P. Hardy, Dr Emily Flashman, Wendy J. Sobey and Herminio Manso Jubier. Various members of the Schofield Group have provided chemicals and they are acknowledged in the text.*

A.P.H. provided glycerol stock for the production of $PHD2_{181-402}$. E.F. provided plasmid DNA and competent cells for the production of $PHD2_{181-426}$. W.J.S. packed the columns for FPLC purification. H.M.J. provided 2TY media.

pD = pH meter reading + 0.40

pH adjustments were carried out using a Jenway 3305 pH meter with a Sigma-Aldrich polymer bodied combination pH electrode. Electrodes were calibrated to pH 7.0 and either pH 4.0 or 10.0 before use. All buffers were filter sterilised through 0.22 μm filters (Millipore) and were stored in 15 mL or 50 mL falcon tubes (Sarstedt) at 4 ºC.

6.1.3 General sample preparation and handling

All samples were prepared in Eppendorf microtubes (500 μL or 1.6 mL) and were transferred to NMR tubes using gel-loading tips (Fisher Scientific). The sample volumes for 3 mm and 5 mm NMR tubes were 160 μL and 500 μL respectively. Conventional 3 mm diameter NMR tubes (Norell or Sigma-Aldrich), 3 mm diameter MATCH NMR tubes (Bruker) and conventional 5 mm diameter NMR tubes (Norell) were used throughout. A 5 mm diameter quartz NMR tube (Wilmad) was used for ^{11}B NMR experiments (Chapter 5) and a 5 mm Teflon liner (GPE Scientific) was used in the development of the water relaxation method (Chapter 3).

Unless otherwise stated, all stock solutions were prepared to the appropriate concentrations in advance using the relevant NMR buffer or DMSO-D6. The iron(II) stock solution (250 mM) was freshly prepared for each set of experiments using $(NH_4)_2Fe(SO_4)_2 \cdot 6H_2O$ and 20 mM HCl, which was then diluted down by the relevant NMR buffer to the appropriate concentration just before adding to the reaction mixture. Zinc, manganese, sodium and potassium stock solutions were made from their corresponding chloride salts ($ZnCl_2$, $MnCl_2$, NaCl and KCl) and the relevant NMR buffer. Ascorbate solutions were freshly prepared each day using sodium ascorbate and the relevant NMR buffer and were stored in black Eppendorf microtubes to prevent degradation. 2OG stock solutions were prepared using 2OG monosodium salt and H_2O-based NMR buffer. D_2O-based buffer was not used in order to prevent H-D exchange. α-Chymotrypsin solutions (Chapter 5) were prepared from lyophilised powder (from bovine pancreas; Type II; ≥40 units per mg protein; Sigma-Aldrich) before each experiment. All components were mixed just before the experiment, and enzyme was always added last to the mixture.

For titration experiments, when a 5 mm NMR tube was used, the titratant (typically ~2 μL) was added to the top of the NMR tube using a Discovery 2–20 μL pipette (HTL) and sample mixing was done by rotating the tube up and down. When a 3 mm

MATCH tube was used, the titratant (typically ~1 µL) was added using a 5 µL plunger-in-needle syringe (SGE) and sample mixing was conducted using a 250 µL gas tight syringe (SGE).

6.1.4 Sample acquisition and processing

Unless otherwise stated, all NMR experiments were conducted using either a Bruker Avance III 700 MHz spectrometer equipped with a 5 mm inverse TCI cryoprobe (AV700), a Bruker Avance II 500 MHz spectrometer equipped with a 5 mm inverse $^{1}H/^{19}F(^{13}C)$ TXI probe (AV500) or a Bruker DRX 500 MHz spectrometer equipped with a 5 mm broadband observe BBO probe (DRX500). The AV700 and AV500 were controlled by the TopSpin 2.1 software whilst the DRX500 was controlled by the TopSpin 1.3 software.

The ^{1}H pulse tip-angle was calibrated using the single-pulse nutation method[2] (Bruker *pulsecal* routine; AV500 and AV700 only) with the NMR sample or with the NMR buffer prior to the actual experiment. The ^{19}F and ^{11}B pulses were calibrated using trifluoroacetone and tetramethylborate in the relevant NMR buffer respectively using the Bruker *paropt* method to identify the 90º and 180º pulse.

Typically, exponential multiplication using a line broadening factor of 1 or 2 Hz was applied for processing. Zero filling was used for processing throughout. Unless otherwise stated, no chemical shift reference was used and chemical shift was referenced against the solvent internally.

6.1.5 Characterisation of compounds

NMR characterisations were conducted using the AV500 or AV700 instruments. 3 mm MATCH NMR tubes were used for experiments conducted on the AV700, and 5 mm conventional NMR tubes were used for experiments conducted on the AV500. Enzymatic products were usually characterised *in situ* in the reaction mixture. A combination of the standard experiments including ^{1}H, ^{1}H-^{13}C HSQC, ^{1}H-^{13}C HMBC, ^{1}H-^{1}H COSY, ^{1}H-^{1}H TOCSY and 1D TOCSY were used. NMR parameters such as water suppression, sample temperature, number of transients, acquisition time and mixing time were judged on a per sample basis.

6.1.6 ^{1}H NMR

^{1}H NMR experiments were conducted using the AV500, AV700 or DRX500 spectrometer. 3 mm MATCH NMR tubes were used for experiments conducted on the AV700, and 5 mm conventional NMR tubes were used for experiments conducted on the AV500 and the DRX500. NMR parameters such as water suppression, sample temperature, number of transients, acquisition time and mixing time were determined on a per sample basis, although typically the number of transients usually varied between 8 and 32, and the relaxation delay usually between 1 and 2 seconds. Typically, water suppression was achieved using the excitation sculpting method (2 ms Sinc1.1000 pulse) or the NOESY presaturation method (mixing time 2 ms) for samples containing 90-95% H_2O. For samples in D_2O, experiments were run with no suppression or with presaturation.

6.1.7 ^{19}F NMR

^{19}F NMR experiments were conducted at 470 MHz (for ^{19}F) using the AV500 spectrometer. Standard 5 mm NMR tubes were used. All experiments were conducted at 298 K. If ^{1}H decoupling was required, a 80 μs 90 degree WALTZ16 decoupling routine was used. NMR parameters such as number of transients and acquisition time were judged on a per sample basis, although typical acquisition times were 700 ms, relaxation delay of 2–5 s and the number of transients ranged from 512 to 2048.

6.1.8 ^{11}B NMR

^{11}B NMR experiments (Chapter 5) were conducted at 160 MHz (for ^{11}B) using the DRX500 spectrometer. A 5 mm quartz NMR tube was used. All experiments were conducted at 298 K. Typical experimental parameters were as follows: acquisition time 16 ms, relaxation delay 400 ms, number of transients 4000–16000. Baseline correction was achieved using spline fit processing or backward linear prediction (28–30 points back predicted and 256 linear prediction coefficients).

6.2 Protein NMR experiments

6.2.1 ^{1}H-^{15}N HSQC

^{1}H-^{15}N HSQC experiments (Chapter 4) were conducted using the AV700 spectrometer. The Bruker sequence *hsqcetfpf3gpsi* was used. Typically, the size of the

FID for the ^{1}H dimension was 2048 points, and for the ^{15}N dimension was set as either 128, 256 or 1024 points depending on the resolution required. The spectral width was set as 16 ppm (^{1}H) and 40 ppm (^{15}N) respectively, and the centre of the spectrum was set to 4.7 ppm and 120 ppm. $^{1}J_{NH}$ was set to 90 Hz. ^{15}N decoupling was achieved using a 170 µs 90 degree GARP sequence and the high power ^{15}N 90 degree pulse was achieved using a 40 µs GARP sequence. If the protein was also labelled with ^{13}C, the Bruker pulse programme flag *–DLABEL_CN* was chosen and a 500 µs 90º Crp80,0.5,20.1 (80 kHz sweep, 0.5 ms duration with 20% smoothing) adiabatic CHIRP pulse was used for the ^{13}C dimension. The number of transients was judged on a per sample basis (typically between 2 and 8). The relaxation delay was 1 second. Temperature was 291.8 K.

6.2.2 Triple resonance experiments

Triple resonance experiments (Chapter 4) were conducted using the AV700 spectrometer. Typical experimental parameters are summarised in Table 6-4. The number of transients was judged on a per sample and per experiment basis by running 2D versions of the relevant 3D experiments (by setting the size of FID of the ^{13}C dimension to 1). The relaxation delay was 2 seconds. The temperature was 291.8 K.

$^{1}J_{NH}$ was set to 91 Hz; $^{1}J_{NCO}$ was set to 21 Hz; $^{1}J_{NC\alpha}$ was set to 23 Hz; $^{1}J_{COC\alpha}$ was set to 61 Hz; $^{1}J_{C\alpha C\beta}$ was set to 36 Hz and $^{1}J_{CH}$ was set to 147 Hz.

For ^{1}H pulses, the 90 degree high power pulse was ~8.2 µs (as judged by the *pulsecal* routine). ^{1}H decoupling during the sequences was achieved using a 50 µs 90 degree DIPSI2 scheme. A 1 ms 90 degree Sinc1.1000 water flip-back pulse was used at the water frequency for water suppression during ^{1}H-^{15}N INEPT transfer.

For ^{15}N pulses, the pulse length for the high power ^{15}N 90 degree pulse was 40 µs. ^{15}N decoupling was achieved using a 170 µs 90 degree GARP sequence.

For ^{13}C shaped pulses, a 274 µs 90 degree Q5.1000 pulse was used on-resonance at C_{α}. A 219 µs 180 degree Q3.1000 pulse was used as the on-resonance pulse for C_{α}, and as the off-resonance pulse for C_{α} and CO. The CO chemical shift offset was 173 ppm, the C_{α} chemical shift offset was 54 ppm and the $C_{aliphatic}$ chemical shift offset was 39 ppm.

If required, ^{2}H decoupling was achieved using a 280 µs 90 degree WALTZ16 sequence.

Data obtained from triple resonance experiments were analysed using the CCPN Analysis software (The Collaborative Computing Project for NMR).[3]

HNCO	
Pulse sequence	hncogp3d
Size of FID	2048 (^{1}H), 80 (^{15}N), 80 (^{13}C)
Spectral width	14 ppm (^{1}H), 29 ppm (^{15}N), 14 ppm (^{13}C)
Centre of spectrum	4.7 ppm (^{1}H), 119.5 ppm (^{15}N), 173 ppm (^{13}C)
HN(CA)CO	
Pulse sequence	hncacogp2h3d (for ^{2}H,^{13}C,^{15}N-PHD2$_{181-402}$) hncacogp3d (for ^{13}C,^{15}N-PHD2$_{181-402}$)
Size of FID	2048 (^{1}H), 80 (^{15}N), 80 (^{13}C)
Spectral width	14 ppm (^{1}H), 29 ppm (^{15}N), 14 ppm (^{13}C)
Centre of spectrum	4.7 ppm (^{1}H), 119.5 ppm (^{15}N), 173 ppm (^{13}C)
HN(CO)CA	
Pulse sequence	hncocagp2h3d (for ^{2}H,^{13}C,^{15}N-PHD2$_{181-402}$) hncocagp3d (for ^{13}C,^{15}N-PHD2$_{181-402}$)
Size of FID	2048 (^{1}H), 80 (^{15}N), 128 (^{13}C)
Spectral width	14 ppm (^{1}H), 29 ppm (^{15}N), 32 ppm (^{13}C)
Centre of spectrum	4.7 ppm (^{1}H), 119.5 ppm (^{15}N), 54 ppm (^{13}C)
HNCA	
Pulse sequence	hncagp2h3d (for ^{2}H,^{13}C,^{15}N-PHD2$_{181-402}$) hncagp3d (for ^{13}C,^{15}N-PHD2$_{181-402}$)
Size of FID	2048 (^{1}H), 80 (^{15}N), 128 (^{13}C)
Spectral width	14 ppm (^{1}H), 29 ppm (^{15}N), 32 ppm (^{13}C)
Centre of spectrum	4.7 ppm (^{1}H), 119.5 ppm (^{15}N), 54 ppm (^{13}C)
HN(CO)CACB	
Pulse sequence	hncocacbgp2h3d (for ^{2}H,^{13}C,^{15}N-PHD2$_{181-402}$) hncocacbgp3d (for ^{13}C,^{15}N-PHD2$_{181-402}$)
Size of FID	2048 (^{1}H), 80 (^{15}N), 128 (^{13}C)
Spectral width	14 ppm (^{1}H), 29 ppm (^{15}N), 75 ppm (^{13}C)
Centre of spectrum	4.7 ppm (^{1}H), 119.5 ppm (^{15}N), 39 ppm (^{13}C)
HNCACB	
Pulse sequence	hncacbgp2h3d (for ^{2}H,^{13}C,^{15}N-PHD2$_{181-402}$) hncacbgp3d (for ^{13}C,^{15}N-PHD2$_{181-402}$)
Size of FID	2048 (^{1}H), 80 (^{15}N), 128 (^{13}C)
Spectral width	14 ppm (^{1}H), 29 ppm (^{15}N), 75 ppm (^{13}C)
Centre of spectrum	4.7 ppm (^{1}H), 119.5 ppm (^{15}N), 39 ppm (^{13}C)

Table 6-4 Typical parameters for triple resonance experiments.

6.2.3 ^{1}H-^{15}N TROSY-HSQC

^{1}H-^{15}N TROSY-HSQC experiments (Chapter 4) were conducted using the AV700 spectrometer. The Bruker sequence *trosyf3gpphsi19* was used. The size of the FID for the ^{1}H and ^{15}N dimension was 2048 and 128 points respectively, the spectral width

was set to 16 ppm and 40 ppm respectively, and the centre of the spectrum was set to 4.7 ppm and 120 ppm. $^{1}J_{NH}$ was set to 90 Hz. Watergate was used for water suppression using the 1-3-9-19 binomial sequence. The null was set at the water frequency and a 10000 Hz (~14 ppm) window was set between nulls. Typically the number of transients was 8 and the relaxation delay 2 seconds. The temperature was 291.8 K.

6.3 NMR Binding experiments

6.3.1 CPMG displacement experiments

The CPMG displacement experiments (Chapter 3) were conducted using the AV700 instrument. 3 mm MATCH NMR tubes were used. All experiments were conducted at 298 K. The PROJECT-CPMG sequence (90^{o}_{x}–[τ–180^{o}_{y}–τ–90^{o}_{y}– τ–180^{o}_{y}–τ]$_{n}$–acq) was applied as described by Augilar *et al.*[4] Typical experimental parameters were as follows: total echo time 48 ms (τ = 2 ms, n = 6), acquisition time 2.94 seconds, relaxation delay 2 seconds, number of transients 128. Water suppression was achieved by presaturation.

6.3.2 1D HSQC displacement experiments

The 1D HSQC displacement experiments (Chapter 3) were conducted using the AV700 instrument. 3 mm MATCH NMR tubes were used. All experiments were conducted at 298 K. The reporter molecule contained at least one ^{13}C label. The CLIP-HSQC sequence was used for 1D HSQC experiments (without ^{13}C decoupling).[5] Typical experimental parameters were as follows: acquisition time 0.58 seconds, relaxation delay 2 seconds, number of transients 256–1600. The $^{1}J_{CH}$ was set to 145 or 160 Hz. For the selective version of the experiment, a 6.8 ms Q3.1000 180 degree pulse was used and selective irradiation was applied at the appropriate ^{13}C chemical shift. For the non-selective version, an adiabatic 180 degree CHIRP (Crp80,0.5,20.1) pulse was used.

6.3.3 Water relaxation experiment

High-field experiments were conducted using the AV500 instrument. Unless otherwise stated, all experiments were conducted at 298 K. Conventional 3 mm diameter NMR tubes or 3 mm MATCH tubes were used. Unless otherwise stated, the H_2O to D_2O ratio was 12.5% H_2O and 87.5% D_2O. Inversion recovery (180^{o}–τ–90^{o}–

acq) or saturation recovery (90^{o}_{x}–G_1–90^{o}_{y}–G_2–90^{o}_{x}–G_3–τ–acq) experiments were performed with 1–2 scans with a relaxation delay of at least 5 times T_1 between transients. For the saturation recovery experiment, the gradient pulses were achieved using 1 ms SINE.100 gradient pulse (G_1 = 40%; G_2 = 27.1%; G_3 = 15%). The receiver gain was set to minimum value (rg = 1) to prevent radiation damping.[6,7] Typically, 10 to 16 delay points varied between 100 ms and 60 s was used. T_1 values were obtained using the Bruker *T1/T2 Relaxation* option and peak area was used for curve fitting. The fitting function for the inversion recovery experiment was *invrec*:

$$I_{(\tau)} = I_{(0)}(1 - 2Ae^{-\tau/T_1})$$

In which $I_{(\tau)}$ is the signal intensity at time τ, $I_{(0)}$ is the fully relaxed signal intensity, A is the correction factor to compensate for imperfect inversion and τ is the time delay.

The fitting function for the saturation recovery experiment was *uxnmrt1*:

$$I_{(\tau)} = I_{(0)}(1 - Ae^{-\tau/T_1})$$

In which $I_{(\tau)}$ is the signal intensity at time τ, $I_{(0)}$ is the fully relaxed signal intensity, A is the correction factor to compensate for imperfect saturation and τ is the time delay.

Low-field experiments were conducted using an Oxford Instruments MQC benchtop spectrometer operating at 23 MHz. Conventional 5 mm diameter tubes were used. Inversion recovery experiments were performed with 8 transients with a relaxation delay of at least 5 times T_1. All experimental details were identical to those used for the high field work, except that the experiments were conducted in 100% H_2O and at 313 K.

6.3.4 STD-NMR

STD-NMR experiments were conducted using the AV500 or the AV700 instrument. 3 mm MATCH NMR tubes were used when the experiment was conducted at 700 MHz, and 5 mm conventional NMR tubes were used for experiments conducted at 500 MHz. Unless otherwise stated, all experiments were conducted at 298 K. The pulse sequence used was identical to that published by Mayer and Meyer.[8] Selective saturation of the protein was achieved by a train of Gaussian shaped pulses of 50 ms length. Typical experimental parameters were as follows: saturation time 2–5 seconds, number of transients 64–256, relaxation delay 7–10 seconds. If necessary, water

suppression was achieved by the excitation sculpting method using a 2 ms 180 degree selective Sinc1.1000 pulse at the H_2O frequency.

6.3.5 WaterLOGSY

WaterLOGSY experiments were conducted using AV500 or AV700 spectrometers using the pulse sequence as described by Dalvit *et al.*[9] 3 mm MATCH NMR tubes were used for experiments conducted on the AV700, and 5 mm conventional NMR tubes were used for experiments conducted on the AV500. Unless otherwise stated, all experiments were conducted at 298 K. Typical experimental parameters were as follows: mixing time 0.8–1 second, relaxation delay 5 seconds, number of transients 64–256. Solvent excitation was achieved using a 16 ms 180 degree selective rectangular shape pulse with 100% truncation level and 1000 points (Squa100.1000) set at the H_2O frequency. Water suppression was achieved by the excitation sculpting method using a 2 ms 180 degree selective Squa100.1000 or Sinc1.1000 pulse at the H_2O frequency. If necessary, protein background suppression was achieved by a 30 ms spin-lock.

6.4 Data treatment

6.4.1 ^{1}H NMR time course

Time course experiments were monitored by ^{1}H NMR as described in Section 6.1.6. The lag time between sample mixing and the end of the first experiment was usually between 3.5 and 5 minutes. Typically, the total experiment time for each spectrum was shorter than 2 minutes. Initial rates were calculated by linear fitting using Excel 2003 (Microsoft) for data points up to 20% turnover.

6.4.2 Kinetic parameters by NMR for BBOX

^{1}H NMR spectra were measured as described in Section 6.1.6. The initial rate was calculated as percentage turnover divided by time. The percentage turnover was less than 20% to ensure the reaction was in the initial phase.

When measuring the kinetic parameters of 2OG, the percentage turnover of 2OG at different 2OG concentrations was monitored by comparing the ^{1}H resonance signals of 2OG and succinate. The substrate (GBB / D-3-fluoro-GBB; Chapter 2) concentration remained constant throughout and was at least twice the K_M value.

When the kinetic parameters of the substrate (GBB / D-3-fluoro-GBB) were measured, the percentage turnover of the relevant substrate at different substrate concentrations was monitored by comparing the methyl signals of the substrate and the product. The 2OG concentration remained constant and was at least twice the 2OG K_M value.

In both experiments, the concentrations of Fe(II), ascorbate and potassium ions were present in excess at constant concentrations. The kinetic parameters were obtained using the Hanes plot.[10] Linear fitting was done using Excel 2003 (Microsoft).

6.4.3 IC_{50} measurement for BBOX inhibitor

^{1}H spectra were measured as described in Section 6.1.6. The initial rate was calculated as percentage turnover of GBB (substrate) to L-carnitine (product) divided by time. The percentage turnover was monitored by integrating the methyl signal of GBB against the methyl signal of L-carnitine. The percentage turnover was less than 20% to ensure the reaction was in the initial phase.

For IC_{50} measurement using ^{19}F NMR (Chapter 2), the reaction mixture was prepared in H_2O-based buffer and the reaction was quenched using 20% acetonitrile-D3. Samples were locked onto acetonitrile-D3. The ^{19}F signals of fluoromethyl-GBB and fluoromethyl-carnitine were monitored.

IC_{50} values were obtained using a standard sigmoid curve. Curve fitting was done using OriginPro 8.0 (OriginLab).

6.4.4 pK_a measurement

pK_a was measured by either ^{1}H NMR (Section 6.1.6) or ^{11}B NMR (Section 6.1.8). Typically, 10 to 15 mL of stock solution was made up in either H_2O or D_2O (no buffer) using a universal tube (Sarstedt). pH were adjusted as described in Section 6.1.2. 500 µL solution was aliquoted at each pH for NMR experiments. pK_a values were obtained using a standard sigmoid curve. Curve fitting was done using OriginPro 8.0 (OriginLab).

6.4.5 Binding constant measurement

Binding constant (K_D) measurements using the water relaxation method (Chapter 3) were obtained using the equation described by Morton *et al*.[11]

$$\Delta_{obs} = \Delta_{max} \times \frac{(K_D + [L]_0 + [P]_0) - \sqrt{(K_D + [L]_0 + [P]_0)^2 - (4 \times [P]_0 \times [L]_0)}}{2 \times [P]_0}$$

Δ_{obs} indicates changes in any observable NMR parameter from the titration, in this case 1-(R_1/$R_{1(0)}$). Δ_{max} indicates the maximum change of the monitored NMR parameter. $[L]_0$ is the titrated ligand concentration. $[P]_0$ is the protein concentration. R_1 is the measured R_1 value at $[L]_0$ and $R_{1(0)}$ is the measured R_1 value when no ligand is present. Typically, a 5 to 10% error in protein concentration was allowed in the curve fitting process, which was conducted using OriginPro 8.0 (OriginLab).

The affinity constants (K_A) between boronic acid and diol (Chapter 5) were fitted using the same equation. In this case, $[P]_0$ is the boronic acid concentration, $[L]_0$ is the diol concentration and K_A is defined as $1/K_D$.

Binding constant (K_D) measurements using the reporter ligand displacement method (Chapter 3) were achieved as described by Dalvit *et al.*[12]

The free concentration of the inhibitor at 50% displacement of the reporter ligand ($K_{D,app}$) is described by:

$$K_{D,app} = \frac{[E_T] \times [L] - [E_T] \times [EL] + [EL]^2 - [L] \times [EL]}{[EL]}$$

In which $[E_T]$ is the total enzyme concentration, [L] is the concentration of the competitive inhibitor and [EL] is the concentration of the enzyme-inhibitor complex. The next step is to correlate the apparent dissociation constant of the competitive inhibitor ($K_{D,app}$) with the total concentration of the reporter ligand used ($[R_T]$) and the dissociation constant of the reporter ligand ($K_{D,rep}$), so that the actual dissociation constant of the inhibitor (K_D) can be determined. Because the concentration of the reporter ligand used in this assay was comparable to the total enzyme concentration, the commonly employed Cheng-Prusoff correlation was not valid due to its assumption of a large excess of reporter ligand.[13] Instead, the correlation described by Nikolovska-Coleska *et al.*[14] and Cer *et al.*[15] was used, in which both the enzyme and reporter concentrations were taken into account.

$$K_D = \frac{K_{D,app}}{\frac{[R_{50}]}{K_{D,rep}} + \frac{[E_0]}{K_{D,rep}} + 1}$$

In which $[R_{50}]$ is the free reporter ligand concentration when 50% of the reporter ligand is displaced from the enzyme and $[E_0]$ is the free enzyme concentration in the presence of the reporter ligand but no inhibitor. $[R_{50}]$ is described by the following equation:

$$[R_{50}] = [R_T] - \frac{[E_T] - [E_0]}{2}$$

In which $[R_T]$ is the total concentration of the reporter ligand. $[E_0]$ can be obtained from the following equation:

$$[E_0] = \frac{-(K_{D,rep} + [R_T] - [E_T]) + \sqrt{(K_{D,rep} + [R_T] - [E_T])^2 + 4 \times [E_T] \times K_{D,rep}}}{2}$$

6.5 Mass spectrometry

6.5.1 Identification of BBOX catalysed reaction products

Scanning mode mass spectrometry (MS) detection was carried out using the LCT Premier ToF mass spectrometer (Waters). MS detection was performed in positive V mode. The capillary and cone voltages were 3000 V and 100 V respectively. The desolvation temperature was 250 ºC and the source temperature was 120 ºC. The cone gas flow and the desolvation gas flow were 30 L min^{-1} and 550 L min^{-1} respectively. The scanning range was set between 80 and 250 amu. The mobile phase contained 50% acetonitrile and 0.1% formic acid in water. Samples were injected bypassing the chromatographic column. 10 µL injection was used.

The reaction mixture was essentially the same as NMR experiments, except it was buffered in 100% H_2O Tris-D11 (pH 7.5). The reaction was quenched by addition of 80% MeCN (final concentration).

6.6 General protein methods

6.6.1 Materials

All chemicals were obtained from Sigma-Aldrich unless otherwise stated.

If necessary, pipette tips (Rainin) and microtubes (Eppendorf) were sterilised using a Falcon benchtop autoclave (LTE Scientific) at 121 ºC for 20 min.

6.6.2 Sodium dodecyl sulfate polyacrylamide gel electrophoresis

The compositions of the SDS-PAGE separating gel and stacking gel are described in Table 6-5 and Table 6-6 respectively. Tris solutions were obtained from Dr Emily Flashman and Andrea Szöllössi. SDS and ammonium persulphate (APS) solutions were freshly made for each gel preparation. The setting of the gel was initiated by the addition of APS and tetramethylethylenediamine (TEMED). A 10-well comb (Bio-rad) was usually used.

Component	Amount required per gel
1.5 M Tris (pH 8.8)	1.25 mL
Milli-Q H_2O	1.57 mL
Acrylamide	2.08 mL
10% (w/v) SDS	50 µL
10% (w/v) APS	50 µL
TEMED	4 µL

Table 6-5 Components for the SDS-PAGE separating gel.

Component	Amount required per gel
0.5 M Tris (pH 6.8)	0.63 mL
Milli-Q H_2O	1.57 mL
Acrylamide	0.25 mL
10% (w/v) SDS	25 µL
10% (w/v) APS	25 µL
TEMED	2.5 µL

Table 6-6 Components for the SDS-PAGE stacking gel.

Typically, 10 to 20 µL of the analyte was mixed with 10 µL of the SDS-PAGE protein loading buffer (Table 6-7). The mixture was then heated for at least 5 minutes at 95 ºC using a Dri-Block DB-1 heat block (Techne). 5 to 10 µL of the mixture was then loaded onto a gel and the electrophoresis was run on a Bio-Rad Mini Protean II system at a constant potential of 220 V (Bio-Rad Power Pac 300) for 50 minutes. The SeeBlue pre-stained protein standard (Invitrogen) was used for molecular weight visualisation. The components of the SDS-PAGE protein loading buffer and the running buffer are summaried in Table 6-7 and Table 6-8 respectively.

The gel was then removed from the cast and was stained (Table 6-9) for at least 15 minutes. It was then transferred to a destain solution (Table 6-10) to destain overnight.

Component	Amount per 100 mL
0.5 M Tris (pH 6.8)	10 mL
Milli-Q H_2O	20 mL
Glycerol	40 mL
10% (w/v) SDS	20 mL
β-Mercaptoethanol	10 mL
Bromophenol blue	~1 mg

Table 6-7 Components for the SDS-PAGE protein loading buffer.

Component	Amount per litre
Tris	3.03 g
Glycine	1.44 g
SDS	1 g

Table 6-8 SDS-PAGE running buffer included 25 mM Tris, 19.2 mM glycine and 0.1% SDS. The solution was buffered at pH 8.8.

Component	Amount per litre
Coomassie blue	5 g
Methanol	500 mL
Acetic acid	100 mL
Milli-Q H_2O	400 mL

Table 6-9 Coomassie stain solution contained 0.5% coomassie blue, 50% methanol and 10% acetic acid.

Component	Amount per litre
Methanol	100 mL
Acetic acid	100 mL
Milli-Q H_2O	800 mL

Table 6-10 Destain solution contained 10% methanol and 10% acetic acid.

6.6.3 Protein concentration determination

Concentrations of purified proteins were determined by measuring the A_{280} using an ND-1000 spectrophotometer (NanoDrop Technologies). The *Protein A280* and *Other protein (E & MW)* options were used. Protein buffer solution was used as blank. Protein molecular weights and extinction coefficients were calculated using the ProtParam tool.[16] Typically, 2 µL of the analyte was used per measurement. All measurements were conducted at least three times.

6.7 Production and purification of $PHD2_{181-426}$

6.7.1 Transformation

Modified pET-24a(+) construct (obtained from Dr Emily Flashman) was used to generate $PHD2_{181-426}$, and was transformed into *Escherichia coli* BL21 (DE3)

competent cell (obtained from Dr Emily Flashman). The general transformation protocol was as follows. 1 µL of the plasmid DNA was first added to 35 µL of competent cell in a 500 µL sterilised Eppendorf microtube on ice. The mixture was incubated on ice for 20 minutes. The mixture was then 'heat shocked' in a 42 ºC water bath for 45 seconds, and was returned to ice immediately afterwards for one minute. 200 µL of super optimal broth with catabolite repression (SOC) medium (obtained from Dr Emily Flashman) was then added to the mixture, followed by incubation in a water bath at 37 ºC for 30 minutes. Finally, 100 µL of the transformation mixture was plated on a kanamycin agar plate (obtained from Dr Emily Flashman, Dr Anna Boleininger, Sarah L. Davies and Andrea Szöllössi) in a HeraSafe KS12 Class II Biosafety Cabinet laminar flow hood (Thermo Fisher Scientific). The plate was then left to dry in the flow hood. Once the plate was dried, it was transferred to a Hereus TypB 6030 incubator (Thermo Fisher Scientific) and was incubated overnight at 37 ºC.

6.7.2 2TY growth media

The composition of making the 2TY growth medium shown in Table 6-11.

Component	Amount per litre
Tryptone	16 g
Yeast Extract	10 g
NaCl	5 g

Table 6-11 2TY medium composition (1 L).

Growth medium was autoclaved using a TouchClave autoclave (LTE Scientific; operated by Herminio Manso Jubier) at 121 ºC for 20 min before use.

6.7.3 Starter culture

A single colony from the agar plate was picked and inoculated into a starting culture containing 100 mL 2TY medium and 3 mg kanamycin (Melford Laboratories) in a 500 mL Erlenmeyer culture flask (Schott) in the flow hood. It was then incubated overnight at 37 ºC in a G25 environmental incubator shaker (New Brunswick Scientific) with a shaking rate typically between 180 and 250 rpm.

6.7.4 Large scale growth

Large scale growth were conducted using 2000 mL Erlenmeyer culture flasks (Schott) each containing 600 mL 2TY medium and 18 mg kanamycin (typically, 12 flasks

were used per production). 7 mL of the starting culture were added to each flask, which were then incubated at 37 ºC in a Innova 44 Incubator Shaker (New Brunswick Scientific) with a shaking rate typically between 180 and 220 rpm until the cell density reached an OD_{600} between 0.6 and 0.8 (typically around 2 hours). OD_{600} was measured using a Novaspec II spectrophotometer (Pharmacia) at 600 nm wavelength using 1 mL cuvettes (Bio-rad). Once the OD_{600} was reached, 71.4 mg of the promoter isopropyl-β-D-thiogalactopyranoside (IPTG; Melford Laboratories) was added to each flask (500 µM final concentration). The flasks were then incubated at 37 ºC for another 3 to 5 hours. The cells were harvested by centrifugation using Avanti J-25 centrifuge (Beckman Coulter) and a JLA 9.1000 rotor (Beckman Coulter) at a speed of 8500 rpm at 4 ºC for 25 minutes. The cells were stored in a resealable plastic bag at -80 ºC in a U570 premium ultra low temperature freezer (New Brunswick Scientific).

6.7.5 Protein purification by cation exchange chromatography

The components of the start and elution buffers for S-Sepharose cation exchange chromatography are described in Table 6-12 and Table 6-13. All buffers were prepared using Milli-Q H_2O, filtered through a 0.22 µm filter (Millipore) and degassed under vacuum before use.

Component	Amount per litre
MES hydrate	19.5 g

Table 6-12 The start buffer contained 100 mM MES (pH 5.8).

Component	Amount per litre
MES hydrare	19.5 g
NaCl	58.4 g

Table 6-13 The elution buffer contained 100 mM MES and 1 M NaCl (pH 5.8).

Typically, around 20 g of cells were resuspended using 120 mL start buffer. Approximately 1 mg DNAse 1 (Roche Diagnostics) and 1 µM $MgCl_2$ (final concentration) were added to the mixture. The mixture was then stirred on a hotplate stirrer in a cold room at 4 ºC until the cells were re-suspended. The cells were lysed on ice by sonication (4 × 45 seconds bursts at 60% amplitude with 45 seconds rest in between) using a Vibra Cell VCX 500 equipped with a 13 mm probe (Sonics). Debris was removed by centrifugation, first at 15000 rpm for 20 minutes at 4 ºC (JLA 16.250 rotor; Beckman Coulter) and then at 21000 rpm for 20 minutes at 4 ºC (JA 25.50

rotor; Beckman Coulter). The supernatant was then filtered using a 0.45 µM filter (Millipore).

Protein purification was carried out using a AKTA fast protein liquid chromatography system (FPLC; GE Healthcare) in a cold room at 4 ºC. A 50 mL S-Sepharose column (provided by Wendy J. Sobey) was used with a flow rate no higher than 4 mL per minute. The column was initially prepared by washing with 2 column volumes of Milli-Q H_2O, 2 column volumes of 1M NaCl and 2 column volumes of the start buffer. The cell lysate was then loaded onto the column and was washed with the start buffer until the A_{280} trace flattened out. The protein was eluted in 5 mL fractions using the elution buffer at a gradient of 0 to 100% over 35 minutes. The A_{280} trace and SDS-PAGE were used to determine which fractions contained the purified protein.

6.7.6 *Apo*-protein production

The fractions containing the purified protein were then diluted to a final concentration of <1 mg/mL in 200 mM EDTA and 15 mM ammonium acetate (pH 7.0 to 8.0). The mixture was incubated overnight at 4 ºC. Finally, the mixture was concentrated to 2 mL volume using Amicon Ultra-4 or Amicon Ultra-15 centrifugal filter units (Molecular weight cut-off: 10 kDa; Millipore) in an Allegra 21R centrifuge (Beckman Coulter; S4180 rotor; 4000 rpm; 4 ^{o}C; 20 minutes per run).

6.7.7 Protein purification by size exclusion chromatography

The components of the buffer used for size exclusion chromatography are described in Table 6-14. The buffer was filtered through a 0.22 µm filter (Millipore) and degassed under vacuum before use.

Component	Amount per litre
Tris	12.1 g
NaCl	5.84 g

Table 6-14 The size exclusion buffer contained 100 mM Tris and 100 mM NaCl (pH 7.5).

Size exclusion chromatography was conducted using a 300 mL Superdex 75 size exclusion chromatography column (GE Healthcare; provided by Wendy J. Sobey) at a flow rate of 2 mL per minute. The column was prepared by washing with 1 column volume of Milli-Q H_2O and 1 column volume of the gel filtration buffer. The protein (2 mL) was loaded onto the column with a 2 mL injection loop. The protein was

eluted over 1 column volume of the size exclusion buffer, and 5 mL fractions were collected. A_{280} trace and SDS-PAGE were used to determine the fractions that contained the purified protein. Finally, the proteins were buffer exchanged into NMR buffer (50 mM Tris-D11 pH 7.5 and 0.02% NaN_3 in either H_2O or D_2O) by spin concentration using Amicon Ultra-4 or Amicon Ultra-15 centrifugal filter units (Molecular weight cut-off: 10 kDa; Millipore). At least five rounds of dilution and concentration were performed at 4 ºC. Purified proteins were stored at -80 ºC until use.

6.8 Production and purification of ^{15}N-labelled and ^{13}C,^{15}N-labelled PHD2$_{181-402}$

6.8.1 M9 minimal media

M9 salt solution (Table 6-15) was prepared and autoclaved using a Falcon benchtop autoclave (LTE Scientific) at 121 ºC for 20 min. The phosphate salts were obtained from BDH Chemicals. ^{15}N-labelled HN_4Cl was obtained from Cambridge Isotope Laboratories, Euriso-Top or Cortecnet.

Component	Amount per litre
Na_2HPO_4	6.0 g
KH_2PO_4	3.0 g
NH_4Cl	1.0 g
NaCl	0.5 g
$CaCl_2$	0.3 mg

Table 6-15 Composition of M9 salt solution (1 L).

The solutions described in Table 6-16 were then added to the M9 salt solution after it was cooled down to room temperature. These solutions were syringe filtered (0.22 µm filter; Millipore) because they were heat sensitive and could not be autoclaved. Isotopic labelled glucose was obtained from Cortecnet.

Component	Amount per litre
1M $MgSO_4 \cdot H_2O$	500 µL
20% (w/v) glucose	50 mL (20 mL)
0.5% (w/v) vitamin B1	50 µL

Table 6-16 Amount of solutions to be added to per litre of the M9 salt solution. If isotopic labelled glucose was used, a reduced amount (20 mL) was added.

6.8.2 Starter culture

A glycerol stock of *E. coli* BL21 (DE3) containing the pET-28a(+) construct was used for the production of isotopic labelled $PHD2_{181-402}$ (obtained from Dr Adam P. Hardy). Normal 2TY growth medium was used for the starter culture and the growth procedure used was identical to that described in Section 6.7.3.

6.8.3 Large scale growth

The large scale growth procedure was largely identical to that described in Section 6.7.4. 2000 mL Erlenmeyer culture flasks (Schott) each containing 600 mL M9 minimal medium and 18 mg kanamycin (typically 12 flasks were used per production) were used. 12 mL of the starting culture was added to each flask, which were then incubated at 37 ºC until the cell density reached an OD_{600} between 0.6 and 0.8 (typically around 4.5 hours). Once the OD_{600} was reached, 28.6 mg IPTG was added to each flask (200 µM final concentration). The cultures were then incubated at 28 ºC overnight (typically around 15 hours).

6.8.4 Protein purification using gravity flow nickel affinity chromatography

A small scale gravity flow nickel affinity column containing 2 mL His·Bind resin (Novagen) was used for purification (obtained from Dr Adam P. Hardy).

The preparation of cell lysate largely follows the procedure described in Section 6.7.5. Typically, 20 g of cells were resuspended in 100 mL binding buffer (Table 6-17) and 1 mg DNAse 1. The cells were lysed on ice by sonication (4× 20 seconds bursts at 60% amplitude with 40 seconds rest in between). Debris was removed by centrifugation at 21000 rpm for 25 minutes and the supernatant was filtered using a 0.45 µm filter (Millipore).

Component	Amount per litre
Imidazole	0.34 g
NaCl	29.2 g
HEPES	11.9 g

Table 6-17 Binding buffer contained 5 mM imidazole, 500 mM NaCl and 50 mM HEPES buffered at pH 7.8.

The gravity flow column was prepared by washing with 40 mL Milli-Q H_2O. The resin was charged using 5 mL nickel charge buffer (Table 6-18), followed by 9 mL binding buffer. The cell lysate was then loaded onto the column. It was then washed

with 15 mL wash buffer (Table 6-19). Proteins were eluted in 6× 1 mL fractions using elution buffer (Table 6-20).

Component	Amount per litre
$NiSO_4 \cdot 7H_2O$	14.0 g

Table 6-18 Charge buffer contained 50 mM $NiSO_4$ (no buffer).

Component	Amount per litre
Imidazole	2.0 g
NaCl	29.2 g
HEPES	11.9 g

Table 6-19 Wash buffer contained 30 mM imidazole, 500 mM NaCl and 50 mM HEPES buffered at pH 7.8.

Bradford reagent (obtained from Dr Adam P. Hardy) and SDS-PAGE were used to determine the fractions that contained the purified protein. Bradford reagent was measured using a Novaspec II spectrophotometer (Pharmacia) at 595 nm wavelength using 1 mL cuvettes (Bio-rad). Finally, the column was stored in strip buffer (Table 6-21).

Component	Amount per litre
Imidazole	34.0 g
NaCl	29.2 g
HEPES	11.9 g

Table 6-20 Elute buffer contained 500 mM imidazole, 500 mM NaCl and 50 mM HEPES buffered at pH 7.8.

Component	Amount per litre
EDTA	37.2 g
NaCl	29.2 g
HEPES	11.9 g

Table 6-21 Strip buffer contained 500 mM imidazole, 500 mM NaCl and 50 mM HEPES buffered at pH 7.8.

6.8.5 Removal of the His-tag

Thrombin (Novagen) was used to remove the His-tag from the purified protein. 0.5 unit of the protease was added per mg of purified protein, and the 10× thrombin cleavage buffer (Novagen) was diluted to 1× with the protein solution accordingly. The mixture was then incubated at 4 ºC for around 20 hours.

6.8.6 *Apo*-protein production

Apo-protein production was achieved as described in Section 6.7.6.

6.8.7 Buffer exchange

After thrombin and EDTA treatments, the protein was concentrated to a volume of 2.5 mL. Buffer exchange into the NMR buffer (50 mM Tris-D11 pH 6.6 and 0.02% NaN_3 in H_2O) was achieved in two steps.

The first step involved the use of a gravity flow PD10 column (GE Healthcare). The column was prepared by washing with 20 mL Milli-Q H_2O and 20 mL NMR buffer. 2.5 mL of the protein was then loaded onto the column, which was then eluted with 3.5 mL of the NMR buffer.

The second step involved spin concentration using Amicon Ultra-4 or Amicon Ultra-15 centrifugal filter units (Molecular weight cut-off: 10 kDa; Millipore). At least five rounds of dilution and concentration were performed at 4 ºC. The purity of the protein was checked by SDS-PAGE and the purified protein was stored at -80 ºC until use.

6.9 Production and purification of $^{2}H,^{13}C,^{15}N$-labelled $PHD2_{181-402}$

6.9.1 M9 minimal media

The components of the M9 minimal media is identical to those described in Section 6.8.1, except all solutions were made up in D_2O. In order to prevent H-D exchange, all solutions were not autoclaved, instead they were syringe filter sterilised with a 0.22 μm filter (Millipore) in the flow hood. The culture flasks were autoclaved separately.

6.9.2 Starter culture

The procedure was similar to that described in Section 6.8.2, except the overnight incubation was conducted at 30 ºC. Typically, 200 mL of starter culture was prepared.

6.9.3 Large scale growth

The overnight culture (200 mL) was divided into eight 50 mL falcon tubes (25 mL each) and was gently spun down at 2000 rpm at 4 ºC. The supernatants were then discarded. For each tube, the cells were resuspended with 12.5 mL D_2O-based M9

minimal media containing 375 µg kanamycin. The resuspended cells were then incubated at 30 ºC for a further 30 minutes.

Large scale growth was conducted using ten 2000 mL Erlenmeyer culture flasks (Schott). Each flask contained 500 mL D_2O-based M9 minimal medium and 15 mg kanamycin. 10 mL of the resuspended starting culture were added to each flask, and the flasks were then incubated at 30 ºC until the cell density reached an OD_{600} of 1.0. Once the OD_{600} was reached, 59.6 mg IPTG was added to each flask (500 µM final concentration). The flasks were then incubated at 28 ºC for 15 hours.

6.9.4 Protein purification

Protein purification, His-tag removal, metal removal and buffer exchange were achieved as described in Sections 6.8.4 to 6.8.7.

6.10 Expression trials

6.10.1 Starter culture

The procedure was identical to that described in Section 6.8.2. The overnight incubations were conducted at 37 ºC for the trials of ^{15}N and ^{13}C,^{15}N-labelled $PHD2_{181-402}$, and at 30 ºC for the trial of the triple ^{2}H,^{13}C,^{15}N-labelled $PHD2_{181-402}$.

6.10.2 Expression trial for the production of ^{15}N-labelled $PHD_{181-402}$

The trial was conducted using six 500 mL Erlenmeyer culture flasks (Schott). Each flask contained 100 mL M9 minimal media, 1 g glucose and 3 mg kanamycin.

1 mL of the starter culture was added to each flask. Cultures were incubated at 37 ºC until they reached an OD_{600} between 0.6 and 0.8. The cultures were then divided into two sets of three flasks, and IPTG was added to each flask (200 µM, 500 µM and 1 mM final concentrations for each set). The two sets of flasks were then transferred to different incubators (28 ºC and 37 ºC) and were further incubated at the new temperatures overnight.

The conditions tested are summarised in Table 6-22.

IPTG concentration	200 µM, 500 µM and 1 mM
Incubation temperature	28 ºC and 37 ºC

Table 6-22 Conditions tested for the production of ^{15}N-labelled $PHD2_{181-402}$.

6.10.3 Expression trial for the production of $^{15}N,^{13}C$-labelled $PHD_{181-402}$

The trial was conducted using eight 500 mL Erlenmeyer culture flasks (Schott). The flasks were divided into two sets of four flasks. Each flask contained 100 mL M9 minimal media and 3 mg of kanamycin but different glucose concentrations (200 mg, 400 mg, 700 mg and 1 g for each set).

1 mL of the starter culture was added to each flask. Cultures were incubated at 37 ºC until they reached an OD_{600} between 0.6 and 0.8. IPTG was then added to each flask (200 µM final concentration for one set, and 500 µM final concentration for the other set). The cultures were then incubated at 28 ºC overnight. The conditions tested are summarised in Table 6-23.

Glucose concentration	2 g/L, 4 g/L, 7 g/L and 10 g/L
IPTG concentration	200 µM and 500 µM

Table 6-23 Conditions tested for the production of $^{13}C,^{15}N$-labelled $PHD2_{181-402}$.

6.10.4 Expression trial for the production of $^{2}H,^{15}N,^{13}C$-labelled $PHD_{181-402}$

The overnight culture (100 mL) was gently spun down in four 50 mL falcon tubes (25 mL each) at 2000 rpm at 4 ºC. The supernatants were discarded. For each tube, the cells were resuspended with 12.5 mL D_2O-based M9 minimal media containing 50 mg glucose and 375 µg kanamycin. The resuspended cells were then incubated at 30 ºC for a further 30 minutes.

The trial was conducted using eight 250 mL Erlenmeyer culture flasks (Schott), each containing 50 mL D_2O-based M9 minimal medium containing 200 mg glucose and 1.5 mg kanamycin. 1 mL of the resuspended starting culture was added to each flask, and they were incubated at 30 ºC. The flasks were initially divided into two sets of four flasks. For one set, the flasks were removed from the incubator when the OD_{600} reached 0.6; and for the other set, when the OD_{600} reached 1.0. For each set, once the desired OD_{600} was reached, they were sub-divided into two subsets of two flasks. IPTG was then added to each flask (200 µM and 500 µM final concentrations per subset). One subset was then incubated at 15 ºC and the other subset was incubated at 28 ºC.

5 mL samples were removed from each flask 15 hours, 24 hours and 48 hours after the addition of IPTG. The conditions tested are summarised in Table 6-24.

OD_{600} for induction	0.6 and 1.0
IPTG concentration	200 µM and 500 µM
Incubation temperature	15 ºC and 28 ºC

Table 6-24 Conditions tested for the production of triple ^{2}H,^{13}C,^{15}N-labelled $PHD2_{181-402}$.

6.10.5 Analysis

For each condition tested, 1.5 mL of the culture was transferred to a 1.6 mL Eppendorf microtube. It was then centrifuged for 5 minutes using an accuSpin Micro benchtop centrifuge (Thermo Fisher Scientific) at 13000 rpm at room temperature. The supernatant was discarded and the sample was stored at -80 ºC for at least one hour. It was then thawed on ice and the cells were resuspended in 300 µL of binding buffer (Table 6-17). After the resuspension, 25 µL of the sample was removed to a separate Eppendorf microtube to be analysed as the "whole cell sample". The rest of the resuspended cells were lysed by sonication on ice (1× 30 second burst) using a Soniprep 150 sonicator (Sanyo) at 10 microns amplitude. The tube was then centrifuged at room temperature for 5 minutes. The cell lysate was removed to a separate Eppendorf microtube to be analysed as the "soluble fraction sample".

The protein production levels of both the "whole cell sample" and the "soluble fraction sample" were analysed by SDS-PAGE as described in Section 6.6.2.

6.11 References

1. Glasoe, P. K.; Long, F. A. Use of glass electrodes to measure acidities in deuterium oxide. *J. Phys. Chem.* **1960**, *64*, 188–190.
2. Wu, P. S. C.; Otting, G. Rapid Pulse Length Determination in High-Resolution NMR. *J. Magn. Reson.* **2005**, *176*, 115–119.
3. Vranken, W. F.; Boucher, W.; Stevens, T. J.; Fogh, R. H.; Pajon, A.; Llinas, M.; Ulrich, E. L.; Markley, J. L.; Ionides, J.; Laue, E. D. The CCPN data model for NMR spectroscopy: development of a software pipeline. *Proteins Struct. Funct. Bioinf.* **2005**, *59*, 687–696.
4. Aguilar, J. A.; Nilsson, M.; Bodenhausen, G.; Morris, G. A. Spin echo NMR spectra without J modulation. *Chem. Commun.* **2012**, *48*, 811–813.
5. Enthart, A.; Freudenberger, J. C.; Furrer, J.; Kessler, H.; Luy, B. The CLIP/CLAP-HSQC: pure absorptive spectra for the measurement of one-bond couplings. *J. Magn. Reson.* **2008**, *192*, 314–322.
6. Mao, X; Guo, J.; Ye, C. Competition Between Radiation Damping and Transverse Relaxation Effects on NMR Signal Intensities. *Chem. Phys. Lett.* **1994**, *218*, 249–253.
7. Mao, X.; Guo, J.; Ye, C. Radiation Damping Effects on Spin-Lattice Relaxation Time Measurements. *Chem. Phys. Lett.* **1994**, *222*, 417–421.
8. Mayer, M.; Meyer, B. Characterization of ligand binding by saturation transfer difference NMR spectroscopy. *Angew. Chem. Int. Ed.* **1999**, *38*, 1784–1788.
9. Dalvit, C.; Pevarello, P.; Tató, M.; Veronesi, M.; Vulpetti, A.; Sundström, M. Identification of compounds with binding affinity to proteins via magnetization transfer from bulk water. *J. Biomol. NMR* **2000**, *18*, 65–68.
10. Hanes, C. S. Studies on plant amylases: The effect of starch concentration upon the velocity of hydrolysis by the amylase of germinated barley. *Biochem. J.* **1932**, *26*, 1406–1421.
11. Morton, C. J.; Pugh, D. J. R.; Brown, E. L. J.; Kahmann, J. D.; Renzoni, D. A. C.; Campbell, I. D. Solution structure and peptide binding of the SH3 domain from human Fyn. *Structure* **1996**, *4*, 705–714.
12. Dalvit, C.; Flocco, M.; Knapp, S.; Mostardini, M.; Perego, R.; Stockman, B. J.; Veronesi, M.; Varasi, M. High-throughput NMR-based screening with competition binding experiments. *J. Am. Chem. Soc.* **2002**, *124*, 7702–7709.
13. Cheng, Y.-C.; Prusoff, W. H. Relationship between the inhibition constant (KI) and the concentration of inhibitor which causes 50 per cent inhibition (I50) of an enzymatic reaction. *Biochem. Pharmacol.* **1973**, *22*, 3099–3108.
14. Nikolovska-Coleska, Z.; Wang, R.; Fang, X.; Pan, H.; Tomita, Y.; Li, P.; Roller, P. P.; Krajewski, K.; Saito, N. G.; Stuckey, J. A.; Wang, S. Development and optimization of a binding assay for the XIAP BIR3 domain using fluorescence polarization. *Anal. Biochem.* **2004**, *332*, 261–273 http://sw16.im.med.umich.edu/software/calc_ki (accessed Aug 31, 2012).
15. Cer, R. Z.; Mudunuri, U.; Stephens, R.; Lebeda, F. J. IC_{50}-to-K_i: a web-based tool for converting IC_{50} to K_i values for inhibitors of enzyme activity and ligand binding. *Nucl. Acids Res.* **2009**, *37*, W441–W445 http://botdb.abcc.ncifcrf.gov (accessed Aug 31, 2012).
16. Gasteiger, E.; Hoogland, C.; Gattiker, A.; Duvaud, S.; Wilkins, M. R.; Appel, R. D.; Bairoch, A. Protein Identification and Analysis Tools on the ExPASy Server. In *The Proteomics Protocols Handbook*; Walker, J. M., Ed.; Humana Press: New Jersey, 2005; Chapter 52, pp 571–607 http://expasy.org (accessed Aug 31, 2012).

Appendix I. Protein backbone assignment for $PHD2_{181-402}$-Zn(II)-2OG-alanine substituted CODD variants

Protein backbone assignment for $PHD2_{181-402}$-Zn(II)-2OG-D556A CODD (sequence: ALDLEMLAPYIPMDDDFQL).

Transfer of ^{1}H and ^{15}N assignment				
	^{15}N-$PHD2_{181-402}$-Zn(II)-2OG-CODD		^{15}N-$PHD2_{181-402}$-Zn(II)-2OG-D556A CODD	
Residue	^{1}H	^{15}N	^{1}H	^{15}N
G				
S	8.54	115.47	8.54	115.47
H	8.61	120.70	8.61	120.73
M	8.32	122.67	8.31	122.69
A	8.36	126.06	8.36	126.06
S	8.25	116.25	8.24	116.22
P181				
N182	8.60	119.73	8.60	119.73
G183	8.30	109.27	8.30	109.26
Q184	8.16	119.61	8.16	119.61
T185				
K186	8.19	125.08	8.18	125.05
P187				
L188				
P189				
A190	8.32	123.08	8.31	123.01
L191	7.94	116.86	7.93	116.89
K192	7.21	117.45	7.21	117.56
L193				
A194	8.06	119.86	8.07	119.82
L195	7.97	112.82	7.98	112.80
E196				
Y197	7.21	117.10	7.21	117.16
I198	8.63	121.20	8.60	121.09
V199	8.44	116.09	8.42	116.04
P200				
C201	7.70	116.41	7.68	116.40
M202	8.54	117.76	8.54	117.77
N203	8.43	117.02	8.42	116.95
K204	7.86	117.25	7.85	117.29
H205	8.40	112.54	8.38	112.64
G206	8.52	111.15	8.49	111.11
I207	6.58	115.82	6.58	115.83
C208				
V209	8.69	130.40	8.70	130.43
V210				
D211	8.36	125.70	8.36	125.69
D212	8.57	117.75	8.57	117.80
F213	8.42	117.37	8.43	117.40
L214				
G215	10.19	115.52	10.19	115.55
K216	8.12	117.94	8.11	117.93
E217	8.47	119.25	8.47	119.25
T218	8.64	118.59	8.63	118.56
G219	8.50	108.66	8.50	108.67
Q220	8.44	120.83	8.45	120.82
Q221	7.51	120.11	7.50	120.14
I222	7.99	119.90	7.99	119.87
G223	8.33	107.24	8.32	107.21
D224	8.45	122.58	8.44	122.64
E225	8.11	122.24	8.11	122.38
V226				
R227	8.20	120.42	8.20	120.42
A228	7.79	121.00	7.79	120.99
L229	7.74	119.21	7.73	119.23
H230	8.41	119.59	8.41	119.64
D231	8.80	121.52	8.80	121.52
T232	7.35	108.27	7.35	108.27
G233	7.47	108.03	7.47	108.04
K234	7.45	115.88	7.45	115.88
F235	8.55	121.08	8.55	121.06
T236	9.40	113.47	9.41	113.47
D237	8.48	121.18	8.47	121.18
G238	8.04	109.25	8.05	109.25
Q239				
L240				
V241				
S242				
Q243				
K244				
S245	8.13	116.16	8.14	116.27
D246	8.37	120.83	8.38	120.91
S247	8.00	114.05	7.99	113.95
S248	8.47	119.99	8.45	119.86
K249	7.94	121.75	7.94	121.78
D250	8.03	117.11	8.04	117.00
I251	7.75	121.72	7.74	121.61
R252	7.92	114.05	7.92	114.04
G253	8.73	110.46	8.73	110.52
D254	9.35	116.28	9.35	116.26
K255				
I256	9.59	114.96	9.59	114.95
T257	7.93	113.06	7.93	113.07
W258	7.88	124.78	7.87	124.78
I259	9.74	126.04	9.74	126.03
E260	11.23	129.03	11.24	129.08
G261	9.91	109.41	9.91	109.40
K262	6.71	116.63	6.70	116.63
E263	10.54	126.65	10.54	126.68
P264				
G265	8.98	113.83	8.99	113.91
C266	7.54	115.01	7.55	115.05
E267	9.03	120.57	9.03	120.51

T268	9.79	120.90	9.89	121.16
I269				
G270	8.38	106.99	8.38	106.95
L271	7.55	125.49	7.55	125.53
L272				
M273				
S274				
S275				
M276				
D277				
D278				
L279				
I280				
R281				
H282	7.58	113.99	7.58	114.08
C283	7.57	115.76	7.57	115.73
N284	7.52	117.03	7.53	117.06
G285	8.63	112.69	8.63	112.78
K286	7.91	116.16	7.92	116.21
L287	7.56	120.34	7.55	120.34
G288	8.71	114.34	8.70	114.33
S289	7.70	118.88	7.70	118.94
Y290	7.16	120.13	7.16	120.12
K291	9.07	126.01	9.06	125.99
I292	8.48	125.11	8.48	125.08
N293	8.31	125.27	8.31	125.21
G294	7.79	108.73	7.79	108.76
R295	9.04	115.23	9.04	115.21
T296	7.86	108.60	7.86	108.62
K297	7.90	115.46	7.91	115.48
A298	8.34	121.00	8.34	121.00
M299	9.70	124.93	9.71	124.96
V300	8.49	129.83	8.49	129.84
A301	8.89	127.80	8.89	127.79
C302	9.14	120.27	9.14	120.24
Y303	9.03	129.91	9.03	129.98
P304				
G305				
N306				
G307				
T308				
G309				
Y310				
V311	8.07	119.18	8.07	119.11
R312	8.06	120.24	8.06	120.29
H313	8.72	122.03	8.70	122.00
V314	8.17	117.17	8.19	117.18
D315	9.11	128.94	9.11	128.97
N316	7.12	106.18	7.13	106.12
P317				
N318	8.36	118.78		
G319	8.20	112.80	8.21	112.89
D320	8.92	119.45	8.89	119.33
G321	9.15	106.62	9.18	106.69
R322				
C323	9.69	121.22	9.70	121.14
V324	7.29	125.71	7.29	125.72
T325				
C326				
I327				
Y328				
Y329				
L330				
N331				
K332				
D333				
W334				
D335				
A336				
K337				
V338				
S339				
G340				
G341				
I342				
L343	7.63	127.15	7.63	127.13
R344	8.82	130.87	8.82	130.90
I345	8.82	125.98	8.82	125.98
F346	8.48	125.42	8.48	125.38
P347				
E348	9.25	123.75	9.24	123.92
G349	8.91	111.72	8.90	111.83
K350	7.55	119.05	7.55	119.00
A351	8.28	122.42	8.29	122.42
Q352	7.35	115.83	7.35	115.78
F353	7.03	118.96	7.02	118.98
A354	9.00	124.43	9.00	124.43
D355	8.25	123.39	8.25	123.42
I356	9.67	126.42	9.68	126.49
E357	8.31	125.65	8.31	125.67
P358				
K359	7.44	122.37	7.44	122.33
F360	7.14	119.19	7.13	119.30
D361	7.63	125.75	7.63	125.73
R362				
L363				
L364				
F365				
F366				
W367	7.15	117.83	7.16	117.87
S368	7.53	114.30	7.53	114.30
D369	7.74	119.49	7.74	119.52
R370	7.64	110.69	7.63	110.69
R371	8.30	118.79	8.27	118.72
N372	7.39	110.84	7.38	110.82
P373				
H374	8.95	118.35	8.95	118.36
E375	9.01	116.19	9.02	116.26
V376	9.21	123.12	9.19	123.09
Q377	8.66	127.84	8.66	127.87
P378				
A379				
Y380				
A381	7.65	121.78	7.65	121.74
T382	8.18	116.06	8.18	116.04
R383	8.37	130.46	8.36	130.45

Y384	9.70	127.04	9.69	127.07
A385	8.52	121.81	8.52	121.81
I386				
T387				
V388				
W389				
Y390				
F391	8.73	121.18	8.73	121.17
D392	8.36	119.49	8.36	119.51
A393	9.35	128.87	9.35	128.83
D394	8.28	118.05	8.27	118.06
E395	8.78	122.10	8.77	122.11
R396	8.75	118.22	8.76	118.21
A397	7.41	118.58	7.40	118.55
R398	7.44	116.98	7.44	117.02
A399	7.63	121.35	7.64	121.35
K400	7.09	114.94	7.08	114.91
V401	7.21	118.00	7.21	118.01
K402	7.60	129.41	7.59	129.54

Table I-i Protein backbone assignments of $PHD2_{181-402}$-Zn(II)-2OG-CODD and $PHD2_{181-402}$-Zn(II)-2OG-D556A CODD.

Protein backbone assignment for $PHD2_{181-402}$-Zn(II)-2OG-L557A CODD (sequence: DADLEMLAPYIPMDDDFQL).

Transfer of ^{1}H and ^{15}N assignment				
	^{15}N-$PHD2_{181-402}$-Zn(II)-2OG-CODD		^{15}N-$PHD2_{181-402}$-Zn(II)-2OG-L557A CODD	
Residue	^{1}H	^{15}N	^{1}H	^{15}N
G				
S	8.54	115.47	8.54	115.47
H	8.61	120.70	8.61	120.71
M	8.32	122.67	8.31	122.68
A	8.36	126.06	8.36	126.06
S	8.25	116.25	8.24	116.24
P181				
N182	8.60	119.73	8.60	119.73
G183	8.30	109.27	8.30	109.26
Q184	8.16	119.61	8.16	119.61
T185				
K186	8.19	125.08	8.18	125.08
P187				
L188				
P189				
A190	8.32	123.08	8.32	123.04
L191	7.94	116.86	7.94	116.86
K192	7.21	117.45	7.21	117.56
L193				
A194	8.06	119.86	8.06	119.86
L195	7.97	112.82	7.97	112.82
E196				
Y197	7.21	117.10	7.21	117.08
I198	8.63	121.20		
V199	8.44	116.09	8.43	116.04
P200				
C201	7.70	116.41	7.69	116.42
M202	8.54	117.76	8.53	117.77
N203	8.43	117.02	8.43	117.01
K204	7.86	117.25	7.86	117.23
H205	8.40	112.54	8.39	112.51
G206	8.52	111.15	8.51	111.15
I207	6.58	115.82	6.58	115.83
C208				
V209	8.69	130.40	8.72	130.42
V210				
D211	8.36	125.70		
D212	8.57	117.75	8.57	117.81
F213	8.42	117.37	8.44	117.34
L214				
G215	10.19	115.52	10.19	115.50
K216	8.12	117.94	8.11	117.91
E217	8.47	119.25	8.47	119.26
T218	8.64	118.59	8.63	118.56
G219	8.50	108.66	8.50	108.67
Q220	8.44	120.83	8.44	120.83
Q221	7.51	120.11	7.50	120.13
I222	7.99	119.90	7.99	119.89
G223	8.33	107.24	8.33	107.19
D224	8.45	122.58	8.45	122.58
E225	8.11	122.24	8.11	122.24
V226				
R227	8.20	120.42	8.20	120.42
A228	7.79	121.00	7.79	121.00
L229	7.74	119.21	7.74	119.19
H230	8.41	119.59	8.41	119.62
D231	8.80	121.52	8.80	121.53
T232	7.35	108.27	7.35	108.28
G233	7.47	108.03	7.47	108.03
K234	7.45	115.88	7.45	115.88
F235	8.55	121.08	8.55	121.09
T236	9.40	113.47	9.41	113.49
D237	8.48	121.18	8.47	121.19
G238	8.04	109.25	8.04	109.25
Q239				
L240				
V241				
S242				
Q243				
K244				
S245	8.13	116.16	8.11	116.08
D246	8.37	120.83	8.37	120.89
S247	8.00	114.05	7.99	114.00
S248	8.47	119.99	8.50	120.23
K249	7.94	121.75	7.94	121.74
D250	8.03	117.11	8.02	117.18
I251	7.75	121.72	7.75	121.77
R252	7.92	114.05	7.92	114.01
G253	8.73	110.46	8.73	110.50
D254	9.35	116.28	9.35	116.25
K255				
I256	9.59	114.96	9.59	114.95
T257	7.93	113.06	7.93	113.07
W258	7.88	124.78	7.87	124.78
I259	9.74	126.04	9.74	126.04
E260	11.23	129.03	11.23	129.03
G261	9.91	109.41	9.91	109.39
K262	6.71	116.63	6.70	116.62
E263	10.54	126.65	10.54	126.65
P264				
G265	8.98	113.83	8.97	113.80
C266	7.54	115.01	7.54	115.01
E267	9.03	120.57	9.03	120.55
T268	9.79	120.90	9.79	120.93
I269				
G270	8.38	106.99	8.38	107.03
L271	7.55	125.49	7.55	125.50
L272				
M273				
S274				
S275				
M276				
D277				
D278				

L279				
I280				
R281				
H282	7.58	113.99	7.57	114.02
C283	7.57	115.76	7.57	115.78
N284	7.52	117.03	7.52	117.03
G285	8.63	112.69	8.62	112.70
K286	7.91	116.16	7.91	116.18
L287	7.56	120.34	7.56	120.36
G288	8.71	114.34	8.71	114.35
S289	7.70	118.88	7.70	118.87
Y290	7.16	120.13	7.16	120.11
K291	9.07	126.01	9.06	125.98
I292	8.48	125.11	8.47	125.10
N293	8.31	125.27	8.32	125.34
G294	7.79	108.73	7.79	108.74
R295	9.04	115.23	9.03	115.22
T296	7.86	108.60	7.87	108.62
K297	7.90	115.46	7.90	115.45
A298	8.34	121.00	8.33	120.97
M299	9.70	124.93	9.70	124.94
V300	8.49	129.83	8.49	129.83
A301	8.89	127.80	8.89	127.79
C302	9.14	120.27	9.14	120.27
Y303	9.03	129.91	9.02	129.96
P304				
G305				
N306				
G307				
T308				
G309				
Y310				
V311	8.07	119.18	8.08	119.14
R312	8.06	120.24	8.07	120.17
H313	8.72	122.03	8.73	122.21
V314	8.17	117.17	8.15	117.20
D315	9.11	128.94	9.09	128.87
N316	7.12	106.18	7.10	106.22
P317				
N318	8.36	118.78	8.41	118.94
G319	8.20	112.80	8.19	112.69
D320	8.92	119.45	8.93	119.54
G321	9.15	106.62	9.15	106.63
R322				
C323	9.69	121.22	9.70	121.18
V324	7.29	125.71	7.29	125.69
T325				
C326				
I327				
Y328				
Y329				
L330				
N331				
K332				
D333				
W334				
D335				
A336				
K337				
V338				
S339				
G340				
G341				
I342				
L343	7.63	127.15	7.65	127.15
R344	8.82	130.87	8.82	130.89
I345	8.82	125.98	8.81	125.98
F346	8.48	125.42	8.48	125.43
P347				
E348	9.25	123.75	9.25	123.78
G349	8.91	111.72	8.91	111.74
K350	7.55	119.05	7.55	119.04
A351	8.28	122.42	8.28	122.43
Q352	7.35	115.83	7.35	115.84
F353	7.03	118.96	7.02	118.96
A354	9.00	124.43	8.99	124.43
D355	8.25	123.39	8.25	123.42
I356	9.67	126.42	9.68	126.45
E357	8.31	125.65	8.31	125.68
P358				
K359	7.44	122.37	7.43	122.34
F360	7.14	119.19	7.14	119.22
D361	7.63	125.75	7.63	125.78
R362				
L363				
L364				
F365				
F366				
W367	7.15	117.83	7.14	117.84
S368	7.53	114.30	7.53	114.30
D369	7.74	119.49	7.73	119.47
R370	7.64	110.69	7.64	110.70
R371	8.30	118.79	8.35	118.94
N372	7.39	110.84	7.39	110.88
P373				
H374	8.95	118.35	8.94	118.34
E375	9.01	116.19	9.01	116.22
V376	9.21	123.12	9.20	123.15
Q377	8.66	127.84	8.66	127.86
P378				
A379				
Y380				
A381	7.65	121.78	7.64	121.69
T382	8.18	116.06	8.18	116.05
R383	8.37	130.46	8.37	130.50
Y384	9.70	127.04	9.70	127.00
A385	8.52	121.81	8.51	121.82
I386				
T387				
V388				
W389				
Y390				
F391	8.73	121.18	8.72	121.18
D392	8.36	119.49	8.37	119.47
A393	9.35	128.87	9.35	128.88
D394	8.28	118.05	8.28	118.05

E395	8.78	122.10	8.78	122.10
R396	8.75	118.22	8.76	118.22
A397	7.41	118.58	7.40	118.58
R398	7.44	116.98	7.43	116.98
A399	7.63	121.35	7.63	121.34
K400	7.09	114.94	7.08	114.94
V401	7.21	118.00	7.21	117.99
K402	7.60	129.41	7.60	129.41

Table I-ii Protein backbone assignments of $PHD2_{181-402}$-Zn(II)-2OG-CODD and $PHD2_{181-402}$-Zn(II)-2OG-$L_{557}A$ CODD.

Protein backbone assignment for $PHD2_{181-402}$-Zn(II)-2OG-D558A CODD (sequence: DLALEMLAPYIPMDDDFQL).

Transfer of ^{1}H and ^{15}N assignment				
	^{15}N-$PHD2_{181-402}$-Zn(II)-2OG-CODD		^{15}N-$PHD2_{181-402}$-Zn(II)-2OG-D558A CODD	
Residue	^{1}H	^{15}N	^{1}H	^{15}N
G				
S	8.54	115.47	8.54	115.47
H	8.61	120.70	8.61	120.73
M	8.32	122.67	8.31	122.70
A	8.36	126.06	8.36	126.06
S	8.25	116.25	8.24	116.21
P181				
N182	8.60	119.73	8.60	119.73
G183	8.30	109.27	8.30	109.26
Q184	8.16	119.61	8.16	119.60
T185				
K186	8.19	125.08	8.17	125.03
P187				
L188				
P189				
A190	8.32	123.08	8.32	123.12
L191	7.94	116.86	7.94	116.89
K192	7.21	117.45	7.18	117.41
L193				
A194	8.06	119.86	8.06	119.83
L195	7.97	112.82	7.98	112.84
E196				
Y197	7.21	117.10	7.21	117.27
I198	8.63	121.20	8.63	121.13
V199	8.44	116.09	8.42	116.04
P200				
C201	7.70	116.41	7.68	116.38
M202	8.54	117.76	8.54	117.78
N203	8.43	117.02	8.42	116.94
K204	7.86	117.25	7.85	117.26
H205	8.40	112.54	8.40	112.64
G206	8.52	111.15	8.50	111.08
I207	6.58	115.82	6.58	115.81
C208				
V209	8.69	130.40	8.71	130.41
V210				
D211	8.36	125.70		
D212	8.57	117.75	8.58	117.73
F213	8.42	117.37	8.42	117.28
L214				
G215	10.19	115.52	10.20	115.51
K216	8.12	117.94	8.12	117.95
E217	8.47	119.25	8.47	119.25
T218	8.64	118.59	8.63	118.55
G219	8.50	108.66	8.50	108.65
Q220	8.44	120.83	8.44	120.87
Q221	7.51	120.11	7.49	120.14
I222	7.99	119.90	7.99	119.86
G223	8.33	107.24	8.33	107.20
D224	8.45	122.58	8.44	122.63
E225	8.11	122.24	8.12	122.38
V226				
R227	8.20	120.42	8.21	120.41
A228	7.79	121.00	7.79	121.00
L229	7.74	119.21	7.73	119.20
H230	8.41	119.59	8.40	119.56
D231	8.80	121.52	8.81	121.54
T232	7.35	108.27	7.35	108.26
G233	7.47	108.03	7.47	108.02
K234	7.45	115.88	7.45	115.87
F235	8.55	121.08	8.55	121.02
T236	9.40	113.47	9.41	113.44
D237	8.48	121.18	8.47	121.17
G238	8.04	109.25	8.06	109.31
Q239				
L240				
V241				
S242				
Q243				
K244				
S245	8.13	116.16	8.10	116.21
D246	8.37	120.83	8.40	120.92
S247	8.00	114.05	8.00	113.99
S248	8.47	119.99	8.38	119.30
K249	7.94	121.75	7.94	121.84
D250	8.03	117.11		
I251	7.75	121.72	7.72	121.60
R252	7.92	114.05	7.91	114.20
G253	8.73	110.46	8.74	110.57
D254	9.35	116.28	9.34	116.27
K255				
I256	9.59	114.96	9.59	114.92
T257	7.93	113.06	7.93	113.06
W258	7.88	124.78	7.87	124.77
I259	9.74	126.04	9.74	126.05
E260	11.23	129.03	11.25	129.07
G261	9.91	109.41	9.92	109.41
K262	6.71	116.63	6.69	116.61
E263	10.54	126.65	10.55	126.70
P264				
G265	8.98	113.83	8.99	113.90
C266	7.54	115.01	7.54	115.06
E267	9.03	120.57	9.03	120.51
T268	9.79	120.90	9.91	121.16
I269				
G270	8.38	106.99	8.39	106.95
L271	7.55	125.49	7.55	125.52
L272				
M273				
S274				
S275				
M276				
D277				
D278				

L279				
I280				
R281				
H282	7.58	113.99	7.58	114.10
C283	7.57	115.76	7.57	115.76
N284	7.52	117.03	7.53	117.05
G285	8.63	112.69	8.63	112.75
K286	7.91	116.16	7.91	116.17
L287	7.56	120.34	7.55	120.36
G288	8.71	114.34	8.70	114.33
S289	7.70	118.88	7.71	118.91
Y290	7.16	120.13	7.15	120.11
K291	9.07	126.01	9.05	125.98
I292	8.48	125.11	8.48	125.06
N293	8.31	125.27	8.31	125.32
G294	7.79	108.73	7.79	108.75
R295	9.04	115.23	9.04	115.20
T296	7.86	108.60	7.88	108.61
K297	7.90	115.46	7.91	115.50
A298	8.34	121.00	8.33	120.99
M299	9.70	124.93	9.71	124.96
V300	8.49	129.83	8.49	129.85
A301	8.89	127.80	8.90	127.77
C302	9.14	120.27	9.15	120.25
Y303	9.03	129.91	9.03	129.97
P304				
G305				
N306				
G307				
T308				
G309				
Y310				
V311	8.07	119.18	8.07	119.11
R312	8.06	120.24	8.06	120.36
H313	8.72	122.03	8.69	121.83
V314	8.17	117.17		
D315	9.11	128.94	9.11	128.87
N316	7.12	106.18	7.15	106.00
P317				
N318	8.36	118.78		
G319	8.20	112.80	8.25	113.24
D320	8.92	119.45	8.81	118.90
G321	9.15	106.62	9.21	106.75
R322				
C323	9.69	121.22	9.69	121.11
V324	7.29	125.71	7.29	125.84
T325				
C326				
I327				
Y328				
Y329				
L330				
N331				
K332				
D333				
W334				
D335				
A336				
K337				
V338				
S339				
G340				
G341				
I342				
L343	7.63	127.15	7.64	127.10
R344	8.82	130.87	8.81	130.89
I345	8.82	125.98	8.82	126.01
F346	8.48	125.42	8.49	125.40
P347				
E348	9.25	123.75	9.24	123.84
G349	8.91	111.72	8.91	111.79
K350	7.55	119.05	7.55	119.00
A351	8.28	122.42	8.30	122.47
Q352	7.35	115.83	7.35	115.78
F353	7.03	118.96	7.02	118.99
A354	9.00	124.43	9.00	124.45
D355	8.25	123.39	8.25	123.44
I356	9.67	126.42	9.69	126.50
E357	8.31	125.65	8.32	125.68
P358				
K359	7.44	122.37	7.44	122.32
F360	7.14	119.19	7.13	119.28
D361	7.63	125.75	7.62	125.73
R362				
L363				
L364				
F365				
F366				
W367	7.15	117.83	7.16	117.87
S368	7.53	114.30	7.54	114.28
D369	7.74	119.49	7.76	119.51
R370	7.64	110.69	7.61	110.66
R371	8.30	118.79	8.26	118.86
N372	7.39	110.84	7.39	110.83
P373				
H374	8.95	118.35	8.96	118.39
E375	9.01	116.19	9.01	116.18
V376	9.21	123.12	9.20	123.13
Q377	8.66	127.84	8.66	127.85
P378				
A379				
Y380				
A381	7.65	121.78	7.65	121.75
T382	8.18	116.06	8.18	116.00
R383	8.37	130.46	8.37	130.44
Y384	9.70	127.04	9.71	127.01
A385	8.52	121.81	8.52	121.85
I386				
T387				
V388				
W389				
Y390				
F391	8.73	121.18	8.73	121.17
D392	8.36	119.49		
A393	9.35	128.87	9.36	128.87
D394	8.28	118.05	8.27	118.03

E395	8.78	122.10	8.76	122.10
R396	8.75	118.22	8.76	118.22
A397	7.41	118.58	7.40	118.51
R398	7.44	116.98	7.44	117.01
A399	7.63	121.35	7.64	121.28
K400	7.09	114.94	7.07	114.95
V401	7.21	118.00	7.21	118.19
K402	7.60	129.41	7.61	129.62

Table I-iii Protein backbone assignments of $PHD2_{181-402}$-Zn(II)-2OG-CODD and $PHD2_{181-402}$-Zn(II)-2OG-D558A CODD.

Protein backbone assignment for $PHD2_{181-402}$-Zn(II)-2OG-L559A CODD (sequence: DLDAEMLAPYIPMDDDFQL).

Transfer of ^{1}H and ^{15}N assignment				
	^{15}N-$PHD2_{181-402}$-Zn(II)-2OG-CODD		^{15}N-$PHD2_{181-402}$-Zn(II)-2OG-L559A CODD	
Residue	^{1}H	^{15}N	^{1}H	^{15}N
G				
S	8.54	115.47	8.54	115.47
H	8.61	120.70	8.61	120.70
M	8.32	122.67	8.31	122.71
A	8.36	126.06	8.36	126.07
S	8.25	116.25	8.24	116.23
P181				
N182	8.60	119.73	8.60	119.73
G183	8.30	109.27	8.30	109.26
Q184	8.16	119.61	8.16	119.62
T185				
K186	8.19	125.08	8.18	125.07
P187				
L188				
P189				
A190	8.32	123.08	8.33	123.14
L191	7.94	116.86	7.94	116.87
K192	7.21	117.45	7.18	117.41
L193				
A194	8.06	119.86	8.06	119.83
L195	7.97	112.82	7.98	112.83
E196				
Y197	7.21	117.10	7.22	117.25
I198	8.63	121.20	8.61	121.08
V199	8.44	116.09	8.43	116.08
P200				
C201	7.70	116.41	7.69	116.35
M202	8.54	117.76	8.53	117.76
N203	8.43	117.02	8.43	117.00
K204	7.86	117.25	7.86	117.25
H205	8.40	112.54	8.38	112.56
G206	8.52	111.15	8.50	111.13
I207	6.58	115.82	6.58	115.84
C208				
V209	8.69	130.40	8.68	130.41
V210				
D211	8.36	125.70		
D212	8.57	117.75	8.57	117.75
F213	8.42	117.37	8.42	117.34
L214				
G215	10.19	115.52	10.18	115.54
K216	8.12	117.94	8.11	117.93
E217	8.47	119.25	8.48	119.23
T218	8.64	118.59	8.63	118.58
G219	8.50	108.66	8.50	108.67
Q220	8.44	120.83	8.44	120.82
Q221	7.51	120.11	7.50	120.14
I222	7.99	119.90	7.99	119.88
G223	8.33	107.24	8.33	107.22
D224	8.45	122.58	8.44	122.61
E225	8.11	122.24	8.11	122.31
V226				
R227	8.20	120.42	8.20	120.41
A228	7.79	121.00	7.79	121.01
L229	7.74	119.21	7.74	119.28
H230	8.41	119.59	8.41	119.59
D231	8.80	121.52	8.80	121.51
T232	7.35	108.27	7.35	108.27
G233	7.47	108.03	7.47	108.04
K234	7.45	115.88	7.45	115.90
F235	8.55	121.08	8.55	121.12
T236	9.40	113.47	9.40	113.48
D237	8.48	121.18	8.47	121.18
G238	8.04	109.25	8.03	109.19
Q239				
L240				
V241				
S242				
Q243				
K244				
S245	8.13	116.16	8.16	116.09
D246	8.37	120.83	8.34	120.64
S247	8.00	114.05	8.00	114.20
S248	8.47	119.99	8.47	119.90
K249	7.94	121.75	7.94	121.73
D250	8.03	117.11	8.06	117.29
I251	7.75	121.72	7.77	121.84
R252	7.92	114.05	7.90	113.94
G253	8.73	110.46	8.72	110.46
D254	9.35	116.28	9.36	116.28
K255				
I256	9.59	114.96	9.58	114.92
T257	7.93	113.06	7.93	113.06
W258	7.88	124.78	7.87	124.76
I259	9.74	126.04	9.74	126.04
E260	11.23	129.03	11.23	129.06
G261	9.91	109.41	9.92	109.38
K262	6.71	116.63	6.70	116.64
E263	10.54	126.65	10.54	126.67
P264				
G265	8.98	113.83	8.98	113.86
C266	7.54	115.01	7.54	115.04
E267	9.03	120.57	9.03	120.55
T268	9.79	120.90	9.78	120.92
I269				
G270	8.38	106.99	8.38	106.96
L271	7.55	125.49	7.55	125.52
L272				
M273				
S274				
S275				
M276				
D277				
D278				

L279				
I280				
R281				
H282	7.58	113.99	7.58	114.08
C283	7.57	115.76	7.57	115.74
N284	7.52	117.03	7.53	117.05
G285	8.63	112.69	8.63	112.70
K286	7.91	116.16	7.91	116.17
L287	7.56	120.34	7.56	120.37
G288	8.71	114.34	8.71	114.34
S289	7.70	118.88	7.70	118.89
Y290	7.16	120.13	7.16	120.15
K291	9.07	126.01	9.06	126.01
I292	8.48	125.11	8.48	125.10
N293	8.31	125.27	8.29	125.26
G294	7.79	108.73	7.79	108.73
R295	9.04	115.23	9.03	115.23
T296	7.86	108.60	7.86	108.57
K297	7.90	115.46	7.91	115.48
A298	8.34	121.00	8.34	120.90
M299	9.70	124.93	9.71	124.95
V300	8.49	129.83	8.50	129.83
A301	8.89	127.80	8.89	127.81
C302	9.14	120.27	9.14	120.26
Y303	9.03	129.91	9.04	130.00
P304				
G305				
N306				
G307				
T308				
G309				
Y310				
V311	8.07	119.18	8.07	119.19
R312	8.06	120.24	8.07	120.06
H313	8.72	122.03	8.73	122.15
V314	8.17	117.17	8.16	117.21
D315	9.11	128.94		
N316	7.12	106.18	7.05	106.36
P317				
N318	8.36	118.78		
G319	8.20	112.80	8.15	112.65
D320	8.92	119.45	8.90	119.60
G321	9.15	106.62	9.16	106.70
R322				
C323	9.69	121.22	9.68	121.25
V324	7.29	125.71	7.29	125.62
T325				
C326				
I327				
Y328				
Y329				
L330				
N331				
K332				
D333				
W334				
D335				
A336				
K337				
V338				
S339				
G340				
G341				
I342				
L343	7.63	127.15	7.62	127.11
R344	8.82	130.87	8.82	130.91
I345	8.82	125.98	8.81	126.01
F346	8.48	125.42	8.48	125.42
P347				
E348	9.25	123.75	9.25	123.80
G349	8.91	111.72	8.92	111.81
K350	7.55	119.05	7.55	119.04
A351	8.28	122.42	8.28	122.45
Q352	7.35	115.83	7.35	115.81
F353	7.03	118.96	7.02	119.03
A354	9.00	124.43	9.01	124.52
D355	8.25	123.39	8.25	123.41
I356	9.67	126.42	9.68	126.50
E357	8.31	125.65	8.31	125.67
P358				
K359	7.44	122.37	7.44	122.35
F360	7.14	119.19	7.13	119.23
D361	7.63	125.75	7.63	125.75
R362				
L363				
L364				
F365				
F366				
W367	7.15	117.83	7.15	117.91
S368	7.53	114.30	7.53	114.25
D369	7.74	119.49		
R370	7.64	110.69	7.63	110.71
R371	8.30	118.79	8.28	118.41
N372	7.39	110.84	7.38	110.94
P373				
H374	8.95	118.35	8.90	118.28
E375	9.01	116.19	9.00	116.20
V376	9.21	123.12	9.22	123.12
Q377	8.66	127.84	8.67	127.89
P378				
A379				
Y380				
A381	7.65	121.78	7.64	121.77
T382	8.18	116.06	8.18	116.08
R383	8.37	130.46	8.37	130.47
Y384	9.70	127.04	9.70	127.03
A385	8.52	121.81	8.52	121.83
I386				
T387				
V388				
W389				
Y390				
F391	8.73	121.18	8.73	121.18
D392	8.36	119.49	8.36	119.49
A393	9.35	128.87	9.35	128.87
D394	8.28	118.05	8.28	118.06

E395	8.78	122.10	8.76	122.11
R396	8.75	118.22	8.76	118.22
A397	7.41	118.58	7.41	118.58
R398	7.44	116.98	7.43	117.00
A399	7.63	121.35	7.63	121.36
K400	7.09	114.94	7.08	114.95
V401	7.21	118.00	7.21	118.04
K402	7.60	129.41	7.60	129.46

Table I-iv Protein backbone assignments of $PHD2_{181-402}$-Zn(II)-2OG-CODD and $PHD2_{181-402}$-Zn(II)-2OG-L559A CODD.

Protein backbone assignment for $PHD2_{181-402}$-Zn(II)-2OG-E560A CODD (sequence: DLDLAMLAPYIPMDDDFQL).

Transfer of ^{1}H and ^{15}N assignment				
	^{15}N-$PHD2_{181-402}$-Zn(II)-2OG-CODD		^{15}N-$PHD2_{181-402}$-Zn(II)-2OG-E560A CODD	
Residue	^{1}H	^{15}N	^{1}H	^{15}N
G				
S	8.54	115.47	8.54	115.47
H	8.61	120.70	8.61	120.72
M	8.32	122.67	8.31	122.72
A	8.36	126.06	8.36	126.07
S	8.25	116.25	8.24	116.21
P181				
N182	8.60	119.73	8.60	119.73
G183	8.30	109.27	8.30	109.25
Q184	8.16	119.61	8.16	119.62
T185				
K186	8.19	125.08	8.18	125.05
P187				
L188				
P189				
A190	8.32	123.08	8.32	123.07
L191	7.94	116.86	7.93	116.88
K192	7.21	117.45	7.19	117.39
L193				
A194	8.06	119.86	8.06	119.84
L195	7.97	112.82	7.98	112.84
E196				
Y197	7.21	117.10	7.22	117.21
I198	8.63	121.20	8.62	121.13
V199	8.44	116.09	8.43	116.03
P200				
C201	7.70	116.41	7.68	116.35
M202	8.54	117.76	8.54	117.76
N203	8.43	117.02	8.42	116.95
K204	7.86	117.25	7.84	117.29
H205	8.40	112.54	8.38	112.65
G206	8.52	111.15	8.50	111.09
I207	6.58	115.82	6.58	115.80
C208				
V209	8.69	130.40	8.69	130.40
V210				
D211	8.36	125.70		
D212	8.57	117.75	8.57	117.74
F213	8.42	117.37	8.44	117.41
L214				
G215	10.19	115.52	10.19	115.54
K216	8.12	117.94	8.12	117.96
E217	8.47	119.25	8.48	119.24
T218	8.64	118.59	8.62	118.55
G219	8.50	108.66	8.50	108.65
Q220	8.44	120.83	8.45	120.81
Q221	7.51	120.11	7.49	120.14
I222	7.99	119.90	7.99	119.85
G223	8.33	107.24	8.33	107.20
D224	8.45	122.58	8.44	122.64
E225	8.11	122.24	8.12	122.40
V226				
R227	8.20	120.42	8.21	120.42
A228	7.79	121.00	7.79	121.00
L229	7.74	119.21	7.74	119.19
H230	8.41	119.59	8.41	119.63
D231	8.80	121.52	8.80	121.52
T232	7.35	108.27	7.35	108.28
G233	7.47	108.03	7.47	108.04
K234	7.45	115.88	7.45	115.89
F235	8.55	121.08	8.55	121.11
T236	9.40	113.47	9.41	113.49
D237	8.48	121.18	8.46	121.17
G238	8.04	109.25		
Q239				
L240				
V241				
S242				
Q243				
K244				
S245	8.13	116.16	8.16	116.31
D246	8.37	120.83	8.38	120.83
S247	8.00	114.05	7.99	113.94
S248	8.47	119.99	8.47	119.92
K249	7.94	121.75	7.94	121.76
D250	8.03	117.11		
I251	7.75	121.72	7.74	121.61
R252	7.92	114.05	7.92	114.01
G253	8.73	110.46	8.73	110.54
D254	9.35	116.28	9.35	116.31
K255				
I256	9.59	114.96	9.58	114.91
T257	7.93	113.06	7.93	113.07
W258	7.88	124.78	7.87	124.77
I259	9.74	126.04	9.74	126.03
E260	11.23	129.03	11.23	129.12
G261	9.91	109.41	9.91	109.42
K262	6.71	116.63	6.70	116.61
E263	10.54	126.65	10.54	126.70
P264				
G265	8.98	113.83	9.00	113.94
C266	7.54	115.01	7.55	115.07
E267	9.03	120.57	9.03	120.48
T268	9.79	120.90	9.91	121.20
I269				
G270	8.38	106.99	8.39	106.93
L271	7.55	125.49	7.55	125.53
L272				
M273				
S274				
S275				
M276				
D277				
D278				

L279				
I280				
R281				
H282	7.58	113.99	7.58	114.10
C283	7.57	115.76	7.57	115.75
N284	7.52	117.03	7.53	117.04
G285	8.63	112.69	8.63	112.81
K286	7.91	116.16	7.91	116.19
L287	7.56	120.34	7.56	120.34
G288	8.71	114.34	8.71	114.36
S289	7.70	118.88	7.70	118.92
Y290	7.16	120.13	7.15	120.12
K291	9.07	126.01	9.06	126.00
I292	8.48	125.11	8.48	125.06
N293	8.31	125.27	8.30	125.25
G294	7.79	108.73	7.79	108.75
R295	9.04	115.23	9.04	115.22
T296	7.86	108.60	7.86	108.59
K297	7.90	115.46	7.90	115.51
A298	8.34	121.00	8.34	120.97
M299	9.70	124.93	9.71	125.00
V300	8.49	129.83	8.49	129.85
A301	8.89	127.80	8.88	127.78
C302	9.14	120.27	9.14	120.24
Y303	9.03	129.91	9.03	129.92
P304				
G305				
N306				
G307				
T308				
G309				
Y310				
V311	8.07	119.18	8.07	119.13
R312	8.06	120.24	8.06	120.31
H313	8.72	122.03	8.70	121.91
V314	8.17	117.17	8.17	117.10
D315	9.11	128.94	9.11	128.89
N316	7.12	106.18	7.12	105.93
P317				
N318	8.36	118.78		
G319	8.20	112.80	8.14	113.05
D320	8.92	119.45	8.85	119.29
G321	9.15	106.62	9.25	106.80
R322				
C323	9.69	121.22	9.68	121.18
V324	7.29	125.71	7.29	125.76
T325				
C326				
I327				
Y328				
Y329				
L330				
N331				
K332				
D333				
W334				
D335				
A336				
K337				
V338				
S339				
G340				
G341				
I342				
L343	7.63	127.15	7.64	127.18
R344	8.82	130.87	8.82	130.90
I345	8.82	125.98	8.82	126.00
F346	8.48	125.42	8.49	125.39
P347				
E348	9.25	123.75	9.24	123.86
G349	8.91	111.72	8.91	111.79
K350	7.55	119.05	7.55	119.01
A351	8.28	122.42	8.28	122.47
Q352	7.35	115.83	7.35	115.78
F353	7.03	118.96	7.02	119.03
A354	9.00	124.43	8.99	124.49
D355	8.25	123.39	8.25	123.42
I356	9.67	126.42	9.69	126.50
E357	8.31	125.65	8.31	125.67
P358				
K359	7.44	122.37	7.44	122.37
F360	7.14	119.19	7.14	119.30
D361	7.63	125.75	7.63	125.72
R362				
L363				
L364				
F365				
F366				
W367	7.15	117.83	7.15	117.81
S368	7.53	114.30	7.52	114.26
D369	7.74	119.49	7.74	119.41
R370	7.64	110.69	7.64	110.80
R371	8.30	118.79	8.27	118.90
N372	7.39	110.84	7.38	110.81
P373				
H374	8.95	118.35	8.95	118.39
E375	9.01	116.19	9.02	116.27
V376	9.21	123.12	9.20	123.09
Q377	8.66	127.84	8.66	127.84
P378				
A379				
Y380				
A381	7.65	121.78	7.65	121.78
T382	8.18	116.06	8.18	116.05
R383	8.37	130.46	8.36	130.44
Y384	9.70	127.04	9.70	126.99
A385	8.52	121.81	8.51	121.79
I386				
T387				
V388				
W389				
Y390				
F391	8.73	121.18	8.73	121.15
D392	8.36	119.49	8.37	119.52
A393	9.35	128.87	9.36	128.87
D394	8.28	118.05	8.26	118.03

E395	8.78	122.10	8.77	122.09
R396	8.75	118.22	8.75	118.22
A397	7.41	118.58	7.41	118.52
R398	7.44	116.98	7.44	117.02
A399	7.63	121.35	7.63	121.18
K400	7.09	114.94	7.06	115.02
V401	7.21	118.00	7.21	118.43
K402	7.60	129.41	7.64	129.74

Table I-v Protein backbone assignments of $PHD2_{181-402}$-Zn(II)-2OG-CODD and $PHD2_{181-402}$-Zn(II)-2OG-E560A CODD.

Protein backbone assignment for $PHD2_{181-402}$-Zn(II)-2OG-M561A CODD (sequence: DLDLEALAPYIPMDDDFQL).

Transfer of ^{1}H and ^{15}N assignment				
	^{15}N-$PHD2_{181-402}$-Zn(II)-2OG-CODD		^{15}N-$PHD2_{181-402}$-Zn(II)-2OG-M561A CODD	
Residue	^{1}H	^{15}N	^{1}H	^{15}N
G				
S	8.54	115.47	8.54	115.47
H	8.61	120.70	8.61	120.68
M	8.32	122.67	8.32	122.56
A	8.36	126.06	8.35	126.04
S	8.25	116.25	8.25	116.36
P181				
N182	8.60	119.73	8.60	119.72
G183	8.30	109.27	8.30	109.25
Q184	8.16	119.61	8.16	119.58
T185				
K186	8.19	125.08	8.23	125.20
P187				
L188				
P189				
A190	8.32	123.08		
L191	7.94	116.86	7.92	116.96
K192	7.21	117.45		
L193				
A194	8.06	119.86	8.06	119.84
L195	7.97	112.82	7.99	112.74
E196				
Y197	7.21	117.10		
I198	8.63	121.20	8.59	121.16
V199	8.44	116.09	8.45	115.96
P200				
C201	7.70	116.41	7.72	116.51
M202	8.54	117.76	8.52	117.79
N203	8.43	117.02	8.45	117.12
K204	7.86	117.25	7.89	117.20
H205	8.40	112.54	8.40	112.31
G206	8.52	111.15	8.52	111.30
I207	6.58	115.82	6.58	115.83
C208				
V209	8.69	130.40	8.68	130.43
V210				
D211	8.36	125.70		
D212	8.57	117.75	8.56	117.80
F213	8.42	117.37		
L214				
G215	10.19	115.52	10.19	115.57
K216	8.12	117.94	8.10	117.95
E217	8.47	119.25	8.45	119.18
T218	8.64	118.59	8.64	118.61
G219	8.50	108.66	8.51	108.72
Q220	8.44	120.83	8.43	120.86
Q221	7.51	120.11	7.53	120.13
I222	7.99	119.90	8.00	120.02
G223	8.33	107.24	8.34	107.25
D224	8.45	122.58	8.46	122.37
E225	8.11	122.24	8.10	121.95
V226				
R227	8.20	120.42	8.18	120.39
A228	7.79	121.00	7.77	121.02
L229	7.74	119.21	7.77	119.16
H230	8.41	119.59	8.42	119.59
D231	8.80	121.52	8.79	121.42
T232	7.35	108.27	7.34	108.28
G233	7.47	108.03	7.47	108.01
K234	7.45	115.88	7.45	115.88
F235	8.55	121.08	8.55	121.18
T236	9.40	113.47	9.40	113.39
D237	8.48	121.18	8.50	121.19
G238	8.04	109.25	8.04	109.36
Q239				
L240				
V241				
S242				
Q243				
K244				
S245	8.13	116.16	8.10	116.20
D246	8.37	120.83	8.36	123.26
S247	8.00	114.05	7.96	113.48
S248	8.47	119.99	8.35	122.97
K249	7.94	121.75	7.92	121.67
D250	8.03	117.11	8.03	115.83
I251	7.75	121.72	7.72	121.41
R252	7.92	114.05	7.91	114.10
G253	8.73	110.46	8.72	110.61
D254	9.35	116.28	9.33	116.21
K255				
I256	9.59	114.96	9.60	115.01
T257	7.93	113.06	7.92	113.07
W258	7.88	124.78	7.88	124.79
I259	9.74	126.04	9.73	125.99
E260	11.23	129.03		
G261	9.91	109.41	9.90	109.39
K262	6.71	116.63	6.74	116.66
E263	10.54	126.65	10.51	126.53
P264				
G265	8.98	113.83	8.92	113.52
C266	7.54	115.01	7.54	114.88
E267	9.03	120.57	9.01	120.67
T268	9.79	120.90	9.53	120.31
I269				
G270	8.38	106.99	8.38	107.16
L271	7.55	125.49	7.54	125.39
L272				
M273				
S274				
S275				
M276				
D277				
D278				

L279				
I280				
R281				
H282	7.58	113.99	7.54	113.86
C283	7.57	115.76	7.56	115.77
N284	7.52	117.03	7.50	116.99
G285	8.63	112.69		
K286	7.91	116.16	7.91	116.11
L287	7.56	120.34	7.57	120.36
G288	8.71	114.34	8.69	114.30
S289	7.70	118.88	7.70	118.85
Y290	7.16	120.13	7.18	120.15
K291	9.07	126.01	9.05	126.00
I292	8.48	125.11	8.48	125.16
N293	8.31	125.27	8.31	125.16
G294	7.79	108.73	7.79	108.69
R295	9.04	115.23	9.03	115.26
T296	7.86	108.60	7.85	108.60
K297	7.90	115.46	7.89	115.39
A298	8.34	121.00	8.33	120.99
M299	9.70	124.93	9.71	124.96
V300	8.49	129.83	8.50	129.80
A301	8.89	127.80	8.90	127.81
C302	9.14	120.27	9.15	120.31
Y303	9.03	129.91	9.03	129.88
P304				
G305				
N306				
G307				
T308				
G309				
Y310				
V311	8.07	119.18	8.07	119.21
R312	8.06	120.24	8.05	120.11
H313	8.72	122.03	8.72	122.04
V314	8.17	117.17	8.16	117.15
D315	9.11	128.94	9.09	128.90
N316	7.12	106.18	7.12	106.24
P317				
N318	8.36	118.78		
G319	8.20	112.80	8.20	112.65
D320	8.92	119.45	8.92	119.45
G321	9.15	106.62	9.04	106.41
R322				
C323	9.69	121.22	9.71	121.33
V324	7.29	125.71	7.28	125.69
T325				
C326				
I327				
Y328				
Y329				
L330				
N331				
K332				
D333				
W334				
D335				
A336				
K337				
V338				
S339				
G340				
G341				
I342				
L343	7.63	127.15	7.61	127.16
R344	8.82	130.87	8.81	130.85
I345	8.82	125.98	8.82	126.00
F346	8.48	125.42	8.49	125.37
P347				
E348	9.25	123.75	9.27	123.59
G349	8.91	111.72	8.91	111.62
K350	7.55	119.05	7.55	119.10
A351	8.28	122.42	8.28	122.42
Q352	7.35	115.83	7.35	115.91
F353	7.03	118.96	7.02	118.83
A354	9.00	124.43	8.98	124.25
D355	8.25	123.39	8.29	123.37
I356	9.67	126.42	9.67	126.30
E357	8.31	125.65	8.31	125.72
P358				
K359	7.44	122.37	7.44	122.36
F360	7.14	119.19	7.14	119.20
D361	7.63	125.75	7.64	125.79
R362				
L363				
L364				
F365				
F366				
W367	7.15	117.83	7.14	117.79
S368	7.53	114.30	7.53	114.26
D369	7.74	119.49	7.72	119.49
R370	7.64	110.69	7.63	110.73
R371	8.30	118.79	8.30	118.88
N372	7.39	110.84	7.39	110.88
P373				
H374	8.95	118.35	8.94	118.36
E375	9.01	116.19	8.99	116.04
V376	9.21	123.12	9.21	123.25
Q377	8.66	127.84	8.65	127.85
P378				
A379				
Y380				
A381	7.65	121.78	7.66	121.78
T382	8.18	116.06	8.18	116.04
R383	8.37	130.46	8.37	130.46
Y384	9.70	127.04	9.71	127.01
A385	8.52	121.81	8.51	121.82
I386				
T387				
V388				
W389				
Y390				
F391	8.73	121.18	8.74	121.34
D392	8.36	119.49	8.37	119.54
A393	9.35	128.87	9.33	128.93
D394	8.28	118.05	8.30	118.07

E395	8.78	122.10	8.78	121.98
R396	8.75	118.22	8.76	118.24
A397	7.41	118.58	7.41	118.67
R398	7.44	116.98	7.43	116.93
A399	7.63	121.35	7.61	121.32
K400	7.09	114.94	7.10	115.09
V401	7.21	118.00	7.23	118.14
K402	7.60	129.41	7.64	129.03

Table I-vi Protein backbone assignments of $PHD2_{181-402}$-Zn(II)-2OG-CODD and $PHD2_{181-402}$-Zn(II)-2OG-M561A CODD.

Protein backbone assignment for $PHD2_{181-402}$-Zn(II)-2OG-L562A CODD (sequence: DLDLEMAAPYIPMDDDFQL).

Transfer of ^{1}H and ^{15}N assignment				
	^{15}N-$PHD2_{181-402}$-Zn(II)-2OG-CODD		^{15}N-$PHD2_{181-402}$-Zn(II)-2OG-L562A CODD	
Residue	^{1}H	^{15}N	^{1}H	^{15}N
G				
S	8.54	115.47	8.54	115.47
H	8.61	120.70	8.61	120.70
M	8.32	122.67	8.31	122.69
A	8.36	126.06	8.36	126.07
S	8.25	116.25	8.24	116.25
P181				
N182	8.60	119.73	8.60	119.73
G183	8.30	109.27	8.30	109.25
Q184	8.16	119.61	8.16	119.61
T185				
K186	8.19	125.08	8.18	125.06
P187				
L188				
P189				
A190	8.32	123.08	8.34	123.26
L191	7.94	116.86	7.94	116.84
K192	7.21	117.45	7.20	117.41
L193				
A194	8.06	119.86	8.04	119.95
L195	7.97	112.82	7.97	112.87
E196				
Y197	7.21	117.10	7.22	117.12
I198	8.63	121.20	8.60	121.04
V199	8.44	116.09	8.41	116.03
P200				
C201	7.70	116.41	7.69	116.36
M202	8.54	117.76	8.52	117.76
N203	8.43	117.02	8.44	117.08
K204	7.86	117.25	7.87	117.17
H205	8.40	112.54	8.39	112.43
G206	8.52	111.15	8.52	111.18
I207	6.58	115.82	6.58	115.75
C208				
V209	8.69	130.40	8.68	130.43
V210				
D211	8.36	125.70	8.40	125.81
D212	8.57	117.75	8.56	117.79
F213	8.42	117.37	8.43	117.36
L214				
G215	10.19	115.52	10.18	115.46
K216	8.12	117.94	8.11	117.94
E217	8.47	119.25	8.46	119.20
T218	8.64	118.59	8.62	118.51
G219	8.50	108.66	8.49	108.63
Q220	8.44	120.83	8.44	120.85
Q221	7.51	120.11	7.51	120.09
I222	7.99	119.90	7.99	119.95
G223	8.33	107.24	8.34	107.28
D224	8.45	122.58	8.45	122.46
E225	8.11	122.24	8.09	122.07
V226				
R227	8.20	120.42	8.18	120.42
A228	7.79	121.00	7.78	121.01
L229	7.74	119.21	7.75	119.16
H230	8.41	119.59	8.41	119.60
D231	8.80	121.52	8.80	121.50
T232	7.35	108.27	7.35	108.25
G233	7.47	108.03	7.47	108.03
K234	7.45	115.88	7.45	115.87
F235	8.55	121.08	8.54	121.01
T236	9.40	113.47	9.40	113.49
D237	8.48	121.18	8.48	121.16
G238	8.04	109.25		
Q239				
L240				
V241				
S242				
Q243				
K244				
S245	8.13	116.16	8.15	116.39
D246	8.37	120.83	8.39	120.97
S247	8.00	114.05	8.01	114.10
S248	8.47	119.99	8.21	121.62
K249	7.94	121.75	7.94	121.69
D250	8.03	117.11	8.04	117.24
I251	7.75	121.72	7.76	121.58
R252	7.92	114.05	7.93	114.49
G253	8.73	110.46	8.68	110.45
D254	9.35	116.28	9.36	116.33
K255				
I256	9.59	114.96	9.57	114.84
T257	7.93	113.06	7.94	113.09
W258	7.88	124.78	7.88	124.80
I259	9.74	126.04	9.73	125.95
E260	11.23	129.03	11.24	128.99
G261	9.91	109.41	9.91	109.40
K262	6.71	116.63	6.72	116.61
E263	10.54	126.65	10.52	126.57
P264				
G265	8.98	113.83	8.95	113.63
C266	7.54	115.01	7.54	114.93
E267	9.03	120.57	9.02	120.63
T268	9.79	120.90	9.65	120.58
I269				
G270	8.38	106.99	8.36	107.05
L271	7.55	125.49	7.55	125.44
L272				
M273				
S274				
S275				
M276				
D277				
D278				

L279				
I280				
R281				
H282	7.58	113.99	7.58	113.99
C283	7.57	115.76	7.57	115.76
N284	7.52	117.03	7.52	117.00
G285	8.63	112.69	8.61	112.59
K286	7.91	116.16	7.89	116.17
L287	7.56	120.34	7.56	120.39
G288	8.71	114.34	8.72	114.45
S289	7.70	118.88	7.68	118.78
Y290	7.16	120.13	7.17	120.11
K291	9.07	126.01	9.06	125.99
I292	8.48	125.11	8.48	125.15
N293	8.31	125.27	8.31	125.31
G294	7.79	108.73	7.78	108.60
R295	9.04	115.23		
T296	7.86	108.60	7.86	108.58
K297	7.90	115.46	7.89	115.43
A298	8.34	121.00	8.31	121.12
M299	9.70	124.93	9.70	125.00
V300	8.49	129.83	8.50	129.83
A301	8.89	127.80	8.89	127.81
C302	9.14	120.27	9.15	120.23
Y303	9.03	129.91	9.03	130.03
P304				
G305				
N306				
G307				
T308				
G309				
Y310				
V311	8.07	119.18	8.12	119.29
R312	8.06	120.24	7.99	118.95
H313	8.72	122.03	8.75	121.99
V314	8.17	117.17	8.16	117.18
D315	9.11	128.94	9.03	129.38
N316	7.12	106.18	7.11	106.27
P317				
N318	8.36	118.78		
G319	8.20	112.80	8.19	112.76
D320	8.92	119.45	8.86	119.26
G321	9.15	106.62	9.10	106.46
R322				
C323	9.69	121.22	9.68	121.19
V324	7.29	125.71	7.28	125.77
T325				
C326				
I327				
Y328				
Y329				
L330				
N331				
K332				
D333				
W334				
D335				
A336				
K337				
V338				
S339				
G340				
G341				
I342				
L343	7.63	127.15	7.63	127.17
R344	8.82	130.87	8.81	130.84
I345	8.82	125.98	8.80	126.00
F346	8.48	125.42	8.48	125.45
P347				
E348	9.25	123.75	9.25	123.51
G349	8.91	111.72	8.91	111.58
K350	7.55	119.05	7.55	119.11
A351	8.28	122.42	8.26	122.26
Q352	7.35	115.83	7.34	115.86
F353	7.03	118.96	7.02	118.92
A354	9.00	124.43	9.00	124.40
D355	8.25	123.39	8.25	123.37
I356	9.67	126.42	9.68	126.34
E357	8.31	125.65	8.30	125.73
P358				
K359	7.44	122.37	7.42	122.33
F360	7.14	119.19	7.14	119.34
D361	7.63	125.75	7.63	125.72
R362				
L363				
L364				
F365				
F366				
W367	7.15	117.83	7.14	117.79
S368	7.53	114.30	7.52	114.28
D369	7.74	119.49	7.71	119.13
R370	7.64	110.69	7.62	110.79
R371	8.30	118.79	8.25	118.86
N372	7.39	110.84	7.39	110.92
P373				
H374	8.95	118.35	8.96	118.41
E375	9.01	116.19	8.97	115.97
V376	9.21	123.12	9.20	123.12
Q377	8.66	127.84	8.66	127.80
P378				
A379				
Y380				
A381	7.65	121.78	7.65	121.70
T382	8.18	116.06	8.19	116.09
R383	8.37	130.46	8.35	130.40
Y384	9.70	127.04	9.71	126.95
A385	8.52	121.81	8.51	121.79
I386				
T387				
V388				
W389				
Y390				
F391	8.73	121.18	8.71	121.12
D392	8.36	119.49	8.35	119.48
A393	9.35	128.87	9.33	128.84
D394	8.28	118.05	8.29	118.07

E395	8.78	122.10	8.77	122.05
R396	8.75	118.22	8.74	118.19
A397	7.41	118.58	7.42	118.67
R398	7.44	116.98	7.44	116.98
A399	7.63	121.35	7.62	121.36
K400	7.09	114.94		
V401	7.21	118.00	7.23	118.18
K402	7.60	129.41	7.63	129.24

Table I-vii Protein backbone assignments of $PHD2_{181-402}$-Zn(II)-2OG-CODD and $PHD2_{181-402}$-Zn(II)-2OG-L562A CODD.

Protein backbone assignment for $PHD2_{181-402}$-Zn(II)-2OG-Y565A CODD (sequence: DLDLEMLAPAIPMDDDFQL).

	Transfer of ^{1}H and ^{15}N assignment			
	^{15}N-$PHD2_{181-402}$-Zn(II)-2OG-CODD		^{15}N-$PHD2_{181-402}$-Zn(II)-2OG-Y565A CODD	
Residue	^{1}H	^{15}N	^{1}H	^{15}N
G				
S	8.54	115.47	8.54	115.47
H	8.61	120.70	8.60	120.68
M	8.32	122.67	8.31	122.68
A	8.36	126.06	8.36	126.07
S	8.25	116.25	8.25	116.25
P181				
N182	8.60	119.73	8.60	119.72
G183	8.30	109.27	8.30	109.26
Q184	8.16	119.61	8.16	119.62
T185				
K186	8.19	125.08	8.18	125.07
P187				
L188				
P189				
A190	8.32	123.08	8.31	123.13
L191	7.94	116.86	7.94	116.81
K192	7.21	117.45	7.20	117.39
L193				
A194	8.06	119.86		
L195	7.97	112.82	7.96	112.88
E196				
Y197	7.21	117.10	7.24	117.04
I198	8.63	121.20	8.60	121.04
V199	8.44	116.09	8.41	116.05
P200				
C201	7.70	116.41	7.69	116.39
M202	8.54	117.76	8.53	117.79
N203	8.43	117.02	8.44	117.13
K204	7.86	117.25	7.88	117.13
H205	8.40	112.54	8.39	112.36
G206	8.52	111.15	8.53	111.22
I207	6.58	115.82	6.57	115.81
C208				
V209	8.69	130.40	8.68	130.36
V210				
D211	8.36	125.70		
D212	8.57	117.75	8.56	117.83
F213	8.42	117.37		
L214				
G215	10.19	115.52	10.17	115.49
K216	8.12	117.94	8.10	117.89
E217	8.47	119.25	8.46	119.15
T218	8.64	118.59	8.63	118.55
G219	8.50	108.66	8.49	108.63
Q220	8.44	120.83	8.44	120.81
Q221	7.51	120.11	7.52	120.09
I222	7.99	119.90	7.98	119.97
G223	8.33	107.24	8.35	107.14
D224	8.45	122.58	8.45	122.38
E225	8.11	122.24	8.08	121.98
V226				
R227	8.20	120.42	8.17	120.36
A228	7.79	121.00	7.77	121.02
L229	7.74	119.21	7.75	119.23
H230	8.41	119.59	8.39	119.51
D231	8.80	121.52	8.79	121.41
T232	7.35	108.27	7.35	108.25
G233	7.47	108.03	7.46	108.05
K234	7.45	115.88	7.45	115.88
F235	8.55	121.08	8.57	120.96
T236	9.40	113.47	9.35	113.76
D237	8.48	121.18	8.45	121.19
G238	8.04	109.25		
Q239				
L240				
V241				
S242				
Q243				
K244				
S245	8.13	116.16	8.10	116.24
D246	8.37	120.83	8.36	120.53
S247	8.00	114.05	8.01	114.27
S248	8.47	119.99	8.50	119.94
K249	7.94	121.75	7.96	121.84
D250	8.03	117.11	8.02	117.16
I251	7.75	121.72	7.70	121.17
R252	7.92	114.05	7.89	113.91
G253	8.73	110.46	8.74	110.44
D254	9.35	116.28	9.33	116.25
K255				
I256	9.59	114.96	9.58	114.86
T257	7.93	113.06	7.89	113.06
W258	7.88	124.78	7.85	124.54
I259	9.74	126.04	9.75	126.05
E260	11.23	129.03	11.24	128.92
G261	9.91	109.41	9.91	109.38
K262	6.71	116.63	6.72	116.60
E263	10.54	126.65	10.52	126.54
P264				
G265	8.98	113.83	8.92	113.56
C266	7.54	115.01	7.54	114.90
E267	9.03	120.57	9.01	120.61
T268	9.79	120.90	9.58	120.41
I269				
G270	8.38	106.99	8.37	107.14
L271	7.55	125.49	7.54	125.40
L272				
M273				
S274				
S275				
M276				
D277				
D278				

L279				
I280				
R281				
H282	7.58	113.99	7.58	113.96
C283	7.57	115.76	7.57	115.77
N284	7.52	117.03	7.52	116.95
G285	8.63	112.69	8.61	112.20
K286	7.91	116.16	7.88	116.16
L287	7.56	120.34	7.60	120.46
G288	8.71	114.34	8.74	114.46
S289	7.70	118.88	7.68	118.73
Y290	7.16	120.13	7.20	120.10
K291	9.07	126.01	9.06	125.97
I292	8.48	125.11	8.46	125.16
N293	8.31	125.27	8.28	125.21
G294	7.79	108.73	7.80	108.75
R295	9.04	115.23	9.01	115.22
T296	7.86	108.60	7.91	108.63
K297	7.90	115.46	7.94	115.43
A298	8.34	121.00	8.34	120.99
M299	9.70	124.93	9.70	125.11
V300	8.49	129.83	8.47	129.71
A301	8.89	127.80	8.84	127.69
C302	9.14	120.27	9.13	120.26
Y303	9.03	129.91	9.03	129.81
P304				
G305				
N306				
G307				
T308				
G309				
Y310				
V311	8.07	119.18	8.08	119.11
R312	8.06	120.24	8.04	120.15
H313	8.72	122.03	8.71	122.11
V314	8.17	117.17	8.15	117.15
D315	9.11	128.94	9.05	129.05
N316	7.12	106.18	7.14	106.36
P317				
N318	8.36	118.78		
G319	8.20	112.80	8.19	112.61
D320	8.92	119.45	8.94	119.65
G321	9.15	106.62	9.05	106.47
R322				
C323	9.69	121.22	9.71	121.28
V324	7.29	125.71	7.29	125.72
T325				
C326				
I327				
Y328				
Y329				
L330				
N331				
K332				
D333				
W334				
D335				
A336				
K337				
V338				
S339				
G340				
G341				
I342				
L343	7.63	127.15	7.64	127.17
R344	8.82	130.87	8.82	130.84
I345	8.82	125.98	8.82	126.04
F346	8.48	125.42	8.49	125.27
P347				
E348	9.25	123.75	9.28	123.51
G349	8.91	111.72	8.91	111.54
K350	7.55	119.05	7.55	119.10
A351	8.28	122.42	8.26	122.30
Q352	7.35	115.83	7.35	115.90
F353	7.03	118.96	7.04	118.87
A354	9.00	124.43	8.99	124.35
D355	8.25	123.39	8.26	123.36
I356	9.67	126.42	9.67	126.36
E357	8.31	125.65	8.31	125.71
P358				
K359	7.44	122.37	7.42	122.31
F360	7.14	119.19	7.14	119.23
D361	7.63	125.75	7.63	125.72
R362				
L363				
L364				
F365				
F366				
W367	7.15	117.83	7.13	117.72
S368	7.53	114.30	7.54	114.26
D369	7.74	119.49	7.73	119.53
R370	7.64	110.69	7.63	110.76
R371	8.30	118.79	8.31	118.79
N372	7.39	110.84	7.40	110.90
P373				
H374	8.95	118.35	8.92	118.32
E375	9.01	116.19	9.00	116.08
V376	9.21	123.12	9.21	123.22
Q377	8.66	127.84	8.66	127.80
P378				
A379				
Y380				
A381	7.65	121.78	7.64	121.80
T382	8.18	116.06	8.18	116.05
R383	8.37	130.46	8.37	130.40
Y384	9.70	127.04	9.69	126.96
A385	8.52	121.81	8.50	121.83
I386				
T387				
V388				
W389				
Y390				
F391	8.73	121.18	8.73	121.19
D392	8.36	119.49		
A393	9.35	128.87	9.34	128.83
D394	8.28	118.05	8.27	117.98

E395	8.78	122.10	8.80	121.96
R396	8.75	118.22	8.76	118.29
A397	7.41	118.58	7.44	118.88
R398	7.44	116.98	7.40	116.69
A399	7.63	121.35	7.58	121.46
K400	7.09	114.94	7.24	116.02
V401	7.21	118.00	7.33	118.73
K402	7.60	129.41	7.66	129.04

Table I-viii Protein backbone assignments of $PHD2_{181-402}$-Zn(II)-2OG-CODD and $PHD2_{181-402}$-Zn(II)-2OG-Y565A CODD.

Protein backbone assignment for $PHD2_{181-402}$-Zn(II)-2OG-I566A CODD (sequence: DLDLEMLAPYAPMDDDFQL).

Transfer of ^{1}H and ^{15}N assignment				
	^{15}N-$PHD2_{181-402}$-Zn(II)-2OG-CODD		^{15}N-$PHD2_{181-402}$-Zn(II)-2OG-I566A CODD	
Residue	^{1}H	^{15}N	^{1}H	^{15}N
G				
S	8.54	115.47	8.54	115.47
H	8.61	120.70	8.60	120.69
M	8.32	122.67	8.31	122.67
A	8.36	126.06	8.36	126.06
S	8.25	116.25	8.24	116.24
P181				
N182	8.60	119.73	8.60	119.74
G183	8.30	109.27	8.30	109.27
Q184	8.16	119.61	8.16	119.62
T185				
K186	8.19	125.08	8.18	125.03
P187				
L188				
P189				
A190	8.32	123.08	8.31	123.08
L191	7.94	116.86	7.94	116.86
K192	7.21	117.45	7.20	117.30
L193				
A194	8.06	119.86	8.06	119.86
L195	7.97	112.82	7.96	112.83
E196				
Y197	7.21	117.10	7.22	117.16
I198	8.63	121.20	8.62	121.12
V199	8.44	116.09	8.41	116.03
P200				
C201	7.70	116.41	7.69	116.40
M202	8.54	117.76	8.53	117.76
N203	8.43	117.02	8.43	117.05
K204	7.86	117.25	7.86	117.21
H205	8.40	112.54	8.39	112.47
G206	8.52	111.15	8.50	111.13
I207	6.58	115.82	6.58	115.85
C208				
V209	8.69	130.40	8.69	130.38
V210				
D211	8.36	125.70		
D212	8.57	117.75	8.56	117.79
F213	8.42	117.37		
L214				
G215	10.19	115.52	10.18	115.46
K216	8.12	117.94	8.11	117.90
E217	8.47	119.25	8.47	119.21
T218	8.64	118.59	8.63	118.55
G219	8.50	108.66	8.49	108.62
Q220	8.44	120.83	8.44	120.82
Q221	7.51	120.11	7.51	120.11
I222	7.99	119.90	7.99	119.90
G223	8.33	107.24	8.33	107.24
D224	8.45	122.58	8.44	122.53
E225	8.11	122.24	8.10	122.16
V226				
R227	8.20	120.42	8.19	120.40
A228	7.79	121.00	7.78	121.00
L229	7.74	119.21	7.75	119.22
H230	8.41	119.59	8.42	119.60
D231	8.80	121.52	8.79	121.50
T232	7.35	108.27	7.35	108.29
G233	7.47	108.03	7.47	108.04
K234	7.45	115.88	7.45	115.91
F235	8.55	121.08	8.57	121.14
T236	9.40	113.47	9.41	113.52
D237	8.48	121.18	8.48	121.16
G238	8.04	109.25	8.06	109.06
Q239				
L240				
V241				
S242				
Q243				
K244				
S245	8.13	116.16	8.13	116.14
D246	8.37	120.83	8.36	120.82
S247	8.00	114.05	8.00	114.09
S248	8.47	119.99	8.47	119.99
K249	7.94	121.75	7.94	121.77
D250	8.03	117.11	8.05	117.16
I251	7.75	121.72		
R252	7.92	114.05	7.93	114.03
G253	8.73	110.46		
D254	9.35	116.28	9.35	116.22
K255				
I256	9.59	114.96	9.62	115.14
T257	7.93	113.06	7.94	113.11
W258	7.88	124.78	7.90	124.68
I259	9.74	126.04	9.75	125.79
E260	11.23	129.03	11.22	128.84
G261	9.91	109.41	9.89	109.23
K262	6.71	116.63	6.70	116.64
E263	10.54	126.65	10.52	126.60
P264				
G265	8.98	113.83	8.97	113.75
C266	7.54	115.01	7.54	115.00
E267	9.03	120.57	9.02	120.56
T268	9.79	120.90	9.77	120.84
I269				
G270	8.38	106.99	8.38	107.03
L271	7.55	125.49	7.55	125.48
L272				
M273				
S274				
S275				
M276				
D277				
D278				

L279				
I280				
R281				
H282	7.58	113.99	7.59	114.02
C283	7.57	115.76	7.56	115.78
N284	7.52	117.03	7.52	116.95
G285	8.63	112.69	8.61	112.34
K286	7.91	116.16	7.88	116.17
L287	7.56	120.34	7.60	120.49
G288	8.71	114.34	8.73	114.44
S289	7.70	118.88	7.67	118.68
Y290	7.16	120.13	7.17	120.15
K291	9.07	126.01	9.05	125.97
I292	8.48	125.11	8.45	125.11
N293	8.31	125.27		
G294	7.79	108.73	7.74	108.45
R295	9.04	115.23	8.90	115.12
T296	7.86	108.60	7.83	108.42
K297	7.90	115.46		
A298	8.34	121.00		
M299	9.70	124.93	9.64	124.80
V300	8.49	129.83	8.51	129.78
A301	8.89	127.80	8.87	127.69
C302	9.14	120.27	9.17	120.29
Y303	9.03	129.91	9.03	129.85
P304				
G305				
N306				
G307				
T308				
G309				
Y310				
V311	8.07	119.18	8.08	119.10
R312	8.06	120.24	8.06	120.18
H313	8.72	122.03	8.66	122.06
V314	8.17	117.17	8.15	117.18
D315	9.11	128.94	9.04	129.26
N316	7.12	106.18		
P317				
N318	8.36	118.78		
G319	8.20	112.80	8.22	112.85
D320	8.92	119.45	9.03	119.79
G321	9.15	106.62	9.15	107.20
R322				
C323	9.69	121.22		
V324	7.29	125.71	7.36	125.52
T325				
C326				
I327				
Y328				
Y329				
L330				
N331				
K332				
D333				
W334				
D335				
A336				
K337				
V338				
S339				
G340				
G341				
I342				
L343	7.63	127.15	7.63	127.13
R344	8.82	130.87	8.81	130.90
I345	8.82	125.98	8.81	125.98
F346	8.48	125.42	8.48	125.40
P347				
E348	9.25	123.75	9.27	123.72
G349	8.91	111.72	8.91	111.72
K350	7.55	119.05	7.55	119.05
A351	8.28	122.42	8.28	122.42
Q352	7.35	115.83	7.35	115.84
F353	7.03	118.96	7.03	118.91
A354	9.00	124.43	8.99	124.40
D355	8.25	123.39	8.24	123.42
I356	9.67	126.42	9.67	126.37
E357	8.31	125.65	8.31	125.69
P358				
K359	7.44	122.37	7.43	122.28
F360	7.14	119.19	7.14	119.20
D361	7.63	125.75	7.63	125.70
R362				
L363				
L364				
F365				
F366				
W367	7.15	117.83	7.15	117.73
S368	7.53	114.30		
D369	7.74	119.49	7.77	119.62
R370	7.64	110.69	7.60	110.70
R371	8.30	118.79	8.30	119.07
N372	7.39	110.84	7.42	110.99
P373				
H374	8.95	118.35	8.93	118.28
E375	9.01	116.19	9.00	116.16
V376	9.21	123.12	9.20	123.13
Q377	8.66	127.84	8.66	127.84
P378				
A379				
Y380				
A381	7.65	121.78	7.65	121.82
T382	8.18	116.06	8.18	116.03
R383	8.37	130.46	8.38	130.43
Y384	9.70	127.04	9.70	127.00
A385	8.52	121.81	8.51	121.74
I386				
T387				
V388				
W389				
Y390				
F391	8.73	121.18	8.75	119.83
D392	8.36	119.49		
A393	9.35	128.87	9.33	128.76
D394	8.28	118.05	8.27	117.90

E395	8.78	122.10	8.67	122.05
R396	8.75	118.22	8.74	118.51
A397	7.41	118.58	7.41	118.36
R398	7.44	116.98	7.44	117.08
A399	7.63	121.35	7.70	121.51
K400	7.09	114.94	7.13	114.99
V401	7.21	118.00	7.23	117.77
K402	7.60	129.41	7.57	129.26

Table I-ix Protein backbone assignments of $PHD2_{181-402}$-Zn(II)-2OG-CODD and $PHD2_{181-402}$-Zn(II)-2OG-I566A CODD.

Protein backbone assignment for $PHD2_{181-402}$-Zn(II)-2OG-P567A CODD (sequence: DLDLEMLAPYIAMDDDFQL).

Transfer of ^{1}H and ^{15}N assignment				
	^{15}N-$PHD2_{181-402}$-Zn(II)-2OG-CODD		^{15}N-$PHD2_{181-402}$-Zn(II)-2OG-P567A CODD	
Residue	^{1}H	^{15}N	^{1}H	^{15}N
G				
S	8.54	115.47	8.54	115.47
H	8.61	120.70	8.61	120.69
M	8.32	122.67	8.31	122.71
A	8.36	126.06	8.36	126.06
S	8.25	116.25	8.24	116.21
P181				
N182	8.60	119.73	8.60	119.73
G183	8.30	109.27	8.30	109.25
Q184	8.16	119.61	8.16	119.62
T185				
K186	8.19	125.08	8.17	125.02
P187				
L188				
P189				
A190	8.32	123.08	8.33	123.16
L191	7.94	116.86	7.94	116.89
K192	7.21	117.45	7.19	117.45
L193				
A194	8.06	119.86	8.06	119.85
L195	7.97	112.82	7.98	112.83
E196				
Y197	7.21	117.10	7.22	117.23
I198	8.63	121.20	8.62	121.09
V199	8.44	116.09	8.43	116.08
P200				
C201	7.70	116.41	7.67	116.39
M202	8.54	117.76	8.55	117.76
N203	8.43	117.02	8.42	116.95
K204	7.86	117.25	7.84	117.30
H205	8.40	112.54	8.38	112.72
G206	8.52	111.15	8.51	111.09
I207	6.58	115.82	6.58	115.84
C208				
V209	8.69	130.40	8.70	130.41
V210				
D211	8.36	125.70	8.36	125.70
D212	8.57	117.75	8.58	117.82
F213	8.42	117.37	8.43	117.40
L214				
G215	10.19	115.52	10.18	115.51
K216	8.12	117.94	8.12	117.92
E217	8.47	119.25	8.48	119.25
T218	8.64	118.59	8.63	118.56
G219	8.50	108.66	8.49	108.65
Q220	8.44	120.83	8.44	120.82
Q221	7.51	120.11	7.49	120.14
I222	7.99	119.90	7.99	119.84
G223	8.33	107.24	8.33	107.19
D224	8.45	122.58	8.44	122.67
E225	8.11	122.24	8.12	122.45
V226				
R227	8.20	120.42	8.20	120.41
A228	7.79	121.00	7.80	121.01
L229	7.74	119.21	7.73	119.24
H230	8.41	119.59	8.39	119.61
D231	8.80	121.52	8.81	121.55
T232	7.35	108.27	7.35	108.28
G233	7.47	108.03	7.46	108.04
K234	7.45	115.88	7.45	115.88
F235	8.55	121.08	8.56	121.07
T236	9.40	113.47	9.41	113.47
D237	8.48	121.18	8.47	121.17
G238	8.04	109.25	8.03	109.17
Q239				
L240				
V241				
S242				
Q243				
K244				
S245	8.13	116.16	8.12	116.18
D246	8.37	120.83	8.38	120.93
S247	8.00	114.05	7.99	113.94
S248	8.47	119.99	8.48	120.08
K249	7.94	121.75	7.94	121.74
D250	8.03	117.11	8.03	117.18
I251	7.75	121.72	7.72	121.70
R252	7.92	114.05	7.92	114.02
G253	8.73	110.46	8.74	110.51
D254	9.35	116.28	9.34	116.24
K255				
I256	9.59	114.96	9.59	114.98
T257	7.93	113.06	7.93	112.96
W258	7.88	124.78	7.89	124.63
I259	9.74	126.04	9.73	125.90
E260	11.23	129.03		
G261	9.91	109.41	9.90	109.66
K262	6.71	116.63	6.74	116.73
E263	10.54	126.65	10.52	126.65
P264				
G265	8.98	113.83	9.01	113.94
C266	7.54	115.01	7.52	115.06
E267	9.03	120.57	9.02	120.52
T268	9.79	120.90	9.97	121.35
I269				
G270	8.38	106.99	8.44	106.97
L271	7.55	125.49	7.55	125.55
L272				
M273				
S274				
S275				
M276				
D277				
D278				

L279				
I280				
R281				
H282	7.58	113.99	7.60	114.17
C283	7.57	115.76	7.57	115.75
N284	7.52	117.03	7.53	117.07
G285	8.63	112.69	8.62	112.84
K286	7.91	116.16	7.92	116.17
L287	7.56	120.34	7.55	120.36
G288	8.71	114.34	8.73	114.43
S289	7.70	118.88	7.70	118.95
Y290	7.16	120.13	7.16	120.13
K291	9.07	126.01	9.06	125.96
I292	8.48	125.11	8.48	125.10
N293	8.31	125.27	8.29	125.05
G294	7.79	108.73	7.77	108.71
R295	9.04	115.23	8.98	115.09
T296	7.86	108.60	7.84	108.48
K297	7.90	115.46	7.90	115.31
A298	8.34	121.00		
M299	9.70	124.93	9.76	125.16
V300	8.49	129.83	8.49	129.84
A301	8.89	127.80	8.89	127.80
C302	9.14	120.27	9.15	120.33
Y303	9.03	129.91	9.03	129.97
P304				
G305				
N306				
G307				
T308				
G309				
Y310				
V311	8.07	119.18	8.07	119.16
R312	8.06	120.24	8.06	120.33
H313	8.72	122.03	8.71	122.06
V314	8.17	117.17	8.17	117.15
D315	9.11	128.94	9.10	128.95
N316	7.12	106.18	7.13	106.12
P317				
N318	8.36	118.78		
G319	8.20	112.80	8.20	112.85
D320	8.92	119.45	8.91	119.39
G321	9.15	106.62	9.19	106.75
R322				
C323	9.69	121.22	9.70	121.16
V324	7.29	125.71	7.29	125.69
T325				
C326				
I327				
Y328				
Y329				
L330				
N331				
K332				
D333				
W334				
D335				
A336				
K337				
V338				
S339				
G340				
G341				
I342				
L343	7.63	127.15	7.64	127.07
R344	8.82	130.87	8.82	130.95
I345	8.82	125.98	8.82	125.98
F346	8.48	125.42	8.48	125.44
P347				
E348	9.25	123.75	9.25	123.93
G349	8.91	111.72	8.91	111.82
K350	7.55	119.05	7.55	119.01
A351	8.28	122.42	8.29	122.47
Q352	7.35	115.83	7.35	115.77
F353	7.03	118.96	7.02	119.08
A354	9.00	124.43	9.00	124.55
D355	8.25	123.39	8.24	123.43
I356	9.67	126.42	9.68	126.49
E357	8.31	125.65	8.30	125.63
P358				
K359	7.44	122.37	7.43	122.39
F360	7.14	119.19	7.13	119.25
D361	7.63	125.75	7.62	125.72
R362				
L363				
L364				
F365				
F366				
W367	7.15	117.83	7.15	117.84
S368	7.53	114.30	7.53	114.27
D369	7.74	119.49	7.74	119.50
R370	7.64	110.69	7.63	110.68
R371	8.30	118.79	8.31	118.84
N372	7.39	110.84	7.39	110.83
P373				
H374	8.95	118.35	8.94	118.35
E375	9.01	116.19	9.02	116.27
V376	9.21	123.12	9.20	123.05
Q377	8.66	127.84	8.65	127.82
P378				
A379				
Y380				
A381	7.65	121.78	7.65	121.73
T382	8.18	116.06	8.18	116.00
R383	8.37	130.46	8.36	130.47
Y384	9.70	127.04	9.71	126.95
A385	8.52	121.81	8.52	121.87
I386				
T387				
V388				
W389				
Y390				
F391	8.73	121.18	8.70	121.06
D392	8.36	119.49	8.35	119.48
A393	9.35	128.87	9.36	128.86
D394	8.28	118.05	8.27	118.08

E395	8.78	122.10	8.75	122.12
R396	8.75	118.22	8.75	118.20
A397	7.41	118.58	7.42	118.49
R398	7.44	116.98	7.42	117.02
A399	7.63	121.35	7.65	121.34
K400	7.09	114.94	7.07	114.77
V401	7.21	118.00	7.20	117.93
K402	7.60	129.41	7.58	129.56

Table I-x Protein backbone assignments of $PHD2_{181-402}$-Zn(II)-2OG-CODD and $PHD2_{181-402}$-Zn(II)-2OG-P567A CODD.

Protein backbone assignment for $PHD2_{181-402}$-Zn(II)-2OG-M568A CODD (sequence: DLDLEMLAPYIPADDDFQL).

Transfer of ^{1}H and ^{15}N assignment				
	^{15}N-$PHD2_{181-402}$-Zn(II)-2OG-CODD		^{15}N-$PHD2_{181-402}$-Zn(II)-2OG-M568A CODD	
Residue	^{1}H	^{15}N	^{1}H	^{15}N
G				
S	8.54	115.47	8.54	115.47
H	8.61	120.70		
M	8.32	122.67	8.32	122.65
A	8.36	126.06	8.36	126.05
S	8.25	116.25	8.25	116.26
P181				
N182	8.60	119.73	8.60	119.74
G183	8.30	109.27	8.30	109.27
Q184	8.16	119.61	8.16	119.61
T185				
K186	8.19	125.08	8.19	125.10
P187				
L188				
P189				
A190	8.32	123.08	8.32	123.05
L191	7.94	116.86	7.94	116.83
K192	7.21	117.45	7.19	117.31
L193				
A194	8.06	119.86	8.06	119.82
L195	7.97	112.82	7.97	112.80
E196				
Y197	7.21	117.10	7.20	116.99
I198	8.63	121.20	8.61	121.07
V199	8.44	116.09	8.45	116.02
P200				
C201	7.70	116.41	7.69	116.43
M202	8.54	117.76	8.53	117.75
N203	8.43	117.02	8.43	117.04
K204	7.86	117.25	7.87	117.28
H205	8.40	112.54	8.40	112.49
G206	8.52	111.15	8.51	111.23
I207	6.58	115.82	6.58	115.85
C208				
V209	8.69	130.40	8.67	130.42
V210				
D211	8.36	125.70		
D212	8.57	117.75	8.57	117.76
F213	8.42	117.37		
L214				
G215	10.19	115.52	10.19	115.50
K216	8.12	117.94	8.11	117.93
E217	8.47	119.25	8.47	119.21
T218	8.64	118.59	8.63	118.62
G219	8.50	108.66	8.50	108.68
Q220	8.44	120.83	8.44	120.82
Q221	7.51	120.11	7.51	120.15
I222	7.99	119.90	7.99	119.89
G223	8.33	107.24	8.32	107.24
D224	8.45	122.58	8.45	122.54
E225	8.11	122.24	8.11	122.22
V226				
R227	8.20	120.42	8.19	120.40
A228	7.79	121.00	7.78	121.02
L229	7.74	119.21	7.75	119.20
H230	8.41	119.59	8.41	119.59
D231	8.80	121.52	8.80	121.48
T232	7.35	108.27	7.35	108.28
G233	7.47	108.03	7.46	108.04
K234	7.45	115.88	7.45	115.88
F235	8.55	121.08	8.55	121.12
T236	9.40	113.47	9.40	113.45
D237	8.48	121.18	8.47	121.19
G238	8.04	109.25	8.03	109.27
Q239				
L240				
V241				
S242				
Q243				
K244				
S245	8.13	116.16	8.13	116.15
D246	8.37	120.83	8.37	120.85
S247	8.00	114.05	8.00	114.04
S248	8.47	119.99	8.46	119.96
K249	7.94	121.75	7.94	121.77
D250	8.03	117.11	8.04	117.15
I251	7.75	121.72	7.74	121.75
R252	7.92	114.05	7.92	114.00
G253	8.73	110.46	8.71	110.34
D254	9.35	116.28	9.36	116.27
K255				
I256	9.59	114.96	9.59	114.97
T257	7.93	113.06	7.92	113.07
W258	7.88	124.78	7.87	124.72
I259	9.74	126.04	9.74	126.05
E260	11.23	129.03	11.23	129.03
G261	9.91	109.41	9.92	109.40
K262	6.71	116.63	6.71	116.64
E263	10.54	126.65	10.53	126.63
P264				
G265	8.98	113.83	8.97	113.81
C266	7.54	115.01	7.54	115.01
E267	9.03	120.57	9.03	120.57
T268	9.79	120.90	9.78	120.86
I269				
G270	8.38	106.99	8.38	107.00
L271	7.55	125.49	7.55	125.50
L272				
M273				
S274				
S275				
M276				
D277				
D278				

L279				
I280				
R281				
H282	7.58	113.99	7.57	114.00
C283	7.57	115.76	7.56	115.75
N284	7.52	117.03	7.52	117.00
G285	8.63	112.69	8.62	112.60
K286	7.91	116.16	7.90	116.10
L287	7.56	120.34	7.57	120.35
G288	8.71	114.34	8.71	114.39
S289	7.70	118.88	7.70	118.90
Y290	7.16	120.13	7.18	120.12
K291	9.07	126.01	9.07	126.01
I292	8.48	125.11	8.48	125.08
N293	8.31	125.27		
G294	7.79	108.73	7.79	108.78
R295	9.04	115.23	9.02	115.24
T296	7.86	108.60	7.89	108.61
K297	7.90	115.46	7.93	115.39
A298	8.34	121.00	8.33	120.92
M299	9.70	124.93	9.69	124.88
V300	8.49	129.83	8.48	129.78
A301	8.89	127.80	8.89	127.76
C302	9.14	120.27	9.14	120.29
Y303	9.03	129.91	9.03	129.93
P304				
G305				
N306				
G307				
T308				
G309				
Y310				
V311	8.07	119.18	8.09	119.15
R312	8.06	120.24	8.06	120.18
H313	8.72	122.03	8.71	122.01
V314	8.17	117.17	8.16	117.19
D315	9.11	128.94	9.10	129.02
N316	7.12	106.18	7.14	106.27
P317				
N318	8.36	118.78		
G319	8.20	112.80	8.20	112.76
D320	8.92	119.45	8.93	119.59
G321	9.15	106.62	9.11	106.49
R322				
C323	9.69	121.22	9.69	121.13
V324	7.29	125.71	7.29	125.74
T325				
C326				
I327				
Y328				
Y329				
L330				
N331				
K332				
D333				
W334				
D335				
A336				
K337				
V338				
S339				
G340				
G341				
I342				
L343	7.63	127.15	7.64	127.24
R344	8.82	130.87	8.82	130.90
I345	8.82	125.98	8.81	126.01
F346	8.48	125.42	8.48	125.40
P347				
E348	9.25	123.75	9.26	123.79
G349	8.91	111.72	8.91	111.75
K350	7.55	119.05	7.55	119.04
A351	8.28	122.42	8.29	122.45
Q352	7.35	115.83	7.35	115.82
F353	7.03	118.96	7.03	118.94
A354	9.00	124.43	9.00	124.36
D355	8.25	123.39	8.26	123.43
I356	9.67	126.42	9.66	126.40
E357	8.31	125.65	8.30	125.64
P358				
K359	7.44	122.37	7.43	122.30
F360	7.14	119.19	7.14	119.28
D361	7.63	125.75	7.62	125.82
R362				
L363				
L364				
F365				
F366				
W367	7.15	117.83	7.15	117.84
S368	7.53	114.30	7.54	114.31
D369	7.74	119.49	7.74	119.55
R370	7.64	110.69	7.63	110.70
R371	8.30	118.79	8.29	118.77
N372	7.39	110.84	7.39	110.87
P373				
H374	8.95	118.35	8.94	118.34
E375	9.01	116.19	9.00	116.20
V376	9.21	123.12	9.21	123.16
Q377	8.66	127.84	8.66	127.88
P378				
A379				
Y380				
A381	7.65	121.78	7.66	121.80
T382	8.18	116.06	8.18	116.05
R383	8.37	130.46	8.36	130.45
Y384	9.70	127.04	9.71	127.08
A385	8.52	121.81	8.51	121.81
I386				
T387				
V388				
W389				
Y390				
F391	8.73	121.18		
D392	8.36	119.49	8.39	119.50
A393	9.35	128.87	9.34	128.90
D394	8.28	118.05	8.24	118.02

E395	8.78	122.10	8.81	122.05
R396	8.75	118.22	8.73	118.24
A397	7.41	118.58	7.39	118.73
R398	7.44	116.98	7.45	117.00
A399	7.63	121.35	7.58	121.43
K400	7.09	114.94	7.19	116.02
V401	7.21	118.00	7.34	118.69
K402	7.60	129.41	7.64	129.39

Table I-xi Protein backbone assignments of $PHD2_{181-402}$-Zn(II)-2OG-CODD and $PHD2_{181-402}$-Zn(II)-2OG-M568A CODD.

Protein backbone assignment for $PHD2_{181-402}$-Zn(II)-2OG-F572A CODD (sequence: DLDLEMLAPYIPMDDDAQL).

Transfer of ^{1}H and ^{15}N assignment				
	^{15}N-$PHD2_{181-402}$-Zn(II)-2OG-CODD		^{15}N-$PHD2_{181-402}$-Zn(II)-2OG-F572A CODD	
Residue	^{1}H	^{15}N	^{1}H	^{15}N
G				
S	8.54	115.47	8.54307	115.47385
H	8.61	120.70		
M	8.32	122.67	8.31352	122.67663
A	8.36	126.06	8.35723	126.06747
S	8.25	116.25	8.24447	116.25968
P181				
N182	8.60	119.73	8.59552	119.73017
G183	8.30	109.27	8.29951	109.26698
Q184	8.16	119.61	8.15804	119.62788
T185				
K186	8.19	125.08	8.1845	125.08361
P187				
L188				
P189				
A190	8.32	123.08	8.31842	123.07948
L191	7.94	116.86	7.9336	116.85451
K192	7.21	117.45	7.20166	117.31992
L193				
A194	8.06	119.86	8.05596	119.87976
L195	7.97	112.82	7.95691	112.82546
E196				
Y197	7.21	117.10	7.21758	117.13421
I198	8.63	121.20		
V199	8.44	116.09	8.42636	116.0923
P200				
C201	7.70	116.41	7.69068	116.42088
M202	8.54	117.76	8.53537	117.79254
N203	8.43	117.02	8.43161	117.06034
K204	7.86	117.25	7.87106	117.19823
H205	8.40	112.54	8.39131	112.43317
G206	8.52	111.15	8.50463	111.20057
I207	6.58	115.82	6.58187	115.79394
C208				
V209	8.69	130.40	8.69426	130.39184
V210				
D211	8.36	125.70		
D212	8.57	117.75	8.55887	117.77362
F213	8.42	117.37		
L214				
G215	10.19	115.52	10.18735	115.49932
K216	8.12	117.94	8.11335	117.93505
E217	8.47	119.25	8.4654	119.22304
T218	8.64	118.59	8.63188	118.53018
G219	8.50	108.66	8.49879	108.6374
Q220	8.44	120.83	8.44007	120.79289
Q221	7.51	120.11	7.5208	120.11213
I222	7.99	119.90	7.99248	119.92346
G223	8.33	107.24	8.34208	107.22977
D224	8.45	122.58	8.4569	122.48545
E225	8.11	122.24	8.10046	122.12857
V226				
R227	8.20	120.42	8.18769	120.38222
A228	7.79	121.00	7.78169	121.04788
L229	7.74	119.21	7.75858	119.17942
H230	8.41	119.59	8.41877	119.61926
D231	8.80	121.52	8.7986	121.51466
T232	7.35	108.27	7.34758	108.26734
G233	7.47	108.03	7.46481	108.03001
K234	7.45	115.88	7.44851	115.88163
F235	8.55	121.08	8.54628	121.03911
T236	9.40	113.47	9.4053	113.44596
D237	8.48	121.18	8.48754	121.19276
G238	8.04	109.25	8.04257	109.28474
Q239				
L240				
V241				
S242				
Q243				
K244				
S245	8.13	116.16	8.13288	116.15301
D246	8.37	120.83	8.36695	120.75573
S247	8.00	114.05	8.00504	114.13173
S248	8.47	119.99	8.46517	119.97574
K249	7.94	121.75	7.93778	121.75452
D250	8.03	117.11	8.03532	117.06152
I251	7.75	121.72	7.75737	121.68742
R252	7.92	114.05	7.91946	114.07435
G253	8.73	110.46	8.71841	110.42624
D254	9.35	116.28	9.35188	116.25696
K255				
I256	9.59	114.96	9.58059	114.91407
T257	7.93	113.06	7.91879	113.0938
W258	7.88	124.78	7.86289	124.75718
I259	9.74	126.04	9.76542	126.04945
E260	11.23	129.03	11.32	130.00925
G261	9.91	109.41	10.01875	109.57148
K262	6.71	116.63	6.85963	116.99058
E263	10.54	126.65	10.58156	126.49976
P264				
G265	8.98	113.83	8.96411	113.74226
C266	7.54	115.01	7.54148	115.03442
E267	9.03	120.57	9.02922	120.68396
T268	9.79	120.90	9.70268	120.61699
I269				
G270	8.38	106.99	8.43786	107.18972
L271	7.55	125.49	7.59049	125.59444
L272				
M273				
S274				
S275				
M276				
D277				
D278				

L279				
I280				
R281				
H282	7.58	113.99	7.57184	114.04115
C283	7.57	115.76	7.55745	115.75673
N284	7.52	117.03	7.51348	117.02967
G285	8.63	112.69	8.62943	112.51922
K286	7.91	116.16	7.89172	116.14288
L287	7.56	120.34	7.54725	120.36117
G288	8.71	114.34	8.66484	114.22657
S289	7.70	118.88	7.6693	118.72151
Y290	7.16	120.13	7.177	120.19425
K291	9.07	126.01	9.03645	125.96184
I292	8.48	125.11	8.47788	125.183
N293	8.31	125.27		
G294	7.79	108.73	7.79452	108.37399
R295	9.04	115.23	8.64702	114.98896
T296	7.86	108.60	7.94038	108.61913
K297	7.90	115.46	7.85067	115.80519
A298	8.34	121.00		
M299	9.70	124.93	9.71623	125.08475
V300	8.49	129.83	8.49536	129.90693
A301	8.89	127.80	8.89629	127.79275
C302	9.14	120.27	9.13272	120.2588
Y303	9.03	129.91	9.03572	129.97785
P304				
G305				
N306				
G307				
T308				
G309				
Y310				
V311	8.07	119.18	8.07982	119.11502
R312	8.06	120.24	8.05501	120.2062
H313	8.72	122.03	8.72302	122.0781
V314	8.17	117.17	8.1608	117.19364
D315	9.11	128.94	9.1012	128.92535
N316	7.12	106.18	7.11492	106.10643
P317				
N318	8.36	118.78		
G319	8.20	112.80	8.2041	112.77667
D320	8.92	119.45	8.91706	119.4067
G321	9.15	106.62	9.09703	106.53591
R322				
C323	9.69	121.22		
V324	7.29	125.71	7.24179	125.73183
T325				
C326				
I327				
Y328				
Y329				
L330				
N331				
K332				
D333				
W334				
D335				
A336				
K337				
V338				
S339				
G340				
G341				
I342				
L343	7.63	127.15	7.64118	127.19692
R344	8.82	130.87	8.81882	130.88305
I345	8.82	125.98	8.81118	126.01179
F346	8.48	125.42	8.49401	125.2829
P347				
E348	9.25	123.75	9.2559	123.61761
G349	8.91	111.72	8.91227	111.63056
K350	7.55	119.05	7.54787	119.05656
A351	8.28	122.42	8.27223	122.34886
Q352	7.35	115.83	7.34601	115.8874
F353	7.03	118.96	7.03726	118.8949
A354	9.00	124.43	9.00317	124.31144
D355	8.25	123.39	8.25405	123.38336
I356	9.67	126.42	9.67016	126.3514
E357	8.31	125.65	8.30592	125.69358
P358				
K359	7.44	122.37	7.43911	122.32645
F360	7.14	119.19	7.14882	119.26249
D361	7.63	125.75	7.62691	125.7314
R362				
L363				
L364				
F365				
F366				
W367	7.15	117.83	7.16045	117.92962
S368	7.53	114.30	7.51064	114.27081
D369	7.74	119.49	7.72821	119.55637
R370	7.64	110.69	7.62891	110.78098
R371	8.30	118.79	8.28338	118.78306
N372	7.39	110.84	7.38729	110.85992
P373				
H374	8.95	118.35	8.94336	118.35847
E375	9.01	116.19	8.998	116.06591
V376	9.21	123.12	9.21274	123.24412
Q377	8.66	127.84	8.66723	127.85186
P378				
A379				
Y380				
A381	7.65	121.78	7.6416	121.76763
T382	8.18	116.06	8.17832	116.08933
R383	8.37	130.46	8.36728	130.40927
Y384	9.70	127.04	9.71372	126.93193
A385	8.52	121.81	8.52182	121.84349
I386				
T387				
V388				
W389				
Y390				
F391	8.73	121.18	8.85635	121.90648
D392	8.36	119.49		
A393	9.35	128.87	9.34294	129.13178
D394	8.28	118.05	8.28186	118.03665

E395	8.78	122.10	8.74941	122.0424
R396	8.75	118.22	8.76376	118.2823
A397	7.41	118.58	7.40915	118.65472
R398	7.44	116.98	7.43481	116.97772
A399	7.63	121.35	7.6252	121.35569
K400	7.09	114.94	7.08251	114.99534
V401	7.21	118.00	7.2047	118.0165
K402	7.60	129.41	7.6136	129.29101

Table I-xii Protein backbone assignments of $PHD2_{181-402}$-Zn(II)-2OG-CODD and $PHD2_{181-402}$-Zn(II)-2OG-F572A CODD.

Protein backbone assignment for $PHD2_{181-402}$-Zn(II)-2OG-Q573A CODD (sequence: DLDLEMLAPYIPMDDDFAL).

	Transfer of ^{1}H and ^{15}N assignment			
	^{15}N-$PHD2_{181-402}$-Zn(II)-2OG-CODD		^{15}N-$PHD2_{181-402}$-Zn(II)-2OG-Q573A CODD	
Residue	^{1}H	^{15}N	^{1}H	^{15}N
G				
S	8.54	115.47	8.54	115.47
H	8.61	120.70		
M	8.32	122.67	8.32	122.63
A	8.36	126.06	8.36	126.05
S	8.25	116.25	8.24	116.26
P181				
N182	8.60	119.73	8.59	119.74
G183	8.30	109.27	8.30	109.24
Q184	8.16	119.61	8.16	119.61
T185				
K186	8.19	125.08	8.20	125.11
P187				
L188				
P189				
A190	8.32	123.08	8.31	123.11
L191	7.94	116.86	7.93	116.84
K192	7.21	117.45		
L193				
A194	8.06	119.86	8.07	119.82
L195	7.97	112.82	7.98	112.81
E196				
Y197	7.21	117.10	7.22	117.05
I198	8.63	121.20	8.62	121.22
V199	8.44	116.09	8.43	116.06
P200				
C201	7.70	116.41	7.69	116.38
M202	8.54	117.76	8.53	117.77
N203	8.43	117.02	8.44	117.02
K204	7.86	117.25	7.87	117.28
H205	8.40	112.54	8.40	112.50
G206	8.52	111.15	8.51	111.16
I207	6.58	115.82	6.58	115.83
C208				
V209	8.69	130.40		
V210				
D211	8.36	125.70		
D212	8.57	117.75	8.58	117.76
F213	8.42	117.37	8.44	117.30
L214				
G215	10.19	115.52	10.18	115.59
K216	8.12	117.94	8.11	117.93
E217	8.47	119.25	8.47	119.24
T218	8.64	118.59	8.63	118.60
G219	8.50	108.66	8.51	108.67
Q220	8.44	120.83	8.44	120.82
Q221	7.51	120.11	7.52	120.18
I222	7.99	119.90	7.99	119.88
G223	8.33	107.24	8.34	107.19
D224	8.45	122.58	8.45	122.58
E225	8.11	122.24	8.11	122.22
V226				
R227	8.20	120.42	8.20	120.41
A228	7.79	121.00	7.78	121.00
L229	7.74	119.21	7.75	119.18
H230	8.41	119.59	8.41	119.55
D231	8.80	121.52	8.80	121.53
T232	7.35	108.27	7.35	108.27
G233	7.47	108.03	7.47	108.03
K234	7.45	115.88	7.45	115.90
F235	8.55	121.08	8.55	121.12
T236	9.40	113.47	9.41	113.44
D237	8.48	121.18	8.48	121.19
G238	8.04	109.25	8.04	109.24
Q239				
L240				
V241				
S242				
Q243				
K244				
S245	8.13	116.16	8.13	116.13
D246	8.37	120.83	8.37	120.83
S247	8.00	114.05	8.00	114.04
S248	8.47	119.99	8.47	120.00
K249	7.94	121.75	7.94	121.75
D250	8.03	117.11	8.04	117.12
I251	7.75	121.72	7.75	121.69
R252	7.92	114.05	7.93	114.03
G253	8.73	110.46	8.72	110.59
D254	9.35	116.28	9.34	116.27
K255				
I256	9.59	114.96	9.60	114.99
T257	7.93	113.06	7.93	113.06
W258	7.88	124.78	7.88	124.78
I259	9.74	126.04	9.74	126.03
E260	11.23	129.03	11.23	128.97
G261	9.91	109.41	9.92	109.51
K262	6.71	116.63	6.70	116.56
E263	10.54	126.65	10.53	126.65
P264				
G265	8.98	113.83	8.97	113.82
C266	7.54	115.01	7.55	115.02
E267	9.03	120.57	9.03	120.57
T268	9.79	120.90	9.77	120.92
I269				
G270	8.38	106.99	8.37	106.99
L271	7.55	125.49	7.55	125.51
L272				
M273				
S274				
S275				
M276				
D277				
D278				

L279				
I280				
R281				
H282	7.58	113.99	7.57	114.01
C283	7.57	115.76	7.56	115.75
N284	7.52	117.03	7.52	117.04
G285	8.63	112.69	8.62	112.74
K286	7.91	116.16	7.91	116.13
L287	7.56	120.34	7.55	120.32
G288	8.71	114.34	8.69	114.29
S289	7.70	118.88	7.72	119.00
Y290	7.16	120.13	7.17	120.16
K291	9.07	126.01	9.06	126.00
I292	8.48	125.11	8.48	125.09
N293	8.31	125.27	8.27	125.84
G294	7.79	108.73	7.82	109.24
R295	9.04	115.23	9.06	115.58
T296	7.86	108.60	7.89	108.61
K297	7.90	115.46	7.90	115.35
A298	8.34	121.00	8.33	120.96
M299	9.70	124.93	9.71	124.92
V300	8.49	129.83	8.49	129.83
A301	8.89	127.80	8.89	127.80
C302	9.14	120.27	9.15	120.26
Y303	9.03	129.91	9.03	129.97
P304				
G305				
N306				
G307				
T308				
G309				
Y310				
V311	8.07	119.18	8.08	119.17
R312	8.06	120.24	8.05	120.24
H313	8.72	122.03	8.71	122.00
V314	8.17	117.17	8.15	117.13
D315	9.11	128.94	9.10	128.97
N316	7.12	106.18	7.13	106.18
P317				
N318	8.36	118.78	8.34	118.81
G319	8.20	112.80	8.20	112.80
D320	8.92	119.45	8.93	119.44
G321	9.15	106.62	9.16	106.64
R322				
C323	9.69	121.22	9.66	121.20
V324	7.29	125.71	7.28	125.72
T325				
C326				
I327				
Y328				
Y329				
L330				
N331				
K332				
D333				
W334				
D335				
A336				
K337				
V338				
S339				
G340				
G341				
I342				
L343	7.63	127.15	7.63	127.14
R344	8.82	130.87	8.83	130.91
I345	8.82	125.98	8.81	125.97
F346	8.48	125.42	8.48	125.37
P347				
E348	9.25	123.75	9.25	123.80
G349	8.91	111.72	8.91	111.75
K350	7.55	119.05	7.55	119.04
A351	8.28	122.42	8.28	122.44
Q352	7.35	115.83	7.35	115.83
F353	7.03	118.96	7.03	118.90
A354	9.00	124.43	8.99	124.31
D355	8.25	123.39	8.26	123.44
I356	9.67	126.42	9.67	126.38
E357	8.31	125.65	8.30	125.68
P358				
K359	7.44	122.37	7.43	122.31
F360	7.14	119.19	7.13	119.26
D361	7.63	125.75	7.62	125.81
R362				
L363				
L364				
F365				
F366				
W367	7.15	117.83	7.16	117.86
S368	7.53	114.30	7.53	114.29
D369	7.74	119.49	7.73	119.48
R370	7.64	110.69	7.63	110.72
R371	8.30	118.79	8.30	118.84
N372	7.39	110.84	7.39	110.86
P373				
H374	8.95	118.35	8.95	118.40
E375	9.01	116.19	9.00	116.15
V376	9.21	123.12	9.21	123.19
Q377	8.66	127.84	8.65	127.87
P378				
A379				
Y380				
A381	7.65	121.78	7.64	121.78
T382	8.18	116.06	8.18	116.05
R383	8.37	130.46	8.37	130.48
Y384	9.70	127.04	9.70	127.00
A385	8.52	121.81	8.51	121.83
I386				
T387				
V388				
W389				
Y390				
F391	8.73	121.18	8.71	121.22
D392	8.36	119.49	8.36	119.45
A393	9.35	128.87	9.32	128.76
D394	8.28	118.05	8.28	118.05

E395	8.78	122.10	8.77	122.09
R396	8.75	118.22	8.75	118.25
A397	7.41	118.58	7.40	118.58
R398	7.44	116.98	7.44	117.00
A399	7.63	121.35	7.63	121.33
K400	7.09	114.94	7.08	114.96
V401	7.21	118.00	7.21	118.00
K402	7.60	129.41	7.60	129.41

Table I-xiii Protein backbone assignments of $PHD2_{181-402}$-Zn(II)-2OG-CODD and $PHD2_{181-402}$-Zn(II)-2OG-Q_{573}A CODD.

Protein backbone assignment for $PHD2_{181-402}$-Zn(II)-2OG-L574A CODD (sequence: DLDLEMLAPYIPMDDDFQA).

	Transfer of ^{1}H and ^{15}N assignment			
	^{15}N-$PHD2_{181-402}$-Zn(II)-2OG-CODD		^{15}N-$PHD2_{181-402}$-Zn(II)-2OG-L574A CODD	
Residue	^{1}H	^{15}N	^{1}H	^{15}N
G				
S	8.54	115.47	8.54	115.47
H	8.61	120.70		
M	8.32	122.67	8.31	122.66
A	8.36	126.06	8.36	126.05
S	8.25	116.25	8.24	116.22
P181				
N182	8.60	119.73	8.60	119.73
G183	8.30	109.27	8.30	109.27
Q184	8.16	119.61	8.16	119.59
T185				
K186	8.19	125.08	8.19	125.08
P187				
L188				
P189				
A190	8.32	123.08	8.32	123.07
L191	7.94	116.86	7.92	116.61
K192	7.21	117.45	7.18	117.17
L193				
A194	8.06	119.86		
L195	7.97	112.82	7.99	112.88
E196				
Y197	7.21	117.10	7.24	116.94
I198	8.63	121.20		
V199	8.44	116.09	8.44	116.09
P200				
C201	7.70	116.41	7.70	116.46
M202	8.54	117.76	8.55	117.80
N203	8.43	117.02	8.44	117.19
K204	7.86	117.25	7.88	117.20
H205	8.40	112.54	8.39	112.42
G206	8.52	111.15	8.49	111.09
I207	6.58	115.82	6.58	115.85
C208				
V209	8.69	130.40	8.71	130.42
V210				
D211	8.36	125.70		
D212	8.57	117.75	8.58	117.83
F213	8.42	117.37	8.41	117.45
L214				
G215	10.19	115.52	10.19	115.51
K216	8.12	117.94	8.11	117.92
E217	8.47	119.25	8.47	119.19
T218	8.64	118.59	8.64	118.55
G219	8.50	108.66	8.49	108.64
Q220	8.44	120.83	8.44	120.79
Q221	7.51	120.11	7.52	120.15
I222	7.99	119.90	8.01	119.96
G223	8.33	107.24	8.34	107.30
D224	8.45	122.58	8.45	122.53
E225	8.11	122.24	8.08	122.13
V226				
R227	8.20	120.42	8.19	120.41
A228	7.79	121.00	7.77	121.08
L229	7.74	119.21	7.72	119.59
H230	8.41	119.59	8.40	119.60
D231	8.80	121.52	8.86	121.47
T232	7.35	108.27	7.41	108.14
G233	7.47	108.03	7.46	108.13
K234	7.45	115.88	7.45	115.92
F235	8.55	121.08	8.57	120.98
T236	9.40	113.47	9.31	113.02
D237	8.48	121.18	8.49	121.25
G238	8.04	109.25		
Q239				
L240				
V241				
S242				
Q243				
K244				
S245	8.13	116.16	8.10	116.16
D246	8.37	120.83	8.38	120.97
S247	8.00	114.05		
S248	8.47	119.99	8.27	120.98
K249	7.94	121.75	7.94	121.82
D250	8.03	117.11	8.04	117.08
I251	7.75	121.72	7.83	121.12
R252	7.92	114.05		
G253	8.73	110.46		
D254	9.35	116.28		
K255				
I256	9.59	114.96		
T257	7.93	113.06		
W258	7.88	124.78	7.89	124.64
I259	9.74	126.04	9.74	125.85
E260	11.23	129.03		
G261	9.91	109.41	9.96	109.56
K262	6.71	116.63	6.76	116.59
E263	10.54	126.65	10.49	126.48
P264				
G265	8.98	113.83	8.95	113.74
C266	7.54	115.01	7.57	115.02
E267	9.03	120.57	9.05	120.59
T268	9.79	120.90	9.71	120.67
I269				
G270	8.38	106.99	8.37	107.27
L271	7.55	125.49	7.58	125.51
L272				
M273				
S274				
S275				
M276				
D277				
D278				

L279				
I280				
R281				
H282	7.58	113.99	7.56	114.33
C283	7.57	115.76	7.54	115.45
N284	7.52	117.03	7.54	117.13
G285	8.63	112.69		
K286	7.91	116.16	7.92	116.22
L287	7.56	120.34	7.58	120.47
G288	8.71	114.34		
S289	7.70	118.88	7.71	119.29
Y290	7.16	120.13		
K291	9.07	126.01	9.09	125.94
I292	8.48	125.11	8.51	124.89
N293	8.31	125.27		
G294	7.79	108.73		
R295	9.04	115.23		
T296	7.86	108.60		
K297	7.90	115.46		
A298	8.34	121.00	8.33	120.96
M299	9.70	124.93	9.71	125.42
V300	8.49	129.83	8.52	129.92
A301	8.89	127.80	8.90	127.64
C302	9.14	120.27	9.13	120.15
Y303	9.03	129.91	9.01	129.83
P304				
G305				
N306				
G307				
T308				
G309				
Y310				
V311	8.07	119.18	8.09	119.15
R312	8.06	120.24	8.04	120.14
H313	8.72	122.03	8.75	121.96
V314	8.17	117.17		
D315	9.11	128.94	9.10	129.36
N316	7.12	106.18		
P317				
N318	8.36	118.78	8.31	119.08
G319	8.20	112.80	8.17	112.48
D320	8.92	119.45	8.99	119.52
G321	9.15	106.62		
R322				
C323	9.69	121.22	9.65	120.78
V324	7.29	125.71	7.20	125.36
T325				
C326				
I327				
Y328				
Y329				
L330				
N331				
K332				
D333				
W334				
D335				
A336				
K337				
V338				
S339				
G340				
G341				
I342				
L343	7.63	127.15	7.65	127.11
R344	8.82	130.87	8.82	130.79
I345	8.82	125.98	8.83	126.01
F346	8.48	125.42	8.47	125.40
P347				
E348	9.25	123.75	9.23	123.68
G349	8.91	111.72	8.91	111.72
K350	7.55	119.05	7.55	119.05
A351	8.28	122.42	8.28	122.38
Q352	7.35	115.83	7.35	115.88
F353	7.03	118.96	7.05	118.86
A354	9.00	124.43	8.97	124.27
D355	8.25	123.39	8.26	123.40
I356	9.67	126.42	9.66	126.26
E357	8.31	125.65		
P358				
K359	7.44	122.37	7.43	122.37
F360	7.14	119.19	7.13	119.31
D361	7.63	125.75	7.64	125.74
R362				
L363				
L364				
F365				
F366				
W367	7.15	117.83	7.11	117.81
S368	7.53	114.30	7.53	114.29
D369	7.74	119.49	7.73	119.79
R370	7.64	110.69	7.61	110.90
R371	8.30	118.79	8.21	119.05
N372	7.39	110.84	7.42	110.86
P373				
H374	8.95	118.35	9.02	119.49
E375	9.01	116.19	9.01	116.32
V376	9.21	123.12	9.17	122.92
Q377	8.66	127.84	8.65	127.95
P378				
A379				
Y380				
A381	7.65	121.78	7.65	121.79
T382	8.18	116.06	8.19	116.04
R383	8.37	130.46	8.35	130.48
Y384	9.70	127.04	9.71	127.15
A385	8.52	121.81	8.53	121.97
I386				
T387				
V388				
W389				
Y390				
F391	8.73	121.18	8.79	121.48
D392	8.36	119.49	8.38	119.63
A393	9.35	128.87	9.23	126.50
D394	8.28	118.05	8.31	116.66

E395	8.78	122.10	8.81	122.02
R396	8.75	118.22	8.66	118.21
A397	7.41	118.58	7.54	119.74
R398	7.44	116.98	7.50	115.90
A399	7.63	121.35	7.59	121.83
K400	7.09	114.94		
V401	7.21	118.00	7.08	117.88
K402	7.60	129.41	7.76	129.22

Table I-xiv Protein backbone assignments of $PHD2_{181-402}$-Zn(II)-2OG-CODD and $PHD2_{181-402}$-Zn(II)-2OG-$L_{574}A$ CODD.

Appendix II. Protein backbone assignments for $PHD2_{181-402}$-Zn(II), $PHD2_{181-402}$-Zn(II)-2OG and $PHD2_{181-402}$-Zn(II)-BIQ

Comparison of the protein backbone assignments for $PHD2_{181-402}$-Zn(II) and $PHD2_{181-402}$-Zn(II)-2OG.

Transfer of ^{1}H and ^{15}N assignment				
	^{15}N-labelled $PHD2_{181-402}$-Zn(II)-2OG		^{15}N-labelled $PHD2_{181-402}$-Zn(II)	
Residue	^{1}H	^{15}N	^{1}H	^{15}N
G				
S	8.54	115.50		
H	8.57	121.01	8.62	120.99
M	8.27	123.11	8.16	122.86
A	8.37	126.20	8.39	126.08
S	8.23	115.93	8.22	115.96
P181				
N182	8.32	118.24	8.32	118.28
G183	8.21	109.14	8.20	109.16
Q184	8.08	119.69	8.07	119.68
T185	8.07	117.04	8.06	117.00
K186	7.99	122.23	8.00	122.21
P187				
L188	7.33	117.93	7.36	118.50
P189				
A190				
L191				
K192				
L193				
A194				
L195				
E196	8.36	121.28		
Y197				
I198	8.60	121.33	8.64	121.13
V199	8.48	116.22	8.54	116.28
P200				
C201	7.68	116.47	7.65	116.33
M202	8.59	117.70		
N203	8.36	116.80	8.31	116.53
K204	7.76	117.79	7.69	118.12
H205	8.36	113.52	8.51	112.89
G206	8.51	111.36		
I207	6.59	115.84	6.61	116.05
C208	9.31	126.94	9.25	126.68
V209	8.72	130.54	8.68	131.00
V210				
D211	8.41	125.88	8.43	126.08
D212	8.61	117.51	8.60	117.53
F213	8.41	117.09	8.39	116.88
L214				
G215	10.21	115.54	10.21	115.54
K216	8.12	117.86	8.13	117.99
E217	8.54	119.19	8.55	119.17
T218	8.62	118.55	8.61	118.60
G219	8.48	108.64	8.50	108.71
Q220	8.45	120.75	8.45	120.89
Q221	7.48	120.29	7.49	120.43
I222	8.01	119.75	8.02	119.61
G223	8.30	107.14	8.26	107.11
D224	8.37	122.87	8.37	123.07
E225	8.10	123.00	8.11	123.01
V226	8.54	120.35	8.51	120.22
R227	8.22	120.23	8.23	120.00
A228	7.78	120.90	7.91	121.30
L229	7.60	119.60	7.52	119.49
H230	8.13	119.24		
D231	8.91	121.30	8.89	120.95
T232	7.45	107.94	7.46	107.81
G233	7.49	108.27	7.54	108.47
K234	7.51	115.83	7.57	116.01
F235	8.46	119.39		
T236	9.36	113.99		
D237	8.51	121.24	8.48	121.39
G238	8.88	114.59	8.84	114.38
Q239	8.40	118.95	8.43	119.15
L240	7.59	119.99		
V241	7.87	119.20		
S242	7.74	117.16	7.81	117.48
Q243	8.16	121.51	8.16	121.57
K244	8.12	120.82	8.13	120.78
S245	8.16	115.83	8.16	115.84
D246	8.25	121.25	8.22	121.34
S247	8.10	114.93	8.10	115.04
S248	8.09	117.35	8.10	117.33
K249	8.11	122.10	8.15	122.24
D250	8.10	121.79	8.04	121.86
I251	8.05	122.43	8.06	122.64
R252				
G253				
D254	9.02	116.10	9.02	116.15
K255	8.62	121.52		
I256	9.35	114.73		
T257	8.07	113.52	8.04	113.31
W258	7.91	124.20	7.98	124.43
I259	9.78	125.69	9.78	125.18
E260	11.25	129.19	11.25	129.10
G261	9.99	109.64	10.01	109.51
K262	6.76	116.80	6.73	116.68
E263	10.47	126.65	10.45	126.64
P264				
G265	9.07	114.35	9.08	114.51
C266	7.53	115.28	7.55	115.33
E267	8.99	120.18	8.99	120.04

T268	10.48	122.61	10.62	122.96
I269				
G270	8.42	106.91	8.38	106.94
L271	7.60	125.94	7.59	125.97
L272				
M273				
S274	8.30	114.02	8.29	114.17
S275	8.21	120.22	8.20	119.99
M276				
D277				
D278				
L279				
I280				
R281				
H282	7.58	116.14	7.59	116.16
C283	7.50	114.77	7.48	114.31
N284	7.59	117.27	7.56	117.18
G285	8.68	112.47	8.68	113.54
K286	7.92	116.49	8.00	116.80
L287	7.59	120.53	7.59	120.66
G288	8.81	114.62	8.78	114.31
S289	7.70	118.53	7.73	118.83
Y290	7.25	119.99	7.28	120.07
K291	9.14	126.12	9.15	126.15
I292	8.41	125.14	8.41	125.25
N293	8.37	126.80	8.37	126.64
G294	8.01	109.28	8.01	109.29
R295	8.00	112.82	8.02	112.79
T296	8.08	110.05	8.02	109.82
K297	7.82	115.54	7.83	115.48
A298	8.46	121.29	8.41	120.98
M299	9.73	126.15	9.59	125.63
V300	8.53	130.02		
A301	8.88	127.41	8.69	126.33
C302	9.08	119.95		
Y303	9.04	129.44	9.05	129.33
P304				
G305				
N306				
G307	8.69	113.91	8.71	113.99
T308				
G309	8.40	110.65	8.33	110.32
Y310				
V311				
R312	8.34	122.46	8.52	124.05
H313	8.80	123.54	8.61	123.14
V314	8.04	118.82	7.86	117.48
D315	9.07	128.11	9.01	128.30
N316	7.51	110.66		
P317				
N318	8.16	117.57	8.17	117.50
G319	8.16	112.67	8.15	112.71
D320	9.06	119.46	9.03	119.47
G321	9.45	108.73	9.49	108.90
R322	8.02	120.29	8.03	120.33
C323	9.36	120.76	9.24	120.77
V324	7.22	125.34		
T325				
C326				
I327	8.25	121.67		
Y328				
Y329				
L330				
N331	6.41	115.93	6.46	116.21
K332	9.05	129.91	9.12	129.36
D333	8.98	122.44	8.91	122.19
W334	7.56	119.47	7.62	119.48
D335				
A336				
K337				
V338	6.76	113.64	6.76	113.67
S339	8.24	114.08	8.23	113.96
G340				
G341				
I342	7.29	119.57	7.31	119.66
L343	7.64	127.06	7.65	127.10
R344	8.79	130.86	8.76	130.71
I345	8.86	126.06	8.87	126.22
F346	8.44	125.41	8.40	125.38
P347				
E348	9.17	124.57	9.13	124.90
G349	8.90	112.29	8.89	112.52
K350	7.52	118.78	7.49	118.58
A351	8.34	122.86	8.24	122.84
Q352	7.36	115.55	7.34	115.37
F353	6.98	119.39	6.96	119.51
A354	8.98	124.72	8.97	124.65
D355	8.24	123.50	8.27	123.72
I356	9.65	126.56	9.57	125.66
E357				
P358				
K359	7.43	122.39	7.44	122.71
F360	7.15	119.23	7.22	118.58
D361	7.64	125.87		
R362				
L363	8.23	125.20	8.22	125.17
L364				
F365				
F366				
W367	7.08	117.80	7.09	118.12
S368	7.63	114.37	7.70	114.71
D369	7.84	119.84	7.76	119.41
R370	7.60	110.89	7.59	110.82
R371	8.19	120.16	8.17	119.76
N372	7.45	110.69	7.47	110.60
P373				
H374	8.78	117.94	8.60	116.93
E375	9.09	116.84	9.09	116.69
V376	9.12	122.73	9.09	123.22
Q377	8.65	128.12	8.66	127.63
P378				
A379	8.42	123.58		
Y380				
A381	7.68	121.99	7.71	122.09
T382				
R383	8.31	130.72	8.23	129.69

Y384	9.82	127.26		
A385	8.56	122.05	8.65	122.26
I386	8.79	120.92	8.80	121.66
T387				
V388				
W389				
Y390				
F391			8.56	120.50
D392	8.67	119.90	8.67	119.91
A393	9.27	128.50	9.26	128.49
D394	8.13	117.87	8.13	118.01
E395	8.68	122.22	8.71	122.19
R396	8.50	117.89	8.49	117.89
A397	7.45	119.62	7.45	119.67
R398	7.42	116.87	7.42	116.92
A399	7.49	122.74	7.50	122.74
K400	7.83	119.31	7.83	119.41
V401	7.77	120.35	7.77	120.34
K402	7.75	129.65	7.74	129.68

Table II-i Protein backbone assignments of $PHD2_{181-402}$-Zn(II)-2OG and $PHD2_{181-402}$-Zn(II).

Comparison of the protein backbone assignments for $PHD2_{181-402}$-Zn(II) and $PHD2_{181-402}$-Zn(II)-BIQ.

Transfer of ^{1}H and ^{15}N assignment				
	^{15}N-labelled $PHD2_{181-402}$-Zn(II)-BIQ		^{15}N-labelled $PHD2_{181-402}$-Zn(II)	
Residue	^{1}H	^{15}N	^{1}H	^{15}N
G				
S				
H	8.61	121.08	8.62	120.99
M	8.19	123.15	8.16	122.86
A	8.40	126.04	8.39	126.08
S	8.21	115.75	8.22	115.96
P181				
N182	8.32	118.23	8.32	118.28
G183	8.20	109.09	8.20	109.16
Q184	8.08	119.67	8.07	119.68
T185	8.06	116.97	8.06	117.00
K186	7.99	122.19	8.00	122.21
P187				
L188	7.37	118.51	7.36	118.50
P189				
A190				
L191				
K192				
L193				
A194				
L195				
E196				
Y197				
I198	8.65	121.17	8.64	121.13
V199	8.52	116.28	8.54	116.28
P200				
C201	7.67	116.42	7.65	116.33
M202				
N203	8.31	116.51	8.31	116.53
K204	7.70	118.07	7.69	118.12
H205	8.51	112.94	8.51	112.89
G206				
I207	6.61	115.80	6.61	116.05
C208	9.31	126.70	9.25	126.68
V209	8.72	130.56	8.68	131.00
V210				
D211	8.42	125.96	8.43	126.08
D212	8.61	117.63	8.60	117.53
F213	8.41	116.91	8.39	116.88
L214				
G215	10.23	115.51	10.21	115.54
K216	8.12	117.96	8.13	117.99
E217	8.55	119.08	8.55	119.17
T218	8.56	118.45	8.61	118.60
G219	8.53	108.80	8.50	108.71
Q220	8.46	120.99	8.45	120.89
Q221	7.48	120.42	7.49	120.43
I222	8.00	119.70	8.02	119.61
G223	8.15	106.94	8.26	107.11
D224	8.38	122.90	8.37	123.07
E225	8.14	122.81	8.11	123.01
V226	8.48	120.19	8.51	120.22
R227	8.28	120.16	8.23	120.00
A228	7.89	121.06	7.91	121.30
L229	7.54	119.49	7.52	119.49
H230				
D231	8.90	120.67	8.89	120.95
T232	7.65	108.27	7.46	107.81
G233	7.65	108.81	7.54	108.47
K234	7.60	116.19	7.57	116.01
F235				
T236				
D237	8.42	120.94	8.48	121.39
G238			8.84	114.38
Q239	8.32	119.53	8.43	119.15
L240				
V241				
S242	7.80	116.79	7.81	117.48
Q243	8.22	121.96	8.16	121.57
K244	8.08	120.48	8.13	120.78
S245	8.17	115.70	8.16	115.84
D246	8.27	122.05	8.22	121.34
S247	8.27	116.76	8.10	115.04
S248	8.22	117.88	8.10	117.33
K249	8.12	122.24	8.15	122.24
D250	8.06	122.07	8.04	121.86
I251	8.06	122.63	8.06	122.64
R252				
G253				
D254	8.71	118.20	9.02	116.15
K255				
I256				
T257			8.04	113.31
W258			7.98	124.43
I259	9.80	125.56	9.78	125.18
E260	11.25	129.64	11.25	129.10
G261	9.98	109.45	10.01	109.51
K262	6.73	116.68	6.73	116.68
E263	10.49	126.77	10.45	126.64
P264				
G265	9.07	114.53	9.08	114.51
C266	7.57	115.35	7.55	115.33
E267	9.00	120.06	8.99	120.04
T268	10.64	122.96	10.62	122.96
I269				
G270	8.35	106.86	8.38	106.94
L271	7.59	126.00	7.59	125.97
L272				
M273				
S274	8.35	114.04	8.29	114.17
S275	8.22	120.13	8.20	119.99
M276				
D277				
D278				

L279				
I280				
R281				
H282	7.60	116.24	7.59	116.16
C283	7.49	114.37	7.48	114.31
N284	7.53	116.91	7.56	117.18
G285	8.68	113.30	8.68	113.54
K286	7.99	116.68	8.00	116.80
L287	7.57	120.55	7.59	120.66
G288	8.82	114.42	8.78	114.31
S289	7.74	118.84	7.73	118.83
Y290	7.28	120.05	7.28	120.07
K291	9.15	126.09	9.15	126.15
I292	8.44	125.08	8.41	125.25
N293	8.35	126.53	8.37	126.64
G294	7.91	108.78	8.01	109.29
R295	8.01	112.91	8.02	112.79
T296	8.03	110.02	8.02	109.82
K297	7.69	115.45	7.83	115.48
A298	8.32	120.92	8.41	120.98
M299	9.73	127.74	9.59	125.63
V300				
A301	8.79	127.80	8.69	126.33
C302				
Y303	9.04	129.15	9.05	129.33
P304				
G305				
N306				
G307	8.74	114.13	8.71	113.99
T308				
G309	8.35	110.32	8.33	110.32
Y310				
V311				
R312	8.52	124.05	8.52	124.05
H313	8.84	124.36	8.61	123.14
V314	7.80	117.30	7.86	117.48
D315	8.89	129.01	9.01	128.30
N316				
P317				
N318	8.18	117.46	8.17	117.50
G319	8.14	112.64	8.15	112.71
D320	9.02	119.30	9.03	119.47
G321	9.47	108.65	9.49	108.90
R322	8.03	120.49	8.03	120.33
C323	9.31	120.83	9.24	120.77
V324				
T325				
C326				
I327				
Y328				
Y329				
L330				
N331	6.48	116.63	6.46	116.21
K332	9.07	129.14	9.12	129.36
D333	8.90	122.42	8.91	122.19
W334			7.62	119.48
D335				
A336				
K337				
V338	6.77	113.62	6.76	113.67
S339	8.25	113.99	8.23	113.96
G340				
G341				
I342	7.33	119.80	7.31	119.66
L343	7.73	127.20	7.65	127.10
R344	8.74	130.51	8.76	130.71
I345	8.88	125.84	8.87	126.22
F346	8.43	125.16	8.40	125.38
P347				
E348	9.20	124.89	9.13	124.90
G349	8.91	112.43	8.89	112.52
K350	7.51	118.66	7.49	118.58
A351	8.32	122.93	8.24	122.84
Q352	7.37	115.35	7.34	115.37
F353	6.95	119.49	6.96	119.51
A354	8.99	124.31	8.97	124.65
D355	8.23	123.43	8.27	123.72
I356	9.54	125.92	9.57	125.66
E357				
P358				
K359	7.43	122.80	7.44	122.71
F360	7.30	118.24	7.22	118.58
D361				
R362				
L363	8.22	125.03	8.22	125.17
L364				
F365				
F366				
W367	7.11	118.31	7.09	118.12
S368	7.61	114.52	7.70	114.71
D369	7.77	119.76	7.76	119.41
R370	7.60	110.69	7.59	110.82
R371	8.16	119.79	8.17	119.76
N372	7.50	110.81	7.47	110.60
P373				
H374	8.95	118.53	8.60	116.93
E375	9.11	116.94	9.09	116.69
V376	8.91	124.31	9.09	123.22
Q377	8.70	127.88	8.66	127.63
P378				
A379				
Y380				
A381	7.70	121.87	7.71	122.09
T382				
R383	8.41	130.41	8.23	129.69
Y384				
A385	8.68	120.35	8.65	122.26
I386	8.78	122.18	8.80	121.66
T387				
V388				
W389				
Y390				
F391	8.56	120.54	8.56	120.50
D392	8.67	119.91	8.67	119.91
A393	9.24	128.46	9.26	128.49
D394	8.12	117.99	8.13	118.01

E395	8.76	122.20	8.71	122.19
R396	8.49	117.84	8.49	117.89
A397	7.46	119.67	7.45	119.67
R398	7.44	116.91	7.42	116.92
A399	7.50	122.64	7.50	122.74
K400	7.84	119.18	7.83	119.41
V401	7.76	120.25	7.77	120.34
K402	7.73	129.60	7.74	129.68

Table II-ii Protein backbone assignments of $PHD2_{181-402}$-Zn(II)-BIQ and $PHD2_{181-402}$-Zn(II).

Appendix III. Publications

Parts of the work described in this Thesis have been published as follows:

1. Leung, I. K. H.; Demetriades, M.; Hardy, A. P.; Lejeune, C.; Smart, T. J.; Szöllössi, A.; Kawamura, A.; Schofield, C. J.; Claridge, T. D. W. Reporter ligand NMR screening method for 2-oxoglutarate oxygenase inhibitors. *J. Med. Chem.* **2013**, 56, 547–555.

2. Rose, N. R.; Woon, E. C.; Tumber, A.; Walport, L. J.; Chowdhury, R.; Li, X. S.; King, O. N. F.; Lejeune, C.; Ng, S. S.; Krojer, T.; Chan, M. C.; Rydzik, A. M.; Hopkinson, R. J.; Che, K. H.; Daniel, M.; Strain-Damerell, C.; Gileadi, C.; Kochan, G.; Leung, I. K. H.; Dunford, J.; Yeoh, K. K.; Ratcliffe, P. J.; Burgess-Brown, N.; von Delft, F.; Muller, S.; Marsden, B.; Brennan, P. E.; McDonough, M. A.; Oppermann, U.; Klose, R. J.; Schofield, C. J.; Kawamura, A. The plant growth regulator daminozide is a selective inhibitor of the human KDM2/7 histone demethylases. *J. Med. Chem.* **2012**, *55*, 6639–6643.

3. Henry, L.; Leung, I. K. H.; Claridge, T. D. W.; Schofield, C. J. γ-Butyrobetaine hydroxylase catalyses a Stevens type rearrangement. *Bioorg. Med. Chem. Lett.* **2012**, *22*, 4975–4978.

4. Rydzik, A. M.; Leung, I. K. H.; Kochan, G. T.; Thalhammer, A.; Oppermann, U.; Claridge, T. D. W.; Schofield, C. J. Development and application of a fluoride-detection-based fluorescence assay for γ-butyrobetaine hydroxylase. *ChemBioChem* **2012**, *13*, 1559–1563.

5. Demetriades, M.; Leung, I. K. H.; Chowdhury, R.; Chan, M. C.; McDonough, M. A.; Yeoh, K. K.; Tian, Y.-M.; Claridge, T. D. W.; Ratcliffe, P. J.; Woon, E. C. Y.; Schofield, C. J. Dynamic combinatorial chemistry employing boronic acids/boronate esters leads to potent oxygenase inhibitors. *Angew. Chem. Int. Ed.* **2012**, *51*, 6672–6675; *Angew. Chem.* **2012**, *124*, 6776–6779.

6. Rotili, D.; Altun, M.; Kawamura, A.; Wolf, A.; Fischer, R.; Leung, I. K. H.; Mackeen, M. M.; Tian, Y.-M.; Ratcliffe, P. J.; Mai, A.; Kessler, B. M.; Schofield, C. J. A photoreactive small-molecule probe for 2-oxoglutarate oxygenases. *Chem. Biol.* **2011**, *18*, 642–654.

7. Leung, I. K. H.; Brown Jr, T.; Schofield, C. J.; Claridge, T. D. W. An approach to enzyme inhibition employing reversible boronate ester formation. *Med. Chem. Commun.* **2011**, *2*, 390–395.

8. Chowdhury, R.; Yeoh, K. K.; Tian, Y.-M.; Hillringhaus, L.; Bagg, E. A.; Rose, N. R.; Leung, I. K. H.; Li, X. S.; Woon, E. C. Y.; Yang, M.; McDonough, M. A.; King, O. N.; Clifton, I. J.; Klose, R. J.; Claridge, T. D. W.; Ratcliffe, P. J.; Schofield, C. J.; Kawamura, A. The oncometabolite 2-hydroxyglutarate inhibits histone lysine demethylases. *EMBO Rep.* **2011**, *12*, 463–469.

9. Leung, I. K. H.; Krojer, T. J.; Kochan, G. T.; Henry, L.; von Delft, F.; Claridge, T. D. W.; Oppermann, U.; McDonough, M. A.; Schofield, C. J. Structural and mechanistic studies on γ-butyrobetaine hydroxylase. *Chem. Biol.* **2010**, *17*, 1316–1324.

10. Leung, I. K. H.; Flashman, E.; Yeoh, K. K.; Schofield, C. J.; Claridge, T. D. W. Using NMR solvent water relaxation to investigate metalloenzyme–ligand binding interactions. *J. Med. Chem.* **2010**, *53*, 867–875.

Journal of Medicinal Chemistry

Article

pubs.acs.org/jmc

Reporter Ligand NMR Screening Method for 2-Oxoglutarate Oxygenase Inhibitors

Ivanhoe K. H. Leung, Marina Demetriades, Adam P. Hardy, Clarisse Lejeune, Tristan J. Smart, Andrea Szöllössi, Akane Kawamura, Christopher J. Schofield,* and Timothy D. W. Claridge*

Department of Chemistry, University of Oxford, Chemistry Research Laboratory, 12 Mansfield Road, Oxford OX1 3TA, United Kingdom

Supporting Information

ABSTRACT: The human 2-oxoglutarate (2OG) dependent oxygenases belong to a family of structurally related enzymes that play important roles in many biological processes. We report that competition-based NMR methods, using 2OG as a reporter ligand, can be used for quantitative and site-specific screening of ligand binding to 2OG oxygenases. The method was demonstrated using hypoxia inducible factor hydroxylases and histone demethylases, and K_D values were determined for inhibitors that compete with 2OG at the metal center. This technique is also useful as a screening or validation tool for inhibitor discovery, as exemplified by work with protein-directed dynamic combinatorial chemistry.

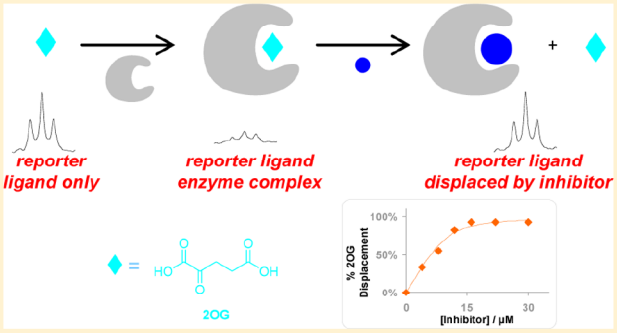

INTRODUCTION

2-Oxoglutarate (2OG) dependent oxygenases are present in plants, microorganisms, and animals.[1−5] In humans, they are involved in a diverse range of important biological roles, including collagen biosynthesis, oxygen sensing, fatty acid metabolism, and epigenetic regulation involving nucleic acid and histone modifications.[5] Several human 2OG oxygenases, including the hypoxia inducible factor (HIF) hydroxylases,[6−10] are current inhibition targets for diseases including cancer, ischemia, inflammation, and anemia.[11−14] The inhibition of γ-butyrobetaine hydroxylase,[15] a 2OG oxygenase involved in human carnitine biosynthesis, is used clinically for the treatment of angina and myocardial infarction.[16]

All 2OG oxygenases utilize 2OG and oxygen as cosubstrates to catalyze two-electron oxidation reactions (mostly hydroxylations), with the release of succinate and carbon dioxide as coproducts (Figure S1, Supporting Information). This property has led to the development of several generic activity-based assays (for reviews see refs 17 and 18). However, activity-based assays are not always well-suited to the initial stages of medicinal chemistry, for example, for fragment-based screening, and are only possible when substrates are available. As an alternative to these activity-based assays, binding assays have also been developed for 2OG oxygenases, studying the binding of metal ions, small molecules, and other biomolecules. Reported methods include nondenaturing electrospray ionization mass spectrometry (ESI-MS; for examples see refs 19−23), protein X-ray crystallography (for reviews see refs 24−26), isothermal titration calorimetry (ITC),[27] surface plasmon resonance (SPR),[28] circular dichroism (CD),[27] electron paramagnetic resonance (EPR),[29] and nuclear magnetic resonance (NMR).[27,30,31] Among these different techniques, nondenaturing ESI-MS has been used by our group as a simple and rapid primary screening method for 2OG oxygenase inhibitors. However, because noncovalent protein−ligand complexes may not always survive the transition from solution phase to gas phase,[32] there is a need for complementary solution-based screening techniques.

NMR spectroscopy is an established technique for the study of protein−ligand binding interactions. Ligand detection methods such as saturation transfer difference (STD)[33] and water ligand observed gradient spectroscopy (waterLOGSY)[34] are widely used for ligand screening because they do not require isotopically labeled protein and are relatively quick and sensitive. However, many ligand-based NMR methods suffer from limited detection ranges of binding affinities, false positives arising from nonspecific binding,[35] and complications with binding constant determination that arise from, for instance, ligand rebinding events and dependencies on ligand spin relaxation rates and saturation times.[36,37] NMR reporter screening methods are useful alternatives for the site-specific detection of both high- and low-affinity ligands. By observing changes in the NMR parameter(s) (such as chemical shift or relaxation rate) associated with a reporter ligand, it is possible to obtain qualitative and quantitative information on the binding of ligands that compete with the reporter ligand for the target protein (Figure 1). Several nuclei, including proton,[38−40] phosphorus,[41] fluorine,[42] and carbon,[43] have been proposed for reporter screening by NMR.

Received: October 26, 2012
Published: December 12, 2012

ACS Publications © 2012 American Chemical Society

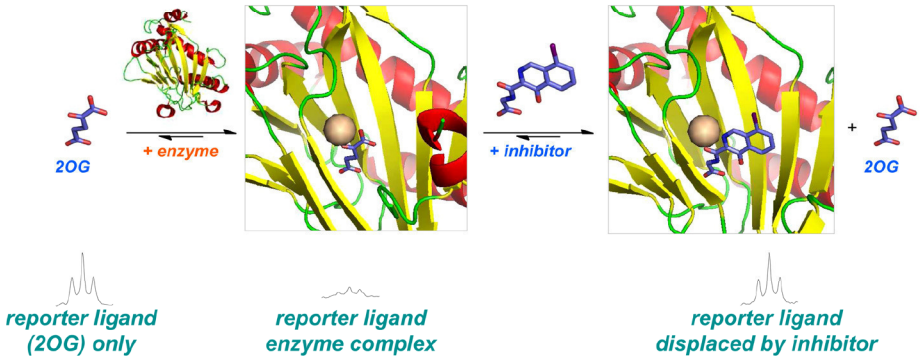

Figure 1. Schematic representation for the NMR reporter screening method. When the reporter ligand is bound to the protein, the corresponding ^{1}H NMR resonance is broadened, and its intensity is lowered. In the presence of a competitive inhibitor, the reporter ligand is displaced from the protein binding site, and its signal intensity is recovered.

We reasoned that 2OG is a potentially good reporter ligand candidate for generic NMR binding assays for 2OG oxygenases because they all utilize it as a cosubstrate. Using unlabeled and commercially available [1,2,3,4-$^{13}C_4$]-labeled 2OG ([^{13}C]-2OG), we have optimized the experimental conditions and demonstrated the feasibility of applying the reporter ligand method for high-throughput screening and binding constant (K_D) measurements for a selection of 2OG oxygenases.

RESULTS

Methodology. The HIF hydroxylases, in particular, the prolyl hydroxylase domain containing enzyme isoform 2 (PHD2; EC 1.14.11.29; for reviews see refs 6−8) and factor inhibiting HIF (FIH; EC 1.14.11.30; for reviews see refs 9 and 10), play key roles in human oxygen/hypoxia sensing. Their inhibition is of therapeutic interest;[11−14] hence, they were chosen as model systems.

It is known that the catalytically essential Fe^{II} at the active site of 2OG oxygenases can be substituted by different transition metals.[21] Because many (but not all) 2OG oxygenases catalyze 2OG turnover in the absence of substrates, native Fe^{II} was substituted with the diamagnetic Zn^{II} in order to block enzyme-catalyzed 2OG turnover and to avoid the oxidation of Fe^{II} to paramagnetic Fe^{III}. In the assays, an 8-fold molar excess of Zn^{II} was used relative to PHD2 to ensure that only the metal-bound holo form was present. It should be noted that a caveat of our method is that it does not employ the native metal ion, although the binding affinity of ligands, including 2OG, is not substantially affected by the use of Zn^{II} as the active site metal (see below; Figure S2, Supporting Information).

Both PHD2 and FIH form stable complexes with 2OG that saturate at a ∼1:1 ratio (Figure S3, Supporting Information).[23,31] Under these conditions, the ^{1}H NMR spectra were dominated by the protein resonances (Figure S4, Supporting Information). In order to observe the reporter ligand (2OG) signal, the Carr−Purcell−Meiboom−Gill (CPMG)[44−46] sequence was applied to attenuate any broad (protein) resonances (Figure S4, Supporting Information). In particular, the recently proposed Periodic Refocusing Of J Evolution by Coherence Transfer (PROJECT) method,[47] which uses an additional 90°$_y$ pulse at the midpoint of a double spin echo to refocus and suppress J modulation, provided unperturbed line shapes and was therefore used in assays described herein. This method provides a means to distinguish free from bound 2OG.

When 2OG was bound to the protein, significant broadening of the 2OG ^{1}H resonances was observed due to a high ^{1}H transverse relaxation rate in the bound state, so the resultant CPMG-edited ^{1}H spectrum displayed near-complete diminution of the 2OG signal intensity. In the presence of a competitive binder, however, 2OG was displaced from the binding site into the bulk solution, leading to sharpening of the signals and recovery of the 2OG signal intensity (Figure 2a). The simplicity and sensitivity of the experiment make it well-suited to the primary screening of 2OG oxygenases. In addition, by monitoring the intensity of the 2OG reporter signal as a function of increasing concentrations of an inhibitor (Figure 2b), it is possible to obtain quantitative binding information for the inhibitor (Figure 2c).

When using this method for inhibitor screening, we define the percentage 2OG displacement as

$$\%\text{2OG displacement} = \frac{I_{2OG} - I_{2OG(0)}}{I_{2OG(blank)} - I_{2OG(0)}} \times 100\% \quad (1)$$

where I_{2OG} is the integral of the 2OG ^{1}H signal in the presence of both the inhibitor and the protein, $I_{2OG(0)}$ is the integral of 2OG in the presence of the protein but in the absence of the inhibitor, and $I_{2OG(blank)}$ is the integral of 2OG in the absence of both protein and inhibitor. For the ideal scenario in which the 2OG signal is fully attenuated in the presence of the protein (and absence of inhibitor), $I_{2OG(0)}$ should tend toward zero.

Screening for Inhibitor Binding. By monitoring the level of 2OG displacement, it is possible to compare the relative strength of binding for different compounds at a single inhibitor concentration in an efficient manner, as was demonstrated herein using several known PHD2/2OG oxygenase inhibitors (Figure 3). Compounds were screened at a concentration of 400 μM in the presence of 10 μM Zn(II)-holo-enzyme and 10 μM 2OG.

N-Oxalylglycine (NOG; Figure 3)[48] is a nonreactive 2OG analogue, with a NH group replacing the CH_2 at the C-3 position of 2OG. It is a relatively nonselective 2OG oxygenase inhibitor[49] and gave ∼85% 2OG displacement for both PHD2 and FIH (Figure 4). In contrast, the bicyclic isoquinolinyl inhibitor (BIQ; Figure 3)[50,51] is reported as a potent PHD2 inhibitor. The reporter assay results demonstrate it to be more selective for PHD2 compared with FIH, consistent with literature reports.[52,53] Full recovery of the 2OG reporter signal was observed with PHD2, but only ∼55% 2OG displacement was observed with FIH (Figure 4). The assay was also tested

dx.doi.org/10.1021/jm301583m | J. Med. Chem. 2013, 56, 547−555

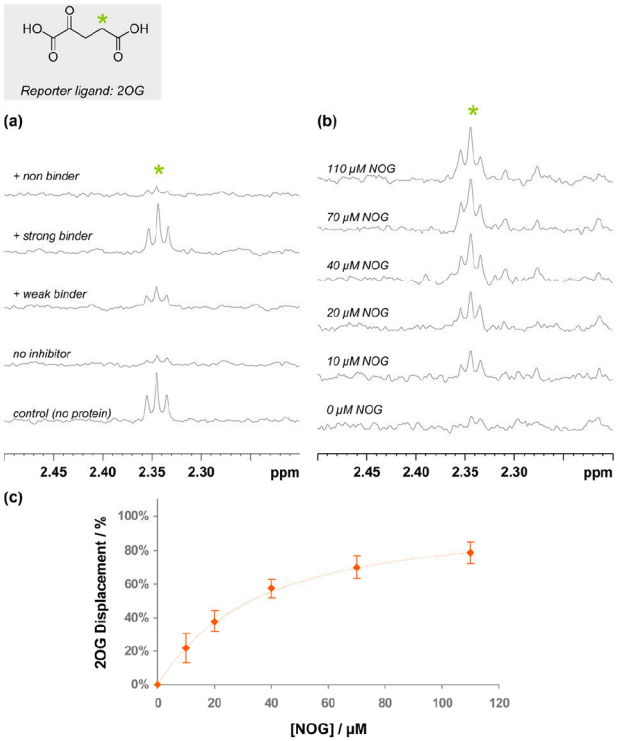

Figure 2. 2OG displacement from human PHD2 as monitored by CPMG-edited ^{1}H analyses. (a) Single concentration screening at 400 μM inhibitor concentration. The nonbinder is *cis*-aconitate; the strong binder is the bicyclic naphthalenylsulfonyl inhibitor (BNS), and the weaker binder is fumarate; (b) titration experiment monitoring 2OG signal recovery at different inhibitor (*N*-oxalyglycine; NOG) concentrations; (c) corresponding plot of the NOG titration data. The percentage 2OG displacement is defined in eq 1. Samples contained 10 μM apo-PHD2, 80 μM Zn^{II}, 10 μM 2OG, and 50 mM Tris-D11 pH 7.5 in 90% H_2O and 10% D_2O. The asterisk indicates the 2OG CH_2 resonance at 2.35 ppm that is being monitored.

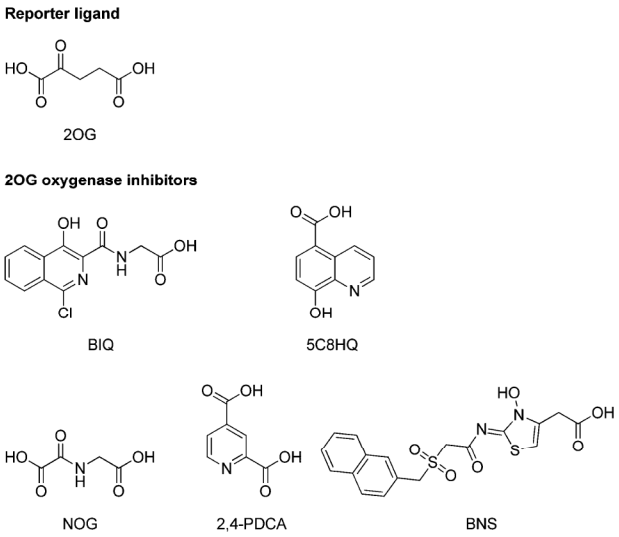

Figure 3. Structures of compounds used in this study.

with 5-carboxy-8-hydroxyquinoline (5C8HQ; Figure 3),[54] which is a generic inhibitor for histone demethylases[55,56] but a weaker inhibitor for HIF hydroxylases.[54] The single

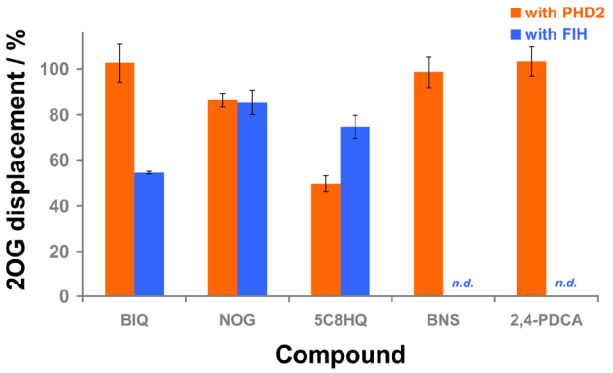

Figure 4. Single concentration 2OG displacement experiments using CPMG-edited ^{1}H analyses. The assay mixture contained 10 μM apo-PHD2 or apo-FIH, 80 μM Zn^{II}, 10 μM (nonlabeled) 2OG, 400 μM inhibitor, and 50 mM Tris-D11 pH 7.5 in 10% D_2O and 90% H_2O. The errors shown are the standard deviation from three separate measurements. The percentage 2OG displacement is defined in eq 1. n.d. = not determined.

concentration 2OG displacement assay confirms that 5C8HQ binds to both PHD2 and FIH but its binding is weaker than with NOG (~50% and ~75% 2OG displacement with PHD2 and FIH, respectively; Figure 4). Finally, we tested two other known PHD2 inhibitors: 2,4-pyridine dicarboxylic acid (2,4-PDCA; Figure 3)[57] and the bicyclic naphthalenylsulfonyl inhibitor (BNS; Figure 3).[58] Both compounds caused complete 2OG displacement when tested with PHD2 under standard conditions (Figure 4).

Quantification of Binding. By monitoring the intensity of the 2OG reporter signal at different inhibitor concentrations, it is possible to obtain the dissociation constant (K_D) for the inhibitor, provided the dissociation constant ($K_{D,rep}$) of the reporter ligand (2OG) is known.

By using the methods of Morton et al.[59] and Dalvit et al.,[39] the apparent dissociation constant of the inhibitor ($K_{D,app}$; which is defined as the free concentration of the inhibitor when 50% of the enzyme is bound with the inhibitor) can be obtained by nonlinear curve fitting of the titration data (Figure 2b,c) according to the following equation:

$$K_{D,app} = \frac{[E_T] \times [L] - [E_T] \times [EL] + [EL]^2 - [L] \times [EL]}{[EL]} \quad (2)$$

in which $[E_T]$ is the total enzyme concentration, $[L]$ is the concentration of the inhibitor, and $[EL]$ is the concentration of the enzyme–inhibitor complex.

From the experimentally determined $K_{D,app}$, it is possible to derive the K_D of an inhibitor from knowledge of the dissociation constant of the reporter ligand ($K_{D,rep}$). However, because the concentration of the reporter ligand used in this assay is comparable to the total enzyme concentration, the Cheng–Prusoff correlation[60] is not valid due to its assumption of a large excess of reporter ligand. Instead, we used the correlation described by Nikolovska-Coleska et al.[61] and Cer et al.,[62] which considers all the variables including enzyme and reporter ligand concentrations. A full description of the data treatment can be found in the Supporting Information (Figure legend of Figure S5).

dx.doi.org/10.1021/jm301583m | J. Med. Chem. 2013, 56, 547–555

In order to obtain an accurate K_D value for a ligand of interest, it is crucial that the K_D value of the reporter ligand is measured accurately. The K_D values of 2OG with PHD2 (900 nM) and FIH (4 μM) used in this study were obtained using the solvent water relaxation method,[31] in which native Fe^{II} was replaced by paramagnetic Mn^{II}. The binding constants of 2OG to PHD2-Mn^{II} (900 nM) and PHD2-Zn^{II} (<2 μM obtained by $^1H-^{15}N$ heteronuclear single quantum correlation (HSQC) titration; Figure S2, Supporting Information) were essentially the same.

The K_D values for the inhibitors tested are summarized in Table 1. The K_D values obtained for NOG with PHD2 and FIH are 3 and 4 μM, respectively (Figures S5 and S6, Supporting Information), which are comparable to the reported K_D values (3 μM for PHD2 and 2 μM for FIH).[31,63] In agreement with the result obtained from the single concentration screening and previous reported work,[52] BIQ was found to be more potent against PHD2 than FIH: the K_D obtained for BIQ with PHD2 is 80 nM (Figure S7, Supporting Information), which is ~1800 times lower than the value obtained with FIH (140 μM; Figure S8, Supporting Information). The K_D values obtained for 5C8HQ are 60 and 30 μM with PHD2 and FIH, respectively (Figures S9 and S10, Supporting Information), supporting the result obtained from the single concentration screening (Figure 4) and are comparable to reported IC_{50} values (15 μM for PHD2 and 20 μM for FIH).[54]

Table 1. Binding Constants (K_D) for the Catalytic Domain of Human PHD2 and FIH Measured by NMR in This Study[a]

compound	K_D	reported IC_{50} (or K_D)
	Binding to PHD2	
NOG	3 ± 1 μM	20 μM (3 μM)
BIQ	80 ± 5 nM	70 nM (<1 μM)
5C8HQ	60 ± 5 μM	15 μM
BNS	100 ± 10 nM	20 nM (<1 μM)
2,4-PDCA	420 ± 130 nM	2 μM
fumarate	200 ± 70 μM	220 μM
	Binding to FIH	
NOG	4 ± 1 μM	50 μM (2 μM)
BIQ	140 ± 10 μM	>25 μM
5C8HQ	30 ± 10 μM	20 μM

[a]The errors shown are the standard deviation from three separate measurements. The obtained K_D values are based on the K_D values for 2OG binding to PHD2-Mn^{II} and FIH-Mn^{II}, which are 900 nM and 4 μM, respectively. Reported IC_{50} and K_D values were obtained from refs 22, 31, 53, 54, and 58.

Titrations were also conducted for BNS and 2,4-PDCA with PHD2. The K_D value obtained for BNS is 100 nM (Figure S11, Supporting Information). BNS is reported as a potent PHD2 inhibitor (IC_{50} 20 nM),[58] and the low K_D value obtained here confirmed that it is a very strong binder to PHD2 and that it binds in the 2OG binding pocket. The K_D value obtained for 2,4-PDCA is 420 nM (Figure S12, Supporting Information), supporting previous inhibition studies that reported 2,4-PDCA as a weaker inhibitor than BIQ but more potent than NOG.[53]

HIF Hydroxylases and Tricarboxylic Acid Cycle Intermediates. After demonstrating that the method is applicable for generic 2OG oxygenase inhibitors, we conducted screening against tricarboxylic acid (TCA) cycle intermediates (except succinyl coenzyme A; Figure S13, Supporting Information). Information on the binding of TCA cycle intermediates to HIF hydroxylases (and other 2OG oxygenases) is of biological interest because there is evidence that TCA cycle intermediates may influence the regulation of HIF hydroxylase activities or other 2OG oxygenases.[22,64−67]

At an inhibitor concentration of 400 μM, the only TCA cycle intermediate that shows significant 2OG displacement is fumarate with PHD2 (~25% 2OG displacement; Figure S14, Supporting Information). This is in agreement with our previous inhibition data, which found that fumarate is the only compound among TCA cycle intermediates that inhibits PHD2 in the micromolar range.[22] A titration was also conducted for fumarate with PHD2. The K_D value obtained was 200 μM (Table 1 and Figure S15, Supporting Information; reported IC_{50} = 220 μM[22]), confirming it is a weak PHD2 binder, although the role of fumarate-mediated PHD inhibition may become significant, for instance, in cancers that are involved in the mutations of fumarate hydratase where fumarate concentrations are reported to exceed 10 mM.[68−70]

Previous inhibition data also suggested succinate and isocitrate may be weak PHD2 inhibitors, with IC_{50} values greater than 10 mM.[22,65] Our results suggest that, at least at the concentration used (40-fold molar excess), no 2OG displacement by these compounds was observed (Figure S14, Supporting Information). Under our screening conditions, citrate, isocitrate, and malate also did not appear to displace 2OG in solution (Figure S14, Supporting Information), although previous nondenaturing ESI-MS data suggested they form binary complexes with PHD2 but not ternary complexes with PHD2 and its peptidyl substrate.[22] These data suggest that citrate, isocitrate, and malate may not bind to the 2OG binding pocket but could form "nonspecific" weak binding interactions to PHD2 (possibly to the peptidyl substrate binding site). Ascorbate, a commonly used reducing agent in 2OG oxygenase activity assays,[71] does not appear to compete with 2OG. In agreement with previous inhibition data,[22] none of the TCA cycle intermediates appeared to bind substantially to FIH (Figure S14, Supporting Information).

Using [^{13}C]-2OG as a Reporter Ligand. One potential problem associated with CPMG-edited ^1H NMR screening is signal overlap of the reporter and ligand resonances such that it is not possible to reliably monitor reporter ligand recovery in response to its displacement. In order to address this issue, we investigated the use of commercially available [1,2,3,4-$^{13}C_4$]-labeled 2OG as an alternative reporter ligand (Figure S16, Supporting Information), using the [^{13}C]-label for spectral editing (Figure S17, Supporting Information). However, aside from cost, the penalty of using [^{13}C] for editing is a loss of sensitivity and a loss of additional T_2 filtering (as in the CPMG T_2-edited experiments) to distinguish the free and bound ligands. In order to tackle this issue, one-dimensional (1D) $^1H-^{13}C$ HSQC was chosen in favor of direct carbon observation.[72] A ^{13}C selective version of the 1D $^1H-^{13}C$ HSQC experiment was used to ensure clean selection of the 2OG CH_2 resonance, in which a Q3 shaped 180° pulse was applied as the selective inversion pulse in the INEPT transfer stages. In general, a slightly higher concentration of protein and 2OG was used so that a reasonable signal-to-noise ratio can be achieved while keeping the experiment time relatively short (<30 min).

By applying selective ^{13}C irradiation on C-4 of 2OG (30.5 ppm), it was possible to selectively observe free 2OG (Figure S18, Supporting Information). Titrations were conducted for BNS and NOG with PHD2 (Figure S19, Supporting

dx.doi.org/10.1021/jm301583m | J. Med. Chem. 2013, 56, 547−555

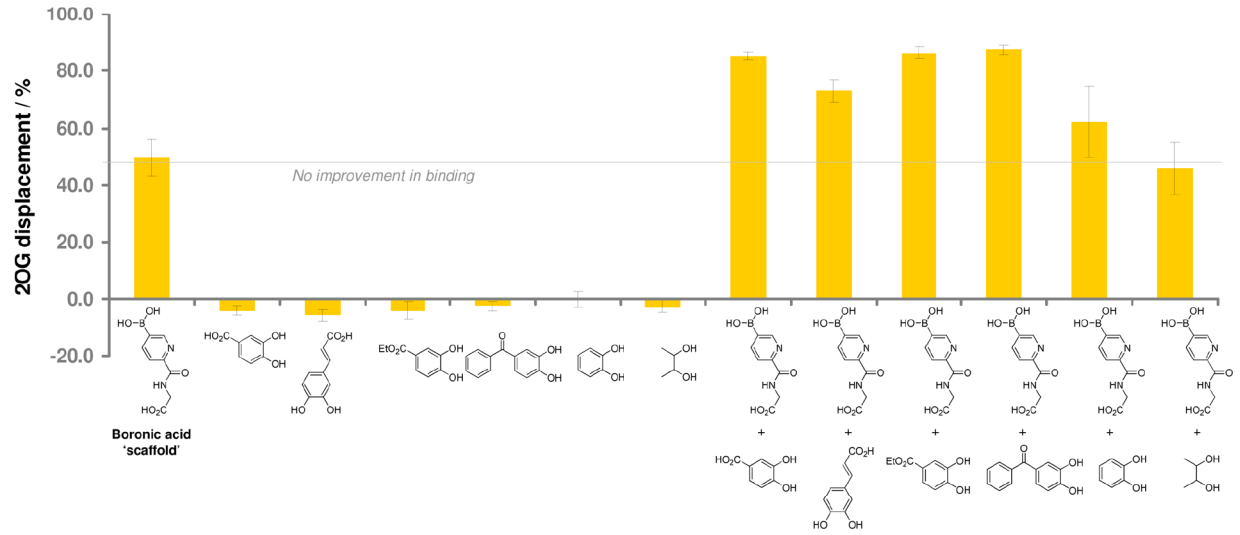

Figure 5. Addition of certain diols improves the binding of the boronic acid scaffold to PHD2-Zn^{II}, as reflected by the improvement in 2OG displacement as monitored by the reporter ligand screening method using CPMG-edited ^{1}H analyses. The final sample mixtures contained 10 μM apo-PHD2, 80 μM Zn^{II}, 10 μM (nonlabeled) 2OG, 50 μM boronic acid, and 150 μM diol where applicable. Solutions were buffered using 50 mM Tris-D11 (pH 7.5) in 90% H_2O and 10% D_2O. The percentage 2OG displacement is defined in eq 1.

Information), whereby the K_D values obtained (~110 nM for BNS and ~2 μM for NOG; Figures S20 and S21, Supporting Information) were comparable to those obtained using CPMG-edited ^{1}H NMR (100 nM for BNS and 3 μM for NOG), thus demonstrating its potential use as an alternative approach in case of signal overlap.

Application to Other 2OG Oxygenases. In order to test the wider applicability of the 2OG displacement method across the 2OG oxygenase family, we investigated qualitative binding with the histone demethylase F-box and leucine-rich repeat protein 11 (FBXL11; EC 1.14.11.27) using CPMG-edited ^{1}H NMR.[73] Histone lysine methylation status is linked to cancer,[74] and therefore, a reliable screening assay would be useful for future inhibitor development against FBXL11 and related 2OG dependent demethylases such as Jimonji (JmjC) domain containing enzymes.

In experiments with FBXL11, excess enzyme was found to be needed to ensure most of the 2OG signal was attenuated (Figure S22, Supporting Information), indicating FBXL11 is a relatively weak 2OG binder. Single-point screening experiments (at 800 μM inhibitor concentration) were performed using five of the inhibitors tested with PHD2 (Figure 3).

The results reveal that BNS and 2,4-PDCA, two potent PHD2 inhibitors, are relatively strong binders to FBXL11 (~90% and ~70% 2OG displacement, respectively; Figure S23, Supporting Information). NOG and 5C8HQ are also binders of FBXL11 (~30% and ~65% 2OG displacement, respectively; Figure S23, Supporting Information). Interestingly, the PHD2 inhibitor BIQ does not seem to displace 2OG when tested with FBXL11 (Figure S23, Supporting Information). These results demonstrate the wider applicability of the 2OG displacement assay across 2OG oxygenases and will help to provide a basis for future FBXL11 inhibitor development.

Application in Inhibitor Discovery. Finally, we applied the 2OG reporter method to inhibitor discovery for hit validation. Protein-directed dynamic combinatorial chemistry (DCC), which is related to the fragment-based drug discovery (FBDD) method, is an emerging technique for inhibitor discovery.[75−80] DCC is an approach to the generation and identification of protein ligands via reversible interconversions of simple building blocks in the presence of a target protein template (Figure S24, Supporting Information). Previously, we have successfully applied protein-directed DCC to identify ligands produced by reversible boronate ester formation that led to novel nanomolar inhibitors for PHD2.[81,82] This work involved the use of a boronic acid "scaffold", which binds in the 2OG binding pocket and is a weak inhibitor of PHD2. However, upon addition of appropriate diols, boronate esters form reversibly, which can bind tightly to PHD2 (Figure S25, Supporting Information).[82]

As a proof-of-principle study, the boronic acid scaffold and the reported diol hits were subjected to the NMR reporter analyses using CPMG-edited ^{1}H NMR (Figure S25, Supporting Information).[82] At 50 μM concentration, the boronic acid appeared to cause ~50% 2OG displacement (Figure 5), confirming it is a weak binder to PHD2. A slightly higher concentration (150 μM) of diols (than the boronic acid scaffold) was used to ensure the generation of the boronate ester species. In the absence of the boronic acid, none of the diols appeared to displace 2OG from PHD2 (Figure 5). However, in the presence of the boronic acid and the diols, a significant improvement in 2OG displacement was observed (~75% to ~85% 2OG displacement; Figure 5), in agreement with the results obtained from nondenaturing ESI-MS.[82] As negative controls, in the presence of the boronic acid scaffold and butane-2,3-diol, no improvement in 2OG displacement was observed (Figure 5), and in the presence of the boronic acid scaffold and catechol, only a moderate improvement in 2OG displacement was observed (~60%; Figure 5), again in good agreement with the ESI-MS result.[82]

These results validate previous screening results obtained by nondenaturing ESI-MS[82] and support the proposal that it is the boronate ester species that are responsible for the improvement in binding and inhibition and validate the potential of the reporter method for hit identification.

dx.doi.org/10.1021/jm301583m | J. Med. Chem. 2013, 56, 547−555

CONCLUSIONS

In this study, we have demonstrated the development and application of reporter ligand ^{1}H NMR analyses to the study of ligand binding to 2OG oxygenases, using the natural cosubstrate 2OG as a reporter ligand. This method relies on the displacement of 2OG on binding of competitive ligand and direct ^{1}H NMR observation of unbound 2OG. It can provide site-specific binding information and may also provide an accurate determination of dissociation constants for both strong and weak binders, which is otherwise difficult to estimate using other ligand-based NMR techniques. We have further shown that signal overlap, a problem associated with many ^{1}H NMR based screening methods, can be overcome by the use of commercially available [1,2,3,4-$^{13}C_4$]-labeled 2OG combined with a 1D selective HSQC experiment for editing.

The reporter method has been applied to different members of the 2OG oxygenase superfamily, including HIF hydroxylases (PHD2 and FIH) and histone demethylases (FBXL11), and is proposed as a generic NMR-based screening method for this superfamily. A caveat of the method is that it does not employ the native metal Fe^{II}, and it should be noted that use of an alternative metal could affect binding modes. Nevertheless, our results demonstrated a good correlation between binding data from the NMR reporter method employing Zn^{II} and that from catalytic turnover assays using native Fe^{II}. To date, most 2OG oxygenase inhibitors are designed as 2OG competitors,[17] and this method can also be applied to validate the binding mode of these compounds. We have also screened and quantified the binding affinities of TCA cycle intermediates that may be involved in HIF regulation in certain cancers and have shown that this method can be applied as a screening or validation tool in hit discovery, as exemplified by protein-directed DCC. Finally, we also propose that this NMR-based approach of using cofactors/cosubstrates as reporters could be more widely applied in general NMR screening assays for other superfamilies of enzymes including kinases and ATPases.

EXPERIMENTAL SECTION

Materials. Chemicals were from Acros, Alfa Aesar, Apollo Scientific, Cambridge Isotope Laboratories, or Sigma–Aldrich. BNS, BIQ, 5C8HQ, NOG (Figure 3), and the scaffold boronic acid (Figure 5) were synthesized by the reported methods.[48,50,54,58,82] The purity of all compounds synthesized were ≥95% as determined by analytical reverse-phase high-performance liquid chromatography (UltiMate 3000; Dionex).

Expression and Purification of PHD2, FIH, and FBXL11. The catalytic domains of PHD2 (residues 181–426) and FBXL11 (residues 1–517) and full length FIH were expressed in *Escherichia coli* and purified by metal-affinity, cation-exchange, and size-exclusion chromatographies, essentially as described.[18,63,83]

NMR Experiments. NMR experiments were conducted at a ^{1}H frequency of 700 MHz using a Bruker Avance III spectrometer equipped with a TCI inverse cryoprobe. All experiments were conducted at 298 K. MATCH NMR tubes (3 mm diameter, Bruker) using a sample volume of 160 μL were used in all experiments. Solutions were buffered using 50 mM Tris-D11 (pH 7.5) dissolved in 90% H_2O and 10% D_2O. The pulse tip-angle calibration using the single-pulse nutation method[84] (Bruker *pulsecal* routine) was undertaken for each sample.

CMPG-Edited Screening Experiments. Samples contained 10 μM apo-PHD2/apo-FIH, 80 μM Zn^{II}, 10 μM 2OG, and 400 μM potential inhibitor. In the case of FBXL11, 35 μM apo-protein was used, and inhibitors were screened at 800 μM concentration. The PROJECT-CPMG sequence ($90°_x$–[τ–$180°_y$–τ–$90°_y$–τ–$180°_y$–τ]$_n$–acq) was applied as described by Augilar et al.[47] Typical experimental parameters were as follows: total echo time, 48 ms (τ = 2 ms; n = 6); acquisition time, 2.94 s; relaxation delay, 2 s; number of transients, 128. Water suppression was achieved by presaturation. All experiments were conducted at 298 K.

1D Selective HSQC. Samples contained 150 μM apo-PHD2, 200 μM Zn^{II}, and 150 μM 2OG. The CLIP-HSQC sequence was used for 1D HSQC experiments (without ^{13}C decoupling).[85] Typical experimental parameters were as follows: acquisition time, 0.58 s; relaxation delay, 2 s; number of transients, 256–1600. The $^1J_{CH}$ was set to 145 or 160 Hz. A 6.8 ms Q3 180° pulse was used, and ^{13}C selective irradiation was applied at 30.5 ppm (2OG C-4). All experiments were conducted at 298 K.

Dissociation Constant Determination. Experiments were conducted under the same conditions as described above, except for varying inhibitor concentrations. An inhibitor stock solution of 0.5–1.5 μL was titrated into NMR tubes. $K_{D,app}$ curves were fitted using OriginPro 8.0 (OriginLab, USA).

ASSOCIATED CONTENT

Supporting Information

Additional information as noted in the text. This material is available free of charge via the Internet at http://pubs.acs.org.

AUTHOR INFORMATION

Corresponding Author

*Phone: +44 (0)1865 285 000 (C.J.S.). Fax: +44 (0)1865 285 002 (C.J.S.). E-mail: christopher.schofield@chem.ox.ac.uk (C.J.S.); tim.claridge@chem.ox.ac.uk. (T.D.W.C.).

Notes

The authors declare no competing financial interest.

ACKNOWLEDGMENTS

We thank the British Heart Foundation, the Engineering and Physical Sciences Research Council (EPSRC), the Wellcome Trust, the European Research Council (ERC), and the Open Horizons program of the Dinu Patriciu Foundation for funding.

ABBREVIATIONS USED

2,4-PDCA, 2,4-pyridine dicarboxylic acid; 2OG, 2-oxoglutarate; 5C8HQ, 5-carboxy-8-hydroxyquinoline; BIQ, bicyclic isoquinolinyl inhibitor; BNS, bicyclic naphthalenylsulfonyl inhibitor; CD, circular dichroism; CPMG, Carr–Purcell–Meiboom–Gill; DCC, dynamic combinatorial chemistry; ESI-MS, electrospray ionization mass spectrometry; EPR, electron paramagnetic resonance; FBDD, fragment-based drug discovery; FIH, factor inhibiting hypoxia inducible factor; FBXL11, F-box and leucine-rich repeat protein 11; NOG, *N*-oxalylglycine; HSQC, heteronuclear single quantum correlation; HIF, hypoxia inducible factor; ITC, isothermal titration calorimetry; NMR, nuclear magnetic resonance; PHD2, prolyl hydroxylase domain containing enzyme isoform 2; PROJECT, periodic refocusing of J evolution by coherence transfer; SPR, surface plasmon resonance; STD, saturation transfer difference; TCA, tricarboxylic acid; waterLOGSY, water ligand observed gradient spectroscopy

REFERENCES

(1) Costas, M.; Mehn, M. P.; Jensen, M. P.; Que, L., Jr. Dioxygen activation at mononuclear nonheme iron active sites: enzymes, models, and intermediates. *Chem. Rev.* **2004**, *104*, 939–986.

(2) Prescott, A. G.; Lloyd, M. D. The iron(II) and 2-oxoacid-dependent dioxygenases and their role in metabolism. *Nat. Prod. Rep.* **2000**, *17*, 367–383.

(3) Hausinger, R. P. Fe(II)/α-ketoglutarate-dependent hydroxylases and related enzymes. *Crit. Rev. Biochem. Mol. Biol.* **2004**, *39*, 21−68.
(4) Kovaleva, E. G.; Lipscomb, J. D. Versatility of biological non-heme Fe(II) centers in oxygen activation reactions. *Nat. Chem. Biol.* **2008**, *4*, 186−193.
(5) Loenarz, C.; Schofield, C. J. Expanding chemical biology of 2-oxoglutarate oxygenases. *Nat. Chem. Biol.* **2008**, *4*, 152−156.
(6) Epstein, A. C. R.; Gleadle, J. M.; McNeill, L. A.; Hewitson, K. S.; O'Rourke, J.; Mole, D. R.; Mukherji, M.; Metzen, E.; Wilson, M. I.; Dhanda, A.; Tian, Y.-M.; Masson, N.; Hamilton, D. L.; Jaakkola, P.; Barstead, R.; Hodgkin, J.; Maxwell, P. H.; Pugh, C. W.; Schofield, C. J.; Ratcliffe, P. J. *C. elegans* EGL-9 and mammalian homologs define a family of dioxygenases that regulate HIF by prolyl hydroxylation. *Cell* **2001**, *107*, 43−54.
(7) Bruick, R. K.; McKnight, S. L. A conserved family of prolyl-4-hydroxylases that modify HIF. *Science* **2001**, *294*, 1337−1340.
(8) Ivan, M.; Haberberger, T.; Gervasi, D. C.; Michelson, K. S.; Günzler, V.; Kondo, K.; Yang, H.; Sorokina, I.; Conaway, R. C.; Conaway, J. W.; Kaelin, W. G., Jr. Biochemical purification and pharmacological inhibition of a mammalian prolyl hydroxylase acting on hypoxia-inducible factor. *Proc. Natl. Acad. Sci. U.S.A.* **2002**, *99*, 13459−13464.
(9) Hewitson, K. S.; McNeill, L. A.; Riordan, M. V.; Tian, Y.-M.; Bullock, A. N.; Welford, R. W.; Elkins, J. M.; Oldham, N. J.; Bhattacharya, S.; Gleadle, J. M.; Ratcliffe, P. J.; Pugh, C. W.; Schofield, C. J. Hypoxia-inducible factor (HIF) asparagine hydroxylase is identical to factor inhibiting HIF (FIH) and is related to the cupin structural family. *J. Biol. Chem.* **2002**, *277*, 26351−26355.
(10) Mahon, P. C.; Hirota, K.; Semenza, G. L. FIH-1: a novel protein that interacts with HIF-1α and VHL to mediate repression of HIF-1 transcriptional activity. *Genes Dev.* **2001**, *15*, 2675−2686.
(11) Semenza, G. L. Targeting HIF-1 for cancer therapy. *Nat. Rev. Cancer* **2003**, *3*, 721−732.
(12) Nagel, S.; Talbot, N. P.; Mecinović, J.; Smith, T. G.; Buchan, A. M.; Schofield, C. J. Therapeutic manipulation of the HIF hydroxylases. *Antioxid. Redox Signaling* **2010**, *12*, 481−501.
(13) Hewitson, K. S.; Schofield, C. J. The HIF pathway as a therapeutic target. *Drug Discovery Today* **2004**, *9*, 704−711.
(14) Fraisl, P.; Aragonés, J.; Carmeliet, P. Inhibition of oxygen sensors as a therapeutic strategy for ischaemic and inflammatory disease. *Nat. Rev. Drug Discovery* **2009**, *8*, 139−152.
(15) Leung, I. K. H.; Krojer, T. J.; Kochan, G. T.; Henry, L.; von Delft, F.; Claridge, T. D. W.; Oppermann, U.; McDonough, M. A.; Schofield, C. J. Structural and mechanistic studies on γ-butyrobetaine hydroxylase. *Chem. Biol.* **2010**, *17*, 1316−1324.
(16) Simkhovich, B. Z.; Shutenko, Z. V.; Meirena, D. V.; Khagi, K. B.; Mezapuķe, R. J.; Molodchina, T. N.; Kalviņs, I. J.; Lukevics, E. 3-(2,2,2-Trimethylhydrazinium) propionate (THP)−a novel gamma-butyrobetaine hydroxylase inhibitor with cardioprotective properties. *Biochem. Pharmacol.* **1988**, *37*, 195−202.
(17) Rose, N. R.; McDonough, M. A.; King, O. N. F.; Kawamura, A.; Schofield, C. J. Inhibition of 2-oxoglutarate dependent oxygenases. *Chem. Soc. Rev.* **2011**, *40*, 4364−4397.
(18) Hewitson, K. S.; Schofield, C. J.; Ratcliffe, P. J. Hypoxia-inducible factor prolyl-hydroxylase: purification and assays of PHD2. *Methods Enzymol.* **2007**, *435*, 25−42.
(19) Rose, N. R.; Woon, E. C. Y.; Kingham, G. L.; King, O. N. F.; Mecinović, J.; Clifton, I. J.; Ng, S. S.; Talib-Hardy, J.; Oppermann, U.; McDonough, M. A.; Schofield, C. J. Selective inhibitors of the JMJD2 histone demethylases: combined nondenaturing mass spectrometric screening and crystallographic approaches. *J. Med. Chem.* **2010**, *53*, 1810−1818.
(20) Mecinović, J.; Loenarz, C.; Chowdhury, R.; Schofield, C. J. 2-Oxoglutarate analogue inhibitors of prolyl hydroxylase domain 2. *Bioorg. Med. Chem. Lett.* **2009**, *19*, 6192−6195.
(21) Mecinović, J.; Chowdhury, R.; Liénard, B. M. R.; Flashman, E.; Buck, M. R. G.; Oldham, N. J.; Schofield, C. J. ESI-MS studies on prolyl hydroxylase domain 2 reveal a new metal binding site. *ChemMedChem* **2008**, *3*, 569−572.
(22) Hewitson, K. S.; Liénard, B. M. R.; McDonough, M. A.; Clifton, I. J.; Butler, D.; Soares, A. S.; Oldham, N. J.; McNeill, L. A.; Schofield, C. J. Structural and mechanistic studies on the inhibition of the hypoxia-inducible transcription factor hydroxylases by tricarboxylic acid cycle intermediates. *J. Biol. Chem.* **2007**, *282*, 3293−3301.
(23) McNeill, L. A.; Flashman, E.; Buck, M. R. G.; Hewitson, K. S.; Clifton, I. J.; Jeschke, G.; Claridge, T. D. W.; Ehrismann, D.; Oldham, N. J.; Schofield, C. J. Hypoxia-inducible factor prolyl hydroxylase 2 has a high affinity for ferrous iron and 2-oxoglutarate. *Mol. BioSyst.* **2005**, *1*, 321−324.
(24) McDonough, M. A.; Loenarz, C.; Chowdhury, R.; Clifton, I. J.; Schofield, C. J. Structural studies on human 2-oxoglutarate dependent oxygenases. *Curr. Opin. Struct. Biol.* **2010**, *20*, 1−14.
(25) Schofield, C. J.; Zhang, Z. Structural and mechanistic studies on 2-oxoglutarate-dependent oxygenases and related enzymes. *Curr. Opin. Struct. Biol.* **1999**, *9*, 722−731.
(26) Clifton, I. J.; McDonough, M. A.; Ehrismann, D.; Kershaw, N. J.; Granatino, N.; Schofield, C. J. Structural studies on 2-oxoglutarate oxygenases and related double-stranded β-helix fold proteins. *J. Inorg. Biochem.* **2006**, *100*, 644−669.
(27) Bleijlevens, B.; Shivarattan, T.; Flashman, E.; Yang, Y.; Simpson, P. J.; Koivisto, P.; Sedgwick, B.; Schofield, C. J.; Matthews, S. J. Dynamic states of the DNA repair enzyme AlkB regulate product release. *EMBO Rep.* **2008**, *9*, 872−877.
(28) Ehrismann, D.; Flashman, E.; Genn, D. N.; Mathioudakis, N.; Hewitson, K. S.; Ratcliffe, P. J.; Schofield, C. J. Studies on the activity of the hypoxia-inducible-factor hydroxylases using an oxygen consumption assay. *Biochem. J.* **2007**, *401*, 227−234.
(29) Flagg, S. C.; Martin, C. B.; Taabazuing, C. Y.; Holmes, B. E.; Knapp, M. J. Screening chelating inhibitors of HIF-prolyl hydroxylase domain 2 (PHD2) and factor inhibiting HIF (FIH). *J. Inorg. Biochem.* **2012**, *113*, 25−30.
(30) Hardy, A. P.; Prokes, I.; Kelly, L.; Campbell, I. D.; Schofield, C. J. Asparaginyl β-hydroxylation of proteins containing ankyrin repeat domains influences their stability and function. *J. Mol. Biol.* **2009**, *392*, 994−1006.
(31) Leung, I. K. H.; Flashman, E.; Yeoh, K. K.; Schofield, C. J.; Claridge, T. D. W. Using NMR solvent water relaxation to investigate metalloenzyme-ligand binding interactions. *J. Med. Chem.* **2010**, *53*, 867−875.
(32) Loo, J. A. Studying noncovalent protein complexes by electrospray ionization mass spectrometry. *Mass Spectrom. Rev.* **1997**, *16*, 25−49.
(33) Mayer, M.; Meyer, B. Characterization of ligand binding by saturation transfer difference NMR spectroscopy. *Angew. Chem., Int. Ed.* **1999**, *38*, 1784−1788.
(34) Dalvit, C.; Pevarello, P.; Tatò, M.; Veronesi, M.; Vulpetti, A.; Sundström, M. Identification of compounds with binding affinity to proteins via magnetization transfer from bulk water. *J. Biomol. NMR* **2000**, *18*, 65−68.
(35) Ji, Z.; Yao, Z.; Liu, M. Saturation transfer difference nuclear magnetic resonance study on the specific binding of ligand to protein. *Anal. Biochem.* **2009**, *385*, 380−382.
(36) Angulo, J.; Enríquez-Navas, P. M.; Nieto, P. M. Ligand-receptor binding affinities from saturation transfer difference (STD) NMR spectroscopy: the binding isotherm of STD initial growth rates. *Chem.—Eur. J.* **2010**, *16*, 7803−7812.
(37) Fielding, L.; Rutherford, S.; Fletcher, D. Determination of protein−ligand binding affinity by NMR: observation from serum albumin model systems. *Magn. Reson. Chem.* **2005**, *43*, 463−470.
(38) Jahnke, W.; Floersheim, P.; Ostermeier, C.; Zhang, X.; Hemmig, R.; Hurth, K.; Uzunov, D. P. NMR reporter screening for the detection of high-affinity ligands. *Angew. Chem., Int. Ed.* **2002**, *41*, 3420−3423.
(39) Dalvit, C.; Flocco, M.; Knapp, S.; Mostardini, M.; Perego, R.; Stockman, B. J.; Veronesi, M.; Varasi, M. High-throughput NMR-based screening with competition binding experiments. *J. Am. Chem. Soc.* **2002**, *124*, 7702−7709.
(40) Dalvit, C.; Flocco, M.; Stockman, B. J.; Veronesi, M. Competition binding experiments for rapidly ranking lead molecules

for their binding affinity to human serum albumin. *Comb. Chem. High Throughput Screening* **2002**, *5*, 645−650.
(41) Manzenrieder, F.; Frank, A. O.; Kessler, H. Phosphorus NMR spectroscopy as a versatile tool for compound library screening. *Angew. Chem., Int. Ed.* **2008**, *47*, 2608−2611.
(42) Dalvit, C. Ligand- and substrate-based ^{19}F NMR screening: principles and applications to drug discovery. *Prog. Nucl. Magn. Reson. Spectrosc.* **2007**, *51*, 243−271.
(43) Araç, D.; Murphy, T.; Rizo, J. Facile detection of protein−protein interactions by one-dimensional NMR spectroscopy. *Biochemistry* **2003**, *42*, 2774−2780.
(44) Carr, H. Y.; Purcell, E. M. Effects of diffusion on free precession in nuclear magnetic resonance experiments. *Phys. Rev.* **1954**, *94*, 630−638.
(45) Meiboom, S.; Gill, D. Modified spin-echo method for measuring nuclear relaxation times. *Rev. Sci. Instrum.* **1958**, *29*, 688−691.
(46) Hajduk, P. J.; Olejniczak, E. T.; Fesik, S. W. One-dimensional relaxation- and diffusion-edited NMR methods for screening compounds that bind to macromolecules. *J. Am. Chem. Soc.* **1997**, *119*, 12257−12261.
(47) Aguilar, J. A.; Nilsson, M.; Bodenhausen, G.; Morris, G. A. Spin echo NMR spectra without J modulation. *Chem. Commun.* **2012**, *48*, 811−813.
(48) Mole, D. R.; Schlemminger, I.; McNeill, L. A.; Hewitson, K. S.; Pugh, C. W.; Ratcliffe, P. J.; Schofield, C. J. 2-Oxoglutarate analogue inhibitors of HIF prolyl hydroxylase. *Bioorg. Med. Chem. Lett.* **2003**, *13*, 2677−2680.
(49) Rose, N. R.; Woon, E. C.; Tumber, A.; Walport, L. J.; Chowdhury, R.; Li, X. S.; King, O. N. F.; Lejeune, C.; Ng, S. S.; Krojer, T.; Chan, M. C.; Rydzik, A. M.; Hopkinson, R. J.; Che, K. H.; Daniel, M.; Strain-Damerell, C.; Gileadi, C.; Kochan, G.; Leung, I. K. H.; Dunford, J.; Yeoh, K. K.; Ratcliffe, P. J.; Burgess-Brown, N.; von Delft, F.; Muller, S.; Marsden, B.; Brennan, P. E.; McDonough, M. A.; Oppermann, U.; Klose, R. J.; Schofield, C. J.; Kawamura, A. The plant growth regulator daminozide is a selective inhibitor of the human KDM2/7 histone demethylases. *J. Med. Chem.* **2012**, *55*, 6639−6643.
(50) Warshakoon, N. C.; Wu, S.; Boyer, A.; Kawamoto, R.; Sheville, J.; Renock, S.; Xu, K.; Pokross, M.; Evdokimov, A. G.; Walter, R.; Mekel, M. A novel series of imidazo[1,2-a]pyridine derivatives as HIF-1α prolyl hydroxylase inhibitors. *Bioorg. Med. Chem. Lett.* **2006**, *16*, 5598−5601.
(51) Yan, L.; Colandrea, V. J.; Hale, J. J. Prolyl hydroxylase domain-containing protein inhibitors as stabilizers of hypoxia-inducible factor: small molecule-based therapeutics for anemia. *Expert Opin. Ther. Pat.* **2010**, *20*, 1219−1245.
(52) Tian, Y.-M.; Yeoh, K. K.; Lee, M. K.; Eriksson, T.; Kessler, B. M.; Kramer, H. B.; Edelmann, M. J.; Willam, C.; Pugh, C. W.; Schofield, C. J.; Ratcliffe, P. J. Differential sensitivity of hypoxia inducible factor hydroxylation sites to hypoxia and hydroxylase inhibitors. *J. Biol. Chem.* **2011**, *286*, 13041−13051.
(53) Stubbs, C. J.; Loenarz, C.; Mecinović, J.; Yeoh, K. K.; Hindley, N.; Liénard, B. M.; Sobott, F.; Schofield, C. J.; Flashman, E. Application of a proteolysis/mass spectrometry method for investigating the effects of inhibitors on hydroxylase structure. *J. Med. Chem.* **2009**, *52*, 2799−2805.
(54) King, O. N. F.; Li, X. S.; Sakurai, M.; Kawamura, A.; Rose, N. R.; Ng, S. S.; Quinn, A. M.; Rai, G.; Mott, B. T.; Beswick, P.; Klose, R. J.; Oppermann, U.; Jadhav, A.; Heightman, T. D.; Maloney, D. J.; Schofield, C. J.; Simeonov, A. Quantitative high-throughput screening identifies 8-hydroxyquinolines as cell-active histone demethylase inhibitors. *PLoS ONE* **2010**, *5*, e15535.
(55) Tsukada, Y.; Fang, J.; Erdjument-Bromage, H.; Warren, M. E.; Borchers, C. H.; Tempst, P.; Zhang, Y. Histone demethylation by a family of JmjC domain-containing proteins. *Nature* **2006**, *439*, 811−816.
(56) Klose, R. J.; Kallin, E. M.; Zhang, Y. JmjC-domain-containing proteins and histone demethylation. *Nat. Rev. Genet.* **2006**, *7*, 715−727.
(57) Hirsila, M.; Koivunen, P.; Gunzler, V.; Kivirikko, K. I.; Myllyharju, J. Characterization of the human prolyl 4-hydroxylases that modify the hypoxia-inducible factor. *J. Biol. Chem.* **2003**, *278*, 30772−30780.
(58) Tegley, C. M.; Viswanadhan, V. N.; Biswas, K.; Frohn, M. J.; Peterkin, T. A. N.; Chang, C.; Bürli, R. W.; Dao, J. H.; Veith, H.; Rogers, N.; Yoder, S. C.; Biddlecome, G.; Tagari, P.; Allen, J. R.; Hungate, R. W. Discovery of novel hydroxy-thiazoles as HIF-α prolyl hydroxylase inhibitors: SAR, synthesis, and modeling evaluation. *Bioorg. Med. Chem. Lett.* **2008**, *18*, 3925−3928.
(59) Morton, C. J.; Pugh, D. J. R.; Brown, E. L. J.; Kahmann, J. D.; Renzoni, D. A. C.; Campbell, I. D. Solution structure and peptide binding of the SH3 domain from human Fyn. *Structure* **1996**, *4*, 705−714.
(60) Cheng, Y.-C.; Prusoff, W. H. Relationship between the inhibition constant (K_I) and the concentration of inhibitor which causes 50% inhibition (I_{50}) of an enzymatic reaction. *Biochem. Pharmacol.* **1973**, *22*, 3099−3108.
(61) Nikolovska-Coleska, Z.; Wang, R.; Fang, X.; Pan, H.; Tomita, Y.; Li, P.; Roller, P. P.; Krajewski, K.; Saito, N. G.; Stuckey, J. A.; Wang, S. Development and optimization of a binding assay for the XIAP BIR3 domain using fluorescence polarization. *Anal. Biochem.* **2004**, *332*, 261−273.
(62) Cer, R. Z.; Mudunuri, U.; Stephens, R.; Lebeda, F. J. IC_{50}-to-K_i: a web-based tool for converting IC_{50} to K_i values for inhibitors of enzyme activity and ligand binding. *Nucleic Acids Res.* **2009**, *37*, W441−W445.
(63) Koivunen, P.; Hirsila, M.; Gunzler, V.; Kivirikko, K. I.; Myllyharju, J. Catalytic properties of the asparaginyl hydroxylase (FIH) in the oxygen sensing pathway are distinct from those of its prolyl 4-hydroxylases. *J. Biol. Chem.* **2004**, *279*, 9899−9904.
(64) Koivunen, P.; Hirsilä, M.; Remes, A. M.; Hassinen, I. E.; Kivirikko, K. I.; Myllyharju, J. Inhibition of hypoxia-inducible factor (HIF) hydroxylases by citric acid cycle intermediates. Possible links between cell metabolism and stabilization of HIF. *J. Biol. Chem.* **2007**, *282*, 4524−4532.
(65) Selak, M. A.; Armour, S. M.; MacKenzie, E. D.; Boulahbel, H.; Watson, D. G.; Mansfield, K. D.; Pan, Y.; Simon, M. C.; Thompson, C. B.; Gottlieb, E. Succinate links TCA cycle dysfunction to oncogenesis by inhibiting HIF-α prolyl hydroxylase. *Cancer Cell* **2005**, *7*, 77−85.
(66) Chowdhury, R.; Yeoh, K. K.; Tian, Y.-M.; Hillringhaus, L.; Bagg, E. A.; Rose, N. R.; Leung, I. K. H.; Li, X. S.; Woon, E. C. Y.; Yang, M.; McDonough, M. A.; King, O. N.; Clifton, I. J.; Klose, R. J.; Claridge, T. D. W.; Ratcliffe, P. J.; Schofield, C. J.; Kawamura, A. The oncometabolite 2-hydroxyglutarate inhibits histone lysine demethylases. *EMBO Rep.* **2011**, *12*, 463−469.
(67) Koivunen, P.; Lee, S.; Duncan, C. G.; Lopez, G.; Lu, G.; Ramkissoon, S.; Losman, J. A.; Joensuu, P.; Bergmann, U.; Gross, S.; Travins, J.; Weiss, S.; Looper, R.; Ligon, K. L.; Verhaak, R. G. W.; Yan, H.; Kaelin, W. G., Jr. Transformation by the (*R*)-enantiomer of 2-hydroxyglutarate linked to EGLN activation. *Nature* **2012**, *483*, 484−488.
(68) Isaacs, J. S.; Jung, Y. J.; Mole, D. R.; Lee, S.; Torres-Cabala1, C.; Chung, Y.-L.; Merino, M.; Trepel, J.; Zbar, B.; Toro, J.; Ratcliffe, P. J.; Linehan, W. M.; Neckers, L. HIF overexpression correlates with biallelic loss of fumaratehydratase in renal cancer: novel role of fumarate in regulation of HIF stability. *Cancer Cell* **2005**, *8*, 143−153.
(69) King, A.; Selak, M. A.; Gottlieb, E. Succinate dehydrogenase and fumarate hydratase: linking mitochondrial dysfunction and cancer. *Oncogene* **2006**, *25*, 4675−4682.
(70) Sudarshan, S.; Linehan, W. M.; Neckers, L. HIF and fumarate hydratase in renal cancer. *Br. J. Cancer* **2007**, *96*, 403−407.
(71) Flashman, E.; Davies, S. L.; Yeoh, K. K.; Schofield, C. J. Investigating the dependence of the hypoxia-inducible factor hydroxylases (factor inhibiting HIF and prolyl hydroxylase domain 2) on ascorbate and other reducing agents. *Biochem. J.* **2010**, *427*, 135−142.

(72) Swann, S. L.; Song, D.; Sun, C.; Hajduk, P. J.; Petros, A. M. Labeled ligand displacement: extending NMR-based screening of protein targets. *ACS Med. Chem. Lett.* **2010**, *1*, 295−299.
(73) Tsukada, Y.-I.; Fang, J.; Erdjument-Bromage, H.; Warren, M. E.; Borchers, C. H.; Tempst, P.; Zhang, Y. Histone demethylation by a family of JmjC domain-containing proteins. *Nature* **2006**, *439*, 811−816.
(74) Varier, R. A.; Timmers, H. T. Histone lysine methylation and demethylation pathways in cancer. *Biochim. Biophys. Acta* **2010**, *1815*, 75−89.
(75) Lehn, J.-M.; Eliseev, A. V. Dynamic combinatorial chemistry. *Science* **2001**, *291*, 2331−2332.
(76) Ramström, O.; Lehn, J.-M. Drug discovery by dynamic combinatorial libraries. *Nat. Rev. Drug Discovery* **2002**, *1*, 26−36.
(77) Otto, S.; Furlan, R. L. E.; Sanders, J. K. M. Dynamic combinatorial chemistry. *Drug Discovery Today* **2002**, *7*, 117−125.
(78) Greaney, M. F.; Bhat, V. T. Protein-directed dynamic combinatorial chemistry. In *Dynamic Combinatorial Chemistry: In Drug Discovery, Bioinorganic Chemistry, and Materials Sciences*; Miller, B. L., Ed.; John Wiley & Sons, Inc.: Hoboken, NJ, 2010; Chapter 2, pp 43−82.
(79) Hochgürtel, M.; Lehn, J.-M. Dynamic combinatorial diversity in drug discovery. In *Fragment-Based Approaches in Drug Discovery*; Jahnke, W., Erlanson, D. A., Eds.; Wiley-VCH: Weinheim, Germany, 2006; Chapter 16, pp 341−364.
(80) Corbett, P. T.; Leclaire, J.; Vial, L.; West, K. R.; Wietor, J.-L.; Sanders, J. K. M.; Otto, S. Dynamic combinatorial chemistry. *Chem. Rev.* **2006**, *106*, 3652−3711.
(81) Leung, I. K. H.; Brown, T., Jr.; Schofield, C. J.; Claridge, T. D. W. An approach to enzyme inhibition employing reversible boronate ester formation. *Med. Chem. Commun.* **2011**, *2*, 390−395.
(82) Demetriades, M.; Leung, I. K. H.; Chowdhury, R.; Chan, M. C.; Yeoh, K. K.; Tian, Y.-M.; Claridge, T. D. W.; Ratcliffe, P. J.; Woon, E. C. Y.; Schofield, C. J. Dynamic combinatorial chemistry employing boronic acids/boronate esters leads to potent oxygenase inhibitors. *Angew. Chem., Int. Ed.* **2012**, *51*, 6672−6675.
(83) Rotili, D.; Altun, M.; Kawamura, A.; Wolf, A.; Fischer, R.; Leung, I. K. H.; Mackeen, M. M.; Tian, Y.-M.; Ratcliffe, P. J.; Mai, A.; Kessler, B. M.; Schofield, C. J. A photoreactive small-molecule probe for 2-oxoglutarate oxygenases. *Chem. Biol.* **2011**, *18*, 642−654.
(84) Wu, P. S. C.; Otting, G. Rapid pulse length determination in high-resolution NMR. *J. Magn. Reson.* **2005**, *176*, 115−119.
(85) Enthart, A.; Freudenberger, J. C.; Furrer, J.; Kessler, H.; Luy, B. The CLIP/CLAP-HSQC: pure absorptive spectra for the measurement of one-bond couplings. *J. Magn. Reson.* **2008**, *192*, 314−322.

Journal of Medicinal Chemistry

Brief Article

pubs.acs.org/jmc

Plant Growth Regulator Daminozide Is a Selective Inhibitor of Human KDM2/7 Histone Demethylases

Nathan R. Rose,[†,‡,#] Esther C. Y. Woon,[‡,#,∞] Anthony Tumber,[§,#] Louise J. Walport,[‡] Rasheduzzaman Chowdhury,[‡] Xuan Shirley Li,[†] Oliver N. F. King,[‡] Clarisse Lejeune,[‡,§] Stanley S. Ng,[§,∥] Tobias Krojer,[§] Mun Chiang Chan,[‡] Anna M. Rydzik,[‡] Richard J. Hopkinson,[‡] Ka Hing Che,[§,∥] Michelle Daniel,[§] Claire Strain-Damerell,[§] Carina Gileadi,[§] Grazyna Kochan,[§] Ivanhoe K. H. Leung,[‡] James Dunford,[∥] Kar Kheng Yeoh,[⊥] Peter J. Ratcliffe,[⊥] Nicola Burgess-Brown,[§] Frank von Delft,[§] Susanne Muller,[§] Brian Marsden,[§] Paul E. Brennan,[§] Michael A. McDonough,[‡] Udo Oppermann,[§,∥] Robert J. Klose,[†] Christopher J. Schofield,*[,‡] and Akane Kawamura*[,‡]

[†]Epigenetic Regulation of Chromatin Function Group, Department of Biochemistry, University of Oxford, South Parks Road, Oxford OX1 3QU, U.K.

[‡]Chemistry Research Laboratory, Department of Chemistry, University of Oxford, Mansfield Road, Oxford OX1 3TA, U.K.

[§]Structural Genomics Consortium, University of Oxford, Headington OX3 7DQ, U.K.

[∥]Oxford Biomedical Research Unit, Botnar Research Centre, University of Oxford, Oxford OX3 7LD, U.K.

[⊥]Henry Wellcome Building for Molecular Physiology, Department of Clinical Medicine, University of Oxford, Roosevelt Drive, Oxford OX3 7BN, U.K.

Supporting Information

ABSTRACT: The JmjC oxygenases catalyze the *N*-demethylation of N^{ε}-methyl lysine residues in histones and are current therapeutic targets. A set of human 2-oxoglutarate analogues were screened using a unified assay platform for JmjC demethylases and related oxygenases. Results led to the finding that daminozide (*N*-(dimethylamino)succinamic acid, 160 Da), a plant growth regulator, selectively inhibits the KDM2/7 JmjC subfamily. Kinetic and crystallographic studies reveal that daminozide chelates the active site metal via its hydrazide carbonyl and dimethylamino groups.

INTRODUCTION

Histone modifications are central to the regulation of eukaryotic gene expression. The dynamic methylation of lysine and arginine residues in histones has diverse transcriptional outcomes, with different methylation sites and states being associated with promotion or repression of transcription. There are two classes of histone lysine demethylases (KDMs), the largest of which uses 2-oxoglutarate (2OG) as a cosubstrate (the JmjC enzymes) and comprises ~18 human enzymes grouped into five subfamilies (Figure 1). Several JmjC demethylases are targets for the treatment of diseases including leukemia, breast, and prostate cancers[1,2] and inflammation.[3] However, only limited inhibition data have been reported for the JmjC enzymes with few reports of selective inhibitors.[4−8]

2OG oxygenases have been targeted for therapeutic and agricultural applications:[9] an inhibitor of γ-butyrobetaine hydroxylase, BBOX1, is used clinically as a "cardioprotectant", inhibition of the collagen prolyl hydroxylases has been investigated for treating fibrotic disease, and inhibitors of the hypoxia inducible factor hydroxylases are in clinical trials for the treatment of anemia. These examples provide evidence that 2OG oxygenases are viable targets for therapeutic inhibition by small molecules in vivo. 2OG oxygenases involved in the biosynthesis of gibberellins, plant hormones involved in growth regulation, have also been targeted using small molecule inhibitors for agricultural and horticultural applications. Here we report that daminozide, *N*-(dimethylamino)succinamic acid, which was once widely used as a plant growth retardant but later withdrawn because of toxicity concerns, is a highly selective inhibitor of the KDM2/7 family of human JmjC histone demethylases.

RESULTS

To enable the identification of selective JmjC demethylase subfamily inhibitors, we developed a unified screening platform containing representatives of each of the five human demethylase subfamilies (KDM2A/FBXL11, KDM3A/JMJD1A, KDM4E/JMJD2E, KDM5C/JARID1C, KDM6B/JMJD3) (Supporting Information). Active enzymes were expressed using bacterial or eukaryotic expression systems and purified to near homogeneity (Supporting Information). Kinetic parameters for 2OG and histone fragment substrates were determined (Table 1), and activity AlphaScreens (amplified luminescence proximity homogeneous assays) were developed (Figure S1).[10] This assay is based on immunodetection of the lysine methylation state of biotin-conjugated histone peptide product, using streptavidin- and protein A-

Received: May 15, 2012
Published: June 25, 2012

ACS Publications © 2012 American Chemical Society

dx.doi.org/10.1021/jm300677j | J. Med. Chem. 2012, 55, 6639−6643

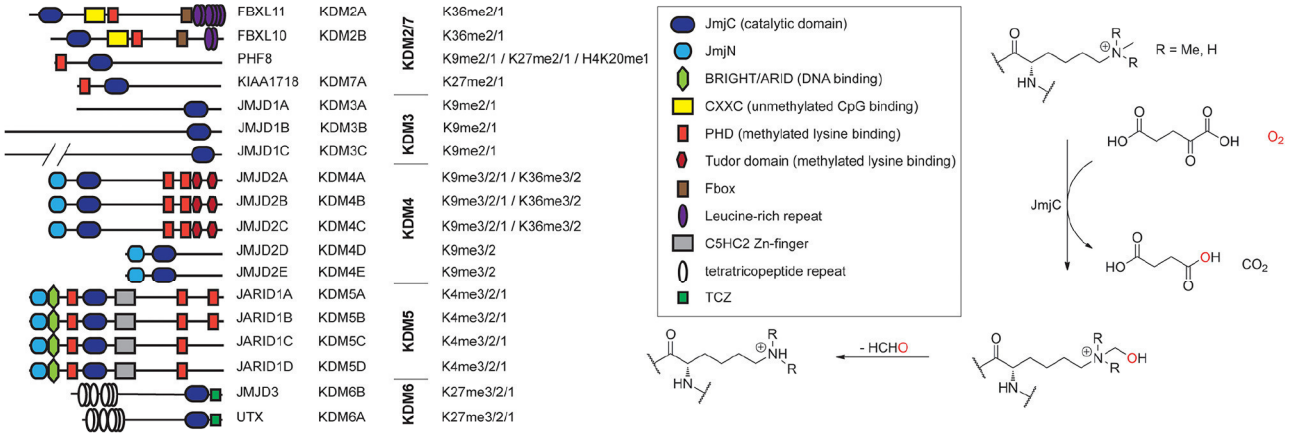

Figure 1. Subfamilies of the human 2-oxoglutarate (JmjC) histone demethylases, showing their domain architecture. Not all proposed family members are shown. Each demethylation reaction is coupled to 2OG decarboxylation and formaldehyde production. KIAA1718 has recently been assigned as KDM7A;[11] however, its JmjC domain shows high sequence and structural similarity with the KDM2 subfamily members.

Table 1. Inhibition Data (IC_{50}) for Daminozide and Its Analogues across KDMs and Other 2OG Oxygenases[a]

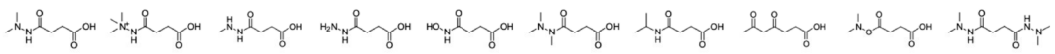

	Daminozide	22	23	24	25	26	27	28	29	30
KDM2A	1.5	63	0.37	0.25	0.43	3.7	>100	0.57	9.1	>100
PHF8	0.55	35	3.4	0.48	1.7	11.5	>100	2.3	6.9	117
KDM7A	(2.1)	-	-	-	-	-	-	-	-	-
KDM3A	>100	>100	>100	>100	3.0	>100	>100	12.7	>100	>100
KDM4E	>100	>100	4.3	0.2	0.4	>100	>100	23.9	>100	>100
KDM5C	>100	>100	1.1	0.48	1.9	>100	>100	4.5	42	>100
KDM6B	>100	>100	>100	>100	1.1	>100	>100	16.5	41.7	>100
FIH	(>100)	(>100)	(>100)	(>100)	(>100)	(>100)	(>100)	(>100)	(>100)	(>100)
PHD2	>100	>100	14.2	>100	19.6	>100	>100	>100	6.3	>100
BBOX1*	>100	>100	>100	>100	>100	>100	>100	>100	>100	>100

[a]Data are reported as IC_{50} in μM. AlphaScreen was used for all IC_{50} determinations except where values are given in parenthesis where a MALDI assay was used. All BBOX assays were run using a fluorescence based assay.[12] AlphaScreen assays were optimized to run at the linear range of the reaction. Assays were performed at concentrations of 2OG near experimentally determined 2OG K_m^{app} values. Where K_m^{app} values for 2OG for enzymes were unknown, the kinetic parameter was determined by using the FDH assay: KDM2A (12.5 ± 1.4 μM), PHF8 (16.6 ± 1.8 μM), KDM3A (5.3 ± 2.2 μM), KDM5C (41.7 ± 6.3 μM), and KDM6B (5.4 ± 0.4 μM).

conjugated beads for quantification. For counterscreening, we selected three clinically relevant oxygenases, the hypoxic response oxygenases PHD2 and FIH (prolyl and asparaginyl hydroxylases acting on hypoxia inducible factor, respectively), and BBOX1 (γ-butyrobetaine hydroxylase) for which AlphaScreen or fluorescence assays[12] were also developed. This screening platform is a significant improvement on previous methods for human 2OG oxygenases;[9] it enables the oxygenases to be used at low nanomolar concentrations. Standardization of the analytical methods for enzymes employing different types of substrates enabled quantitative comparisons of inhibitor potencies to be made.

In work aimed at identifying inhibitor scaffolds for the JmjC histone demethylases, we assembled a set of 2OG analogues known to inhibit 2OG oxygenases (Figure 2) and screened these against the 2OG oxygenase panel using the assay platform. As expected, known "generic" 2OG oxygenase inhibitors[9] including pyridine 2,4-dicarboxylic acid (**11**) and *N*-oxalylglycine (**12**) showed inhibition across the 2OG oxygenases tested, validating this assay platform. Interestingly, the clinically used histone deacetylase (HDAC) inhibitor Vorinostat/SAHA (suberoylanilide hydroxamic acid, **15**) inhibited several histone demethylases (Figure 2).

Unexpectedly, the plant growth regulator daminozide (**19**) stood out as a selective inhibitor of KDM2A (IC_{50} = 1.5 μM), which is selective for dimethyl lysine residues. Daminozide was identified as a plant growth retardant in the 1960s[14] and used to control stem growth, plant size, and fruit ripening for over 20 years.[15] In vivo, daminozide is proposed to inhibit 2OG oxygenases involved in gibberellin, and possibly ethylene, biosynthesis in plants.[16,17] However, daminozide usage in food crops was curtailed because of the potential carcinogenicity of its metabolite, 1,1-dimethylhydrazine (although is still used for ornamental plants).[18−20] A formaldehyde dehydrogenase (FDH) coupled assay monitoring formaldehyde production confirmed the potency of daminozide against KDM2A (IC_{50} = 1.5 μM). To test further for subfamily selectivity, daminozide was screened against two other members of the KDM2/7 subfamily (PHF8 and KDM7A, Table 1) which are structurally highly related to KDM2A and KDM2B and are also selective

dx.doi.org/10.1021/jm300677j | J. Med. Chem. 2012, 55, 6639−6643

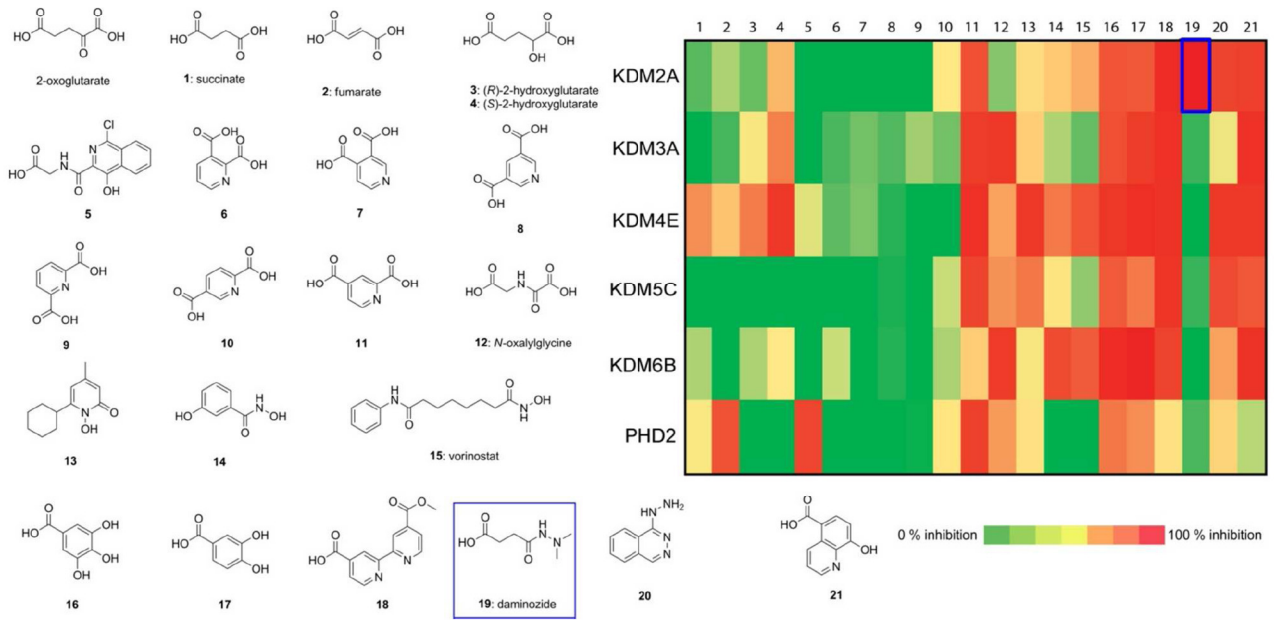

Figure 2. Heat map of JmjC demethylase inhibition by a set of 2OG analogues. Daminozide **19** is selective for KDM2A. Tricarboxylic acid cycle intermediates succinate **1** and fumarate **2** were generally poor demethylase inhibitors, though KDM4E[7] was an exception to this trend. The (*R*)- and (*S*)-2-hydroxyglutarate enantiomers, produced by gain-of-function mutations to isocitrate dehydrogenase, were inhibitors of the KDM2, KDM3, and KDM4 histone demethylases.[13] Catechols **16** and **17**, bipyridyl **18**, and 8-hydroxyquinoline **21** inhibited all demethylases screened. By contrast, **5** most potently inhibited PHD2 (prolyl hydroxylase domain enzyme isoform 2). Each compound was screened in an AlphaScreen assay and is represented as % inhibition of the enzyme at 20 μM compound. Details of the assays are in the Supporting Information.

for demethylation of dimethyl lysine residues but have different sequence specificities.[21−23] The results indicate that daminozide is at least 60-fold selective as an inhibitor of the KDM2/7 subfamily over the other demethylase subfamily members tested, with IC_{50} of 2 μM or less against KDM2A, PHF8, and KIAA1718 and IC_{50} of 127 μM for KDM3A (a different subfamily of dimethyl lysine demethylase) or greater (millimolar range) against other demethylases. No inhibition was observed (at 1 mM) against other biologically important 2OG oxygenases that catalyze hydroxylation, i.e., PHD2, FIH, and BBOX1. Given its simple achiral structure and low molecular weight (160 Da), the degree of selectivity exhibited by daminozide is remarkable.

Kinetic analyses revealed that daminozide is predominantly a competitive inhibitor with respect to 2OG (K_i = 1.97 μM) for KDM2A but shows mixed inhibition with respect to peptide substrate, binding predominantly to the enzyme-peptide complex (K_i = 85 μM, α = 0.13) (Figure 3). The latter observation is notable given that daminozide contains a dimethylamino group as do the KDM2/7 subfamily dimethyl

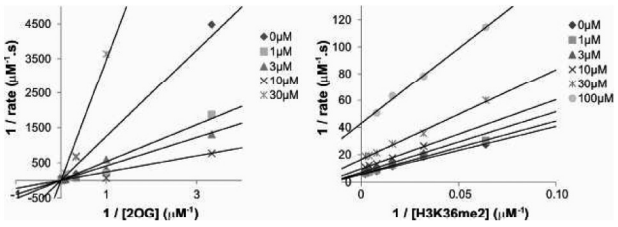

Figure 3. Mode of inhibition of the KDM2/7 subfamily by daminozide. Inhibition of KDM2A by daminozide is competitive with 2OG but not peptide substrate.

lysine substrates and might thus be expected to compete with the dimethylated lysine substrate. The pK_a of the daminozide hydrazide amine is 2.8 while that of its carboxylate is 4.6,[24] suggesting that it may bind the active site iron; NMR analyses show daminozide complexes to Fe(II) in solution (Figure S2).

We then investigated the structural basis of the selective inhibition by daminozide on the KDM2/7 subfamily. We obtained structures of daminozide complexed with two demethylases, PHF8 and KDM4A, and a hydroxylase, FIH (Figure 4). The structures support the proposed general mode of inhibition by daminozide, i.e., by binding in the 2OG binding pocket and chelating to the active site metal via its acylhydrazide carbonyl and dimethylamino groups (Figure 4). While the coordinate position of the daminozide carbonyl was invariant, i.e., in all cases trans to the Asp/Glu protein-based ligand, in the KDM4A structure the dimethylamino group was observed to complex trans to His276 or trans to His188 in the two different molecules present in the asymmetric unit. Although in the cases of PHF8 and FIH the daminozide dimethylamino group was only observed to bind trans to the histidine equivalent to His276 of KDM4A, previous work[25] on complexes of 2OG oxygenases with 2OG and the cosubstrate analogue **12** demonstrates that the 1-carboxylate can bind in either of the two conformational positions, in a manner analogous to that observed for the dimethylamino group in the KDM4A structure. We propose that the selectivity of daminozide for the KDM2/7 subfamily could, at least in part, arise from a "snug fit" obtained via binding in the position trans to His247 wherein its two methyl groups are accommodated in a tight hydrophobic pocket (formed by Val255, Ile313, and Tyr257), which is conserved in the KDM2/7subfamily (Figure 4). This pocket might bind the daminozide methyl groups less tightly in other demethylases/oxygenases because it is more hydrophilic (as demonstrated by crystallographic analysis) or

dx.doi.org/10.1021/jm300677j | *J. Med. Chem.* 2012, 55, 6639−6643

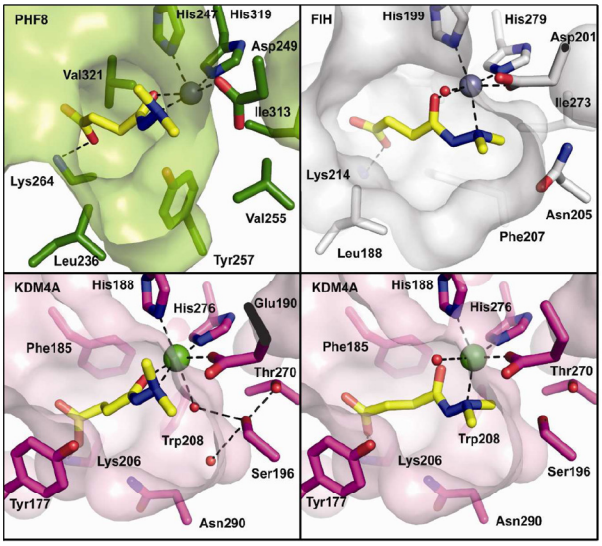

Figure 4. Crystal structures reveal the mode of inhibition of the KDM2/7 subfamily by daminozide: PHF8 (with Zn(II) substituting for Fe(II)) and KDM4A (with Ni(II) substituting for Fe(II)) and FIH (with Zn(II) substituting for Fe(II)) (Table S3). Daminozide binds the metal through its hydrazide amine lone pair and carbonyl oxygen. Two distinct orientations of daminozide are observed in the two KDM4A molecules in the asymmetric unit; both are shown (see Table S2 for electron density maps). Selectivity of daminozide for the KDM2/7 subfamily may arise because they possess a hydrophobic region (Tyr257, Val255, and Ile313) into which the two daminozide methyl groups bind. In contrast, the equivalent regions of KDM4A, FIH, and the other tested demethylases/oxygenases are more hydrophilic.

predicted to be more hydrophilic (by structure based on sequence alignments) for all the other 2OG oxygenases tested (Figure 1) (e.g., for KDM4A, they are Ser196, Thr270, and Asn198; for KDM6B, they are Ser225, Ile291, and Asn227; for FIH, they are Asn205, Ile273, and Phe257).

We also synthesized and tested analogues of daminozide (Table 1 and Table S3). The trimethylated analogue **22** and **27**, both of which lack the terminal amine lone pair, displayed little/no KDM inhibition, consistent with the proposed mode of daminozide inhibition involving chelation by its terminal hydrazide amine. The monomethylated **23** and unmethylated analogues **24** were more potent than daminozide against KDM2A. However, when tested against other 2OG subfamilies, these compounds were substantially less selective than daminozide (and were somewhat unstable in aqueous solution). Succinylhydroxamic acid **25** and dioxoheptanoic acid **28**, in which the acylhydrazinamide of daminozide is replaced by metal-chelating hydroxamic acid and malonyl groups, respectively, were also relatively potent but nonselective inhibitors (Table 1). Notably, **26**, in which the amide nitrogen of daminozide is N-methylated, is also selective for the KDM2/7demethylases, albeit with reduced potency. Like daminozide, **26** has two methyl groups on the acylhydrazide amine, suggesting that their presence confers selectivity. The other tested analogues were less active (Table S3).

■ CONCLUSIONS

Overall, we have demonstrated how the development of a screening platform employing multiple human 2OG oxygenases can enable the discovery of compounds selective for particular subfamilies. In the long term, we aim to help develop screens for all human 2OG oxygenases and see them applied to the discovery of medicinally useful inhibitors. By use of a relatively focused set of 2OG analogues, the screening platform led to the discovery that daminozide is a selective inhibitor of the KDM2/7demethylase subfamily. While daminozide itself is unlikely to be of medicinal use, the work has revealed a new class of 2OG oxygenase inhibitor, which employs alkylamino iron chelation. Of particular note is the high degree of selectivity exhibited by daminozide, especially given its achiral nature and low molecular weight. The precise mode of action of daminozide as a plant growth regulator[16,17] and its potential human toxicity (if any) under physiologically relevant conditions are unknown. We have no evidence that our results are directly relevant to the toxicity issues relating to daminozide. However, the results do suggest a potential of daminozide or its derivatives to exert biological effects via the inhibition of 2OG oxygenases involved in epigenetics in animals and, potentially, in other organisms including plants. Given the link between JmjC enzymes and diseases including cancer,[2,3] further work on the biological effects of daminozide is of interest.

■ ASSOCIATED CONTENT

Ⓢ Supporting Information

Protein expression and purification methods, assay methods, synthetic procedures, characterization of all synthesized compounds, ^{1}H NMR spectra of daminozide and analogues with iron(II), and crystalllographic data collection and refinement statistics. This material is available free of charge via the Internet at http://pubs.acs.org.

Accession Codes

PDB codes: 4AI9, 4AI8, 4DO0 for complex of daminozide with KDM4A, FIH, PHF8 proteins, respectively.

■ AUTHOR INFORMATION

Corresponding Author

*For C.J.S.: phone, (01865) 275625; e-mail, christopher.schofield@chem.ox.ac.uk. For A.K.: phone, (01865) 275677; e-mail, akane.kawamura@chem.ox.ac.uk.

Present Address

[∞]Department of Pharmacy, National University of Singapore, 18 Science Drive 4, Singapore 117543.

Author Contributions

[#]These authors contributed equally to the work.

Notes

The authors declare no competing financial interest.

■ ACKNOWLEDGMENTS

This research was supported in part by the The Wellcome Trust, The Commonwealth Scholarship Commission in the United Kingdom, the Biotechnology and Biological Research Council (U.K.), and the European Research Council. The Structural Genomics Consortium is a registered charity (No. 1097737) that receives funds from the Canadian Institutes for Health Research, the Canadian Foundation for Innovation, Genome Canada through the Ontario Genomics Institute, GlaxoSmithKline, Karolinska Institutet, the Knut and Alice Wallenberg Foundation, the Ontario Innovation Trust, the Ontario Ministry for Research and Innovation, Merck & Co., Inc., the Novartis Research Foundation, the Swedish Agency for Innovation Systems, the Swedish Foundation for Strategic Research, and the Wellcome Trust.

■ ABBREVIATIONS USED

2OG, 2-oxoglutarate; BBOX, γ-butyrobetaine hydroxylase; FBXL, F-box, leucine-rich repeat protein; FIH, factor inhibiting hypoxia inducible factor; HDAC, histone deacetylase; JARID, jumonji, AT rich interactive domain containing protein; JmjC, jumonji-C domain; JMJD, jumonji-C domain containing protein; PHD2, human prolyl hydroxylase; PHF, plant homeodomain containing protein

■ REFERENCES

(1) He, J.; Nguyen, A. T.; Zhang, Y. KDM2b/JHDM1b, an H3K36me2-specific demethylase, is required for initiation and maintenance of acute myeloid leukemia. *Blood* **2011**, *117* (14), 3869−3880.

(2) Yang, J.; Jubb, A. M.; Pike, L.; Buffa, F. M.; Turley, H.; Baban, D.; Leek, R.; Gatter, K. C.; Ragoussis, J.; Harris, A. L. The histone demethylase JMJD2B is regulated by estrogen receptor alpha and hypoxia, and is a key mediator of estrogen induced growth. *Cancer Res.* **2010**, *70* (16), 6456−6466.

(3) De Santa, F.; Totaro, M. G.; Prosperini, E.; Notarbartolo, S.; Testa, G.; Natoli, G. The histone H3 lysine-27 demethylase Jmjd3 links inflammation to inhibition of polycomb-mediated gene silencing. *Cell* **2007**, *130* (6), 1083−1094.

(4) Chang, K. H.; King, O. N.; Tumber, A.; Woon, E. C.; Heightman, T. D.; McDonough, M. A.; Schofield, C. J.; Rose, N. R. Inhibition of histone demethylases by 4-carboxy-2,2′-bipyridyl compounds. *ChemMedChem* **2011**, *6* (5), 759−764.

(5) Hamada, S.; Suzuki, T.; Mino, K.; Koseki, K.; Oehme, F.; Flamme, I.; Ozasa, H.; Itoh, Y.; Ogasawara, D.; Komaarashi, H.; Kato, A.; Tsumoto, H.; Nakagawa, H.; Hasegawa, M.; Sasaki, R.; Mizukami, T.; Miyata, N. Design, synthesis, enzyme-inhibitory activity, and effect on human cancer cells of a novel series of jumonji domain-containing protein 2 histone demethylase inhibitors. *J. Med. Chem.* **2010**, *53* (15), 5629−5638.

(6) Luo, X.; Liu, Y.; Kubicek, S.; Myllyharju, J.; Tumber, A.; Ng, S.; Che, K. H.; Podoll, J.; Heightman, T. D.; Oppermann, U.; Schreiber, S. L.; Wang, X. A selective inhibitor and probe of the cellular functions of Jumonji C domain-containing histone demethylases. *J. Am. Chem. Soc.* **2011**, *133* (24), 9451−9456.

(7) Rose, N. R.; Ng, S. S.; Mecinovic, J.; Liénard, B. M. R.; Bello, S. H.; Sun, Z.; McDonough, M. A.; Oppermann, U.; Schofield, C. J. Inhibitor scaffolds for 2-oxoglutarate-dependent histone lysine demethylases. *J. Med. Chem.* **2008**, *51* (22), 7053−7056.

(8) Sekirnik, R.; Rose, N. R.; Mecinovic, J.; Schofield, C. J. 2-Oxoglutarate oxygenases are inhibited by a range of transition metals. *Metallomics* **2010**, *2* (6), 397−399.

(9) Rose, N. R.; McDonough, M. A.; King, O. N.; Kawamura, A.; Schofield, C. J. Inhibition of 2-oxoglutarate dependent oxygenases. *Chem. Soc. Rev.* **2011**, *40* (8), 4364−4397.

(10) Kawamura, A.; Tumber, A.; Rose, N. R.; King, O. N.; Daniel, M.; Oppermann, U.; Heightman, T. D.; Schofield, C. Development of homogeneous luminescence assays for histone demethylase catalysis and binding. *Anal. Biochem.* **2010**, *404* (1), 86−93.

(11) Huang, C.; Xiang, Y.; Wang, Y.; Li, X.; Xu, L.; Zhu, Z.; Zhang, T.; Zhu, Q.; Zhang, K.; Jing, N.; Chen, C. D. Dual-specificity histone demethylase KIAA1718 (KDM7A) regulates neural differentiation through FGF4. *Cell Res.* **2010**, *20* (2), 154−165.

(12) Rydzik, A.; Leung, I. K. H.; Kochan, G. T.; Thalhammer, A.; Opperman, U.; Claridge, T. D. W.; Schofield, C. J. Development and application of a fluoride detection based fluorescence assay for gamma-butyrobetaine hydroxylase. *ChemBioChem* [Online early access]. DOI: 10.1002/cbic.201200256. Published Online: Jun 22, **2012**.

(13) Chowdhury, R.; Yeoh, K. K.; Tian, Y. M.; Hillringhaus, L.; Bagg, E. A.; Rose, N. R.; Leung, I. K. H.; Li, X. S.; Woon, E. C.; Yang, M.; McDonough, M. A.; King, O. N.; Clifton, I. J.; Klose, R. J.; Claridge, T. D. W.; Ratcliffe, P. J.; Schofield, C. J.; Kawamura, A. The oncometabolite 2-hydroxyglutarate inhibits histone lysine demethylases. *EMBO Rep.* **2011**, *12* (5), 463−469.

(14) Riddell, J. A.; Hageman, H. A.; J'Anthony, C. M.; Hubbard, W. L. Retardation of plant growth by a new group of chemicals. *Science* **1962**, *136* (3514), 391.

(15) Rademacher, W. Growth retardants: effects on gibberellin biosynthesis and other metabolic pathways. *Ann. Rev. Plant Physiol. Plant Mol. Biol.* **2000**, *51* (1), 501−531.

(16) Brown, R. G. S.; Kawaide, H.; Yang, Y.-Y.; Rademacher, W.; Kamiya, Y. Daminozide and prohexadione have similar modes of action as inhibitors of the late stages of gibberellin metabolism. *Physiol. Plant.* **1997**, *101*, 309−313.

(17) Looney, N. E. Inhibition of apple ripening by succinic acid, 2,2-dimethyl hydrazide and its reversal by ethylene. *Plant Physiol* **1968**, *43*, 1133−1137.

(18) Hasegawa, R.; Cabral, R.; Hoshiya, T.; Hakoi, K.; Ogiso, T.; Boonyaphiphat, P.; Shirai, T.; Ito, N. Carcinogenic potential of some pesticides in a medium-term multi-organ bioassay in rats. *Int. J. Cancer* **1993**, *54* (3), 489−493.

(19) Mott, L. Alar again: science, the media, and the public's right to know. *Int. J. Occup. Environ. Health* **2000**, *6* (1), 68−70.

(20) Toth, B.; Wallcave, L.; Patil, K.; Schmeltz, I.; Hoffmann, D. Induction of tumors in mice with the herbicide succinic acid 2,2-dimethylhydrazide. *Cancer Res.* **1977**, *37* (10), 3497−3500.

(21) Horton, J. R.; Upadhyay, A. K.; Qi, H. H.; Zhang, X.; Shi, Y.; Cheng, X. Enzymatic and structural insights for substrate specificity of a family of jumonji histone lysine demethylases. *Nat. Struct. Mol. Biol.* **2010**, *17* (1), 38−43.

(22) Liu, W.; Tanasa, B.; Tyurina, O. V.; Zhou, T. Y.; Gassmann, R.; Liu, W. T.; Ohgi, K. A.; Benner, C.; Garcia-Bassets, I.; Aggarwal, A. K.; Desai, A.; Dorrestein, P. C.; Glass, C. K.; Rosenfeld, M. G. PHF8 mediates histone H4 lysine 20 demethylation events involved in cell cycle progression. *Nature* **2010**, *466* (7305), 508−512.

(23) Qi, H. H.; Sarkissian, M.; Hu, G. Q.; Wang, Z.; Bhattacharjee, A.; Gordon, D. B.; Gonzales, M.; Lan, F.; Ongusaha, P. P.; Huarte, M.; Yaghi, N. K.; Lim, H.; Garcia, B. A.; Brizuela, L.; Zhao, K.; Roberts, T. M.; Shi, Y. Histone H4K20/H3K9 demethylase PHF8 regulates zebrafish brain and craniofacial development. *Nature* **2010**, *466* (7305), 503−507.

(24) Schoenherr, J.; Bukovac, M. J. Dissociation constants of succinic acid 2,2-dimethylhydrazide. *J. Agric. Food Chem.* **1972**, *20* (6), 1263−1265.

(25) Zhang, Z.; Ren, J.; Harlos, K.; McKinnon, C. H.; Clifton, I. J.; Schofield, C. J. Crystal structure of a clavaminate synthase−Fe(II)−2-oxoglutarate−substrate−NO complex: evidence for metal centred rearrangements. *FEBS Lett.* **2002**, *517* (1−3), 7−12.

Bioorganic & Medicinal Chemistry Letters 22 (2012) 4975–4978

Contents lists available at SciVerse ScienceDirect

Bioorganic & Medicinal Chemistry Letters

journal homepage: www.elsevier.com/locate/bmcl

γ-Butyrobetaine hydroxylase catalyses a Stevens type rearrangement

Luc Henry [†], Ivanhoe K. H. Leung [†], Timothy D. W. Claridge [*], Christopher J. Schofield [*]

Department of Chemistry, University of Oxford, Chemistry Research Laboratory, 12 Mansfield Road, Oxford OX1 3TA, United Kingdom

ARTICLE INFO

Article history:
Received 4 May 2012
Revised 10 June 2012
Accepted 11 June 2012
Available online 16 June 2012

Keywords:
BBOX
Carnitine
THP
Stevens rearrangement
Formaldehyde
Fatty acid oxidation
2-Oxoglutarate (2OG) oxygenase
Trimethyl L-lysine

ABSTRACT

γ-Butyrobetaine hydroxylase (BBOX) is a 2-oxoglutarate and Fe(II)-dependent oxygenase that catalyses the final step of L-carnitine biosynthesis in animals. BBOX catalyses the oxidation of 3-(2,2,2-trimethylhydrazinium)propionate (THP), a clinically used BBOX inhibitor, to form multiple products including 3-amino-4-(methyamino)butanoic acid (AMBA), which is proposed to be formed via a Stevens type rearrangement mechanism. We report the synthesis of AMBA and confirm that it is a product of the BBOX catalysed oxidation of THP. AMBA reacts with formaldehyde, which is produced enzymatically by BBOX, to give a cyclic adduct.

© 2012 Elsevier Ltd. All rights reserved.

γ-Butyrobetaine hydroxylase (BBOX) is a 2-oxoglutarate (2OG) and Fe(II)-dependent oxygenase that catalyses the final step of L-carnitine (L-Car) biosynthesis in animals (Scheme 1).[1] 3-(2,2,2-Trimethylhydrazinium)propionate (THP) is a BBOX inhibitor that is used clinically for the treatment of angina and myocardial infarction.[2] THP was recently demonstrated to be a substrate for recombinant BBOX,[3] an observation that is consistent with rat tissue studies on THP metabolism.[4] Our NMR and mass spectrometric studies identified malonic acid semialdehyde, formaldehyde, dimethyl amine and an unanticipated compound, 3-amino-4-(methylamino)butanoic acid **1** (AMBA), as products of the oxidation of THP as catalysed by recombinant human BBOX (Scheme 1).[3] The structures were assigned on the basis of NMR and mass spectrometric analyses using ^{13}C-labelled THP.[3] The proposed formation of AMBA **1** suggests that BBOX catalyses an oxidative rearrangement reaction involving N–N bond cleavage and C–C bond formation, likely via a radical mechanism in a process related to a Stevens type rearrangement (Scheme 2).[5] However, under the incubation conditions, free AMBA **1** was not observed. Instead, the product was provisionally assigned as an AMBA-formaldehyde adduct **2** or derivative there of (Scheme 1), with the formaldehyde being produced by BBOX-catalysed N-demethylation.[3] To test the proposed structure of **2**, we synthesised both enantiomers of AMBA **1** ((*S*)-AMBA **1a** and (*R*)-AMBA **1b**) and studied their reaction with formaldehyde. The results validate the proposed production of AMBA **1** by BBOX-catalysed THP oxidation. They also reveal that formaldehyde reacts with AMBA **1** to form the cyclic adduct **3**, which likely exists in equilibrium with the previously proposed hemiaminal **2**.[3]

Enantiomerically enriched (3*S*)-AMBA **1a** and (3*R*)-AMBA **1b** were obtained in six steps with overall yields of ~50% from commercially available (3*S*) and (3*R*)-aspartic acid 4-*tert*-butyl esters **4a** and **4b** (Scheme 3). Thus, following protection of the amino group of **4** with a *N*-*tert*-butoxycarbonyl group, the carboxylic acid of **5** was reacted with *iso*-butyl chloroformate to give a mixed anhydride, which was reduced in situ with sodium borohyride to give the homoserine derivative **6**.[6] β-Aminoalcohol **6** was oxidised to aldehyde **7**, using the Dess–Martin periodinane. Attempted reductive amination using monomethylamine and sodium triacetoxyborohydride did not yield detectable amounts of the desired product **8**. However, use of neat benzylmethylamine and sodium triacetoxyborohydride gave (*S*)-*tert*-butyl 4-(benzyl(methyl)amino)-3-(*tert*-butoxycarbonylamino)butanoate **9** in good yield. The benzyl group of **9** was removed by hydrogenation to give **8** which was converted to the hydrochloride salt of AMBA **1**.

The synthetic AMBA enantiomers **1a** and **1b** were then separately analysed by NMR in the absence and in the presence of formaldehyde under buffered conditions identical to those used for the

Abbreviations: AMBA, 3-amino-4-(methylamino)butanoic acid; BBOX, γ-butyrobetaine hydroxylase; THP, 3-(2,2,2-trimethylhydrazinium)propionate.

* Corresponding authors. Tel.: +44 (0)1865 275 625; fax: +44 (0)1865 275 674.
E-mail addresses: tim.claridge@chem.ox.ac.uk (T.D.W. Claridge), christopher.schofield@chem.ox.ac.uk (C.J. Schofield).
† These authors contributed equally to this work.

0960-894X/$ - see front matter © 2012 Elsevier Ltd. All rights reserved.
http://dx.doi.org/10.1016/j.bmcl.2012.06.024

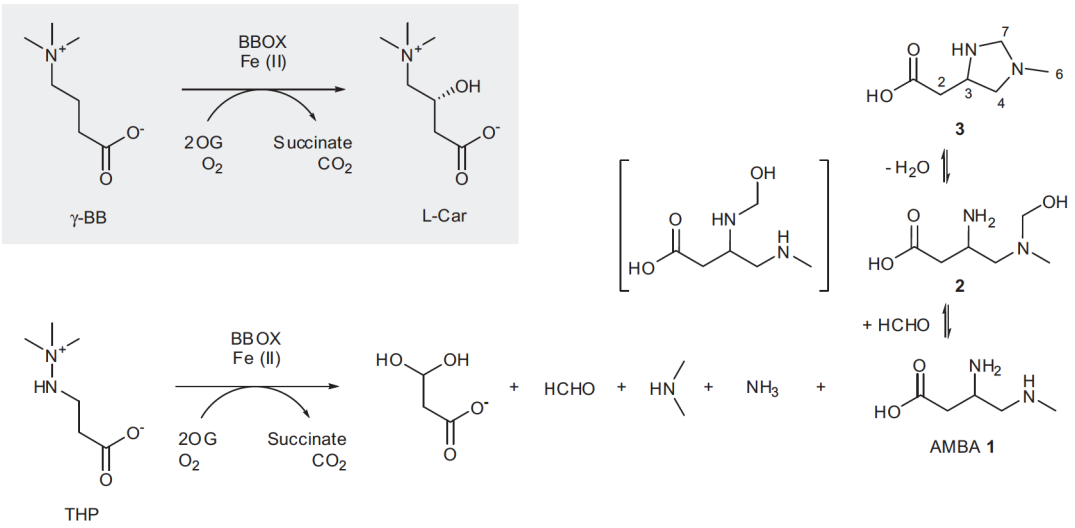

Scheme 1. BBOX catalyses the hydroxylation of γ-butyrobetaine (γ-BB) in the final step of L-carnitine (L-Car) biosynthesis in animals (shaded box). The clinically used compound 3-(2,2,2-trimethylhydrazinium)propionate (THP) is a BBOX substrate. The unexpected product of BBOX catalysis, AMBA **1**, reacts with formaldehyde to give heterocycle **3**, likely via the branched hemiaminal **2**.

BBOX assay (Fig. 1 and Supplementary Figs. S1–S4). The NMR analyses validate the proposal that AMBA **1** is a product of the oxidation of THP by BBOX and forms a cyclic adduct **3** by reaction with formaldehyde (Supplementary Figs. S1 and S2). When comparing free AMBA **1** and the AMBA-formaldehyde adduct **3**, striking variations are observed in the tertiary C-3 chemical shifts ($\delta^{13}C_{AMBA\ 1}$ = 46.1 ppm; $\delta^{13}C_{AMBA\text{-}formaldehyde\ 2}$ = 55.1 ppm) and *N*-methyl C-6 ($\delta^{13}C_{AMBA\ 1}$ = 33.3 ppm; $\delta^{13}C_{AMBA\text{-}formaldehyde\ 2}$ = 39.4 ppm),

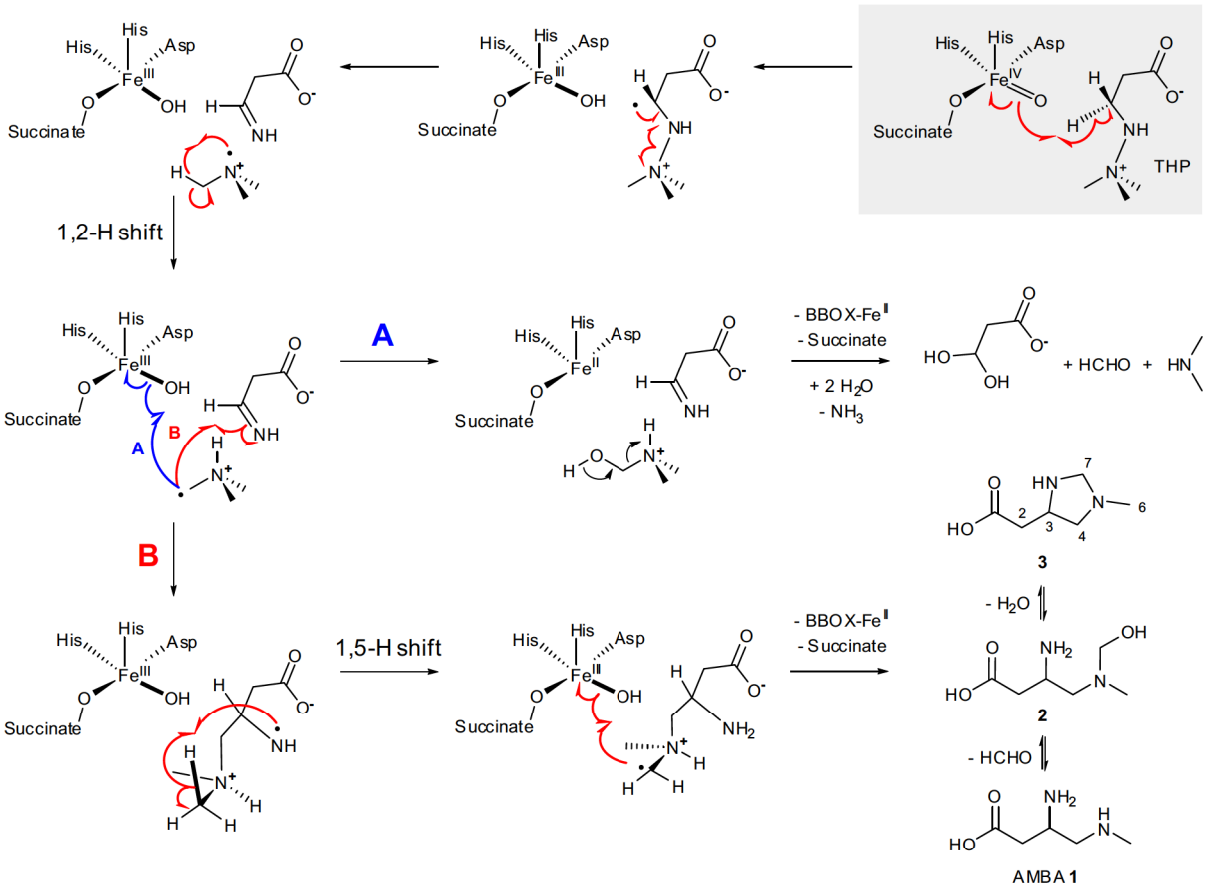

Scheme 2. Proposed mechanism for the BBOX catalysed oxidative rearrangement of THP. The proposed Fe(IV)-oxo intermediate (shaded box) is formed by oxidative decarboxylation of 2OG likely via the consensus mechanism for 2OG and Fe(II)-dependent oxygenases.[11] The operation of two divergent reaction pathways A and B give rise to all the observed THP derived products. In pathway A, the methylene radical rebounds to the iron-hydroxyl intermediate to give the hydroxylation product. In pathway B, the methylene radical adds into the imine to generate the rearranged C–C framework for AMBA. Although not observed, NH_3 is expected to be formed in path A, according to the proposed mechanism.

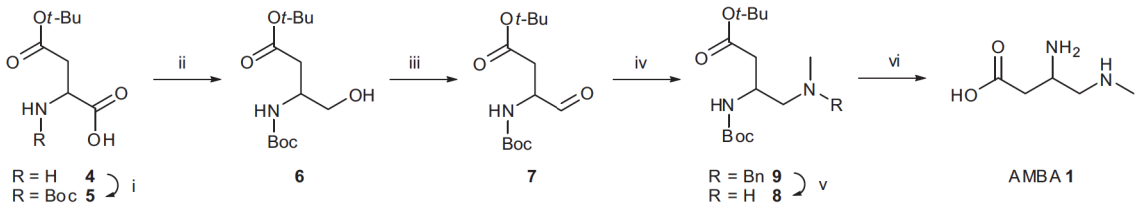

Scheme 3. Synthesis of 3-amino-4-(methyamino)butanoic acid **1** (AMBA). Reagents: (i) $(Boc)_2O$, Na_2CO_3; (ii) *i*-BuOCOCl, $NaBH_4$; (iii) Dess–Martin periodinane; (iv) BnMeNH, $NaBH(OAc)_3$; (v) H_2 (1 bar), Pd/C; (vi) 2 M HCl in Et_2O. Compounds **1a**, **4a**–**9a** correspond to the (3*S*)-series of compounds; **1b**, **4b**–**9a** correspond to the (3*R*)-series of compounds.

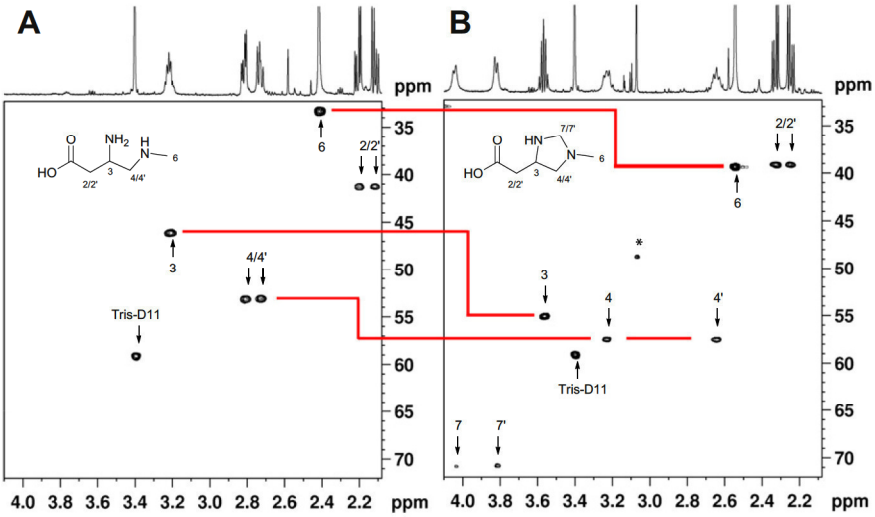

Figure 1. Reaction of 3-amino-4-(methyamino)butanoic acid **1** (AMBA) with formaldehyde. Addition of [^{12}C]-formaldehyde to AMBA induces substantial chemical shift differences, indicating substitution on both AMBA nitrogen atoms. (A) 2D ^{1}H–^{13}C HSQC NMR for AMBA in the absence of formaldehyde; (B) 2D ^{1}H–^{13}C HSQC NMR for AMBA in the presence of stoichiometric [^{12}C]-formaldehyde. Except for C-2, all aliphatic carbons show a large positive $\Delta\delta$. The same results were obtained for both (*S*)- and (*R*)-AMBA. An impurity from the formaldehyde solution is indicated by an asterisk (*).

which differ by ~9 ppm and ~6 ppm, respectively (Fig. 1). These observations suggest that both nitrogen atoms of the AMBA-formaldehyde adduct **3** are substituted. However, when [^{12}C]-formaldehyde is added to AMBA **1**, no HMBC correlations were observed from H-3 or H4/4' to the aminal/hemiaminal C-7 (Supplementary Fig. S3), likely due in part to the fast transverse relaxation of the broad resonances (see below). In an attempt to observe the HMBC correlations predicted for a cyclic structure, AMBA **1** was titrated with a stoichiometric amount of [^{13}C]-labelled formaldehyde. Subsequently ^{1}H–^{13}C HSQC analysis revealed that the only [^{13}C]-enriched position in the resultant adduct is the aminal/hemiaminal C-7 carbon (Supplementary Fig. S4). Notably, HMBC correlations are observed between H-3 and H4/4' and the aminal/hemiaminal ^{13}C-7 of the formaldehyde adduct **3**, implying ring formation (Supplementary Fig. S4). It has previously been observed that the reactions between formaldehyde and amines are highly pH dependent,[7,8] and the broad ^{1}H resonances of the aminal/hemiaminal CH_2 suggest that this is a dynamic system, which may reflect the pK_a of a protonated amino group of AMBA (pK_a ~7.2; Supplementary Fig. S5). Indeed, the ^{1}H resonances of the N–CH_2–N group in **3** sharpen significantly when treated with deuterated hydrochloric acid (Supplementary Fig. S6). Thus, at pH 7.5 the AMBA-formaldehyde adduct probably exists as an equilibrium between the favoured cyclic aminal **3** and acyclic hemiaminal forms such as **2** (Scheme 2).

In conclusion, enantiomerically enriched (*S*)-AMBA **1a** and (*R*)-AMBA **1b** were synthesised from commercially available enantiomers of aspartic acid 4-*tert*-butyl ester **4**. By reacting both enantiomers of the synthetic AMBA **1** with stoichiometric amounts of [^{12}C]- or [^{13}C]-formaldehyde and using NMR for analyses, our results demonstrate that AMBA **1** is indeed a rearrangement product of BBOX catalysed THP-oxidation, and that the observed adduct is predominately present in its five-membered cyclic aminal form **3** at pH 7.5. Formaldehyde is proposed to be formed via *N*-methyl hydroxylation followed by fragmentation (Scheme 2, paths A and B). It is likely that the AMBA-formaldehyde adduct **3** is present in equilibrium between the branched hemiaminal(s) and the cyclic aminal forms. The observation of compound **3** is notable given the concentrations of formaldehyde are relatively low; only small amounts of the hemiaminal adduct formed by reaction of formaldehyde with tris(hydroxymethyl)aminomethane (Tris buffer), which is present in large excess as a buffer, were observed. Formaldehyde is also produced by other 2OG and Fe(II)-dependent oxygenases, that is, histone lysine demethylases and DNA demethylases.[9] Demethylation of histone lysines is catalysed by the ubiquitous JmjC subfamily. Given that histone proteins contain a high content of nucleophilic/basic residues including lysines, the results presented herein raise the possibility of the formation of formaldehyde-mediated cross-linking of histone lysine (and other) side-chains. Heterocycles have also been shown to be formed by reacting formaldehyde with the tripeptide reducing agent glutathione.[8] Although the precise mechanisms of formaldehyde toxicity remain unclear, it is proposed to involve the formation of DNA adducts, possibly by cross-linking.[10] Thus, together with other work,

our results suggest that under physiological conditions, biomolecules may react rather often with formaldehyde to produce N–CH_2–N (or X–CH_2–X) linkages.

Acknowledgments

We thank Dr. Grazyna T. Kochan and Professor Udo Oppermann for recombinant human BBOX and Dr. Filippo Sladojevich for chiral HPLC analyses. We thank the Berrow Foundation, the Biotechnology and Biological Sciences Research Council (BBSRC) and the Engineering and Physical Sciences Research Council (EPSRC) for funding.

Supplementary data

Supplementary data (figures, experimental details of synthesis and NMR experiments.) associated with this article can be found, in the online version, at http://dx.doi.org/10.1016/j.bmcl.2012.06.024.

References and notes

1. Vaz, F. M.; Wanders, R. J. A. *Biochem. J.* **2002**, *361*, 417; Strijbis, K.; Vaz, F. M.; Distel, B. *IUBMB Life* **2010**, *62*, 357; Vaz, F. M.; van Gool, S.; Ofman, R.; IJlst, L.; Wanders, R. J. *Biochem. Biophys. Res. Commun.* **1998**, *250*, 506.
2. Simkhovich, B. Z.; Shutenko, Z. V.; Meirena, D. V.; Khagi, K. B.; Mezapuķe, R. J.; Molodchina, T. N.; Kalviņs, I. J.; Lukevics, E. *Biochem. Pharmacol.* **1988**, *37*, 195; Sesti, C.; Simkhovich, B. Z.; Kalvinsh, I.; Kloner, R. A. *J. Cardiovasc. Pharmacol.* **2006**, *47*, 493; Liepinsh, E.; Vilskersts, R.; Loca, D.; Kirjanova, O.; Pugovichs, O.; Kalvinsh, I.; Dambrova, M. *J. Cardiovasc. Pharmacol.* **2006**, *48*, 314; Hayashi, Y.; Kirimoto, T.; Asaka, N.; Nakano, M.; Tajima, K.; Miyake, H.; Matsuura, N. *Eur. J. Pharmacol.* **2000**, *395*, 217.
3. Leung, I. K. H.; Krojer, T. J.; Kochan, G. T.; Henry, L.; von Delft, F.; Claridge, T. D. W.; Oppermann, U.; McDonough, M. A.; Schofield, C. J. *Chem. Biol.* **2010**, *17*, 1316.
4. Spaniol, M.; Brooks, H.; Auer, L.; Zimmermann, A.; Solioz, M.; Stieger, B.; Krähenbühl, S. *Eur. J. Biochem.* **2001**, *268*, 1876; Yoshisue, K.; Yamamoto, Y.; Yoshida, K.-I.; Saeki, M.; Minami, Y.; Esumi, Y.; Kawaguchi, Y. *Drug Metab. Dispos.* **2000**, *28*, 687.
5. Stevens, T. S.; Creighton, E. M.; Gordon, A. B.; MacNicol, M. *J. Chem. Soc.* **1928**, 3193; Vanecko, J. A.; Hayley, W.; West, F. G. *Tetrahedron* **2006**, *62*, 1043.
6. Bowers, A. A.; Greshock, T. J.; West, N.; Estiu, G.; Schreiber, S. L.; Wiest, O.; Williams, R. M.; Bradner, J. E. *J. Am. Chem. Soc.* **2009**, *131*, 2900.
7. Kallen, R. G.; Jencks, W. P. *J. Biol. Chem.* **1966**, *241*, 5864.
8. Hopkinson, R. J.; Barlow, P. S.; Schofield, C. J.; Claridge, T. D. W. *Org. Biomol. Chem.* **2010**, *8*, 4915; Naylor, S.; Mason, R. P.; Sanders, J. K. M.; Williams, D. H.; Moneti, G. *Biochem. J.* **1988**, *249*, 573; Bateman, R.; Rauh, D.; Shokat, K. M. *Org. Biomol. Chem.* **2007**, *5*, 3363.
9. Hopkinson, R. J.; Hamed, R. B.; Rose, N. R.; Claridge, T. D. W.; Schofield, C. J. *ChemBioChem* **2010**, *11*, 506; Hamm, S.; Just, G.; Lacoste, N.; Moitessier, N.; Szyf, M.; Mamer, O. *Bioorg. Med. Chem. Lett.* **2008**, *18*, 1046.
10. Conaway, C. C.; Whysner, J.; Verna, L. K.; Williams, G. M. *Pharmacol. Ther.* **1996**, *71*, 29.
11. Hausinger, R. P. *Crit. Rev. Biochem. Mol. Biol.* **2004**, *39*, 21.

DOI: 10.1002/cbic.201200256

Development and Application of a Fluoride-Detection-Based Fluorescence Assay for γ-Butyrobetaine Hydroxylase

Anna M. Rydzik,[a] Ivanhoe K. H. Leung,[a] Grazyna T. Kochan,[b] Armin Thalhammer,[a] Udo Oppermann,[b] Timothy D. W. Claridge,[a] and Christopher J. Schofield*[a]

2-Oxoglutarate (2OG)-dependent oxygenases are a large enzyme superfamily, the members of which play a range of important biological roles in animals, plants and bacteria. In humans, their functions include oxygen sensing, collagen biosynthesis, fatty acid metabolism, and DNA/RNA repair and modification. Several human 2OG-dependent hydroxylases and histone demethylases are inhibition targets for therapeutic intervention in diseases including myocardial infarction, anaemia, inflammation and cancer.[1–6]

We and others are interested in the functional assignment of 2OG-dependent oxygenases and are attempting to identify selective small-molecule inhibitors. However, this work is limited by a lack of effective and cost-efficient assays. Reported assays for 2OG-dependent oxygenases can be broadly divided into those measuring cosubstrate (2OG, O_2)/coproduct (succinate, CO_2) consumption/production and those measuring substrate/product consumption/formation. The first type of assay commonly employs radiolabelled 2OG.[7–10] Other assays employ the detection of oxidised products by mass spectrometry,[11–13] NMR spectroscopy,[11,14] or fluorescence-/luminescence-based methods.[15,16] However, these techniques are often not suitable for high-throughput studies (e.g., NMR-based assays) or require difficult to access reagents (e.g., antibodies) or expensive equipment (e.g., LC-MS, NMR).

γ-Butyrobetaine hydroxylase (BBOX) catalyses the final step in the biosynthesis of carnitine, which is essential in fatty acid metabolism (Figure S1). BBOX is important for the development of clinically useful 2OG oxygenase inhibitors because its inhibition is likely to have physiological effects. Indeed 3-(2,2,2-trimethylhydrazinium)propionate (THP), which is used clinically to treat angina and myocardial infarction,[17–19] is proposed to target BBOX in cells.[20,21] Hence, work on BBOX inhibition and selectivity screens of inhibitors targeted towards other 2OG oxygenases would both benefit from an efficient BBOX assay. Various techniques, including NMR spectroscopy and assays employing isotope-labelled 2OG or substrate, have been applied to study the kinetics and inhibition of BBOX;[22–28] however, these techniques are low throughput and not efficient for inhibitor screening.

The detection of fluoride ions is of interest because of their pharmacological and environmental importance. Chemosensors have attracted attention because they can enable the fluorescence-based detection of fluoride ions.[29] Here, we report the synthesis and evaluation of fluorinated substrate analogues for recombinant human BBOX.[30–34] Based on the results, we developed a fluorescence-based fluoride-release assay that is suitable for high-throughput studies on BBOX and other 2OG-dependent oxygenases.

Previous studies on the hypoxia-inducible factor prolyl hydroxylase domain containing enzyme 2 (PHD2) and a collagen prolyl 4-hydroxylase (P4H) have reported that these oxygenases can accept substrate analogues that are fluorinated on the same carbon as that undergoing hydroxylation.[35,36] For both P4H and PHD2, it was shown that peptides containing (4*S*)-4-fluoroproline are hydroxylated to yield peptidyl-4-oxoproline with the release of a fluoride ion (Figure S2 A).[36] We postulated that analogous fluoride-release reactions could not only occur with peptide substrates, but could also be general for other 2OG hydroxylases, including those employing small-molecule substrates. BBOX catalyses the hydroxylation of γ-butyrobetaine **1 d** (GBB or 4-(trimethylammonio)butanoic acid) to give (*R*)-carnitine **1 e** ((3*R*)-3-hydroxy-4-(trimethylammonio)butanoate; Scheme 1 and Figure S1).[30–34,37,38] Therefore (3*S*)-3-

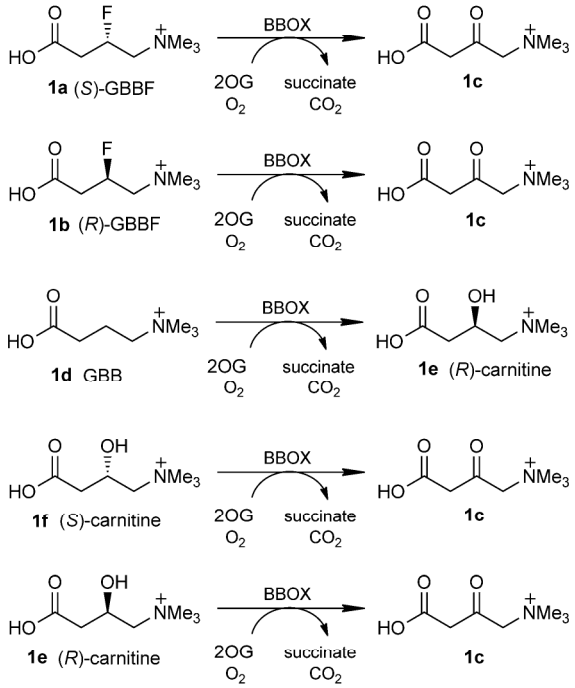

Scheme 1. Reactions catalysed by BBOX.

[a] A. M. Rydzik, I. K. H. Leung, A. Thalhammer, Dr. T. D. W. Claridge, Prof. C. J. Schofield
Department of Chemistry, University of Oxford
12 Mansfield Road, Oxford, OX1 3TA (UK)
E-mail: christopher.schofield@chem.ox.ac.uk

[b] Dr. G. T. Kochan, Prof. U. Oppermann
Structural Genomics Consortium, University of Oxford
Old Road Campus, Roosvelt Drive, Headington, OX3 7DQ (UK)

Supporting information for this article is available on the WWW under http://dx.doi.org/10.1002/cbic.201200256.

© 2012 Wiley-VCH Verlag GmbH & Co. KGaA, Weinheim

fluoro-4-(trimethylammonio)butanoate **1a** ((*S*)-GBBF) was prepared and analysed as a BBOX substrate. To evaluate the reaction stereospecificity, the enantiomer of **1a** ((*R*)-GBBF **1b**) was also prepared. The results demonstrate that the *S* stereoisomer **1a** is the preferred substrate and can be used efficiently in assays for BBOX activity.

The synthesis of β-fluorinated acid derivatives by direct fluorodehydroxylation can be challenging because fluoride is a strong base that induces elimination to give α,β-unsaturated compounds.[39] We investigated several routes based on 3-hydroxy-4-aminobutyric acid derivatives, but these were unsuccessful (Scheme S1). We thus employed a route in which fluorine was introduced prior to the carboxylic acid (Scheme 2).

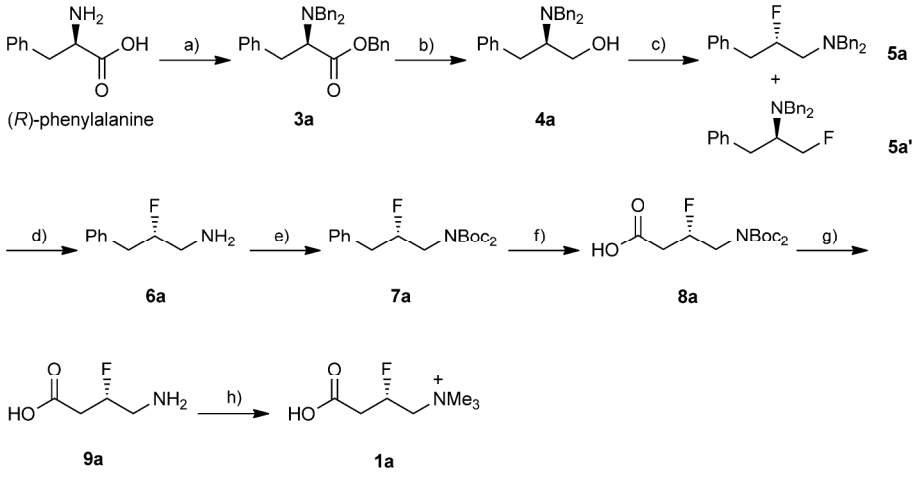

Scheme 2. Synthesis of (3*S*)-3-fluoro-4-(trimethylammonio)butanoate (**1a**, (*S*)-GBBF). Reagents and conditions: a) BnBr, K_2CO_3, EtOH, H_2O, 62%; b) $LiAlH_4$, THF, 76%; c) Deoxo-Fluor, CH_2Cl_2, **5a**: 46%, **5a**′: 10%; d) H_2, Pd(C), MeOH, 84%; e) Boc_2O, DMAP, MeCN, 88%; f) $RuCl_3$, $NaIO_4$, CCl_4/MeCN/H_2O, 52%; g) CH_2Cl_2, HCl, 54%; h) CH_3I, K_2CO_3, MeOH, apparently quantitative (by NMR).

(3*S*)-3-Fluoro-4-aminobutanoic acid (**9a**) and (3*R*)-3-fluoro-4-aminobutanoic acid (**9b**) were synthesised according to Deniau et al.,[40] starting from (*R*)- and (*S*)-phenylalanine, respectively. In this synthetic route, ring opening of the aziridinium intermediate by a fluoride ion to give regioisomers **5a** and **5a**′ was utilised. The desired potential substrates (*S*)-GBBF (**1a**) and (*R*)-GBBF (**1b**) were obtained by N-methylation of **9a** and **9b** with an excess of iodomethane in the presence of potassium carbonate.

We evaluated both (*S*)-GBBF (**1a**) and (*R*)-GBBF (**1b**) as human BBOX substrates, and (*S*)-GBBF was found to be a good substrate. ^{1}H NMR studies revealed the formation of 3-oxo-4-(trimethylammonio)butanoate (**1c**) with subsequent decarboxylation leading to *N*,*N*,*N*-trimethylammonio acetone (Figures 1 and S3). ^{19}F NMR analyses revealed that the only detectable fluorine-containing species formed in the reaction of (*S*)-GBBF with BBOX are fluoride ions (Figure 1B). This observation is consistent with previous studies in which BBOX was shown to catalyse the hydroxylation of (*S*)-carnitine (**1f**), an analogue of (*S*)-GBBF, to give 3-oxo-4-(trimethylammonio)butanoate (**1c**) and water (Scheme 1 and Figure S2B).[41] However, the reaction with (*S*)-GBBF (Figure S2C) was approximately twice as rapid as the reaction with (*S*)-carnitine (Figure S4). (*R*)-GBBF was found to be a poorer substrate (< 5% turnover after 3 h under standard assay conditions as monitored by ^{1}H and ^{19}F NMR spectroscopy—higher levels of (*R*)-GBBF turnover (~20%) are obtained with a higher concentration of BBOX and prolonged incubation; Figure S5). ^{1}H and ^{19}F NMR analyses determined that the products of the reaction of (*R*)-GBBF were the same as for the reaction of its enantiomer. Although we cannot entirely rule out the possibility of BBOX-catalysed racemisation, the observation that (*S*)-GBBF (**1a**) is a BBOX substrate is consistent with crystallographic studies revealing that the pro-*R* C–H bond of GBB is directed towards the iron centre, which is responsible for hydroxylation to give (*R*)-carnitine.[41] Assuming that this reaction proceeds through C–H bond oxidation, the observation that (*R*)-GBBF is a poor substrate implies that this substrate can adopt a catalytically productive arrangement other than that observed in the reported BBOX–GBB complex crystal structure.[41]

Notably, although the reaction products of (*S*)-GBBF and (*R*)-GBBF as BBOX substrates are the same as those of (*S*)- and (*R*)-carnitine (Figure S2C), the rate of (*S*)-GBBF hydroxylation by BBOX is significantly higher than that of (*S*)-carnitine. This observation suggested that fluoride release from (*S*)-GBBF might enable the development of efficient assays for BBOX activity.

A fluoride-ion-selective electrode-based method has been reported for use in P4H assays,[36] but this method is not, at least readily, suitable for inhibitor screening in plate format. We therefore investigated the use of *tert*-butyldimethylsilyl-protected fluorescein (**2**) for fluoride ion detection. When **2** is subjected to increasing fluoride ion concentration, a proportional increase in fluorescence is observed following the removal of the silyl protective groups (Figure S6);[29] this method has been used to determine fluoride concentrations in toothpaste.[42] We adapted this method to a multiwell system suitable for high-throughput screening. The method was optimised such that it can employ organic solvent–buffer mixtures and low volumes and amounts of reagents (Figures S7 and S13).

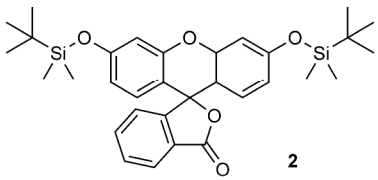

2

 © 2012 Wiley-VCH Verlag GmbH & Co. KGaA, Weinheim

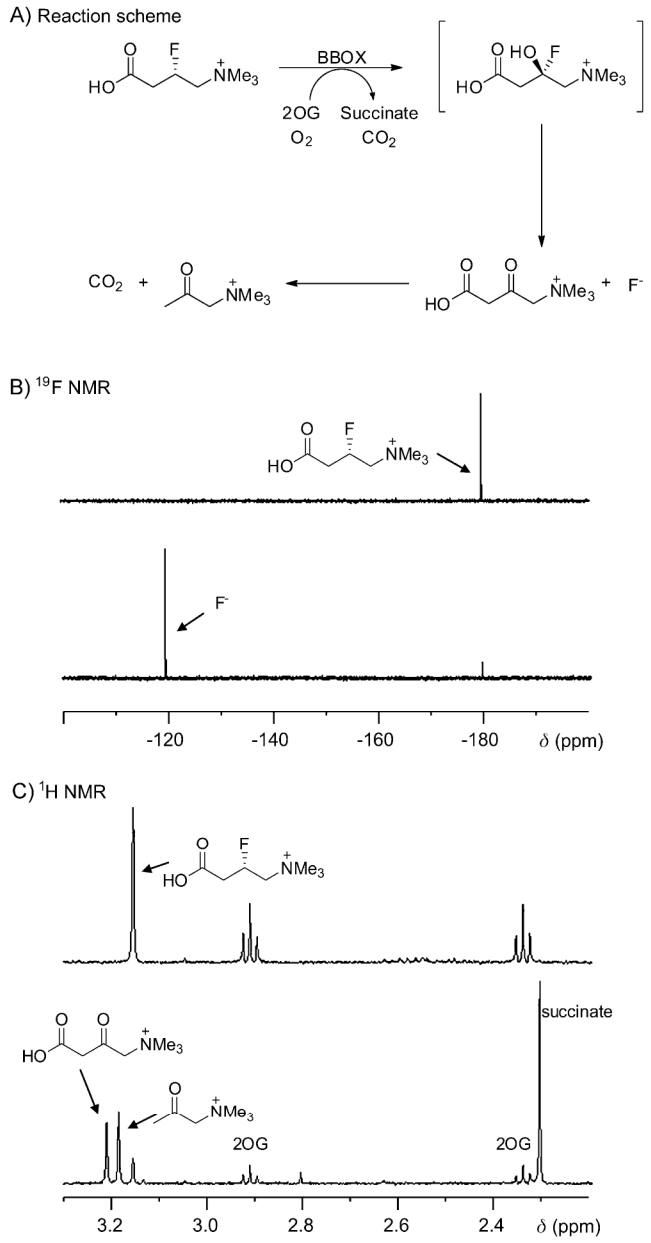

Figure 1. BBOX catalyses fluoride release from (*S*)-GBBF. A) The reaction of (*S*)-GBBF with BBOX; B) ^{19}F NMR spectra of the reaction showing the release of F^-; C) ^{1}H NMR spectra of the corresponding reaction showing the formation of 3-oxo-4-(trimethylammonio)butanoate and *N*,*N*,*N*-trimethylammonio acetone. The assay mixture included BBOX (100 nM), Fe^{II} (50 μM), 2OG (500 μM), (*S*)-GBBF (200 μM), ascorbate (500 μM), KCl (80 mM) and Tris·D11 (50 mM, pH 7.5) in 90% H_2O and 10% D_2O.

Standard kinetic time-course and Michaelis–Menten kinetics can be readily obtained from the fluorescence intensity by using this method (Figure 2). The K_M and V_{max} values obtained for 2OG and (*S*)-GBBF (**1a**) by fluorescence are comparable to those obtained by NMR spectroscopy under similar conditions (Table 1, Figure 2B and C, and Figure S8). Although the V_{max} of (*S*)-GBBF is reduced compared to that of GBB, the K_M value of (*S*)-GBBF is similar to that of GBB (Table 1 and Figure S8); this suggests that the fluoride substituent does not substantially affect the binding of (*S*)-GBBF in the substrate binding pocket of BBOX. Previous kinetic studies have reported that the activity of human BBOX is stimulated by potassium ions and reducing agents.[43] Our results reveal that human BBOX has the same requirements when (*S*)-GBBF is used: potassium ions and reducing agents such as ascorbate increase activity (Figure S9). Thus, high-throughput and quantitative determination of enzyme kinetics for BBOX appear feasible with fluorinated substrate analogues.

We investigated the applicability of this assay for inhibitor screening by determining the IC_{50} values of potential BBOX inhibitors. By monitoring the change in fluorescence intensity at different inhibitor concentrations, sigmoidal curves for inhibition were observed (Figure 2D). We initially evaluated BBOX inhibition by using 3-(2,2,2-trimethylhydrazine)propionate (THP)[20] and *N*-oxalylglycine (NOG), a 2OG analogue. We obtained IC_{50} values of 65 and 389 μM for THP and NOG, respectively; these are consistent with the values obtained previously by NMR spectroscopy using recombinant human BBOX (Table 2 and Figure S11C and D).[41] Aromatic inhibitors such as pyridine 2,4-dicarboxylate (2,4-PDCA) and the bicyclic isoquinolinyl inhibitor (BIQ),[1,44] which were being investigated as inhibitors of human prolyl hydroxylases, were then tested. Using our assay, we found that they are also inhibitors of BBOX, with IC_{50} values of 82 and 18 μM, respectively (Table 2 and Figure S11A and B).

We then investigated if the fluorescence-based fluoride detection assay is applicable to other 2OG-dependent oxygenases. It is reported that PHD2 accepts a fluorinated peptide analogue as a substrate to yield the 4-oxoprolyl product (Figure S2).[13] We thus carried out a reaction of PHD2 with an appropriate peptide substrate bearing a *cis*-4-fluoroprolyl residue at the canonical hydroxylation site. Fluoride ions were released with PHD2 catalysis, and the amount of fluoride released could be quantified by using the chemical probe (Figure S12). This result demonstrates the utility of the fluorescence-based fluoride detection assay for 2OG-dependent oxygenases with oligomeric substrates.

In conclusion we have developed a fluorescence assay based on the detection of fluoride released from reactions of fluorinated substrates with BBOX by the use of *tert*-butyldimethylsilyl-protected fluorescein. (*S*)-GBBF (**1a**) is a sufficiently good substrate for BBOX, releasing fluoride when subjected to the enzyme. Thus it can be used for kinetic and inhibition studies. The assay was adapted to an efficient multiwall-plate format by using fluoride detection by a chemical probe method of desilylation and resulting in an increase in fluorescence. (*S*)-GBBF (**1a**) can be synthesised from the readily available (*R*)-phenylalanine in eight steps, and the sensitivity of the method is such that many assays can be performed with a small amount of material.

We used the assay as a proof of principle with THP and broad-spectrum 2OG oxygenase inhibitors (NOG and 2,4-PDCA) and the PHD2 inhibitor BIQ. Interestingly, we found that BIQ is a better BBOX inhibitor than THP. Indeed, as found both by our assay methodology and in previous work, THP is not a particularly potent BBOX inhibitor with IC_{50} values of 65 μM (fluoride release assay), 34 μM (NMR-based assay), or 62 μM.[34]

 © 2012 Wiley-VCH Verlag GmbH & Co. KGaA, Weinheim

It should be noted that THP is a competitive substrate for BBOX undergoing catalytic oxidation to give multiple products, proceeding via a Stevens-type rearrangement.[41,45] It is thus possible that the physiological effects of THP are mediated by targets other than BBOX, for example, carnitine transporters.[46] If so, the metabolism of THP by BBOX catalysis might, in fact, reduce its biological activity. Thus, the observation that (*R*)-GBBF (**1b**) is a poor substrate for BBOX, suggests that suitably fluorinated THP analogues might present improved therapeutic opportunities.

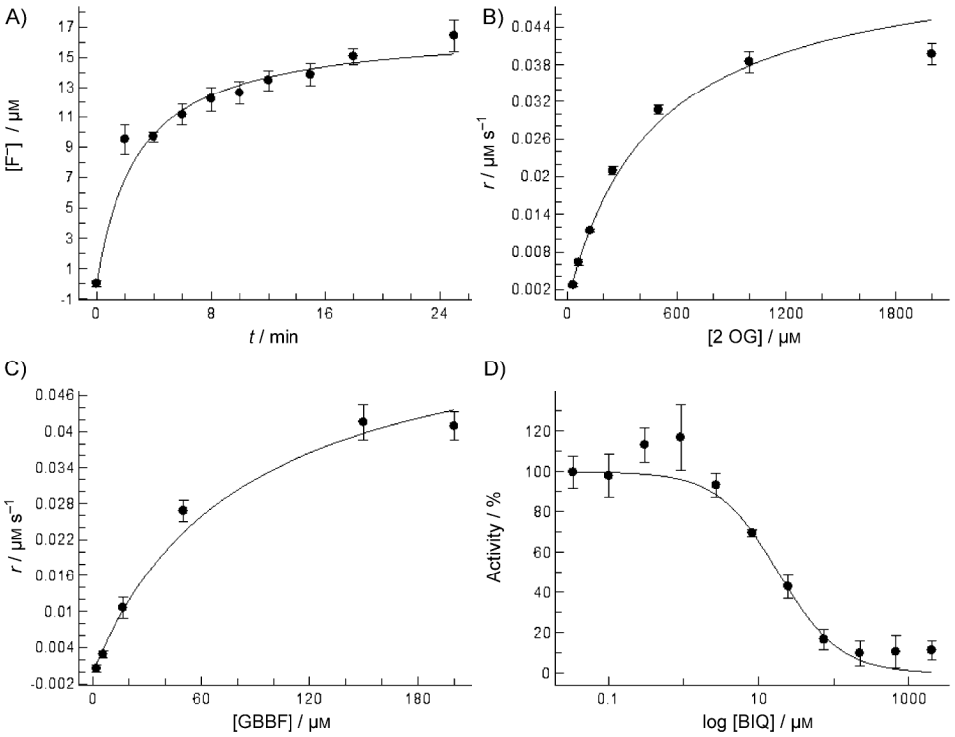

Figure 2. Kinetic analyses of BBOX. A) Enzyme kinetics can be measured by using the fluoride-release assay. B) The turnover of (*S*)-GBBF is dependent on the 2OG concentration. C) (*S*)-GBBF is a substrate for BBOX, but is an inhibitor at high concentrations. D) IC_{50} measurements can be made by using this assay; the curve obtained for BIQ inhibition is shown. For details on fitting and experimental conditions see Figures S10 and S11.

Experimental Section

NMR spectroscopy assay: ^{1}H and ^{19}F spectroscopy experiments were conducted at 500 and 470 MHz, respectively, by using a Bruker Avance II spectrometer equipped with a standard 5 mm *z*-gradient $^{1}H/^{19}F(^{13}C)$ TXI probe. All experiments were conducted at 298 K, and conventional 5 mm diameter NMR tubes (Norell) were used.

Fluoride-release assays: Enzymatic reactions were performed with the following final concentrations: 40 μM (*S*)-GBBF, 40 μM ammonium iron(II) sulfate hexahydrate, 250 μM ascorbic acid disodium salt, 160 mM potassium chloride, 500 μM 2-oxoglutarate disodium salt, 100 nM BBOX and 50 mM Tris·HCl buffer (pH 7.5). Fe^{II} solution was kept as a 100 mM stock solution in HCl (20 mM) and was diluted freshly with Tris·HCl buffer before use. Reagents and BBOX were mixed at room temperature in a 96-well plate, and the reaction was initiated by the addition of 2OG. The reaction was quenched by addition of 20% acetonitrile. The quenched reaction mixture (20 μL) was then transferred to a separate solid black 96-well round-bottom plate, and was incubated with bis(*tert*-butyldimethylsilyloxy)fluorescein (80 μL, 5 μM) for 1 h at room temperature. HEPES at (50 μL, 50 mM, pH 7.0) was then added, and the mixture was incubated for a further 2 min prior to fluorescence being measured by using an EnVision Multilabel plate reader (PerkinElmer) fitted with FITC FP 480/30 (480 nm, bandwidth 30 nm) and FITC FP 535/40 emission (535 nm, bandwidth 40 nm) filters. For each enzymatic reaction, a corresponding control containing all reagents but no enzyme was also recorded. The normalised fluorescence signal was defined as the observed fluorescence signal minus the control signal.

Table 2. IC_{50} measurements (see also Figure S11).

Name	Structure	IC_{50} fluoride assay [μM]	IC_{50} NMR assay [μM]
BIQ	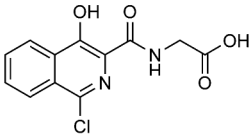	18	22
NOG	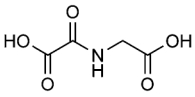	390	124
2,4-PDCA	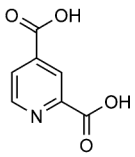	82	n.d.
THP	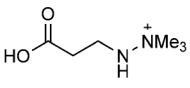	65	34

n.d. = not determined.

Table 1. Comparison of kinetic values for BBOX obtained with different assays (see also Figure S10).

	(*S*)-GBBF and 2OG fluoride assay			(*S*)-GBBF and 2OG NMR assay			GBB and 2OG NMR assay		
	K_M [μM]	V_{max} [μM s^{-1}]	k_{cat} [s^{-1}]	K_M [μM]	V_{max} [μM s^{-1}]	k_{cat} [s^{-1}]	K_M [μM]	V_{max} [μM s^{-1}]	k_{cat} [s^{-1}]
2OG	470	0.055	0.55	150	0.039	0.39	160	0.13	5.1
substrate	83	0.062	0.62	12	0.010	0.10	26	0.13	5.3

 © 2012 Wiley-VCH Verlag GmbH & Co. KGaA, Weinheim

BBOX expression and purification: BBOX was expressed and purified according to the protocol described by Leung et al.[41]

Kinetic assays: Standard kinetic assays were conducted at 298 K in solutions containing (*S*)-GBBF 40 μM), ammonium iron(II) sulfate hexahydrate (40 μM), ascorbic acid disodium salt (250 μM), potassium chloride (160 mM), 2-oxoglutarate disodium salt (500 μM), BBOX (100 nM) and Tris·HCl buffer (50 mM, pH 7.5). Reactions were initiated by the addition of 2OG. All measurements were repeated four times.

Inhibition assays: Inhibition assays were conducted at 298 K in solutions containing (*S*)-GBBF (40 μM), ammonium iron(II) sulfate hexahydrate (40 μM), ascorbic acid disodium salt (250 μM), potassium chloride (160 mM), 2-oxoglutarate disodium salt (500 μM), BBOX (100 nM) and Tris·HCl buffer (50 mM, pH 7.5) and varying concentrations of inhibitor. Reactions were initiated by 2OG addition, and quenched by the addition of 20% acetonitrile after 10 min. Response curves were fitted by using OriginPro 8.0 (OriginLab, Northampton, MA, USA) and XLfit (ID Business Solution, Guildford, UK). Each measurement was repeated four times.

Acknowledgements

The authors gratefully acknowledge support of this project by the Engineering and Physical Sciences Research Council and the Biotechnology and Biological Sciences Research Council. We thank Naomi Rippengale for the synthesis and purification of the fluorinated peptide substrate for PHD2.

Keywords: carnitine · fatty acids · fluorescence · inhibition · metabolism · oxygenases

[1] N. R. Rose, M. A. McDonough, O. N. F. King, A. Kawamura, C. J. Schofield, *Chem. Soc. Rev.* **2011**, *40*, 4364–4397.
[2] E. Flashman, C. J. Schofield, *Nat. Chem. Biol.* **2007**, *3*, 86–87.
[3] I. J. Clifton, M. A. McDonough, D. Ehrismann, N. J. Kershaw, N. Granatino, C. J. Schofield, *J. Inorg. Biochem.* **2006**, *100*, 644–669.
[4] R. P. Hausinger, *Crit. Rev. Biochem. Mol. Biol.* **2004**, *39*, 21–68.
[5] M. A. McDonough, C. Loenarz, R. Chowdhury, I. J. Clifton, C. J. Schofield, *Curr. Opin. Struct. Biol.* **2010**, *20*, 659–672.
[6] C. Loenarz, C. J. Schofield, *Nat. Chem. Biol.* **2008**, *4*, 152–156.
[7] K. S. Hewitson, L. A. McNeill, M. V. Riordan, Y. M. Tian, A. N. Bullock, R. W. Welford, J. M. Elkins, N. J. Oldham, S. Bhattacharya, J. M. Gleadle, P. J. Ratcliffe, C. W. Pugh, C. J. Schofield, *J. Biol. Chem.* **2002**, *277*, 26351–26355.
[8] J. H. Zhang, R. C. C. Qi, T. M. Chen, T. D. Y. Chung, A. M. Stern, G. F. Hollis, R. A. Copeland, K. R. Oldenburg, *Anal. Biochem.* **1999**, *271*, 137–142.
[9] G. Kaule, V. Gunzler, *Anal. Biochem.* **1990**, *184*, 291–297.
[10] R. Wirthner, K. Balamurugan, D. P. Stiehl, S. Barth, P. Spielmann, F. Oehme, I. Flarnme, D. M. Katschinski, R. H. Wenger, G. Camenisch in *Methods in Enzymology, Vol. 435: Oxygen Biology and Hypoxia* (Eds.: H. Sies, B. Brüne), Elsevier, San Diego, **2007**, pp. 43–60.
[11] E. Flashman, L. M. Hoffart, R. B. Hamed, J. M. Bollinger, C. Krebs, C. J. Schofield, *FEBS J.* **2010**, *277*, 4089–4099.
[12] N. R. Rose, S. S. Ng, J. Mecinovic, B. M. R. Lienard, S. H. Bello, Z. Sun, M. A. McDonough, U. Oppermann, C. J. Schofield, *J. Med. Chem.* **2008**, *51*, 7053–7056.
[13] C. J. Stubbs, C. Loenarz, J. Mecinović, K. K. Yeoh, N. Hindley, B. M. Liénard, F. Sobott, C. J. Schofield, E. Flashman, *J. Med. Chem.* **2009**, *52*, 2799–2805.
[14] I. K. H. Leung, E. Flashman, K. K. Yeoh, C. J. Schofield, T. D. W. Claridge, *J. Med. Chem.* **2010**, *53*, 867–875.
[15] J. H. Dao, R. J. M. Kurzeja, J. M. Morachis, H. Veith, J. Lewis, V. Yu, C. M. Tegley, P. Tagari, *Anal. Biochem.* **2009**, *384*, 213–223.
[16] A. Kawamura, A. Tumber, N. R. Rose, O. N. F. King, M. Daniel, U. Oppermann, T. D. Heightman, C. Schofield, *Anal. Biochem.* **2010**, *404*, 86–93.
[17] C. Sesti, B. Z. Simkhovich, I. Kalvinsh, R. A. Kloner, *J. Cardiovasc. Pharmacol.* **2006**, *47*, 493–499.
[18] E. Liepinsh, R. Vilskersts, D. Loca, O. Kirjanova, O. Pugovichs, I. Kalvinsh, M. Dambrova, *J. Cardiovasc. Pharmacol.* **2006**, *48*, 314–319.
[19] Y. Hayashi, K. Tajima, T. Kirimoto, H. M. N. Matsuura, *Pharmacology* **2000**, *61*, 238–243.
[20] B. Z. Simkhovich, Z. V. Shutenko, D. V. Meirena, K. B. Khagi, R. J. Mezapuke, T. N. Molodchina, I. J. Kalvins, E. Lukevics, *Biochem. Pharmacol.* **1988**, *37*, 195–202.
[21] M. Dambrova, E. Liepinsh, I. Kalvinsh, *Trends Cardiovasc. Med.* **2002**, *12*, 275–279.
[22] G. Lindstedt, S. Lindstedt, S. Tofft, *Biochemistry* **1970**, *9*, 4336–4342.
[23] G. Lindstedt, S. Lindstedt, I. Nordin, *Biochemistry* **1977**, *16*, 2181–2188.
[24] G. Cederblad, S. Lindstedt, *Clin. Chim. Acta* **1972**, *37*, 235–243.
[25] T. Böhmer, A. Rydning, H. E. Solberg, *Clin. Chim. Acta* **1974**, *57*, 55–61.
[26] J. D. McGarry, D. W. Foster, *J. Lipid Res.* **1976**, *17*, 277–281.
[27] R. Parvin, S. V. Pande, *Anal. Biochem.* **1977**, *79*, 190–201.
[28] S. Englard, L. J. Horwitz, J. T. Mills, *J. Lipid Res.* **1978**, *19*, 1057–1063.
[29] M. Cametti, K. Rissanen, *Chem. Commun.* **2009**, 2809–2829.
[30] F. M. Vaz, S. van Gool, R. Ofman, L. IJlst, R. J. A. Wanders, *Biochem. Biophys. Res. Commun.* **1998**, *250*, 506–510.
[31] C. Rigault, F. Le Borgne, J. Demarquoy, *Biochim. Biophys. Acta Mol. Cell Biol. Lipids* **2006**, *1761*, 1469–1481.
[32] G. Lindstedt, S. Lindstedt, I. Nordin, *Scand. J. Clin. Lab. Invest.* **1982**, *42*, 477–485.
[33] G. Lindstedt, S. Lindstedt, B. Olander, M. Tofft, *Biochim. Biophys. Acta Gen. Subj.* **1968**, *158*, 503–505.
[34] K. Tars, J. Rumnieks, A. Zeltins, A. Kazaks, S. Kotelovica, A. Leonciks, J. Sharipo, A. Viksna, J. Kuka, E. Liepinsh, M. Dambrova, *Biochem. Biophys. Res. Commun.* **2010**, *398*, 634–639.
[35] C. Loenarz, J. Mecinovic, R. Chowdhury, L. A. McNeill, E. Flashman, C. J. Schofield, *Angew. Chem.* **2009**, *121*, 1816–1819; *Angew. Chem. Int. Ed.* **2009**, *48*, 1784–1787.
[36] K. L. Gorres, R. T. Raines, *Anal. Biochem.* **2009**, *386*, 181–185.
[37] K. Strijbis, F. M. Vaz, B. Distel, *IUBMB Life* **2010**, *62*, 357–362.
[38] F. M. Vaz, R. J. A. Wanders, *Biochem. J.* **2002**, *361*, 417–429.
[39] H. R. Hoveyda, J.-F. Pinault, *Org. Lett.* **2006**, *8*, 5849–5852.
[40] G. Deniau, A. M. Z. Slawin, T. Lebl, F. Chorki, J. P. Issberner, T. van Mourik, J. M. Heygate, J. J. Lambert, L. A. Etherington, K. T. Sillar, D. O'Hagan, *ChemBioChem* **2007**, *8*, 2265–2274.
[41] I. K. H. Leung, T. J. Krojer, G. T. Kochan, L. Henry, F. von Delft, T. D. W. Claridge, U. Oppermann, M. A. McDonough, C. J. Schofield, *Chem. Biol.* **2010**, *17*, 1316–1324.
[42] X. F. Yang, S. J. Ye, Q. Bai, X. Q. Wang, *J. Fluoresc.* **2007**, *17*, 81–87.
[43] R. S. Wehbie, N. S. Punekar, H. A. Lardy, *Biochemistry* **1988**, *27*, 2222–2228.
[44] N. C. Warshakoon, S. D. Wu, A. Boyer, R. Kawamoto, J. Sheville, S. Renock, K. Xu, M. Pokross, S. Zhou, C. Winter, R. Walter, M. Mekel, A. G. Evdokimov, *Bioorg. Med. Chem. Lett.* **2006**, *16*, 5517–5522.
[45] L. Henry, I. K. H. Leung, T. D. W. Claridge, C. J. Schofield, *Bioorg. Med. Chem. Lett.* **2012**; DOI: 10.1016/j.bmcl.2012.06.024.
[46] K. Jaudzems, J. Kuka, A. Gutsaits, K. Zinovjevs, I. Kalvinsh, E. Liepinsh, E. Liepinsh, M. Dambrova, *J. Enzyme Inhib. Med. Chem.* **2009**, *24*, 1269–1275.

Received: April 18, 2012
Published online on June 22, 2012

 © 2012 Wiley-VCH Verlag GmbH & Co. KGaA, Weinheim

Boron Chemistry

DOI: 10.1002/anie.201202000

Dynamic Combinatorial Chemistry Employing Boronic Acids/Boronate Esters Leads to Potent Oxygenase Inhibitors**

Marina Demetriades, Ivanhoe K. H. Leung, Rasheduzzaman Chowdhury, Mun Chiang Chan, Michael A. McDonough, Kar Kheng Yeoh, Ya-Min Tian, Timothy D. W. Claridge, Peter J. Ratcliffe, Esther C. Y. Woon, and Christopher J. Schofield**

The application of dynamic reactions is a promising approach for the discovery of small-molecule ligands for proteins. To date, however, this method is limited by the few appropriate reactions and the techniques used for the analysis of protein–ligand complexes.[1] "Dynamic" functional group interconvertions that have been employed include the conversion of thiols to disulfides, the aldol reaction, and the addition of nucleophiles to ketones and aldehydes.[2] The reaction of boronic acids with diols to form boronate esters is attractive for dynamic-library formation, because it is reversible in aqueous solution in a pH-dependent manner.[3] The dynamic boronic acid/boronate ester system has been used to form supramolecular switches, some of which have been used for sugar detection.[4,5] However, this system has not been used for the identification of protein ligands. Proof of principle work with proteases, which react reversibly with boronic acids, suggests that boronic acid/boronate ester systems might be useful for the identification of enzyme inhibitors.[6]

One issue with the application of reversible reactions for ligand identification is the need to analyze labile complexes that are derived from mixtures. High-resolution techniques, such as NMR spectroscopy and X-ray crystallography, are applicable, but these are time-consuming.[7] Our research group and that of Poulsen, have used non-denaturing protein mass spectrometry to identify protein–ligand complexes formed from equilibrating mixtures of thiols/disulfides[8–11] and aldehydes/hydrazones.[7] The dynamic-combinatorial mass spectrometry (DCMS) technique has the advantages of being efficient and providing information on mass shifts, which can be used for assigning structures to the ligands that bind preferentially.

Herein we demonstrate that boronic acid/boronate ester dynamic systems coupled with protein mass spectrometry analysis are useful for the identification of protein inhibitors (Scheme 1). Our target model enzyme was prolyl hydroxylase domain isoform 2 (PHD2), which is a Fe^{II} and 2-oxoglutarate (2OG) oxygenase that regulates the human hypoxic response. PHD2 inhibition is of therapeutic interest for the treatment of anemia and ischemia-related diseases.[12]

DCMS experiments were carried out using "support ligands" **2** and **3** (Scheme 2), which were designed to participate in Fe^{II} chelation in the active site and, through the incorporation of a boronic acid moiety, participate in boronate ester exchange. We selected the 2-(picolinamido)-acetic acid scaffold because, based on crystal structures of PHD2,[13] it is predicted to fit into the active site through its chelation with Fe^{II}. The low potency of 2-(picolinamido)acetic acid ($IC_{50} > 1$ mM) enabled the effect of boronate ester substitution to be monitored.

Modeling studies suggested that whereas the boronic acid group in support ligand **2** would fit into the active-site subpocket, that of **3** would clash with the active-site wall.[14] Hence, it was envisaged that the reactivity of **3** might serve as a control to investigate possible non-specific binding. The analysis of mixtures of **2** or **3** with PHD2·Fe^{II} through the use of non-denaturing ESI-MS led to the observation of a new peak at 27 887 Da (187 ± 2 Da shift), corresponding to a small molecule/protein adduct, in which the OH groups of the boronic acids moiety are cleaved. We have previously observed, through the use of non-denaturing ESI-MS, analogous apparent fragmentation of boronic acids complexed with other enzymes.[15] Notably, the mixture of boronate ester **4** and PHD2·Fe^{II} gave the same mass shift (187 ± 2 Da) as that observed with **2** and **3** at a cone voltage of 80 V.[14] However, when a lower cone voltage was used (30 V), the mass shift corresponding to an adduct of **4** with the protein, without fragmentation, was apparent (358 ± 2 Da), demonstrating that boronate ester formation can be observed when sufficiently mild ionization is used.

Both **2** and **3** compete with the 2OG analogue *N*-oxalylglycine (NOG) for the 2OG binding site of PHD2.[14] To ensure that boronate ester formation involving **2** and **3** was favorable under the conditions used (NH_4OAc

[*] M. Demetriades, I. K. H. Leung,[+] Dr. R. Chowdhury,[+] M. C. Chan, Dr. M. A. McDonough, Dr. K. K. Yeoh, Dr. T. D. W. Claridge, Prof. C. J. Schofield
Chemistry Research Laboratory, University of Oxford
12 Mansfield Road, Oxford, OX1 3TA (UK)
E-mail: christopher.schofield@chem.ox.ac.uk
Dr. Y. M. Tian, Prof. P. J. Ratcliffe
Nuffield Department of Clinical Medicine, University of Oxford
Roosevelt Drive, OX3 7BN (UK)
Dr. E. C. Y. Woon
Department of Pharmacy, National University of Singapore
18 Science Drive 4, 117543 Singapore (Singapore)
E-mail: phaewcy@nus.edu.sg
[+] These authors contributed equally to this work.

[**] We thank Dr. T. Brown Jr. for the initial work and Dr. R. J. Hopkinson for discussions, Dr. M. K. Lee for providing a sample of HyAsn803 antibody, and the Universiti Sains Malaysia (fellowship to K.K.Y).

Supporting information, including syntheses and characterizations, MS methods, inhibition assays, protein purification, crystallization, and structure solution methods for this article is available on the WWW under http://dx.doi.org/10.1002/anie.201202000.

© 2012 Wiley-VCH Verlag GmbH & Co. KGaA, Weinheim

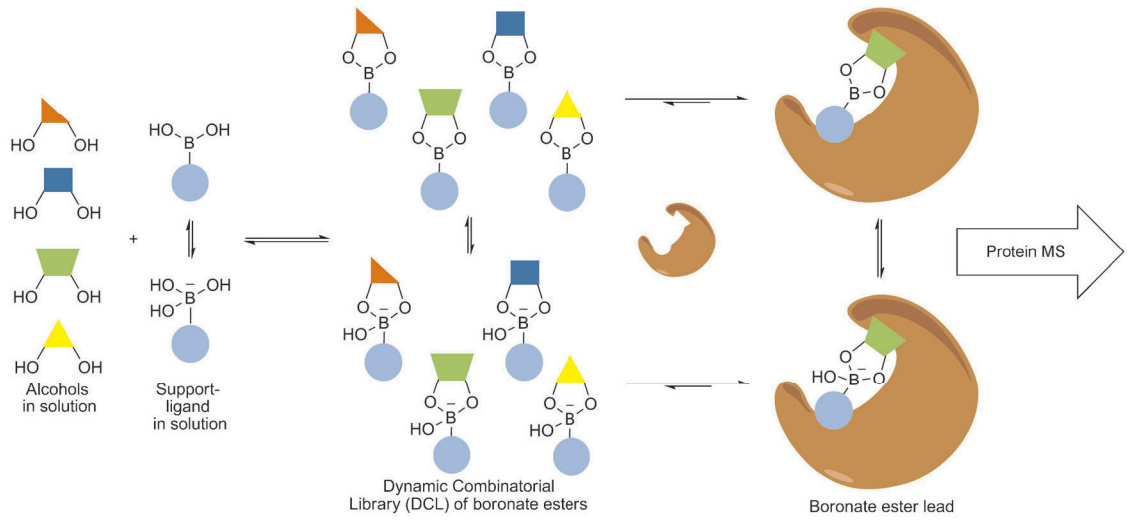

Scheme 1. Schematic representation of the dynamic combinatorial mass spectrometry (DCMS) method that uses the conversion between boronic acids and boronate esters as the reversible reaction.

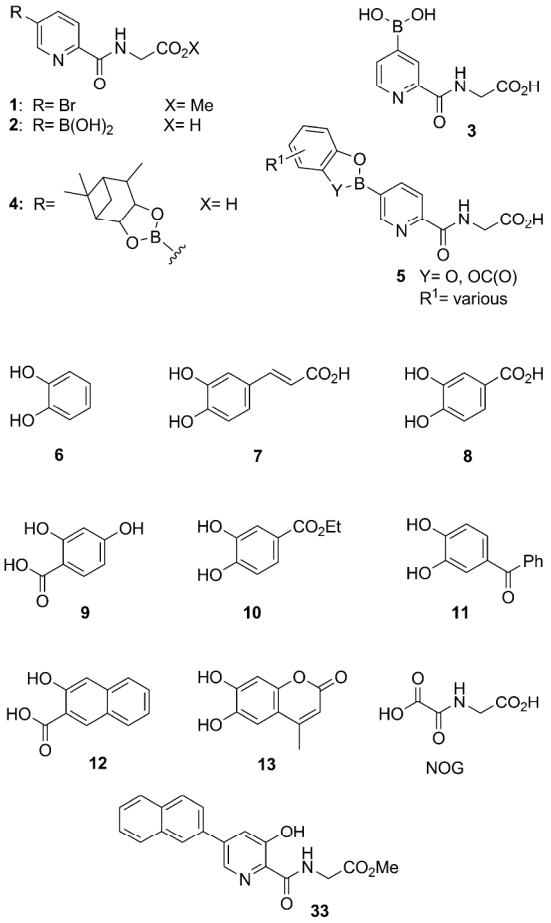

Scheme 2. Structures of selected compounds used in this work.

buffer, pH 7.5), the pK_as of the boronic acids were measured by NMR spectroscopy. The pK_a values of **2** (approximately 7.4) and **3** (approximately 6.9) [14] are appropriate for boronate ester formation under the incubation conditions.[14]

We then investigated whether boronate esters could be used in DCMS. Forty diols were separated into four sets (i–iv) of ten diols[14] according to molecular weight (see the Supporting Information for details). Each set was treated with either support ligands, **2** or **3**, in the presence of PHD2·Fe^{II}. ESI-MS was then used to determine which of the in situ formed boronate esters bind preferentially to PHD2·Fe^{II} (Figure 1).

The reaction of support ligand **2** with the diol sets i–iv resulted in the observation of peaks with mass shifts corresponding to complexes of PHD2 with boronate esters of **2** (**5**, Scheme 2), which were derived from 7 diols (**7**–**13**, Scheme 2). ESI-MS analysis of mixtures of **2** with the individual diols validated the above DCMS results.[14] In some cases, diols were observed to bind to PHD2·Fe^{II} in the absence of **2**, presumably through Fe chelation (Figure 1).[14]

In contrast to the results with **2**, when **3** was employed, no binding of boronate esters was observed in the corresponding assay. Direct binding of some diols to PHD2·Fe^{II} was again observed (Figure 1). The results imply that the mass shifts observed with **2** represent protein adducts involving boronate esters derived from support ligand **2** rather than adducts derived from simultaneous binding of **2** and diols. In the case of diol **8**, which was observed to bind to PHD2·Fe^{II} both in the absence of a support ligand (**2** and **3**) and in the form of the boronate ester derived from **2**, addition of the 2OG competitor NOG to the PHD2/Fe^{II}/**8** mixture resulted in separate peaks representing the adducts derived from the binding of PHD2·Fe^{II} with both **8** and NOG; no peak derived from simultaneous binding of **8** and NOG was observed. These observations support the hypothesis that boronate esters derived from **2** are formed and bind to the protein and that, in the absence of **2**, diol **8** and also the diols **11**, **13**, and **34**–**38** (see the Supporting Information for details) bind to PHD2 through chelation with Fe^{II}.[14]

The results of ESI-MS analyses are not always representative of what exists in solution,[16] therefore the DCMS results were validated by solution studies. NMR-based water

 © 2012 Wiley-VCH Verlag GmbH & Co. KGaA, Weinheim

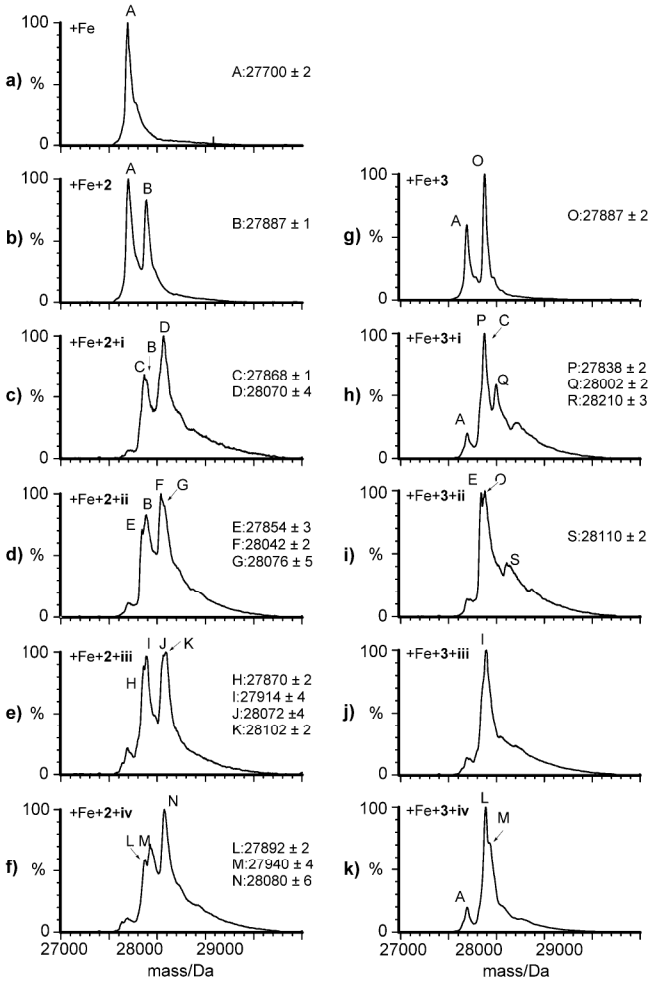

Figure 1. DCMS analyses of PHD2 with boronic acids **2**/**3** and diol sets i–iv. Spectra of deconvoluted non-denaturing ESI-MS (cone voltage 30 V) showing: a) PHD2·Fe^{II}; b) PHD2·Fe^{II} with **2** (1:1); c–f) PHD2·Fe^{II} with **2** and i–iv (1:1:1), respectively; g) PHD2·Fe^{II} with **3** (1:1), h–k) PHD2·Fe^{II} with **3** and diols i–iv (1:1:1), respectively. Assignment of labeled peaks: PHD2·Fe·**2** (peak B); PHD2·Fe·**3** (peak O); PHD2·Fe··diol (peaks C, E, H, I, L, M, P, and Q); PHD2·Fe·**5** (peaks D, F, G, J, K, and N).

relaxation experiments [17,18] were used for the measurement of the apparent binding constants ($K_{D,app}$) of **2** with PHD2, in the presence of different diols. In this method, paramagnetic Mn^{II} was used as a substitute for the diamagnetic Fe^{II}; $K_{D,app}$ values were determined by monitoring the bulk water relaxation rate, which decreases when water access to the paramagnetic metal center is hindered through binding of compounds to the metal. The support ligand **3** displayed no significant PHD2 binding, as determined by NMR spectroscopy.[14] When the NMR experiments were carried out using **2** in the absence or in the presence of diols (**6**–**13**), it was found that its apparent affinity for PHD2 ($K_{D,app}$ = 24.8 μM) was enhanced in the presence of the diols that had been identified by DCMS as being able to form boronate esters (e.g. **2**/**12**: $K_{D,app}$ = 3.0 μM, **2**/**10**: $K_{D,app}$ = 1.3 μM, **2**/**11**: $K_{D,app}$ = 0.6 μM). The presence of diols that were not observed to form boronate esters in the DCMS assays caused a much weaker increase in the apparent binding affinity of **2** (**2**/**6**: $K_{D,app}$ = 13.2 μM, **2**/**39**: $K_{D,app}$ = 18.2 μM).[14] Hence there is qualitative agreement between the gas-phase and solution studies.

To verify the potential of the boronic acid/boronate ester-based DCMS for identification of PHD2 inhibitors, the synthesis of stable analogues that mimic the structure of the identified hits (boronate esters derived from **2** and diols **7**–**13**) from DCMS experiments was attempted. To prepare stable analogues of the boronate esters, we made use of the boronic acid functional group, which was also employed in the DCMS chemistry, in Suzuki cross-coupling reactions.[14] Benzofuran- and naphthalene-based analogues, **16** and **18**, respectively, were prepared; the benzofuran and naphthalene moieties function as 6/5- and 6/6-fused bicyclic mimics of the catechol boronate ester moiety in the boronate ester derived from **2** and catechol (**6**). The binding constants of **16** and **18** were similar (**16**: K_D = 9.5 μM, **18**: K_D = 7.0 μM) suggesting that both ring systems are accommodated in the protein binding pocket. The 5-methoxynaphthalene derivative **20** was used as a mimic of the boronate esters derived from 4-substituted catechols (**7**–**11**) and, notably, **20** (IC_{50} = 107 μM, K_D = 1.6 μM) showed greater inhibition and binding affinity than **16** and **18**; these results are consistent with the DCMS results. NMR water relaxation measurements showed that all the stable analogues bind significantly stronger to PHD2 than the parent compound **2** (Table 1); however they were generally poorer binders than the boronate esters identified by DCMS.[14]

Analysis of PHD2 structures[14] suggests that hydrogen-bonding interactions between the inhibitor and the side chain

Table 1: Binding constants (K_D) as measured by NMR spectroscopy and IC_{50} values for selected inhibitors.[14]

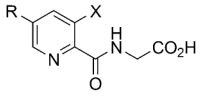

Compound	R	X	K_D [μM]	IC_{50} [μM]
14	H	H	N/A	>1000
16	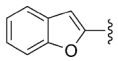	H	9.5	>500
18	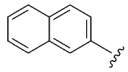	H	7.0	>500
2	$B(OH)_2$	H	24.8	126
20	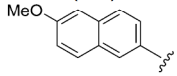	H	1.6	107
22	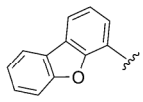	H	8.7	>100
23	H	OH	3.5	409
30	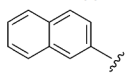	OH	0.5	0.017
28	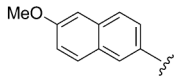	OH	0.8	0.013
32	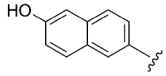	OH	0.9	0.004

© 2012 Wiley-VCH Verlag GmbH & Co. KGaA, Weinheim

hydroxy group of Tyr303 might promote inhibitor binding.[13] Thus, a derivative of inhibitor **20** containing a hydroxy group at the C3 position, **28**, was prepared.[14] Compound **28** showed significantly higher potency and affinity ($IC_{50} = 13$ nM, $K_D = 0.8$ μM) than **20**. As indicated by DCMS, the aryl substituent at the 5-position is important: **28** showed higher potency than **23** (Table 1).[11] In the presence of the C3 hydroxy group, the methoxy group on the naphthalene ring, which improved the activity of the initial inhibitors, is less important, as shown by the similar potency of **28** and **30** (Table 1). However, substitution at the C5 position of the naphthalene moiety remains important as indicated by the higher activity of **32** relative to **30**.

To investigate the mode of binding of **28**, it was crystalized in complex with the PHD2 catalytic domain incorporating Mn^{II}, which substitutes for Fe^{II}.

The crystal structure reveals that **28** complexes to the metal in a bidentate manner, with the C3 hydroxy group interacting with Tyr303 through a hydrogen bond. The naphthalene group of **28** is twisted relative to the pyridinyl ring (torsion angle 52.8°), thus allowing the naphthalene moiety to occupy the substrate-binding site (Figure 2).

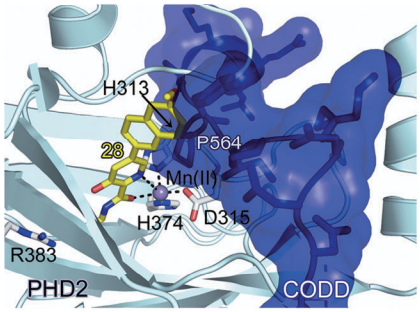

Figure 2. View from a crystal structure of PHD2·Mn^{II} (light blue) complexed with **28** (yellow) superimposed with a structure of PHD2·Mn^{II} in complex with HIF-1α residues 558-574 ("CODD": blue surface; PDB ID 3HQR). The image shows the proximity of the C5 substituent of **28** (5-methoxynaphthalene) to the substrate binding site. The active-site metal is in purple and Pro564 of HIF-1α is labeled.

Finally, to investigate the efficacy of the C5 pyridyl compounds in cells, we tested the methyl ester derivative of **30** (**33**, Scheme 2) owing to its better cell penetration. **33** was shown to upregulate HIF1α in cells by selectively inhibiting PHDs but not Factor Inhibiting Hypoxia (FIH).[14]

Overall, we have demonstrated the potential of boronic acids/boronate esters for inhibitor discovery using a biologically relevant human hydroxylase. We envision that similar approaches that use this boron chemistry will be applicable to other proteins. Suitably protected boronic acids were also used for the synthesis of stable analogues through organometallic chemistry. We have found that there are potential limitations of the DCMS approach, for example, boronic acids can sometimes fragment under the conditions of MS. However, we foresee that improved MS screening methods that give results that are more representative of the composition of the analyte in solution will become available as the technology develops. We have also shown that NMR-based screening methods, and other types of analysis, can also be employed in the evaluation of boronate ester binding.

Received: March 13, 2012
Published online: May 25, 2012

Keywords: boron · combinatorial chemistry · mass spectrometry · oxygenase · prolyl hydroxylase

[1] O. Ramstrom, J. M. Lehn, *Nat. Rev. Drug Discovery* **2002**, *1*, 26.
[2] P. T. Corbett, J. Leclaire, L. Vial, K. R. West, J. L. Wietor, J. K. M. Sanders, S. Otto, *Chem. Rev.* **2006**, *106*, 3652.
[3] G. Springsteen, B. H. Wang, *Tetrahedron* **2002**, *58*, 5291.
[4] H. G. Kuivila, A. H. Keough, E. J. Soboczenski, *J. Org. Chem.* **1954**, *19*, 780.
[5] J. Z. Zhao, T. M. Fyles, T. D. James, *Angew. Chem.* **2004**, *116*, 3543; *Angew. Chem. Int. Ed.* **2004**, *43*, 3461.
[6] I. K. H. Leung, T. Brown, C. J. Schofield, T. D. W. Claridge, *Med. Chem. Commun.* **2011**, *2*, 390.
[7] S. A. Poulsen, *J. Am. Soc. Mass Spectrom.* **2006**, *17*, 1074.
[8] B. M. R. Liénard, N. Selevsek, N. J. Oldham, C. J. Schofield, *ChemMedChem* **2007**, *2*, 175.
[9] N. R. Rose, E. C. Y. Woon, G. L. Kingham, O. N. F. King, J. Mecinovic, I. J. Clifton, S. S. Ng, J. Talib-Hardy, U. Oppermann, M. A. McDonough, C. J. Schofield, *J. Med. Chem.* **2010**, *53*, 1810.
[10] B. M. R. Liénard, R. Hueting, P. Lassaux, M. Galleni, J. M. Frere, C. J. Schofield, *J. Med. Chem.* **2008**, *51*, 684.
[11] E. C. Y. Woon, M. Demetriades, E. A. L. Bagg, W. S. Aik, S. M. Krylova, J. H. Y. Ma, M. C. Chan, L. J. Walport, D. Wegman, K. N. Dack, M. A. McDonough, S. N. Krylov, C. J. Schofield, *J. Med. Chem.* **2012**, accepted, DOI: 10.1021/jm201417e.
[12] N. R. Rose, M. A. McDonough, O. N. F. King, A. Kawamura, C. J. Schofield, *Chem. Soc. Rev.* **2011**, *40*, 4364.
[13] R. Chowdhury, M. A. McDonough, J. Mecinovic, C. Loenarz, E. Flashman, K. S. Hewitson, C. Domene, C. J. Schofield, *Structure* **2009**, *17*, 981.
[14] For more details see the Supporting Information.
[15] T. Brown, Jr., D.Phil Thesis, University of Oxford (UK), **2009**.
[16] J. M. Daniel, S. D. Friess, S. Rajagopalan, S. Wendt, R. Zenobi, *Int. J. Mass Spectrom.* **2002**, *216*, 1.
[17] I. K. H. Leung, E. Flashman, K. K. Yeoh, C. J. Schofield, T. D. W. Claridge, *J. Med. Chem.* **2010**, *53*, 867.
[18] I. Bertini, M. Fragai, C. Luchinat, E. Talluri, *Angew. Chem.* **2008**, *120*, 4609; *Angew. Chem. Int. Ed.* **2008**, *47*, 4533.

 © 2012 Wiley-VCH Verlag GmbH & Co. KGaA, Weinheim

Chemistry & Biology
Article

A Photoreactive Small-Molecule Probe for 2-Oxoglutarate Oxygenases

Dante Rotili,[1,2] Mikael Altun,[3] Akane Kawamura,[1,4] Alexander Wolf,[1,4] Roman Fischer,[3] Ivanhoe K.H. Leung,[1] Mukram M. Mackeen,[3] Ya-min Tian,[3] Peter J. Ratcliffe,[3] Antonello Mai,[2] Benedikt M. Kessler,[3,*] and Christopher J. Schofield[1,*]

[1]Department of Chemistry and the Oxford Centre for Integrative Systems Biology, Chemistry Research Laboratory, University of Oxford, 12 Mansfield Road, Oxford OX1 3TA, UK

[2]Department of Chemistry and Technologies of Drugs, Pasteur Institute-Cenci Bolognetti Foundation, University of Rome "La Sapienza," Piazzale Aldo Moro 5, 00185 Rome, Italy

[3]Nuffield Department of Medicine, University of Oxford, Henry Wellcome Building for Molecular Physiology, Roosevelt Drive, Oxford OX3 7BN, UK

[4]These authors contributed equally to this work

*Correspondence: bmk@ccmp.ox.ac.uk (B.M.K.), christopher.schofield@chem.ox.ac.uk (C.J.S.)

DOI 10.1016/j.chembiol.2011.03.007

SUMMARY

2-oxoglutarate (2-OG)-dependent oxygenases have diverse roles in human biology. The inhibition of several 2-OG oxygenases is being targeted for therapeutic intervention, including for cancer, anemia, and ischemic diseases. We report a small-molecule probe for 2-OG oxygenases that employs a hydroxyquinoline template coupled to a photoactivable crosslinking group and an affinity-purification tag. Following studies with recombinant proteins, the probe was shown to crosslink to 2-OG oxygenases in human crude cell extracts, including to proteins at endogenous levels. This approach is useful for inhibitor profiling, as demonstrated by crosslinking to the histone demethylase FBXL11 (KDM2A) in HEK293T nuclear extracts. The results also suggest that small-molecule probes may be suitable for substrate identification studies.

INTRODUCTION

Oxygenases that employ 2-oxoglutarate (2-OG) as a cosubstrate and ferrous iron as a cofactor have emerged as a large enzyme superfamily (Hausinger, 2004). In humans there are predicted to be >60 oxygenases. To date, human oxygenases have been found to have roles in collagen biosynthesis, fatty acid metabolism, DNA/RNA repair and modifications, histone modification, and the hypoxic response (Loenarz and Schofield, 2008).

In the hypoxic response in animals, 2-OG oxygenases play important roles by catalyzing posttranslational hydroxylation of the hypoxia-inducible transcription factor (HIF), which orchestrates the expression of a large gene array. The oxygen dependence of these hydroxylases is proposed to enable them to act as oxygen sensors for the HIF system (Kaelin and Ratcliffe, 2008). *trans*-4-prolyl hydroxylation, catalyzed by the prolyl hydroxylase domain-containing enzymes PHD1–3, of either of two prolyl residues in the oxygen-dependent degradation domain of HIF-α signals for degradation via the proteasome. HIF-α asparaginyl hydroxylation is catalyzed by the factor inhibiting HIF (FIH) and reduces the interaction of HIF-α with transcriptional coactivator proteins (Kaelin and Ratcliffe, 2008). The upregulation of HIF and/or increases in its activity (through inhibition of HIF hydroxylases or by other means) may be beneficial for ischemic diseases, anemia, and gastrointestinal inflammatory diseases (Nagel et al., 2010). On the other hand, the therapeutic inhibition of HIF through increasing HIF hydroxylase activity (or by other means) is an approach for tumor treatment because HIF-α expression is increased in hypoxia.

2-OG oxygenases also play roles in fatty acid metabolism, namely in carnitine biosynthesis and chlorophyll metabolism, and in modification of nucleic acids via *N*-demethylation and t-RNA and 5-methylcytosine hydroxylation (for a review, see Loenarz and Schofield, 2008). 2-OG oxygenases (the JmjC family) have emerged as important in the modification of histones by catalyzing the *N*-demethylation of N^{ε}-methyllysine residues. Different human subfamilies of 2-OG-dependent N^{ε}-lysine demethylases have been identified (Klose and Zhang, 2007), the members of which have a range of proposed roles, including in cellular differentiation and development. Mutations to two of the JmjC domain-containing demethylases (JARID1C and PHF8) are associated with X-linked human mental retardation, indicating that these 2-OG oxygenases are important for normal neuronal function (Jensen et al., 2005; Laumonnier et al., 2005). The observation that JmjC proteins are often deleted, translocated, mutated, and aberrantly expressed in human cancers, and that some of these histone demethylases regulate the proliferation of cancer cell lines, suggests that their activation or inactivation (some are proposed to be oncoproteins and others as tumor suppressors) contributes to tumor development. For these reasons, the therapeutic potential of JmjC histone demethylase inhibitors as anticancer agents is being considered (for a review, see Spannhoff et al., 2009).

The diverse roles and substrates of 2-OG oxygenases make functional assignation work challenging. It is desirable to develop more efficient methods both for their identification in different cell types and for the identification of their substrates.

 ©2011 Elsevier Ltd All rights reserved

One approach that has been applied to other enzyme families is the use of small-molecule "chemical" probes based on inhibitor templates specific for particular active sites (Kessler et al., 2001; Evans and Cravatt, 2006; Sadaghiani et al., 2007). However, to date, the development of compounds that are selective for human 2-OG oxygenases over other enzyme families is at an early stage.

Despite recent advancements in mass spectrometric (MS) and bioinformatic methods, there remains a need to reduce the complexity of the proteome prior to detailed proteomic analysis. "Classical" approaches include 2D electrophoresis, affinity chromatography, and immunoprecipitation methods. Although these techniques are powerful, they suffer from limitations; for example, 2D electrophoresis is not selective from a functional perspective and is not well suited for the analysis of lipophilic proteins, and affinity chromatography and immunoprecipitation methods normally require knowledge of the target proteins and can be difficult to apply to complexes. Small-molecule-based probes which are selective for specific protein families are complementary to established techniques (Evans and Cravatt, 2006), and have long been used for profiling proteins, and particularly enzymes, in antibiotic research (e.g., penicillin binding proteins). More recently, they have been shown to be useful in profiling enzymes in eukaryotic cells. One strategy has employed the use of irreversible inhibitors derivatized with an affinity tag that enables efficient purification (Evans and Cravatt, 2006). A development of this strategy employs reversible inhibitors coupled to an affinity tag and a photoreactive group that "locks" the protein-inhibitor complex by irreversible crosslinking to enable purification (Salisbury and Cravatt, 2008; Xu et al., 2009; Fischer et al., 2010).

Here we report on the development of a small-molecule probe for human 2-OG oxygenases (Table 1A) based on a reversibly binding inhibitor coupled to an affinity-purification tag and a photoreactive group. We demonstrate the viability of the method for identifying 2-OG oxygenases in crude cell extracts and for profiling 2-OG oxygenase inhibitors.

RESULTS

Probe Selection

We began by preparing molecules with a common scaffold consisting of a substituted phenyl azide as a photocrosslinking group capable of forming a covalent bond with the target protein after UV irradiation and a biotin derivative as an affinity-purification tag (Table 1A). We chose this approach because it has been useful in analogous studies on kinases by Koester and coworkers (Fischer et al., 2010). We investigated two "inhibitor templates" in order to achieve selective and reversible binding to 2-OG oxygenases (selectivity function). In one series, we generated *N*-oxalylglycine (NOG) derivatives because of the close relationship of NOG with 2-OG, and because NOG/NOG derivatives inhibit a range of 2-OG oxygenases (Rose et al., 2010). In another series, we synthesized 8-hydroxyquinoline (8-HQ) derivatives, because 8-HQ is a known iron chelator and is present in inhibitors of 2-OG oxygenases, including PHD2 and FIH (Warshakoon et al., 2006; Smirnova et al., 2010) and some histone demethylases (King et al., 2010) (Table 1A). As for the kinase work (Fischer et al., 2010), a spacer was introduced between the inhibitor/selectivity function and the phenyl azide in order to reduce potential reactions of the photocrosslinker, with the intention of enabling crosslinking close to but not within the inhibitor/selectivity function binding site on the target oxygenases. Both epimers at the *C*-α chiral center of the *N*-oxalyllysine group of the NOG-based probe were prepared, because chirality at this center is a means of achieving selective inhibition of some 2-OG oxygenases, including the HIF hydroxylases (Tables 1A and 1B) (McDonough et al., 2005). Details of the synthesis of the probes are given in Supplemental Experimental Procedures available online.

We then investigated the capability of the probes to bind to recombinant PHD2 and JMJD2E (JMJD2E is likely not expressed, but its catalytic domain is representative of the JMJD2 histone demethylases). Initially, we tested for inhibition of/interaction with PHD2 using an MS-based hydroxylation assay (Flashman et al., 2010) and an NMR-based binding assay (Leung et al., 2010), and for inhibition of JMJD2E using a formaldehyde dehydrogenase (FDH)-coupled assay (Rose et al., 2008) (Table 1B; Figures S1A–S1C).

The two NOG-based probes were at most only weakly active against both JMJD2E and, consistent with structural studies (McDonough et al., 2005), PHD2 (Table 1B; Figure S1C). In contrast, the 8-HQ derivative DR025 displayed promising binding/inhibition of both enzymes (IC_{50} = 58.4 μM against JMJD2E and K_D = 17.7 μM and IC_{50} = 41.8 μM against PHD2), and hence was selected for further work. In the absence of the selectivity function, the common scaffold DR024 (see Supplemental Experimental Procedures) was not observed to bind to PHD2 (NMR-based assay) and to inhibit JMJD2E (FDH-coupled assay), and was therefore used as a negative control in subsequent experiments (Table 1B). In contrast, the synthetic 8-HQ intermediate DR016 displayed a comparable binding/inhibition capacity to PHD2 and JMJD2E (Table 1B). This property made this compound useful for subsequent "competition" control experiments.

Photocrosslinking Experiments

To test the suitability of DR025 as a crosslinker, we carried out studies with purified PHD2, using Mn(II) to substitute for Fe(II) because the PHD2-Mn(II) complex is not catalytically active. The extent of crosslinking was analyzed by protein MS through the observation of a mass shift approximately corresponding to the mass of the probe after the loss of N_2. Prior to UV irradiation, only a mass peak corresponding to PHD2 ($\sim$28 kDa) was observed (Figure 1Ai). After irradiation, an additional peak with a mass shift of >800 Da was observed, consistent with a covalent adduct formation with DR025 (*m/z* 861 for [*M*-N_2]) (Figure 1Aii). The extent of crosslinking by DR025 was substantially reduced in competition experiments (1:1 ratio with DR025) with a reported PHD2 inhibitor ([1-chloro-4-hydroxyisoquinoline-3-carbonyl]-amino)-acetic acid (Warshakoon et al., 2006) and with the 8-HQ-containing DR016 (10:1 ratio with DR025) (Table 1B). These experiments provide evidence that this probe binds to the PHD2 active site (Figure 1Aiii and 1Aiv). No crosslinking was observed for the scaffold DR024 without the 8-HQ group (Table 1B and Figure 1Av). The presence of metal was important for efficient crosslinking (Figure 1Bii and 1Biii). The low level of crosslinking in the absence of Mn(II) (Figure 1Bii) may be due to residual Fe(II) in the PHD2 sample (McNeill et al., 2005). Using

Table 1. Structures and Biological Validation of Photoreactive Small-Molecule Probes Used in the Study

A

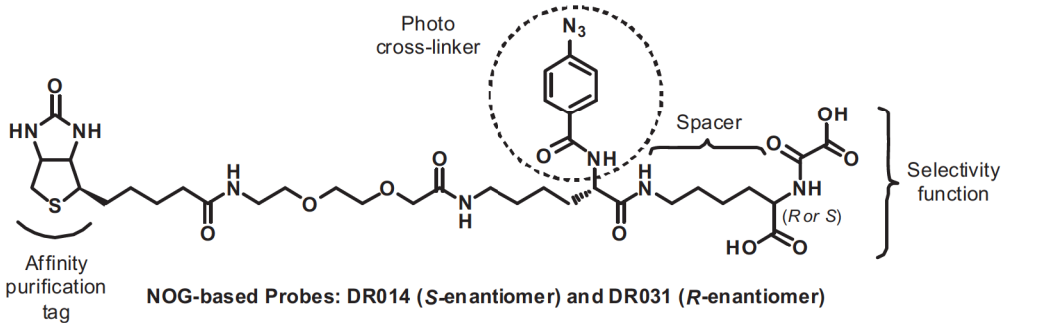

NOG-based Probes: DR014 (*S*-enantiomer) and DR031 (*R*-enantiomer)

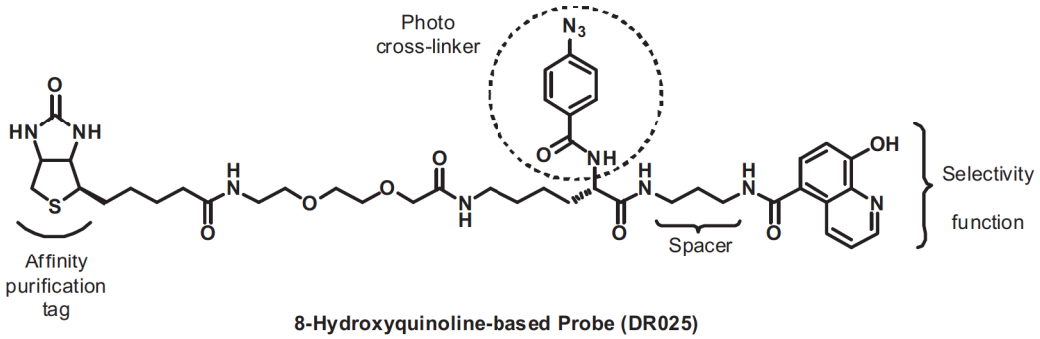

8-Hydroxyquinoline-based Probe (DR025)

B

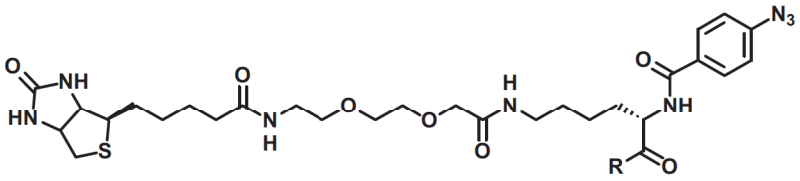

Compound	R	JMJD2E FDH-Coupled Assay IC_{50}[a]	PHD2 NMR-Based Binding Assay K_D[a]	PHD2 MS-Based Hydroxylation Assay IC_{50}[a]
DR014	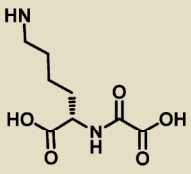	3870 μM	No binding at 250 μM	No inhibition at 300 μM
DR031	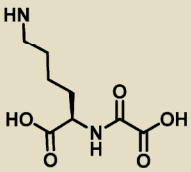	625 μM	No binding at 250 μM	No inhibition at 300 μM

 ©2011 Elsevier Ltd All rights reserved

Table 1. *Continued*

DR025	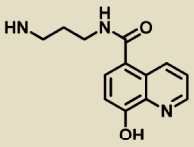	58.5 μM	17.7 μM	41.8 μM
DR024 (scaffold)[b]	OH	No inhibition at 300 μM	No binding at 250 μM	No inhibition at 300 μM
DR016 (competitor)	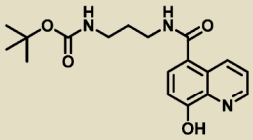	40.7 μM	0.7 μM	20.8 μM

[a] See also Figures S1A–S1C.
[b] See also Scheme S1.

the MS method, it was also possible to demonstrate selectivity for the formation of a covalent adduct between DR025 and PHD2 in protein mixtures containing additional enzymes (e.g., lysozyme, lactic dehydrogenase) unrelated to oxygenases (Figure S2A).

The efficiency of crosslinking was investigated under conditions of varying wavelengths, concentrations of the target and the probe, incubation times, and buffer. After some optimization, the following conditions were selected for further investigation: 20 min of irradiation at 365 nm with an energy of 5 mW/cm^2, conditions which led to 35% crosslinking relative to unmodified protein (Figure S2B). This level is in agreement with reported data for phenyl azide-mediated photocrosslinking; incomplete crosslinking is likely, at least in part, due to quenching of the reactive intermediates by solvent/buffer (Fleming, 1995).

Photoaffinity Labeling and Enrichment of Purified 2-OG Oxygenases

We then investigated the capability of the probe to enable enrichment of a target protein by means of avidin-coated beads. Following irradiation, the protein-probe mixture was incubated with avidin-coated agarose beads; after washing, the beads were then mixed with the MALDI matrix and analyzed; after the affinity-purification step, there was enrichment of crosslinked

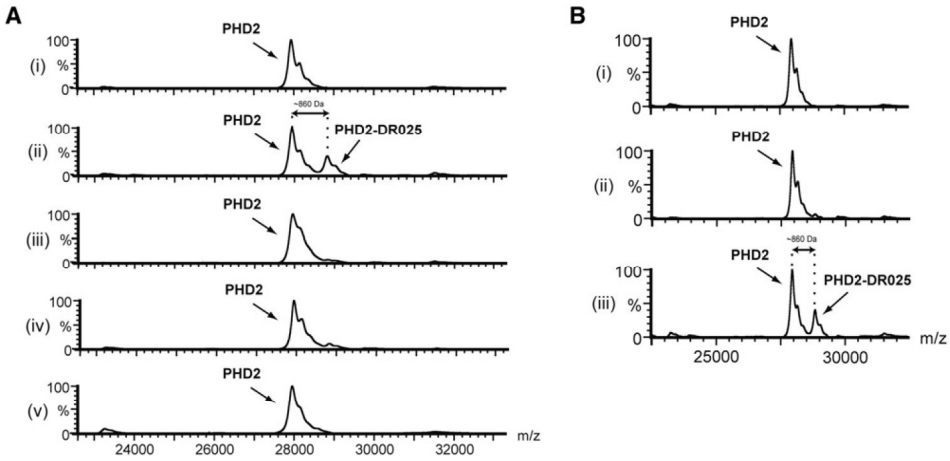

Figure 1. Crosslinking between DR025 and PHD2 Is Dependent on Irradiation and Mn(II)

(A) MALDI TOF MS spectra for photolabeling of PHD2$_{181–426}$ by DR025. PHD2$_{181–426}$ (5 μM) and DR025 (25 μM) were incubated (45 min, r.t.) in Tris buffer in the presence of Mn(II) (5 μM). After irradiation on ice (20 min, 365 nm), the resulting solutions were analyzed by MS. (i and ii) Results before and after irradiation. (iii) Results after irradiation in the presence of an inhibitor ([1-chloro-4-hydroxyisoquinoline-3-carbonyl]-amino)-acetic acid (Warshakoon et al., 2006) (25 μM) in a 1:1 concentration ratio with DR025. (iv) Competition experiment with DR016 (250 μM) in a 10:1 molar ratio with DR025. (v) Control with DR024 (25 μM). For selectivity and efficiency of PHD2 capture by DR025, see Figure S2.

(B) Effect of Mn(II) on the efficiency of PHD2$_{181–426}$ capture by DR025. (i and iii) Effects relative to a mixture in Tris buffer of PHD2 (5 μM), DR025 (25 μM), and Mn(II) (5 μM) before and after irradiation, respectively. (ii) Effects of the irradiation on the same mixture without Mn(II).

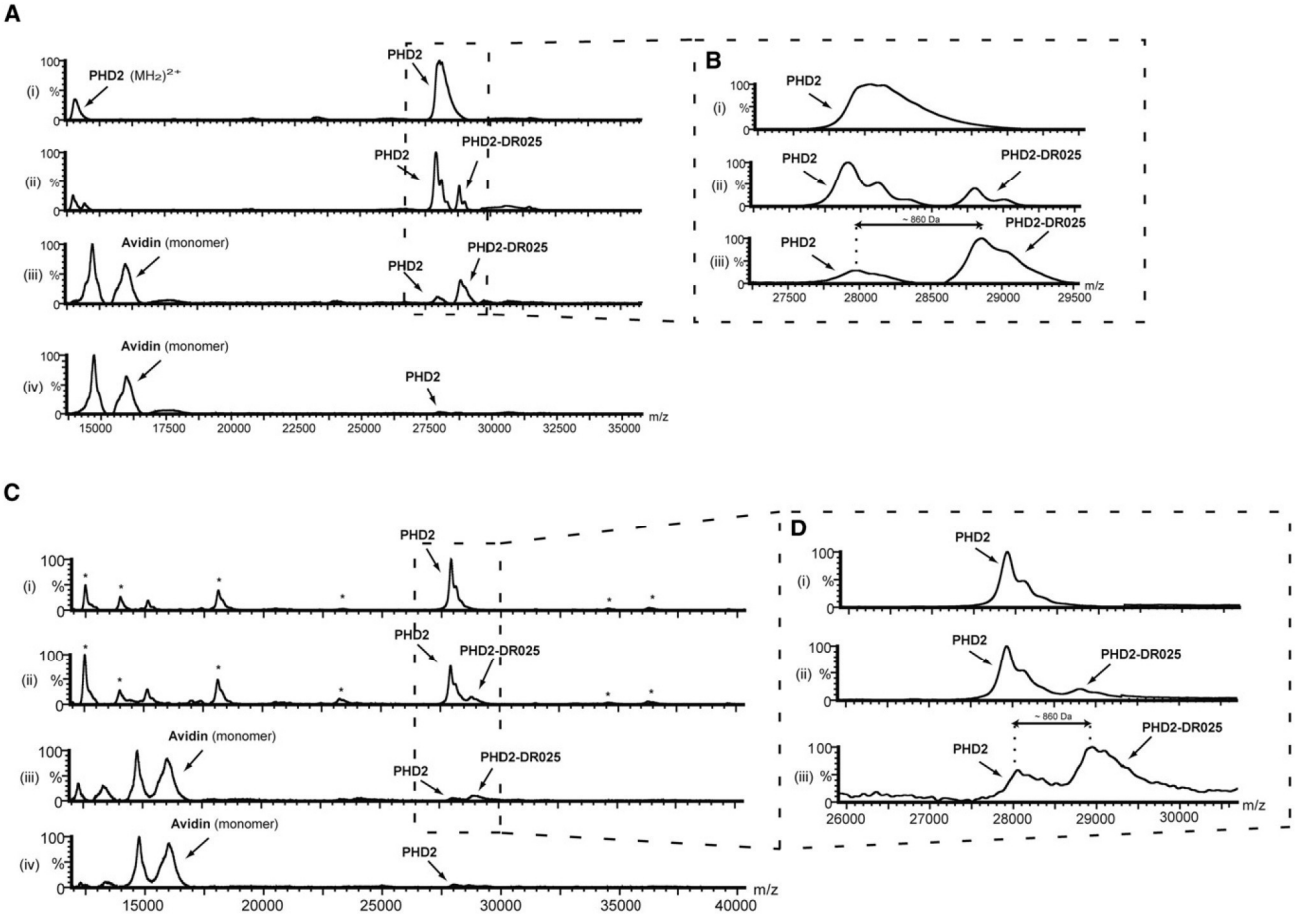

Figure 2. Photoaffinity Labeling and Enrichment of Purified PHD2 by DR025

(A) MALDI TOF MS spectra for the crosslinking of purified $PHD2_{181–426}$ by DR025. $PHD2_{181–426}$ (5 μM) and DR025 (15 μM) were incubated (45 min, r.t.) in Tris buffer in the presence of Mn(II) (5 μM). After irradiation on ice (20 min, 365 nm) the solutions were divided, with one part being analyzed by MALDI TOF and the other incubated (30 min, r.t.) with avidin-coated agarose beads. After washing (see Experimental Procedures), the beads were mixed with the MALDI matrix and analyzed. (i) Before irradiation in the presence of DR025. (ii) After irradiation in the presence of DR025. (iii) After irradiation and avidin-bead-mediated purification. (iv) After irradiation in the presence of DR024 at the same concentration (15 μM) as DR025 and affinity purification. For the identification of the PHD2 region covalently crosslinked by DR025, see Figure 5 and the text.

(B) Magnification of the $PHD2_{181–426}$ region of spectra in (A).

(C) MALDI TOF spectra of the crosslinking of $PHD2_{181–426}$ by DR025 in the presence of HEK293T cell lysates. $PHD2_{181–426}$ (5 μM, 5.2 μg), Mn(II) (5 μM), and DR025 (15 μM) were incubated (45 min, r.t.) in Tris buffer in the presence of HEK293T cell lysates (~50 μg total protein). After UV treatment on ice (20 min, 365 nm) the resulting solutions were divided, with one part being analyzed by MALDI TOF and the other incubated (30 min, r.t.) with avidin-coated agarose beads. After washing, the beads were mixed with the MALDI matrix and spotted. (i) Before irradiation in the presence of DR025. (ii) After irradiation in the presence of DR025. (iii) After irradiation and affinity purification in the presence of DR025. (iv) Same as (iii) but in the presence of DR024 at the same concentration (15 μM) as DR025.

(D) Magnification of the $PHD2_{181–426}$ region of the spectra in (C).

PHD2 material (Figure 2Aii and 2Aiii; magnifications in Figure 2B). However, after crosslinking and affinity purification, unmodified PHD2 was still observed (Figures 2Aiii and 2Biii); unmodified PHD2 was also observed, to a small extent, after the same treatment when using the scaffold DR024 (Figure 2Aiv). This is likely due to relatively nonspecific capture of PHD2 by the beads at the relatively high PHD2 concentrations used in these analyses (see below). Note that the limit of detection by MALDI-TOF MS requires protein concentrations (5 μM in this case) that are likely higher than the endogenous levels of most proteins in biologically relevant samples.

We then carried out the analyses in the presence of HEK293T cell lysates as a background to test whether the probe can selectively target proteins in a complex mixture. Comparison of the spectra in Figure 2Ci–2Ciii shows that after affinity purification there is selective enrichment of the tagged PHD2 over background proteins (indicated with an asterisk). A limitation of this experiment was that the concentration of PHD2 was likely higher (5 μM) as compared to other "background" proteins. As stated above, this may account for some of the apparent nonspecific capture observed (Figure 2Diii). Low levels of nonspecific capture (but not crosslinking) were observed with the scaffold control DR024 (Figure 2Civ).

Labeling of purified PHD2 (alone and when added to HEK293T cell lysates) was also analyzed by simultaneous western blotting using anti-biotin and anti-PHD2 antibodies. As indicated in the

anti-biotin blots (Figures 3A, right and 4B, central), biotinylation of PHD2 by DR025 was apparent in both experiments and was selective for PHD2 in the presence of the "background" proteins of HEK293T cell lysates (Figure 3B, central). Crosslinking was significantly reduced in the presence of a 10-fold excess of the 8-HQ competitor DR016 and absent in the control with the scaffold DR024 and in the experiment without irradiation. The anti-PHD2 blots confirmed that capture of PHD2 by DR025 was substantially reduced in the presence of DR016, in controls with the scaffold (DR024) alone, and without irradiation (Figures 3A and 3B, left). In the latter two experiments (i.e., DR024 alone and without irradiation), as previously found (Figures 2A–2D), a low level of nonspecific PHD2 capture was observed, as demonstrated by comparison of the corresponding lanes in the anti-biotin blots that show a complete absence of biotinylation (Figures 3A, right, and 3B, central). It was notable that, compared to those with isolated proteins, nonspecific PHD2 capture was reduced in the experiments with cell lysates, probably because of competition for "nonspecific" binding exerted by the other proteins (compare corresponding lanes in the left panels of Figures 3A and 3B). SDS-PAGE and silver staining (Figure 3B, right) supported the capability of DR025 to selectively capture PHD2 in the presence of irradiated HEK293T cell-lysate proteins (Figure 3B, right). Identification of the labeled protein band at 28 kDa as the supplemented PHD2 was verified by LC-MS/MS analysis (see Experimental Procedures).

We then tested the versatility of the probe for crosslinking to 2-OG oxygenases by carrying out experiments with the 2-OG-dependent histone demethylase JMJD2E. Closely analogous results to those obtained with PHD2 were obtained with JMJD2E (Figures S3A and S3B), providing preliminary evidence for the suitability of DR025 as a general probe for the 2-OG oxygenase superfamily.

Validation of the Functional Probe by Detecting Endogenous Levels of Target Proteins

To investigate the utility of DR025 in a more biologically relevant context, we then carried out analyses of crude extracts prepared from human HEK293T cells (grown under normoxic conditions) that either overexpressed full-length PHD2 or were untransfected (Figures 3C and 3D, respectively). The MALDI MS analysis method was not applicable, at least with our current capability, because of the complexity of the system and the low abundance of the target protein. In cell extracts from both untransfected and PHD2-overexpressing HEK293T cells, anti-PHD2 immunoblotting (Figures 3C and 3D, left) revealed PHD2 capture by DR025. A strong reduction in capture was observed in competition experiments using DR016, and a complete absence of any labeling was observed in controls with the inactive probe DR014 or without irradiation. These controls imply that the nonspecific capture observed at the high PHD2 concentrations used in the preliminary analyses (Figures 2, 3A, and 3B) is not, at least under the conditions tested, a problem when the target concentration is at relatively low "endogenous" levels. It was necessary to use a more sensitive chemiluminescence kit for immunoblotting to observe the same degree of capture in the lysates from the cells not overexpressing PHD2 than in those doing so (see Experimental Procedures for details). The two anti-biotin immunoblots (Figures 3C and 3D, right) showed more than one band in the capture assay. Some of them were substantially reduced or absent in the competition (DR016) and scaffold (DR024) controls, indicating a specific enrichment of more than one protein as a result of the crosslinking process (see below). In the lanes with the input lysates and the experiments without irradiation, we did not detect any bands even from the naturally present biotinylated proteins, likely because the lysate was subjected to a "preclearing" with avidin-coated beads prior to probe treatment.

Mapping the PHD2 Probe Photocrosslinking Site

We then investigated the photocrosslinking site of the probe DR025 with recombinant $PHD2_{181–426}$ by performing photocrosslinking followed by purification and tryptic digestion/MS analysis to map the region(s) that is covalently modified. LC-MS/MS analysis of the digested photocrosslinked $PHD2_{181–426}$ material revealed three coeluting precursor ion masses that may contain crosslinked species (Figure 4A): (1) a doubly charged ion at m/z = 817.42 Da (MW = 1632.84 Da) was identified by MS/MS analysis as VELNKPSDSVGKDVF (Figure 4B), which corresponds to the C-terminal sequence of $PHD2_{411–426}$; (2) a triply charged precursor ion at m/z = 755.40 Da (MW = 2263.20 Da) exhibited the same fragmentation pattern under normal MS/MS conditions as the ion at 817.42 Da (MW = 1632.84 Da), but with additional ions in the low molecular range (Figure 4C); and (3) a singly charged ion at m/z = 631.35 Da (MW = 630.35 Da) corresponding to the exact mass difference (MW = 2263.20 – 1632.84 = 630.36 Da) between the ions at 755.40 Da (MW = 2263.20 Da) and 817.42 (MW = 1632.84 Da). In the MS/MS spectrum of the precursor ion for the latter species (817.42 Da), we did not observe proteotypic immonium ions, suggesting that it is not derived from a proteotypic peptide (Figure S4). We compared the MS/MS spectra in the low molecular range of all three precursor ions (Figure S4), and observed that fragment ions derived from the precursor at 631.35 Da (MW = 630.35 Da) were also present in the MS/MS spectrum of the triply charged precursor ion at 755.40 Da (MW = 2263.20 Da) but not in the spectrum of the doubly charged precursor ion at 817.42 Da (MW = 1632.84 Da). These observations imply that the C-terminal region of $PHD2_{411–426}$ (VELNKPSDSVGKDVF) is reacted with DR025. We noted that during the ionization, the majority of the crosslinked peptides undergo fragmentation releasing a nonproteotypic fragment (630.35 Da). To confirm this, we produced an MS/MS spectrum of the precursor at 755.40 Da $[M+3H]^{3+}$ (MW = 2263.20 Da) with reduced collision energy (Figure 4D). Under these conditions, we observed only a doubly charged fragment ion at 817.42 Da (MW = 1632.84 Da) and a singly charged ion at 631.35 Da (MW = 630.35 Da), implying that the peptide does not (normally) fragment, and the DR025-derived fragment at 631.35 Da is separated in an intact form from the precursor ion at 755.40 Da (Figure 4D). Taken together, the spectra show that the precursors at 755.40 Da $[M+3H]^{3+}$ (MW = 2263.20 Da) and 817.42 Da $[M+2H]^{2+}$ (MW = 1632.84 Da) correspond to the same PHD2-derived peptide with and without a linked nonproteotypic adduct with a molecular weight of 630.35 Da. The precursor ion for the triply charged adduct at 755.40 Da was not observed in the non-UV-irradiated PHD2 protein control sample. The instability of the peptide-probe adduct under MS/MS conditions did not allow the exact

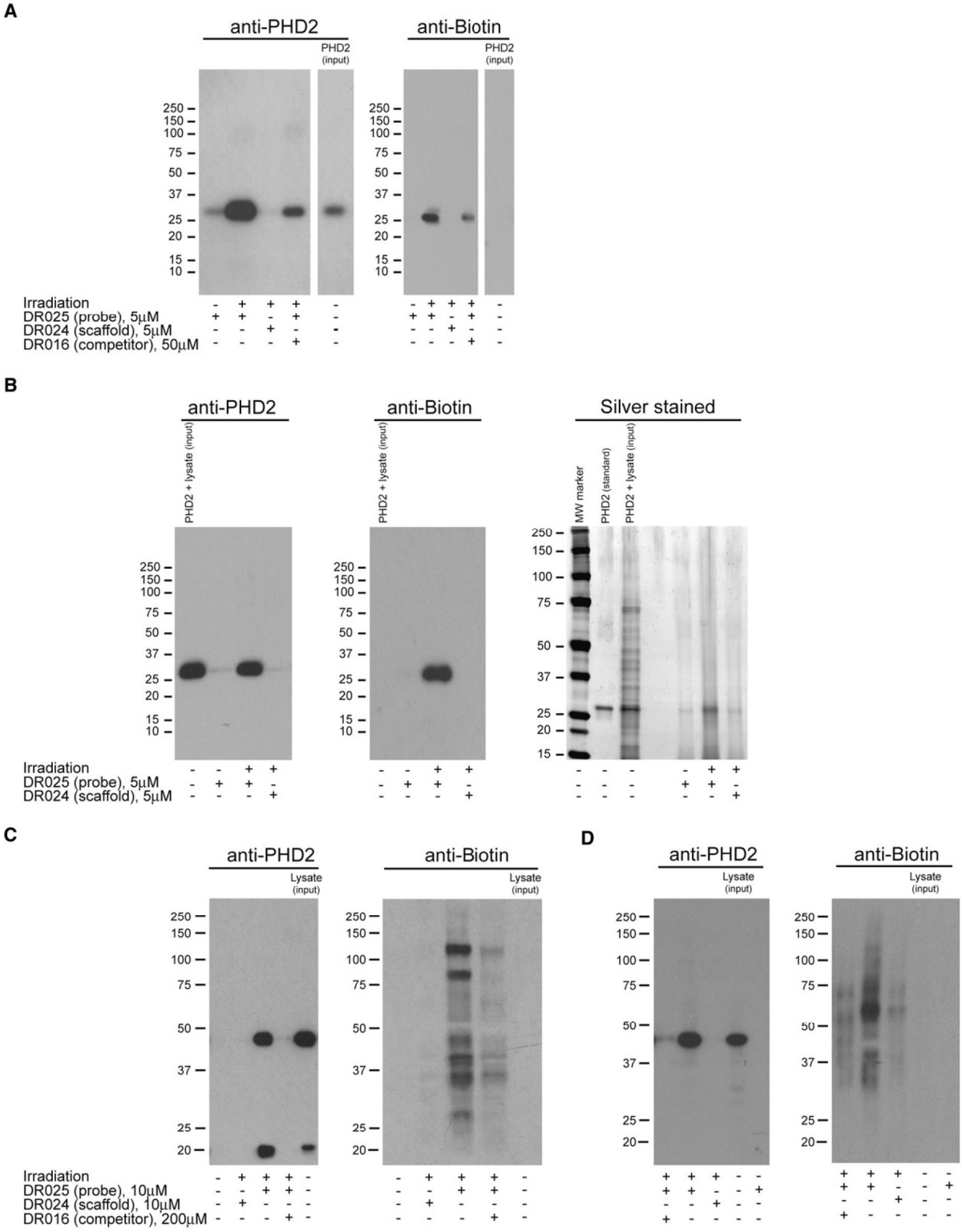

Figure 3. Photoaffinity Labeling and Enrichment of Purified and Endogenous Human PHD2 by DR025

(A) Western blot analysis of the capture of purified $PHD2_{181–426}$ by DR025. $PHD2_{181–426}$ (5 μM, 5.2 μg) and DR025 (5 μM) were incubated in the presence of Mn(II) (5 μM) at room temperature. After irradiation and purification by streptavidin-coated beads, proteins were separated by SDS-PAGE and analyzed by anti-PHD2 (polyclonal antibody from rabbit; left) and anti-biotin (right) immunoblotting. The input purified $PHD2_{181–426}$ was ~4% of the protein corresponding to the other lanes. For an analogous experiment with JMJD2E, see Figure S3A.

 ©2011 Elsevier Ltd All rights reserved

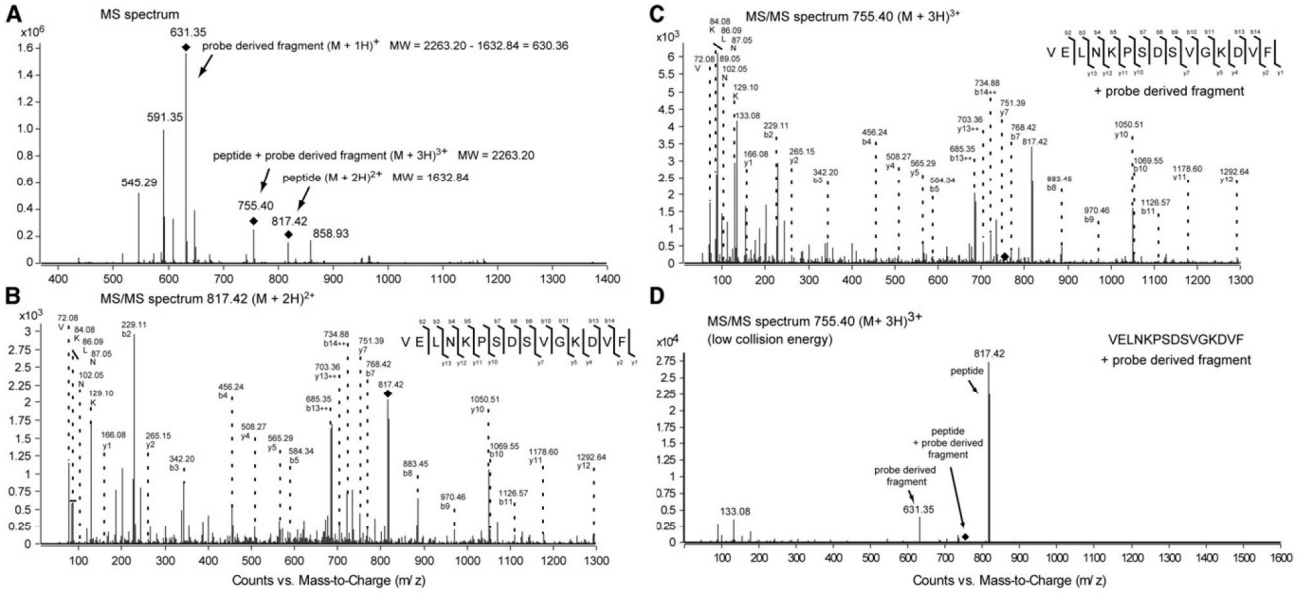

Figure 4. Identification by MS of the PHD2 Peptide Sequence Covalently Crosslinked by the Probe

(A) MS spectrum of $PHD2_{181–426}$ covalently crosslinked by DR025. $PHD2_{181–426}$ (5 μM), Mn(II) (5 μM), and DR025 (25 μM) were incubated (45 min, r.t.) in Tris buffer. After irradiation (20 min, 365 nm) and purification by means of streptavidin beads, photocrosslinked $PHD2_{181–426}$ was digested on the beads with trypsin and analyzed by LC-MS/MS.

(B) MS/MS spectrum of the doubly charged precursor ion at m/z = 817.42 Da. The doubly charged precursor ion at m/z = 817.42 Da was identified as the peptide VELNKPSDSVGKDVF, which represents the C-terminal region of $PHD2_{181–426}$. The b and y fragment ion series and the detected immonium ions are shown.

(C) MS/MS spectrum of the triply charged precursor ion at m/z = 755.40 Da. The triply charged precursor ion at m/z = 755.40 Da exhibits the same fragmentation pattern as the coeluting precursor at m/z = 817.42 Da with additional ions in the low molecular mass range. The b and y fragment ion series and the detected immonium ions are shown as in (B).

(D) MS/MS spectrum of the triply charged precursor ion at m/z = 755.40 Da with reduced collision energy. Under these conditions, the triply charged precursor loses a singly charged fragment at m/z = 631.35 Da, which generates the doubly charged precursor at m/z = 817.42 Da (MW = 1632.84 Da). For MS/MS spectra in the low molecular range of the precursor ion masses associated with the crosslinked PHD2, see Figure S4.

assignment of the modified amino acid residue. Nonetheless, the results reveal a major site of crosslinking of the probe as the C-terminal region of $PHD2_{411–426}$.

Profiling of 2-OG Oxygenases in Human Cells

We investigated whether DR025 could be used to identify 2-OG oxygenases present in a human cell line (HEK293T cells grown under normoxic conditions) using MS (Wu and MacCoss, 2002). To differentiate between specifically enriched and "nonspecifically" captured proteins (see Table 2 and Experimental Procedures for details), we compared the results obtained from proteomic analyses in labeling experiments using DR025 with controls, including proteomic analyses of the digested input lysate. The identified 2-OG oxygenases were divided into three groups on the basis of the controls: enrichment, possible enrichment, and no enrichment. There was clear evidence for enrichment of PHD2 (Epstein et al., 2001) for two N^{ε}-methyl histone lysyl demethylases, JARID1C (Jensen et al., 2005) and FBXL11(Tsukada et al., 2006), and for the collagen lysyl hydroxylase LH3 (Risteli et al., 2009). These oxygenases were identified only in the labeling experiment with DR025, that is, they were not identified in the DR016 competition control or in the other controls (scaffold DR024 and no irradiation). In the cases of PHD2 and LH3, we did not accrue evidence for them in the input lysate. For two other oxygenases, TET2 (Loenarz and Schofield, 2009) and the N^{ε}-methyl histone lysyl demethylase PHF8 (Yu et al., 2010), we observed evidence for possible enrichment due to their identification when captured by the

(B) Immunoblotting and silver-staining analysis showing capture of purified $PHD2_{181–426}$ by DR025 in HEK293T cell lysates. The anti-PHD2 (polyclonal antibody from rabbit; left), anti-biotin (center), and silver-stained SDS-PAGE gels (right) are relative to an experiment carried out under the same conditions as in (A) but in the presence of HEK293T cell lysates (~43 μg total proteins). The input lysate supplemented with recombinant $PHD2_{181–426}$ was ~4% of the total protein corresponding to the other lanes; the purified $PHD2_{181–426}$ as standard was ~4% of the protein corresponding to the other lanes. For an analogous experiment with JMJD2E, see Figure S3B.

(C) Crosslinking with full-length PHD2 in HEK293T cell lysates overexpressing full-length PHD2. DR025 (10 μM) was incubated (45 min, r.t.) with an HEK293T cell lysate overexpressing human full-length PHD2 (~40 μg total protein). After UV treatment (20 min, 365 nm) and purification by means of avidin-coated agarose beads, proteins released from the beads were analyzed by SDS-PAGE and western blots using anti-PHD2 (monoclonal antibody from mouse; left) and anti-biotin (right) antibodies. The input lysate overexpressing full-length PHD2 was ~2% of the total protein corresponding to the other lanes.

(D) Crosslinking of endogenous full-length PHD2 in HEK293T cell lysates (i.e., not overexpressing PHD2). Conditions are as in (C) but employing HEK293T cell lysates (~200 μg total protein) not overexpressing PHD2. The input lysate was ~3% of the total protein corresponding to the other lanes.

Table 2. 2-OG Oxygenases Identified by DR025 in HEK293T Cell Lysates

		DR025 (Probe)			DR016 (Competition)			DR024 (Scaffold)			No Irradiation			Lysate (Input)			
ID	2-OG Oxygenase	Spectral Counts[b]	Number of Peptides[c]	Coverage (%)[d]	Spectral Counts	Number of Peptides	Coverage (%)	Spectral Counts	Number of Peptides	Coverage (%)	Spectral Counts	Number of Peptides	Coverage (%)	Spectral Counts	Number of Peptides	Coverage (%)	Result[a]
Q9GZT9	PHD2[e]	2	1	4	Absent			Absent			Absent			Absent			E
P41229	JARID1C (KDM5C)	2	2	1	Absent			Absent			Absent			5	5	2	E
Q9Y2K7	FBXL11[e] (KDM2A)	1	1	0.9	Absent			Absent			Absent			8	7	6	E
O60568	LH3	2	1	2	Absent			Absent			Absent			Absent			E
Q6N021	TET2	2	2	1	9	9	4	Absent			Absent			Absent			PE
Q9UPP1	PHF8	2	2	2	11	7	3	Absent			Absent			Absent			PE
Q15652	JMJD1C	5	1	0.6	27	14	5	21	14	5	29	20	8	22	14	7	NE
Q9UGL1	JARID1B (KDM5B)	1	1	1	8	8	6	11	11	7	Absent			6	5	2	NE
O94953	JMJD2B (KDM4B)	4	2	2	18	8	7	Absent			11	8	6	Absent			NE

DR025 (10 μM) was incubated with a whole lysate from HEK293T cells grown under normoxic conditions (~950 μg total protein, 45 min, r.t.). After irradiation (20 min, 365 nm) and purification by avidin-coated agarose beads, trypsin digestion and LC-MS/MS analysis comparison with the human protein database were performed. The columns reflect the following conditions. DR025 (probe), complete experiment in the presence of DR025. No Irradiation, same as DR025 but without UV treatment. DR024 (scaffold), negative control experiment in the presence of scaffold DR024 (10 μM). DR016 (competitor), control experiment with the competitor DR016 (200 μM) in a 20:1 molar ratio with DR025. Lysate, input lysate (5% of the total protein corresponding to the other columns). Note that detection corresponds to the observation of at least one peptide with the correct predicted mass for the identified oxygenases. See also Table S1.

[a] E, enrichment; enzyme not detected in the DR024 and No Irradiation negative controls. PE, possible enrichment; enzyme not detected in the DR024 and No Irradiation negative controls, but detected with the DR016 competitor control. NE, no enrichment; enzyme detected in at least one of the negative controls (DR024 or No Irradiation).

[b] Spectral counts: number of MS/MS spectra identified.

[c] Number of unique peptides identified by MS/MS.

[d] Protein sequence coverage (%).

[e] Confirmed by immunoblotting (Figures 3 and 4).

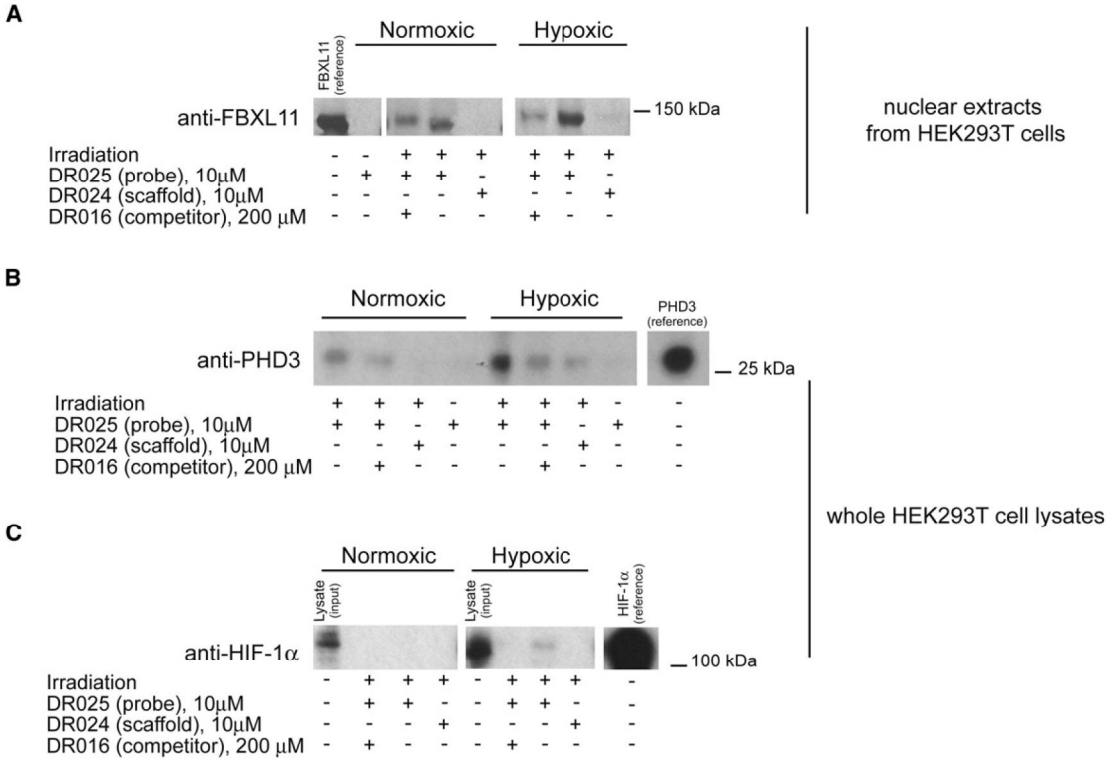

Figure 5. Photoaffinity Crosslinking Experiments in Lysates from HEK293T Cells Grown under Normoxic and Hypoxic Conditions

(A) Crosslinking of endogenous FBXL11 (KDM2A) in nuclear protein extracts of HEK293T cells. DR025 (10 μM) was incubated (45 min, r.t.) with nuclear extracts (~200 μg total protein) of HEK293T cells grown under normoxic (left) and hypoxic (right) conditions. After irradiation (20 min, 365 nm) and purification with streptavidin beads, the proteins released were analyzed by SDS-PAGE and subsequent anti-FBXL11 (polyclonal antibody from rabbit) immunoblotting. The reference protein was a nuclear protein extract of HEK293T cells overexpressing FBXL11 (KDM2A). For the entire immunoblot, see Figure S5A.

(B) Crosslinking of PHD3 at endogenous levels in HEK293T cell lysates. DR025 (10 μM) was incubated (45 min, r.t.) with cell lysates (~200 μg total protein) of HEK293T cells grown under normoxic (left) and hypoxic (right) conditions. After irradiation (20 min, 365 nm) and purification by streptavidin beads, released proteins were analyzed by SDS-PAGE and anti-PHD3 (monoclonal antibody from mouse) immunoblotting. The protein reference was a cell lysate (RCC4) overexpressing PHD3. For the entire immunoblot, see Figure S5B.

(C) Identification of endogenous HIF-1α in HEK293T cell lysates. DR025 (10 μM) was incubated (45 min, r.t.) with a whole lysate (~200 μg total protein) of HEK293T cells grown under normoxic (left) and hypoxic (1% O_2) (right) conditions. After irradiation (20 min, 365 nm) and purification by streptavidin beads, released proteins were analyzed by SDS-PAGE and anti-HIF-1α (monoclonal antibody from mouse) immunoblotting. The input HEK293T lysate was ~3% of the total protein corresponding to the other lanes; the protein reference was a cell lysate (RCC4) overexpressing HIF-1α. For the entire immunoblot, see Figure S5C.

probe (DR025), but both were absent in the scaffold, no irradiation, and input lysate controls. They were, however, observed in the competition (DR016) control experiments, but we cannot rule out the possibility that this is because of incomplete competition. Three 2-OG oxygenases were considered as likely not enriched because they were identified in at least one of the scaffold or no irradiation controls (Table 2).

Overall, the MS results suggest that appropriately functionalized probes can capture and enrich endogenous levels of PHD2 and other 2-OG oxygenases. However, the identified 2-OG oxygenases had a low number of spectral counts relative to background proteins, which is in part due to the fact that these enzymes are not expressed at abundant levels in cells. Hence, to further validate the approach, we employed western blotting to confirm the enrichment of at least one 2-OG oxygenase other than PHD2. We focused our attention on the histone demethylase FBXL11 (KDM2A), an enzyme involved in epigenetic regulation (Tsukada et al., 2006). As shown Figure 5A (see also Figure S5A), western blotting demonstrated that the probe was able to specifically capture FBXL11 in nuclear extracts of HEK293T cells grown under both normoxic conditions and, to a greater extent, hypoxic conditions. The results with FBXL11 are important because they reveal the potential of the method to profile 2-OG oxygenase inhibitors.

To test whether 8-HQ is indeed an inhibitor of FBXL11 (KDM2A), we produced FBXL11 in a recombinant form and carried out tests using an assay that monitors formaldehyde production (see Experimental Procedures). The results revealed inhibition of FBXL11 with IC_{50} values in the micromolar range (IC_{50} = 9.1 μM for DR016 and IC_{50} = 16.7 μM for DR025; Figure S1D), but a lack of inhibition by the scaffold control DR024 (no inhibition at 100 μM). These results reveal the potential of the method for profiling 2-OG oxygenase inhibitors.

Discrimination between Different Levels of PHD3 Expression Depending on Oxygenation Conditions

The finding that FBXL11 (KDM2A) was more efficiently captured by DR025 under hypoxic than normoxic conditions (Figure 5A;

Figure S5A) led us to test the capability of the probe to discriminate between different target protein expression levels under different oxygenation conditions. We chose to analyze PHD3, which is known to be strongly induced by hypoxia in some cell lines (Pescador et al., 2005, Pollard et al., 2008; Appelhoff, et al., 2004). The anti-PHD3 immunoblot in HEK293T whole-cell lysates prepared under normoxic or hypoxic conditions clearly showed that the probe DR025 (or a derivative thereof) is a valid tool to detect the difference of expression between normoxic and reduced oxygenation conditions (Figure 5B; Figure S5B). On the basis of this evidence and studies on the inhibition of histone demethylation by 8-HQ derivatives, DR025 can be proposed as a potentially useful probe to profile different expression levels of 2-OG oxygenases in tissues.

Detection of the 2-OG Oxygenase PHD2 Substrate HIF-1α at Endogenous Levels

Although we cannot rule out the possibility of other sites of crosslinking, the demonstration that the C terminus of PHD2 is involved is interesting because this region interacts with its HIF-α substrate (Chowdhury et al., 2009). The available evidence suggests the extent to which PHD inhibitors block HIF-α substrate binding varies (Chowdhury et al., 2009). We therefore considered whether DR025 might be capable of "capturing" the HIF-α substrate of the PHDs along with the enzymes. As shown by anti-HIF-1α western blotting (Figure 5C; Figure S5C), DR025 is capable of capturing (by an unknown mechanism), albeit not strongly, endogenous levels of HIF-1α in HEK293T cell lysates at least when cultured under hypoxic conditions, where HIF-1α levels are increased relative to normoxic conditions (Figure 5C) (Kaelin and Ratcliffe, 2008).

DISCUSSION

Overall, the results demonstrate the potential of a small-molecule probe-based approach for identifying 2-OG oxygenases in crude cell extracts via photocrosslinking and affinity purification coupled to MS analysis. Importantly, we were able to demonstrate that the probe is able to capture human 2-OG oxygenases in cell extracts at endogenous levels (Figures 3D and 5). Thus, with appropriate development, such as by optimization of the active site binding groups and crosslinking conditions, the photocrosslinking probe method could be used for profiling 2-OG oxygenases from different cell types. This application is potentially useful for (patho)physiological analysis because levels of some 2-OG oxygenases (e.g., JMJD2C and PHD3) vary in diseased and hypoxic cells (Pollard et al., 2008). DR025 showed the capability to discriminate between different levels of expression of PHD3 and, to a lesser extent, of FBXL11 (KDM2A) in lysates from cells (HEK293T) grown under normoxic and hypoxic conditions (Figures 5A and 5B). These results support work showing that some 2-OG oxygenases, including PHD3 and JMJD1A (Pollard et al., 2008), are induced by hypoxia.

Modifications of our lead probe designed to enable cell penetration by introducing postlysis an affinity-purification tag via "click" chemistry or other ligation techniques are possible, as reported in work on probes for proteases (Sadaghiani et al., 2007; Sieber et al., 2006). Although it is unlikely that DR025 itself will be a useful probe for all human 2-OG oxygenases, our results suggest that it may be useful for a significant subset. In principle, the probe approach could also be useful for identifying enzymes from the superfamily not already annotated as 2-OG oxygenases.

Various 2-OG oxygenases are being targeted for therapeutic intervention. γ-butyrobetaine hydroxylase is a target for the clinically used compound mildronate (Liepinsh et al., 2006), and HIF-α hydroxylases and histone demethylases are being explored as targets for anemia/ischemic diseases and cancer, respectively. One application of the probe methodology may be to profile oxygenases that a particular inhibitor/modulator targets inside a cell, including "off-target" interactions of lead compounds. One problem with this approach is that a modification of a "small molecule" with relatively large photocrosslinking/affinity-purification groups will inevitably modify binding characteristics, potentially leading to false-negative results. However, given the high cost of pharmaceutical development, the effort of applying this, or related approaches, to potential leads in order to identify potentially deleterious interactions would seem to be small.

In support of the approach, we found that DR025 crosslinked to the histone demethylase FBXL11 (KDM2A) in HEK293T cell lysates, as initially identified by MS analysis (Table 2) and confirmed by antibody analysis (Figure 5A). We subsequently demonstrated that DR025 and the 8-HQ derivative which acts as a selectivity function (DR016) actually inhibit FBXL11 (KDM2A) to a significant extent (IC_{50} = 16.7 μM for DR025 and IC_{50} = 9.1 μM for DR016). To our knowledge, this is the first reported inhibition study on FBXL11 (KDM2A) and supports the proposal that 8-HQs may be useful generic templates for the inhibition of 2-OG oxygenases (King et al., 2010).

Finally, we note that the photocrosslinking approach may have applications for functional assignment studies of 2-OG oxygenases and other enzymes. Analyses on purified PHD2 after crosslinking and affinity purification with DR025 demonstrate that crosslinking occurs between DR025 and the C-terminal region of $PHD2_{411–426}$ (Figure 4; Figure S4). The C terminus of PHD2 is involved in HIF-α substrate binding (Chowdhury et al., 2009). This suggests that the probe may be useful in "capturing" a substrate from the cell extract. Indeed, western blotting analyses revealed that HIF-1α was purified along with PHD2 at least from whole lysates of HEK293T cells cultured under hypoxic conditions (Figure 5C; Figure S5C), consistent with the reported reduced degradation of HIF-1α under hypoxia. This preliminary evidence of an active site-directed probe capable of identifying endogenous levels of the natural substrate of a target enzyme, on the basis of our knowledge, is one of the first reported to date. As for the crosslinking to PHD2 itself, the mechanism of the apparent crosslinking to HIF-1α is uncertain; however, analysis of a PHD2-substrate structure (Chowdhury et al., 2009) suggests that it is possible that it occurs by crosslinking of the probe with HIF-1α that is simultaneously bound to PHD2. An application of the chemical probe strategy reported here may therefore be to identify (new) substrates for 2-OG oxygenases (or indeed other protein interactors).

SIGNIFICANCE

2-Oxoglutarate (2-OG)-dependent oxygenases catalyze a range of hydroxylation and *N*-methyl demethylation reactions that are important in oxygen sensing and the

epigenetic control of gene expression. These enzymes are being targeted for modulation by small molecules as novel potential therapeutic targets for the treatment of anemia, ischemic diseases, and cancer. We demonstrate that a small-molecule probe-based approach employing photocrosslinking and affinity purification is useful for the identification of 2-OG oxygenases present in human cell extracts and for identifying 2-OG oxygenases that interact with inhibitors. The approach was validated by studies on a transcription factor hydroxylase (PHD2, EGLN1) and by the finding that the probe binds to and inhibits the N^{ε}-methyl lysine histone demethylase FBXL11 (KDM2A). We also demonstrate the potential of this photocrosslinking small-molecule probe-based approach to "capture" the 2-OG oxygenase (PHD2) substrate HIF-1α, suggesting that it may be useful in substrate capture and discovery studies.

EXPERIMENTAL PROCEDURES

Synthesis of Probes

Details of the synthesis of the probes DR014, DR031, and DR025 are given in Supplemental Experimental Procedures, along with analytical data. The PHD2 inhibitor ([1-chloro-4-hydroxyisoquinoline-3-carbonyl]-amino)-acetic acid was synthesized as reported (Stubbs et al., 2009).

Photocrosslinking Experiments

The photocrosslinking procedure is described here for purified $PHD2_{181–426}$ and DR025. For the other purified enzyme, JMJD2E, experiments in the presence of non-2-OG enzymes (Figure S2A), experiments with HEK293T whole-cell lysates as background, and tests in the presence of HEK293T whole-cell lysates or nuclear protein extracts, capture was performed in an analogous manner. $PHD2_{181–426}$ (5 μM) and $MnCl_2$ (5 μM) were incubated with DR025 (25 μM) in Tris buffer (50 mM Tris, 100 mM NaCl [pH 7.4]) with shaking at room temperature (r.t.) (45 min). The samples were then irradiated (20 min) on ice with UV light at 365 nm at an irradiance of 5 mW/cm^2 (Spectrolinker XL-1500). Controls in the presence of the scaffold DR024 or of the competitive inhibitor DR016 were treated in the same way. After exposure to UV light, the samples were either directly analyzed by MALDI-TOF MS or subjected to purification using (strept)avidin-coated beads.

Affinity-Purification Experiments

The complete labeling and enrichment procedure is described here for purified $PHD2_{181–426}$ and the probe (DR025) in the presence of HEK293T cell lysates. In experiments with purified enzymes and in the presence of only HEK293T whole-cell lysates or nuclear protein extracts, the labeling and enrichment processes were performed in an analogous way. $PHD2_{181–426}$ (7.5 μl of 25 μM in Tris buffer solution, final concentration 5 μM) and $MnCl_2$ (1.5 μl of 125 μM in water, final concentration 5 μM) were incubated with DR025 (1.5 μl of 125 μM in water, final concentration 5 μM) in the presence of 27 μl of HEK293T whole-cell lysates (1.6 μg/μl total protein) with shaking at r.t. for 45 min. The scaffold (DR024) control sample was prepared in the same way. The mixture was then UV irradiated as described above, and incubated with streptavidin-coated magnetic beads (50 μl; Dynabeads MyOne Streptavidin C1; Invitrogen) for 30 min at r.t. in a shaker incubator. The beads were collected using a magnetic device (Dynal DynaMag Spin; Invitrogen) and washed five times with washing buffer (10 mM HEPES [pH 7.2], 1 M NaCl, 1% Triton X-100, 2 mM EDTA, 4 mM dithiothreitol) and then three times with water. In other experiments, after the photocrosslinking, the mixtures were incubated with avidin-coated agarose beads (Pierce monomeric avidin agarose; Thermo Scientific). In these cases, the washing was performed with the same buffer but without any device, and the supernatant was removed by pipetting. Beads were stored at −20°C.

In the experiments aimed at labeling and enriching endogenous levels of target proteins, the final concentrations of probe (DR025) and scaffold control (DR024) were 10 μM and the total protein amounts in the HEK293T whole-cell lysates and in the nuclear protein extracts were 200 μg. In the capture experiment carried out on the lysate obtained from HEK293T cells overexpressing PHD2 the total protein amount was 40 μg, whereas in the profiling of the 2-OG oxygenases present in the HEK293T whole-cell lysates the total quantity of proteins was 950 μg per sample in the presence of 10 μM DR025 and DR024. The competition control tests were performed using the competitive inhibitor DR016 (final concentration 10 or 40 times higher than DR025) (see figure legends for details). Negative control experiments were carried out by incubating with DR025 under the same conditions as the "capture" experiments but without irradiation.

SUPPLEMENTAL INFORMATION

Supplemental Information includes Supplemental Experimental Procedures, five figures, and two tables and can be found with this article online at doi:10.1016/j.chembiol.2011.03.007.

ACKNOWLEDGMENTS

C.J.S. was supported by the European Union, The Wellcome Trust, and the Biotechnology and Biological Research Council. B.M.K. and R.F. were supported by the Biomedical Research Centre (NIHR), Oxford, UK and by a grant from Action Medical Research. M.A. was supported by the Swedish Research Council, The Loo and Hans Ostermans Foundation for Geriatric Research, and the Foundation for Geriatric Diseases at Karolinska Institutet. A.W. was a recipient of an EMBO long-term fellowship. A.M. was supported by Fondazione Roma. The nuclear protein extract of HEK293T cells overexpressing FBXL11 (KDM2A) as a protein reference was a kind gift of Dr. Rob Klose. We thank Dr. Oliver King, Dr. Nathan Rose, and Tristan Smart for assistance in recombinant protein production and peptide synthesis.

Received: November 22, 2010
Revised: March 1, 2011
Accepted: March 2, 2011
Published: May 26, 2011

REFERENCES

Appelhoff, R.J., Tian, Y.M., Raval, R.R., Turley, H., Harris, A.L., Pugh, C.W., Ratcliffe, P.J., and Gleadle, J.M. (2004). Differential function of the prolyl hydroxylases PHD1, PHD2, and PHD3 in the regulation of hypoxia-inducible factor. J. Biol. Chem. *279*, 38458–38465.

Chowdhury, R., McDonough, M.A., Mecinovic, J., Loenarz, C., Flashman, E., Hewitson, K.S., Domene, C., and Schofield, C.J. (2009). Structural basis for binding of hypoxia-inducible factor to the oxygen-sensing prolyl hydroxylases. Structure *17*, 981–989.

Epstein, A.C.R., Gleadle, J.M., McNeill, L.A., Hewitson, K.S., O'Rourke, J., Mole, D.R., Mukherji, M., Metzen, E., Wilson, M.I., Dhanda, A., et al. (2001). *C. elegans* EGL-9 and mammalian homologs define a family of dioxygenases that regulate HIF by prolyl hydroxylation. Cell *107*, 43–54.

Evans, M.J., and Cravatt, B.F. (2006). Mechanism-based profiling of enzyme families. Chem. Rev. *106*, 3279–3301.

Fischer, J.J., Graebner (neé Baessler), O.Y., Dalhoff, C., Michaelis, S., Schrey, A.K., Ungewiss, J., Andrich, K., Jeske, D., Kroll, F., Glinski, M., et al. (2010). Comprehensive identification of staurosporine-binding kinases in the hepatocyte cell line HepG2 using capture compound mass spectrometry (CCMS). J. Proteome Res. *9*, 806–817.

Flashman, E., Davies, S.L., Yeoh, K.K., and Schofield, C.J. (2010). Investigating the dependence of the hypoxia-inducible factor hydroxylases (factor inhibiting HIF and prolyl hydroxylase domain 2) on ascorbate and other reducing agents. Biochem. J. *427*, 135–142.

Fleming, S.A. (1995). Chemical reagents in photoaffinity labeling. Tetrahedron *51*, 12479–12520.

Hausinger, R.P. (2004). Fe(II)/α-ketoglutarate-dependent hydroxylases and related enzymes. Crit. Rev. Biochem. Mol. Biol. *39*, 21–68.

Jensen, L.R., Amende, M., Gurok, U., Moser, B., Gimmel, V., Tzschach, A., Janecke, A.R., Tariverdian, G., Chelly, J., Fryns, J.P., et al. (2005). Mutations in the JARID1C gene, which is involved in transcriptional regulation and chromatin remodeling, cause X-linked mental retardation. Am. J. Hum. Genet. *76*, 227–236.

Kaelin, W.G., Jr., and Ratcliffe, P.J. (2008). Oxygen sensing by metazoans: the central role of the HIF hydroxylase pathway. Mol. Cell *30*, 393–402.

Kessler, B.M., Tortorella, D., Altun, M., Kisselev, A.F., Fiebiger, E., Hekking, B.G., Ploegh, H.L., and Overkleeft, H.S. (2001). Extended peptide-based inhibitors efficiently target the proteasome and reveal overlapping specificities of the catalytic β-subunits. Chem. Biol. *8*, 913–929.

King, O.N.F., Li, X.S., Sakurai, M., Kawamura, A., Rose, N.R., Ng, S.S., Quinn, A.M., Rai, G., Mott, B.T., Beswick, P., et al. (2010). Quantitative high-throughput screening identifies 8-hydroxyquinolines as cell-active histone demethylase inhibitors. PLoS One *5*, e15535.

Klose, R.J., and Zhang, Y. (2007). Regulation of histone methylation by demethylimination and demethylation. Nat. Rev. Mol. Cell Biol. *8*, 307–317.

Laumonnier, F., Holbert, S., Ronce, N., Faravelli, F., Lenzner, S., Schwartz, C.E., Lespinasse, J., Van Esch, H., Lacombe, D., Goizet, C., et al. (2005). Mutations in PHF8 are associated with X linked mental retardation and cleft lip/cleft palate. J. Med. Genet. *42*, 780–786.

Leung, I.K.H., Flashman, E., Yeoh, K.K., Schofield, C.J., and Claridge, T.D.W. (2010). Using NMR solvent water relaxation to investigate metalloenzyme-ligand binding interactions. J. Med. Chem. *53*, 867–875.

Liepinsh, E., Vilskersts, R., Loca, D., Kirjanova, O., Pugovichs, O., Kalvinsh, I., and Dambrova, M. (2006). Mildronate, an inhibitor of carnitine biosynthesis, induces an increase in γ-butyrobetaine contents and cardioprotection in isolated rat heart infarction. J. Cardiovasc. Pharmacol. *48*, 314–319.

Loenarz, C., and Schofield, C.J. (2008). Expanding chemical biology of 2-oxoglutarate oxygenases. Nat. Chem. Biol. *4*, 152–156.

Loenarz, C., and Schofield, C.J. (2009). Oxygenase catalyzed 5-methylcytosine hydroxylation. Chem. Biol. *16*, 580–583.

McDonough, M.A., McNeill, L.A., Tilliet, M., Papamicael, C.A., Chen, Q.-Y., Banerji, B., Hewitson, K.S., and Schofield, C.J. (2005). Selective inhibition of factor inhibiting hypoxia-inducible factor. J. Am. Chem. Soc. *127*, 7680–7681.

McNeill, L.A., Flashman, E., Buck, M.R.G., Hewitson, K.S., Clifton, I.J., Jeschke, G., Claridge, T.D.W., Ehrismann, D., Oldham, N.J., and Schofield, C.J. (2005). Hypoxia-inducible factor prolyl hydroxylase 2 has a high affinity for ferrous iron and 2-oxoglutarate. Mol. Biosyst. *1*, 321–324.

Nagel, S., Talbot, N.P., Mecinovic, J., Smith, T.G., Buchan, A.M., and Schofield, C.J. (2010). Therapeutic manipulation of the HIF hydroxylases. Antioxid. Redox Signal. *12*, 481–501.

Pescador, N., Cuevas, Y., Naranjo, S., Alcaide, M., Villar, D., Landazuri, M.O., and Del Peso, L. (2005). Identification of a functional hypoxia-responsive element that regulates the expression of the egl nine homologue 3 (egln3/phd3) gene. Biochem. J. *390*, 189–197.

Pollard, P.J., Loenarz, C., Mole, D.R., McDonough, M.A., Gleadle, J.M., Schofield, C.J., and Ratcliffe, P.J. (2008). Regulation of Jumonji-domain-containing histone demethylases by hypoxia-inducible factor (HIF)-1α. Biochem. J. *416*, 387–394.

Risteli, M., Ruotsalainen, H., Salo, A.M., Sormunen, R., Sipilä, L., Baker, N.L., Lamandé, S.R., Vimpari-Kauppinen, L., and Myllylä, R. (2009). Reduction of lysyl hydroxylase 3 causes deleterious changes in the deposition and organization of extracellular matrix. J. Biol. Chem. *284*, 28204–28211.

Rose, N.R., Ng, S.S., Mecinovic, J., Lienard, B.M., Bello, S.H., Sun, Z., McDonough, M.A., Oppermann, U., and Schofield, C.J. (2008). Inhibitor scaffolds for 2-oxoglutarate-dependent histone lysine demethylases. J. Med. Chem. *51*, 7053–7056.

Rose, N.R., Woon, E.C.Y., Kingham, G.L., King, O.N.F., Mecinovic, J., Clifton, I.J., Ng, S.S., Talib-Hardy, J., Oppermann, U., McDonough, M.A., et al. (2010). Selective inhibitors of the JMJD2 histone demethylases: combined nondenaturing mass spectrometry screening and crystallographic approaches. J. Med. Chem. *53*, 1810–1818.

Sadaghiani, A.M., Verhelst, S.H.L., and Bogyo, M. (2007). Tagging and detection strategies for activity-based proteomics. Curr. Opin. Chem. Biol. *11*, 20–28.

Salisbury, C.M., and Cravatt, B.F. (2008). Optimization of activity-based probes for proteomic profiling of histone deacetylase complexes. J. Am. Chem. Soc. *130*, 2184–2194.

Sieber, S.A., Niessen, S., Hoover, H.S., and Cravatt, B.F. (2006). Proteomic profiling of metalloprotease activities with cocktails of active-site probes. Nat. Chem. Biol. *2*, 274–281.

Smirnova, N.A., Rakhman, I., Moroz, N., Basso, M., Payappilly, J., Kazakov, S., Hernandez-Guzman, F., Gaisina, I.N., Kozikowski, A.P., Ratan, R.R., et al. (2010). Utilization of an in vivo reporter for high throughput identification of branched small molecule regulators of hypoxic adaptation. Chem. Biol. *17*, 380–391.

Spannhoff, A., Hauser, A.T., Heinke, R., Sippl, W., and Jung, M. (2009). The emerging therapeutic potential of histone methyltransferase and demethylase inhibitors. ChemMedChem *4*, 1568–1582.

Stubbs, C.J., Loenarz, C., Mecinovic, J., Yeoh, K.K., Hindley, N., Lienard, B.M., Sobott, F., Schofield, C.J., and Flashman, E. (2009). Application of a proteolysis/mass spectrometry method for investigating the effects of inhibitors on hydroxylase structure. J. Med. Chem. *52*, 2799–2805.

Tsukada, Y., Fang, J., Erdjument-Bromage, H., Warren, M.E., Borchers, C.H., Tempst, P., and Zhang, Y. (2006). Histone demethylation by a family of JmjC domain-containing proteins. Nature *439*, 811–816.

Warshakoon, N.C., Wu, S., Boyer, A., Kawamoto, R., Sheville, J., Renock, S., Xu, K., Pokross, M., Zhou, S., Winter, C., et al. (2006). Structure-based design, synthesis, and SAR evaluation of a new series of 8-hydroxyquinolines as HIF-1α prolyl hydroxylase inhibitors. Bioorg. Med. Chem. Lett. *16*, 5517–5522.

Wu, C.C., and MacCoss, M.J. (2002). Shotgun proteomics: tools for the analysis of complex biological systems. Curr. Opin. Mol. Ther. *4*, 242–250.

Xu, C., Soragni, E., Chou, C.J., Herman, D., Plasterer, H.L., Rusche, J.R., and Gottesfeld, J.M. (2009). Chemical probes identify a role for histone deacetylase 3 in Friedreich's ataxia gene silencing. Chem. Biol. *16*, 980–989.

Yu, L., Wang, Y., Huang, S., Wang, J., Deng, Z., Zhang, Q., Wu, W., Zhang, X., Liu, Z., Gong, W., et al. (2010). Structural insights into a novel histone demethylase PHF8. Cell Res. *20*, 166–173.

 ©2011 Elsevier Ltd All rights reserved

MedChemComm

Dynamic Article Links

Cite this: *Med. Chem. Commun.*, 2011, **2**, 390

www.rsc.org/medchemcomm

CONCISE ARTICLE

An approach to enzyme inhibition employing reversible boronate ester formation†

Ivanhoe K. H. Leung,‡ Tom Brown Jr,‡ Christopher J. Schofield* and Timothy D. W. Claridge*

Received 17th January 2011, Accepted 15th February 2011
DOI: 10.1039/c1md00011j

Dynamic combinatorial chemistry (DCC) is a potentially useful method for the identification of biomacromolecule ligands; however, the number of reactions applicable to DCC in aqueous solution is limited. We report studies that investigate the reversible reaction of boronic acids with alcohols as an approach to enzyme inhibition, employing α-chymotrypsin as a model system. NMR techniques (^{11}B NMR and ^{1}H waterLOGSY) were used to observe ternary complexes of boronic acids, sugars and α-chymotrypsin, and were useful for distinguishing preferentially binding combinations of boronic acids and sugars. The results reveal that both the propensity of boronate ester formation in solution and affinity of the boronate ester for the target enzyme determine whether ternary complex formation is observed. The results also provide proof of principle for the boronate ester approach to DCC *versus* protein targets.

Introduction

The electrophilic nature of boronic acids has been exploited for the inhibition of enzymes containing nucleophilic active site residues, including serine proteases, proteasomes and serine β-lactamases.[1,2] Boronic acids can react reversibly with an active site nucleophile to form a tetrahedral complex which can act as an analogue of the tetrahedral intermediates in catalysis.[2] Boronic acids, and the tetrahedral ions formed by their reaction with water, also react with alcohols to form boronate esters. In aqueous solution at neutral pH the reactions of boronic acids with alcohols, including diols, are reversible (ESI Figure S1†),[3] with the equilibrium position dependent upon on the pK_a values of the boronic acid and the alcohol.[4] The structure of the alcohol can also be important, with diols that are conformationally locked in a *syn*-periplanar arrangement, as in some furanoses, forming more stable complexes.[4]

The generation of libraries of new molecules formed by the reversible reaction of relatively simple components is an emerging tool for the generation of novel protein ligands that may, for example, be used as leads for the generation of potent and selective enzyme inhibitors. When large numbers of compounds are generated and screened, this method is referred to as dynamic combinatorial chemistry (DCC). Various reversible reactions have been used for generating protein ligands in aqueous solution including thiol-disulfide exchange and addition-elimination reactions including carbonyl groups (for reviews, see ref. 5). However, the development of appropriate reversible reactions in the context of pharmaceutical applications can be challenging because they must occur in aqueous solution under conditions that remain compatible with biomacromolecules. The analysis of ligand binding in DCC experiments involving biomacromolecules is also not always straightforward. Although indirect methods involving library analysis have been developed,[5] the reversible nature of DCC reactions means that direct analyses on the target biomacromolecule are attractive. Biophysical techniques including mass spectrometry[6] and X-ray crystallography[7] have been applied to study such interactions with target enzymes. NMR spectroscopy may also be used to monitor such interactions[8] and has been applied to study binding interactions in systems based on hemithioacetal formation.[9,10]

We reasoned that reversible boronate ester formation may represent a suitable class of reaction for the development of protein ligands or enzyme inhibitors. Evidence for this proposal comes from reports that the addition of specific diols/sugars, such as D-fructose (ESI Figure S2†), can improve the potency of inhibition of nucleophilic enzymes by boronic acids.[11] Here we report on NMR-based investigations into reversible boronate ester formation and its application to enzyme inhibition using the serine protease α-chymotrypsin (αCT) as a model system.

Results and discussion

Initial experiments were undertaken to observe ternary enzyme-boronic acid-sugar complex formation by NMR spectroscopy. 1-Benzothiophen-2-ylboronic acid (**1**) (Fig. 1) is an inhibitor of

Department of Chemistry, University of Oxford, Chemistry Research Laboratory, 12 Mansfield Road, Oxford, OX1 3TA, United Kingdom. E-mail: christopher.schofield@chem.ox.ac.uk; tim.claridge@chem.ox.ac.uk; Fax: +44 (0)1865 285 002; Tel: +44 (0)1865 285 000

† Electronic supplementary information (ESI) available. See DOI: 10.1039/c1md00011j

‡ These authors made equal contributions to the work.

This journal is © The Royal Society of Chemistry 2011

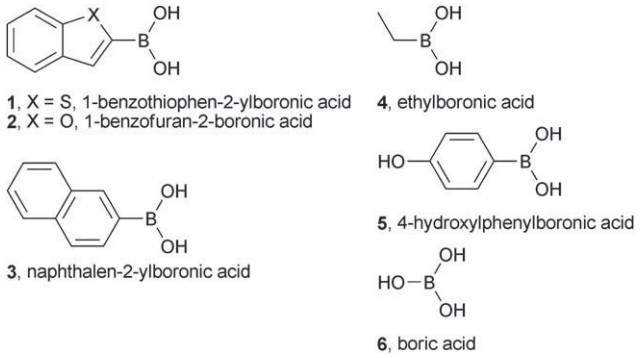

Fig. 1 Structures of the boronic acids used in this study.

some serine proteases (IC_{50} for αCT = 5 μM) and serine β-lactamases (IC_{50} for the AmpC serine β-lactamase = 27 nM),[12] and was therefore used as a model boronic acid. Boronic acids form covalent complexes with serine proteases, and ^{11}B NMR is a useful technique for the direct observation of the free and protein bound boron-species.[13] ^{11}B is quadrupolar ($I = 3/2$) and this property can be exploited to probe the hybridisation state of the boron atom.[14] In NMR analyses, broad peaks are often observed if the ^{11}B nucleus is in a sp^2-hybridised trigonal planar environment, whereas relatively sharper peaks are often observed for the ^{11}B nucleus in the more highly symmetrical sp^3-hybridised tetrahedral environment;[14] The slow rotational correlation time associated with protein-boronic acid/boronate ester complexes may further contribute to line-narrowing.[15]

The pK_a of **1** (corresponding to $RB(OH)_2 + H_2O \rightleftharpoons RB(OH)_3^- + H^+$) was found to be ~7.4 (ESI Figure S3†), therefore initial experiments were conducted at pH 5.8 to ensure the free boronic acid was predominantly in the sp^2-hybridised form (ESI Figure S4a†: peak A; 26.4 ppm; linewidth >300 Hz). Upon addition of D-fructose to **1**, the ^{11}B signal was sharpened and was shifted to lower ppm, indicating the formation of a tetrahedral, sp^3 hybridised boronate ester species (ESI Figure S4b†: peak B; 6.72 ppm; linewidth ~190 Hz). A similar peak sharpening and shift was observed when αCT was added to **1** at pH 5.8 to form a binary αCT-**1** complex (ESI Figure S4c†: peak D; 2.35 ppm; linewidth ~90 Hz), suggesting that the boronic acid is in a tetrahedral boronate form when bound to αCT. The addition of D-fructose to the αCT-**1** binary complex further sharpened and shifted the ^{11}B signal (ESI Figure S4d†: peak C; 6.47 ppm; linewidth ~60 Hz), consistent with the formation of a ternary αCT-**1**-D-fructose complex in which the αCT-bound ^{11}B nucleus is in an sp^3-hydribised tetrahedral environment. These results support previous studies employing kinetic and X-ray crystallographic analyses[11,16] providing evidence for the formation of ternary boronic acid-sugar complexes with nucleophilic enzymes.

In screening experiments employing reversible boronate ester formation, the distribution of boronate esters reflects their respective thermodynamic stabilities. When a mixture of boronic acids and diols is exposed to an external influence, such as the presence of a protein, the equilibrium shifts and those components (*i.e.* boronate esters) that interact with the template are stabilized. Using ^{11}B NMR, we observed that the presence of αCT appeared to move the equilibrium towards the formation of the **1**-D-fructose boronate ester. Thus, in the absence of αCT, ~140 mM D-fructose was required to observe the formation of **1**-D-fructose boronate ester, but in the presence of 1 mM αCT, only ~2 mM D-fructose was required (Fig. 2). Analogous changes to the equilibrium position have been observed by NMR in

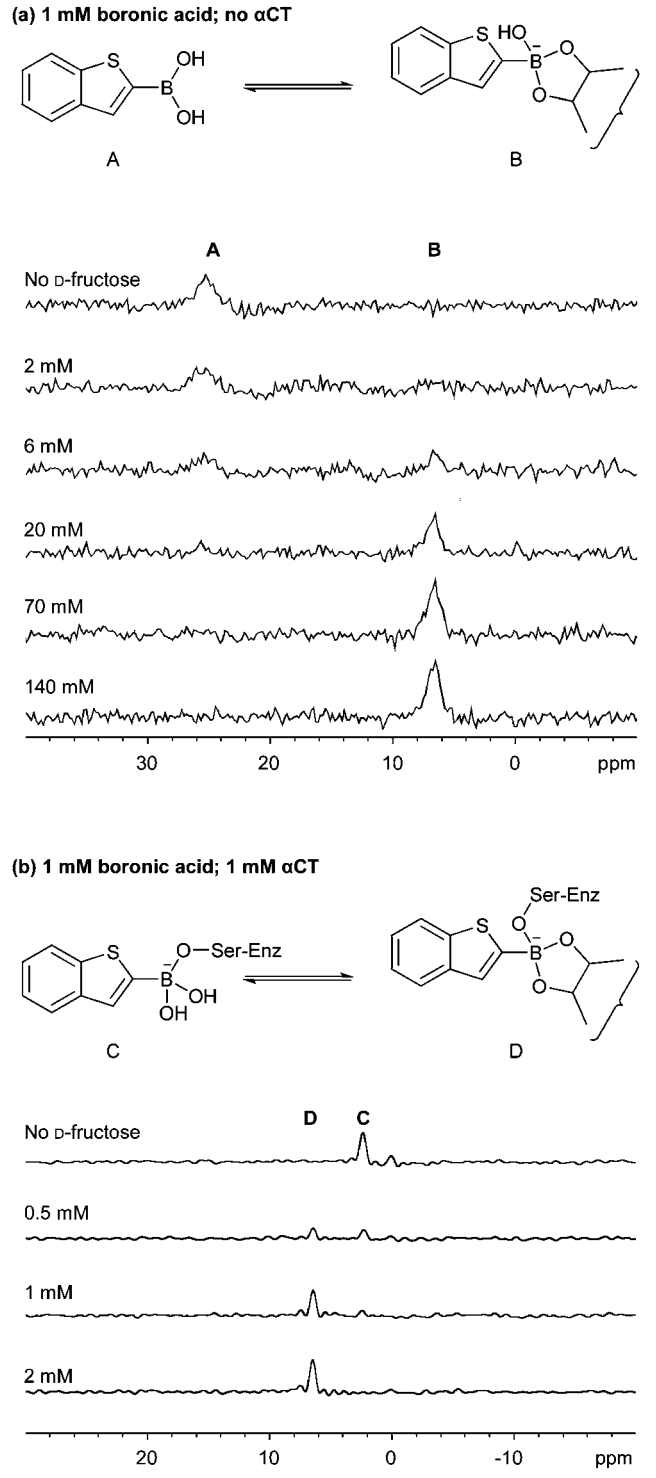

Fig. 2 The presence of αCT moves the equilibrium position towards the formation of the 1-D-fructose boronate ester. ^{11}B NMR spectra of (a) the addition of D-fructose to boronic acid **1** and (b) the addition of D-fructose to boronic acid **1** in the presence of one equivalent of α-CT.

a dynamic compound library system involving hemithioacetal formation with *Mycobacterium tuberculosis* pantothenate synthetase.[9]

In subsequent experiments we investigated the correlation between αCT inhibition and boronate ester binding. Sugars, including D-fructose, on their own do not bind to αCT to any significant extent as observed by ligand based NMR analyses (data not shown). It has been proposed[11] that the efficacy of sugars in increasing the inhibitory effect of boronic acids depends on both: (i) the propensity of the boronate ester to form in solution and (ii) the affinity of the boronate ester complex for the enzyme. We found that only D-fructose improved substantially the inhibitory effect of **1** (78 ± 2.4% activity, relative to that in the absence of sugar), with D-glucose (97 ± 4.8%), L-glucose (94 ± 3.5%) and L-fructose (97 ± 0.6%) having little effect. These results imply selectivity in the formation of ternary αCT-boronic acid-sugar complexes. The affinities of these same sugars for **1** were determined by conducting a series of titrations monitored by ^{1}H and ^{11}B NMR. The affinities of D-fructose and L-fructose for **1** were similar (K_A = ~52 M), but those of D-glucose and L-glucose were weaker (K_A = <2 M) (ESI Figure S5†), consistent with previous studies on the reaction of phenylboronic acid with polyols.[17] These data further suggest that the more potent inhibition observed in the presence of D-fructose relative to L-fructose results from more efficient recognition by αCT of either D-fructose or of the D-fructose-boronate ester complex. In accordance with this, we found that D-fructose readily forms a ternary αCT-**1**-fructose complex, whereas use of L-fructose resulted in the formation of only a small amount of a ternary complex under similar conditions (Fig. 3). Titrations revealed that at least 30 times more L-fructose (than D-fructose) was required to fully form the ternary αCT-**1**-fructose complex (Fig. 3). We also observed stereoselectivity for boronate ester formation in the case of αCT-**1** and L-/D-sorbose (ESI Figure S2†), in which case the αCT-**1**-L-sorbose complex is preferentially formed over the αCT-**1**-D-sorbose complex (ESI Figure S6†). The relative increase in potency observed for D-fructose over (both D- and L-) glucose may reflect, at least in part, the higher affinity of D-fructose for boronic acids in solution. This follows from the increased population (~25% of the total) of the β-furanose form in which the C-1 and C-2 hydroxyl groups are in a *syn*-periplanar arrangement for D- (and L-) fructose, compared to the ~0.1% of the α-furanose form present in (both D- and L-) glucose solution.[18]

Further investigations revealed the selectivity of the αCT active site for particular boronic acids. 1-Benzofuran-2-boronic acid (**2**) (Fig. 1), the oxygen analogue of boronic acid **1**, is also an inhibitor of serine proteases (IC_{50} for αCT = 14 μM) and serine β-lactamases (IC_{50} for AmpC β-lactamase = 220 nM).[12] It has a similar pK_a value to **1** (pK_a ~ 7.3, ESI Figure S3†) and both **1** and **2** are equally reactive to boronate ester formation in solution as demonstrated by NMR analyses (ESI S5†). ^{11}B NMR was used to monitor the interaction of αCT with boronic acids **1** and **2** in the presence and absence of sugars (Fig. 4a and ESI Figure S7†). Addition of D-fructose revealed the preferential formation of the αCT-**1**-D-fructose over the αCT-**2**-D-fructose ternary complex, demonstrating subtle active site selectivity and illustrating the potential of this technique to analyse equilibrium mixtures.

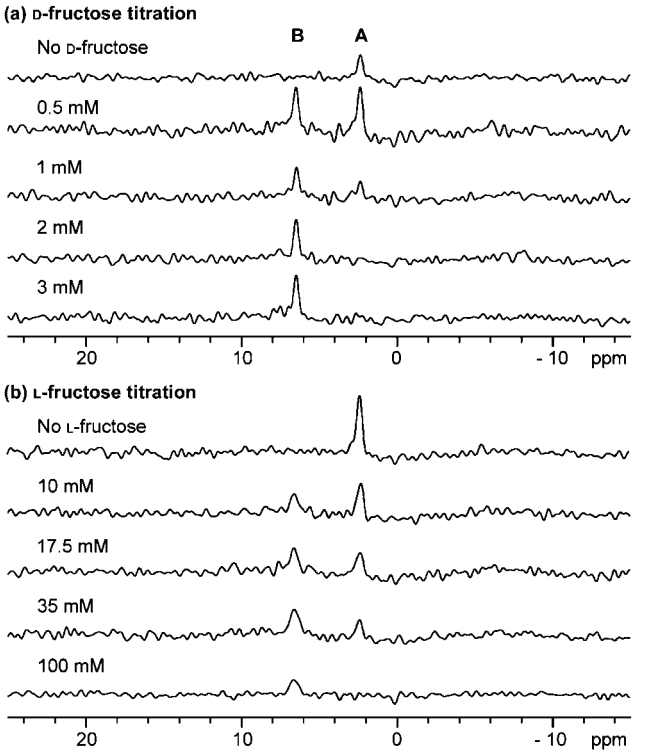

Fig. 3 Formation of an αCT-**1**-fructose ternary complex as monitored by ^{11}B NMR. The formation of a ternary enzyme–boronic acid–sugar complex on titration of (a) D-fructose and (b) L-fructose (at the concentrations shown) into a mixture of **1** (1 mM) and αCT (1.3 mM). Peak A is the αCT-**1** binary complex and peak B is the αCT-**1**-fructose ternary complex.

A particular requirement for the use of boronic acids as templates in the development of protein ligands or enzyme inhibitors is that they readily form boronate esters under the solution conditions appropriate to the target enzyme. The dynamics of boronate ester formation depends upon the structure and pK_a of the boronic acid, and the solution pH (ESI Figure S1†). For instance, the pK_a of naphthalen-2-ylboronic acid (**3**) (Fig. 1) is ~8.8 (ESI Figure S3†) and at pH 5.8, a ~1 : 500 **3**/D-fructose ratio was required to form 50% of the **3**-D-fructose boronate ester complex (compared to 1 : 6 for **1**); at pH 7.0 this was reduced to ~1 : 50, and at pH 8.0, ~1 : 10 (as determined by ^{1}H and ^{11}B NMR, ESI Figure S8†). Thus, in addition to the selection of suitable chelating alcohols, the properties of the boronic acid should be appropriate for boronate ester formation to enable assessment of any enhanced inhibitory potency. To demonstrate the dependencies on pK_as and to investigate the utility of NMR for the screening of a set of simple boronic acids, we selected four structurally different boronic acids including **1**, ethylboronic acid (**4**), 4-hydroxyphenylboronic acid (**5**), and boric acid (**6**) (Fig. 1), and monitored the formation of ternary enzyme-boronic acid-sugar complexes by ^{11}B NMR at pH 5.8 in the presence and absence of sugars (Fig. 5). Upon addition of αCT to the mixture of bor(on)ic acids (without sugar), boronic acid **1** was identified as the only compound leading to an observable complex with αCT. Addition of D-fructose revealed the formation of a αCT-**1**-D-fructose ternary complex. These results suggest that αCT binds

This journal is © The Royal Society of Chemistry 2011

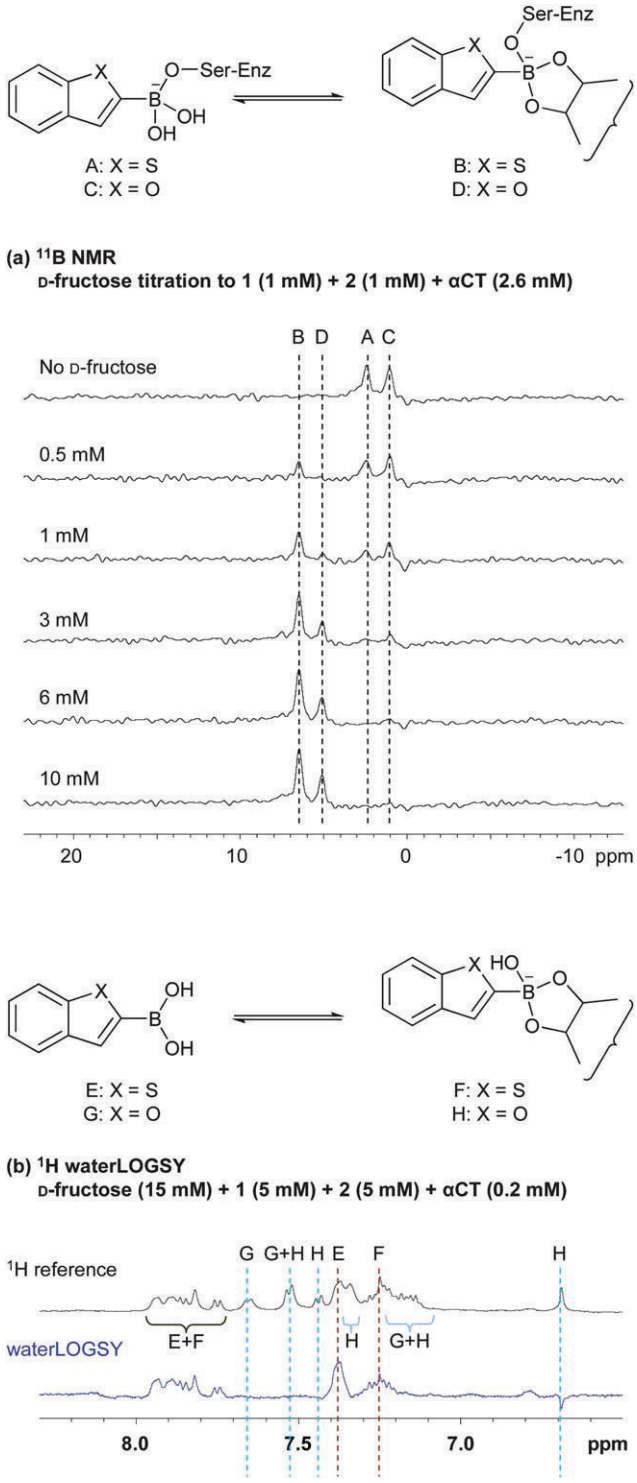

Fig. 4 αCT preferentially binds to **1** and **1**-D-fructose boronate ester, as shown by (a) ^{11}B NMR: (Peak A: αCT-**1** binary complex; Peak B: αCT-**1**-D-fructose ternary complex; Peak C: αCT-**2** binary complex; Peak D: αCT-**2**-D-fructose ternary complex), and (b) ^{1}H waterLOGSY analyses: (Peak E: **1**; Peak F: **1**-D-fructose boronate ester; Peak G: **2**; Peak H: **2**-D-fructose boronate ester).

preferentially with **1** out of the tested mixture of boronic acids, and, in support of the previous inhibition analyses, further demonstrate the preferential binding of **1** with D-fructose. In part

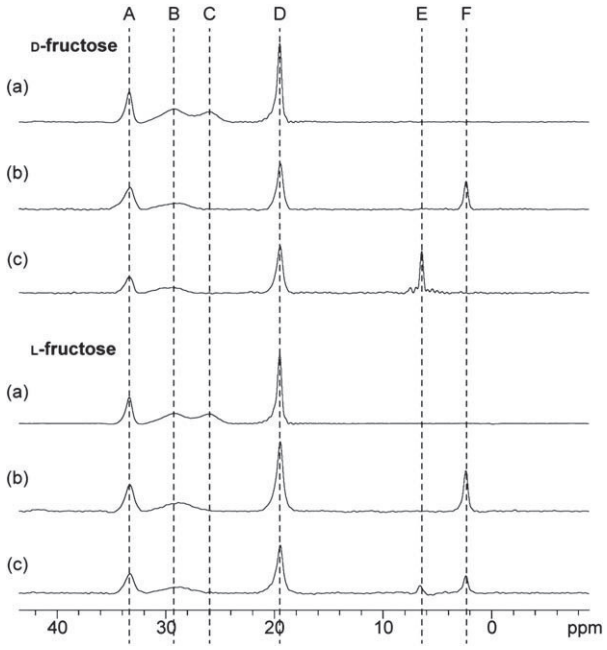

Fig. 5 Equilibrium mixture analysis by ^{11}B NMR: (a) boronic acids only; (b) boronic acids + αCT; (c) boronic acids + αCT + D/L-fructose. Assays included the following bor(on)ic acids (at 2 mM concentration each): **1** (peak C), **4** (peak A), **5** (peak B), **6** (peak D). Addition of αCT (~2 mM) led to the selective formation of a binary enzyme-boronic acid complex with **1** (peak F). Addition of fructose (12 mM) leads to the selective formation of a ternary αCT-boronic acid-fructose complex with **1** (peak E). Addition of D-fructose gives full conversion to the ternary αCT-**1**-D-fructose complex whilst <50% conversion is observed for L-fructose.

this selectivity likely reflects the low efficacy of **4**, **5** and **6** in forming boronate esters at pH 5.8 due to their pK_a values (typically 10–12 for alkylboronic acids) and, in the case of **5**, the electron-donating nature of its 4-hydroxyphenyl substituent.

Whilst the use of reversible boronate ester formation shows potential for the development of inhibitors of greater affinity, it is apparent that the use of ^{11}B NMR spectroscopy is likely not an optimal general method for screening in most cases. Whilst enabling the direct observation of the ternary boronate-enzyme complexes, ^{11}B NMR resonances are broad, owing to the quadrupolar ^{11}B nucleus,[14] meaning boronic acids with similar structures often cannot be distinguished owing to signal overlap. In addition, high concentrations of boronic acids and protein are necessary to compensate for the relatively low sensitivity of ^{11}B NMR. Alternatively, ^{1}H-based screening techniques such as waterLOGSY (water-ligand observed *via* gradient spectroscopy)[19] offer superior resolution and sensitivity and may represent a more attractive NMR methodology. Furthermore, waterLOGSY employs observation of the free ligand, and has the further benefit of requiring relatively small amounts of protein. We therefore investigated the use of waterLOGSY for detection of binding of boronate esters/boronic acids to αCT. As in the previous ^{11}B experiment, the boronic acid pair **1** and **2** was used to investigate waterLOGSY screening at pH 5.8. A slight excess of D-fructose was used to ensure the formation of some boronate ester species. In agreement with the ^{11}B NMR experiments, the waterLOGSY analyses revealed that αCT

preferentially selects **1**-D-fructose boronate ester over the **2**-D-fructose boronate ester (Fig. 4b and ESI Figure S9†). In contrast, no selectivity was observed in the equivalent waterLOGSY experiment with L-fructose; Presumably all four components (**1**, **1**-L-fructose, **2** and **2**-L-fructose) bind weakly to αCT (ESI Figure S10†).

Conclusions

Overall, the results of our work validate the potential of the reversible reaction of boronic acids with alcohols to produce boronate esters for exploring active site ligand interactions. In the presence of a target protein, the most favourable combination of boronic acids and sugars that combine to give a ternary enzyme-bound complex can be identified by NMR analyses. The observation of selective complex formation provides leads for further biophysical analysis involving, for example, protein crystallography and/or the development of stable analogues, as employed in DCC approaches.[5,20] The model enzyme that we used, αCT, possess a nucleophilic serine residue at its active site, enabling reversible formation of a ternary protein-ligand complex that has been monitored by NMR. It is important to note, however, that the observation of a ternary complex depends not only on the affinity of the boronate ester for the target protein, but also on the propensity of the boronate ester to form in solution, which in turn is dependent upon the pK_a of the boronic acid and on solution pH.

The development of efficient methods for the screening of members of a DCC library that bind to a target macromolecule can be challenging. We have shown that ^{11}B NMR and ^{1}H waterLOGSY can be used to monitor the formation of ternary enzyme-boronate ester complexes. ^{11}B NMR allows direct detection of the protein-bound boronic acids and, despite suffering from low intrinsic sensitivity and broad resonances (ESI Figures S1 and S4†), ^{11}B NMR is sensitive to the local ^{11}B environment, is free from protein background signals and is useful for distinguishing free and bound species. ^{1}H based techniques such as waterLOGSY have superior sensitivity but may be limited by the exchange kinetics of the reversibly forming protein-ligand complex and remain prone to signal overlap from large compound libraries.

In our study the enhanced inhibition of αCT by boronic acids in the presence of D-fructose in particular was shown to correlate with greater stability of the enzyme-boronate ester ternary complex. The relative lack of enhanced inhibition in the presence of L-fructose likewise correlates with a significantly lower propensity for the ternary complex to form with this stereoisomer, despite similar affinities for the formation of the binary boronate ester complexes for both D- and L- fructose in the absence of αCT.

Finally we note that the dynamic nature of the boronic acid-ester interconversions suggests that reversible reactions including boronic acids may be useful for the development of dynamic combinatorial libraries of potential inhibitors. Various reversible reactions have been used in the context of dynamic combinatorial chemistry and related approaches to enzyme inhibition, including thiol-disulfide exchange and addition-elimination reactions involving carbonyl groups.[5] Provided suitable methods for library screening can be developed, the boronic acid template may become another scaffold for protein-ligand investigations utilising dynamic combinatorial chemistry.

Experimental

Materials

Chemicals were purchased from Sigma-Aldrich or Alfa Aesar, with the exceptions of Tris-D_{11} (Cambridge Isotope Laboratories), and D_2O (Apollo Scientific). αCT was purchased as lyophilized powder (from bovine pancreas, Type II, ≥40 units/mg protein).

Inhibition assay

The hydrolysis of succinyl-Ala-Ala-Pro-Phe-*para*-nitroanilide was monitored by measuring the increase in absorbance at 405 nm as a function of time. The temperature was kept constant at 25 °C. Measurements were performed using an Envision microplate reader (Perkin-Elmer, Waltham, MA, USA) and using 96-well plates (Corning, Lowell, MA, USA). Assays were started by adding substrate to either enzyme or a mixture of enzyme and inhibitor (in either case incubated at 25 °C for 10 min). The contents of each well were mixed manually using a multi-channel pipette (Eppendorf, Hamburg, Germany) immediately after adding substrate. Measurements were performed in triplicate. Initial rates were taken by measuring the slope of a line of best fit through the first six data points, which were recorded at 10–20 s intervals. Residual activities were calculated by dividing the initial rate of the reaction in the presence of inhibitor by that in the absence of inhibitor. Activities relative to the activity in the absence of sugar were calculated by dividing the rate of the reaction in the presence of sugar by that in the absence of sugar. Concentrations were as follows: enzyme (5 nM), substrate (100 μM), boronic acid (25 μM), sugar (2.5 mM).

^{11}B NMR experiments

Experiments were conducted at 160 MHz (for ^{11}B) using a Bruker DRX 500 MHz spectrometer equipped with a standard 5 mm broadband probe. Typical experimental parameters were as follows: acquisition time 16 ms, relaxation delay 400 ms, number of scans 4000–16000. The baselines were corrected by spline fit processing or backward linear prediction (28–30 points back predicted and 256 linear prediction coefficients).

^{1}H WaterLOGSY experiments

Experiments were conducted using a Bruker Avance II 500 MHz spectrometer equipped with a 5 mm TXI probe. Typical experimental parameters were as follows: mixing time 1 s, relaxation delay 5 s, number of scans 64. Samples were prepared in 90% H_2O/10% D_2O and solvent excitation was achieved using a 16 ms, 180 degree selective rectangular shape pulse (Squa100.1000) set at the H_2O frequency. Protein background suppression was achieved by a 30 ms spin-lock and water suppression was achieved by the excitation sculpting method using a 2 ms 180 degree selective Squa100.1000 pulse at the H_2O frequency.

This journal is © The Royal Society of Chemistry 2011

Abbreviations

αCT	α-chymotrypsin
DCC	Dynamic Combinatorial Chemistry
waterLOGSY	water-ligand observed *via* gradient spectroscopy.

Acknowledgements

The authors gratefully acknowledge support of this project by the EPSRC and the BBSRC.

Bibliographic references and notes

1 P. C. Trippier and C. McGuigan, *Med. Chem. Commun.*, 2010, **1**, 183–198; W. Yang, X. Gao and B. Wang, *Med. Res. Rev.*, 2003, **23**, 346–368.

2 L. Hedstrom, *Chem. Rev.*, 2002, **102**, 4501–4524; D. A. Matthews, R. A. Alden, J. J. Birktoft, S. T. Freer and J. Kraut, *J. Biol. Chem.*, 1975, **250**, 7120–7126; C. A. Kettner, R. Bone, D. A. Agard and W. W. Bachovchin, *Biochemistry*, 1988, **27**, 7682–7688; W. W. Bachovchin, W. Y. L. Wong, S. Farr-Jones, A. B. Shenvi and C. A. Kettner, *Biochemistry*, 1988, **27**, 7689–7697; V. K. Antonov, T. V. Ivanina, I. V. Berezin and K. Martinek, *FEBS Lett.*, 1970, **7**, 23–25; M. Philipp and M. L. Bender, *Proc. Natl. Acad. Sci. U. S. A.*, 1971, **68**, 478–480; K. A. Koehler and G. E. Lienhard, *Biochemistry*, 1971, **10**, 2477–2483.

3 G. Springsteen and B. H. Wang, *Tetrahedron*, 2002, **58**, 5291–5300; T. D. James, M. D. Phillips and S. Shinkai, in *Boronic Acids in Saccharide Recognition*; RSC Publishing: 2006.

4 J. Yan, G. Springsteen, S. Deeter and B. Wang, *Tetrahedron*, 2004, **60**, 11205–11209.

5 P. T. Corbett, J. Leclaire, L. Vial, K. R. West, J. L. Wietor, J. K. Sanders and S. Otto, *Chem. Rev.*, 2006, **106**, 3652–3711; O. Ramström and J.-M. Lehn, *Nat. Rev. Drug Discovery*, 2002, **1**, 26–36; S. J. Rowan, S. J. Cantrill, G. R. L. Cousins and J. K. M. Sanders, *Angew. Chem., Int. Ed.*, 2002, **41**, 898–952; J.-M. Lehn and A. V. Eliseev, *Science*, 2001, **291**, 2331–2332; G. R. L. Cousins, S. A. Poulsen and J. K. M. Sanders, *Curr. Opin. Chem. Biol.*, 2000, **4**, 270–279; J.-M. Lehn, *Chem.–Eur. J.*, 1999, **5**, 2455–2463; B. Klekota and B. L. Miller, *Trends Biotechnol.*, 1999, **17**, 205–209; M. F. Greaney and V. T. Bhat, in *Dynamic Combinatorial Chemistry: In Drug Discovery, Bioinorganic Chemistry, and Materials Sciences*, ed. B. L. Miller, Wiley, New Jersey, 2010. ch. 2, pp. 43–82.

6 S. A. Poulsen and L. F. Bornaghi, *Bioorg. Med. Chem.*, 2006, **14**, 3275–3284; S. A. Poulsen, *J. Am. Soc. Mass Spectrom.*, 2006, **17**, 1074–1080; R. D. Sussmuth and G. Jung, *J. Chromatogr., Biomed. Appl.*, 1999, **725**, 49–65.

7 M. S. Congreve, D. J. Davis, L. Devine, C. Granata, M. O'Reilly, P. G. Wyatt and H. Jhoti, *Angew. Chem.*, 2003, **115**, 4617–4620; A. M. Davis, S. J. Teague and G. J. Kleywegt, *Angew. Chem., Int. Ed.*, 2003, **42**, 2718–2736.

8 B. Meyer and T. Peters, *Angew. Chem., Int. Ed.*, 2003, **42**, 864–890; M. J. Shapiro and J. R. Wareing, *Curr. Opin. Chem. Biol.*, 1998, **2**, 372–375; H. Kessler, *Angew. Chem., Int. Ed. Engl.*, 1997, **36**, 829–831.

9 D. E. Scott, G. J. Dawes, M. Ando, C. Abell and A. Ciulli, *ChemBioChem*, 2009, **10**, 2772–2779.

10 R. Caraballo, H. Dong, J. P. Ribeiro, J. Jiménez-Barbero and O. Ramström, *Angew. Chem. Int. Ed.*, 2010, **49**, 589–593.

11 H. Suenaga, K. Nakashima and S. Shinkai, *J. Chem. Soc., Chem. Commun.*, 1995, 29–30; H. Suenaga, M. Mikami, H. Yamamoto, T. Harada and S. Shinkai, *J. Chem. Soc., Perkin Trans. 1*, 1995, 1733–1738.

12 G. S. Weston, J. Blázquez, F. Baquero and B. K. Shoichet, *J. Med. Chem.*, 1998, **41**, 4577–4586.

13 S. Zhong, F. Jordan, C. Kettner and L. Polgar, *J. Am. Chem. Soc.*, 1991, **113**, 9429–9435; J. E. Baldwin, T. D. W. Claridge, A. E. Derome, B. D. Smith, M. Twyman and S. G. Waley, *J. Chem. Soc., Chem. Commun.*, 1991, 573–574; J. E. Baldwin, T. D. W. Claridge, A. E. Derome, C. J. Schofield and B. D. Smith, *Bioorg. Med. Chem. Lett.*, 1991, **1**, 9–12.

14 R. R. Gupta and M. D. Lechner, in *Chemical Shifts and Coupling Constants for Boron-11 and Phosphorus-31*, Springer-Verlag: 1997.

15 P. S. Hubbard, *J. Chem. Phys.*, 1970, **53**, 985–987; T. E. Bull, *J. Magn. Reson.*, 1972, **8**, 344–353.

16 T. R. Transue, J. M. Krahn, S. A. Gabel, E. F. DeRose and R. E. London, *Biochemistry*, 2004, **43**, 2829–2839.

17 J. P. Lorand and J. O. Edwards, *J. Org. Chem.*, 1959, **24**, 769–774.

18 P. M. Collins and R. J. Ferrier, in *Monosaccharides: Their Chemistry and their Roles in Natural Products*; Wiley: Chichester, 1995; S. J. Angyal, *Adv. Carbohydr. Chem. Biochem.*, 1984, **42**, 15–68.

19 C. Dalvit, P. Pevarello, M. Tatò, M. Veronesi, A. Vulpetti and M. Sundström, *J. Biomol. NMR*, 2000, **18**, 65–68.

20 R. Caraballo, M. Sakulsombat and O. Ramström, *ChemBioChem*, 2010, **11**, 1600–1606; B. M. R. Liénard, R. Hüting, P. Lassaux, M. Galleni, J.-M. Frère and C. J. Schofield, *J. Med. Chem.*, 2008, **51**, 684–688; B. M. R. Liénard, N. Selevsek, N. J. Oldham and C. J. Schofield, *ChemMedChem*, 2007, **2**, 175–179; N. R. Rose, E. C. Y. Woon, G. L. Kingham, O. N. F. King, J. Mecinović, I. J. Clifton, S. S. Ng, J. Talib-Hardy, U. Oppermann, M. A. McDonough and C. J. Schofield, *J. Med. Chem.*, 2010, **53**, 1810–1818.

EMBO reports

scientific report

The oncometabolite 2-hydroxyglutarate inhibits histone lysine demethylases

Rasheduzzaman Chowdhury[1], Kar Kheng Yeoh[1], Ya-Min Tian[2]*, Lars Hillringhaus[1], Eleanor A. Bagg[1], Nathan R. Rose[1], Ivanhoe K.H. Leung[1], Xuan S. Li[3], Esther C.Y. Woon[1], Ming Yang[1], Michael A. McDonough[1], Oliver N. King[1], Ian J. Clifton[1], Robert J. Klose[3], Timothy D.W. Claridge[1], Peter J. Ratcliffe[2], Christopher J. Schofield[1+] & Akane Kawamura[1++]*

[1]Chemistry Research Laboratory, Department of Chemistry, [2]Henry Wellcome Building for Molecular Physiology, Department of Clinical Medicine, and [3]Epigenetic Regulation of Chromatin Function Group, Department of Biochemistry, University of Oxford, Oxford, UK

Mutations in isocitrate dehydrogenases (IDHs) have a gain-of-function effect leading to *R*(−)-2-hydroxyglutarate (*R*-2HG) accumulation. By using biochemical, structural and cellular assays, we show that either or both *R*- and *S*-2HG inhibit 2-oxoglutarate (2OG)-dependent oxygenases with varying potencies. Half-maximal inhibitory concentration (IC_{50}) values for the *R*-form of 2HG varied from approximately 25 μM for the histone N^{ε}-lysine demethylase JMJD2A to more than 5 mM for the hypoxia-inducible factor (HIF) prolyl hydroxylase. The results indicate that candidate oncogenic pathways in IDH-associated malignancy should include those that are regulated by other 2OG oxygenases than HIF hydroxylases, in particular those involving the regulation of histone methylation.

Keywords: isocitrate dehydrogenase; 2-hydroxyglutarate; 2-oxoglutarate; oxygenases; hypoxia-inducible factor

EMBO *reports* (2011) **12**, 463–469. doi:10.1038/embor.2011.43

INTRODUCTION

Heterozygous mutations in either of the two isoforms of the Krebs-cycle enzyme isocitrate dehydrogenase (IDH1/2) occur with a high prevalence in glioma, malignant glioblastoma and acute myeloid leukaemia (Dang *et al*, 2010; Reitman & Yan, 2010). The IDH mutations occur at substrate-binding arginine residues (Arg 132 in IDH1; Arg 140 and Arg 172 in IDH2) and inactivate IDH for conversion of isocitrate to 2-oxoglutarate (2OG; Zhao *et al*, 2009). However, they also cause a gain of function comprising catalysis of 2OG to the *R*-enantiomer of 2-hydroxyglutarate (*R*-2HG; Dang *et al*, 2009; Gross *et al*, 2010; Ward *et al*, 2010). The accumulation of *R*-2HG (to more than 10 mM in some cases) is associated with mutations of this type in both malignant glioblastoma and acute myeloid leukaemia, leading to the proposal that *R*-2HG is an 'oncometabolite'.

Increased L(*S*)-2HG or D(*R*)-2HG levels are also caused by germline mutations in L- or D-2-HG dehydrogenases, with excess *S*-2HG being correlated with an increased risk of brain tumour. *R*-2HG aciduria results in a more severe clinical manifestation than *S*-2HG aciduria, possibly precluding observation of tumours (Struys, 2006; Dang *et al*, 2010).

In some tumours, elevated levels of the Krebs-cycle intermediates succinate and fumarate result from mutations in succinate dehydrogenase and fumarate hydratase (Kaelin, 2009), which are proposed to stimulate the hypoxia-inducible factor (HIF)-mediated response. HIF target genes encode proteins that enable tumour growth, including vascular endothelial growth factor (Semenza, 2010). The HIF hydroxylases function as negative regulators of HIF-mediated transcription (Isaacs *et al*, 2005; Selak *et al*, 2005; Hewitson *et al*, 2007); thus, increased levels of succinate and fumarate are thought to promote tumour growth by inhibition of the HIF hydroxylases.

The HIF hydroxylases are Fe(II)- and 2OG-dependent oxygenases that produce succinate and CO_2 as coproducts; the HIF prolyl hydroxylases (PHD/EGLN enzymes) signal for HIF degradation, whereas factor inhibiting-HIF (FIH) is an asparaginyl hydroxylase that reduces HIF activity (Kaelin & Ratcliffe, 2008). Overexpression of IDH1 Arg 132 mutants results in elevated HIFα levels (Zhao *et al*, 2009). Other 2OG oxygenases are associated with cancer, including the JmjC histone demethylases (Varier & Timmers, 2010). This raises the question of whether 2HG inhibits 2OG oxygenases in a pathophysiologically relevant

[1]Chemistry Research Laboratory, Department of Chemistry, University of Oxford, Mansfield Road, Oxford OX1 3TA, UK
[2]Henry Wellcome Building for Molecular Physiology, Department of Clinical Medicine, University of Oxford, Roosevelt Drive, Oxford OX3 7BN, UK
[3]Epigenetic Regulation of Chromatin Function Group, Department of Biochemistry, University of Oxford, South Parks Road, Oxford OX1 3QU, UK
*These authors contributed equally to this work
[+]Corresponding author. Tel: +44 1865 275625; Fax: +44 1865 275674; E-mail: christopher.schofield@chem.ox.ac.uk
[++]Corresponding author. Tel: +44 1865 275631; Fax: +44 1865 275674; E-mail: akane.kawamura@chem.ox.ac.uk

Received 27 October 2010; revised 21 February 2011; accepted 22 February 2011; published online 1 April 2011

©2011 EUROPEAN MOLECULAR BIOLOGY ORGANIZATION

manner (Dang *et al*, 2010; Kaelin & Thompson, 2010). We report biochemical, structural and cellular studies showing that both *R*- and *S*-2HG inhibit 2OG oxygenases, but with different potencies. The results indicate that 2HG is a relatively poor inhibitor of the HIF hydroxylases in comparison to the 2OG-dependent histone lysyl demethylases, suggesting that candidate oncogenic pathways involving 2HG elevation might involve chromatin modifications.

RESULTS

First, we investigated whether *R*- or *S*-2HG inhibit representative human 2OG oxygenases with the following roles: (i) HIF prolyl (PHD2/EGLN1) and asparaginyl (FIH) hydroxylation; (ii) fatty-acid metabolism (γ-butyrobetaine hydroxylase 1, BBOX1); (iii) histone demethylation (JMJD2A, JMJD2C and JHDM1A/FBXL11); and (iv) DNA demethylation activity (AlkB homologue 2, ABH2; Table 1; Fig 1). When using a 2OG concentration at or close to the K_m (2OG) values for the individual enzymes, the half-maximal inhibitory concentration (IC_{50}) values for the *R*-/*S*-2HG ranged from approximately 25 μM to more than 10 mM. We used *N*-oxalylglycine (NOG), an unreactive 2OG analogue, for comparison. Of the two 2HG enantiomers, the *S*-form was the more-potent inhibitor. For *R*-2HG, the most significant inhibition was of JMJD2A, for which the IC_{50} (24 μM) was similar to that observed for NOG (17 μM). By contrast, inhibition of PHD2 and BBOX1 by *R*-2HG was weak, with IC_{50} values of approximately 7 and 13 mM, respectively, consistent with previous work with the PHDs (Mole *et al*, 2003).

The lack of a substantial increase in IC_{50} values at higher (10-fold) iron concentrations (for JMJD2A and BBOX-1), and different values for the two enantiomers imply that the mode of inhibition is not predominantly iron sequestration (Table 1). We investigated whether *R*- or *S*-2HG is oxidized to 2OG by PHD2 and FIH; in our standard conditions, we did not find conversion of 2HG to 2OG by NMR analysis (data not shown). Neither *R*- nor *S*-2HG was a cosubstrate for PHD2 (supplementary Fig S1 online). Although care must be taken in comparing IC_{50} values determined with different assay conditions for the various oxygenases, these results show that both *R*- and *S*-2HG inhibit the 2OG oxygenases, but with different potencies. The weak inhibition of the HIF hydroxylases suggests that the pathological effects of 2HG are probably not, at least predominantly, mediated by direct inhibition of HIF hydroxylases.

We then investigated the structural basis of oxygenase inhibition by 2HG. Structures of FIH and JMJD2A with *R*- or *S*-2HG show that both can bind to the active site iron, or surrogate nickel, in a bidentate manner (Fig 2). The JMJD2A.2HG structures were obtained with a histone H3K36me3 substrate fragment, which bound similarly to previously reported structures (Chen *et al*, 2006; Couture *et al*, 2007; Ng *et al*, 2007). Similarly to 2OG and NOG (Elkins *et al*, 2003; Ng *et al*, 2007), both *R*- and *S*-2HG coordinate the metal with the 2-hydroxyl group *trans* to $D201^{FIH}$/$E190^{JMJD2A}$ and one oxygen of the the C1-carboxylate *trans* to $H199^{FIH}$/$H188^{JMJD2A}$ (Fig 2A,B,D,E). The other oxygen of the 2HG C1-carboxylate is positioned to hydrogen bond to Nδ2 of $N205^{FIH}$ (Fig 2A,B) or to Oγ of $S288^{JMJD2A}$ (Fig 2D,E); the 2HG C5-carboxylate is positioned to hydrogen bond to $K214^{FIH}$ Nζ, $Y145^{FIH}$ OH and $T196^{FIH}$ Oγ1 (Fig 2A,B) and to $K206^{JMJD2A}$ Nζ and $Y132^{JMJD2A}$ OH (Fig 2D,E), as observed for the 2HG C5-carboxylate. In FIH, the remaining metal coordination site is probably occupied by a glycerol molecule derived from the cryoprotectant solution (not shown in Fig 2A,B) and by water in JMJD2A structures (Fig 2D,E). Overall, the crystallographic analyses indicte that, similarly to succinate and fumarate (Fig 2C,F; Hewitson *et al*, 2007), both *R*- and *S*-2HG have the potential to bind to the active site Fe(II) and compete with 2OG for binding. To test this proposal, we performed further kinetic analyses. These indicate that, although NOG is a 2OG competitor, inhibition of JMJD2A by *R*-/*S*-2HG might be more complex; *R*-2HG demonstrated mixed-mode inhibition kinetics and—within the concentration ranges for which we could reliably obtain data—the *S*-2HG seemed to give uncompetitive kinetics with respect to 2OG (supplementary Fig S2 online; at higher *S*-2HG concentrations, inhibition by *S*-2HG might be mixed, but we were unable to obtain reliable data because of the low level of turnover at high *S*-2HG concentrations). A possible explanation for the results of our combined crystallographic and kinetic analyses is that, at least for *R*-2HG, the inhibitor can bind to both the enzyme.Fe(II) complex competing with 2OG and the enzyme.Fe(II).2OG complex. No additional 2HG binding was observed in the JMJD2A crystal structures. However, support for this idea comes from the observation that, at sufficiently high concentrations, 2OG itself inhibits some 2OG oxygenases—including AlkB (Welford *et al*, 2003), JMJD2A and FBXL11 (unpublished data)—and from crystallographic analyses indicating the potential for coordination of two organic molecules at the active-site metal; glycerol to the FIH.Fe(II).2HG complexes and with inhibitor studies on FIH (Conejo-Garcia *et al*, 2010). Work on deacetoxycephalosporin C synthase–succinate complexes also suggests that binding modes of diacids different to that normally observed for 2OG can also occur (Lee *et al*, 2001).

We then investigated inhibition of 2OG oxygenases by 2HG in cells (Fig 3), by testing JMJD2A because its IC_{50} values were lowest (Fig 3A,B). A cell-penetrating ester form of *R*-/*S*-2HG

Table 1|Inhibition of human 2OG oxygenases by *R*- and *S*-2HG

Enzyme	IC_{50} ± s.e.m. (μM)		
	***R*-2HG**	***S*-2HG**	**NOG**
FIH	1,500 ± 400*	189 ± 34	46 ± 8
PHD2	7,300 ± 3,300*	419 ± 150	0.8 ± 0.2
JMJD2A	24 ± 2 (*17 ± 4*)	26 ± 3 (*33 ± 5*)	17 ± 2 (*20 ± 3*)
JMJD2C	79 ± 7	97 ± 24	14 ± 3
FBXL11	106 ± 22	48 ± 15	252 ± 50
ABH2	424 ± 77	150 ± 20	10 ± 2
BBOX1	13,200 ± 1,100	142 ± 30 (*96 ± 10*)	19 ± 2

Substrates used in the assays for JMJD2A/JMJD2C, FBXL11, BBOX1, PHD2, FIH and ABH2 were histone H3 fragment substrates H3(7–14)K9me$_3$ and H3(30–41)K36me$_2$, γ-butyrobetaine, HIF1αCODD (residues 556–574), HIF1αCAD (residues 786–826) and GCXAGGTCCCGTAGTGCG, where X is 1-methyladenylate, respectively. See Fig 1 for dose–response curves and supplementary Table S1 online for the standard assay conditions used for the individual enzymes. Italicized IC_{50} values in parentheses were determined at 10-fold higher Fe(II) concentration than the standard assay conditions.
*Partial dose–response curves.
ABH2, AlkB homologue 2; BBOX1, γ-butyrobetaine hydroxylase 1; FIH, factor inhibiting-hypoxia-inducible factor; HIF, hypoxia-inducible factor; NOG, *N*-oxalylglycine; 2OG, 2-oxoglutarate; PHD2, prolyl hydroxylase 2; *R*-2HG, *R*-enantiomer of 2-hydroxyglutarate; IC_{50}, half-maximal inhibitory concentration.

©2011 EUROPEAN MOLECULAR BIOLOGY ORGANIZATION

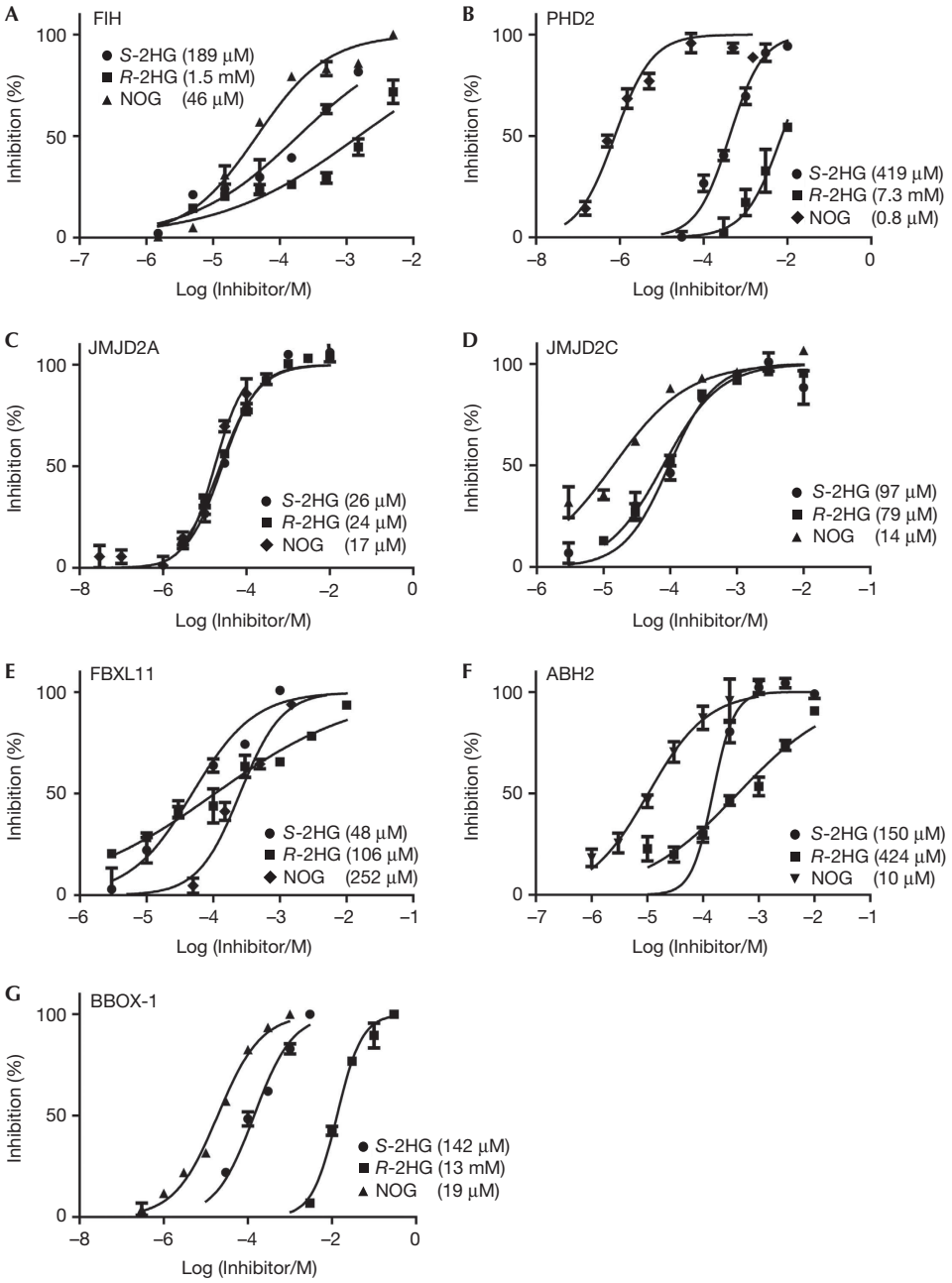

Fig 1 | Inhibition of recombinant forms of 2OG oxygenases by *R*-/*S*-2HG and *N*-oxalylglycine. (**A**) Inhibition of FIH as assessed by measuring hydroxylation of HIF1αCAD using a MALDI–TOF–MS assay. (**B**) Inhibition of PHD2 as assessed by measuring hydroxylation of HIF1αCODD using a MALDI–TOF–MS assay. Inhibition of (**C**) JMJD2A, (**D**) JMJD2C, (**E**) FBXL11 and (**F**) ABH2 by *R*-, *S*-2HG and NOG, as assessed by using formaldehyde dehydrogenase-based assay. (**G**) Inhibition of BBOX1 by *S*-2HG and *R*-2HG as compared with the standard NOG by NMR. All assays were performed in triplicate and are shown as averages with s.e.m. IC_{50} values were calculated using log(inhibitor) compared with normalized response (variable slope), using the program Prism, and are given in parentheses. The assay conditions for each enzyme are described in supplementary Table S1 online. ABH2, AlkB homologue 2; BBOX1, γ-butyrobetaine hydroxylase 1; FIH, factor inhibiting-hypoxia-inducible factor; HIF, hypoxia-inducible factor; 2OG, 2-oxoglutarate; PHD2, prolyl hydroxylase 2; *R*-2HG, *R*-enantiomer of 2-hydroxyglutarate; IC_{50}, half-maximal inhibitory concentration; MALDI–TOF–MS, matrix-assisted laser desorption/ionization–time of flight–mass spectrometry; NOG, *N*-oxalylglycine.

was added to HeLa cells transfected with JMJD2A (Fig 3A). Dimethyloxalylglycine—a cell-penetrating derivative of NOG—was used as a positive control. At high concentrations (8 × 5 mM or 10-mM additions at 30-min intervals), both enantiomers inhibited JMJD2A in a dose-dependent manner (Fig 3B); consistent with the *in vitro* data, the extent of inhibition was similar for

©2011 EUROPEAN MOLECULAR BIOLOGY ORGANIZATION

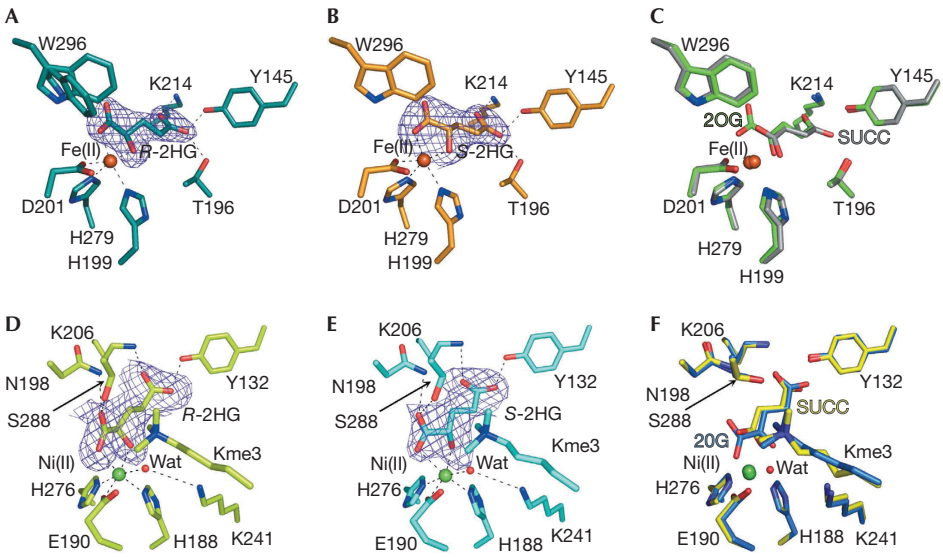

Fig 2 | Crystal structures of FIH and JMJD2A in complex with *R*- and *S*-2HG indicate binding of 2HG to the 2OG-binding site. FIH/JMJD2A folds were similar to those reported (RMSD for Cα ⩽ 0.3 Å for monomers). Dotted lines indicate apparent hydrogen bonds and polar interactions. Data collection and refinement statistics are given in supplementary Table S2 online. (**A**) View of the FIH.Fe(II).*R*-2HG complex showing the *Fo*–*Fc* omit map (contoured to 6 σ) for *R*-2HG. Notably, the side chain of Trp 296^{FIH}, which is involved in substrate binding (Elkins *et al*, 2003), has two conformations. (**B**) FIH.Fe(II).*S*-2HG structure showing the *Fo*–*Fc* omit map contoured to 6 σ around *S*-2HG. (**C**) Overlay of views from structures of FIH in complex with 2OG or succinate. (**D**) View from the active site of the JMJD2A.Ni(II).*R*-2HG.H3K36me_3 structure showing the *Fo*–*Fc* omit map contoured to 3.5 σ around *R*-2HG; Kme3 = N^{ε}-trimethylated lysine substrate residue; Ni(II) substitute for Fe(II). (**E**) JMJD2A.Ni(II).*S*-2HG.H3K36me_3 structure showing the *Fo*–*Fc* omit map contoured to 3.5 σ around *S*-2HG. (**F**) Overlay of views from structures of JMJD2A in complex with 2OG or succinate. (**D**–**F**) Both *R*-/*S*-2HG induce a rotation of approximately 100 ° (relative to other JMJD2A structures) about Cα-Cβ of the Ser 288^{JMJD2A} side chain such that it is positioned to hydrogen bond to 2HG (Ser Oγ-*R*/*S*-2HG O2; 2.8/3.1 Å). Ser 288^{JMJD2A} is proposed to be involved in substrate recognition and a determinant of the specificity of JMJD2 for different methylation states (Chen *et al*, 2006). FIH, factor inhibiting-hypoxia-inducible factor; 2OG, 2-oxoglutarate; *R*-2HG, *R*-enantiomer of 2-hydroxyglutarate; RMSD, root mean square deviation.

R-/S-2HG. We then tested for HIF hydroxylation inhibition using hydroxyl-residue antibodies and von Hippel Lindau protein (VHL)-defective renal cell carcinoma (RCC4) cells to enable simultaneous measurement of Pro- and Asn-hydroxylation (Fig 3C,D). Consistent with *in vitro* data, we observed a clear reduction in HIF1α Asn-hydroxylation, that was greater with *S*- than *R*-2HG. In contrast to these results and consistent with the *in vitro* data, we observed no *R*-2HG and only minimal *S*-2HG inhibition of Pro-hydroxylation, when using the same doses at which JMJD2A was inhibited (exposure to higher 2HG doses was toxic).

These results suggest that 2HG—and in particular the *R*-enantiomer produced by IDH1 mutants (Dang *et al*, 2009)—is probably an ineffective inhibitor of HIF Pro-hydroxylation, and predict that it would be relatively ineffective in inducing HIF1α. To test this, stable RCC4 transfectants re-expressing wild-type VHL (RCC4/VHLHA) and other VHL-competent cell lines (Hep3B/MCF7 cells) were exposed to several 10-mM additions or a single 20-mM addition of the methyl esters of *R*-/*S*-2HG. Neither dose of *R*-2HG induced HIF1α. Modest induction was observed with *S*-2HG (Fig 3E). As both the *in vitro* and cell studies indicate that HIF Asn-hydroxylation is more 2HG-sensitive than Pro-hydroxylation, we suggested that HIF1α induced by 2HG would not be hydroxylated at the site of Asn-hydroxylation in the C-terminal activation domain. We found this is the case (Fig 3F).

DISCUSSION

Overall, our results demonstrate that *R*- and *S*-2HG have the potential to inhibit a range of human 2OG oxygenases, thereby suggesting one mechanism by which elevated 2HG levels might promote oncogenesis. Although the inhibition potencies are generally weak, we observe broad concordance between the *in vitro* and *in vivo* results (Table 1; Figs 1 and 3). As production of 2HG by IDH mutations is stereospecific (Dang *et al*, 2009; Ward *et al*, 2010), the specificity of inhibition by the 2HG enantiomers is relevant to their potential as mediators of oncogenic pathways. For most of the 2OG oxygenases tested *in vitro*, *S*-2HG was more potent than *R*-2HG (Table 1). Only with the histone N^{ε}-methyl lysine demethylases JMJD2A/C were both enantiomers of similar potency, and of the enzymes tested, JMJD2A was the only one for which *R*-2HG showed similar potency to NOG, a 'generic' 2OG oxygenase inhibitor. Interestingly, inactivating mutations and/or reduced expression of JmjC histone demethylases including JARID1C (Dalgliesh *et al*, 2010), UTX (van Haaften *et al*, 2009) and JHDM1B/FBXL10 (Frescas *et al*, 2007), occur in RCCs, multiple myeloma, glioblastoma multiforme and several other cancers. Given the similarity of JMJD2A to some other JmjC histone demethylases, it is likely that *R*-2HG will inhibit at least some other demethylases with a similar or greater potency than JMJD2A. Our results therefore support the candidacy of one or more of these enzymes as targets for pathologically relevant 2HG

©2011 EUROPEAN MOLECULAR BIOLOGY ORGANIZATION

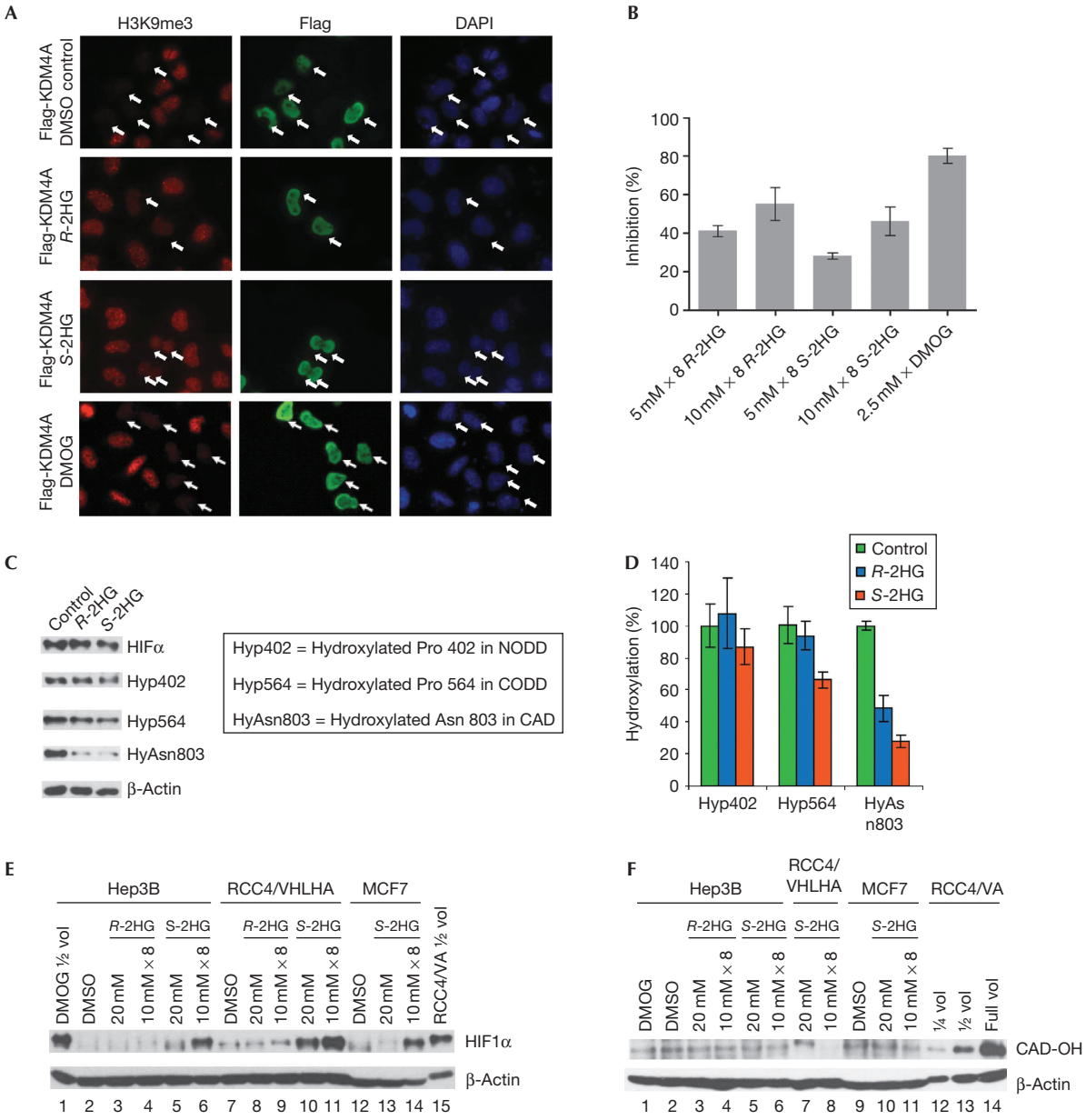

Fig 3 | Inhibition of histone demethylases and HIF hydroxylases by *R*- and *S*-2HG. (**A**,**B**) Inhibition of JMJD2A activity in HeLa cells, as shown by immunofluorescence studies. JMJD2A was expressed as an *N*-terminally Flag-tagged protein. The results for DMOG, a cell-penetrating form of the 'generic' 2OG oxygenase inhibitor NOG, are shown for comparison. (**A**) Indirect immunofluorescence analyses using antibodies against $H3K9me_3$ (left panels) or Flag (middle panels) were used to analyse the inhibition of ectopically expressed JMJD2A. DAPI staining (right panels) indicates location of nuclei. Rows represent control (0.5% DMSO), *R*-/*S*-2HG- and DMOG-treated cells. White arrows in the left and right panels indicate nuclei in which JMJD2A is overexpressed. Higher levels of $H3K9me_3$ were detected in both *R*- and *S*-2HG-treated cells, indicating inhibition of JMJD2A, whereas the control shows only a level of $H3K9me_3$ in nuclei in which JMJD2A is overexpressed. (**B**) Percentage inhibition of JMJD2A activity, using addition of doses of *R*- and *S*-2HG in their dimethyl ester forms (5 or 10 mM × 8); error bars represent standard error ($n > 50$). (**C**,**D**) Effect of *R*-/*S*-2HG on HIF1α hydroxylation in VHL-defective RCC4/VA cells. (**C**) Immunoblots of protein extracts from RCC4 cells treated for 4 h with *R*- and *S*-2HG compared with a DMSO-treated control. The compounds were added using the same dosing regime (10 mM × 8) as was used for the JMJD2A cell-work in their dimethyl ester forms. Signals of total HIF1α and hydroxylated NODD, CODD and CAD were analysed. (**D**) Quantification of data from (**C**) by densitometry; band intensities were normalized to HIF1α signals. Vertical bars represent standard errors ($n > 3$). (**E**) Effect of *R*-/*S*-2HG on HIF1α protein levels in human hepatoma (Hep3B), renal (RCC4/VHLHA, overexpressing haemagglutinin-tagged VHL) and breast cancer (MCF7) cells. (**F**) Immunoblot analyses of HIF1α CAD hydroxylation of selected samples from (**E**). DMOG, dimethyloxalylglycine; HIF, hypoxia-inducible factor; NOG, *N*-oxalylglycine; RCC, renal cell carcinoma; *R*-2HG, *R*-enantiomer of 2-hydroxyglutarate; 2OG, 2-oxoglutarate.

©2011 EUROPEAN MOLECULAR BIOLOGY ORGANIZATION

inhibition. However, they by no means exclude other 2OG oxygenases or other mechanisms of 2HG-mediated tumour promotion from a role in oncogenesis.

The high concentrations of *R*-2HG (more than 10 mM) that have been observed in malignant brain tumours and leukaemias (Dang *et al*, 2009; Gross *et al*, 2010; Ward *et al*, 2010), might be sufficient to inhibit even the less-susceptible 2OG oxygenases. Nevertheless, PHD2 is poorly inhibited *in vitro* by *R*-2HG (Fig 1; Table 1), and we were unable to demonstrate inhibition of the PHDs sufficient to substantially upregulate HIF in cells (Fig 3C–E). HIF is stabilized in IDH-associated gliomas; this has been proposed to be a consequence of intracellular depletion of 2OG following IDH loss of function (Zhao *et al*, 2009). It is possible that the depleted 2OG levels might synergize with *R*-2HG, or that IDH mutations perturb the $NADP^+/NADPH + H^+$ ratio, causing redox stress (Dang *et al*, 2010), inactivating the HIF hydroxylases and upregulating HIF by an unknown mechanism.

In conclusion, our findings argue against upregulation of HIF through PHD inhibition by 2HG being the major factor in IDH mutation-associated oncogenesis. However, they show that elevated 2HG levels might regulate gene expression by inhibition of 2OG-dependent chromatin-modifying enzymes, including the JmjC histone demethylases. Furthermore, they demonstrate that accumulation of *R*-2HG has the potential to modulate the transcriptional activity of the HIF pathway by acting on Asn-hydroxylation. Inhibition of Asn-hydroxylation in the C-terminal transactivation domain of HIFα polypeptides might be predicted to enhance transcriptional activity through the recruitment of p300/CBP coactivators to the C-terminal activation domain (Kaelin & Ratcliffe, 2008). As HIF transcriptional target genes are differently dependent on the activity of this domain, such an action might affect hypoxia pathways.

METHODS

Details of materials used, syntheses, recombinant protein production, additional assay and crystallography are given in supplementary information online.

Biochemical assays. (See supplementary Table S1 online for assay conditions). Assays using mass spectrometry involved incubation of the enzyme in the presence of Fe(II), 2OG, ascorbate and peptide. Product formation was assessed by using matrix-assisted laser desorption/ionization–time of flight–mass spectroscopy assay (Hewitson *et al*, 2007; Rose *et al*, 2008; Chowdhury *et al*, 2009). JMJD2A, JMJD2C, FBXL11 and ABH2 inhibition were assessed using a formaldehyde dehydrogenase-coupled assay (Couture *et al*, 2007; Roy & Bhagwat, 2007; Rose *et al*, 2008).

Histone demethylase assays. HeLa cells grown in Dulbecco's modified eagle's medium containing 10% fetal bovine serum and penicillin/streptomycin were divided into six-well plates and transfected with 2 μg Flag-JMJD2A plasmid per well using Fugene HD (Roche). Compounds were added 5 h after transfection (5- and 10-mM *R*- and *S*-2HG was added at 30-min intervals for 4 h (× 8); 2.5-mM dimethyloxalyl glycine was added once). Cells were fixed 9 h after transfection (20 min in 4% formaldehyde), washed twice with PBS, then permeabilized for 10 min (0.5% Triton X-100/PBS). Permeabilized cells were washed twice in PBS, placed in 3% BSA/PBS (30 min) and then washed twice with PBS. Immunostaining using α-$H3K9me_3$ (1:500; Ab8898, Abcam) and data analysis was carried out as described previously (King *et al*, 2010). Data were normalized by setting DMSO-treated JMJD2A-transfected cells to 100% activity and a catalytically inactive JMJD2A H188A mutant to 0% activity.

HIF hydroxylase assays. Both VHL-defective (RCCs with an empty vector RCC4/VA) and VHL-competent cells, i.e. human heptoma Hep3B, breast cancer MCF7 and RCC4/VHLHA (RCC4 stably transfected with *C*-haemagglutinin-tagged wild-type VHL), were used. In brief (details of this assay will be reported elsewhere), cells were treated with DMSO (control) or *R*-/*S*-2HG dimethyl esters (4 h). Compounds were added at concentrations of 20 mM (× 1) or 10 mM (× 8, at 30-min intervals). Cell extracts were probed with antibodies for hydroxy-Pro 402 (NODD-OH), hydroxy-Pro564 (CODD-OH) and hydroxy Asn 803 (CAD-OH). HIF1α band intensities were used to normalize hydroxylation signals. Antibodies for HIF1α, NODD-OH, CODD-OH and β-actin/horseradish peroxidase were obtained from BD Transduction Laboratories, Millipore Biosciences, New England Biolabs and Abcam, respectively. The CAD-OH antibody was a gift from Dr S.H. Lee (Lee *et al*, 2008).

Supplementary information is available at EMBO *reports* online (http://www.emboreports.org).

ACKNOWLEDGEMENTS

We thank the scientists of Diamond beamline I04, Oxford, UK for assistance.This work was funded by the Wellcome Trust, the Biotechnology and Biological Sciences Research Council, UK, the German Academic Exchange Service (L.H.), the Malaysian Government and Univerisiti Sains Malaysia (K.K.Y.).

Author contributions: R.C., A.K., I.K.H.L., C.J.S. and P.J.R conceived and designed the experiments. R.C., K.K.Y., Y.M.T., A.K., L.H., E.A.B., N.R.R., I.K.H.L., E.C.Y.W. and X.S.L performed the experiments. R.C., K.K.Y., Y.M.T., A.K., L.H., I.K.H.L., C.J.S. and P.J.R analysed the data. M.Y., O.N.K., M.A.M., I.J.C., R.J.K. and T.D.W.C contributed reagents, materials and analysis tools. R.C., A.K., P.J.R. and C.J.S wrote the paper.

CONFLICT OF INTEREST

The authors declare that they have no conflict of interest.

REFERENCES

Chen Z *et al* (2006) Structural insights into histone demethylation by JMJD2 family members. *Cell* **125:** 691–702

Chowdhury R, McDonough MA, Mecinovic J, Loenarz C, Flashman E, Hewitson KS, Domene C, Schofield CJ (2009) Structural basis for binding of hypoxia-inducible factor to the oxygen-sensing prolyl hydroxylases. *Structure* **17:** 981–989

Conejo-Garcia A, McDonough MA, Loenarz C, McNeill LA, Hewitson KS, Ge W, Lienard BM, Schofield CJ, Clifton IJ (2010) Structural basis for binding of cyclic 2-oxoglutarate analogues to factor-inhibiting hypoxia-inducible factor. *Bioorg Med Chem Lett* **20:** 6125–6128

Couture JF, Collazo E, Ortiz-Tello PA, Brunzelle JS, Trievel RC (2007) Specificity and mechanism of JMJD2A, a trimethyllysine-specific histone demethylase. *Nat Struct Mol Biol* **14:** 689–695

Dalgliesh GL *et al* (2010) Systematic sequencing of renal carcinoma reveals inactivation of histone modifying genes. *Nature* **463:** 360–363

Dang L *et al* (2009) Cancer-associated IDH1 mutations produce 2-hydroxyglutarate. *Nature* **462:** 739–744

Dang L, Jin S, Su SM (2010) IDH mutations in glioma and acute myeloid leukemia. *Trends Mol Med* **16:** 387–397

Elkins JM, Hewitson KS, McNeill LA, Seibel JF, Schlemminger I, Pugh CW, Ratcliffe PJ, Schofield CJ (2003) Structure of factor-inhibiting hypoxia-inducible factor (HIF) reveals mechanism of oxidative modification of HIF-1a. *J Biol Chem* **278:** 1802–1806

Frescas D, Guardavaccaro D, Bassermann F, Koyama-Nasu R, Pagano M (2007) JHDM1B/FBXL10 is a nucleolar protein that represses transcription of ribosomal RNA genes. *Nature* **450:** 309–313

©2011 EUROPEAN MOLECULAR BIOLOGY ORGANIZATION

Gross S *et al* (2010) Cancer-associated metabolite 2-hydroxyglutarate accumulates in acute myelogenous leukemia with isocitrate dehydrogenase 1 and 2 mutations. *J Exp Med* **207:** 339–344

Hewitson KS, Lienard BM, McDonough MA, Clifton IJ, Butler D, Soares AS, Oldham NJ, McNeill LA, Schofield CJ (2007) Structural and mechanistic studies on the inhibition of the hypoxia-inducible transcription factor hydroxylases by tricarboxylic acid cycle intermediates. *J Biol Chem* **282:** 3293–3301

Isaacs JS *et al* (2005) HIF overexpression correlates with biallelic loss of fumarate hydratase in renal cancer: novel role of fumarate in regulation of HIF stability. *Cancer Cell* **8:** 143–153

Kaelin WG Jr (2009) SDH5 mutations and familial paraganglioma: somewhere Warburg is smiling. *Cancer Cell* **16:** 180–182

Kaelin WG Jr, Ratcliffe PJ (2008) Oxygen sensing by metazoans: the central role of the HIF hydroxylase pathway. *Mol Cell* **30:** 393–402

Kaelin WG Jr, Thompson CB (2010) Q&A: Cancer: clues from cell metabolism. *Nature* **465:** 562–564

King ONF *et al* (2010) Quantitative high-throughput screening identifies 8-hydroxyquinolines as cell-active histone demethylase inhibitors. *PLoS ONE* **5:** e15535

Lee HJ, Lloyd MD, Harlos K, Clifton IJ, Baldwin JE, Schofield CJ (2001) Kinetic and crystallographic studies on deacetoxycephalosporin C synthase (DAOCS). *J Mol Biol* **308:** 937–948

Lee SH, Jeong Hee M, Eun Ah C, Ryu SE, Myung Kyu L (2008) Monoclonal antibody-based screening assay for factor inhibiting hypoxia-inducible factor inhibitors. *J Biomol Screen* **13:** 494–503

Mole DR, Schlemminger I, McNeill LA, Hewitson KS, Pugh CW, Ratcliffe PJ, Schofield CJ (2003) 2-oxoglutarate analogue inhibitors of HIF prolyl hydroxylase. *Bioorg Med Chem Lett* **13:** 2677–2680

Ng SS *et al* (2007) Crystal structures of histone demethylase JMJD2A reveal basis for substrate specificity. *Nature* **448:** 87–91

Reitman ZJ, Yan H (2010) Isocitrate dehydrogenase 1 and 2 mutations in cancer: alterations at a crossroads of cellular metabolism. *J Natl Cancer Inst* **102:** 932–941

Rose NR, Ng SS, Mecinovic J, Lienard BM, Bello SH, Sun Z, McDonough MA, Oppermann U, Schofield CJ (2008) Inhibitor scaffolds for 2-oxoglutarate-dependent histone lysine demethylases. *J Med Chem* **51:** 7053–7056

Roy TW, Bhagwat AS (2007) Kinetic studies of *Escherichia coli* AlkB using a new fluorescence-based assay for DNA demethylation. *Nucleic Acids Res* **35:** e147

Selak MA, Armour SM, MacKenzie ED, Boulahbel H, Watson DG, Mansfield KD, Pan Y, Simon MC, Thompson CB, Gottlieb E (2005) Succinate links TCA cycle dysfunction to oncogenesis by inhibiting HIF-α prolyl hydroxylase. *Cancer Cell* **7:** 77–85

Semenza GL (2010) Defining the role of hypoxia-inducible factor 1 in cancer biology and therapeutics. *Oncogene* **29:** 625–634

Struys EA (2006) D-2-Hydroxyglutaric aciduria: unravelling the biochemical pathway and the genetic defect. *J Inherit Metab Dis* **29:** 21–29

van Haaften G *et al* (2009) Somatic mutations of the histone H3K27 demethylase gene UTX in human cancer. *Nat Genet* **41:** 521–523

Varier RA, Timmers HT (2010) Histone lysine methylation and demethylation pathways in cancer. *Biochim Biophys Acta* **1815:** 75–89

Ward PS *et al* (2010) The common feature of leukemia-associated IDH1 and IDH2 mutations is a neomorphic enzyme activity converting a-ketoglutarate to 2-hydroxyglutarate. *Cancer Cell* **17:** 225–234

Welford RW, Schlemminger I, McNeill LA, Hewitson KS, Schofield CJ (2003) The selectivity and inhibition of AlkB. *J Biol Chem* **278:** 10157–10161

Zhao S *et al* (2009) Glioma-derived mutations in IDH1 dominantly inhibit IDH1 catalytic activity and induce HIF-1a. *Science* **324:** 261–265

©2011 EUROPEAN MOLECULAR BIOLOGY ORGANIZATION

Chemistry & Biology
Article

Structural and Mechanistic Studies on γ-Butyrobetaine Hydroxylase

Ivanhoe K.H. Leung,[1,4] Tobias J. Krojer,[2,4] Grazyna T. Kochan,[2,4] Luc Henry,[1,4] Frank von Delft,[2,3] Timothy D.W. Claridge,[1] Udo Oppermann,[2,3] Michael A. McDonough,[1,*] and Christopher J. Schofield[1,*]
[1]The Department of Chemistry and the Oxford Centre for Integrative Systems Biology, Chemistry Research Laboratory, University of Oxford, 12 Mansfield Road, Oxford OX1 3TA, UK
[2]Structural Genomics Consortium, University of Oxford, Old Road Campus Roosevelt Drive, Headington OX3 7DQ, UK
[3]The Botnar Research Centre, Oxford Biomedical Research Unit, Oxford OX3 7LD, UK
[4]These authors contributed equally to this work
*Correspondence: michael.mcdonough@chem.ox.ac.uk (M.A.M.), christopher.schofield@chem.ox.ac.uk (C.J.S.)
DOI 10.1016/j.chembiol.2010.09.016

SUMMARY

The final step in carnitine biosynthesis is catalyzed by γ-butyrobetaine (γBB) hydroxylase (BBOX), an iron/2-oxoglutarate (2OG) dependent oxygenase. BBOX is inhibited by trimethylhydrazine-propionate (THP), a clinically used compound. We report structural and mechanistic studies on BBOX and its reaction with THP. Crystallographic and sequence analyses reveal that BBOX and trimethyllysine hydroxylase form a subfamily of 2OG oxygenases that dimerize using an N-terminal domain. The crystal structure reveals the active site is enclosed and how THP competes with γBB. THP is a substrate giving formaldehyde (supporting structural links with histone demethylases), dimethylamine, malonic acid semi-aldehyde, and an unexpected product with an additional carbon-carbon bond resulting from N-demethylation coupled to oxidative rearrangement, likely via an unusual radical mechanism. The results provide a basis for development of improved BBOX inhibitors and may inspire the discovery of additional rearrangement reactions.

INTRODUCTION

In animals, many plants and microorganisms carnitine (L-3-hydroxy-4-*N,N,N*-trimethylaminobutyrate, CAR) plays an essential metabolic role by enabling transport of long-chain fatty acids into the mitochondria. CAR is also involved in transport of the products of β oxidation, fatty acid storage, excretion of toxic products, and maintaining acyl-coenzyme-A/coenzyme-A homeostasis (Vaz and Wanders, 2002). In animals CAR is obtained from the diet and by endogenous biosynthesis. CAR is used as food supplement to promote fatty acid metabolism and is produced either in racemic form by synthesis or in chiral form by fermentation (Naidu et al., 2000; Brass et al., 1994).

In animals CAR biosynthesis occurs from N^{ε}-trimethyllysine, which is produced by hydrolysis of methylated proteins (Figure 1A). Pioneering work demonstrated that two CAR biosynthesis steps are catalyzed by Fe(II) and 2-oxoglutarate (2OG) dependent oxygenases, N^{ε}-trimethyllysine hydroxylase (TMLH) and γ-butyrobetaine (γBB) hydroxylase (BBOX). (Hulse et al., 1978; Lindstedt, 1967, 1977; Englard et al., 1985). BBOX is the target for 3-(2,2,2-trimethylhydrazine)propionate (THP), which is used to treat myocardial infarction (Simkhovich et al., 1988; Dambrova et al., 2002). THP is proposed to lower the levels of reactive oxidizing species associated with fatty acid metabolism by preventing CAR-mediated transport.

We report structural and mechanistic analyses on human BBOX and its inhibition by THP. The results reveal a close relationship between BBOX and TMLH and link the CAR biosynthesis enzymes with the 2OG-dependent histone N^{ε}-methyl lysine demethylases. Studies with γBB analogs and on the mechanism of action of THP reveal that BBOX can catalyze N-methyl demethylation and that the reaction of THP with BBOX involves an unprecedented rearrangement involving N-methyl cleavage and a novel C-*C* bonding forming reaction.

RESULTS

Characterization of BBOX Activity

To investigate its relationship with other human 2OG oxygenases and the mechanism of action of THP, we produced recombinant human BBOX and developed an NMR assay (Figure 1B). The results reveal human BBOX to be highly active and dependent on Fe(II) (see Figure S1A and Table S1A, entry I, available online) and show CAR production to be tightly coupled to 2OG oxidation. BBOX activity was stimulated by potassium ions and reducing agents, including but not limited to ascorbate, and subject to substrate inhibition (Figure S1A), as observed with prokaryotic and partially purified animal BBOX (Lindstedt et al., 1977; Wehbie et al., 1988). The observations with reducing agents are consistent with mouse model work using animals that cannot produce ascorbate (Furusawa et al., 2008).

Overall Structure

We crystallized BBOX employing Zn(II) as an Fe(II) substitute and *N*-oxalylglycine (NOG, an unreactive 2OG analog) (Table S1B, entry I) and γBB. The resultant BBOX.Zn.NOG.γBB structure (resolution 1.82 Å) reveals a homodimer as observed in solution analyses (Galland et al., 1998; Krissinel and Henrick, 2007) (Figure 2). Each monomer comprises N- and C-terminal domains

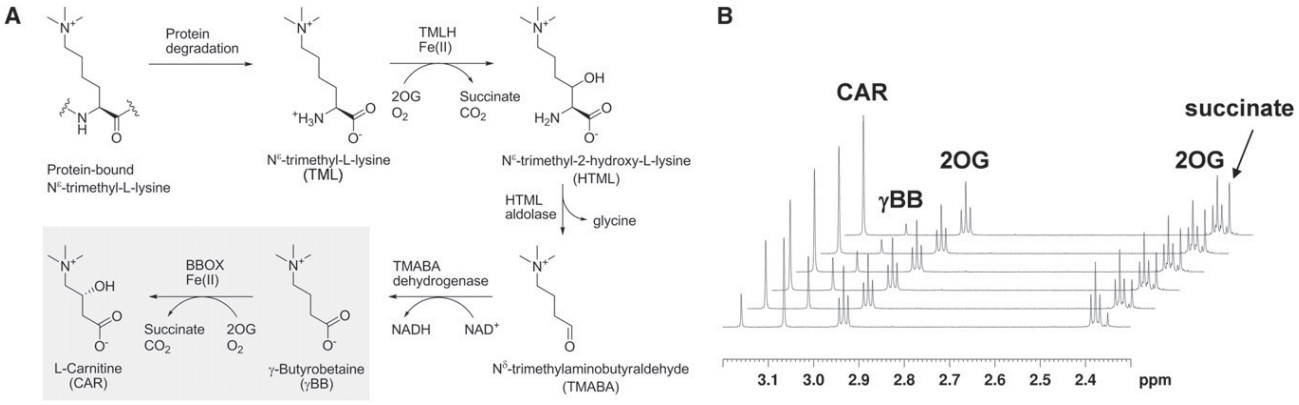

Figure 1. The Role of BBOX in CAR Biosynthesis

(A) The carnitine biosynthesis pathway.

(B) NMR monitoring of BBOX activity in real time: signals for L-Carnitine (CAR), γBB, 2OG, and succinate. Spectra are at 10-min intervals, and the first spectrum is recorded 5 min after sample mixing.

See also Figure S1 for more BBOX characterization.

linked by α-helix α3 (residue range 97–110), positioned close to the C-terminal helix (α10). The N-terminal domain (comprised of secondary elements α1, α2, β1–8) enables dimerization. Whereas dimerization via C-terminal structural elements has been observed for other 2OG oxygenases, BBOX represents the first example of dimerization via an N-terminal domain. Sequence analyses imply that TMLH similarly dimerizes via its N-terminal domain (Figure S2i). The presence of a zinc-binding site in the N-terminal domain was unexpected and is formed by a 3Cys-1His zinc-binding motif (Cys38, Cys40, Cys43, and His82). The C-terminal domain has a double-stranded β-helical core fold (DSBH, β^{I}–β^{VIII}) (Figure 2) forming the major ($\beta11^{I}$, $\beta22^{VIII}$, $\beta13^{III}$, $\beta20^{VI}$, β10, β9) and minor ($\beta12^{II}$, $\beta21^{VII}$, $\beta14^{IV}$, $\beta19^{V}$) β sheets, characteristic of 2OG oxygenases (Clifton et al., 2006). A 94 residue "insert" between DSBH strands $\beta14^{IV}$ and $\beta19^{V}$ contains three α helices (α7, α8, α9), four β strands (β15, β16, β17, β18), and one 3_{10} helix ($3_{10}4$). This insert folds over the more open end of the DSBH, forming both part of the active site and part of the dimerization interface with the N-terminal domain of the other chain in the dimer. A loop and a 3_{10}-helix ($3_{10}3$) links DSBH strand $\beta11^{I}$ with strand $\beta12^{II}$. This region (residues 184–198) also folds over the active site and is involved in substrate binding (Figure 2B); in addition, it interacts with another region comprised of the antiparallel β strands β4-β5 and helix $3_{10}2$ (residues 43–54), which extends from the N-terminal domain zinc-binding site of the other chain in the dimer. Sequence comparison of BBOX with TMLH (26% identity) implies that both the folds and active sites of the two enzymes are similar.

N-Terminal Zinc-Binding Domain

The N-terminal domain fold of BBOX is most related to that of a protein of unknown function from *Acidithiobacillus ferrooxidans* ATCC 23270 (PDB ID 3LUU; PFAM family DUF971, PF06155; DALI Z score = 10.8; rmsd 2.1 Å over 81 residues), which has many homologs (including in prokaryotes), though none other than BBOX or TMLH appear to be 2OG oxygenases. The 3Cys-1His zinc-binding motif is conserved in many of the apparent homologs (Figure S2ii). Although the equivalent N-terminal domain zinc-binding residues in the *Acidithiobacillus* protein structure appear partially disordered, it does have zinc bound, albeit using residues from different secondary structural elements (His36, Glu40, and the C-terminal carboxylate of Glu100). Cys-40 of BBOX is substituted with serine in TMLH, potentially altering metal-binding specificity in TMLH (Figures S2i and S2ii).

Active Site

The active site is enclosed by loops between $\beta11^{I}$–$\beta12^{II}$, β18–$3_{10}4$, and β strand β15 (Figure 3). The opening of a tunnel leading toward the active site, which may enable binding of oxygen and release of CO_2, is "bridged" by the side chains of Val-192 (located between $\beta11^{I}$–$\beta12^{II}$) and Ala-294 (located between β18–$3_{10}4$) (Figure 3C). The small size of the tunnel opening suggests that conformational changes by loop movements may occur to enable substrate binding and product release.

As for other 2OG oxygenases (Clifton et al., 2006), the active site metal is bound by three ligands (His-202, Asp-204, and His-347) (Figure 3). NOG binds to the metal in a bidentate manner with its 1-carboxylate coordinating via a single oxygen (*trans* to His-347) and its C-2 carbonyl oxygen (*trans* to Asp-204). The C-5 carboxylate of NOG interacts with a basic residue (Arg-360) and a hydroxyl group (Ser-229), as observed in other 2OG oxygenases; untypically a second arginine (Arg-349) is also involved in binding of the 2OG C-5 carboxylate. A water completes the octahedral coordination sphere and is positioned to form a hydrogen bond with Gln-215 Oε (2.7 Å) and the Asp-204 carboxylate (2.8 Å), suggesting that both of these residues play a role in O_2 binding. The remainder of the residues around the putative O_2-binding site are hydrophobic (Trp-181, Leu-217, Leu-362). The metal coordination site closest to C-3 of the substrate is occupied by the 2OG C-1 carboxylate. Although it is uncertain whether the crystal structure reflects the solution situation, this arrangement suggests that O_2 may bind at the position occupied by the water, necessitating a rearrangement

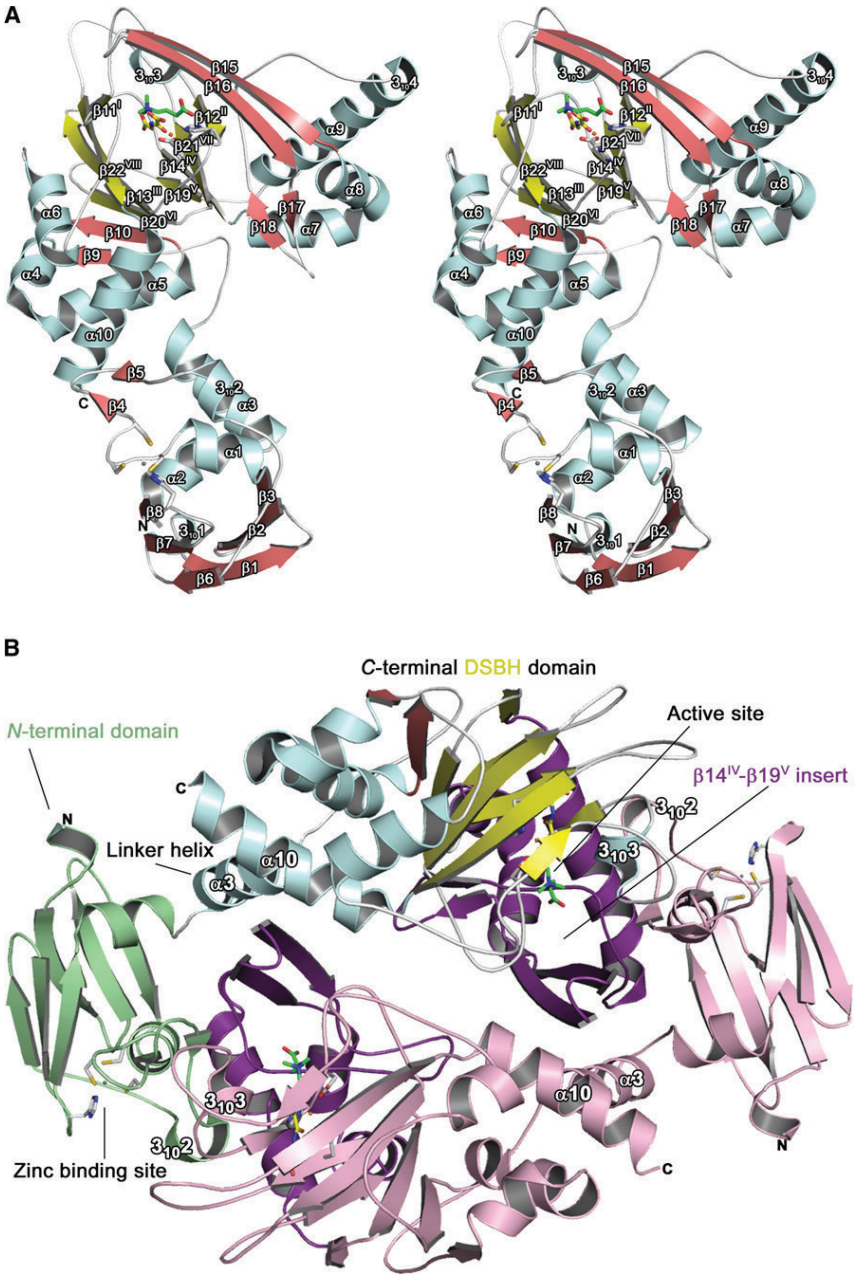

Figure 2. The Overall Fold of BBOX

(A) Stereo view ribbons representation of the BBOX:Zn:NOG:γBB structure. Colored and labeled by secondary structure elements; β strands are pink, and the core DSBH strands are highlighted in yellow, α helices are light blue, and loops are white. Metal binding residues are shown as white sticks, the Zn(II) is displayed as an orange sphere (substituting for iron at the active site) and as a gray sphere in the N-terminal domain. NOG is shown as yellow sticks and γBB as green sticks. (B) Ribbons representation of the BBOX dimer; one monomer is in pink and the other colored as in (A) except for the N-terminal Zn(II) binding domain in light green and the $\beta14^{IV}$-$\beta19^{V}$ insert, which is purple in both molecules.

See also Figure S2 for human BBOX sequence alignments.

(as proposed for other 2OG oxygenases) (Zhang et al., 2002) for the catalytically reactive ferryl intermediate (Hausinger, 2004; Hoffart et al., 2006) to be positioned adjacent to the oxidized bond. γBB binds adjacent to the metal, such that its C-3 *pro-R* C-H bond, which must undergo hydroxylation to give CAR, projects toward the metal (C-3 γBB to metal: 4.7 Å) (Englard et al., 1985) (Figure 3B).

Substrate Specificity

The γBB carboxylate is positioned to interact via hydrogen bonds with the side chains of Asn-292 (2.9 Å), Asn-191 (2.9 Å), and the backbone amide of Tyr-205 (2.9 Å) (Figures 3A and 3B). Structurally informed sequence analyses imply that BBOX and TMLH bind their substrates similarly, except that a modification ($Asn191_{BBOX}$ to $Asp131_{TMLH}$) at the observed C-1 γBB carboxylate-binding site of BBOX enables binding of the α amino group of TMLH's N^{ε}-trimethyllysine substrate (Figures S2i and S2iii).

The positively charged γBB N-trimethyl ammonium group is located in an electron-rich aromatic "cage" formed by the side chains of Tyr177, Tyr-194, and Trp-181 (Figures 3B; Figure S3i) with the side chains of two other aromatic residues positioned nearby (Tyr-205 and Tyr-366). Tyr-366 is also positioned to hydrogen bond to the side chain of Asp-204, suggesting that it may be involved in coordinating γBB binding and reactions at the metal center. The mode of binding of the N-trimethyl group is strikingly similar to the manner in which the same group binds to plant homeobox domain and Tudor domains that bind to modified histones (Huang et al., 2006; Horton et al., 2010) (Figure S3i). N-trimethyl binding also occurs with the 2OG-dependent histone N^{ε}-lysyl demethylases; however, with these enzymes the N-trimethyl binding site is less hydrophobic because one of the substrate methyl groups must be adjacent to the iron to enable demethylation (Ng et al., 2007).

Structural Insights into Specificity and Enzymatic Mechanism

Support for the crystallographically observed substrate binding mode was obtained from substrate analog studies. The carboxylate functionality is an absolute requirement for substrate binding and activity (data not shown), but the requirement for the trimethylamino group is less stringent. γBB analogs with deletion or addition of a methylene group were substrates for

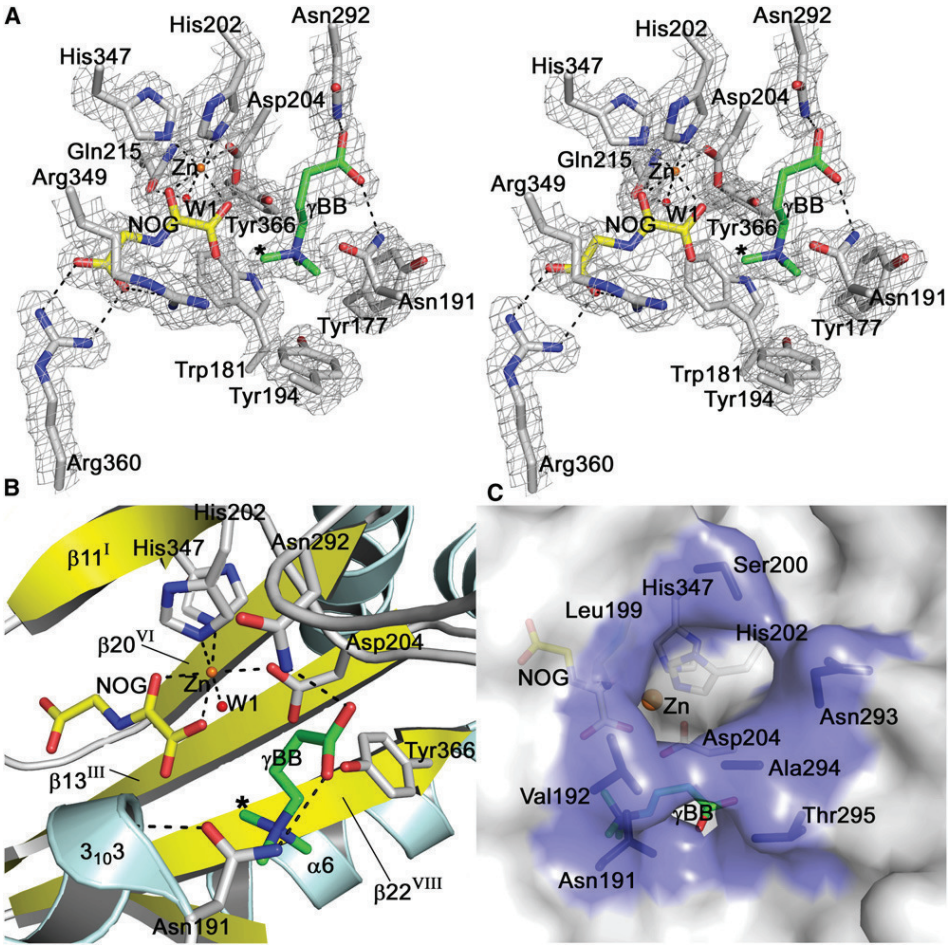

Figure 3. BBOX Active Site

(A) Stereo view representation of the electron density (2Fo-Fc electron density map shown as gray mesh contoured to 1σ) from the 1.82 Å resolution BBOX:γBB structure data. The metal is shown as an orange sphere that is coordinated by three BBOX residues (shown as white sticks), a water (red sphere), and *N*-oxalylglycine (yellow sticks). γBB is shown as green sticks. Black dashes indicate metal coordination and selected hydrogen bonds.

(B) View of the active site of BBOX in complex with Zn(II) (orange sphere), *N*-oxalylglycine (yellow sticks), and γBB (green sticks). Interactions between the γBB carboxylate and Asn-191, Asn-292 and metal coordination interactions are indicated by black dashes. Asn-191 also plays a role in capping the 3_{10} helix ($3_{10}3$) indicated by a dashed line to the backbone amide of Ala-193.

(C) Solvent accessible surface of BBOX (gray and blue) showing the opening of the tunnel bridged by residues Val-192 and Ala-294. The tunnel leads to the active site and is lined by Val-192, Ala-294, Ala-293, Asn-191, Thr-295, Leu-199 (shown as blue surface and sticks).

See also Figure S3 for BBOX ligand binding and a comparison of the BBOX and histone lysine demethylase active sites.

BBOX but were oxidized less efficiently (Table S1A, entries II and III, respectively), as was the γBB analog with two N^{ε}-methyl groups (Table S1A, entry IV).

Analysis of the γBB-binding site revealed the side chain hydrogen bond donor/acceptor atom of Asn-191 is 3.8 Å from the C-3 carbon of γBB (Figure 3), suggesting that BBOX may accept substrates having a polar group at C-3 with "D" stereochemistry; therefore, we tested the D-enantiomer of CAR (D-CAR) as a substrate for BBOX. We found that D-CAR was a substrate for BBOX (Table S1A, entry V) producing *N,N,N*-trimethylaminoacetone, presumably through facile nonenzymatic decarboxylation of an intermediate β carboxyketone formed from the C-3 dihydroxylated product (Figure S4i). Interestingly, we also found that with extended incubation times, CAR itself was a substrate, albeit poorer than γBB or D-CAR, and like the latter producing *N,N,N*-trimethylaminoacetone (Table S1A, entry VI). From a biological perspective these observations are of interest because trimethylaminoacetone has been described as a metabolite of racemic carnitine or D-CAR (Holme et al., 1982). These results rationalize a previous study whereby increased 2OG turnover was observed when D-, L-, or racemic carnitine was reacted with partially purified BBOX from human kidney and *pseudomonas* sp. AK1 (Bremer, 1983). Thus, metabolic production of *N,N,N*-trimethylaminoacetone could be minimized by using pure L-carnitine (CAR), rather than racemic carnitine, as a dietary supplement.

Inhibitor Complex

To investigate its mechanism of action, we then solved a structure of THP in complex with BBOX (1.82 Å resolution). The overall

structure revealed that despite the substitution of an amino group for the C-4 methylene of γBB, THP occupies a near-identical position compared to γBB (Figure S3i). The Tyr-366 phenolic OH is positioned to interact with the secondary amino group of THP (3.6 Å). Notably, as for γBB, the THP C-3 *pro-R* hydrogen projects toward the metal, suggesting that THP may act as a competitive substrate (THP IC_{50} 34 μM) (Table S1B, entry II).

Rearrangement Mechanism

Initial NMR studies on the reaction of THP with BBOX demonstrated that the inhibitor acts as a substrate with the same cofactor requirement as γBB (Table S1A, entry VII), as suggested by previous work conducted with native rat BBOX (Spaniol et al., 2001), and indicated the generation of several products. ^{1}H and ^{13}C NMR studies led to the identification of the hydrated form of malonic acid semi-aldehyde **2** as a major product (Figure 4A). The formation of **2**, which decarboxylates to give acetaldehyde, is consistent with a mechanism involving oxidation at C-3 of THP followed by N-N fragmentation to give a hydrolytically labile imine. However, we did not observe production of 1,1,1-trimethylhydrazinium ions (or trimethylamine), as expected for a "simple" hydroxylation followed by fragmentation; instead, we observed formation of dimethylamine. 2D NMR studies led to the identification of formaldehyde (observed as a tris-(hydroxymethyl)aminomethane buffer adduct). The observation of HCHO and dimethylamine, which must be produced by N-demethylation, provides a mechanistic link between BBOX/TMLH and the histone N^{ε}-methyl lysine demethylases (Figure S3ii). The NMR analyses also indicated the production of another initially unassigned product that was not observed with γBB. The combined NMR data suggested the structure to be $HO_2CCH_2CH(NH_2)CH_2NCH_3(CH_2OH)$ **1**. To support this assignment we prepared THP ^{13}C labeled at one of its N-methyl groups. The resultant analyses confirmed the production of the previously assigned products (formaldehyde and dimethylamine, with partial incorporation of ^{13}C in the anticipated positions) and provided additional evidence for the formation of **1**, with ^{13}C being equally distributed between the N-CH_2 and the N-CH_3 carbons (Figure 4; Figure S4ii). Derivatization of the reaction mixture of labeled THP followed by LC-MS analyses led to the isolation of the derivatized product of **1**, with partial incorporation of ^{13}C in the ratios anticipated (Figures 4D–4F).

DISCUSSION

BBOX and TMLH are closely related 2OG oxygenases belonging to a distinct subfamily that is present in most eukaryotes and many prokaryotes. BBOX is a homodimer mediated by its N-terminal zinc-binding domain. The structural studies also reveal the trimethylamino group-binding site of BBOX to be related to those of histone-binding proteins. Following from pioneering work on their roles in collagen biosynthesis, animal 2OG oxygenases have more recently been shown to play roles in fatty acid metabolism, hypoxic sensing, and nucleic acid modification. In addition to the inhibition of BBOX as a method for cardioprotection, other human 2OG oxygenases are being targeted for small molecule inhibition for the treatment of diseases, including anemia and cancer. The structural information described here will be useful in order to develop potent and selective inhibitors both of BBOX and other human 2OG oxygenases.

Comparison of the structures of BBOX in complex with cofactors, metal, and substrate or inhibitor presented here with that of a recently published apo-BBOX structure provides a possible explanation as to how substrates and products may enter and leave the active site (Tars et al., 2010). The apo-BBOX structure displays disordered loops surrounding the active site, indicating that conformational flexibility of these regions in the absence of substrate or inhibitor is possible. This suggests that an induced fit mechanism may contribute to the catalytic activity of BBOX and may explain the observation of limited accessibility to the active site in the substrate inhibitor complexes.

The analog studies suggest that BBOX accepts a wide range of substrates. In fact, when compared to generic 2OG oxygenase inhibitors such as NOG and succinate (Table S1B, entries I and III), these substrate analogs act as reasonably active competitive inhibitors (Table S1B, entries IV–VII). The observation that BBOX has a less than stringent requirement for a trimethylammonium group may be useful for the design of improved BBOX inhibitors.

In microorganisms and plants, 2OG oxygenases catalyze a very wide range of oxidative reactions (Clifton et al., 2006; Hausinger, 2004). However, to date, their reactions have been limited to hydroxylations and N-demethylations via methyl group hydroxylation in animals. We define the clinically used inhibitor THP as being a competitive substrate for BBOX. THP undergoes N-demethylation and N-N fragmentation leading to a C-C bond forming rearrangement reaction. The closest parallel to the conversion of THP to **1** in established organic reactions is the Stevens rearrangement, wherein an ylide formed by deprotonation of a quaternary amine undergoes rearrangement to give a secondary amine via migration of one of the N-alkyl groups (Figure S5) (Stevens, 1928; Vanecko et al., 2006). However, in contrast to the harsh conditions of the Stevens rearrangement, the BBOX catalyzed oxidative rearrangement of THP occurs in aqueous solution at room temperature. We propose that the BBOX-catalyzed reaction of THP involves initial reaction with an iron-oxo intermediate (Krebs et al., 2007), as involved in other 2OG oxygenase reactions, to give a radical at C-3. In the case of γBB, this can undergo a rebound process to give CAR (Figure 5A). However, with THP the presence of the secondary amine enables fragmentation of the radical intermediate to give an imine and a trimethylamine radical cation (Figure 5B). In the case of THP, fragmentation of the radical must be faster than hydroxylation because we did not observe $Me_3N^{+}NH_2$. In support of the proposed role of the Aza group of THP in inducing fragmentation, the THP analog in which the trimethylamino group was replaced with *t*-butyl or isopropyl groups led to products resulting from "normal" hydroxylation, i.e., formation of *tert*-butylamine or isopropylamine (Figure 5C; Table S1A, entries VIII and IX). Following N-N cleavage, 1,2-hydrogen shift of the trimethylamine radical cation gives a methylene radical that can add into the imine to generate the rearranged C-C framework (Figure 5D). Subsequent 1,5-hydrogen abstraction on one of the N-methyl groups by the resultant amine radical (Figure 5D'), as precedented by the abstraction step in the Hofmann-Löffler-Freytag reaction (Curran et al., 1988), followed by

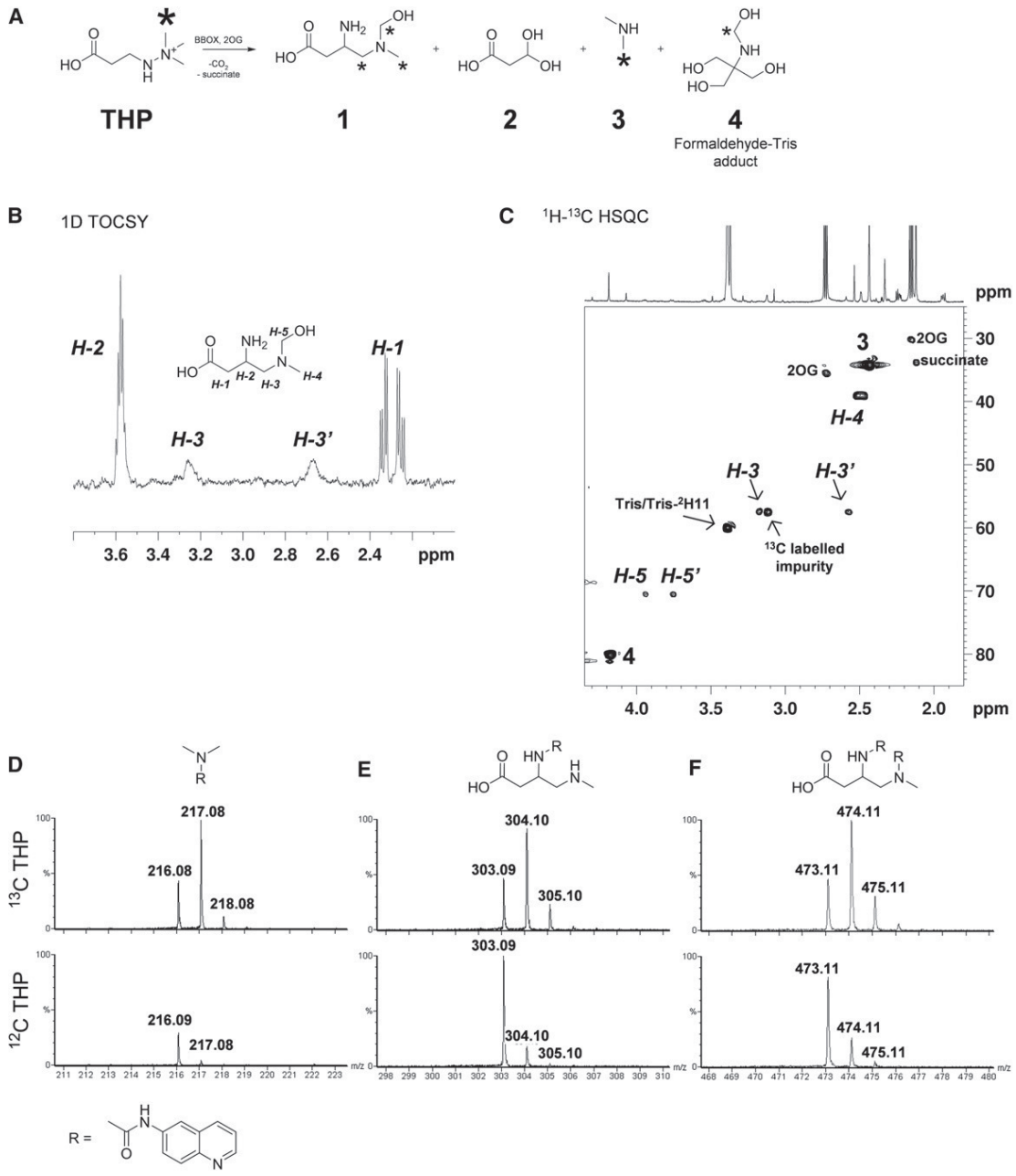

Figure 4. THP Reacts with BBOX in an Unprecedented Reaction

(A) Four products are observed in the THP reaction.

(B) 1D TOCSY of **1** confirming the four carbon chain. Selective excitation is applied on *H*-2 at 3.58 ppm.

(C) 2D HSQC showing the reaction of THP labeled with ^{13}C on one of its methyl groups with BBOX. The ^{13}C label (*) is transferred to **3** ($^{1}J_{CH}$ = 143 Hz) and **4** ($^{1}J_{CH}$ = 160 Hz), and C-3, C-4 ($^{1}J_{CH}$ = 141 Hz) and C-5 of **1**, therefore confirming the formation of a new C-C bond. 2OG, succinate and Tris/Tris-$^{2}H_{11}$ are observed at natural abundance ^{13}C levels. The ^{13}C-labeled impurity was present in the starting material. **1** is shown as its formaldehyde adduct, on the basis of further NMR analyses (Figure S4ii).

Reaction of BBOX with unlabeled THP (bottom row) or ^{13}C-labeled THP (top row) with 6-*N*-aminoquinolyl-*N*-hydroxysuccinimidyl carbamate enabled the identification of the carbamoyl derivatives of: (D) dimethylamine **3** (m/z = ^{12}C 216.1 and ^{13}C 217.1);

(E) a singly derivatized product from **1** (m/z = ^{12}C 303.1 and ^{13}C 304.1), and (F) a doubly derivatized product derived from **1** (m/z = ^{12}C 473.1 and ^{13}C 474.1). In the assay containing ^{13}C-labeled THP, the isotope peak abundance is in accordance with the expected product ratio based on the proposed mechanism (Figure 5). In the assay containing unlabeled THP, the isotope peak abundance reflects natural abundance levels.

See also Table S1 and Figure S4 BBOX product characterization.

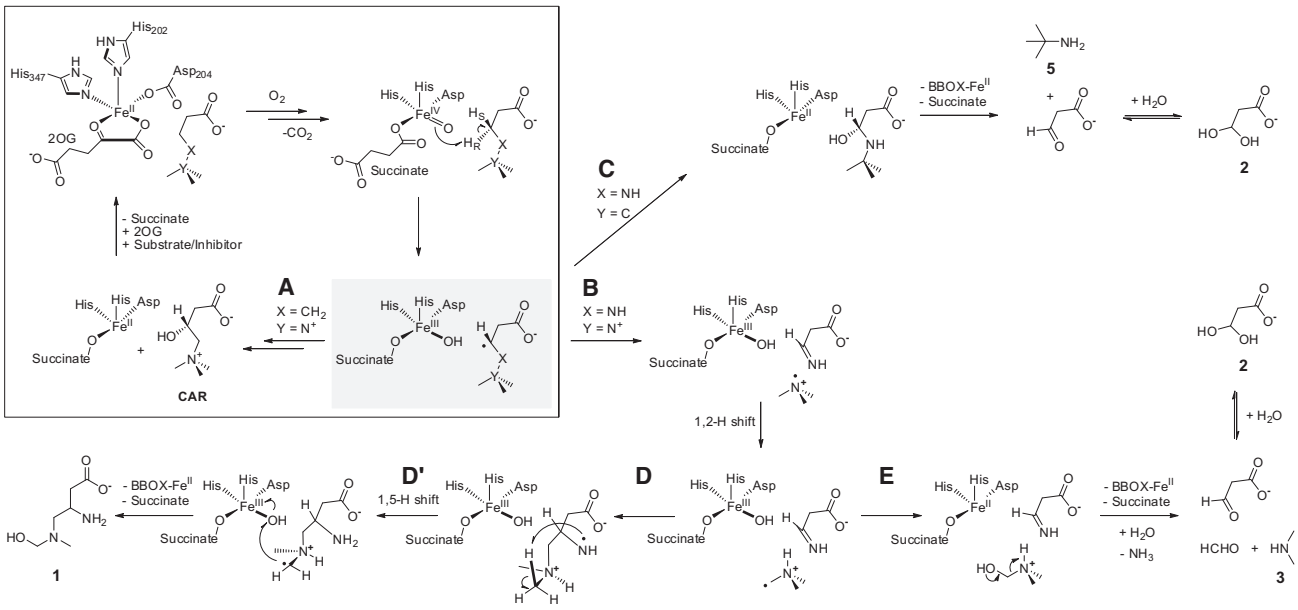

Figure 5. Mechanism for BBOX Catalysis

Proposed mechanisms for the reaction of γBB (route in A), THP (route in B), and 3-*tert*-butylamino propionic acid (route in C) with BBOX. See also Figure S5 for the Stevens rearrangement mechanism.

rebound hydroxylation to give the rearranged product **1**. Analysis of the BBOX-THP structure is consistent with the proposed mechanism; in particular one of the N-methyl groups of THP is close to the metal (N-methyl C to Zn: 5.2 Å cf. C-3 of THP to Zn: 4.7 Å) (Me*) (Figure S3ii). The unprecedented nature of the BBOX-catalyzed THP rearrangement further expands the scope of reactions catalyzed by 2OG oxygenases and may inspire the design of improved inhibitors for BBOX and other 2OG oxygenases.

SIGNIFICANCE

Carnitine plays an essential role in the metabolism of many organisms by enabling transport of fatty acids into mitochondria. Although produced endogenously in humans, carnitine is also used in food supplements. The starting material for carnitine biosynthesis is N^{ε}-trimethyllysine, which is produced from the degradation of posttranslationally modified proteins. Crystallographic studies of γ-butyrobetaine hydroxylase (BBOX), which catalyzes the final step in carnitine biosynthesis, reveal how it binds to its substrates and support prior kinetic analysis. They also highlight structural links between BBOX and histone demethylases, which also employ a ferrous iron cofactor and 2OG and O_2 co-substrates. The structural studies will be useful in the design of improved BBOX inhibitors and more selective inhibitors of other human 2OG oxygenases, which are currently being targeted for therapeutic intervention. Structural and mechanistic studies of the mode of BBOX inhibition by the clinically used compound THP reveal a rearrangement reaction for which there is no direct analog in synthetic chemistry.

EXPERIMENTAL PROCEDURES

Protein Production

The full-length gene of human *BBOX1* was cloned into the pFastBac vector (Invitrogen) containing a tobacco etch virus (TEV) cleavable N-terminal hexahistidine tag. Recombinant baculovirus was produced following the manufacturer's instructions (Invitrogen). High Five cells (Invitrogen) were grown as a suspension in Sf-900 II medium supplemented with 1% fetal calf serum (FCS) at 27°C. Cells were infected at a density of 2×10^6/ml with recombinant baculovirus (1 ml of virus stock/1 liter of cell culture). Seventy-two hours after infection, the cultures were collected and centrifuged (30 min, 2000 rpm, 4°C). The cell pellet was resuspended in cold phosphate-buffered saline (PBS) and centrifuged as before. The pellet from 1 liter of culture was then resuspended in 25 ml lysis buffer (50 mM HEPES [pH 7.5], 500 mM NaCl, 5 mM imidazole, 5% glycerol 0.1% v/v Igepal CA 630 (octylphenoxy)polyethoxyethanol, EDTA-free Complete Protease Inhibitor kit (Roche), benzonase (2.5 U/1 ml of a lysate), and 1 mM TCEP *tris*(2-carboxyethyl)phosphine). Cells were lysed using a Dounce homogenizer, followed by centrifugation (45 min, 20, 000 rpm, 4°C). The supernatant was incubated with the Ni-NTA resin for 1 hr with gentle mixing at 4°C. The resultant resin suspension was loaded on a gravity column, and after washing with 50 volumes of resin with washing buffer containing 50 mM HEPES (pH 7.5), 500 mM NaCl, 5% glycerol, and 10 mM imidazole, protein was eluted with 50 mM HEPES (pH 7.5), 500 mM NaCl, and 5% glycerol containing 250 mM imidazole buffer. Fractions were analyzed by SDS-PAGE. Fractions containing BBOX were combined. After EDTA treatment (final concentration 1 mM) at 4°C to remove excess Ni^{2+}, the protein sample was applied to a Superdex 200 16/60 gel-filtration column, which had been equilibrated in 50 mM HEPES (pH 7.5), 500 mM NaCl, 5% glycerol, and 1 mM TCEP. Fractions containing BBOX were combined, and the N-terminal tag was removed by treatment with TEV protease (o/n digestion at 4°C). The protein was diluted with 25 mM Tris buffer (pH 8.0) to 50 mM NaCl. The cleaved BBOX1, residual uncleaved BBOX1, and TEV protease were separated on HiTrap Q Sepharose column, using NaCl gradient (50–250 mM). Fractions containing purified BBOX were combined and concentrated using 30 kDa MWCO concentrator (Amicon).

Crystallization

Crystallization was performed in crystallization plates (SWISSCI, Zug, Switzerland) in a 96-well (three subwell) format. A Mosquito® (TTP Labtech)

Table 1. Data Collection and Refinement Statistics

	BBOX1: γBB (Hg SAD)	BBOX:THP
Data Collection		
Space group	*H*32	*H*32
Cell dimensions		
a, b, c (Å)	107.39, 107.39, 204.92	107.37, 107.37, 205.05
α, β, γ (°)	90, 90, 120	90, 90, 120
Resolution (Å) (outer shell)	28.98–1.78 (1.88–1.78)	20–1.82 (1.92–1.82)
No. of molecules/ASU	1	1
No. of unique reflections	43,809	40,755
Completeness (%)	100.0 (100.0)	99.4 (96.2)
Redundancy	11.0 (10.7)	5.5 (5.3)
R_{sym} [a]	0.140 (0.865)	0.083 (0.452)
Mean I/σ (I)	12.3 (2.9)	12.3 (3.3)
Wilson B value (Å^2)	18.6	21.0
Phasing		
Resolution (Å)	28.82–1.78	
R_{cullis} [b]	0.846 (iso)/ 0.592 (ano)	
Phasing power	0.909 (iso)/ 2.036 (ano)	
Figure of merit		
Centric	0.10831	
Acentric	0.09341	
After density modification	0.865	
Refinement		
R_{factor} [c]	0.14717	0.14671
R_{free} [d]	0.17633	0.18257
Rmsd		
Bond length (Å)	0.016	0.019
Bond angle (°)	1.554	1.600
No. of atoms		
Protein	3192	3149
Ligand/ion	42	62
Water	437	413
<B_{factor}> (Å^2)		
Protein	26.19	30.70
Ligand/ion	26.23	24.83
Water	28.79	31.46

Numbers in parentheses refer to the highest resolution shell.
[a] R_{sym} is the unweighted R value on I between symmetry mates.
[b] $R_{cullis} = \sum_{hkl} ||FPH \pm FP| - FH(calc)|/ \sum_{hkl} |FPH \pm FP|$.
[c] $R_{factor} = \sum_{hkl} ||Fobs| - k|Fcalc||/ \sum_{hkl} |Fobs|$ for the working set of reflections.
[d] R_{free} is the R value for 5% of the reflections excluded from refinement.

nanoliter liquid handler was used to set up crystallization plates for coarse screening and optimization of hits. The protein (20 mg/ml) was supplemented with *N*-oxalylglycine (8 mM) and γBB or THP (4 mM) prior to crystallization. Crystals were grown at 20°C using the sitting drop vapor diffusion method by mixing 100 nl of the protein solution and 50 nl of a precipitant solution (0.2 M ammonium citrate [pH 7.0], 20% PEG 3350, 6% hexane-1,6-diamine, and 10 mM ZnSO4). Crystals were flash cooled in liquid nitrogen using 25% glycerol in mother liquor as a cryoprotectant.

A mercury derivative was prepared by incubating BBOX:γBB crystals for 60 min in a reservoir solution containing 10 mM thiomersal. Crystals were then transferred for 1 min to a reservoir solution without mercury but supplemented with 25% ethylene glycol, and crystals were immediately flash frozen in liquid nitrogen.

Data Collection and Processing

Data for BBOX crystals in complex with γBB and THP were collected at DIAMOND beamline I02. Single-wavelength anomalous dispersion (SAD) data using 1.0084 Å wavelength X-rays were collected at DIAMOND beamline IO3 on a crystal derivatized with mercury. Data were integrated using XDS and subsequently scaled using SCALA, whereas data of the mercury derivative were integrated and scaled with the HKL2000 package (Table 1).

Crystallographic Phasing and Refinement

SHELXD was used to locate two mercury positions. Heavy atom positions were refined, and initial phases were calculated with SHARP by using a SIRAS method with the data of BBOX serving as the native data set. The final electron density map after phase extension and solvent flattening with SOLOMON was of excellent quality, and automated model building with ARP/wARP resulted in a 95% complete model. Refinement of both structures used REFMAC. After several rounds of manual rebuilding in COOT and subsequent cycles of refinement, the models converged to a final R_{factor}/R_{free} of 14.7%/17.6% and 14.6%/18.3% for BBOX:γBB and BBOX:THP, respectively (Table 1).

Assays

NMR Assays

NMR experiments were conducted at 700 MHz using a Bruker Avance III spectrometer equipped with an inverse TCI cryoprobe optimized for ^{1}H observation and 3 mm diameter Bruker MATCH micro tubes (Hilgenberg) containing 160 μl final sample volume. Solutions were buffered using Tris or Tris-$^2H_{11}$ (pH 7.5) dissolved 100% D_2O or 95% H_2O/5% D_2O. Pulse tip-angle calibration using the single-pulse nutation method was undertaken for each condition using a blank assay sample . Reaction products are identified and assigned by a combination of multiplicity edited HSQC, HMBC, 1D-TOCSY, and COSY where applicable.

Kinetic Analyses

Standard kinetic assays were conducted at 298 K in solutions containing 12.5 nM BBOX, 50 μM Fe(II), 50 μM substrate, 1.5 mM 2OG, 5 mM ascorbate, 50 mM Tris-$^2H_{11}$ (pH 7.5), and 80 mM KCl. Reactions were started by the addition of BBOX. Kinetic time courses were followed by using standard ^{1}H acquisition (ten transients with a relaxation delay of 1.2 s). The total time lapse between addition of the enzyme and the end of the first acquisition was 4 min. Time courses were followed for at least 15 min, and each measurement was repeated at least three times.

Inhibition Assays

Inhibition assays were conducted at 298 K in solutions containing 12.5 nM BBOX, 50 μM Fe(II), 50 μM γBB, 1.5 mM 2OG, 5 mM ascorbate, 50 mM Tris-$^2H_{11}$ (pH 7.5), 80 mM KCl, and varying concentrations of inhibitor. Reactions were initiated by BBOX addition. The extent of turnover of γBB to give CAR was measured 3 min 45 s after mixing by using standard ^{1}H acquisition (ten transients with a relaxation delay of 1.2 s). Response curves were fitted using OriginPro 8.0 (OriginLab, Northampton, MA, USA). Each measurement was repeated at least three times.

MS Assays

MS experiments were conducted using a Waters LCT Premier XE (Waters, Milford, MA, USA) and/or Bruker MicrOTOF. Assay conditions were as for the NMR work, except that the solution was buffered in 100% H_2O Tris-$^2H_{11}$ (pH 7.5); quenching was by addition of 80% MeCN.

Derivatization Assay

The rearrangement product obtained by reacting THP and ^{13}C-labeled THP in the presence of BBOX was identified using the following procedure. Assay conditions were as for the NMR work, and experiments were quenched by addition of 10% MeCN. The samples were freeze-dried, and the mixture was reacted in borate buffer with 6-*N*-aminoquinolyl-*N*-hydroxysuccinimidyl carbamate according to the supplier's instructions (Waters, Milford, MA, USA), followed by MS analysis of the resulting mixture using a Waters LCT Premier XE.

ACCESSION NUMBERS

The structures have been deposited in the RCSB Protein Data Bank as ID 3MS5 and 3O2G.

SUPPLEMENTAL INFORMATION

Supplemental Information includes Supplemental Experimental Procedures, five figures, and one table and can be found with this article online at doi:10.1016/j.chembiol.2010.09.016.

ACKNOWLEDGMENTS

We thank the Engineering and Physical Sciences Research Council, Berrow Foundation, Biotechnology and Biological Sciences Research Council, and the Wellcome Trust for support. The Oxford Structural Genomics Consortium is a registered UK charity (number 1097737) that receives funds from the Canadian Institutes for Health Research, the Canadian Foundation for Innovation, Genome Canada through the Ontario Genomics Institute, GlaxoSmithKline, Karolinska Institutet, the Knut and Alice Wallenberg Foundation, the Ontario Innovation Trust, the Ontario Ministry for Research and Innovation, Merck & Co., Inc., the Novartis Research Foundation, the Swedish Foundation for Strategic Research, and the Wellcome Trust. The work was also supported by the NIHR Biomedical Research Unit. We thank the staff at Diamond Light Source for assistance, support, and access to the beamline. We thank Dr. James McCullagh, Colin Sparrow, and Nikita Loik for their support and advice on this project.

Received: August 11, 2010
Revised: September 9, 2010
Accepted: September 13, 2010
Published: December 21, 2010

REFERENCES

Brass, E.P., Hoppel, C.L., and Hiatt, W.R. (1994). Effect of intravenous L-carnitine on carnitine homeostasis and fuel metabolism during exercise in humans. Clin. Pharmacol. Ther. *55*, 681–692.

Bremer, J. (1983). Carnitine—metabolism and functions. Physiol. Rev. *63*, 1420–1480.

Clifton, I.J., McDonough, M.A., Ehrismann, D., Kershaw, N.J., Granatino, N., and Schofield, C.J. (2006). Structural studies on 2-oxoglutarate oxygenases and related double-stranded β-helix fold proteins. J. Inorg. Biochem. *100*, 644–669.

Curran, D.P., Kim, D., Liu, H.T., and Shen, W. (1988). Translocation of radical sites by intramolecular 1,5-hydrogen atom transfer. J. Am. Chem. Soc. *110*, 5900–5902.

Dambrova, M., Liepinsh, E., and Kalvinsh, I. (2002). Mildronate: cardioprotective action through carnitine-lowering effect. Trends Cardiovasc. Med. *12*, 275–279.

Englard, S., Blanchard, J.S., and Midelfort, C.F. (1985). γ-Butyrobetaine hydroxylase: stereochemical course of the hydroxylation reaction. Biochemistry *24*, 1110–1116.

Furusawa, H., Sato, Y., Tanaka, Y., Inai, Y., Amano, A., Iwama, M., Kondo, Y., Handa, S., Murata, A., Nishikimi, M., et al. (2008). Vitamin C is not essential for carnitine biosynthesis in vivo: verification in vitamin C-depleted senescence marker protein-30/gluconolactonase knockout mice. Biol. Pharm. Bull. *31*, 1673–1679.

Galland, S., Le Borgne, F., Guyonnet, D., Clouet, P., and Demarquoy, J. (1998). Purification and characterization of the rat liver gamma-butyrobetaine hydroxylase. Mol. Cell. Biochem. *178*, 163–168.

Hausinger, R.P. (2004). Fe(II)/α-ketoglutarate-dependent hydroxylases and related enzymes. Crit. Rev. Biochem. Mol. Biol. *39*, 21–68.

Hoffart, L.M., Barr, E.W., Guyer, R.B., Bollinger, J.M., and Krebs, C. (2006). Direct spectroscopic detection of a C-H-cleaving high-spin Fe(IV) complex in a prolyl-4-hydroxylase. Proc. Natl. Acad. Sci. USA *103*, 14738–14743.

Holme, E., Lindstedt, S., and Nordin, I. (1982). Uncoupling in the γ-butyrobetaine hydroxylase reaction by D- and L-carnitine. Biochem. Biophys. Res. Commun. *107*, 518–524.

Horton, J.R., Upadhyay, A.K., Qi, H.H., Zhang, X., Shi, Y., and Cheng, X. (2010). Enzymatic and structural insights for substrate specificity of a family of jumonji histone lysine demethylases. Nat. Struct. Mol. Biol. *17*, 38–43.

Huang, Y., Fang, J., Bedford, M.T., Zhang, Y., and Xu, R.M. (2006). Recognition of histone H3 lysine-4 methylation by the double Tudor domain of JMJD2A. Science *312*, 748–751.

Hulse, J.D., Ellis, S.R., and Henderson, L.M. (1978). Carnitine biosynthesis. β-Hydroxylation of trimethyllysine by an α-ketoglutarate-dependent mitochondrial dioxygenase. J. Biol. Chem. *253*, 1654–1659.

Krebs, C., Fujimori, D.G., Walsh, C.T., and Bollinger, J.M. (2007). Non-heme Fe (IV)-oxo intermediates. Acc. Chem. Res. *40*, 484–492.

Krissinel, E., and Henrick, K. (2007). Inference of macromolecular assemblies from crystalline state. J. Mol. Biol. *372*, 774–797.

Lindstedt, G. (1967). Hydroxylation of γ-butyrobetaine to carnitine in rat liver. Biochemistry *6*, 1271–1282.

Lindstedt, G., Lindstedt, S., and Nordin, I. (1977). Purification and properties of γ-butyrobetaine hydroxylase from Pseudomonas sp AK 1. Biochemistry *16*, 2181–2188.

Naidu, G.S.N., Lee, I.Y., Lee, E.G., Kang, G.H., and Park, Y.H. (2000). Microbial and enzymatic production of L-carnitine. Bioprocess Biosyst. Eng. *23*, 627–635.

Ng, S.S., Kavanagh, K.L., McDonough, M.A., Butler, D., Pilka, E.S., Lienard, B.M.R., Bray, J.E., Savitsky, P., Gileadi, O., von Delft, F., et al. (2007). Crystal structures of histone demethylase JMJD2A reveal basis for substrate specificity. Nature *448*, 87–92.

Simkhovich, B.Z., Shutenko, Z.V., Meirena, D.V., Khagi, K.B., Mezapuķe, R.J., Molodchina, T.N., Kalviņs, I.J., and Lukevics, E. (1988). 3-(2,2,2-Trimethylhydrazinium) propionate (THP)—a novel gamma-butyrobetaine hydroxylase inhibitor with cardioprotective properties. Biochem. Pharmacol. *37*, 195–202.

Spaniol, M., Brooks, H., Auer, L., Zimmermann, A., Solioz, M., Stieger, B., and Krähenbühl, S. (2001). Development and characterization of an animal model of carnitine deficiency. Eur. J. Biochem. *268*, 1876–1887.

Stevens, T.S. (1928). Degradation of quaternary ammonium salts. Part I. J. Chem. Soc., 3193–3197.

Tars, K., Rumnieks, J., Zeltins, A., Kazaks, A., Kotelovica, S., Leonciks, A., Saripo, J., Viksna, A., Kuka, J., Leipinsh, E., and Dambrova, M. (2010). Crystal structure of human gamma-butyrobetaine hydroxylase. Biochem. Biophys. Res. Commun. *398*, 634–639.

Vanecko, J.A., Hayley, W., and West, F.G. (2006). Recent advances in the Stevens rearrangement of ammonium ylides. Tetrahedron *62*, 1043–1062.

Vaz, F.M., and Wanders, R.J.A. (2002). Carnitine biosynthesis in mammals. Biochem. J. *361*, 417–429.

Wehbie, R.S., Punekar, N.S., and Lardy, H.A. (1988). Rat liver γ-butyrobetaine hydroxylase catalyzed reaction: influence of potassium, substrates, and substrate analogues on hydroxylation and decarboxylation. Biochemistry *27*, 2222–2228.

Zhang, Z., Ren, J.-S., Harlos, K., McKinnon, C.H., Clifton, I.J., and Schofield, C.J. (2002). Crystal structure of a clavaminate synthase-Fe(II)-2-oxoglutarate-substrate-NO complex: evidence for metal centered rearrangements. FEBS Lett. *517*, 7–12.

 ©2010 Elsevier Ltd All rights reserved

Journal of Medicinal Chemistry Article

J. Med. Chem. **2010,** *53,* 867–875 **867**
DOI: 10.1021/jm901537q

Using NMR Solvent Water Relaxation to Investigate Metalloenzyme−Ligand Binding Interactions

Ivanhoe K. H. Leung, Emily Flashman, Kar Kheng Yeoh, Christopher J. Schofield, and Timothy D. W. Claridge*

Department of Chemistry, University of Oxford, Chemistry Research Laboratory, 12 Mansfield Road, Oxford OX1 3TA, United Kingdom

Received October 16, 2009

This report demonstrates that solvent water relaxation measurements can be used for quantitative screening of ligand binding and for mechanistic investigations of enzymes containing paramagnetic metal centers by using conventional NMR instrumentation at high field. The method was exemplified using prolyl hydroxylase domain containing enzyme 2 (PHD2), a human enzyme involved in hypoxic sensing, with Mn(II) substituting for Fe(II) at the active site. K_D values were determined for inhibitors that hinder access of water to the paramagnetic center. This technique is also useful for investigating the mechanism of suitable metalloenzymes, including order of ligand binding and modes of inhibition.

Introduction

NMR spectroscopy is widely used for the study of small molecule−protein interactions; saturation transfer difference (STD[a]),[1] transferred NOE,[2] and chemical shift perturbation techniques have emerged over recent years to play useful roles in ligand screening.[3−6] Although widely employed, these techniques may suffer from low intrinsic sensitivity and can require careful optimization of experimental conditions. For instance, STD enhancements can be rather weak and these analyses typically require a large excess of ligand, which may result in nonspecific binding or cause problems if the ligands are of limited solubility. The transferred NOE method requires a delicate ligand−protein ratio, and the results can be difficult to interpret in cases of relatively large ligands such as for peptide−protein or polysaccharide−protein interactions. Chemical shift perturbation using $^{1}H-^{15}N$ HSQC requires access to ^{15}N labeled protein and can be difficult to apply in systems larger than 25 kDa.[7] These factors may limit the applicability of these methods as primary screening tools.

Relaxation enhancement has been used as a tool to study paramagnetic metalloprotein−ligand interactions since the early 1960s;[8] the technique is based on the fact that the magnetic moment of an electron is 658 times greater than that of a proton nuclear spin.[9] Therefore, in the presence of a paramagnetic metalloprotein, the longitudinal and transverse relaxation rates of nuclei within a binding ligand may be enhanced, while for nonbinders the relaxation rates will remain unchanged. The changes in relaxation behavior depend on factors including the applied magnetic field (B_0), molecular correlation times, accessibility of the active site, and the properties of the paramagnetic metal itself.[8,10−12] The same paramagnetic relaxation enhancement (PRE) effect can be observed through solvent water proton relaxation rates. Various groups have made use of this effect to study paramagnetic metal binding interactions with proteins and other macromolecules by monitoring changes in the bulk water relaxation rate.[13−17]

Recently, a novel competition method has been proposed for screening small molecules binding to paramagnetic metalloproteins by employing water as the reporter molecule and monitoring changes in the bulk water proton longitudinal relaxation rate (R_1).[18] In the absence of any ligand, providing that access is possible, water molecules may chelate to the paramagnetic metal and undergo exchange with water molecules in the bulk solvent matrix. This leads to a net increase in the bulk water relaxation rate. The binding of ligands to the active site will normally hinder or prevent access of water molecules to the paramagnetic center and so decrease the observed bulk water relaxation rate.[19] Because the exchange of water will not normally be directly reliant on the exchange kinetics of the reversibly forming protein−ligand complex (as in the case for STD-NMR), this technique does not suffer from the limits imposed by other ligand-based NMR screening methods.[18] For example, while the association of very strongly binding ligands is often difficult to detect directly with ligand-observed methods, alterations in water accessibility may still arise under these conditions and remain readily detectable through water relaxation measurements. Thus, provided the enzyme under investigation contains a paramagnetic center at the binding site, this present approach can overcome the difficulties and limitations often associated with other ligand based NMR screening techniques.

The effect of paramagnetic relaxation is maximized at low field, generally between 0.01 to 100 MHz;[18] hence the original application of this solvent-based method for ligand screening was focused toward the use of specialist low field NMR instruments or fast field-cycling relaxometers.[18,20] While it was demonstrated that it is possible to conduct screening experiments at high field (400 MHz) on very small sample volumes (~2 μL) using an inhibitor with a K_D in the

*To whom correspondence should be addressed. Phone: +44 (0)1865 275 658. Fax: +44 (0)1865 285 002. E-mail: tim.claridge@chem.ox.ac.uk.

[a] Abbreviations: 2OG, 2-oxoglutarate; NOG, *N*-oxalylglycine; PHD, prolyl hydroxylase; STD, saturation transfer difference; PRE, paramagnetic relaxation enhancement; HIF, hypoxia inducible factor; ESI-MS, electrospray ionization mass spectrometry; ILOEs, interligand NOEs; CODD, *C*-terminal oxygen-dependent degradation domain; NODD, *N*-terminal oxygen-dependent degradation domain; BNS, bicyclic naphthalenylsulfonyl compound; BIQ, bicyclic isoquinolinyl compound.

© 2009 American Chemical Society

Published on Web 12/21/2009

Scheme 1. Outline Reaction Scheme for PHD2 Catalysis; 2OG = 2-Oxoglutarate

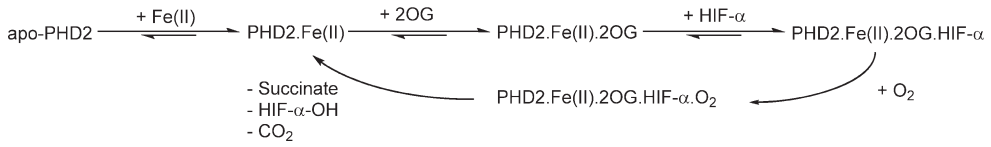

nanomolar region, the application to screen weaker inhibitors has not been demonstrated at high field and may suggest limited applicability in biochemical research laboratories employing conventional high-field NMR spectrometers.

By using the catalytic domain of human prolyl hydroxylase domain 2 ($PHD2_{181-426}$, or PHD2 hereafter) as a model system, we have optimized the experimental conditions of this water relaxation technique at high field and demonstrate its wider application as a NMR screening technique using conventional instrumentation. Furthermore, we have also demonstrated its potential as a method to investigate metalloenzyme reaction and inhibition mechanisms by monitoring the formation of complexes between protein, cofactor and substrates.

Results

Methodology. PHD2 is a Fe(II) and 2-oxoglutarate (2OG) dependent oxygenase that is involved in a key step in human oxygen sensing as part of the response to limiting oxygen levels (hypoxia) (for reviews, see refs 21 and 22). Under normal oxygen levels (normoxia), PHD2 initiates the oxygen dependent degradation of the α-subunit of hypoxia inducible factor (HIF-1α) by catalyzing the hydroxylation of two prolyl residues (positions 402 and 564 in human HIF-1α).[23,24] The PHD2−Fe(II) complex forms a ternary complex with the cofactor 2OG and its protein substrate HIF-α (or the peptide fragments $HIF\text{-}1\alpha_{556-574}$ (*C*-terminal oxygen-dependent degradation domain, CODD) and $HIF\text{-}1\alpha_{395-413}$ (*N*-terminal oxygen-dependent degradation domain, NODD)) (Scheme 1). In the case of the peptide substrates being described here, the hydroxyproline (Hyp) peptides $CODD_{Hyp564}$ or $NODD_{Hyp402}$ are produced, with carbon dioxide and succinate as coproducts.[25] PHD2 is a current pharmaceutical target for new treatments for ischemic disease and anemia.[26,27] Following the finding that PHD activity is inhibited by *N*-oxalylglycine (NOG),[28,29] a 2OG analogue, several groups have described the identification of inhibitors of PHD2.[30−36] Herein we report the application of bulk water relaxation measurements to investigate mechanistic features and inhibition of PHD2.

An absolute requirement for the relaxation-based screening experiment is the presence of a paramagnetic center inside the protein that is accessible to bulk water. PHD2 is unusual among other 2OG oxygenases in that it forms a stable complex with diamagnetic high spin Fe(II).[37] Although there may be small amounts of paramagnetic Fe(III) species inside the PHD2 active site, quantitative information is difficult to extract. Previous studies have indicated that the Fe(II) metal ion in the PHD2 active site can be substituted by different transition metals.[38] Mn(II) forms a 1:1 complex with apo-PHD2[38,39] and was selected as the metal of choice in this study because of its favorable paramagnetic properties.[8,40] By measuring the bulk water relaxation rates at a fixed Mn(II) concentration and varying PHD2 concentrations, we confirmed that the binding of Mn(II) to apo-PHD2 is strong (see Supporting Information, Figure S1). In the screening experiments described below, a 2-fold molar excess of Mn(II) was used to saturate the active site. However, in cases where the small molecule is a nonbinder or a very weak binder, the presence of free paramagnetic metal ions in solution can potentially be a source of artifacts through direct chelation of the free metal and should be avoided. Therefore, in this situation, a 1:1 molar ratio of protein to Mn(II) was used so that any contribution to relaxation rate changes from small molecules chelating to free metal ions was minimized.

Longitudinal relaxation time constants (T_1) were measured at 500 MHz using the standard inversion recovery scheme.[41] Solvent water T_1 constants were measured directly in a H_2O-D_2O mixture as opposed to the originally proposed method in which samples are measured in 100% H_2O.[18] A H_2O-D_2O ratio of 12.5%:87.5% was chosen so that the range of T_1 values could be kept roughly between 1.8 to 3.5 s in order to keep the length of inversion recovery experiments reasonably short. Conventional 3 mm tubes were used to strike a balance between the ease of titration and avoiding radiation damping that may arise from the intense H_2O resonance. The small proportion of H_2O to D_2O would also assist in the avoidance of radiation damping. The reduction of filling factor when using a 5 mm probe was not of concern because of the strong HDO signal being measured.

Ligand Screening. Figure 1a presents solvent water relaxation data for three different 2OG titrations from separate sample preparations by plotting the rate of relaxation (R_1) against the ligand concentration. Analysis in the presence of succinate, a product of PHD2 catalysis and a relatively weak inhibitor,[42] is plotted for comparison purposes. In this presentation format, variability between titration curves is apparent for 2OG and it is not immediately apparent whether 2OG or succinate is the stronger binder. The absolute R_1 values, such as the initial relaxation rate when no ligand is added ($R_{1(0)}$) and the minimum relaxation rate when a 1:1 complex is formed, are strongly influenced by variations in the concentrations of paramagnetic ion and protein. Small variations in Mn(II) and protein concentrations from separate sample preparation stages will therefore influence the ability to identify differences in binding affinities when comparing across samples.

However, the actual parameter of interest is the relative change in observed relaxation rate on titration of the ligand. We therefore propose that in order to normalize these variations, it is advantageous to plot and compare the relative relaxation rates $R_1/R_{1(0)}$ against the titrated ligand concentration, as shown in Figure 1b. With this method of analysis, it is possible to readily distinguish between strong and weak binders. The curve for a strong binder (2OG[37]) is characterized by a steep slope and rapid plateauing at, or close to, a 1:1 protein−ligand ratio, whereas the curve for a weak binder (succinate[42]) is characterized by a gentler slope which does not plateau until a large ligand excess is reached. The R_1 ratio at which this saturating equilibrium condition is reached is likely governed by factors including kinetics of the

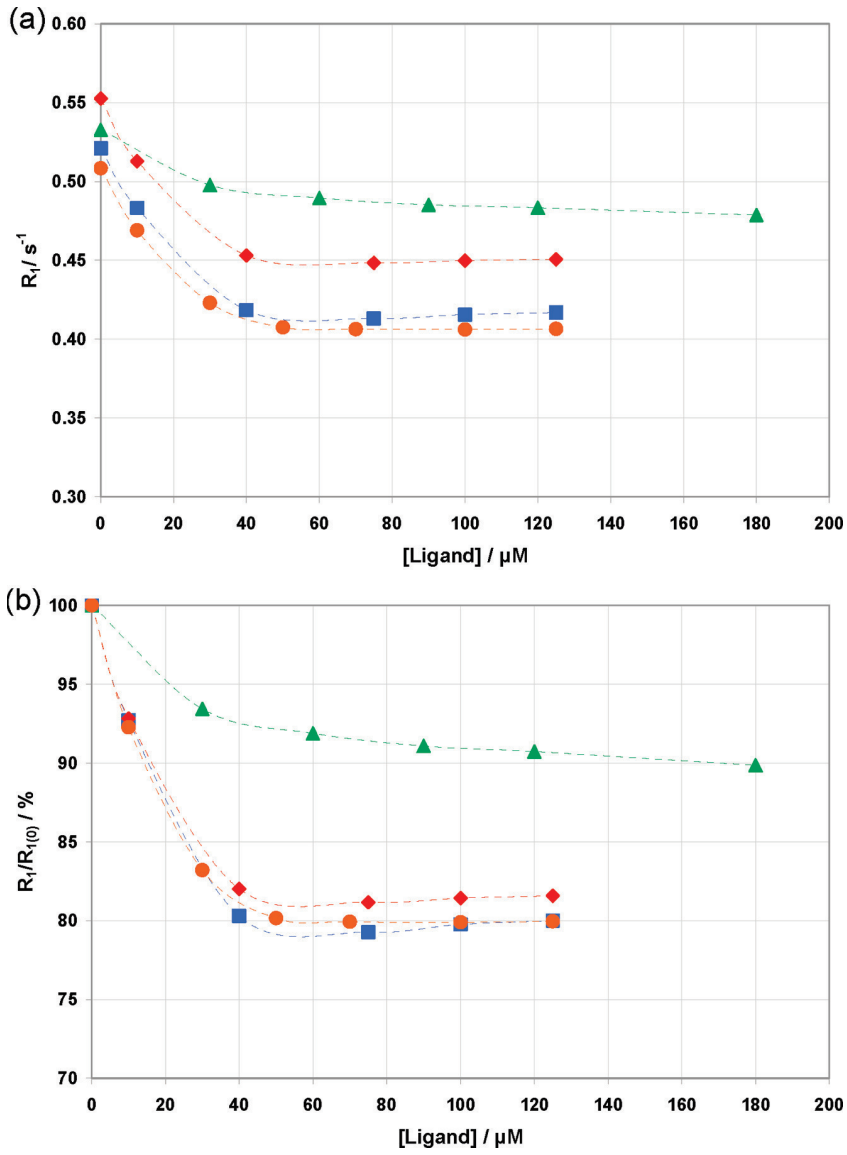

Figure 1. Titrations of 2OG in three separate sample preparations (blue squares, red circles, and red diamonds), and the titration of succinate (green triangles) into 50 μM PHD2. Plotted against ligand concentration is (a) the directly measured solvent relaxation rate (R_1) and (b) the relative relaxation rate $R_1/R_{1(0)}$, in which $R_{1(0)}$ is the initial relaxation rate when no ligand is added. Slight differences in Mn(II) and protein concentrations from different sample preparations complicate comparisons across samples, but by normalizing the rates as $R_1/R_{1(0)}$, binding differences are made apparent. In this and all subsequent figures, dashed lines are included to aid visualization.

reversibly forming protein−ligand complex, the accessibly of water molecules, their mode of binding (e.g., directly to metal or otherwise), and the number of water molecules that are being displaced. The position of the plateau is also somewhat sensitive to the intrinsic variability that occurs between different sample preparations, arising from difficulties in determining protein concentrations accurately and the slight variation in metal ion concentration between different stock solutions. Such variability is apparent for the 2OG titration data in Figure 1b, and we observe this to be typical behavior between discrete sample preparations. For clarity therefore, the normalized rates, $R_1/R_{1(0)}$, versus ligand concentration presentation format is used throughout the remainder of this report.

The amounts of protein and ligand molecules required for this relaxation method are comparable to, or less than, other NMR based screening techniques because it is the intense HDO signal that is being measured. Nevertheless, consideration should be given when choosing the relative amounts of protein and ligand for the experiment because there is trade-off between protein concentration, total experiment time, and the sensitivity of the method in differentiating ligands of similar binding affinity (Figure 2). When using ~25 μM protein and 100 μM Mn(II), the experimental time is shortened because there is a higher concentration of free Mn(II) in solution that is readily accessible to water molecules, thus leading to faster relaxation rates ($R_{1(0)} = 0.60$ s^{-1}). However, in this case, the extent of reduction in relaxation rates on ligand addition is diminished with the titration curve plateauing at around 90%, reducing the separation between the curves of similar affinity ligands. In contrast, by using ~75 μM protein with 100 μM Mn(II), the variation in rates is enhanced, now plateauing at around 65%, and the method becomes more sensitive to small differences in binding affinities. One consequence of this, however, is that the time required for the experiment is greater due to the higher concentration of protein bound Mn(II)

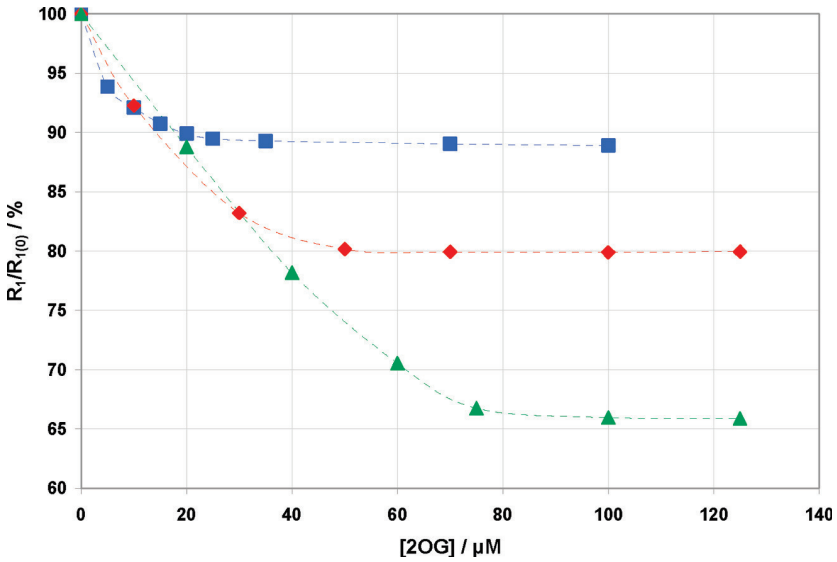

Figure 2. Titration of 2OG into 25 μM PHD2 (blue squares), 50 μM PHD2 (red diamonds), and 75 μM PHD2 (green triangles) with 100 μM Mn(II). The minimum R_1 value depends on the residual relaxation rate of the H_2O-D_2O mixture, which in turn is dependent upon the amount of free Mn(II) present in solution.

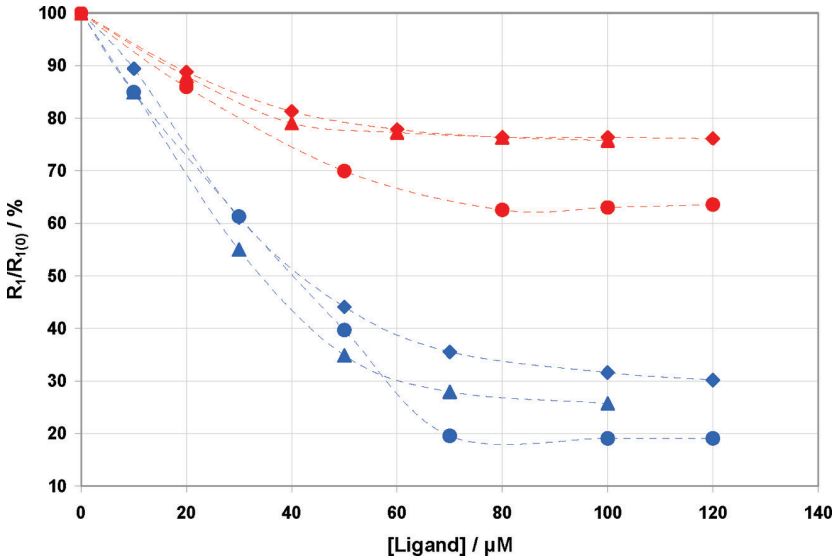

Figure 3. The titration of 2OG (solid triangles), NOG (solid diamonds), and BNS (solid circles) into 50 μM PHD2 with 100 μM Mn(II). The data plotted in red and blue are conducted at 500 and 23 MHz, respectively.

species with correspondingly fewer free ions in solution ($R_{1(0)} = 0.41\ s^{-1}$). As comparison, the water relaxation rate observed for the apo-PHD2 solution (50 μM, 12.5% H_2O) in the absence of Mn(II) was $0.11\ s^{-1}$.

To investigate the validity and sensitivity of the method at high field, we then conducted experiments at low field, as in the work of Bertini et al.,[18] and compared the results with our high field data. Three PHD2−ligand systems were analyzed for comparison. 2OG is a natural cofactor of PHD2 and has a K_D value of about 1 μM as determined by nondenaturing ESI-MS,[37] while *N*-oxalylglycine (NOG) is a 2OG mimic that binds slightly weaker than 2OG.[23] A potent bicyclic naphthalenylsulfonyl inhibitor (BNS) was also tested (Figure 3).[34,36]

The low field experiments were conducted in 100% H_2O at 23 MHz, and both high and low field experiments were measured at 313 K so that the rate of ligand exchange was increased, enabling a more accurate determination of K_D, as suggested by Bertini et al.[18] Such K_D measurements become feasible because only near stoichiometric amounts of ligand are required.

As anticipated, the minimum relaxation rate is smaller at low field, indicating greater sensitivity under these conditions; however, the relative change of R_1 between the three ligands, and hence the calculated K_D values, are essentially the same at both low and high field. Qualitatively, results obtained at high and low fields confirm that the bicyclic inhibitor BNS is a much stronger binder than 2OG and NOG. Quantitatively, the K_D values obtained for 2OG at both low and high field are ~2 μM, while for NOG they are ~3 μM (see Supporting Information, Figures S2−S5). Note that these values are slightly higher than the reported values

Table 1. Dissociation Constants (K_D) Determined by the Solvent Relaxation Technique at 298 K and IC_{50} Values[34,46] for 2OG, Succinate and a Range of Inhibitors

Ligand	Structure	K_D / μM	IC_{50} / μM
2OG	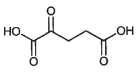	0.9 ± 0.1	N/A
NOG	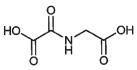	3.1 ± 0.3	18.5
Succinate	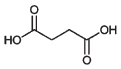	> 100	85.3
BNS	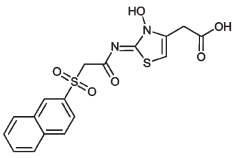	<1	0.021
BIQ	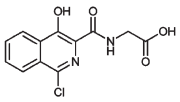	<1	0.073
L-Ala-BIQ	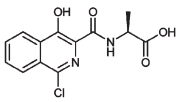	<1	0.512
D-Ala-BIQ	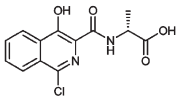	~22	230
L-Val-BIQ	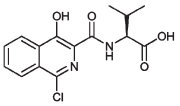	~35	> 400
D-Val-BIQ	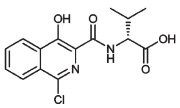	~33	> 400

for 2OG and NOG,[23,37] possibly because in this work we are analyzing binding to a PHD2−Mn(II) rather than a PHD2−Fe(II) complex. Thus, both qualitative screening and the quantitative determination of binding kinetics appear feasible at high field and with conventional, widely used NMR instrumentation.

Determination of Inhibitor Binding Affinities. The bicyclic isoquinolinyl inhibitor (BIQ) is a potent inhibitor of PHD2, with an IC_{50} value of 0.07 μM.[43−45] Most PHD2/HIF hydroxylase inhibitors have amino acid side chains that bind in the 2OG binding pocket, and previous work has shown that the selectivity of these inhibitors can be modified by varying the amino acid moiety.[33] A series of D/L-amino acid substituted BIQ analogues have been synthesized; the binding of some of these to PHD2 is limited by steric constraints.[46] These were screened for their binding affinities using the solvent relaxation technique (Table 1). We found that the introduction of a methyl group (alanine derivative) altered the selectivity of BIQ binding significantly, with L-Ala-BIQ binding to PHD2 in a similar fashion to BIQ, whereas D-Ala-BIQ was a much weaker binder. The relative weaker binding of D-Ala-BIQ is likely due, at least in part, to steric hindrance with the side chain of valine-376 in the 2OG binding pocket.[43,46] Solvent relaxation experiments gave K_D values of $< 1\,\mu M$ and $\sim 22\,\mu M$ for L-Ala-BIQ and D-Ala-BIQ respectively (see Supporting Information, Figure S8), consistent with the binding data obtained from nondenaturing ESI-MS (see Supporting Information, Figure S15).

The substitution of the glycine moiety of BIQ by bulky amino acids such as valine also sterically weakens the binding of BIQ inhibitors to PHD2. In fact, D- and L-Val BIQ show very similar levels of weak binding as indicated by MS analyses (Supporting Information, Figure S15). Solvent relaxation experiments gave K_D values of ~33 μM and ~35 μM for D- and L-Val BIQ, respectively (see Supporting Information, Figures S9−S10). Our results therefore demonstrate and further support the accuracy and sensitivity of this technique while using more conventional NMR instrumentation.

Investigation of PHD2−Mn(II)−2OG−HIF-α Complex Formation. CODD and NODD are 19 amino-acid peptide substrates of PHD2 which are fragments of the natural human HIF-1α; both are hydroxylated by PHD2 at the *trans*-C4 position of a prolyl residue.[23] In studies on the binding of larger peptides such as these, it is often difficult to apply ligand-based NMR techniques; for example, in the transferred NOE method, it becomes difficult to distinguish between NOE signals arising from free and bound peptides because they have the same sign, while in saturation transfer difference (STD) NMR, peak overlap can make it difficult to irradiate selectively the protein resonances. Despite the relatively large size of the NODD and CODD peptide substrates, the application of the solvent relaxation technique at high field is straightforward because only the HDO signal is observed.

Previous biophysical and kinetic studies show that PHD2 has a preference for hydroxylating CODD over NODD,[47−49] and K_m values for CODD and NODD were reported as 37 and 44 μM, respectively.[48] Our results suggest CODD is a significantly stronger binder than NODD, with K_D values of ~14 and ~85 μM, respectively, derived from solvent relaxation data (see Supporting Information, Figures S11−S12). Because neither CODD or NODD directly chelate the metal center,[39] these data demonstrate that it is possible to screen for compounds that bind in the vicinity of the active site metal yet need not interact with this directly, provided that their association displaces water molecules from the active site metal (or indeed enhances their access) or alters their exchange with bulk water. These data are also consistent with the proposed PHD2 mechanism of hydroxylation which, by analogy with work on other 2OG oxygenases, involves displacement of water complexed to the active site iron upon CODD or NODD binding, such that a coordination position becomes free for an oxygen molecule to coordinate to the metal prior to the oxidative decarboxylation step.[50−52]

We have also investigated whether this technique can be used for mechanistic studies. CODD and NODD are both known to form complexes with the PHD2−metal complex and 2OG. CODD binds to PHD2 in a well-defined cleft, adopting a loose and extended conformation; 2OG chelates directly to the metal center in a bidentate fashion.[39] A clear additive effect is observed by the water relaxation technique when CODD is added to PHD2−2OG or when 2OG is added to PHD2−CODD (Figure 4). When CODD is first titrated into PHD2 (red squares, Figure 4a), the curve slowly plateaus to around 90% at a substrate to protein ratio of 2:1, indicating formation of a PHD2−CODD complex. Subsequent addition of 2OG (red triangles, Figure 4a) further decreases the $R_1/R_{1(0)}$ ratio to around 70%, indicating the formation of a PHD2−CODD−2OG complex. An equivalent effect is observed when 2OG is titrated into PHD2

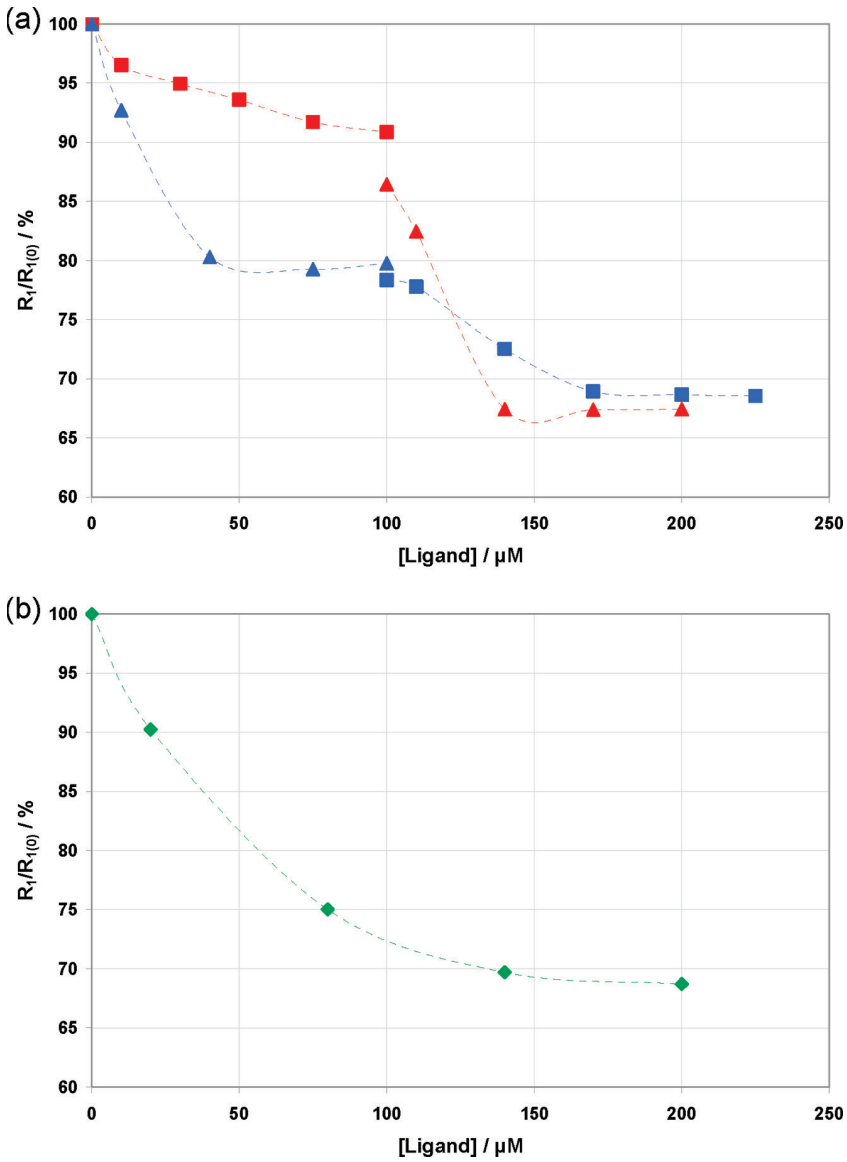

Figure 4. (a) The sequential titration of CODD (solid squares) and 2OG (solid triangles), and (b) simultaneous titration of equal molar CODD and 2OG (solid diamonds) into 50 μM PHD2 as a function of total ligand concentrations. For (a), different colors are used to represent different sequences of addition (red: CODD then 2OG; blue: 2OG then CODD).

first (blue triangles, Figure 4a) in which the $R_1/R_{1(0)}$ ratio plateaus at around 80%, and further titration of CODD (blue squares, Figure 4a) decreases this to around 70%. The titration of an equimolar mixture of 2OG−CODD into PHD2 yields a similar net effect although the profile displays a steeper slope than 2OG or CODD alone due to the binding of both substrate and cofactor throughout. The slight differences in the titration end points observed for the three systems likely arises from the intrinsic variability that occurs between different sample preparations, as described for Figure 1b. The observation of these sequential binding profiles is consistent with previously reported mechanistic and structural studies of PHD2, in which PHD2 forms a ternary complex with 2OG and CODD,[37] and in which 2OG and CODD are observed to bind to neighboring sites in the protein active site.[39,43] It also provides insights into the extent of water accessibility upon the binding of individual substrates. The K_Ds for 2OG in the absence and presence of CODD are measured as 0.9 ± 0.1 and 1.0 ± 0.2 μM, respectively. Similar titration behavior was also observed in ternary systems involving PHD2−2OG−NODD (see Supporting Information, Figure S16).

This additive effect also allows the study of different modes of inhibition. NOG is an unreactive analogue of 2OG, which competes with 2OG for binding to the active site metal.[29,53] As for 2OG, additive effects were observed when CODD was added to PHD2−NOG, indicating the formation of a ternary complex (Figure 5a). In contrast, when CODD (or 2OG) is added to PHD2−BIQ or PHD2−BNS inhibitor complexes, no additive effects were observed (Figure 5b). BIQ and BNS chelate directly to the metal center and therefore compete with 2OG binding, but in addition they also appear able to block CODD from approaching the active site metal, consistent with crystallography studies[39,43] (or alternatively that they serve to completely displace water from around the metal center such that subsequent binding effects cannot be detected, although this

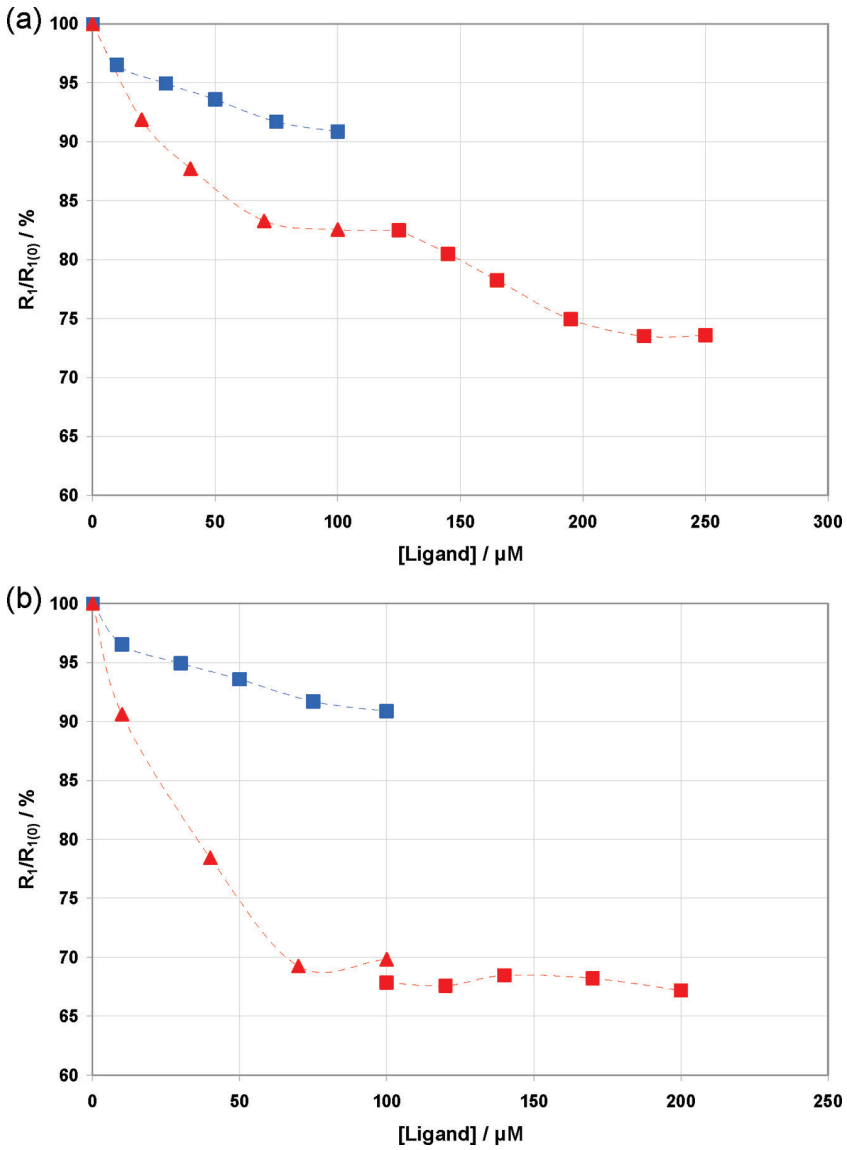

Figure 5. Binding titration curves showing (a) the titration of CODD (red squares) into a solution of PHD2 + NOG (red triangles) and (b) the titration of CODD (red squares) into a solution of PHD2 + BNS (red triangles). In both, the titration of CODD into PHD2 is also plotted as reference (blue squares). Additive effects can be observed in (a) indicating the formation of a PHD2−NOG−CODD complex, while in (b) the BNS inhibitor prevents CODD from approaching the PHD2 active site metal.

seems less likely as they are bidentate metal ligands). Thus, the additional bulk associated with these ligands also offers a second mode of inhibition through blocking substrate binding. Information such as this could prove valuable in inhibitor optimization.

Discussion and Conclusions

We have herein demonstrated the general applicability of ligand screening with paramagnetic metalloproteins through the study of bulk water relaxation, notably using high field NMR spectrometers. It is important to emphasize that the technique is relatively simple to carry out both from experimental and data analysis perspectives. The method is highly sensitive to ligand binding events directly at, and in the vicinity of, the paramagnetic metal center. It enables the differentiation of binding affinities between ligands and, in favorable cases, allows the value of dissociation constants to be determined. Furthermore, it is less restricted than many other screening methods by the upper and lower affinity limits imposed by ligand exchange kinetics.

We have further demonstrated the wider applicability of this technique to detect multiple binding events such as in the formation of ternary protein−substrate complexes, which may have potential applicability in mechanistic studies of enzyme processes and in the design of enzyme inhibitors. Other NMR techniques that are able to identify ternary complex formation, such as interligand NOEs (ILOEs),[54,55] lack the relative simplicity and sensitivity of the solvent relaxation method presented here, requiring very long experiment times and careful optimization of ligand−protein ratios for their success. The ability to screen the formation of ternary complexes in a high throughput fashion is therefore potentially powerful in mechanistic studies on enzymes and in drug design. For instance, Becattini et al. have reported a methodology for drug discovery through the application of ILOEs in which a library of small molecules with simple structures was screened for ternary complex formation.[56] Covalent linkage

of molecules that bind simultaneously may then lead to larger and potentially more potent inhibitors. Provided the target enzyme is a paramagnetic metalloprotein, this solvent screening technique may provide an attractive alternative to ILOEs, in that it may enable the straightforward identification of ternary complex formation.

We also suggest this technique can be applied in a high-throughput fashion for the ligand screening of paramagnetic metalloproteins; by conducting a 2-point assay with and without potential ligands, a significant change in solvent relaxation rate may be correlated with ligand binding. The screening of each potential ligand can be as short as 10 min and may be performed using robotic sample handling.

Experimental Section

Materials. All chemicals were from Sigma-Aldrich, with the exceptions of the CODD (sequence DLDLEMLAPYIPMDDDFQL) and NODD (sequence DALTLLAPAAGDTIISLDF) peptides (Peptide Protein Research Limited), Tris-D11 (Cambridge Isotope Laboratories), and D_2O (Apollo Scientific). BNS was a kind gift from Amgen. BIQ and analogues of BIQ were synthesized by reported methods.[46]

Expression and Purification of PHD2. Recombinant PHD2 was expressed in *Escherichia coli* BL21 (DE3) and purified by cation exchange and size exclusion chromatography as described previously.[37] Apo-proteins were obtained by incubation with EDTA after cation exchange chromatography. Purified PHD2 was buffer exchanged into 50 mM Tris-D11 (100% D_2O, pD 7.1) using Amicon Ultra-4 or Amicon Ultra-15 filter units (MW cutoff: 10 kDa) (Millipore). At least three rounds of dilution and concentration were performed at 277 K. PHD2 aliquots were stored at 193 K.

NMR Experiments. High-field experiments were conducted at 500 MHz using a Bruker Avance II spectrometer equipped with a standard 5 mm *z*-gradient TXI probe. Unless otherwise stated, all experiments were conducted at 298 K. Conventional 3 mm diameter NMR tubes (Norell or Sigma-Aldrich) containing 50 μM PHD2 were used in all experiments unless otherwise indicated. Solutions were buffered using Tris or Tris-D11 (pH 7.5) dissolved in 12.5% H_2O and 87.5% D_2O. A stock solution of 800 μM Mn(II) was used throughout and diluted to final concentrations of 50 or 100 μM. Stock solutions of ligand molecules were made up freshly to concentrations between 1.6 and 2.5 mM. Samples of 1 μL or 2 μL were titrated into NMR tubes. Inversion recovery experiments were performed with two scans with a relaxation delay of at least 5 times T_1 between transients. Pulse tip-angle calibration using the single-pulse nutation method was undertaken for each sample ensuring accurate 90° and 180° pulses.[57] Curve fitting to allow for the possibility of radiation damping[58,59] was used as a check during development work and proved that under the conditions employed there was no contribution from this to the recovery profiles recorded.

Low-field experiments were conducted using an Oxford Instruments MQC spectrometer operating at 23 MHz. Conventional 5 mm diameter tubes (Norell) were used throughout. All experimental details are as for the high field work, except the solution was buffered in 100% H_2O Tris (pH 7.5), and experiments were conducted at 313 K.

Acknowledgment. We thank Oxford Instruments for access to the low-field NMR spectrometer and K. Jassat and Dr. A. Sagidullin (Oxford Instruments) for their advice and technical assistance with low-field NMR experiments. We thank the EPSRC, the BBSRC, European Union, the Wellcome Trust, the Oxford Centre for Advanced Electron Spin Resonance, and Amgen for funding. We thank Amgen for the gift of the BNS compound.

Supporting Information Available: Solvent relaxation measurement for the binding of Mn(II) to PHD2; fitted K_D curves for the binding of small molecule inhibitors to PHD2; ESI-MS data for the binding of BIQ analogues to PHD2; titration data for NODD and 2OG; details for the synthesis of BIQ analogues. This material is available free of charge via the Internet at http://pubs.acs.org.

References

(1) Mayer, M.; Meyer, B. NMR Characterization of Ligand Binding by Saturation Transfer Difference NMR Spectroscopy. *Angew. Chem., Int. Ed.* **1999**, *38*, 1784–1788.
(2) Ni, F. Recent Developments in Transferred NOE Methods. *Prog. Nucl. Magn. Reson. Spectrosc.* **1994**, *26*, 517–606.
(3) Fejzo, J.; Lepre, C.; Xie, X. Application of NMR Screening in Drug Discovery. *Curr. Top. Med. Chem.* **2003**, *3*, 81–97.
(4) Lepre, C. A.; Moore, J. M.; Peng, J. W. Theory and Applications of NMR-Based Screening in Pharmaceutical Research. *Chem. Rev.* **2004**, *104*, 3641–3675.
(5) Zartler, E. R.; Shapiro, M. J. Protein NMR-Based Screening in Drug Discovery. *Curr. Pharm. Des.* **2006**, *12*, 3963–3972.
(6) Ludwig, C.; Guenther, U. L. Ligand Based NMR Methods for Drug Discovery. *Front. Biosci.* **2009**, *14*, 4565–4574.
(7) Kay, L. E.; Gardner, K. H. Solution NMR Spectroscopy Beyond 25 kDa. *Curr. Opin. Struct. Biol.* **1997**, *7*, 722–731.
(8) Burton, D. R.; Forsen, S.; Karlstrom, G.; Dwek, R. A. Proton Relaxation Enhancement (PRE) in Biochemistry: A Critical Survey. *Prog. Nucl. Magn. Reson. Spectrosc.* **1979**, *13*, 1–45.
(9) Mohr, P. J.; Taylor, B. N.; Newell, D. B. CODATA Recommended Values of the Fundamental Physical Constants: 2006. *Rev. Mod. Phys.* **2008**, *80*, 633–730.
(10) Mildvan, A. S.; Engle, J. L. Nuclear Relaxation Measurements of Water Protons and Other Ligands. *Methods Enzymol.* **1972**, *26*, 654–682.
(11) Mildvan, A. S.; Gupta, R. K. Nuclear Relaxation Measurements of the Geometry of Enzyme-Bound Substrates and Analogs. *Methods Enzymol.* **1978**, *49*, 322–359.
(12) Bertini, I.; Luchinat, C.; Parigi, G. *Solution NMR of Paramagnetic Molecules Applications to Metallobiomolecules and Models*; Elsevier Science: Amsterdam, 2001; pp 75−140.
(13) Eisinger, J.; Shulman, R. G.; Blumberg, W. E. Relaxation Enhancement by Paramagnetic Ion Binding to Deoxyribonucleic Acid Solutions. *Nature* **1961**, *192*, 963–964.
(14) Mildvan, A. S.; Cohn, M. Magnetic Resonance Studies of the Interaction of the Manganous Ion with Bovine Serum Albumin. *Biochemistry* **1963**, *2*, 910–919.
(15) Danchim, A.; Guéron, M. Proton Magnetic Relaxation Study of the Manganese−Transfer-RNA Complex. *J. Chem. Phys.* **1970**, *53*, 3599–3609.
(16) Sherry, A. D.; Birnbaum, E. R.; Darnall, D. W. Proton Relaxation Studies in H_2O-D_2O Mixtures The Binding of Manganese(II) to Bovine Serum Albumin. *Anal. Biochem.* **1973**, *52*, 415–420.
(17) Budak, H. Water Proton Relaxation Rate Enhancements and Association Constants for Mn(II) to Serum Proteins Determined by NMR T_1 Measurements. *Z. Naturforsch.* **2005**, *60c*, 807–812.
(18) Bertini, I.; Fragai, M.; Luchinat, C; Talluri, E. Water-Based Ligand Screening for Paramagnetic Metalloproteins. *Angew. Chem., Int. Ed.* **2008**, *47*, 4533–4537.
(19) In some circumstances, it can be envisaged that the binding of ligands will increase access of water to the paramagnetic center.
(20) Kimmich, R.; Anoardo, E. Field-Cycling NMR Relaxometry. *Prog. Nucl. Magn. Reson. Spectrosc.* **2004**, *44*, 257–320.
(21) Semenza, G. L. Hypoxia-Inducible Factor 1 (HIF-1) Pathway. *Sci. STKE* **2007**, *407*, cm8.
(22) Chowdhury, R.; Hardy, A.; Schofield, C. J. The Human Oxygen Sensing Machinery and its Manipulation. *Chem. Soc. Rev.* **2008**, *37*, 1308–1319.
(23) Epstein, A. C. R.; Gleadle, J. M.; McNeill, L. A.; Hewitson, K. S.; O'Rourke, J.; Mole, D. R.; Mukherji, M.; Metzen, E.; Wilson, M. I.; Dhanda, A.; Tian, Y. M.; Masson, N.; Hamilton, D. L.; Jaakkola, P.; Barstead, R.; Hodgkin, J.; Maxwell, P. H.; Pugh, C. W.; Schofield, C. J.; Ratcliffe, P. J. *C. elegans* EGL-9 and Mammalian Homologs Define a Family of Dioxygenases that Regulate HIF by Prolyl Hydroxylation. *Cell* **2001**, *107*, 43–54.
(24) Bruick, R. K.; McKnight, S. L. Oxygen Sensing Gets a Second Wind. *Science* **2002**, *295*, 807–808.
(25) Hausinger, R. P. Fe(II)/α-Ketoglutarate-Dependent Hydroxylases and Related Enzymes. *Crit. Rev. Biochem. Mol. Biol.* **2004**, *39*, 21–68.

(26) Hewitson, K. S.; Schofield, C. J. The HIF Pathway as a Therapeutic Target. *Drug Discovery Today* **2004**, *9*, 704–711.
(27) Fraisl, P.; Aragonás, J.; Carmeliet, P. Inhibition of Oxygen Sensors as a Therapeutic Strategy for Ischaemic and Inflammatory Disease. *Nat. Rev. Drug Discovery* **2009**, *8*, 139–152.
(28) Jaakkola, P.; Mole, D. R.; Tian, Y. M.; Wilson, M. I.; Gielbert, J.; Gaskell, S. J.; von Kriegsheim, A.; Hebestreit, H. F.; Mukherji, M.; Schofield, C. J.; Maxwell, P. H.; Pugh, C. W.; Ratcliffe, P. J. Targeting of HIF-α to the von Hippel−Lindau Ubiquitylation Complex by O_2-Regulated Prolyl Hydroxylation. *Science* **2001**, *292*, 468–472.
(29) Mole, D. R.; Schlemminger, I.; McNeill, L. A.; Hewitson, K. S.; Pugh, C. W.; Ratcliffe, P. J.; Schofield, C. J. 2-Oxoglutarate Analogue Inhibitors of HIF Prolyl Hydroxylase. *Bioorg. Med. Chem. Lett.* **2003**, *13*, 2677–2680.
(30) Ivan, M.; Haberberger, T.; Gervasi, D. C.; Michelson, K. S.; Günzler, V.; Kondo, K.; Yang, H.; Sorokina, I.; Conaway, R. C.; Conaway, J. W.; Kaelin, W. G., Jr. Biochemical Purification and Pharmacological Inhibition of a Mammalian Prolyl Hydroxylase Acting on Hypoxia-Inducible Factor. *Proc. Natl. Acad. Sci. U.S.A.* **2002**, *99*, 13459–13464.
(31) Schlemminger, I.; Mole, D. R.; McNeill, L. A.; Dhanda, A.; Hewitson, K. S.; Tian, Y. M.; Ratcliffe, P. J.; Pugh, C. W.; Schofield, C. J. Analogues of Dealanylalahopcin are Inhibitors of Human HIF Prolyl Hydroxylases. *Bioorg. Med. Chem. Lett.* **2003**, *13*, 1451–1454.
(32) Hewitson, K. S.; McNeill, L. A.; Schofield, C. J. Modulating the hypoxia-inducible factor signaling pathway: Applications from cardiovascular disease to cancer. *Curr. Pharm. Des.* **2004**, *10*, 821–833.
(33) McDonough, M. A.; McNeill, L. A.; Tilliet, M.; Papamicaël, C. A.; Chen, Q. Y.; Banerji, B.; Hewitson, K. S.; Schofield, C. J. Selective Inhibition of Factor Inhibiting Hypoxia-Inducible Factor. *J. Am. Chem. Soc.* **2005**, *127*, 7680–7681.
(34) Tegley, C. M.; Viswanadhan, V. N.; Biswas, K.; Frohn, M. J.; Peterkin, T. A. N.; Chang, C.; Bürli, R. W.; Dao, J. H.; Veith, H.; Rogers, N.; Yoder, S. C.; Biddlecome, G.; Tagari, P.; Allen, J. R.; Hungate, R. W. Discovery of Novel Hydroxy-thiazoles as HIF-α Prolyl Hydroxylase Inhibitors: SAR, Synthesis, and Modeling Evaluation. *Bioorg. Med. Chem. Lett.* **2008**, *18*, 3925–3928.
(35) Liénard, B. M.; Conejo-García, A.; Stolze, I.; Loenarz, C.; Oldham, N. J.; Ratcliffe, P. J.; Schofield, C. J. Evaluation of Aspirin Metabolites as Inhibitors of Hypoxia-Inducible Factor Hydroxylases. *Chem. Commun.* **2008**, *47*, 6393–6395.
(36) Dao, J. H.; Kurzeja, R. J. M.; Morachis, J. M.; Veith, H.; Lewis, J.; Yu, V.; Tegley, C. M.; Tagari, P. Kinetic Characterization and Identification of a Novel Inhibitor of Hypoxia-Inducible Factor Prolyl Hydroxylase 2 Using a Time-Resolved Fluorescence Resonance Energy Transfer-Based Assay Technology. *Anal. Biochem.* **2009**, *384*, 213–223.
(37) McNeill, L. A.; Flashman, E.; Buck, M. R. G.; Hewitson, K. S.; Clifton, I. J.; Jeschke, G.; Claridge, T. D. W.; Ehrismann, D.; Oldham, N. J.; Schofield, C. J. Hypoxia-Inducible Factor Prolyl Hydroxylase 2 has a high affinity for Ferrous Iron and 2-Oxyglutarate. *Mol. BioSyst.* **2005**, *1*, 321–324.
(38) Mecinović, J.; Chowdhury, R.; Liénard, B. M. R.; Flashman, E.; Buck, M. R. G.; Oldham, N. J.; Schofield, C. J. ESI-MS Studies on Prolyl Hydroxylase Domain 2 Reveal a New Metal Binding Site. *ChemMedChem* **2008**, *3*, 569–572.
(39) Chowdhury, R.; McDonough, M. A.; Mecinović, J.; Loenarz, C.; Flashman, E.; Hewitson, K. S.; Domene, C.; Schofield, C. J. Structural Basis for Binding of Hypoxia-Inducible Factor to the Oxygen-Sensing Prolyl Hydroxylases. *Structure* **2009**, *17*, 981–989.
(40) Niccolai, N.; Tiezzi, E.; Valensin, G. Manganese(II) as Magnetic Relaxation Probe in the Study of Biomechanisms and of Biomacromolecules. *Chem. Rev.* **1982**, *82*, 359–384.
(41) Carr, H. Y.; Purcell, E. M. Effects of Diffusion on Free Precession in Nuclear Magnetic Resonance Experiments. *Phys. Rev.* **1954**, *94*, 630–638.
(42) Hewitson, K .S.; Liénard, B. M. R.; McDonough, M. A.; Clifton, I. J.; Butler, D.; Soares, A. S.; Oldham, N. J.; McNeill, L. A.; Schofield, C. J. Structural and Mechanistic Studies on the Inhibition of the Hypoxia-inducible Transcription Factor Hydroxylases by Tricarboxylic Acid Cycle Intermediates. *J. Biol. Chem.* **2007**, *282*, 3293–3301.
(43) McDonough, M. A.; Li, V.; Flashman, E.; Chowdhury, R.; Mohr, C.; Liénard, B. M. R.; Zondlo, J.; Oldham, N. J.; Clifton, I. J.; Lewis, J.; McNeill, L. A.; Kurzeja, R. J. M.; Hewitson, K. S.; Yang, E.; Jordan, S.; Syed, R. S.; Schofield, C. J. Cellular Oxygen Sensing: Crystal Structure of Hypoxia-Inducible Factor Prolyl Hydroxylase (PHD2). *Proc. Natl. Acad. Sci. U.S.A.* **2006**, *103*, 9814–9819.
(44) Warshakoon, N. C.; Wu, S.; Boyer, A.; Kawamoto, R.; Sheville, J.; Renock, S.; Xu, K.; Pokross, M.; Evdokimov, A. G.; Walter, R.; Mekel, M. A Novel Series of Imidazo[1,2-*a*]pyridine Derivatives as HIF-1α Prolyl Hydroxylase Inhibitors. *Bioorg. Med. Chem. Lett.* **2006**, *16*, 5598–5601.
(45) Guenzler, P.; Volkmar, K.; Stephen, J.; Liu, D. Y.; Todd, W. PCT. Int. Appl. WO 2005007192, **2005**.
(46) Stubbs, C. J.; Loenarz, C.; Mecinović, J.; Yeoh, K. K.; Hindley, N.; Liénard, B. M.; Sobott, F.; Schofield, C. J.; Flashman, E. Application of a Proteolysis/Mass Spectrometry Method for Investigating the Effects of Inhibitors on Hydroxylase Structure. *J. Med. Chem.* **2009**, *52*, 2799–2805.
(47) Ehrismann, D.; Flashman, E.; Genn, D. N.; Mathioudakis, N.; Hewitson, K. S.; Ratcliffe, P. J.; Schofield, C. J. Studies on the Activity of the Hypoxia-Inducible-Factor Hydroxylases Using an Oxygen Consumption Assay. *Biochem. J.* **2007**, *401*, 227.
(48) Flashman, E.; Bagg, E. A. L.; Chowdhury, R.; Mecinović, J.; Loenarz, C.; McDonough, M. A.; Hewitson, K. S.; Schofield, C. J. Kinetic Rationale for Selectivity Toward N- and C-terminal Oxygen-Dependent Degradation Domain Substrates Mediated by a Loop Region of Hypoxia-Inducible Factor Prolyl Hydroxylases. *J. Biol. Chem.* **2008**, *283*, 3808–3815.
(49) Chan, D. A.; Sutphin, P. D.; Yen, S. E.; Giaccia, A. J. Coordinate Regulation of the Oxygen-Dependent Degradation Domains of Hypoxia-Inducible Factor 1α. *Mol. Cell. Biol.* **2005**, *25*, 6415–6426.
(50) Zhang, Z.; Ren, J.-S.; Harlos, K.; McKinnon, C. H.; Clifton, I. J.; Schofield, C. J. Crystal Structure of a Clavaminate Synthase-Fe(II)-2-Oxoglutarate-Substrate-NO Complex: Evidence for Metal Centred Rearrangements. *FEBS Lett.* **2002**, *517*, 7–12.
(51) Zhang, Z.; Ren, J.; Stammers, D. K.; Baldwin, J. E.; Harlos, K.; Schofield, C. J. Structural Origins of the Selectivity of the Trifunctional Oxygenase Clavaminic Acid Synthase. *Nat. Struct. Biol.* **2000**, *7*, 127–133.
(52) Zhou, J.; Kelly, W. L.; Bachmann, B. O.; Gunsior, M.; Townsend, C. A.; Solomon, E. I. Spectroscopic Studies of Substrate Interactions with Clavaminate Synthase 2, a Multifunctional Alpha-KG-Dependent Non-Heme Iron Enzyme: Correlation with Mechanisms and Reactivities. *J. Am. Chem. Soc.* **2001**, *123*, 7388–7398.
(53) Cunliffe, C. J.; Franklin, T. J.; Hales, N. J.; Hill, G. B. Novel inhibitors of prolyl 4-hydroxylase. 3. Inhibition by the substrate analog *N*-oxaloglycine and its derivatives. *J. Med. Chem.* **1992**, *35*, 2652–2658.
(54) London, R. E. Theoretical Analysis of the Inter-Ligand Overhauser Effect: A New Approach for Mapping Structural Relationships of Macromolecular Ligands. *J. Magn. Reson.* **1999**, *141*, 301–311.
(55) Li, D.; DeRose, E. F.; London, R. E. The Inter-Ligand Overhauser Effect: A Powerful New NMR Approach For Mapping Structural Relationships of Macromolecular Ligands. *J. Biomol. NMR* **1999**, *15*, 71–76.
(56) Becattini, B.; Pellecchia, M. SAR by ILOEs: An NMR-Based Approach to Reverse Chemical Genetics. *Chem.—Eur. J.* **2006**, *12*, 2658–2662.
(57) Wu, P. S. C.; Otting, G. Rapid Pulse Length Determination in High-Resolution NMR. *J. Magn. Reson.* **2005**, *176*, 115–119.
(58) Mao, X; Guo, J.; Ye, C. Competition Between Radiation Damping and Transverse Relaxation Effects on NMR Signal Intensities. *Chem. Phys. Lett.* **1994**, *218*, 249–253.
(59) Mao, X.; Guo, J.; Ye, C. Radiation Damping Effects on Spin-Lattice Relaxation Time Measurements. *Chem. Phys. Lett.* **1994**, *222*, 417–421.